Jarrah Ali Al-Tubaikh

Internal Medicine

An Illustrated Radiological Guide

Springer

Internal Medicine

Jarrah Ali Al-Tubaikh

Internal Medicine

An Illustrated Radiological Guide

Springer

Dr. Jarrah Ali Al-Tubaikh
Universitätsklinikum München
Klinikum Großhadern
Institut für Klinische Radiologie
Marchioninistr. 15
81377 München
Germany
Tabeebjarah@hotmail.com

Radiologist, Medical Illustrator
Department of Diagnostic Radiology
Sabah Hospital, Kuwait

All illustrations marked with  were drawn by the author.

ISBN: 978-3-642-03708-5 e-ISBN: 978-3-642-03709-2

DOI: 10.1007/978-3-642-03709-2

Springer Heidelberg Dordrecht London New York

Library of Congress Control Number: 2009938956

Cover design: eStudioCalamar, Figueres/Berlin

Printed on acid-free paper

Springer is part of Springer Science+Business Media (www.springer.com)

This book is dedicated to my mother, father, family, and my beloved country "Kuwait".

Preface

In any radiology department worldwide, around 60–70% of investigations deal with surgical cases: trauma, tumors, pre- and postsurgical assessment, surgical follow-ups, and more. In spite of that, radiology has a lot to offer in the field of internal medicine in terms of establishing, confirming, or rejecting diagnoses, or favoring differential diagnoses.

Before I joined radiology, I worked as an internal physician for almost a year and almost another year and half as a general surgeon. This clinical experience leads me to look at radiological images with the eye of a radiologist and the mind of a clinician when I examine patient radiological images. I even take a history and do a clinical examination if I have the chance when the patient is in the ultrasound, CT, or MRI room. I have always believed that the radiologist's role is not confined to writing reports, but it can be broadened to establish the diagnosis in the first hand in the same way as the clinician do.

In the medical library, there are books dedicated to the clinical signs of internal medicine diseases; interestingly, there are no such books in the radiology library. Radiology books concentrate on the radiological signs according to the system involved, not according to the disease or the specialty. For example, looking for signs of multiple myeloma follows the bone marrow tumors in a musculoskeletal radiology book, not a radiological book that discusses diseases of hematology, for example, which is the main target and idea of this book.

This book is designed to put the radiologist in the internal physician's shoes. It teaches radiologists how to think in terms of disease progression and complications, where to look for and to image these complications, and what are the best modalities used to reach a diagnosis. Also, the internal physicians can benefit from this book by learning what help radiology can offer them in establishing a diagnosis. The book also helps internal physicians to think like radiologists, in terms of what investigation they should request to confirm their diagnosis.

Each disease is mentioned with its pathophysiology, symptoms, clinical presentation, and how radiology can be used to establish the diagnosis or to look for the complications of this particular disease. Specialties covered in this book include gastroenterology, neurology, endocrinology, nephrology, cardiology, rheumatology, pulmonology, dermatology, hematology, diabetology, and tropical and infectious medicine.

The book works as a short textbook with an atlas of images. The book is not designed to serve as the only textbook for study. Doctors, or radiologists who are interested in more details about a certain disease, should refer to the standard medical or radiological textbooks.

Although the book's title is *Internal Medicine – An Illustrated Radiological Guide*, the book is not confined to medical diseases alone. Pediatrics, gynecology, genetics, and some surgical cases are discussed in the differentials. Although the world's new direction is toward subspecialties, this is not always the case in radiology. Internal medicine practitioners can refer a patient to a specialist when they feel the case requires it; this is unfortunately not always the case in radiology. Radiology residents may have a request involving an internal medicine case now, and the next case can be a pediatric or a surgical case. This situation of multispecialty diagnosis is faced by so many radiology residents around the world daily. Radiologists can refer the case to a senior, a more experienced, or a specialized radiologist, but again, this is not always the case, especially in hospitals with small radiology departments. I have tried in this book to summarize the diseases that can be in the differential diagnoses or related to a common disease. I have designed the book to mention only the diseases that can be ruled out by history and radiological images, which are the main tools for a radiology resident on duty in a hospital, or without a radiology specialist nearby. Moreover, the differentials are categorized as rare and uncommon diseases. I have specifically chosen these differentials to give the reader more insights and information about rare diseases that can have the same presentation as the disease discussed.

Finally, I hope that this modest work will be of assistance to residents and radiologists worldwide and will work as a quick useful tool to revise the most important signs of radiological diseases in a short time, which is the main goal that I would like to achieve with this book.

Munich, Germany Dr. Jarrah Ali Al-Tubaikh

Contents

Abbreviations

CBCT	Cone-beam computed tomography
CT	Computed tomography
CTA	Computed tomography angiography
DWI	Diffusion-weighted image
FLAIR	Fluid-attenuated inversion recovery sequence
FLASH	Fast low-angle shot sequence
HASTE	Half-Fourier acquisition single-shot turbo spin-echo
HRCT	High-resolution computed tomography
HU	Hounsfield unit
IVU	Intravenous urography
MRA	Magnetic resonance angiography
MRCP	Magnetic resonance cholangiopancreaticography
MRI	Magnetic resonance image
PD	Power Doppler
STIR	Short-tau inversion recovery
True FISP	True fast imaging with steady-state procession
T1W	T1-weighted
T2W	T2-weighted
US	Ultrasound
3D FLASH	Three-dimensional fast low-angle shot images

Contributors

Prof. Dr. Maximilian F. Reiser, FRCR, FACR Universitätsklinikum München, Klinikum Großhadern Institute für Klinische Radiologie, Marchioninistr. 15, 81377 München, Germany

Prof. Tarek Al-Zayat, MD Department of Diagnostic Radiology, Al-Azhar University Hospitals, Cairo, Egypt

Rajae Makar, MD Department of Diagnostic Radiology, Sabah Hospital, Kuwait

Bader Al-Mahdi, MD Cardiologist, Cardiology Care Unit, Adan Hospital, Kuwait

Alaa Abou-Beih, MD Senior Head and Neck Surgeon, Department of Ear, Nose and Throat, Zain Hospital, Kuwait
Lecturer in Otolaryngology Department, Faculty of Medicine, Mansoura University, Mansoura, Egypt

Chapter 1

Gastroenterology

CONTENTS

J. A. Al-Tubaikh: *Internal Medicine* – An Illustrated Radiological Guide
DOI: 10.1007/978-3-642-03709-2_1, © Springer-Verlag Berlin Heidelberg 2010

1.1 Liver Cirrhosis

Liver cirrhosis is a term used to describe the histological development of regenerative hepatic nodules surrounded by fibrous bands in response to chronic liver injury.

Cirrhosis is an advanced, diffuse stage of liver injury, which is characterized by replacement of the normal liver parenchyma by collagenous scar (fibrosis). Cirrhosis is accompanied by diffuse distortion of the hepatic vasculature and architecture, resulting in vascular disturbance between the portal veins and the hepatic veins, plus porta hepatic fibrosis. The major cirrhosis consequences are hepatic function impairment, increased intrahepatic resistance (portal hypertension), and the development of hepatocellular carcinoma (HCC).

Types of Liver Cirrhosis

- *Laennec's cirrhosis* is a type of micro-nodular liver cirrhosis that is seen in patients with malnutrition, alcoholism, or chronic liver steatosis.
- *Posthepatitic cirrhosis* is a micro- and/or macronodular liver cirrhosis commonly seen in patients with hepatitis C virus or uncommonly B virus.
- *Postnecrotic cirrhosis* is macronodular liver cirrhosis that can arise due to fulminating hepatitis infection, or due to toxic liver injury.
- *Primary biliary cirrhosis* (*PBC*) (*Vanishing bile duct syndrome*) is an autoimmune disease of unknown origin characterized by progressive intrahepatic bile duct, nonsuppurative inflammation, and destruction by T-cell lymphocytes, which leads later on to micronodular liver cirrhosis, hepatomegaly, with greenish-stain liver on gross examination due to bile retention. PBC occurs in middle-aged women in up to 90% of cases. In symptomatic PBC, patients may complain of jaundice in the first 2–3 years, which develops later into portal hypertension and hepatosplenomegaly. In the asymptomatic PBC, the only symptom is abnormal serum hepatobiliary enzyme levels. PBC is classified pathologically into four main stages. *Florid duct stage* (*Stage I PBC*) is characterized by vanishing intrahepatic duct and ductopenia due to destruction of the intrahepatic bile ducts basement membrane and cellular bodies by lymphocytes. *Ductular proliferation stage* (*Stage II*) is characterized by small bile ducts proliferation in an attempt to compensate the obstruction of the large bile ducts. The liver characteristically contains few large ducts, and many small bile ducts. *Scarring* (*Stage III*) is characterized by fibrosis and intrahepatic collagen deposition. *Hepatic cirrhosis* (*Stage IV*) is characterized by architectural hepatic disruption, and accumulation of the bile within the hepatocytes. The disease is diagnosed by liver biopsy, plus detecting antimitochondrial antibodies (AMA) in the serum.
- *Secondary biliary cirrhosis* arises due to extrahepatic obstruction of the biliary tree, causing bile stagnation within the liver. This type can be seen in cases of congenital bile duct atresia, chronic biliary stones obstruction, or pancreatic head carcinoma. The inflammation in the secondary biliary cirrhosis arises due to secondary infection of the bile, leading to neutrophilic acute inflammatory reaction. In contrast, PBC is a chronic, autoimmune disease with lymphatic and plasma cell inflammatory reaction.
- *Cirrhosis due to metabolic disease* is seen in glycogen-storage diseases, α1-Antitrypsin deficiency disease, hemochromatosis, and Wilson's disease. All the metabolic cirrhoses are micronodular except Wilson's disease (macronodular).
- *Cirrhosis due to circulatory disorders* is observed in patients with venous congestion due to right-sided heart failure, veno-occlusive disease due to herbal medicine, and Budd-Chiari syndrome. In congestive heart failure, chronic hepatic venous congestion may lead to interahepatic hypertension, which results in sinusoidal congestion, pressure atrophy, and necrosis of pericentral parenchymal cells. Later, there is collapse of the necrotic cells with perisinusoidal and periportal collagen deposition (fibrosis) extending to the central veins. These changes are known as "nutmeg liver" on postmortem liver examination.

Cirrhotic nodules are parenchymal nodules found in cirrhotic liver (seen in 25% of imaging scans only), and they are divided into three main types:

- *Regenerative nodules* represent normal proliferation of liver parenchyma. The development of regenerative nodules can be explained pathologically by cellular repair mechanism known as "cell-to-cell and

cell-to-matrix interaction." Cell-to-cell interaction describes the process of cellular inhibition when two cells touch each other (e.g., skin wound healing). Cell-to-matrix interaction describes the process of cellular proliferation inhibition when the regenerated cells touch the tissue matrix (connective tissue frame). In acute hepatitis, if the connective tissue matrix is preserved, then damage to the liver can be completely repaired without architectural distortion or residuals. In contrast, in chronic hepatitis, both the liver parenchyma and the connective tissue frame are damaged. This matrix damage results in random liver cells regeneration without cell-to-matrix cellular inhibition, which will result in regenerative liver nodules formation with fibrosis in between (liver cirrhosis). These nodules do not function normally because the relationship with the portal vein, hepatic artery, and bile ducts (porta hepatis) is lost.

- *Dysplastic nodules* are regenerative premalignant nodules.
- *HCC nodules* are nodules composed of neoplastic cells and are seen commonly in patients with cirrhosis due to hepatitis C virus.

Patients with cirrhosis are asymptomatic, unless they develop signs of liver failure. Signs of liver failure include yellowish discoloration of the skin (jaundice), development of central arteriole dilatation with radiating vessels on the face (spider navie), white nail bed due to hypoalbuminemia, painful proliferative arthropathy of long bones, gynecomastia and palmar erythema due to reduced estradiol degeneration by the liver, hypogonadism (mainly in cirrhosis due to alcoholism and hemochromatosis), anorexia and wasting (>50% of patients), and diabetes mellitus type 2 (up to 30% of patients). Some patients with liver cirrhosis may develop palmar fibromatosis.

Fibromatosis is a pathological condition characterized by local proliferation of fibroblasts which manifests clinically as soft tissue thickening. Fibromatosis can affect the palmas aponeurosis (*Dupuytren's contracure*), causing limited hand extension and possibly bony erosions (Fig. 1.1.1). Palmar fibromatosis that occurs in a bilateral fashion and is associated with bilateral plantar fibromatosis is called "*Ledderhose disease*" (Fig. 1.1.1). Other forms of fibromatosis in the body include the male genital fibromatosis (*Peyronie's disease*), and fibromatosis of the dorsum of the interphalangeal joint (*Garrod's nodes*).

The development of portal hypertension can result in splenomegaly, ascites, and prominent paraumbilical veins (caput medusae). Multiple intra- and extrahepatic portosystemic collaterals develop to compensate the loss of the large portal venous flow that cannot be maintained longer due to increased intrahepatic venous pressure in portal hypertension. Intrahepatic portosystemic shunts occur when the portal vein communicates with the hepatic vein in or on the surface of the liver

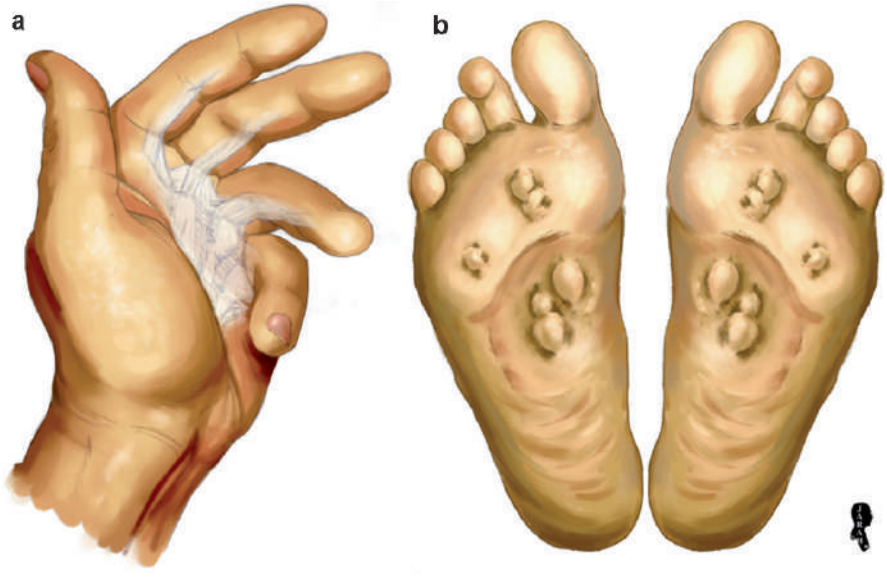

Fig. 1.1.1. An illustration shows the clinical pathological picture of Dupuytren's contracure with illustrated thickening of the palmar aponeurosis (**a**), and bilateral plantar nodules representing the clinical manifestation of Ledderhose disease (**b**)

1.1

through a dilated venous system. In contrast, extrahepatic portosystemic shunts occur when the intrahepatic portal vein runs toward the outside of the liver communicating with the systemic veins. *Cruveilhier-Baumgarten syndrome* is a condition characterized by patent paraumbilical vein as a consequence of portal hypertension, which occurs as a part of porto-systemic shunts. Paraesophageal and paragastric varices develop in patients with advanced liver cirrhosis and can cause life-threatening upper gastrointestinal (GI) bleeding.

Hepatic encephalopathy is a potentially reversible complication seen in advanced liver failure and cirrhosis characterized by motor, cognitive, and psychiatric central nervous system (CNS) dysfunction. Manifestations of hepatic encephalopathy include daytime deterioration (grade 1), disorientation in space (grade 2), or coma (grade 3). Flapping tremor (asterixis) may be seen in patients with hepatic encephalopathy. The neurological manifestations of hepatic encephalopathy are due to inability of the liver to detoxify neurotoxins such as ammonia, phenols, short chained fatty acids, and other toxic metabolites within the blood. These toxic metabolites cross the blood brain barrier and deposits within the basal ganglia causing encephalopathy. Hepatic encephalopathy can be induced or exaggerated by sedation, high protein diet, GI hemorrhage, and the use of diuretics.

Hepatopulmonary syndrome is an end-stage liver disease characterized by pulmonary failure, and it is seen in 15–20% of cirrhosis patients. The diagnosis of hepatopulmonary syndrome requires the following three criteria: chronic liver disease, increased alveolar-arterial gradient on room air, and evidence of intrapulmonary vascular dilatation. Patients with hepatopulmonary syndrome present with liver cirrhosis with hypoxia (30% of decompensated liver patients). This hypoxemia occurs due to pulmonary vascular dilatation and subsequent ventilation-perfusion mismatch due to decreased hepatic clearance, or increased hepatic productions of circulating cytokines and chemical mediators (e.g., nitric oxide). Hypoxic respiratory failure can occur with cases of massive liver necrosis or fulminant hepatic failure.

Hepatitic C virus-related arthritis (HCVrA) may be seen in patients with liver cirrhosis due to hepatitis C virus. HCVrA affects 4% of patients with HCV liver cirrhosis, and it has two forms: a frequent symmetrical polyarthritis affecting small joints similar to rheumatoid arthritis in a lesser form, and an intermittent mono-oligoarthritis that involves medium- and large-sized joints.

Signs on Plain Radiographs

- *Hepatic hydrothorax* is defined as large pleural effusion in a cirrhotic liver disease patient in the absence of cardiac or pulmonary disease. Hepatic hydrothorax is seen in 10% of patients. The pleural effusion can be right-sided (67%), left-sided (17%), or bilateral (17%).
- Hepatopulmonary syndrome is visualized on plain chest radiographs as reticulonodular interstitial pattern located mainly at the lung bases (46–100% of cases).
- Noncardiogenic pulmonary edema can be seen in 37% in patients with fulminant hepatic failure.
- Esophageal varices may manifest on chest radiographs as focal lateral displacement of the mediastinum.
- On abdominal radiographs, ascites is detected as loss of the abdominal gasses and the normal psoas shadows visualization. The abdomen structures are blurry due to the overlying fluid shadow (Fig. 1.1.2).

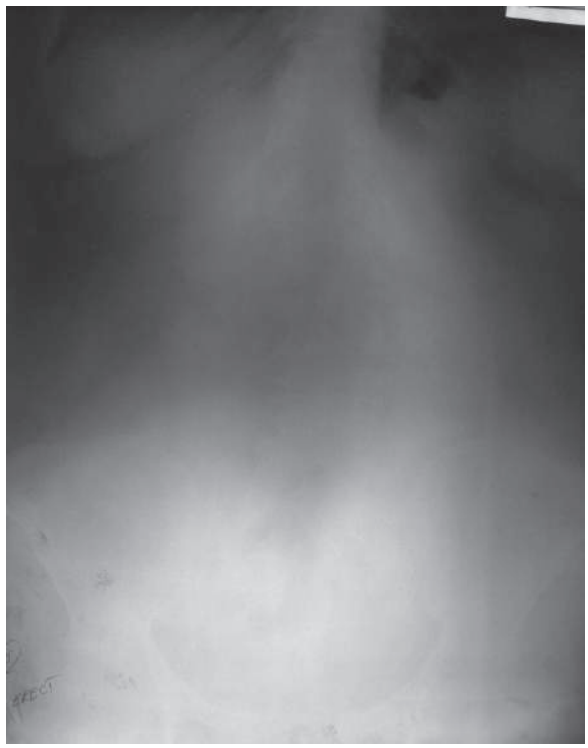

Fig. 1.1.2. Plain abdominal radiograph in a patient with massive ascites shows complete blurry abdomen

Signs on US

- Cirrhosis is detected as irregular nodular liver contour with inhomogeneous echo-texture. Liver right lobe atrophy with enlarged caudate lobe is a typical finding (caudate lobe/right lobe ratio >0.65). (Figs. 1.1.3 and 1.1.4)
- Mixed hypoechoic and hyperechoic texture of the liver parenchyma is detected when regenerative nodules are found.
- Signs of portal hypertension include splenomegaly (>12 cm), ascites, and dilated venous collaterals.

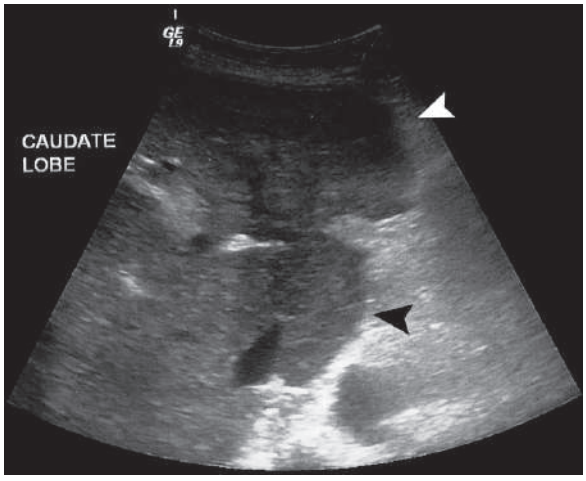

Fig. 1.1.3. Transverse ultrasound image of a patient with liver cirrhosis shows atrophied left lobe (*white arrowhead*), with hypertrophied caudate lobe (*black arrowhead*)

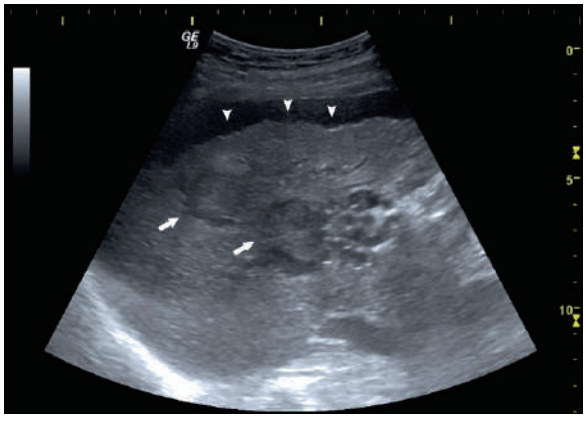

Fig. 1.1.4. Transverse ultrasound image of a patient with liver cirrhosis due to hepatitis C virus shows irregular liver contour (*arrowheads*), with two intrahepatic liver hypoechoic masses, which were diagnosed on liver triphasic CT scan later as hepatocellular carcinoma (HCC) masses (*arrows*)

Signs on Doppler Sonography

- *Hepatic veins*: hepatic veins join immediately the inferior vena cava, which is in direct communication with the left atrium. Due to the previous anatomical fact, the normal hepatic veins waveform is "triphasic," because it is affected by left atrial cardiac motion and Valsalva maneuver (Fig. 1.1.5). In patients with cirrhosis, the triphasic flow pattern is converted into biphasic, and monophasic depending on the severity of cirrhosis.
- *Portal vein*: it supplies 70–80% of the incoming blood to the liver, and the hepatic artery supplies only 20–30%. The normal portal venous flow is always toward the liver (hepatopetal). The fasting mean velocity of normal portal vein is approximately 18 cm/s (range: 13–23 cm/s[3]), and the flow pattern is normally flat or monophasic (Fig. 1.1.6). Mildly pulsatile portal venous flow pattern can be seen normally in tall, thin patients (Fig. 1.1.7). Portal hypertension is detected as hepatic blood flow away from the liver (hepatofugal) due to increased intrahepatic venous flow resistance. Portal vein diameter (>13 mm) and splenic vein diameter (>10 mm) are other signs of portal hypertension. Hepatic vein thrombosis can be seen in patients with HCC, and it is visualized as partial or complete loss of flow signal within the portal vein.
- *Hepatic artery*: the normal hepatic artery in a fasting patient has a systolic velocity of approximately 30–40 cm/s, and a diastolic velocity of 10–15 cm/s. The flow pattern normally is monophasic, low-resistance, with high-diastolic flow (Fig. 1.1.8). The resistance index (RI), which is defined as the maximal systolic velocity minus the end diastolic velocity divided by the maximal velocity, varies normally in a fasting patient from 0.55 to 0.81. There is increase in hepatic artery RI after mean or with age in a healthy person. The hepatic artery diastolic velocity is less than the peak portal vein velocity, and if the hepatic diastolic velocity is greater than the portal vein, one should suspect hepatic parenchymal disease. Also, the RI increases in patients with cirrhosis, and the after meal variation is absent (Fig. 1.1.9).
- *Cruveilhier-Baumgarten syndrome* is detected as a patent vein located at the umbilicus with typical monophasic venous flow (Fig. 1.1.10). The vein can be followed by the probe until identifying its relation to the intrahepatic portal veins passing through the ligamentum teres (Fig. 1.1.11).

1.1

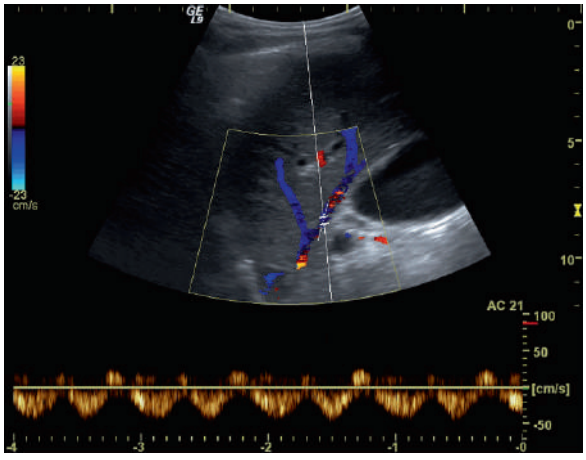

Fig. 1.1.5. Color Doppler waveform spectrum of the hepatic veins shows the normal venous triphasic pattern

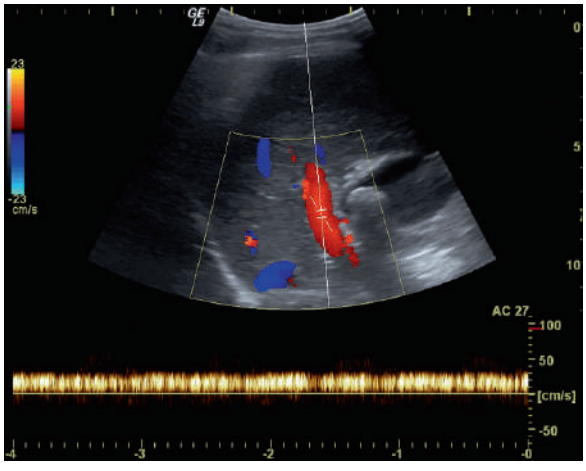

Fig. 1.1.6. Color Doppler waveform spectrum of the portal vein shows the normal monophosaic pattern

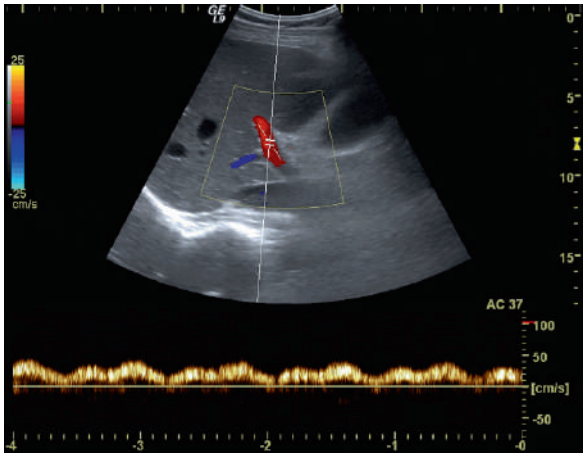

Fig. 1.1.7. Color Doppler waveform spectrum of the portal vein shows the physiologic portal vein pulsation in athletic tall patient who came for a routine abdominal ultrasound check up

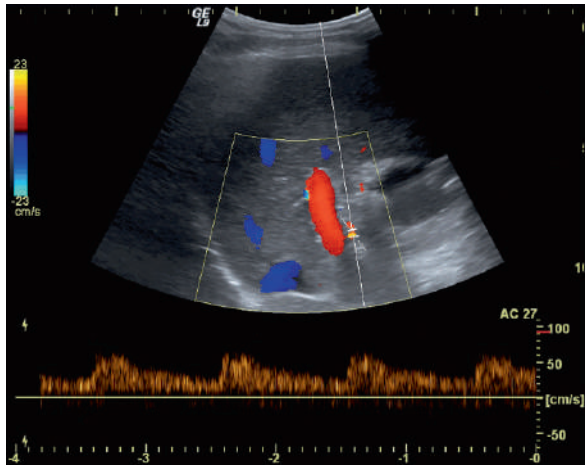

Fig. 1.1.8. Color Doppler waveform spectrum of the hepatic artery shows the normal monophasic, low-resistance with high diastolic flow arterial pattern

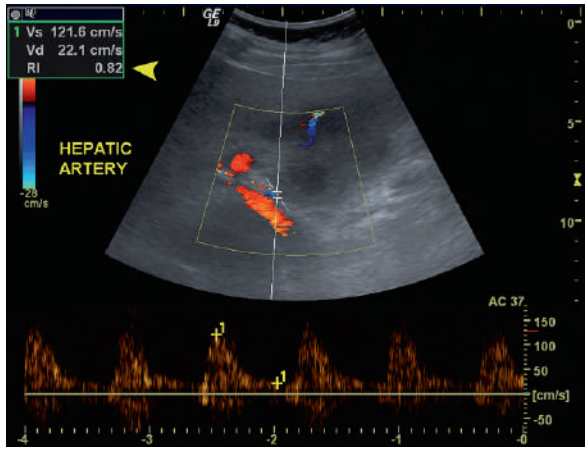

Fig. 1.1.9. Hepatic artery color Doppler waveform spectrum in a patient with alcoholic liver cirrhosis shows high RI (*arrowhead*)

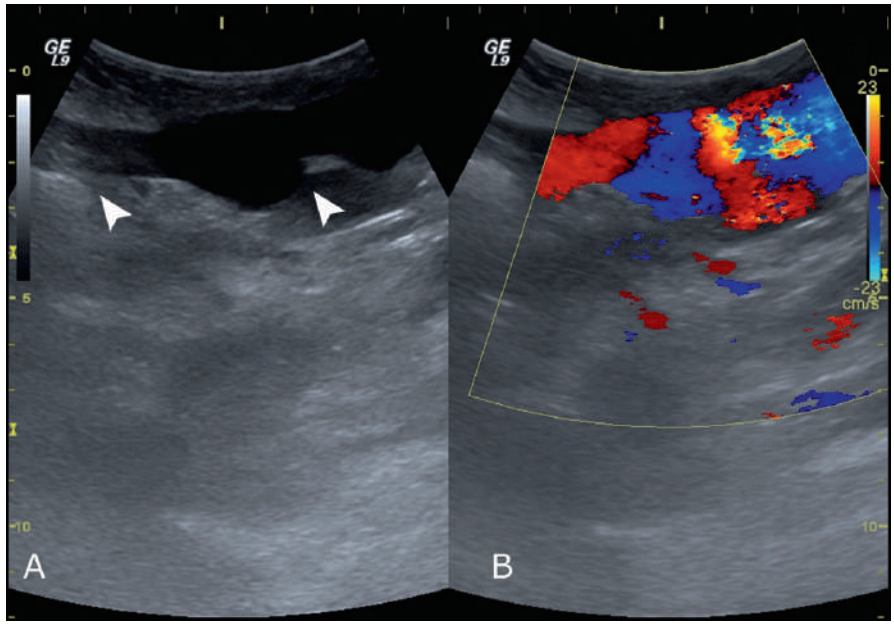

Fig. 1.1.10. Color Doppler sonography image shows patent umbilical vein at the level of the umbilicus (*arrowheads*) in a patient with chronic liver cirrhosis and Cruveilhier-Baumgarten syndrome

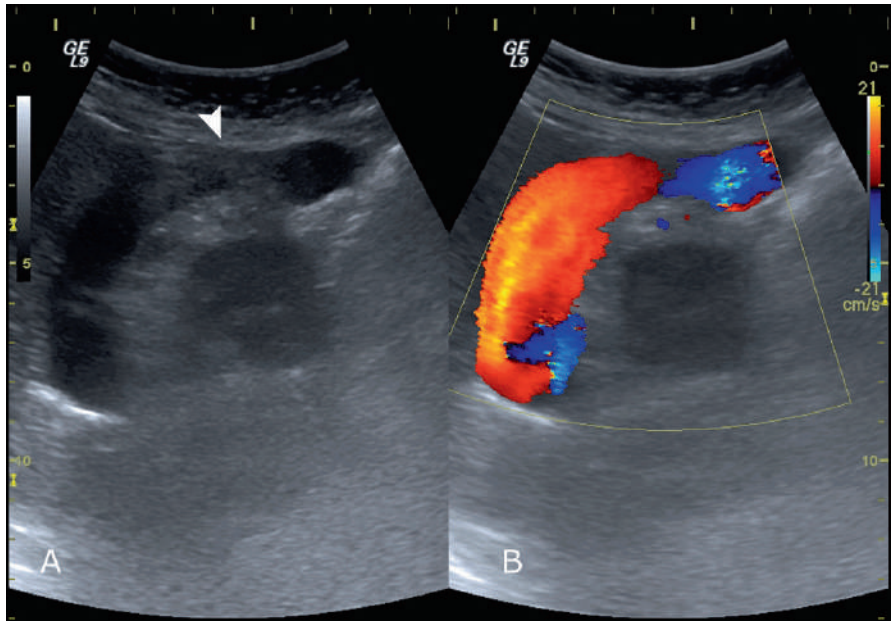

Fig. 1.1.11. The same patient shows the connection of the patent umbilical vein to the dilated portal vein through the ligamentum teres (*arrowhead*)

1.1

Signs on Barium Swallow

- Esophageal varices are visualized as serpigenous filling defects in the esophagus, usually located in the lower third (Fig. 1.1.12).

Signs on CT

- Cirrhotic liver appears small (<15 cm), with atrophied right lobe and enlarged caudate and left lobes. The liver contour is nodular and irregular due to parenchymal atrophy and nodular regeneration (Fig. 1.1.13).
- *Regenerative nodules*: they are divided into micronodules (<3 mm in diameter) and macronodules (>3 mm in diameter). They do not enhance in arterial phase because they are supplied mainly by portal vein and enhance like a normal liver parenchyma. Occasionally, they may accumulate iron within them, which will make them seen in noncontrast scans as hyperdense nodules (*siderotic nodules*), which are typically seen in alcoholic liver cirrhosis.
- *Dysplastic nodules*: a siderotic nodule larger than 1 cm is considered dysplastic nodule. They enhance homogeneously in both arterial and portal phases and are usually not seen in scans. Few nodules may show enhancement in the arterial phase and only differentiated from HCC by biopsy.
- *Hepatocellular nodule* is seen as a hypodense area in nonenhanced CT scan and shows enhancement in the arterial phase, which is the key to HCC diagnosis. Up to 50% of nodules are not detected in the arterial phase because they behave as a normal liver parenchyma in the traiphasic hepatic scan. The nodules become hypodense again in the portal-venous phase of the scan (Fig. 1.1.13).
- *Portal hypertension* can be detected if the Portal vein diameter increases (>13 mm). Also, Splenomegaly, dilated perisplenic collateral venous channels, and ascites may be found as signs of portal hypertension (Fig. 1.1.14).
- *Esophageal varices* are seen as multiple, enhanced nodular or tubular densities inside the esophageal lumen (intraluminal varices), or adjacent to the esophageal wall (paraesophageal varices). (Fig. 1.1.12)
- Enlarged portahepatic lymph nodes might be seen in end-stage cirrhotic liver.
- *Cruveilhier-Baumgarten syndrome* is visualized as an abnormal vein that arises from the right or left intrahepatic portal vein and leaves the liver via ligamentum teres to attach itself to the umbilicus on the portal phase of contrast-enhanced liver CT (Fig. 1.1.15).
- On chest HRCT, *hepatopulmonary syndrome* is visualized as peripheral pulmonary arterioles dilatation with increased numbers of terminal branches extending to the pleura (Fig. 1.1.16).
- Liver venous hypertension due to congestive heart failure (nutmeg liver) may show characteristic reticulo-mosaic pattern of enhancement on postcontrast examinations (Fig. 1.1.17).

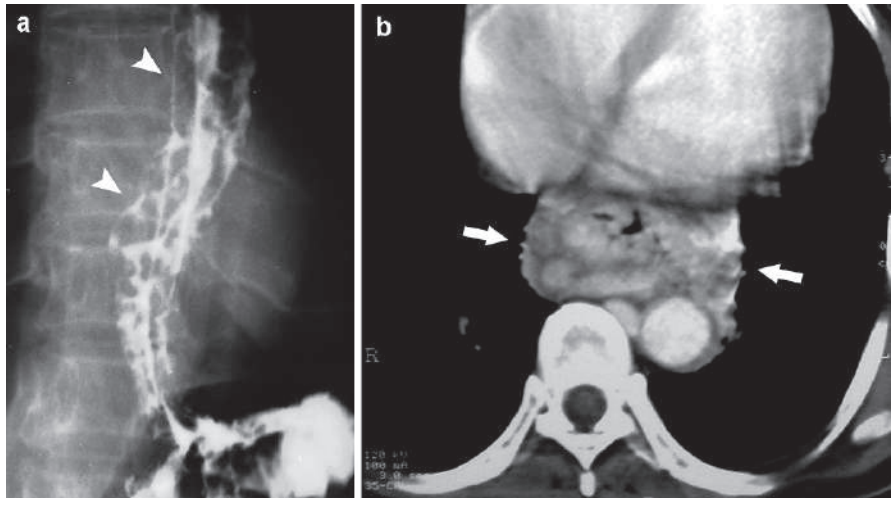

Fig. 1.1.12. Barium swallow (**a**) and axial thoracic-enhanced CT (**b**) images in two patients with esophageal varices. In (**a**), the varices are visualized as serpigenous filling defects in the lower esophagus (*arrowheads*). In (**b**), esophageal varices are visualized as multiple paraesophageal enhanced tubular densities adjacent to the esophageal wall (*arrows*)

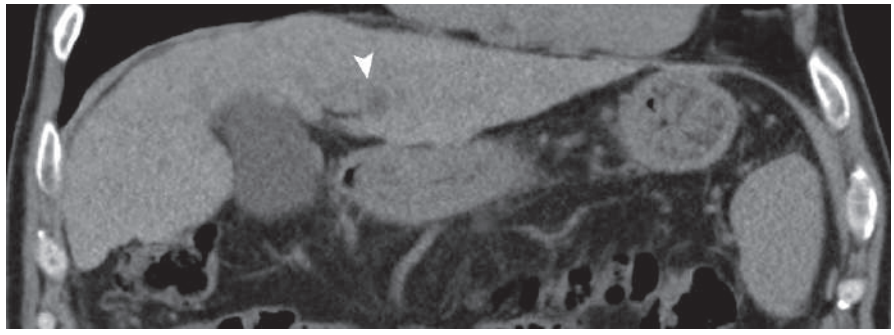

Fig. 1.1.13. Coronal non-enhanced CT image shows mildly shrunken liver due to cirrhosis with mild irregular contour and hypodense nodule in segment IVb (arrowhread), which was proven later to be HCC)

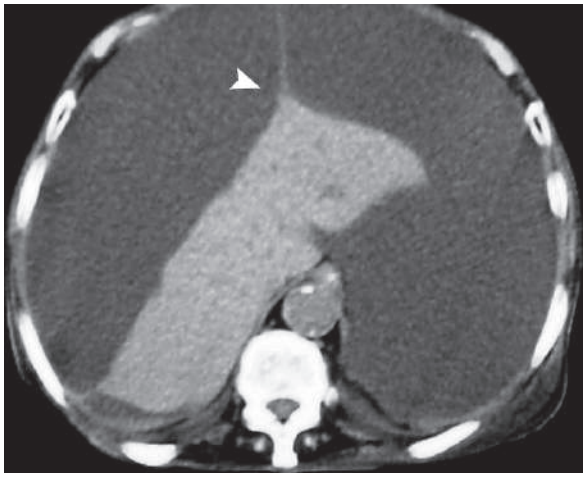

Fig. 1.1.14. Axial CT scan in a patient with liver cirrhosis shows massive ascites that nicely demonstrates Ligamentum teres (*arrowhead*)

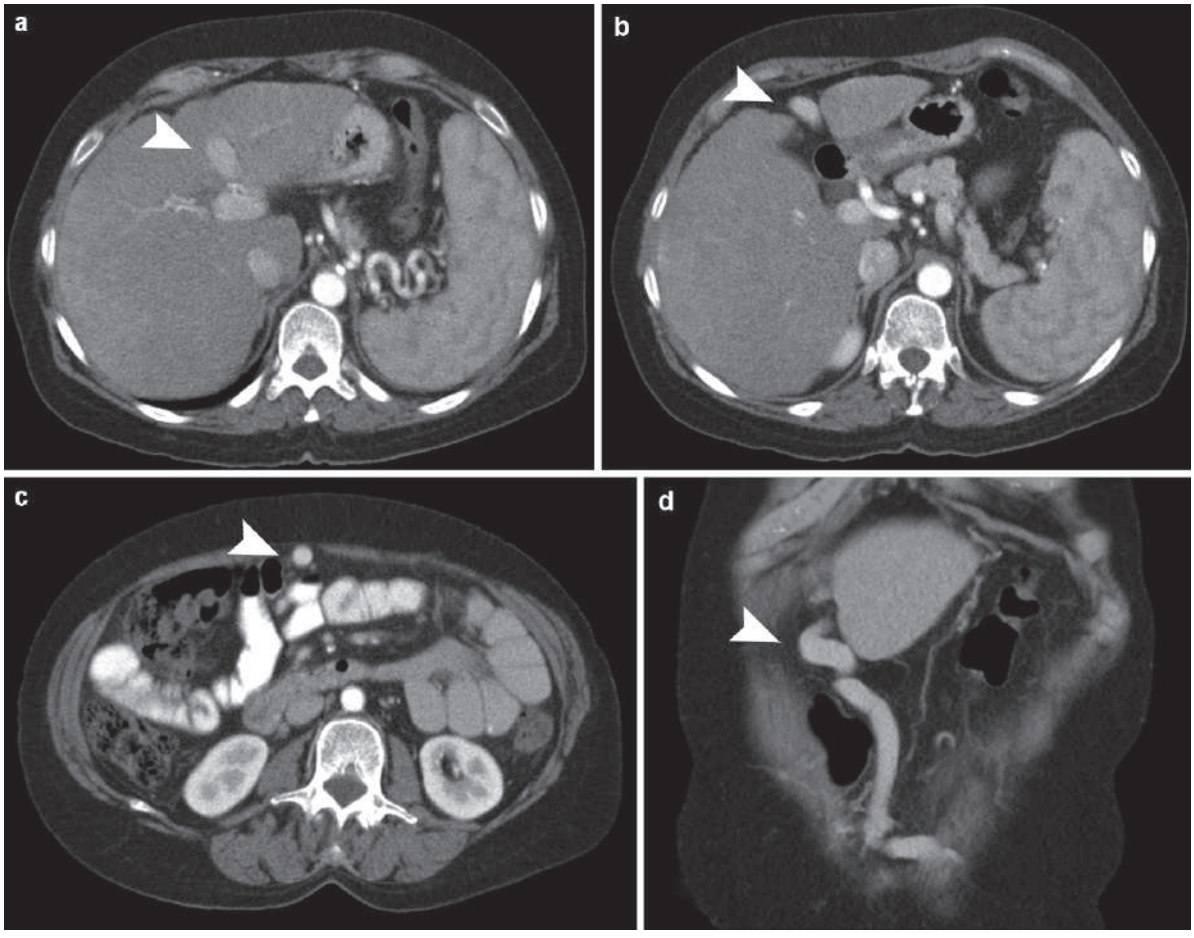

Fig. 1.1.15. Sequential axial abdominal enhanced CT of a patient with liver cirrhosis shows patent umbilical vein arises from the left portal vein (**a**), runs through ligamentum teres (**b**), and joins the umbilicus (**c**). The course of the patent vein can be seen in the coronal image in (**d**)

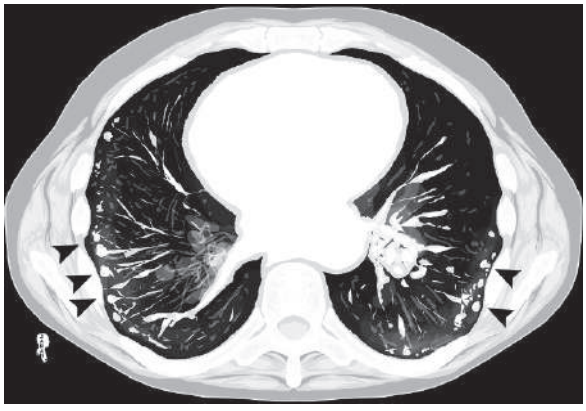

Fig. 1.1.16. Axial chest HRCT illustration shows multiple dilated peripheral pulmonary arterioles demonstrating hepatopulmonary syndrome in patients with liver cirrhosis

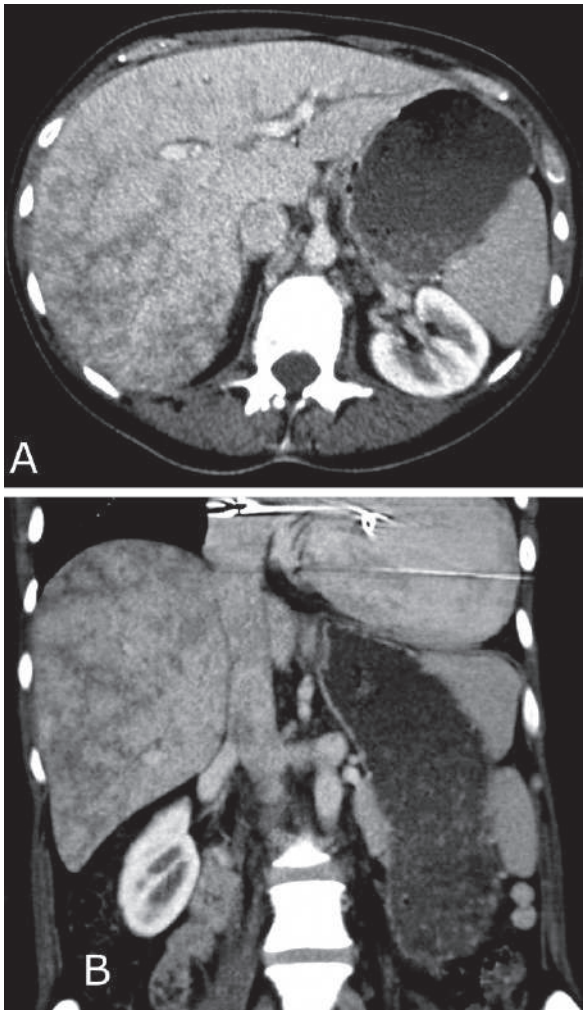

Fig. 1.1.17. Axial (**a**) and coronal (**b**) contrast-enhanced CT in a patient with right-sided heart failure due to tricuspid regurgitation shows the characteristic reticulo-mosaic pattern of enhancement of hepatic venous congestion

Signs on MRI

- *Hepatic encephalopathy* has bilateral and symmetrical high-intensity signal on T1W images in the basal ganglia, especially in the globus pallidus (Fig. 1.1.18). The extent of the basal ganglia disease is related to the plasma level of ammonia. Cerebellar atrophy may be seen in advanced stages.
- Regenerated nodules with or without hemosiderin have low T2 signal intensity. In contrast, a hepatic carcinoma nodule appears hyperintense on T2W images, and shows early arterial phase contrast enhancement.
- In *PBC*, periportal hyperintensity signal on T2W images is observed in the initial stages of the disease (Stage I and II), reflecting active periportal inflammation (Fig. 1.1.19). A *periorbital halo sign* may be seen as low-intensity signal centered around the portal venous branches on T2W images (Fig. 1.1.19). This sign is specific for the diagnosis of PBC. Lastly, a peripheral small wedge-shaped area may be seen in the early phases of liver contrast study, which represents arterial-portal shunting.
- Up to 50% of uncompensated cirrhotic patients show dilated cisterna chyli, which is seen as high T2 signal intensity structure adjacent to the aorta, with delayed enhancement several minutes after gadolinum injection. This sign is detected on CT in 1.7% of uncompensated cirrhotic patients.
- Plantar fibromatosis is visualized as bilateral infiltrative masses located at the deep aponeurosis adjacent to the plantar muscles in the medial aspect of the foot (Fig. 1.1.20). The masses typically show low T1 and T2 signal intensities due to the fibrous nature of the lesion. After contrast injection, enhancement of the masses can be seen in approximately 50% of cases.

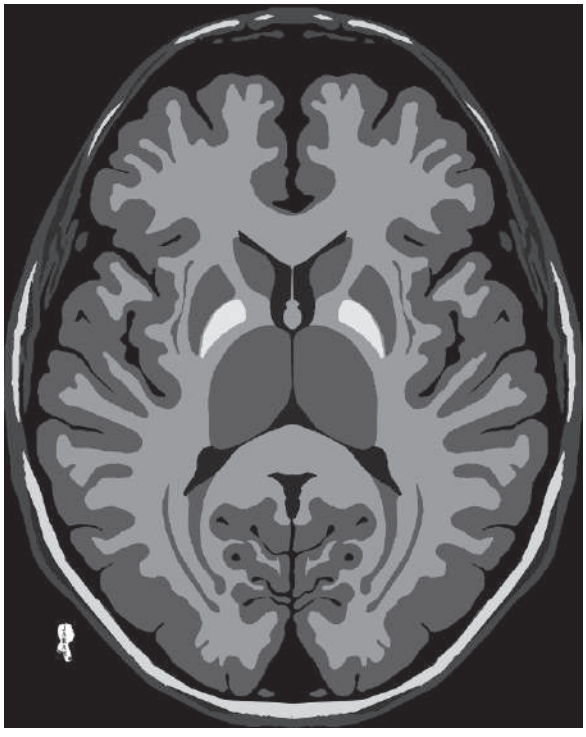

Fig. 1.1.18. Axial T1W MR illustration shows bilateral symmetrical high density in the globus pallidus representing sign of hepatic encephalopathy

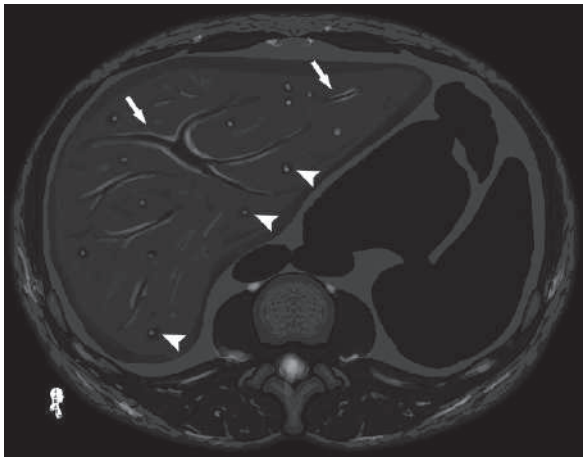

Fig. 1.1.19. Axial T2W MR illustration of the liver demonstrates the periportal hyperintensity (*arrows*), and the periorbital halo sign (*arrowheads*)

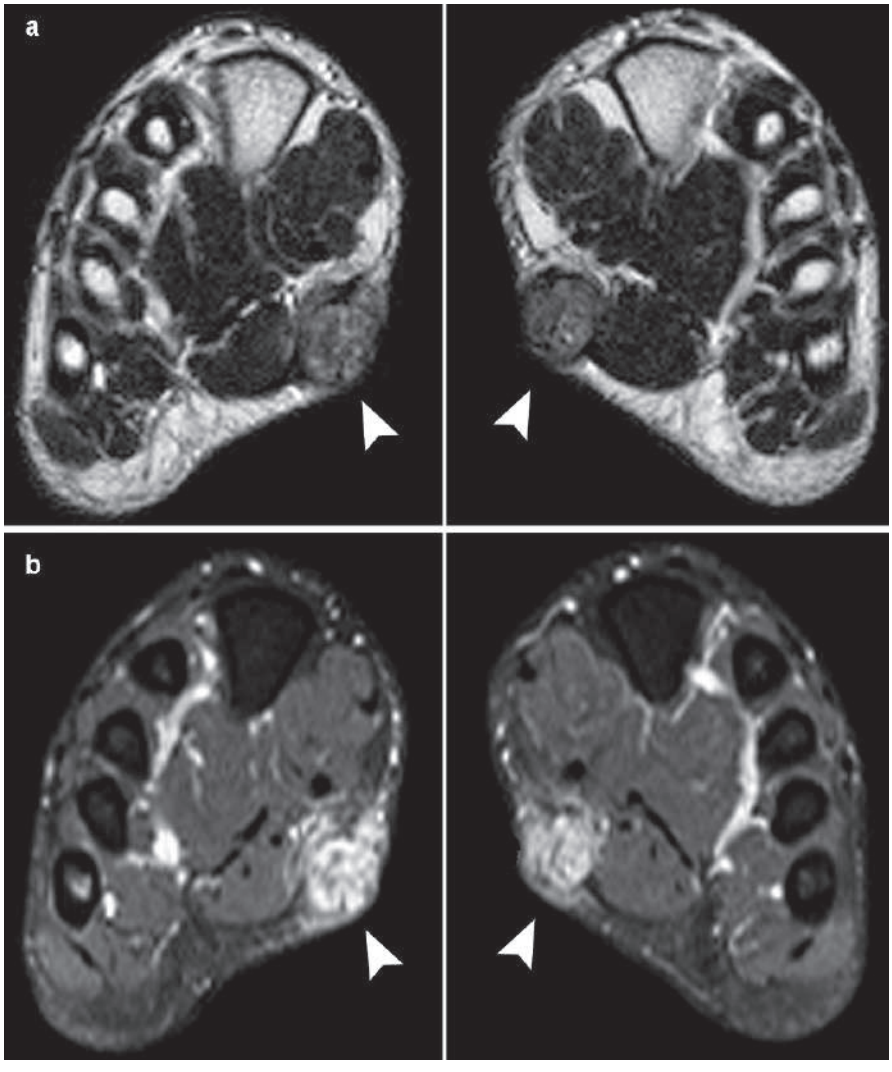

Fig. 1.1.20. Axial-oblique T2W (**a**) and T1W postcontrast MRI of the feet shows bilateral hypointense plantal masses (*arrowheads*) on image (**a**) diagnostic of Ledderhose disease (plantar fibromatosis). The masses show marked contrast enhancement after gadolinium injection (**b**)

For Further Reading

1. Schuppan D et al Liver cirrhosis. Lancet. 2008;371:838–51
2. Colli A et al Severe liver fibrosis or cirrhosis: accuracy of US for detection - analysis of 300 cases. Radiology. 2003; 227:89–94
3. Ito K et al Imaging findings of unusual intra- and extrahepatic portosystemic collaterals. Clin Radiol. 2009;64: 200–07
4. Meyer CA et al Diseases of the hepatopulmonary axis. RadioGraphics. 2000;20:687–98
5. Lim JH et al Regenerative nodules in liver cirrhosis: findings at CT during arterial portography and CT arteriography with histopathologic correlation. Radiology. 1999;210:451–58
6. Martinez-Noguera A et al Doppler in hepatic cirrhosis and chronic hepatitis. Semin Ultrasound CT MR. 2002;23: 19–36
7. Palazzi C et al Hepatitis C virus-related arthritis. Autoimmun Rev 2008;8:48–51
8. Bonekamp S et al Can imaging modalities diagnose and stage hepatic fibrosis and cirrhosis accurately? J Hepatol. 2009;50:17–35
9. Chavhan GB et al Normal Doppler spectral-waves of major pediatric vessels: specific patterns. RadioGraphics 2008;28: 691–706
10. Ba-Ssalamah A et al Dedicated multi-detector CT of the esophagus: spectrum of diseases. Abdom Imaging. 2009;34: 3–18
11. Verma SK et al Dilated cisternae chyli: a sign of uncompensated cirrhosis at MR imaging. Abdom Imaging. 2009;34: 211–16
12. Sharma S et al MRI diagnosis of plantar fibromatosis - a rare anatomic location. The Foot. 2003;13:219–22
13. Mauro MA et al Computed tomography of hepatic venous hypertension: the reticulated-mosaic pattern. Gastrointest Radiol. 1990;15:35–38
14. Kobayashi S et al MRI findings of primary biliary cirrhosis: correlation with Scheuer histologic staging. Abdom Imaging. 2005;30:71–76

1.2

Fatty Liver Disease (Liver Steatosis)

Accumulation of lipid within cells is a pathologic process. Any type of lipid can accumulate within cells, such as cholesterol, triglycerides, and phospholipids. Fatty liver disease (steatosis) is characterized by accumulation of triglycerides within hepatocytes.

Normally, free fatty acids are taken up by the hepatocytes and then converted into cholesterol esters, triglycerides, keton bodies, or phospholipids. Some of the lipids combine with apoproteins to form a specific type of lipoprotein called very low density lipoprotein (VLDL), which is then secreted into the blood. Liver steatosis can result from either excess delivery of free fatty acids into the liver (e.g., diabetes mellitus), increased formation of lipids within the liver (e.g., alcohol ingestion), hepatocytes disease (e.g., hepatitis), or decreased formation of VLDL by the liver (e.g., protein malnutrition).

Types of Liver Steatosis

- *Diffuse fatty infiltration*: the liver is usually enlarged with uniform decrease in density in the liver scan.
- *Focal fatty infiltration*: there is an area of the liver that shows fatty infiltration while the rest of the liver is normal. It usually occurs in the same areas that are supplied by the third inflow systemic veins (porta hepatic, around ligamentum teres, and adjacent to gallbladder). It is seen most commonly in the left lobe of the liver.
- *Multiple fatty infiltrations*: there are scattered low-density areas within a normal density liver. This type can be easily mistaken with metastases on noncontrast-enhanced liver CT scan.
- *Focal sparring*: there are areas of normal liver parenchyma surrounded by large areas of low-density diffuse fatty infiltration. This type also may simulate neoplasms on noncontrast-enhanced liver CT scan.

Signs on US

- Fatty liver is visualized as highly echogenic liver. The high liver echogenicity can be compared to the echogenicity of the right renal cortex, which will show marked difference in echogenicity (Fig. 1.2.1).
- Focal fatty infiltration is seen as a focal, highly echogenic area within a relatively isoechoic (normal) liver parenchyma (Fig. 1.2.2).
- Focal sparring is seen as a focal area which is relatively hypoechoic (normal) within a highly echogenic liver.

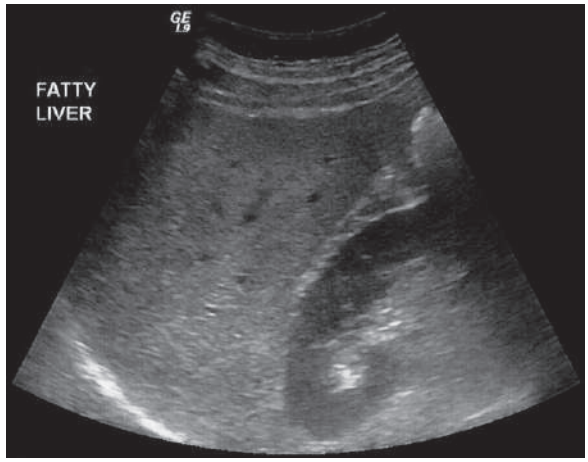

Fig. 1.2.1. Transverse ultrasound image of the liver shows diffuse increase in liver echogenicity compared to the right renal cortex (liver steatosis)

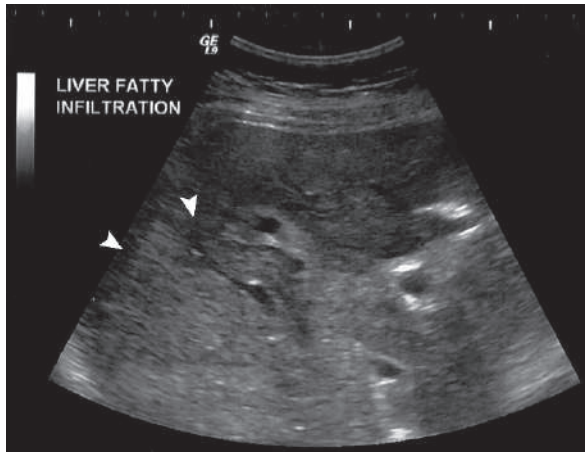

Fig. 1.2.2. Transverse ultrasound image of the liver shows focal fatty infiltration involving segment VI and segment VII

Signs on CT

- Hepatic steatosis is detected as diffuse or focal reduction of the liver normal density on noncontrast-enhanced scan (Fig. 1.2.3). The normal liver density is 8 HU (Hounsfield unit) above that of the spleen (60 HU). Fatty liver density is 10 HU below spleen density on noncontrast-enhanced scan (if the normal spleen is 52 HU, then the fatty liver is <42 HU).
- Focal fatty infiltration is seen as a hypodense area with nonspherical margins (metastases usually have round edge). The hypodense area or the mass does not show mass effect over the parenchyma around it, and shows change over time (seen in films before the current scan or after few months' scan). The same criteria are applied to the focal sparring, but the mass will be isodense within a hypodense liver on noncontrast-enhanced scan.
- In both focal sparring and focal fatty infiltration, hepatic vessels course within the fatty infiltration or focal sparring undisturbed. In contrast, metastases or other hepatic lesions will be cut off the hepatic vessels when they reach them.

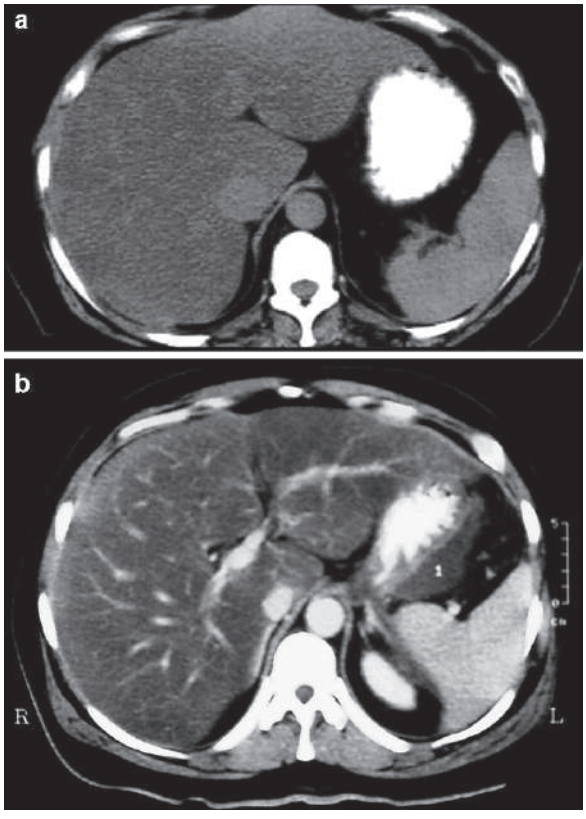

Fig. 1.2.3. Axial precontrast (**a**) and postcontrast (**b**) abdominal CT images show diffuse hepatic steatosis. Notice the density of the liver compared to the spleen in pre- and postcontrast images

Signs on MRI

- Liver steatosis is diagnosed on MRI when the liver intensity drops to >30% difference on both T1W in-phase and T1W out-of-phase images (Fig. 1.2.4).

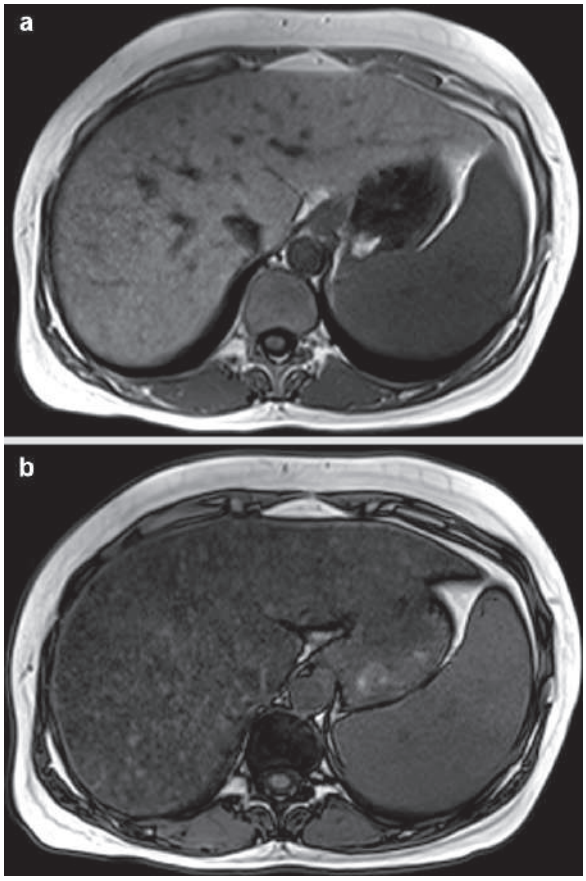

Fig. 1.2.4. Axial T1W in-phase (**a**) and T1W out-of-phase (**b**) MRI in a patient with liver steatosis shows drop in the liver signal intensity >44% in the T1W out-of-phase image (**b**), diagnostic of hepatic steatosis

For Further Reading

1. Karcaaltincaba M et al Imaging of hepatic steatosis and fatty sparing. Eur J Radiol. 2007;61:33–43.
2. Cassidy FH et al Fatty liver disease: MR imaging techniques for the detection and quantification of liver steatosis. RadioGraphics. 2009;29:231–60.
3. Salmonson EC et al Focal periportal liver steatosis. Abdom Imaging. 1993;18:39–41.
4. Yates CH et al Focal fatty infiltration of the liver simulating metastastic disease. Radiology. 1986;159:83–84.
5. Alpern MB et al Focal hepatic masses and fatty infiltration detected by enhanced dynamic CT. Radiology. 1986;158: 45–49.
6. Sabir N et al Correlation of abdominal fat accumulation and liver steatosis: Importance of ultrasonographic and anthropometric measurements. Eur J Ultrasound. 2001;14: 121–28.

1.3 Recurrent Epigastric Pain

Epigastric pain is a term used to describe dull achy pain located at the area of the epigastrium beneath the xyphoid process. Epigastric pain is a very common complaint encountered in both medical and surgical casualty departments. Diagnosis often is established by proper history, examination, and laboratory investigations. This topic discusses some causes of recurrent epigastric pain, in which radiology can play an important role in establishing the underlying diagnosis.

Gastroesophageal Reflux Disease

Gastroesophageal reflux disease (GERD) is a disease characterized by reduction of the lower esophageal sphincter pressure resulting in leaking of the stomach acidity into the lower third of the esophagus, causing esophagitis and epigastric pain.

The most common cause of GERD is hiatus hernia. Four types of hiatus hernias are known: sliding, paraesophageal, sliding and paraesophageal, and complete stomach herniation into the thorax.

Patients with GERD typically present with longstanding mild to moderate epigastric pain with burning sensation, usually postprandial. Severe cases of GERD may manifest due to propagation of gastric acidity to the upper esophagus. Symptoms like aspiration pneumonia, laryngitis, and teeth decay may be seen uncommonly due to advanced GERD. Medical treatments include antacids, histamine (H2) blockers, and proton pump inhibitors. Surgical management with gastric fundoplication is usually advised in cases where the medical therapy fails to control the symptoms.

Barium swallow is the most sensitive method to detect GERD and esophagitis. Esophagitis is defined as defects in the esophageal mucosa due to exposure to the gastric reflux acid and pepsin. *Barrett's esophagus* (BS) is a condition characterized by esophageal mucosal healing in a persistent acid environment. This healing process is characterized by metaplasia of the normal esophageal stratified squamous epithelium into columnar, gastric-like epithelium. Metaplasia is transformation of one cell type to another (e.g., cuboidal cell to columnar cell). BS has the potential for neoplastic transformation. Up to 50% of patients with GERD show esophageal dysmotility disorders (EDM).

On barium swallow, sliding hiatus hernia is detected by identifying Schatzki ring. An esophageal ring is a short annular narrowing of the esophagus <1cm in diameter. *Esophageal A ring* is a ring made up of smooth muscles that is seen at the tubulovestibular junction (muscular ring). *Esophageal B ring* (*Schkatzi ring*) is an esophageal ring that is only visible radiologicaly when there is sliding hiatus hernia, and is caused by propagation of the gastroesophageal junction above the diaphragm. *Esophageal C ring* is the normal abdominal retroperitoneal esophageal part (3 cm long) which makes a groove on the liver. In contrast to esophageal ring, *esophageal stricture* is defined as an esophageal segment with fixed narrowing. *Esophageal web* is an abnormal thick 1–2 mm diaphragm-like membrane that extends partially or completely around the esophageal lumen, and always indents the esophagus anteriorly. The lower esophageal sphincter line where mucosal change is observed between the esophagus and the stomach on barium examination is sometimes referred to as the *Z-line*.

Esophageal dysmotility disorders are a group of diseases characterized by abnormal esophageal peristalsis seen on barium swallow. Types of EDM are: tertiary contractions, crock-screw esophagus, esophageal achalasia, esophageal chalasia, and presbyesophagus.

Tertiary esophageal contraction is a nonpulsatile, uncoordinating contraction of the esophageal circular smooth muscles. The normal primary and secondary contractions of the esophagus help to push the food and fluids through the esophagus. This type of dysmotility is often seen with old age or GERD. *Crock-screw esophagus* is a term used to describe the same dysmotility as in tertiary contractions but arises posterior to the heart, causing pain in the retrocardiac region during swallowing. *Esophageal achalasia* is a disease characterized by contraction and narrowing of the esophagus due to a defect in the normal neuronal plexuses within the esophageal muscles, which results in failure

1.3

of the smooth muscles to relax when the food arrives. Achalasia is commonly seen in the lower third of the esophagus. Achalasia can occur without prior cause (primary), or due to underlying pathology like Chagas' disease or malignancy (secondary). *Esophageal chalasia* is characterized by dilatation and widening of the gastroesophageal junction. *Presbyesophagus* is an asymptomatic condition characterized by failure of the primary peristaltic wave to pass completely through the esophagus, resulting in a combination of tertiary contractions, aperistalsis, and failure of the lower esophageal sphincter to contract (Curling phenomenon).

Hiatus hernia can be congenitally seen in neonates and children. The most common congenital hiatal hernias are Morgagni and Bockdaleck's hernias. *Morgagni hernia* is stomach or bowel herniation into the thorax due to diaphragmatic defects that occurs in the anterior/inferior mediastinum. *Bockdaleck's hernia* is stomach or bowel hernia into the thorax due to diaphragmatic defects that occurs in the inferior/posterior mediastinum.

Differential Diagnoses and Related Diseases

- *Steakhouse syndrome* is a term used to describe acute food impaction of the esophagus, usually at its distal third. The most common cause of food impaction is esophageal webs. Patients often present to the emergency ward with acute esophageal food impaction, especially after meat ingestion, where the name came from. Patients present with intense retrosternal pain, which may be cardiac in origin, especially if the impacted food presses over the posterior cardiac boarder. Plain chest radiographs should be performed to exclude bony material impaction or signs of pulmonary aspiration.
- *Plummer-Vinson syndrome* (*Paterson-Kelly syndrome*) is a disease characterized by dysphagia, iron-deficiency anemia, and esophageal webs. Patients are commonly women (85%), between 30 and 70 years of age. Upper aerodigestive tract carcinoma is seen in 4–16% of cases, with almost all cases occurring at the postcricoid location.

Signs on Chest Radiographs

- Hiatal hernia is diagnosed by finding the stomach bubble within the thorax, rather than under the left hemi-diaphragm (Fig. 1.3.1).
- Morgagni hernia is demonstrated as a mass, bowel loop, or stomach bubble lying in the inferior/anterior mediastinum on lateral radiographs (Fig. 1.3.2). In contrast, Bockdaleck's hernia is demonstrated as mass, bowel loop, or stomach bubble lying in the inferior/posterior mediastinum on lateral radiographs (Fig. 1.3.3).
- In esophageal achalasia, there is paramediastinal shadow (widening of the mediastinum), with air-fluid level seen in the retrocardiac shadow (Fig. 1.3.4).

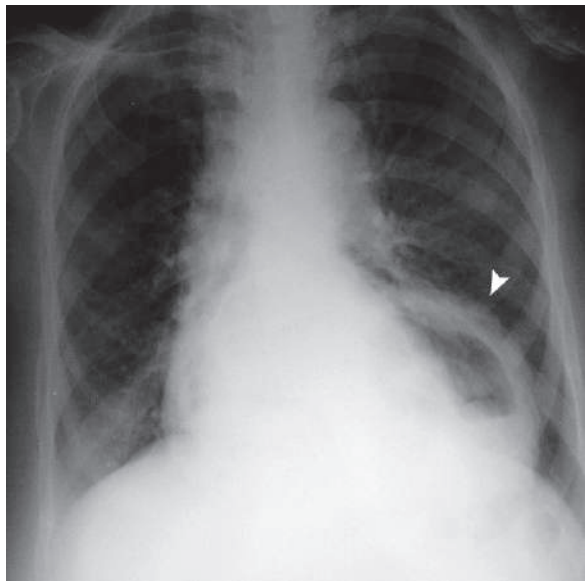

Fig. 1.3.1. Posteroanterior plain chest radiograph shows herniated stomach into the thorax with the gastric bubble observed in the thorax (*arrowhead*)

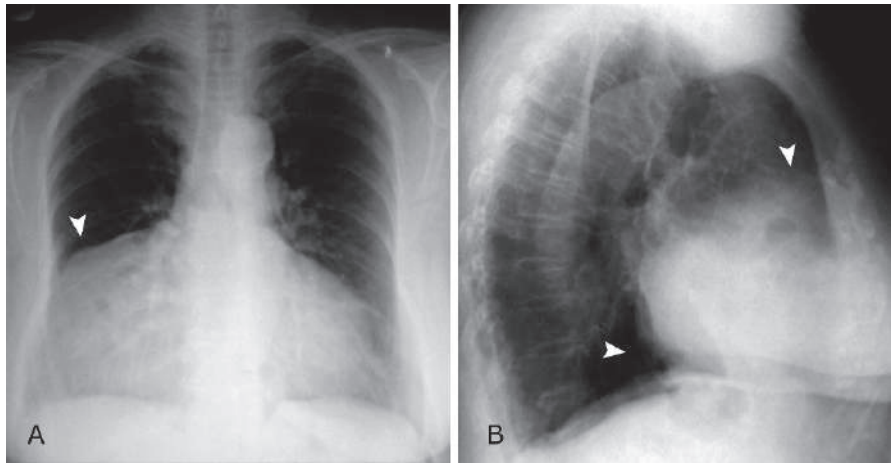

Fig. 1.3.2. Posteroanterior (**a**) and lateral (**b**) plain chest radiographs show right mediastinal mass on (**a**), which is seen located within the anterior/inferior mediastinum on lateral radiographs (*arrows*). The patient is a child, and the mass was omental and bowel herniation due to an anterior congenital diaphragmatic defect (Morgagni hernia)

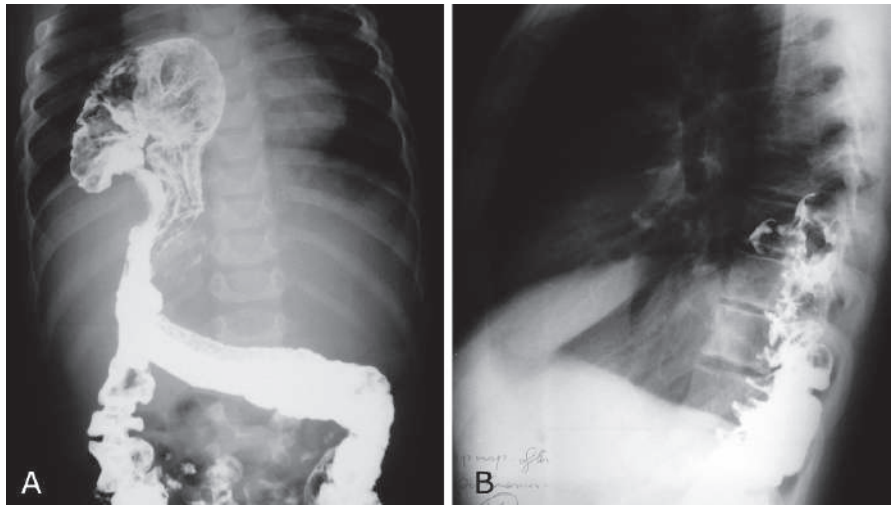

Fig. 1.3.3. Posteroanterior (**a**) and lateral (**b**) barium enema radiographs in a baby with Bockdaleck's hernia show herniation of part of the transverse colon through a posterior/inferior diaphragmatic defect (**b**)

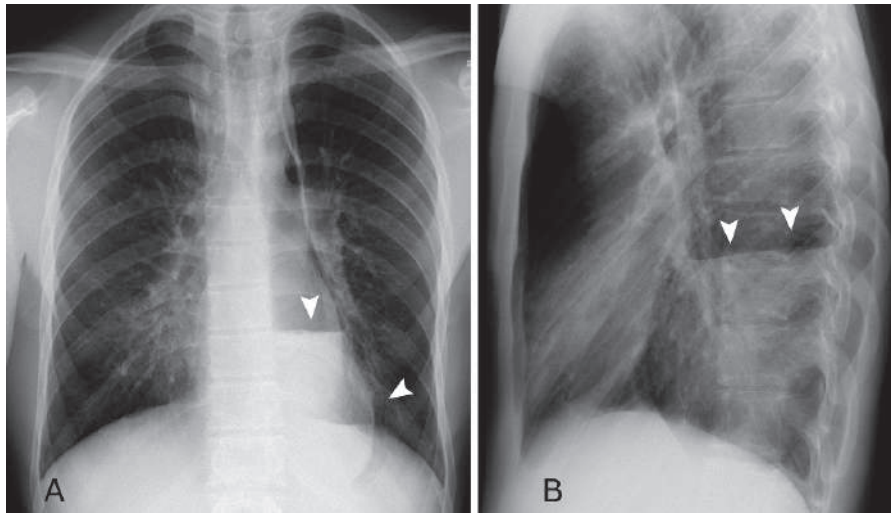

Fig. 1.3.4. Posteroanterior (**a**) and lateral (**b**) plain chest radiographs in a patient with achalasia shows mild widening of the mediastinum and air fluid level behind the cardiac silhouette (*arrowheads*), representing fluid content within the dilated esophagus

1.3

Signs on Barium Swallow

- In *esophagitis*, there is mucosal granularity, thickened mucosal folds due to edema, and linear ulcers seen as linear barium defects. Stricture formation is a sign of chronic ulceration (Fig. 1.3.5).
- Diagnosis of *hiatal hernia* depends upon identification of the gastroesophageal junction, which is typically located at the termination point of the converging gastric mucosa. Schkatzi's ring is seen as a uniform round esophageal narrowing with a distended small pouch representing the herniated stomach above the diaphragm (Fig. 1.3.6). Herniation of the gastric fundus or body into the thorax is a definite sign of hiatus hernia. Esophageal webs are identified as incomplete esophageal narrowing located anteriorly.
- Barrett's esophagus is divided into two types: short-segment and long-segment BS. Short-segment BS is characterized by mucosal metaplasia <3 cm above the gastroesophageal junction, whereas long-segment BS is mucosal metaplasia >3 cm above the gastroesophageal junction. BS is classically suspected when multiple lower esophageal mucosal ulcerations, mid-esophageal stricture, and hiatal hernia are found. The explanation of such suspicion lies in the fact that the new gastric epithelium secretes acid, which causes regional ulcers and esophageal stricture later on. A reticular ring-like pattern of ulceration above the gastroesophageal junction, which mimics areae gastricae, is a relatively specific sign of BS (Fig. 1.3.7).
- In *tertiary contractures*, the esophagus wall is irregular with fine, multiple contractions that run in a wavy appearance (Fig. 1.3.8).
- In *achalasia*, there is narrowing of the distal esophagus with dilation of the esophagus proximal to the narrowing, giving the so-called "mouse-tail appearance" (Fig. 1.3.9).
- In *Plummer-Vinson syndrome*, anterior transverse linear esophageal filling defects (webs) with focal esophageal stenosis and poststenotic dilatation are typically found (Fig. 1.3.10).

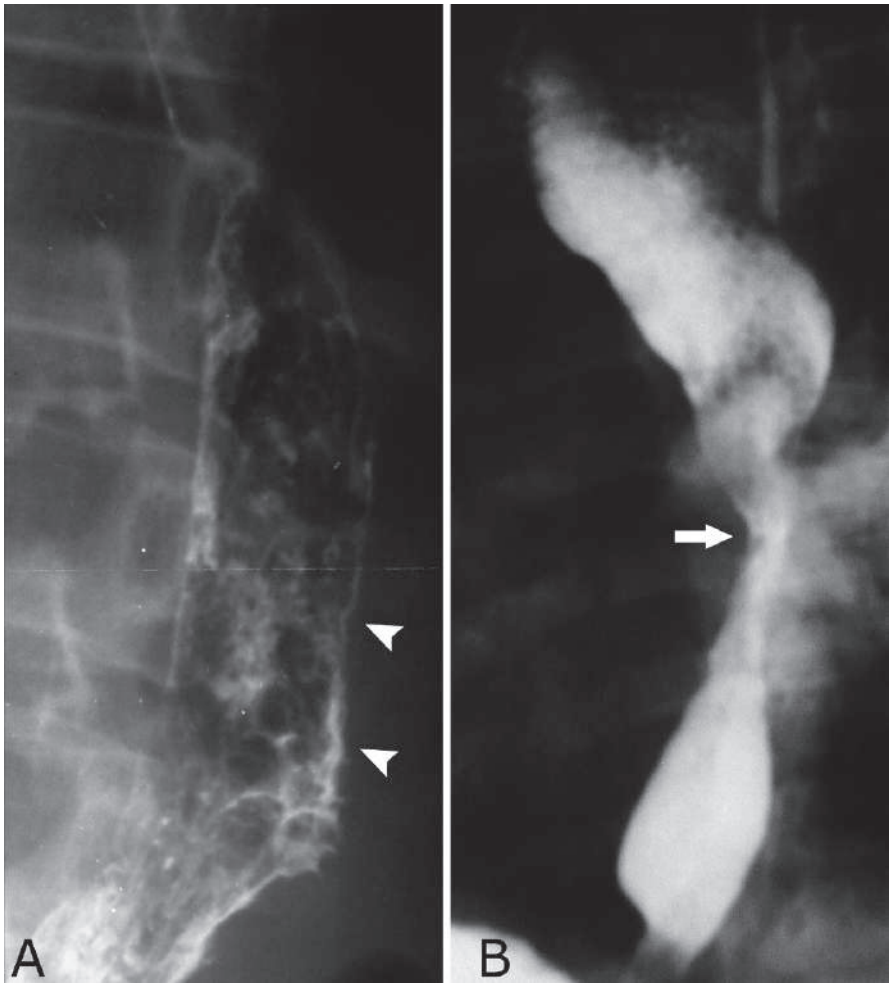

Fig. 1.3.5. Barium swallow examinations show patients with esophagitis. In patient (**a**), there is mucosal granularity with thickened mucosal folds (*arrowheads*). In patient (**b**), there is stricture seen at the distal end of the esophagus (*arrow*)

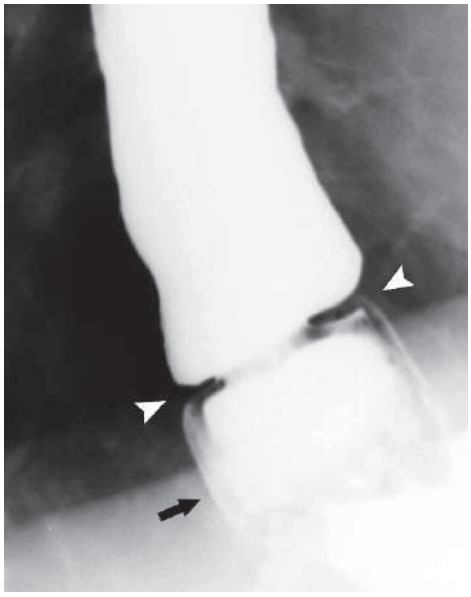

Fig. 1.3.6. Barium swallow image at the distal third of the esophagus in a patient with hiatus hernia shows Schkatzi's ring (*arrowheads*), with the herniated part of the stomach beneath it (*black arrow*)

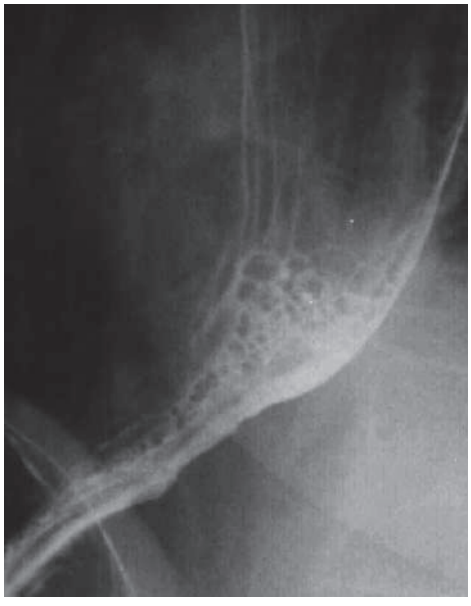

Fig. 1.3.7. Barium swallow image at the gastroesophageal junction shows the specific patter multiple ring-like ulcers and stricture of the esophagus >3 cm above the gastroesophageal junction (long-segment Barrett's esophagus (BS))

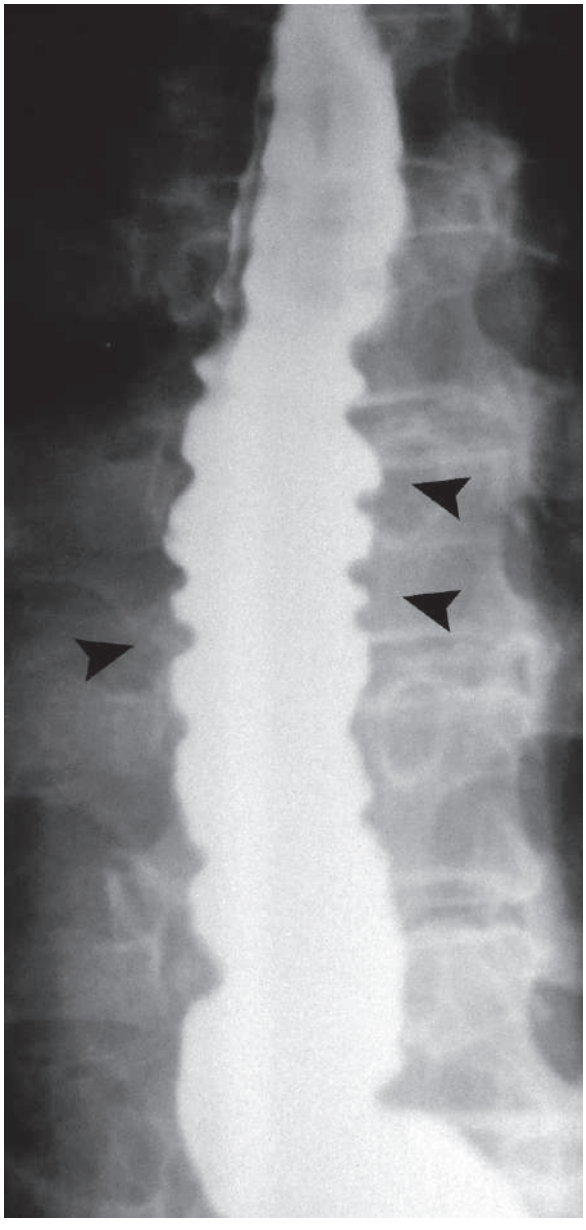

Fig. 1.3.8. Barium swallow image shows the classical appearance of esophageal tertiary contractures as irregular, multiple contractions that run in a wavy appearance

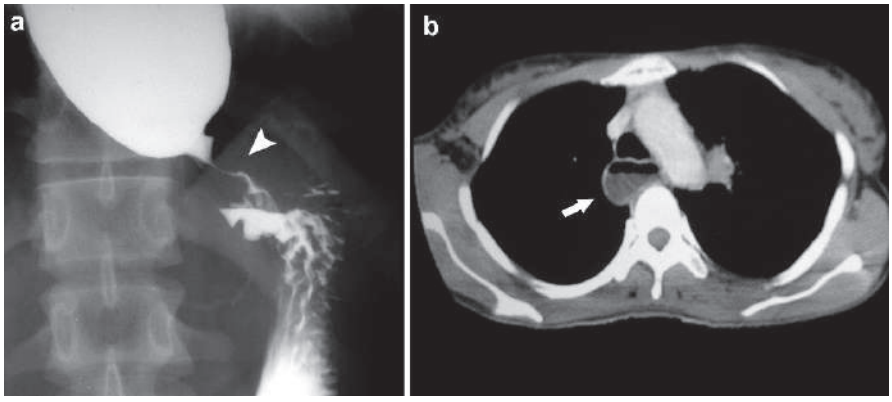

Fig. 1.3.9. Barium swallow (**a**) and enhanced-CT image (**b**) of two patients with achalasia shows the classical "mouse-tail" appearance in patient (**a**) (*arrowhead*), and prestenotic dilatation with fluid residual in patient (**b**) (*arrow*)

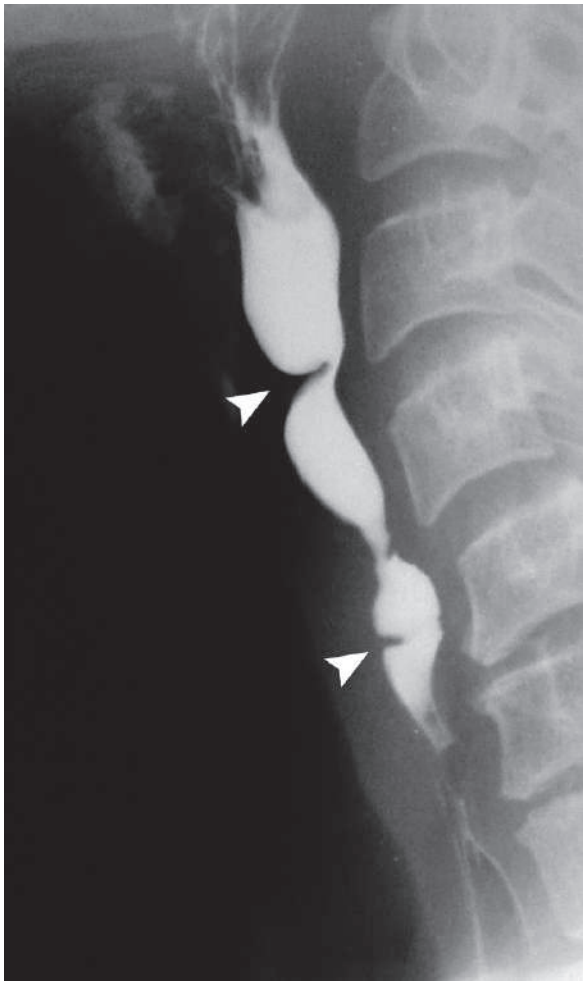

Fig. 1.3.10. Lateral barium swallow image in a patient with Plummer-Vinson syndrome shows multiple anterior esophageal webs (*arrowheads*) with esophageal poststenotic dilatation

Signs on CT

- Hiatus hernia is demonstrated by the stomach fundus or body lying within the posterior mediastinum (Fig. 1.3.11).
- Morgagni hernia is seen as stomach or bowel within the anterior/inferior mediastinum, whereas Bockdaleck's hernia is seen as stomach or bowel within the posterior/inferior mediastinum.
- Esophagitis is visualized as uniform, circumferential wall thickening of the esophagus with a target sign formation.

Peptic Ulcer Disease

Peptic ulcer is a disease characterized by mucosal ulceration of the esophagus, stomach, or duodenum. *Erosion* is defined as an area of mucosal destruction that does not extend beyond the muscularis mucosae into the submucosa, whereas *ulcer* is defined as an area of mucosal destruction that extends beyond the muscularis mucosae into the submucosa or serosa (in perforation).

The gastric mucosa is divided into three types: cardiac mucosa, body-type (oxyntic) mucosa, and antral (pyloric) mucosa. The body-type mucosa contains parietal (oxyntic) cells that secrete hydrochloric acid and intrinsic factor, and chief cells that produce lipase and the proteolytic enzymes pepsinogen I and II. The antral mucosa contains endocrinal cells that produce gastrin (G cells), somatostatin (D cells), histamine (ECL cells), and serotonin (enterochromaffin cells).

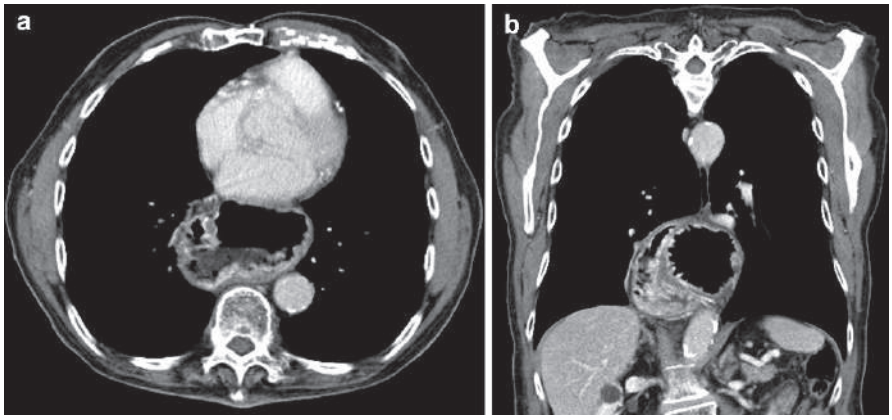

Fig. 1.3.11. Axial and coronal enhanced-CT images show herniation of the stomach into the posterior mediastinum through the esophageal hiatus (hiatus hernia)

The main defensive mechanism against the harmful effects of the acid is the production of the mucus layer. Defects in the mucus layer result in gastritis and peptic ulceration.

Peptic ulcer initially starts as inflammation of the gastric mucosa (gastritis), which, when not properly treated, can progress into gastric ulcer. Causes of gastric ulcers include severe stress situations like burns (*Curling ulcer*), increased intracranial pressure (*Cushing ulcer*), alcoholism, cocaine abuse, nonsteroidal anti-inflammatory drugs (NSAIDs) abuse, and bile salts reflux into the stomach in patients with gastroduodenostomy (Billroth I), and gastrojejunostomy (Billroth II).

Peptic ulcer disease and gastritis are linked to infection of the gastric or duodenal wall with *Helicobacter pylori*, a spiral-shaped gram-negative bacterium which is normally found in the gastric antrum. *H. pylori* gastritis is found in up to 80% of patients with peptic ulcers.

Zollinger-Ellison syndrome (*ZES*) is a disease characterized by severe gastric ulcers due to parietal cell hyperplasia in the body and the fundus of the stomach, mostly due to gastrinomas (>80%). Gastrinomas are gastrin-producing, non-B islet cell tumors that are commonly found within the gastrinoma triangle. The *gastrinoma triangle* is formed by a line joining the confluence of the cystic and common bile ducts superiorly, the junction of the second and third portion of the duodenum inferiorly, and the junction of the neck and body of the pancreas medially. Up to 25% of gastrinoma cases are part of multiple endocrine neoplasia (MEN) syndrome type I, an autosomal dominant disorder with tumors of the parathyroid glands (87%), pancreas (81%), and pituitary gland (65%). Ulcers are detected in the first part of the duodenum in 75% of patients with ZES.

Radiological manifestations of gastric ulcer disease are defined according to the stage of the ulcer. There are signs of acute and chronic ulcers. The usual techniques to detect mucosal abnormalities are the double contrast barium meal, and modern virtual gastroscopy. Virtual gastroscopy is a 3-dimentional (3D) reconstruction rendering technique that uses multiplanar CT sections to reconstruct 3D images of the stomach interior that mimics the images seen in upper gastrointestinal endoscopy of the stomach.

Signs on Plain Radiograph

- Sign of gastrointestinal or peptic ulcer perforation is usually diagnosed by the presence of free air under the diaphragm on erect abdominal or chest films (pneumoperitonium) (Fig. 1.3.12).

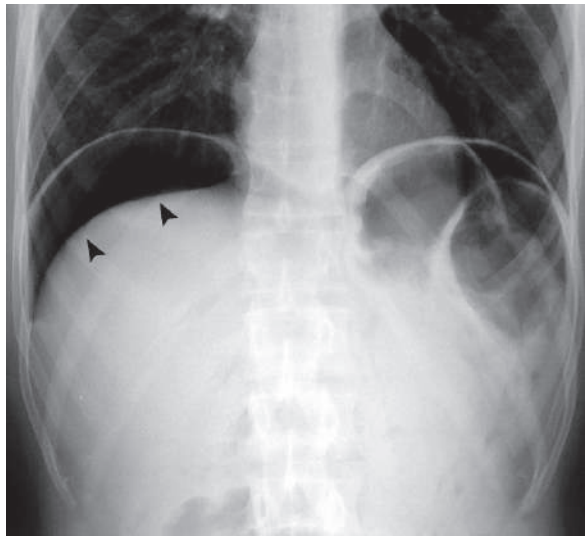

Fig. 1.3.12. Anteroposterior plain abdominal radiograph shows collection of air under the right diaphragm due to duodenal ulcer perforation (*arrowheads*)

Signs on US

- In up to 30% of cases, perforation of a peptic ulcer does not show free pneumoperitonium, but instead penetrate adjacent structures (confined perforation). In suspected cases of perforation, a sonogram of the epigastric region may show an extra-luminal inhomogeneous fluid collection seen within the subhepatic space. This fluid collection represents gastric contents leakage.
- The stomach wall is usually thickened, and the stomach is atonic, dilated, and maybe fluid filled due to gastric outlet obstruction.
- Presence of high echoic areas within the inhomogeneous fluid collection representing air is a pathognomonic finding of perforation.

Signs of Acute Ulcer on Barium Meal

- *Ring sign*: the mucosal edge of the ulcer is covered with barium while the center is not.
- *Arc sign*: occurs when the barium covers part of the ulcer's edge (Fig. 1.3.13).
- *Smudge sign*: shallow smudge barium spot that represents the area of mucosal ulceration (Fig. 1.3.13).
- *Prominent area gastrica*: it is an area of columnar epithelium located in the stomach antrum, which is normally seen as 2–3 mm, sharply edged, polygonal radiolucencies on double barium meal. Prominent area gastrica suggests the possibility of *H. pylori* gastritis.
- In ZES, there are markedly thickened mucosal folds (Rugae), mainly found in the body and the fundus of the stomach.

Signs of Chronic Ulcer on Barium Meal

- *Ulcer crater sign*: seen as a round area filled with barium, with gastric folds radiating from the crater due to fibrosis. This sign arises due to deep chronic ulcer's edge that mimics a volcano crater.
- *Incisura*: it is a fold in the greater curvature due to stricture of the mucosal folds around an ulcer. Incisura may be found as a normal finding in double contrast barium enema as an area of angulation of the lesser curvature (Fig. 1.3.14).
- *Meniscus sign*: the mucosa around the ulcer's crater makes a halo due to edema of the mucosa (Fig. 1.3.15).

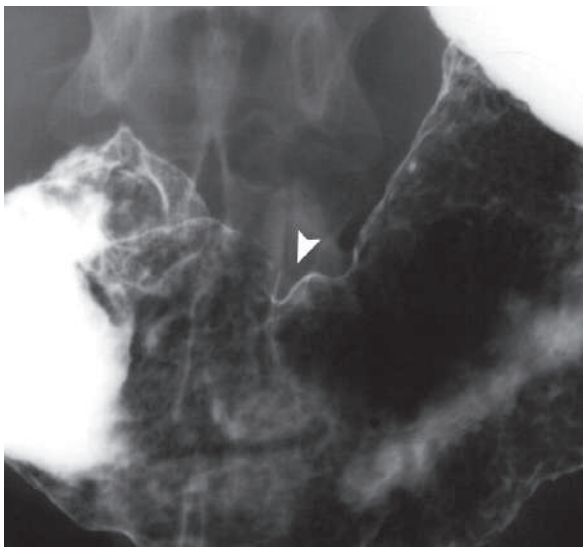

Fig. 1.3.14. Barium meal image in a patient with normal examination shows the incisura (*arrowhead*)

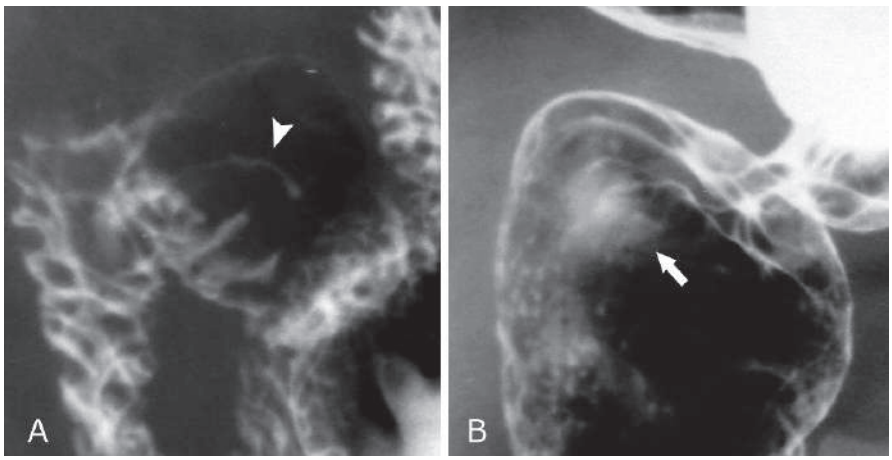

Fig. 1.3.13. Barium meal images of the duodenum in two different patients show duodenal acute ulcer arc sign in patient A (*arrowhead*), and smudge sign in patient B (*arrow*)

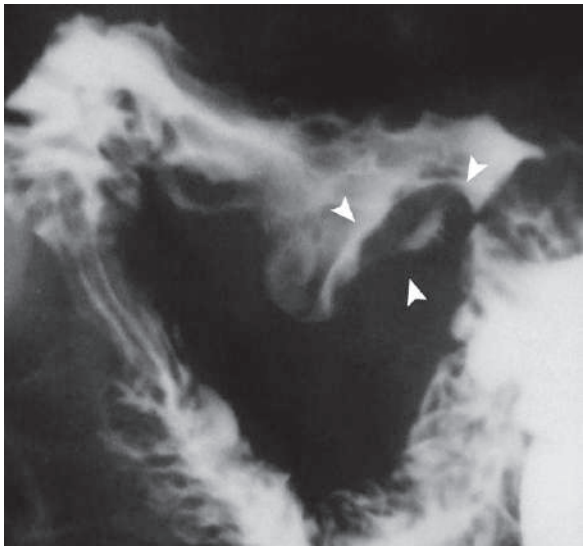

Fig. 1.3.15. Barium meal image of the duodenum in a patient with chronic duodenal ulcer shows the meniscus sign (*arrowheads*)

Signs on Virtual CT Gastroscopy

- The images can be viewed on multiplanar reformation (MPR) images or on 3D reconstructed images.
- In benign ulcers, there is thickening of the stomach wall with preservation of the wall stratification. Mild enhancement may be seen after contrast injection.
- In malignant ulcers, there is marked wall thickening, with strong enhancement more than the adjacent normal gastric wall after contrast injection.

Signs on Conventional CT and MRI

- Gastritis and *H. pylori* infection is detected as a marked thickening and nodularity of the stomach wall, especially in chronic gastritis (Fig. 1.3.16). Biopsy of the nodules by endoscopy is important to exclude malignancy transformation. Up to 80% of patients with stomach cancers that arise outside the cardia have positive antibodies against *H. pylori*.
- In ZES, there is a hypodense nodule with or without calcification often seen in the duodenum or the pancreas on nonenhanced images. After contrast injection, gastrinoma shows intense contrast enhancement in the arterial phase (Fig. 1.3.17). Liver metastasis may be seen. On MRI, gastrinoma shows low T1 and high T2 signal intensities with marked contrast enhancement on the early arterial phase of the scan.

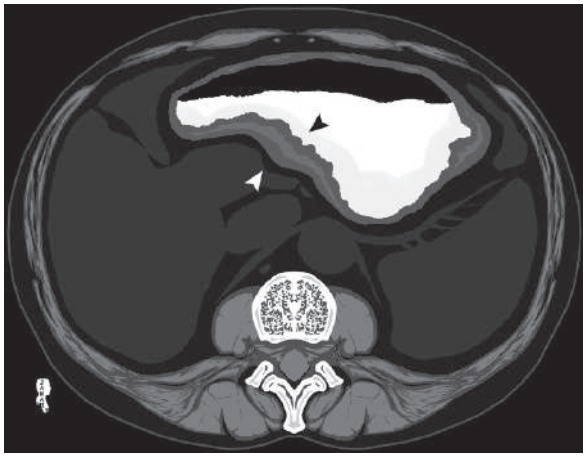

Fig. 1.3.16. Axial CT illustration demonstrates thickening of the stomach wall with nodularity as a sign of chronic gastritis (*arrowheads*)

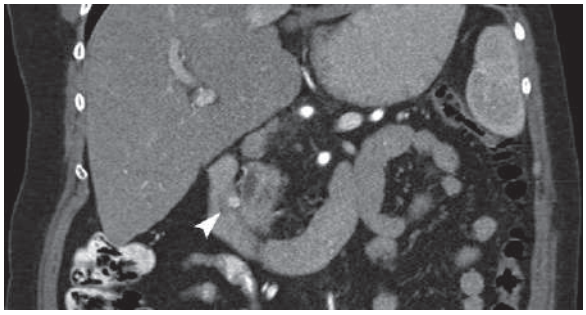

Fig. 1.3.17. Coronal postcontrast CT image of a patient with Zollinger-Ellison syndrome (ZES) shows highly enhanced nodule located between the second part of the duodenum and the pancreatic head within the boundaries of the gastrinoma triangle representing gastrinoma (*arrowhead*)

Superior Mesenteric Artery Syndrome (Wilkie's Syndrome)

Superior mesenteric artery syndrome (SMAS) is a disease characterized by compression of the third part of the duodenum by the superior mesenteric artery axis, causing recurrent, intermittent, or chronic duodenal obstruction.

The left renal vein, the uncinate process of the pancreas, and the third part of the duodenum passes in the space between the retroperitoneal aorta and its branch, the superior mesenteric artery (SMA). The SMA can compress the left renal vein or the third part of the duodenum, a phenomenon known as "nutcracker phenomenon."

1.3

Compression of the third part of the duodenum by SMA is an uncommon clinical situation, and has been attributed to loss of the retroperitoneal and mesenteric fat, exaggerated lumbar lordosis, abnormal high fixation of the ligament of Treitz, or an unusually low origin of the SMA. The theory of loss of the peritoneal fat as a predisposing factor for SMAS is strengthened by the fact that this syndrome is almost never observed in obese patients. SMAS has an incidence of 0.013–0.3%.

The normal aorto-mesenteric angle is about 45° with the SMA-aorta distance of 10–28 mm (Fig. 1.3.18), where the third part of the duodenum passes across the aorta. Any condition that narrows the SMA-aorta distance or the aorto-mesenteric angle can produce SMAS.

Patients with SMAS typically present with postprandial epigastric pain, nausea, bilious vomiting, and abdominal distension. The pain is often relived when the patient lies in the left lateral decubitus, prone, or knee-chest position. Acute presentation of the disease can be seen in patients who suffered a recent rapid weight loss (e.g., aesthetic regime)

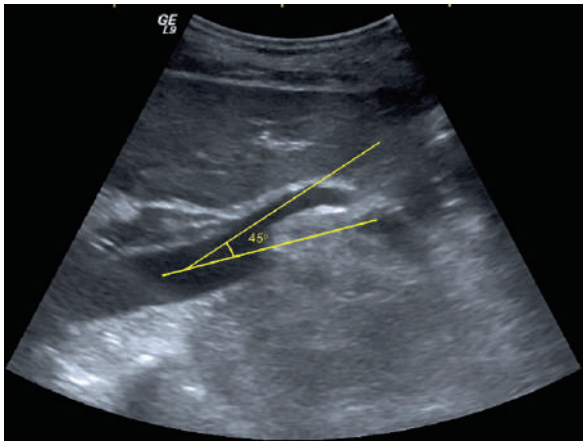

Fig. 1.3.18. Sagittal ultrasound image shows the normal aorto-mesenteric angle

Signs on Doppler US

- The SMA shows high resistant waveform with low diastolic flow in a fasting patient because the intestine is not in vascular demand.
- In a fasting patient, SMA stenosis (>70%) shows peak systolic velocity (PSV) >275 cm/s, and end-diastolic velocity (EDV) >45 cm/s. Also, there is focal increase in velocity, with signs of turbulence. Turbulence within the SMA is observed as aliasing artifact with mosaic color flow.
- Reduced aorto-mesenteric angle (<45°).

Signs on Barium Meal

- Typically, the third part of the duodenum shows sudden, longitudinal filling defect in the middle, at the area where the duodenum passes below the SMA (pathognomonic) (Fig. 1.3.19).
- Dilatation of the first and second part of the duodenum with or without gastric dilatation is commonly seen.

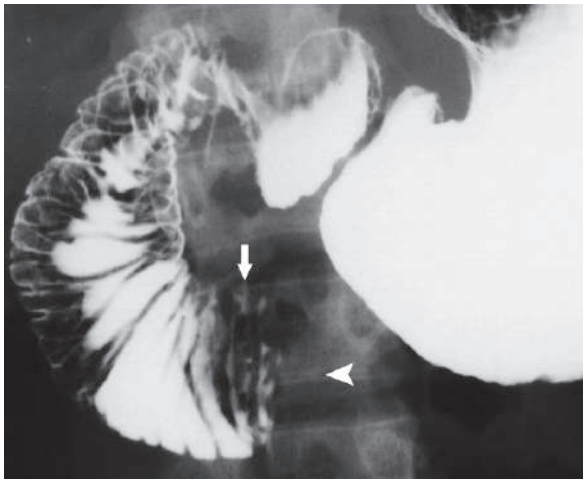

Fig. 1.3.19. Barium meal image in a patient with superior mesenteric artery syndrome (SMAS) shows the classical barium signs. Notice the sudden barium filling cut off of the third part of the duodenum (*arrowhead*) by the superior mesenteric artery (SMA) impression over the duodenum (*arrow*)

Signs on CT

- The CT shows duodenal stenosis at the area where the duodenum passes beneath the SMA, with duodenal poststenotic dilatation (Fig. 1.3.20).

Median Arcuate Ligament Syndrome (Celiac Trunk Compression Syndrome/ Dunbar's Syndrome)

Median arcuate ligament syndrome (MALS) is a rare disease characterized by compression of the celiac trunk by the median arcuate ligament of the diaphragm at the level of the aortic hiatus. In most patients, the celiac artery is displaced cranially, or the diaphragm is displaced caudally. The disease has an incidence of 2:100,000 patients, and has high female incidence between 30 and 50 years of age.

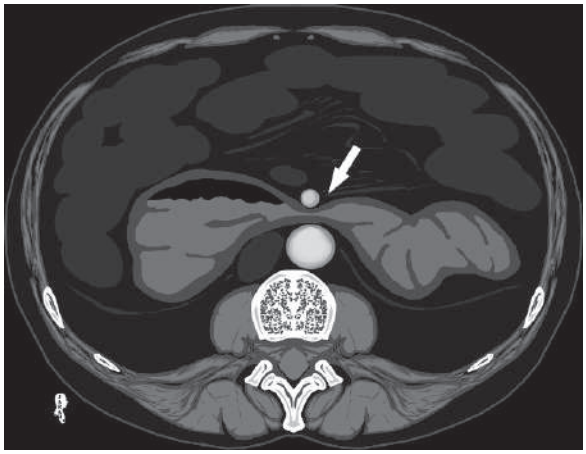

Fig. 1.3.20. Axial CT illustration shows the typical appearance of superior mesenteric artery syndrome. The third part of the duodenum is compressed as it passes beneath the SMA (*arrow*)

Patients with MALS are classically young females (20–40 years) who are very thin presenting with recurrent, nonspecific epigastric pain due to intestinal ischemia and sympathetic-autonomic nerve plexi compression. The pain is often postprandial, and may be accompanied by vomiting, nausea, and weight loss, making the clinical picture more like peptic ulcer disease or gastritis. Postprandial pain typically starts 30 min after eating and may last 1–4 h. The pain can be initiated by exercise, and aggravated by deep expiration. Recurrent diarrhea is frequently seen and explained by the irritation of the celiac plexus. The symptoms appear most frequently in adults.

Clinically, in patients with MALS, an epigastric bruit or thrill may be heard by auscultation, due to the high blood velocity within the compressed celiac trunk.

Because of the rarity of this disease, assumption of MALS must be carried out after excluding all the common causes of epigastric pain like esophagitis, gastritis, and peptic ulcer disease by endoscopy.

MALS sometimes can be associated with cases of Takayasu arteritis due to inflammation of the celiac trunk.

Signs on Doppler US

- The normal celiac artery waveform is low-resistant with high-diastolic flow and no turbulence. In a fasting patient, celiac artery stenosis (>70%) shows PSV >200 cm/s, and EDV >55 cm/s.
- MALS is characterized by celiac artery blood velocity change during inspiration and expiration (*Doppler sign of MALS*). To confirm this sign, the celiac artery velocity during inspiration and expiration must be measured by comparing the velocity difference. The stenosis in MALS typically decreases when the patient stands in upright position, or when he takes deep inspiration because the celiac has a more caudal orientation. In a real celiac trunk stenosis or obstruction, the stenotic velocity does not change with respiration.

Signs on CT Angiography

- The median arcuate ligament shows extrinsic compression of the celiac axis by a MAL (Fig. 1.3.21).
- Pancreaticoduodenal artery aneurysm may occur in 3–18% of cases of MALS.

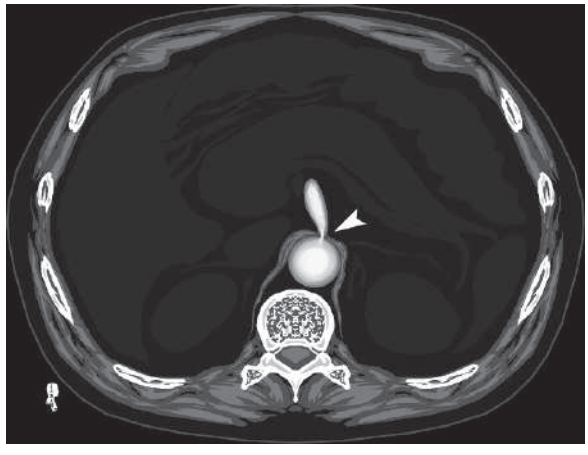

Fig. 1.3.21. Axial CT illustration shows the typical appearance of Median arcuate ligament syndrome (MALS). The diaphragm compresses over the celiac trunk with arterial stenosis (*arrowhead*)

Recurrent Abdominal Pain of Childhood

1.3

Recurrent abdominal pain of childhood is a common complain of school children (8–15%). It is defined as abdominal or epigastic pain that occurs on at least three occasions within a period of at least 3 months. The pain may be severe and associated with pallor. It is mostly psychogenic in origin with no need for radiological diagnosis. Any other pain that does not match this definition should be investigated.

For Further Reading

1. Hayes R. Abdominal pain: General imaging strategies. Eur Radiol. 2004;14:L123–37
2. Foertsch T et al Celiac trunk compression syndrome requiring surgery in 3 adolescent patients. J Pediatr Surg. 2007;42: 709–13
3. Iwazawa J et al Successful embolization of a ruptured pancreaticoduodenal artery aneurysm associated with the median arcuate ligament syndrome. Indian J Radiol Imag. 2008;18:171–4
4. Kohler TR et al Pancreaticoduodenectomy and the celiac trunk compression syndrome. Ann Vasc Surg. 1990;4: 77–80
5. Vaziri K et al Laparoscopic treatment of celiac trunk compression syndrome: Case series and review of current treatment modalities. J Gastrointest Surg. 2009;13:293–98. doi 10.1007/s11605–088–0702–9
6. Frangos SG et al Recurrent celiac trunk compression syndrome. Int J Angiol. 1999;8:150–3
7. Sugiyama K et al Analysis of five cases of splanchnic artery aneurysm associated with celiac artery stenosis due to compression by the median arcuate ligament. Clin Radiol. 2007; 62:688–93
8. Ortiz C et al Familial superior mesenteric artery syndrome. Pediatr Radiol. 1990;20:588–9
9. Bhattacharya D et al Superior mesenteric artery syndrome (Wilkie's syndrome) complicating recovery from posterior fossa surgery in a child - A rare phenomenon. Childs Nerv Syst. 2008;24:365–67
10. Bhattacharjee PK. Wilkie's syndrome: An uncommon cause of intestinal obstruction. Indian J Surg. 2008;70:83–85
11. Santer R et al Computed tomography in superior mesenteric artery syndrome. Pediatr Radiol. 1991;21:154–55
12. Reddy RR et al Superior mesenteric artery syndrome after correction of scoliosis - A case report. Indian J Orthop. 2005;39:59–61
13. Makam R et al Laparoscopic management of superior mesenteric artery syndrome: A case report and review of the literature. J Min Access Surg. 2008;3:80–82
14. Payawal JH et al Superior mesenteric artery syndrome involving the duodenum and jejunum. Emerg Radiol. 2004;10:273–75
15. Lippl F et al Superior mesenteric artery syndrome: Diagnosis and treatment from the gastroenterologist's view. J Gastroenterol. 2002;37:640–43
16. Rubesin SE et al Gastritis from NSAIDS to *Helictobacter pylori*. Abdom Imaging. 2005;30:142–59
17. Chen CY et al Differentiation of gastric ulcers with MDCT. Abdom Imaging. 2007;32:688–93
18. Ranschaert E et al Confined gastric perforation: ultrasound and computed tomographic diagnosis. Abdom Imaging. 1993; 18:318–19
19. Coulier B et al Gastric ulcer penetrating the anterior abdominal wall: Ultrasound diagnosis. Abdom Imaging. 2003;28: 248–51
20. Okada M et al Radiographic findings of intractable gastric ulcers with H_2-receptor antagonists. Abdom Imaging. 1996; 21:133–41
21. Kim JH et al Imaging of various gastric lesions with 2D MPR and CT gastrography performed with multidetector CT. RadioGraphics. 2006;26:1101–18
22. Fishman EK et al CT of the stomach: Spectrum of disease. RadioGraphics. 1996;16:1035–54
23. Thompson WM et al Unusual manifestations of peptic ulcer disease. RadioGraphics. 1981;1:1–16
24. Ellison EC et al The Zollinger-Ellison Syndrome: A comprehensive review of historical, scientific, and clinical considerations. Curr Probl Surg. 2009;46:13–106
25. Canon CL et al Surgical approach to gastroesophageal reflux disease: What the radiologist needs to know. RadioGraphics. 2005;25:1485–99
26. Levine MS. Barrett esophagus: Update for radiologists. Abdom Imaging. 2005;30:133–41
27. Stadler J et al The 'steakhouse syndrome.' Primary and definitive diagnosis and therapy. Surg Endosc. 1989;3: 195–8
28. Anderson SR et al Plummer-Vinson syndrome herald by postcricoid carcinoma. Am J Otolaryngol. 2007;28:22–24
29. Ba-Ssalamah A et al Dedicated multi-detector CT of the esophagus: Spectrum of diseases. Abdom Imaging. 2009; 34:3–18

1.4 Inflammatory Bowel Diseases

Inflammatory bowel diseases (IBDs) are a group of diseases characterized by idiopathic chronic inflammation of the gastrointestinal (GI) tract, extra-intestinal manifestations, and relapsing course. IBDs are divided into Crohn's disease, ulcerative colitis (UC), and indeterminate colitis (6%). Diagnosis of IBDs depends mainly on clinical presentation and biopsy-proved inflammatory changes in a sample taken by colonoscopy. Radiology offers multiple noninvasive methods to monitor the progression of the diseases and their complications through barium studies, CT of the bowel, and MR enteroclysis. Multiple radiographic signs are described in the literature describing different stages of IBDs. An understanding of the basic composition of the bowel wall is mandatory for the radiologist to understand the radiographic signs encountered while investigating IBDs in any radiological modality.

Bowels are hollow organs composed of circumferential wall and circular mucosal folds (Plica circularis in intestines, and haustrations in the colon). The basic layers of the entire GI tract are composed of the innermost layer (mucosa), inner layer (submucosa), middle layer (muscularis), and outer layer (adventitia and serosa). The mucosal layer of the intestine is composed of columnar epithelium with secretory activity, and a thin layer of connective tissue, containing capillaries and lymphatics (Pyer's patches), and usually called "lamina propria." The lamina propria is separated from the submucosa by a thin layer of smooth muscles called the "muscularis mucosa." Beneath the muscularis mucosa lies the submucosa, which is a layer composed of loose areolar connective tissue containing the major lymphatic and vascular channels of the bowel wall. Also, glandular (crypts of Leiberkuhn) and neural structures (Meissner's plexus) lie within the submucosa. Below the submucosa lies the muscular wall, or "muscularis propria," which is divided into an inner circumferential and an outer longitudinal layer. Between layers is the myenteric neural plexus of Auerbach. The outermost layer consists of loose connective tissue called the "adventitia," which is covered by a thin line of peritoneal layer called the "serosa." The normal bowel wall is 3 mm in thickness on radiographic examinations, and the mucosal folds are <3 mm in thickness.

Crohn's Disease

Crohn's disease (CD) is a chronic, granulomatous, idiopathic IBD characterized by the development of multiple GI tract ulcers from mouth to anus.

CD can affect any part of the GI tract. The most common sites for involvement are the terminal ileum and/or cecum (45%), ileo-colonic (13%), or colorectal (30%) region. The disease can be subdivided according to its manifestation into three types: inflammatory, stricturing, and fistulating.

CD is rare before 8 years and after 50 years of age. Patients classically present with diarrhea and abdominal pain. Other symptoms include fever, weight loss, anorexia, and lethargy. Right iliac fossa pain, which occurs 30 min after a meal and reoccurs 3–4 h later, is a common symptom and suggests ileal disease. The right iliac fossa pain may be indistinguishable from the clinical picture of acute appendicitis. Recurrent CD after operation is common.

There is a positive association between CD and tobacco smoking. Also, nonsteroidal anti-inflammatory drugs (NSAIDs) have been reported to exacerbate or lead to reactivation of preexisting IBDs.

MR-enteroclysis or barium studies are used to monitor manifestations of IBDs. Both barium studies and MR-enteroclysis allow detection of subtle mucosal changes. Distension of the bowels by barium or any other contrast media used allows visualization and assessment of the mucosal folds, and detection of ulcers, or newly developed masses as intraluminal filling defects.

Extra-Intestinal Manifestations of CD

- *Arthritis* in IBDs classically has two forms: one that is related to the disease activity, and one that is independent of the disease activity. During an acute episode, a peripheral arthritis may develop in 13% of patients. This type of arthritis resembles rheumatoid arthritis, and should not be confused with arthritis in

a patient with IBDs. The other form, which is independent from the disease activity, presents as radiographic sacroiliitis (10%) or ankylosing spondylitis (3.7%). Up to 15% of patients may experience hip pain due to avascular necrosis of the femoral head. Psoas abscess may occur rarely.

- *Erythema nodosum* (*EN*) is an inflammation of the subcutaneous tissue (panniculitis). It is an immunological reaction that can be triggered by various causes like infections, malignancy, rheumatological disorders, and drugs. EN has an incidence of 1–5 per 100,000. EN typically presents as red, very painful, nonulcerated nodules of the lower extremities, especially over the shin. The lesions may cause difficulty in walking, and usually subside after 2–6 weeks.
- *Pyoderma gangrenosum* (*PG*) is a nodule or pustule that breaks down centrally and forms an expanding ulcer with irregular outline, and a characteristic undermined bluish edge (Fig. 1.4.1). PG is a form of noninfectious ulcer, and can occur during or after the onset of IBDs. PG is often seen in IBDs, multiple myeloma, and leukemia.
- Sclerosing cholangitis
- *Oxalate kidney stones and gallstones* mainly related to the bile stasis and disturbance in the liver-intestine bile cycle.
- *Osteoporosis* is common in patients with CD. This may be attributed to the disease activity, steroids use, and vitamin D malabsorption.

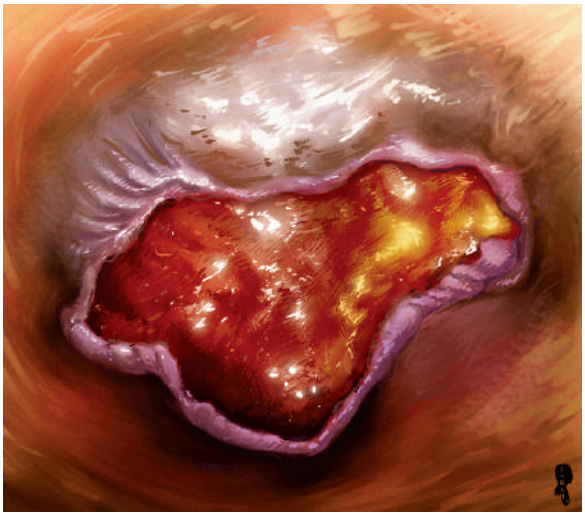

Fig. 1.4.1. An illustration showing the clinical appearance of pyoderma gangrenosum

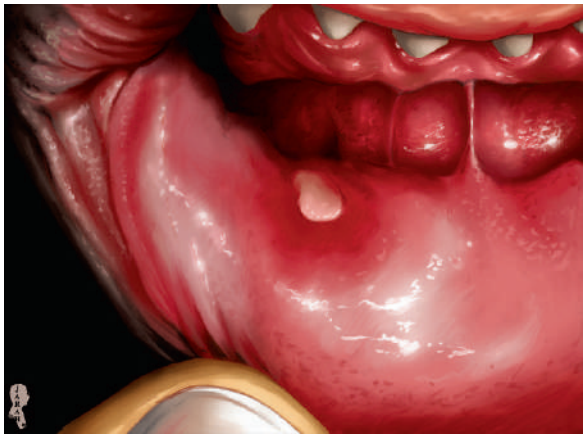

Fig. 1.4.2. An illustration showing the clinical appearance of apthus ulcer of the inner lip mucosal surface

- *Fatty liver and amyloidosis* are changes commonly related to the disease activity. In contrast, sclerosing cholangitis develops in patients with IBDs independent from the diseases activity.
- *Aphthous stomatitis* is a condition in which aphthae are painful buccal ulcers with grayish central fibrinous membrane and erythematous halo (Fig. 1.4.2). They are commonly seen in the "movable buccal mucosa" like the tongue, cheeks, or gutter of the mouth. The pain often subsides within a few days, and the ulcer heals in a week. Aphthae ulcers are seen in around 10% of patients with IBDs.

Signs on Barium (enteroclysis) and Barium Enema

- The maximum diameter of the jejunum is 4.5 cm, and the ileum is 3.5 cm on barium studies. The normal intestinal folds in a normally distended bowel loop are (<3 mm) in thickness. In IBDs, inflammation of the bowel wall affects the mucosal folds, resulting in thickening of the folds (>3 mm) due to edema or hemorrhage. This mucosal fold thickening is seen on barium studies and MR-enteroclysis as an increase in distance between the mucosal folds (plica circularis). Segmental intestinal wall thickening with thickened mucosal folds is a common feature seen on CD.
- *Aphthus ulcer*: the earliest stage of the disease is characterized by lymphoid hyperplasia and lymphadema, which appears radiologicaly as aphthoid ulcers. Aphthus ulcer is an ulcer that

starts as shallow ulceration of the mucosa, and then tunnel deep within the intestinal wall as it progresses. CD ulcers characteristically violate the whole length of the intestinal wall, from the mucosal layer deep into the adventitia (mural ulcer). Barium will accumulate within the ulcer crater, and is surrounded by a barium-free round halo made by mucosal edema (Fig. 1.4.3). When barium enters deep within the intestinal wall due to transmural ulcer, small, white rod-like lines are seen through the intestinal wall, which are called "Rose thorn ulcers."

- *Cobble stone appearance*: seen on barium (enteroclysis) as multiple filling defects grouped together due to aggregation of multiple ulcers in one place with sever edematous mucosa between them (Fig. 1.4.4). The term cobble stone refers to street-like stones arrangement.
- *Multiple skip lesions*: seen as asymmetric distribution of ulceration along the small intestine.
- Narrowing of the lumen with poststenotic dilatation (*String sign)*.
- *String ring of Kantor*: narrowing of the terminal ileum with thick wall separate it from the other loops.
- *Circumferential asymmetry of the bowel lumen*: part of the intestinal lumen will be straight without mucosal folds, while the other preserves its mucosal folds (Fig. 1.4.5).
- In the colon, CD mainly affects the ascending color with relative sparing of the rectum (Fig. 1.4.6).
- *Apple-core appearance*: this appearance is classic for circumferential mass within the bowel lumen. Can be seen due to carcinoma or hypertrophied polyps.

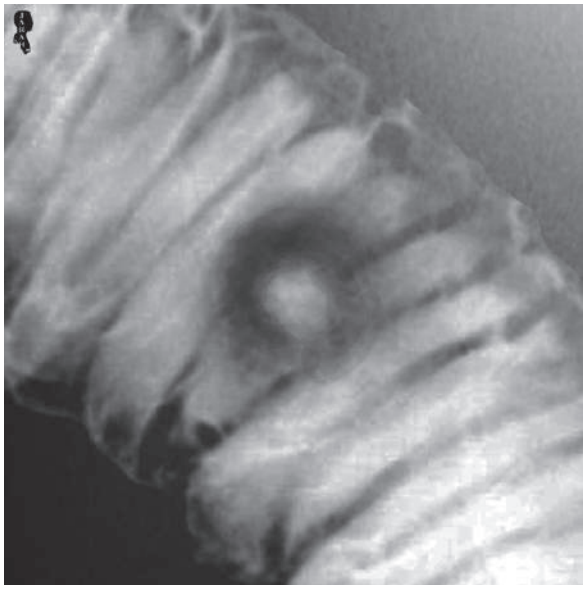

Fig. 1.4.3. Barium (enteroclysis) illustration demonstrating the barium sign of aphthus ulcer

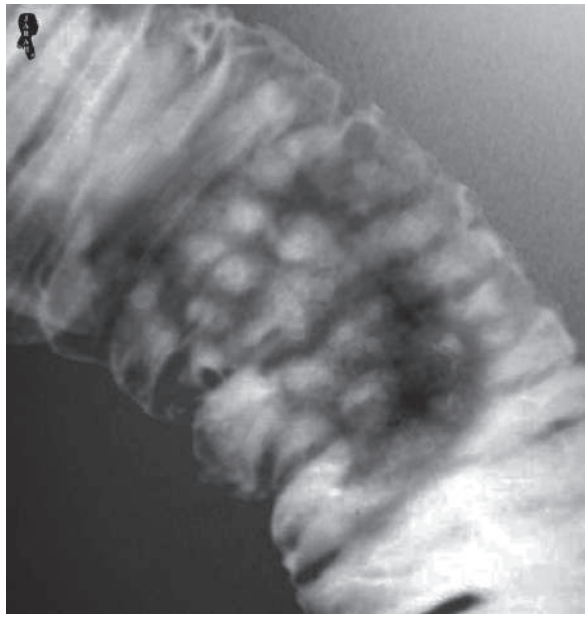

Fig. 1.4.4. Barium (enteroclysis) illustration demonstrating the barium sign of cobble-stone appearance

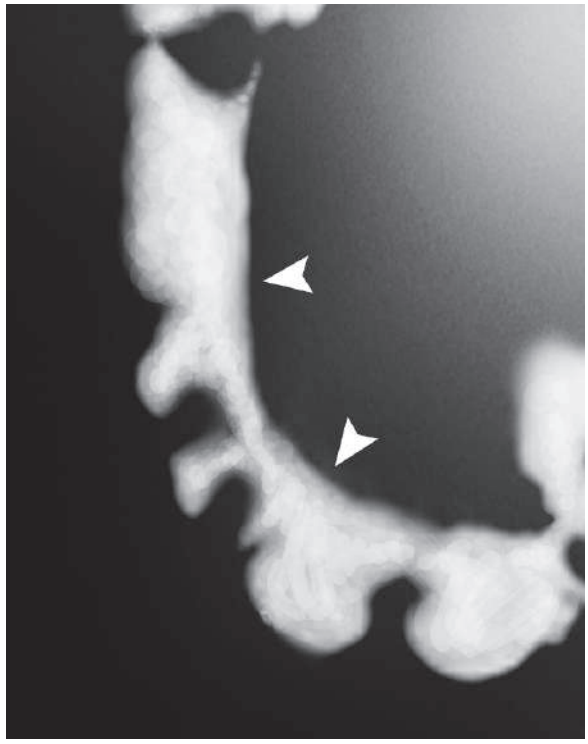

Fig. 1.4.5. Barium (enteroclysis) illustration demonstrating the barium sign of circumferential asymmetry of the bowel lumen

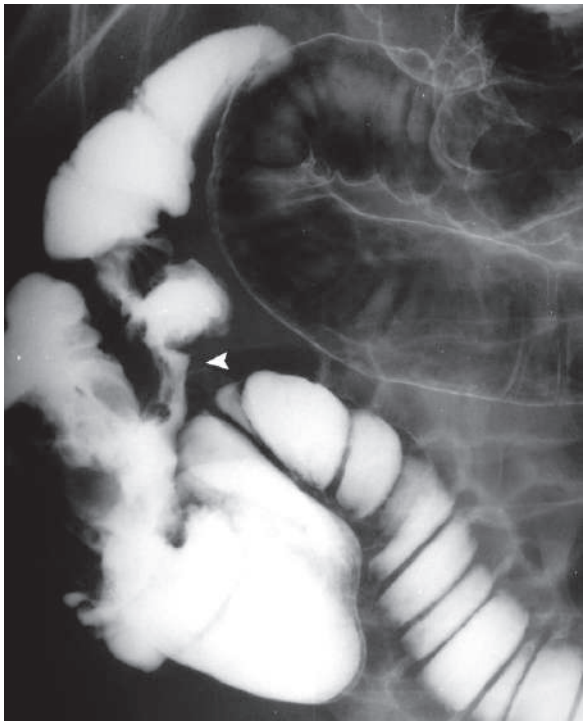

Fig. 1.4.6. Barium enema image in a patient with Crohn's disease (CD) affecting the ascending colon resulting is stricture (*arrowhead*)

Signs on US

- In active CD, ultrasound of the colon or the small intestine shows thickened intestinal wall on the B-mode sonography, mostly in the affected areas. The normal bowel wall thickness on US is equal to or less than 3 mm. Bowel wall thickness is considered pathological when it is >5 mm. Rectal wall thickness is considered normal up to 6 mm in thickness. Reactive lymphadenopathy may be found within the mesentery, which is identified as parallel hyperechogenic structures, about 1 cm thick.
- On PD, the inflamed thickened intestinal walls show high Doppler flow signal on both PD and color-Doppler modes, reflecting the hyperemia of the active inflammation. This hypervasculatization and abnormal Doppler signal within the wall is due to dilatation of small irregular vascular wall vessels <1 mm in diameter.

Signs on CT

- After contrast enhancement, the bowel wall may show five different types of contrast-enhancement patterns (Fig. 1.4.7). The first pattern is characterized by hyperdens (white) enhancement, and is often seen in cases of bowel wall vascular dilatation, or intramural injury with interstitial contrast leakage into the bowel wall, as in cases of ischemic "shock bowel." The second pattern is gray attenuation, where the wall shows little enhancement. This pattern is often seen in cases of neoplastic infiltration (e.g., lymphoma), especially when the wall thickness exceeds 3 cm. The third pattern is the water halo, where the bowel shows intraluminal water-density rings (commonly known as *target sign*). These rings represent edema within the submucosal layer, and they are commonly seen in inflammatory reactions and IBDs. The fourth pattern is the fat halo, which is characterized by deposition of fat within the submucosal layer (HU < -10). This sign is diagnostic of chronic CD. Also, this fat halo may present as a "normal variant" in the distal ileum and colon. The last sign is the black halo, where there is intramural black density that fails to enhance. This sign presents air within the bowel lumen (pneumatosis) and is commonly seen after intestinal infarction.
- *Bowel wall thickness*: this is one of the most common and early signs seen in CD. When the lumen is distended, normal bowel wall thickness is 1–2 mm; when the lumen is collapsed, normal thickness is 3–4 mm. Bowel wall thickness is diagnosed when the bowel wall thickness is >4 mm on distended bowel.
- *Creeping fat*: it refers to fibro-fatty proliferation seen in the mesentery around an inflamed bowel segment, which will cause separation of bowel loops (Fig. 1.4.8).
- *Coomb sign (perienteric hypervascularity)*: this sign is characterized by increased number of dilated mesenteric vessels around a thick bowel loop with intramural target sign (Fig. 1.4.9).
- *Abscess formation*: formation of an abscess commonly seen in patients with intestinal fistulas, where the bacterial flora start to invade the sterile peritoneal organs. Abscess is seen as a soft-tissue density lesion with thick wall, and typical uniform ring enhancement after contrast injection. Air within the lesion is not a common sign but pathognomonic, reflecting gas-producing organism proliferation within the abscess. Abscess formation commonly occurs in the abdominal wall, psoas muscle, small bowel mesentery, and around the anus. The same picture is found on MRI.

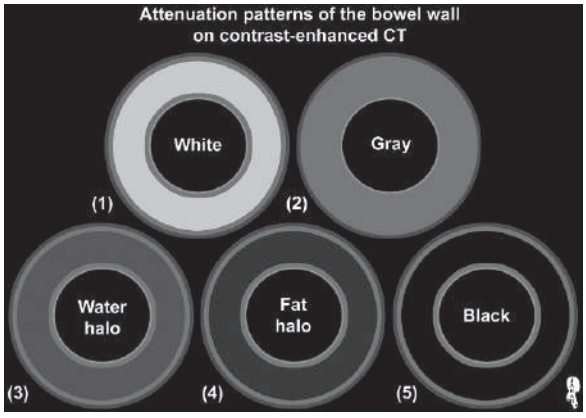

Fig. 1.4.7. An illustration demonstrating the five patterns of bowel wall attenuation: (1) hyperdense, (2) gray density, (3) water density, (4) fat density, and (5) black or air density

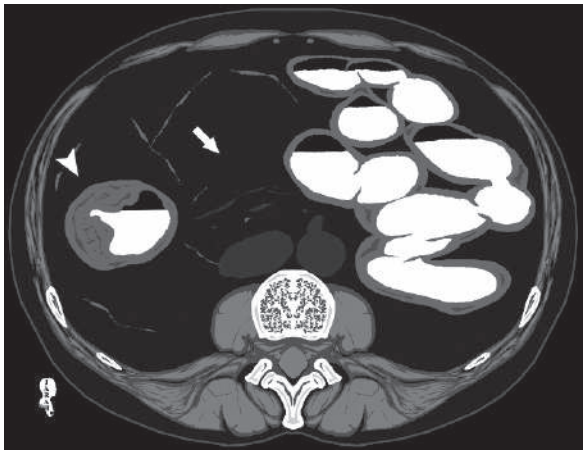

Fig. 1.4.8. Axial contrast-enhanced CT illustration demonstrates bowel wall thickening in CD (*arrow*), with surrounded creeping fatty proliferation that pushes the bowel loops to the left side of the abdomen (*arrow*)

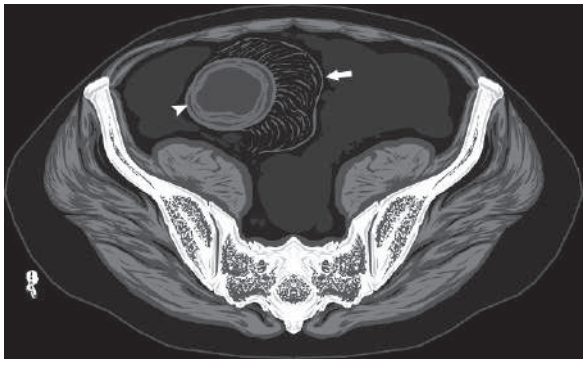

Fig. 1.4.9. Axial contrast-enhanced CT illustration demonstrates the bowel target sign in CD (*arrowhead*), with coomb sign (*arrow*)

Signs on MRI and MR-Enteroclysis

- *Fistula formation*: the main advantages of MR examination over CT are lack of radiation, and high soft-tissue details that make it ideal to detect fistulas. Fistula is an abnormal tract between two surfaces. In CD, fistulas are formed between the organs (e.g., vesicoenteric fistula), or between the internal organs and the skin surface (e.g., fistula-in-ano). Fistula-in-ano typically arises due to rectal crypts infection and abscess formation, which tunnels deep within the perineal tissues until it opens into the skin surface. Fistula-in-ano is identified as an abnormal longitudinal or linear tract that typically runs parallel to the rectum and opens into the skin surface. Thick granulation tissue line may be found surrounding the fistula in chronic cases. Active fistulas show signs of local inflammation and enhancement after gadolinium injection (Fig. 1.4.10).
- Thickening of the iliocecal valve can be nicely demonstrated on coronal MR-enteroclysis images (Fig. 1.4.11).
- *Star sign*: this sign is observed in MR-enteroclysis and represents multiple enter-enteric fistulae with wall-to-wall adhesions (Fig. 1.4.12). The central attachment point between the intersected collapsed bowel loops will result in a star-like configuration.
- *Mucosal polyp formation* is seen in advanced stages of CD as signs of mucosal regeneration (Fig. 1.4.13).
- *Mesenteric lymphadenopathy*: enlargement of the mesenteric lymph node is a common sign in CD (3–8 mm in size) (Fig. 1.4.14). When the lymph nodes are >10 mm in size, carcinoma or lymphoma should be suspected.

Ulcerative Colitis

UC is a chronic inflammatory disease of unknown origin, characterized by rectal and colonic mucosal ulceration.

In contrast to CD, UC affects only the inner wall of the colon (superficial ulceration) and does not extend beyond the muscularis propria layer, and affects the whole colon diffusely with no skip lesions. The rectum is involved in 95–100% of cases. Patients commonly present with bloody diarrhea with mucus. Lower abdominal pain, tenesmus, and urgency are also common symptoms. *Backwash ileitis* refers to mucosal inflammation of the terminal ileum in patients with UC. *Fulminant UC* is a form of severe UC characterized by severe erosions that may lead to muscularis propria damage, causing loss of the haustra and colonic dilatation. Fulminant UC is seen in 15–20% of cases.

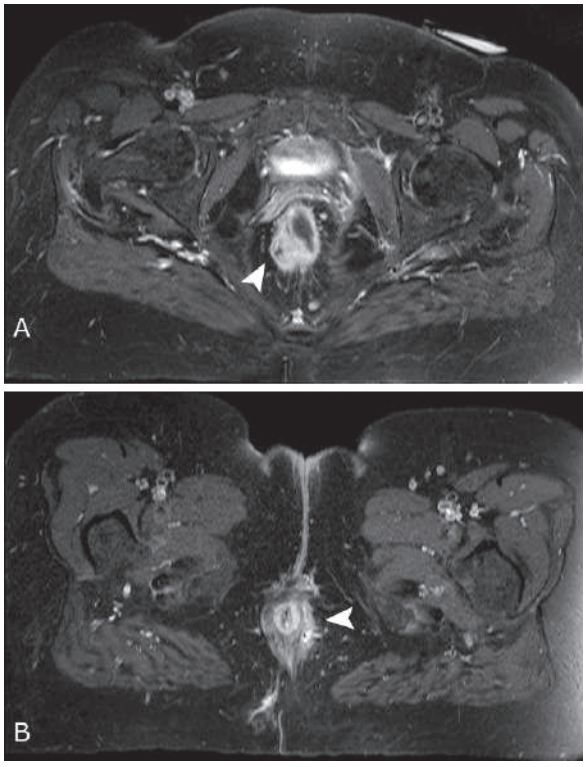

Fig. 1.4.10. Axial T1W postcontrasts with fat-saturation pelvic MRI in a patient with CD and fistula-in-ano seen as abnormal tract parallel to the anus in (**b**) and extends up to the rectum in (**a**) with contrast enhancement of the fistula wall (*arrowheads*)

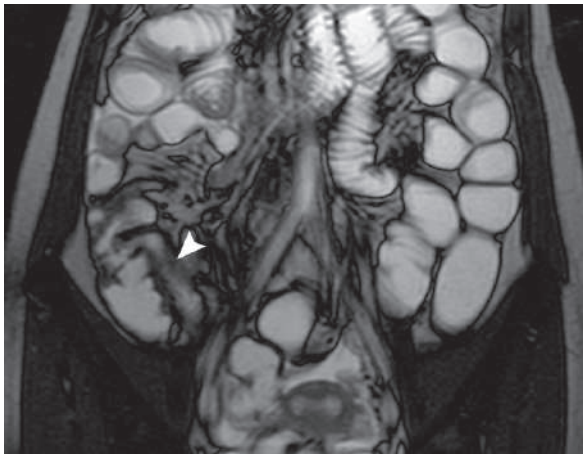

Fig. 1.4.11. Coronal MR-enteroclysis image in a patient with CD shows thickening of the mucosa of the iliocecal valve (*arrowhead*)

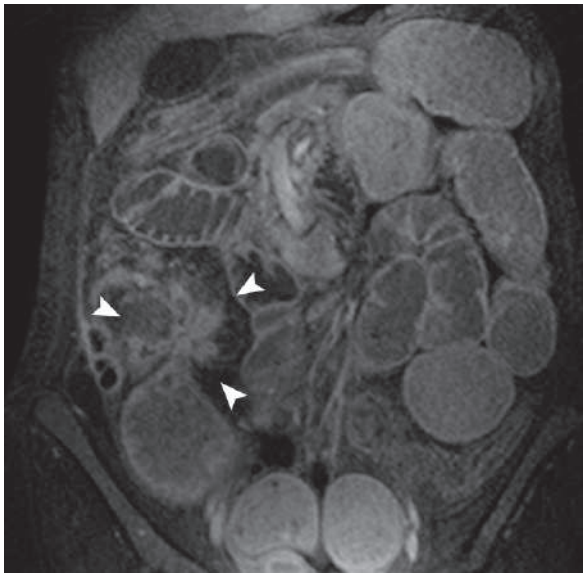

Fig. 1.4.12. Coronal MR-enteroclysis image in a patient with CD shows the star-sign (courtesy of Dr. K. Hermann, Klinikum Großhadern, Munich, Germany)

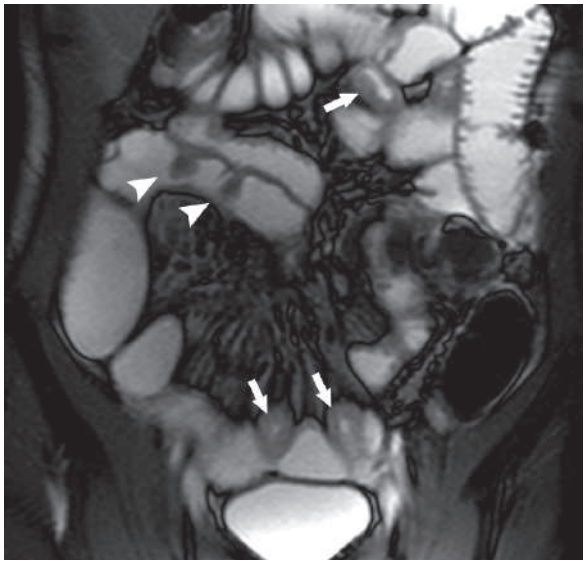

Fig. 1.4.13. Coronal MR-enteroclysis image in a patient with CD shows mucosal polyps formation (*arrowheads*) and bowel wall thickening (*arrows*)

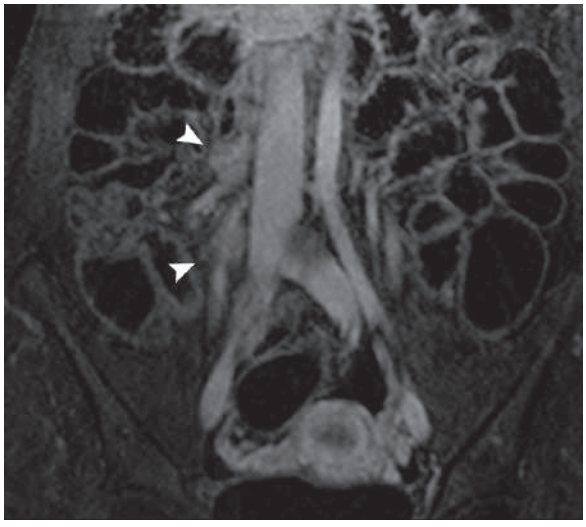

Fig. 1.4.14. Coronal MR-enteroclysis image in a patient with CD shows periaortic lymphadenopathy (*arrowheads*)

CT is indicated in patients with UC when colonoscopy and barium enema are not possible; for example, in cases of sever inflammation, where the risk of perforation is high.

Both UC and CD carry the risk of malignant transformation. The risk of cancer in UC is 0.5–1% after 10 years of universal colonic disease. Surveillance with CT or barium enema is recommended for chronic patients with UC to detect early colonic cancer that may present simulating strictures, or infiltrative process.

Extra-Intestinal Manifestations of UC

- *Arthritis*: same as CD.
- *Sclerosing cholangitis*: sclerosing chlangitis can be seen in association with US in up to 70% of patients with UC.
- *Central nervous system manifestations*: neurological manifestations of UC are rare and patient may presents with seizures. On brain MRI, multiple, periventricular, intra-spinal, and cerebellar hyperintense lesions may be seen (Fig. 1.4.15).
- *Pyostomatitis vegetans* (*PV*): PV is a rare oral ulcerative lesion seen in UC patients, and less frequently in patients with CD. PV is characterized by pustules (visible pus in a blister), erosions, and vegetative plaques appear on the buccal and gingival mucosa forming a "snail-track" appearance. PV is a specific marker for IBDs (Fig. 1.4.16).

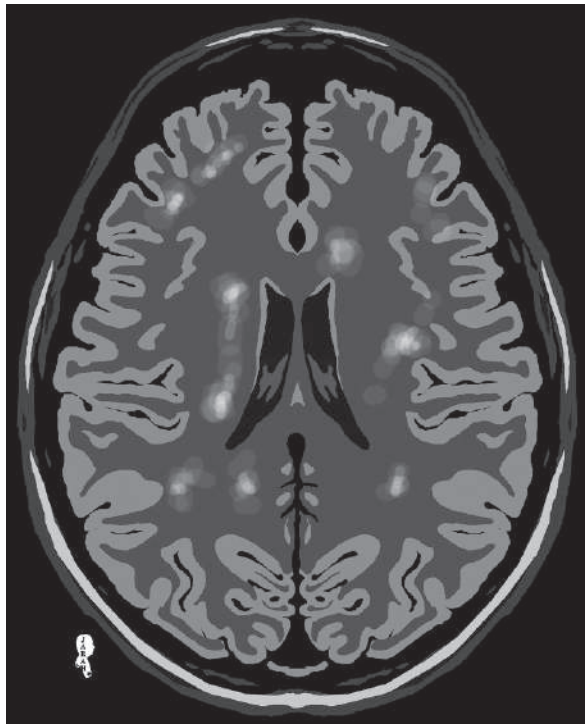

Fig. 1.4.15. Axial FLAIR illustration demonstrates multiple T2 hyperintense signal intensity lesions in a patient with ulcerative colitis (UC)

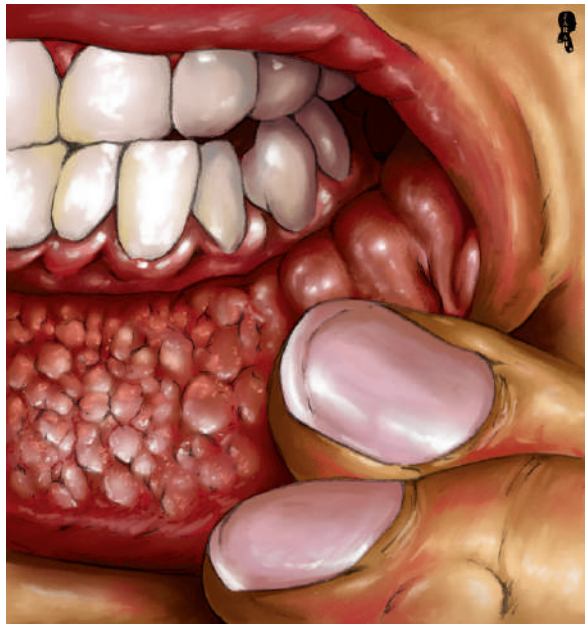

Fig. 1.4.16. An illustration shows the clinical appearance of Pyostomatitis vegetans (PV)

Signs on Plain Radiograph

- Dilated colonic segments with no haustation (*adult toxic dilatation of the colon*).
- *Gasless abdomen*: due to chronic diarrhea.
- *Absence of fecal materials*: because the bowel is not functioning well.
- *Toxic megacolon*: abnormal distention of the colon with air (Fig. 1.4.17).

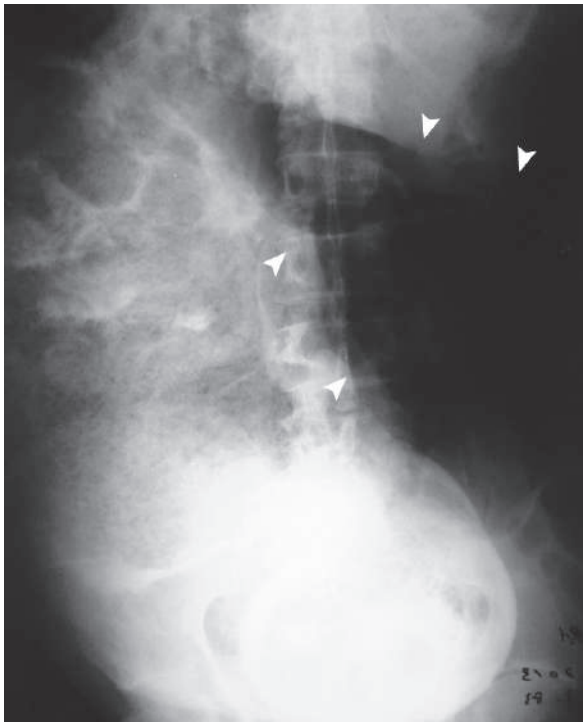

Fig. 1.4.17. Plain abdominal radiograph shows toxic megacolon (*arrowheads*)

Signs on Barium Enema

- *Collar button ulcer*: is a flask-shaped ulcer that is commonly seen in intermediate stage of UC. This type of ulcer is characterized by button-like shape barium appearance. This appearance is seen because UC causes erosions that extend until the muscularis propria, with some intact mucosal layer in between. The intact mucosal layer will have a mushroom-like shape. In barium enema, the barium will fill the erosion gaps between the intact mucosal layers, giving this collar-button appearance (Fig. 1.4.18). This sign is not specific for UC, as it can be seen in duodenal and gastric ulcers.
- *Pipe stem colon*: this refers to rigidity and narrowing of the colon due to longitudinal muscle spasm and hypertrophy (Fig. 1.4.19). This deformity is often seen in the mucosal regenerative stage of the disease.
- *Toxic megacolon*: toxic mega colon is one of the devastating complications of UC, and seen in <5% of cases. Toxic megacolon is diagnosed when the bowel wall shows dilatation >6 cm. Up to 30% of toxic megacolon develops during the first 3 months of the disease. Toxic megacolon is a contraindication for barium enema because of the risk of perforation during air inflation. A plain radiograph should be done in any patient with UC planned for barium enema to exclude the presence of megacolon (Fig. 1.4.17).

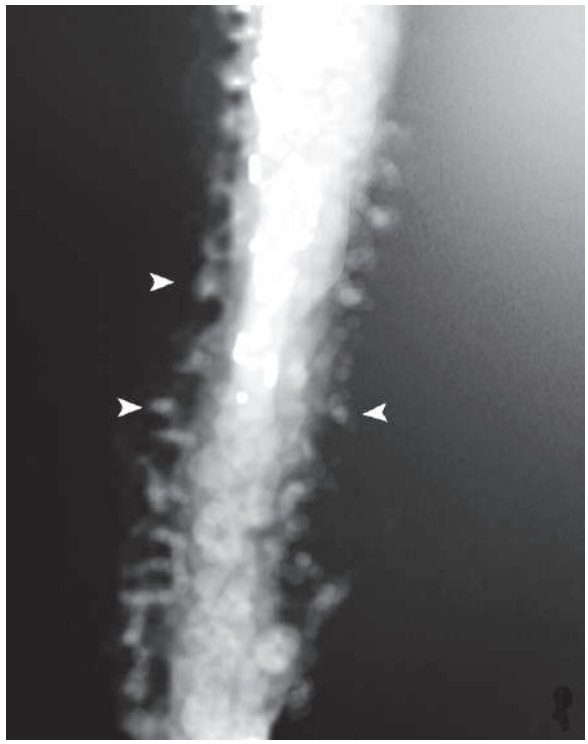

Fig. 1.4.18. Barium enema illustration demonstrates the barium sign of collar button ulcer (*arrowheads*)

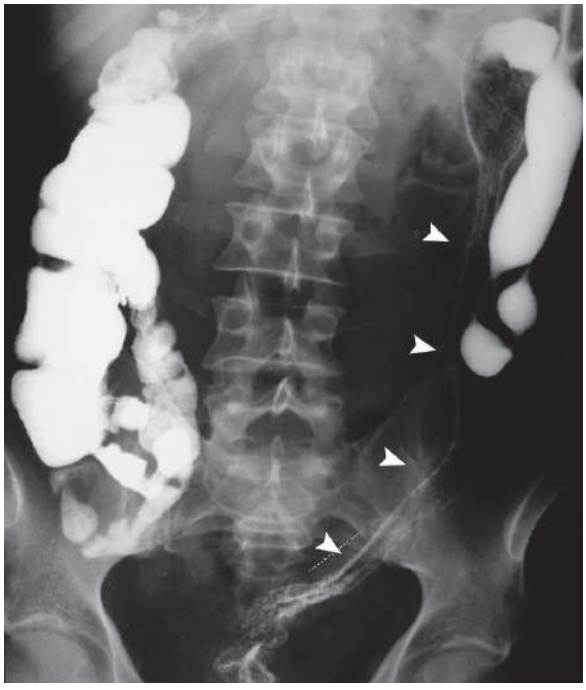

Fig. 1.4.19. Barium enema examination in a patient with chronic US shows marked stenosis and pipe-stem rigidity of the sigmoid colon and the rectum (*arrowheads*)

Signs on CT

- The bowel wall thickness is diffuse, and may affect the entire colon. In contrast, bowel wall thickness in CD may be eccentric and segmental with skip lesions.
- Perirectal fatty proliferation is seen as increased fatty tissues around the rectum (Fig. 1.4.20).

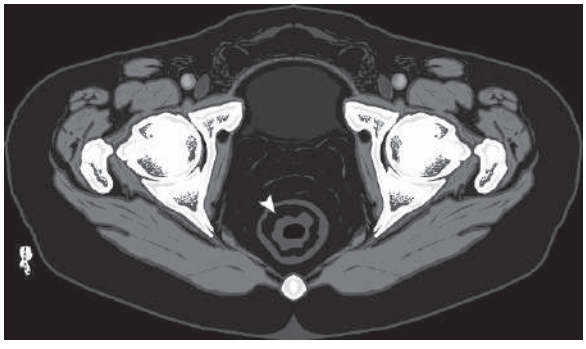

Fig. 1.4.20. Axial CT illustration demonstrates perirectal fatty proliferation with fatty infiltration of the rectal wall (*arrowhead*)

Signs on Colonic MRI (MRI is Used to Diagnose and Monitor UC When Endoscopy Cannot be Performed for Whatever the Reason)

- Hyperintensity and thickening of the colonic mucosa and submucosa on T1W and T2W images, caused by severe hemorrhagic changes.
- T1W post-Gd images show enhancement of the intestinal wall (Fig. 1.4.21). Postcontrast images can be used to monitor the severity and the activity of the disease; the stronger the signal, the higher the severity of the disease.
- Bowel wall thickening >10 mm with loss of the normal haustration may be seen.
- Increase in the peri-rectal fibro-fatty content with widening of the pre-sacral space as a sign of long standing disease.
- Wall stratification is seen in 60% of cases as a hyperintense line on postcontrast T1W images located between two hypointense stripes (Fig. 1.4.22), representing edema and inflammation between the mucosa and the muscularis propria layers.

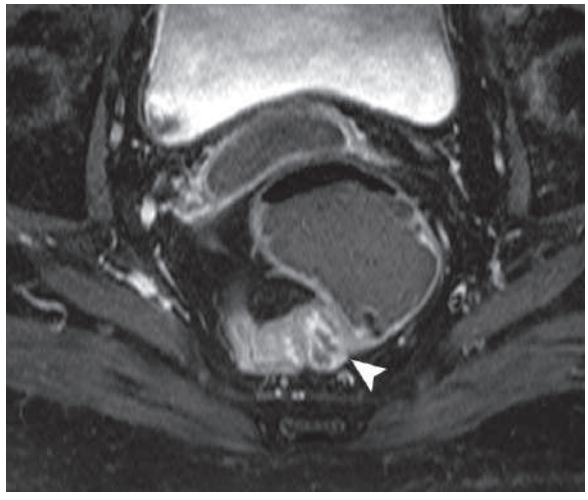

Fig. 1.4.21. Axial T1W, fat-saturated, postcontrast MRI in a patient with UC shows focal rectosigmoidal bowel wall enhancement indicating acute inflammation (*arrowhead*)

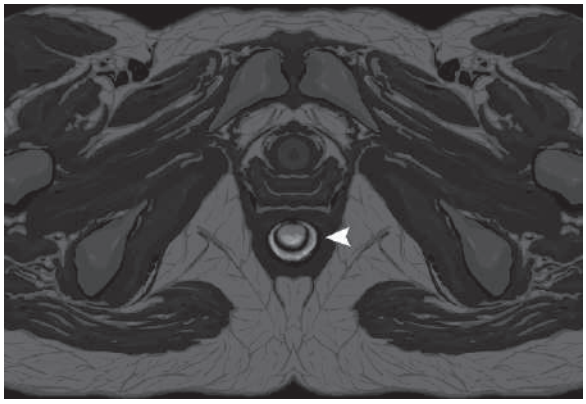

Fig. 1.4.22. Axial T1 W, fat-saturated, postcontrast MR-illustration of a female pelvis demonstrates the rectal wall stratification

Differences Between Ulcerative Colitis and Crohn's Disease

- CD commonly affects the ileum and the ascending colon, and causes transmural (through the whole wall) inflammation. In contrast, UC affects the left colonic side, and causes only inner mucosal layer erosions. Also, backwash ileitis is rare in CD.
- Enlarged mesenteric lymph nodes are commonly seen with CD.
- The rectum is involved in 95% of cases in UC, while only 15–20% of cases in CD.

Differential Diagnoses and Related Diseases

PAPA syndrome is a rare, pediatric, autosomic dominant inherited auto-inflammatory disorder characterized by *Pyogenic* aseptic *Artheritis*, *PG*, and cystic *Acne*. Patients present with recurrent destructive arthritis. The synovial fluid analysis shows purulent content with neutrophils accumulation, but cultures are invariably negative. The cystic acne is seen in the forehead, cheeks, nose, and chin. Humoral markers of inflammatory diseases, including anti-nuclear antibodies and erythrocytes sedimentation rate can be negative. Up to 78% of patients presented with at least one additional inflammatory disorder like: IBD, monoclonal gammopathy, acne conglobata, or hidradenitis suppurativa.

For Further Reading

1. Horton KM et al CT evaluation of the colon: Inflammatory diseases. RadioGraphics 2000;20:399–418
2. Roggeveen MJ et al Ulcerative colitis. RadioGraphics 2006;26:947–51
3. Furukawa A et al Cross-sectional imaging in Crohn disease. RadioGraphics 2004;24:689–702
4. Prassopoulos P et al MR enteroclysis imaging of Crohn disease. RadioGraphics 2001;21:S161–72
5. Wittenberg J et al Algorithmic approach to CT diagnosis of the abnormal bowel wall. RadioGraphics 2002;22:1093–9
6. Javors BR et al Crohn's disease: Less common radiographic manifestations. RadioGraphics 1988;8:259–75
7. Sun MR et al Current techniques in imaging of fistula in ano: Three dimensional endoanal ultrasound and magnetic resonance imaging. Semin Ultrasound CT MR. 2008;29: 454–71
8. Campa A et al Management of a rare ulcerated erythema nodosum in a patient affected by crohn's disease and tuberculosis. J Plast Reconstr Aesthet Surg. 2008;doi:10.1016/j.bjps.2008.11.024
9. Al Roujayee A. Cutaneous manifestations of inflammatory bowel disease. Saudi J Gastroenterol. 2007;13:159–62
10. Maglinte DD et al Classification of small bowel Crohn's subtypes based on multimodality imaging. Radiol Clin North Am. 2003;41:285–303
11. Dekker BJ et al Prevalence of peripheral arthritis, sacroiliitis and ankylosing spondylitis in patients suffering from inflammatory bowel disease. Ann Rheum Dis. 1978;37:33–5
12. Lichtenstein JE et al The collar button. A radiographic-pathologic correlation. Gastrointest Radiol. 1979;4:79–84
13. Maccioni F et al Ulcerative colitis: Value of MR imaging. Abdom Imaging. 2005;30:584–92
14. Giovagnoni A et al MR imaging of ulcerative colitis. Abdom Imaging. 1993;18:371–75
15. Druschky A et al Severe neurological complications of ulcerative colitis. J Clin Neurosci. 2002;9:84–6
16. Koulentaki M et al Ulcerative colitis associated with primary biliary cirrhosis. Dig Dis Sci. 1999;44:1953–56
17. Herrmann KA et al The "star-sign" in magnetic resonance enteroclysis: A characteristic finding of internal fistulae in Crohn's disease. Scand J Gastroenterol. 2006;41:239–41
18. Neye H et al Evaluation of criteria for the activity of Crohn's disease by power Doppler sonography. Dig Dis. 2004;22: 67–72
19. Cammarota T et al US evaluation of patients affected by IBD: How to do it, methods and findings. Eur J Radiol. 2009; 69:429–37
20. Yeon HB et al Pyogenic arthritis, pyoderma gangrenosum, and acne syndrome maps to chromosome 15q. Am J Hum Genet. 2000;66:1443–8.

1.5 Gastrointestinal Hemorrhage

Gastrointestinal (GI) bleeding is classically divided into upper and lower GI bleeding. Upper GI bleeding is defined as bleeding proximal to the ligament of Treitz, and lower GI bleeding is bleeding distal to the ligament of Treitz.

Causes of upper GI bleeding include erosions or ulcers, esophageal varices, Mallory-Weiss tear, and neoplasms. Lower GI bleeding causes include diverticulitis, ulcerative colitis, angiodysplasia, and neoplasms.

Patients with GI bleeding are often asymptomatic until blood loss exceeds 100 mL per day. Tachycardia and hypotension occur when bleeding exceeds 500 mL per day, and systemic shock develops when >15% of the circulation blood volume is lost. Symptoms of upper GI bleeding include vomiting blood (hematemesis) and passing dark stool due to blood digestion (melena). Severe lower GI bleeding may present with passing fresh blood (hematochezia). In up to 75% of upper GI bleeding cases and 80% of lower GI bleeding cases, the bleeding will stop spontaneously with conservative treatment alone. In the remaining 20–25% of cases, further intervention is required.

In recent years, the role of multidetector CT in detecting the source and the cause of bleeding has increased dramatically. CT-angiography is commonly performed to detect the source of bleeding due to its fast scanning time and greater anatomical coverage. Disadvantages of CT-angiography include radiation exposure and inability to perform intervention.

In the classical catheter angiography, bleeding rates as low as 0.5 mL/min can be detected with sensitivity of 63–90% for upper GI bleeding and 40–86% for lower GI bleeding. Conventional angiography specificity of up to 100% is established for both. Active bleeding is detected by extravasation of the contrast material into bowel lumen (pathognomonic sign). Indirect signs of bleeding include detection of aneurysms, arteriovenous fistula, neovascularity, and extravasation of the contrast material into confined space. CT-angiography can detect active bleeding rate as low as 0.3 mL/min.

Signs on CT-Angiography

- Active GI bleeding is detected in the arterial phase of the scan when the contrast material is seen within the bowel lumen (91–274 HU). The extravasated contrast material may demonstrate jet-like, linear, swirled, or pooled configuration (Fig. 1.5.1).
- The presence of hyperattenuated material within the bowel lumen in postcontrast images that was not seen in the precontrast images is diagnostic of acute GI bleeding (Fig. 1.5.1).
- For GI bleeding CTA, only intravenous contrast injection is used. CTA is performed without prior oral administration of water or contrast material. Water can dilute the extravasated contrast material, causing false negative results.
- Clotted blood attenuation is 28–82 HU, which can be differentiated from active bleeding (>90 HU).

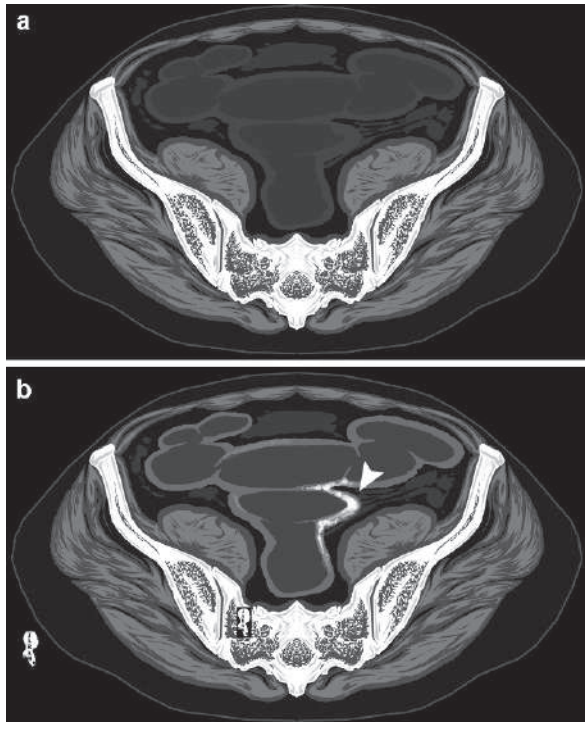

Fig. 1.5.1. Axial abdominal CTA illustration precontrast (**a**) and postcontrast (**b**). GI bleeding is detected in the arterial phase of the scan as an extravasation of the contrast material within the bowel lumen (*arrowhead*)

For Further Reading

1. Jaeckle T et al Acute gastrointestinal bleeding: value of MDCT. Abdom Imaging. 2008;33:285–93.
2. Laing CJ et al Acute gastrointestinal bleeding: emerging role of multidetector CT angiography and review of current imaging techniques. RadioGraphics. 2007;27:1055–70.
3. Yoon W et al Acute gastrointestinal bleeding: contrast-enhanced MDCT. Abdom Imaging. 2006;31:1–8.
4. Yoon W et al Acute massive gastrointestinal bleeding: detection and localization with arterial phase multi-detector row helical CT. Radiology. 2006;239:160–67.
5. Scheffel H et al Acute gastrointestinal bleeding: detection of source and etiology with multi-detector-row CT. Eur Radiol. 2007;17:1555–65.
6. Ha HK et al Radiologic features of vasculitis involving the gastrointestinal tract. RadioGraphics. 2000;20:779–94.
7. Ernst O et al Helical CT in acute lower gastrointestinal bleeding. Eur Radiol. 2003;13:114–17.
8. Yamaguchi T et al Enhanced CT for initial localization of active lower gastrointestinal bleeding. Abdom Imaging. 2003;28:634–36.

Chapter 2

Neurology

CONTENTS

J. A. Al-Tubaikh: *Internal Medicine* – An Illustrated Radiological Guide
DOI: 10.1007/978-3-642-03709-2_2, © Springer-Verlag Berlin Heidelberg 2010

2.1 Stroke (Brain Infarction)

Stroke means the death of brain cells (infarction) due to ischemia or emboli.

The most common causes of stroke are: atherosclerosis, embolic vascular occlusion, hypertension, and inflammatory vascular diseases (vasculitis). Patients present with sudden neurological deficits in the body according to the area of the brain affected. Up to 75% of all cerebral infarctions occur due to middle cerebral artery occlusion. Occlusion of the posterior inferior cerebellar artery (PICA) causes infarction of the lateral medulla plus the inferior cerebellar peduncles (*Wallenberg's syndrome*).

Imaging strokes involves the assessment of 4 Ps:

- *Parenchyma*: assess the area of stroke and exclude hemorrhage (Checked by unenhanced CT).
- *Pipes*: assess the extra- and intracerebral blood vessels (carotid and vertebral arteries). Scanning for CTA should start from the head to the aortic arch.
- *Perfusion*: assess cerebral blood volume (CBV), cerebral blood flow (CBF), and mean transient time (MTT)
- *Penumbra*: the concept of penumbra in stroke refers to the salvageable brain tissue. When a vascular insult occurs, the infracted tissue is surrounded by a region of stunned tissue due to reduction of the blood flow within the affected region. The identification of the penumbra helps the decision of using thrombolytics in acute stroke cases. On CT, the penumbra is assessed by showing parameters mismatch, while on MR, it is assessed by showing diffusion/perfusion mismatch. Pneumbra = MTT minus CBV.

Thrombolytics are not given to stroke patients beyond 3 h from starting of the symptoms due to the risk of hemorrhage. Hemorrhage is an absolute contraindication for thrombolytic therapy. Stroke is evaluated on unenhanced CT, CT-angiography, and CT perfusion study.

Hemorrhagic infarction is usually caused by hypertension or embolic occlusion. Hemorrhagic infarctions arise due to two mechanisms:

- *Venous thrombosis*: the high flowing arterial blood is obstructed by a blocked vein, which raises the intracapillary pressure causing them to rupture and bleed.
- *Arterial embolism*: the embolus blocks the artery, and in some times a small hole develops within the embolus making blood gush into the capillaries with high speed and pressure, causing them to rupture and bleed.

Lacunar infarctions (*cerebral microangiopathy*) are infarctions less than 1 cm in size and occur due to occlusion of the penetrating arterioles of the brain parenchyma. Usually, they are seen in the basal ganglia, the thalamus, and the internal capsule. Lacunar infarctions are commonly seen in diabetic patients.

Differential Diagnoses and Related Diseases

Pusher syndrome: is a very specific disease of postural orientation, commonly affecting poststroke hemiparetic patients. In the pusher syndrome, patients use their nonparetic arm and/or leg to actively push from the nonparalyzed side toward the paralyzed, which results in loss of balance and falling toward the paralyzed side (Fig. 2.1.1). These patients also resist any attempt to correct their tilted body posture toward the vertical upright position. Pusher syndrome can be seen in up to 10% of patients with hemiparesis due to strokes. Pusher syndrome may be also arising due to brain trauma or tumors.

Signs on CT

- *Hyperacute stage* (the first 3–6 h): unenhanced CT usually is normal. It must be repeated after this period within 24–48 h.
- *Acute stage* (from 6 to 24 h): nonenhanced CT shows a wedge-shaped hypodense area surrounded by edema that may cause mass effect on the ventricles with effacement of the cerebral sulci (Fig. 2.1.2a). The hypodense lesion follows a vascular territory (Fig. 2.1.3). Cytotoxic edema starts after 30 min from the stroke attack, and vasogenic edema starts from 4 to 6 h postattack. Each increase in 1% of parenchymal edema reduces the Hounsfield unit (HU) by 2.5 HU.
- *Subacut stage* (days to weeks): there is a hypodense lesion without edema (Fig. 2.1.2b). Edema resolve and the mass effect decrease at 7–10 days postattack.
- *Chronic stage* (more than 3 months postattack): the tissues around the lesion will loose their volume (gliosis), which will cause negative pressure upon the adjacent ventricles, causing

their dilatation (*Evacuee Dilatation*) (Fig. 2.1.2c). When the evacuee dilatation is massive, the negative pressure causes the ventricle to open into the infarction, creating a porencephalic cyst (Fig. 2.1.2d). *Porencephalic cyst* is a cerebrospinal fluid cyst that is communicating with the ventricles.

- *Hyperdense vessel sign*: on nonenhanced CT, a thrombosed vessel may appear as a hyperdense structure due to the thrombus within it. Normal blood measures (40–60 HU) and is normally not seen on nonenhanced CT, while thrombosed blood measures (77–80 HU) and can appear on nonenhanced CT. The thrombosed blood vessels usually asymmetric, bilateral symmetrical hyperdense vessel is unlikely to be thrombosis.
- *Obscuration of the lentiform nucleus*: hypoattenuation and obscuration of the lentiform nucleus due to cytotoxic edema is another sign of acute infarction.
- *Insular ribbon sign*: it refers to hypoattenuation of the insular region with loss of the gray-white matter definition.
- *HU window alteration*: the standard HU window setting is (80 HU widths, and 20 HU center). If no abnormality in attenuation is seen in the image, lower the window to (8 HU widths, and 32 HU center). The last settings increase the sensitivity for detection of hypodense areas.
- *Luxury perfusion*: When you inject contrast into an acute infarction, you'll get contrast diffusion as multiple lines into the gyri (Fig. 2.1.4). This sign appears within the first 3 days of the attack. It is best recalled by Elster's Rule of 3 (as early as 3 days, maximum at 3 days to 3 weeks and gone by 3 months).
- *Hemorrhagic infarction* is seen as an area of hyperdense blood within the brain parenchyma surrounded by hypodense area of cytotoxic edema.
- *Lacunar infarction* is seen as a small (<2 cm), hypodense area within the brain parenchyma with no mass effect (Fig. 2.1.5).
- Disruption of the normal circle of Willis branches is classically detected in stroke (Fig. 2.1.6).

Fig. 2.1.1. An illustration demonstrates pusher syndrome; the patient is actively pushing and extending his right side (nonparalytic side) toward the left side (paralytic side), which is assisted by the nurse

2.1

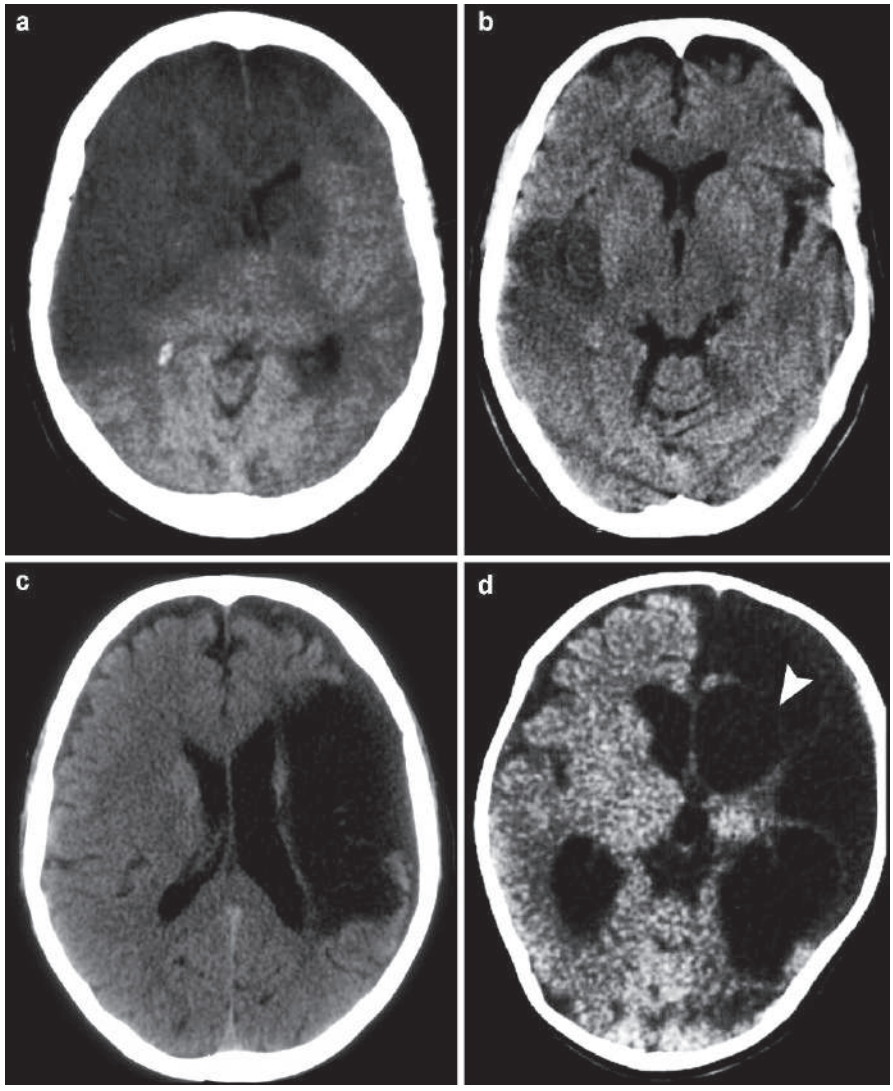

Fig. 2.1.2. Multiple axial CT of the brain with different stages of infarction: (**a**) acute infarction, (**b**) subacute infarction, (**c**) chronic infarction with gliosis, (**d**) chronic infarction with formation of porencephalic cyst (*arrowhead*)

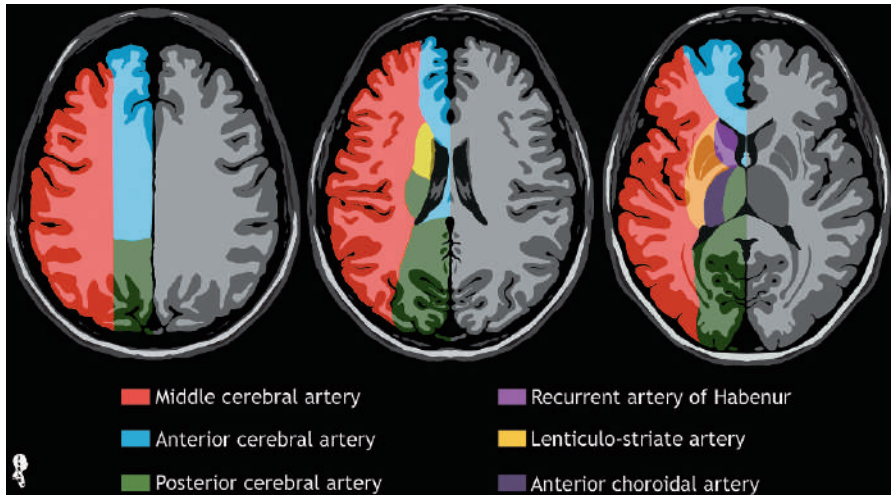

Fig. 2.1.3. Sequential axial brain MR-illustrations demonstrates different vascular territories of the brain parenchyma

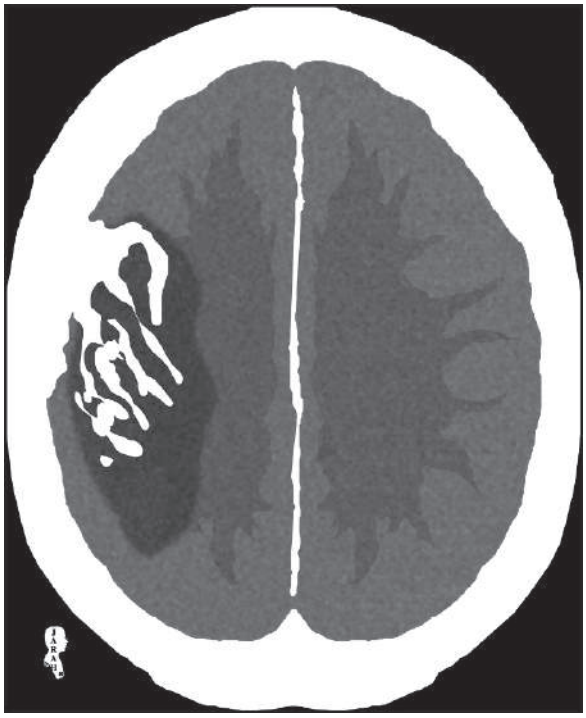

Fig. 2.1.4. Axial brain CT illustration demonstrates infarction within the vascular region of the middle cerebral artery with multiple enhanced lines inside it representing luxury perfusion

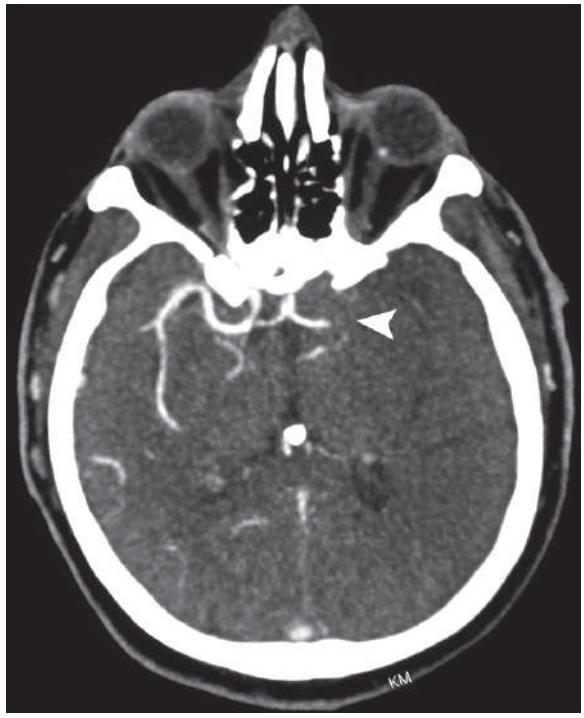

Fig. 2.1.6. Axial brain CTA image of a patient with left brain infarction shows blockage of the left middle cerebral artery (M1) segment (*arrowhead*)

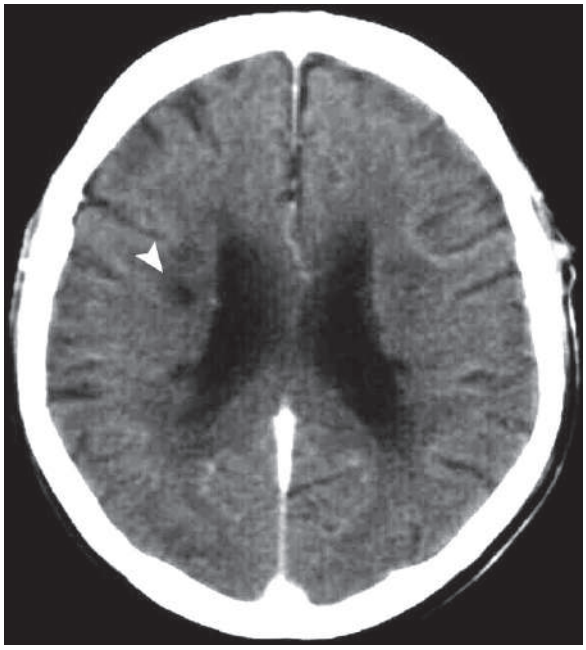

Fig. 2.1.5. Axial brain CT image shows acute lacunar infarction in the right centrum semiovale with small ring of cytotoxic edema around it (*arrowhead*)

Signs on MRI and DWI

- *Hyperattenuated vessel sign*: it is seen on T2* images as hyperintense vessel (like on unenhanced CT images).
- *T2* images*: are very sensitive to detect hemorrhage and microhemorrhages. Hemorrhage is seen as areas of abnormal blooming, while hemosiderin is seen as areas of low signal intensities.
- *DWI*: areas of infarction are seen as areas of high signal intensity due to water motion impedance (cytotoxic edema), usually 30 min from the start of the attack (Fig. 2.1.7). On the ADC map, the areas of high signal intensity on DWI show low signal intensity. Chronic infarction shows low signal intensity on DWI, and high signal intensity on ACD maps. The two must be assessed together to diagnose chronic infarction. DWI is accurate in detecting brain stem and lacunar infarctions.
- *MR Spectroscopy* in infarction shows high lactate, and low *N*-acetyl aspartate, cholin, and creatine (present up to 5 weeks postattack).

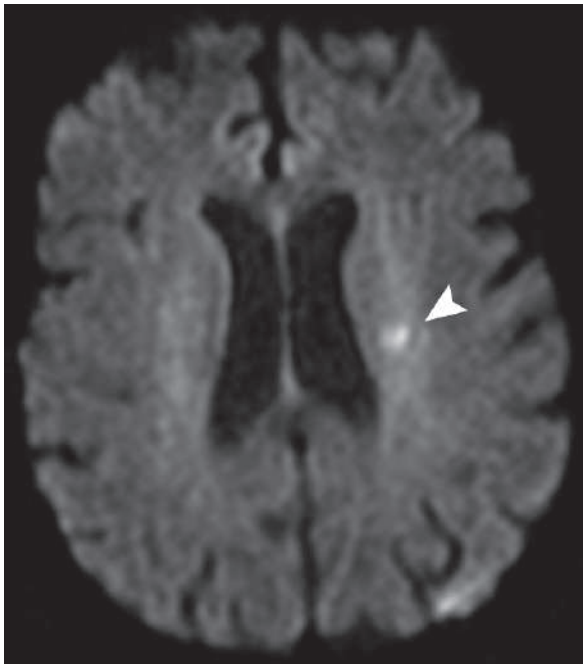

Fig. 2.1.7. Axial brain DWI shows acute lacunar infarction in the left paraventricular area (*arrowhead*)

For Further Reading

1. Srinivasan A et al State-of-the-art imaging of acute stroke. RadioGraph. 2006;26:S75–95
2. Vu D et al Non-contrast CT in acute stroke. Semin Ultrasound CT MRI. 2005;26:380–6
3. Mullins ME. The hyperdense cerebral artery sign on CT scan. Semin Ultrasound CT MRI 2005;26:394–403
4. Shetty SK et al CT perfusion in acute stroke. Neuroimaging Clin N Am. 2005;15:481–501
5. de Lucas EM et al CT protocol for acute stroke: tips and tricks for general radiologists. RadioGraph. 2008;28: 1673–87
6. Karnath H-O. Pusher syndrome – a frequent but little-known disturbance of body orientation reception. J Neurol. 2007; 254:414–24
7. Johannsen L et al "Pusher syndrome" following cortical lesions that spare the thalamus. J Neurol. 2006;253:455–63

2.2 Stroke Diseases and Syndromes

Stroke can be a symptom rather than an actual disease. Some systemic diseases present in the form of stroke. Other diseases or syndromes are associated with stroke as one of their diagnostic criteria. Some syndromes or diseases arise due to stroke in a certain area of the brain. This topic discusses some of the known and uncommon causes, syndromes, and diseases of stroke.

Moyamoya Disease (Progressive Occlusive Arteritis)

Moyamoya disease is characterized by a progressive occlusion of arteries of the circle of Willis due to intimal wall thickening of the distal internal carotid artery and its proximal anterior cerebral artery branch bilaterally, with the formation of abnormal collateral networks that develop adjacent to the stenotic vessel. These collaterals give the shape of puff of smoke, which is called "Moyamoya" in Japanese.

Moyamoya disease is a rare disease worldwide, but with high incidence in Japanese. Occlusion usually occurs in both hemispheres, but unilateral occlusion can occur. The disease can be seen in association with sickle cells disease and neurofibromatosis.

The disease peaks in the first decade and dips in the fourth decade. Patients present in young age with recurrent strokes, headaches, and behavioral disturbance. The disease can be suspected in a young adult presenting with stroke, with no predisposing factors. Diagnosis is essentially established by angiography or MR-angiography.

Signs on CT, MRI, and MR-Angiography

- Large network of collaterals in the basal ganglia and brain stem fed by the internal carotid artery, the basilar artery, and the anterior cerebral artery giving the appearance of a puff of smoke (Pathognomonic) (Fig. 2.2.1).
- On T1W images, there are multiple hypointense, flow void lesions located in the basal ganglia representing the abnormal collaterals networks (Fig. 2.2.2).

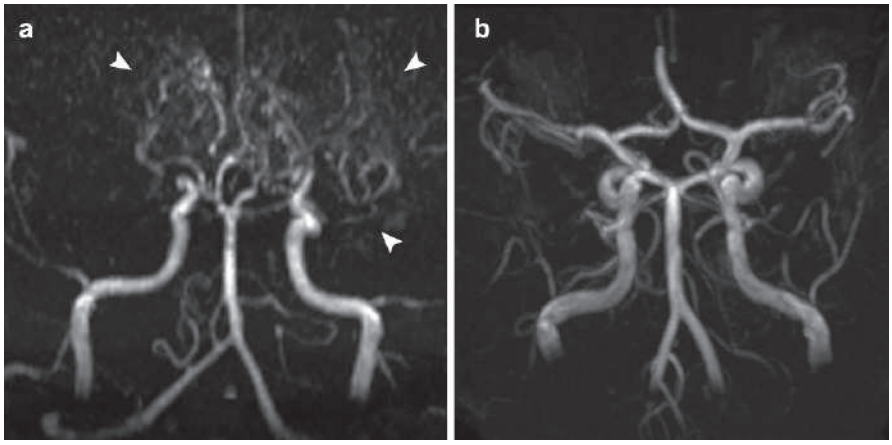

Fig 2.2.1. MR-angiography of a patient with moyamoya disease (**a**) and MR-angiography in a normal healthy patient (**b**) for comparison. In (**a**), there is irregular arterial collateral formation in the region of the anterior cerebral arteries bilaterally in figure (**a**) (*arrowheads*), with complete disappearance of the middle cerebral artery (MCA) (M1 segment). Compare the image in (**a**) with the normal MRI appearance of the circle of Willis in (**b**)

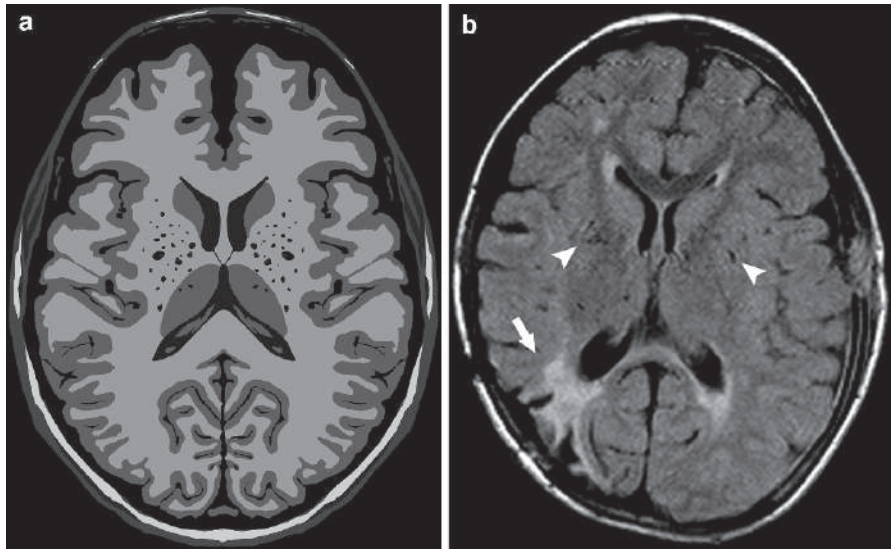

Fig. 2.2.2. Axial T1W brain MR-illustration (**a**) with axial FLAIR MRI of a patient with moyamoya disease shows multiple flow void signal intensities in the region of the basal ganglia bilaterally representing the abnormal collateral formation (*arrowheads*). Leuko-encephalopathy at the region of the posterior horns of the lateral ventricles can be seen (*arrow*) affecting the right side more than the left side

Cerebral Amyloid Angiopathy

Cerebral amyloid angiopathy (CAA) is a disease that occurs due to deposition of a protein (AB peptide) or amyloid substance in the arteriolar wall of the cerebral vessels, causing weakening and fragility of blood vessel walls. Later, intracerebral bleeding develops due to spontaneous blood vessels rupture.

In CAA, amyloid proteins replace the contractile element of the arteriolar muscle layer, leading to increased fragility of the walls. CAA is not a part of systemic amyloidosis, and it is the most common cause of spontaneous, nontraumatic intracranial bleeding in nonhypertensive elderly patients.

CAA should be suspected when an elderly patient (60 years) presents with unexplained spontaneous intracranial bleeding that is lobar and located very superficial in the cortex. It is responsible for up to 20% of nontraumatic brain hemorrhage and hemorrhagic infarction, and up to 30% of lobar bleeding.

CAA can be associated with Alzheimer's disease, with dementia occuring in up to 40% of cases. Dementia in CAA patients occurs and progresses much faster than dementia in patients with Alzheimer's disease. Diagnosis of CAA is usually done by clinical history and the radiological features of the CT or the MRI.

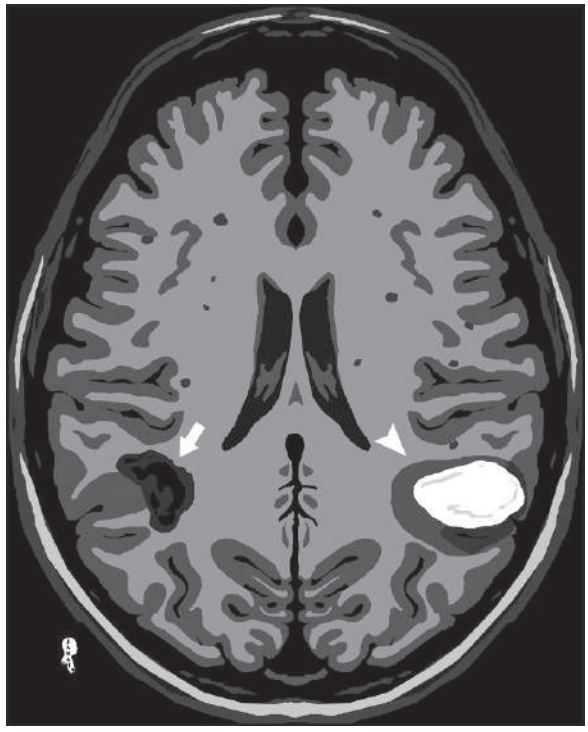

Fig. 2.2.3. Axial T1W brain MR-illustration demonstrates cerebral amyloid angiopathy (CAA). There is corticomedullary bleeding in the left parieto-occipital area surrounded by cytotoxic edema (*arrowhead*). Multiple areas of hypointense signal intensities scattered within the white matter representing chronic micro-hemorrhages. An area of low signal intensity is seen in the right parieto-occipital area representing gliosis (*arrow*)

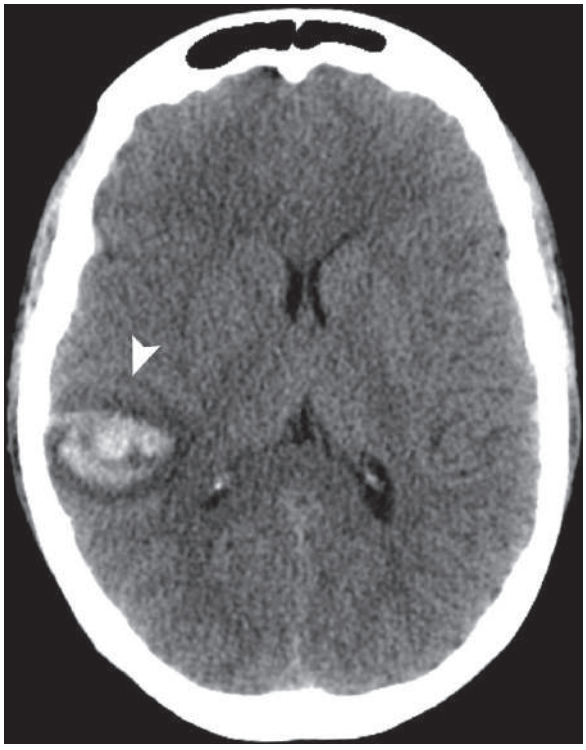

Fig. 2.2.4. Axial brain nonenhanced CT in a patient with intracranial bleeding due to CAA shows an area of bleeding in the right temporo-occipital region involving the cortices and the corticomedullary junction with a rim of cytotoxic edema (*arrowhead*)

CADASIL (Cerebral Autosomal Dominant Arteriopathy with Subcortical Infarcts and Leukodystrophy)

CADASIL is the most common form of familial strokes with progressive dementia due to vasculopathy of the deep perforating arteries of the cerebral white matter. Patient with CADASIL presents with multiple attacks of strokes beginning usually between 40 and 60 years of life. Patients typically have no risk factors for stroke. Psychiatric symptoms occur in 30% of cases (e.g., depression).

Diagnostic Criteria for CADASIL

- Young age (<50 years).
- Two of the following clinical findings: stroke-like episodes with permanent neurological defects, migrainous headache, major mood disturbance, or subcortical dementia.
- No risk factors for stroke.
- Positive family history for such stroke attacks.
- On MRI, white matter changes without cortical infarcts.

Signs on CT and MRI

- Acute intracranial bleeding area (Lobar hemorrhage), seen as high density area on CT images or with high T1/T2 signal intensities on MRI that is located in the superficial cortex and the subcortical white matter (Figs. 2.2.3 and 2.2.4), with a distribution different from those resulting from hypertensive bleeding (usually deep within the brain). Bleeding due to CAA is characteristically multiple, spares the basal ganglia and brain stem, and is located at the corticomedullary junction.
- On MRI, multiple chronic micro-hemorrhages are seen as signal void, a few millimeters in size hypointense lesions in the deep white and the subcortical white matter on T2* images (Fig. 2.2.3).
- CAA affects commonly the frontal and the parietal lobes. Up to 10–50% of cases bleed in more than one lobe.

Signs on MRI

- Extensive white matter lesions and basal ganglia abnormalities in the absence of cortical infarcts typically seen in the temporal lobes and the extreme and external capsule (Fig. 2.2.5). The lesions do not enhance after contrast injection.
- Widening of the periventricular spaces (*Virchow-Robin spaces*) (Fig. 2.2.6).
- MR-angiography is typically normal (no vascular lesion).

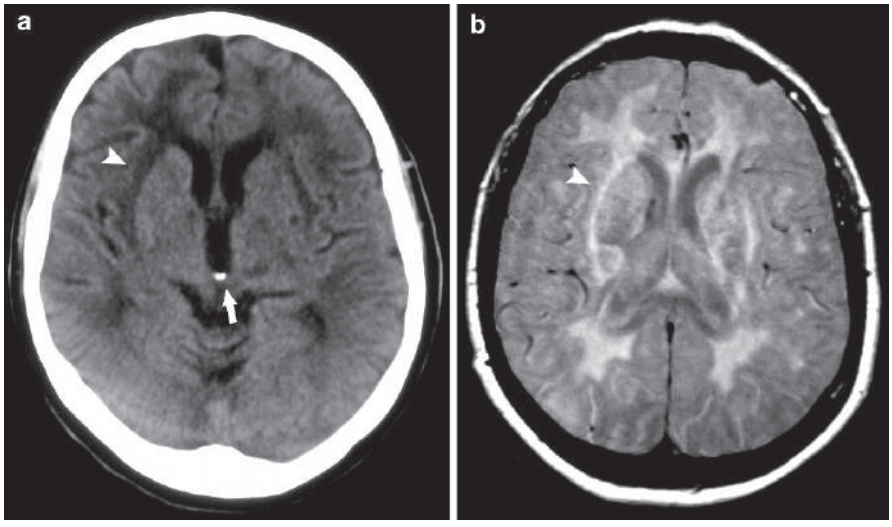

Fig. 2.2.5. Axial nonenhanced brain CT (**a**) and axial FLAIR MRI (**b**) of a patient with cerebral autosomal dominant arteriopathy with subcortical infarcts and leukodystrophy (CADASIL) shows bilateral diffuse white matter lesions with affection of the right external capsule (*arrowheads*). Pineal calcification can be seen as a secondary finding (*arrow*)

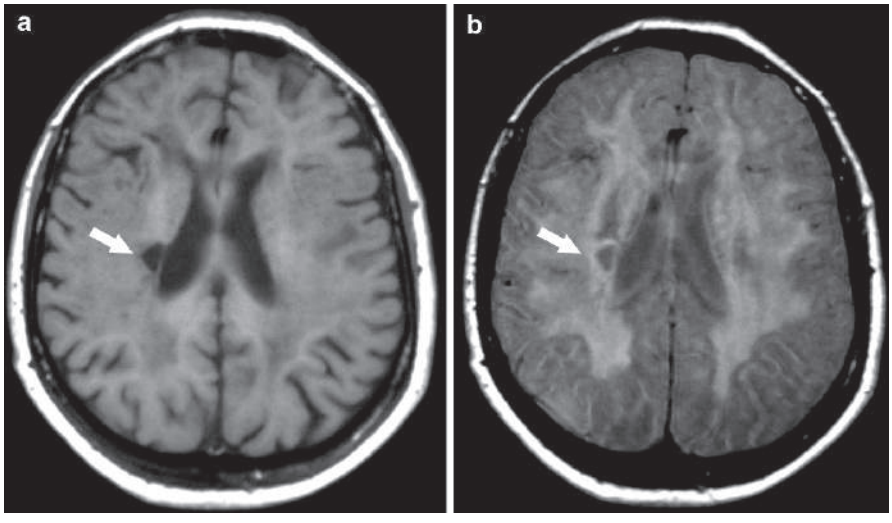

Fig. 2.2.6. Axial T1W (**a**) and FLAIR (**b**) brain MRI of another patient with CADASIL shows bilateral diffuse white matter lesions (leukoencephalopathy) with dilated right Virchow–Robin space (*arrowhead*)

MELAS (Mitochondrial Myopathy, Encephalopathy, Lactic Acidosis, and Stroke-Like Episodes)

MELAS is a mitochondrial disease characterized by episodes of infarction-like cerebral injuries causing hemiparesis or hemiplegia, hearing loss, or cortical blindness. The disease is characterized by elevated serum levels of lactic acid (lactic acidosis).

MELAS starts during early infancy or between the ages of 2–5 years. The child presents with vomiting, seizures, failure to thrive, and infarction-like injuries that can occur anywhere in the brain. Interestingly, angiography reveals no vascular occlusion or vascular disease. The infarction-like episodes are due to abnormal physiology rather than abnormal anatomy or vascular occlusion.

Signs on CT and MRI

- There are hypodense, asymmetric areas on CT located mainly in the occipito-temporal areas representing infarction that does not follow a vascular territory (Fig. 2.2.7). The same area shows low T1/high T2 signal intensities. Diffuse brain atrophy can be seen.
- On CT, bilateral basal ganglia calcification may be seen due to old infarctions (Fig. 2.2.7).
- MR-angiography is typically normal (exclude vasculitis or moyamoya).
- High lactic acidosis peak in MR spectroscopy.

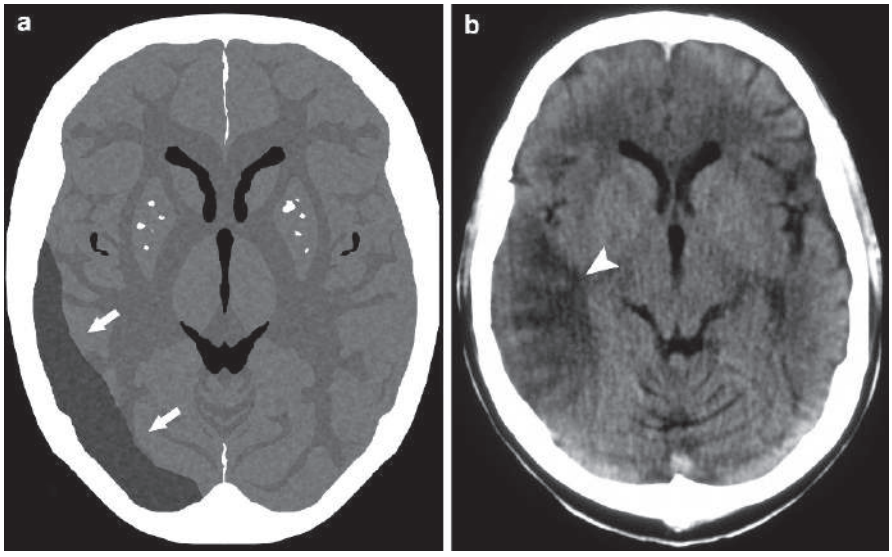

Fig. 2.2.7. Axial nonenhanced brain CT illustration (**a**) and image (**b**) of a patient with mitochondrial myopathy, encephalopathy, lactic acidosis and stroke-like episodes (MELAS) demonstrates the radiological features of MELAS. In (**a**), there is hypodense lesion in the right temporo-parietal region that does not follow a vascular territory (*arrows*) with bilateral basal ganglia calcifications, as typical signs of MELAS. In (**b**), a young patient diagnosed with MELAS shows hypodense lesions in the right temporal area representing infarction (*arrowhead*)

Cortical Laminar Necrosis

Cortical laminar necrosis (CLN) is a disease characterized by destruction of different layers of the cerebral cortex; most prominently the third cortical layer.

On histopathological examination, CLN show brain infarction of the cortical neuronal elements and the blood vessels (pan-necrosis) without hemorrhage or calcification. CLN has been reported in patients with Reye's syndrome.

Reye's syndrome is a rare condition characterized by acute noninflammatory encephalopathy and fatty degeneration of the viscera, commonly the liver. It commonly affects children between 2 months to 15 years of age. The classical clinical presentation is a child presenting with vomiting, headache, convulsions, and signs of encephalopathy, associated with hepatic dysfunction and elevated liver enzymes. Liver biopsy classically shows fatty infiltration. A liver biopsy can help to rule out other conditions that may be affecting the liver and causing liver dysfunction.

The explanation of Reye's syndrome pathology is linked to hepatic and neuronal mitochondrial dysfunction triggered by certain toxins or infections. The most common causes of Reye's syndrome are reaction to salicylate (aspirin), or infections like Influenza B and chickenpox (varicella-zoster virus infection). Chickenpox encephalitis can lead to the development of Reye's syndrome among other cerebral complications.

Signs on MRI

- Typically, CLN lesions show hyperintense curvilinear lines along the cortical gyri and convolutions on both T1W and FLAIR images (Fig. 2.2.8), usually seen from 1 month to 1 year after the ischemic event.
- CLN lesions show contrast enhancement after contrast injection, classically 2 weeks after the initial attack.
- In Reye's syndrome, the brain shows diffuse or focal ischemia in a laminar pattern similar to CLN. Multiple abnormal white matter lesions with heterogeneous signal intensities may be found reflecting different stages of Wallerian degeneration. The latter finding is commonly seen in chronic stage of the disease. *Wallerian degeneration* is a type of neurological degeneration that is seen after an axonal injury. The distal and the proximal segments of the damaged axon with its myelin are fragmented until the first node of Ranvier.

Man-in-the-Barrel Syndrome

Man-in-the-barrel syndrome (MIBS) is a rare disease characterized by paralysis of both arms while the cranial nerves and motor functions of the legs are functioning, giving the patient appearance of a man being confined to a barrel.

MIBS is caused by bilateral ischemia or infarction involving the border-zone areas between the anterior

2.2

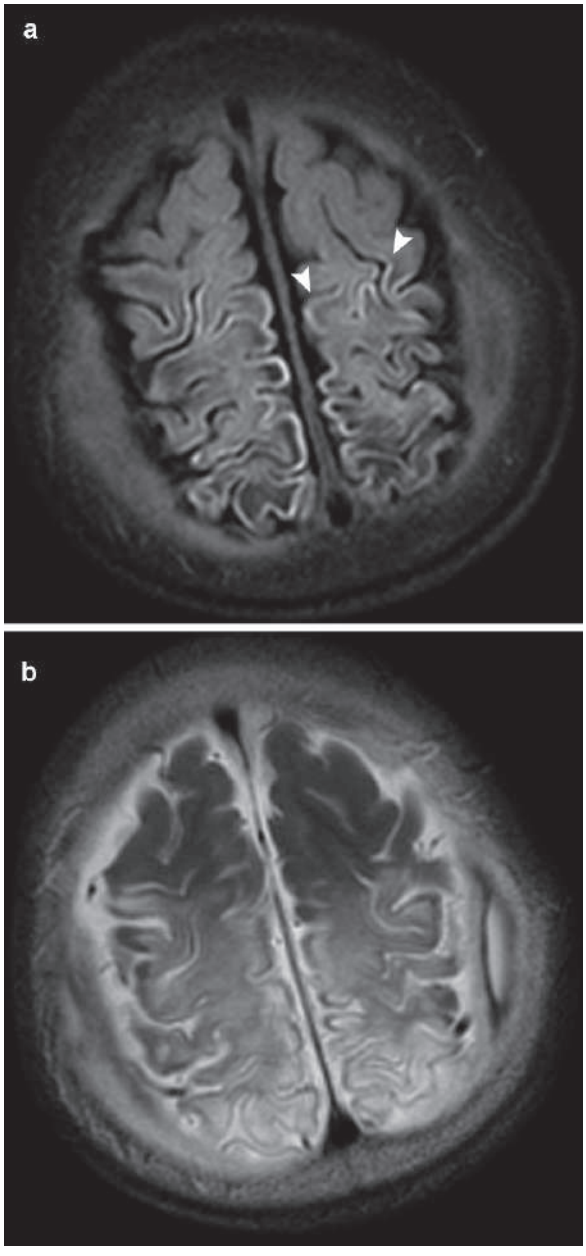

Fig. 2.2.8. Axial T1W (**a**) and T2W (**b**) brain MRI in a 7-year-old child with chickenpox encephalitis shows cortical laminar necrosis (CLN). Notice the curvilinear hyperintense signal intensity lines that follow the convolutions of the gyri on both hemispheres (*arrowheads*), with diffuse white matter lesions seen on T2W images

cerebral artery and the middle cerebral artery (MCA) (watershed zones) at the level of the motor cortex of the arm. Spinal cord disease paralyzing both brachial plexus can cause this disease, but it is extremely rare.

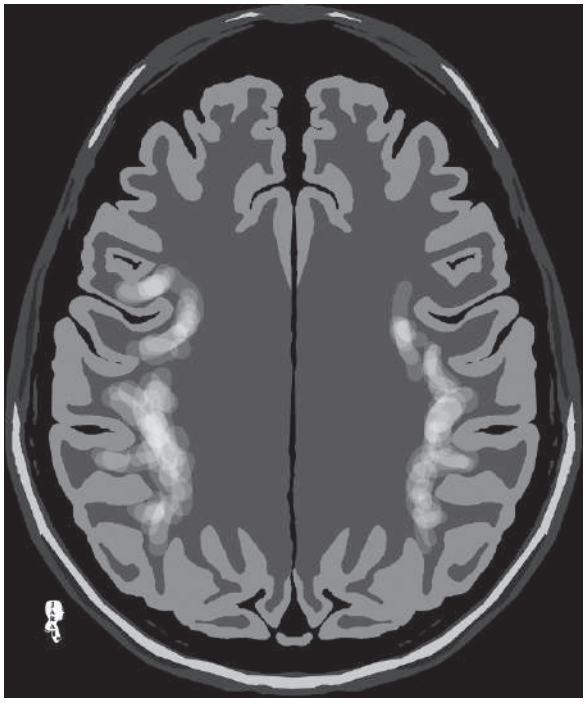

Fig. 2.2.9. Axial brain FLAIR MR-illustration shows the radiological findings in patients with man-in-the-barrel syndrome (MIBS)

The most common cause of MIBS is systemic hypotension following cardiac surgeries or cardiac arrest. MIBS association with pontine myelinolysis, head trauma, and cerebral metastasis has been reported.

Signs on CT and MRI

- CT can be normal.
- MRI typically shows bilateral low T1 and high T2 signal intensities in the parieto-temporal, sensorimotor cortical areas of the arm and hand in the brain (Fig. 2.2.9).

Locked-in Syndrome

Locked-in syndrome (LIS) is a rare disease characterized by normal wakefulness and cognition, anarthria, quadriplegia, and gaze paralysis, caused by ventral pontine infarction.

Patients with LIS are fully conscious, yet they experience almost complete motor paralysis. Typically, patients are able to communicate via vertical gaze

movement and blinking. LIS is classically caused by infarction or hemorrhage involving the pontine perforating arteries arising from the basilar artery. Other causes of LIS include Guillain-Barré syndrome, West Nile encephalitis, and amyotrophic lateral sclerosis.

Signs on CT and MRI

Brain scan typically shows infarction or hemorrhage involving the ventral pontine region, or the cerebral peduncles.

Brain Stem Infarction Syndromes

The brain stem holds nuclei of the cranial nerves. The midbrain contains the nuclei of the cranial nerves 3 and 4. The pons contains the nuclei of the cranial nerves 5–8, and the medulla contains the nuclei of the cranial nerves 9–12. Infarction within the brain stem can result in cranial nerves palsies among other complications. Different syndromes may arise according to the infracted region within the brain stem. A summary of the most common disorders arising due to brain stem infarction is presented below:

- *Millard-Gubler syndrome*: unilateral hemiplegia or hemiparesis with contralateral lower motor neuron facial (CN 7) paralysis due to hemorrhage, tumor, or infarction of the pons.
- *Claude syndrome*: unilateral oculomotor (CN 3) nerve palsy with contralateral hemiataxia due to paramedial midbrain infarction. (Fig. 2.2.10)
- *Benedikt syndrome*: unilateral oculomotor (CN 3) nerve palsy with contralateral limb tremor or paralysis. It can be caused by pontine infarction due to posterior cerebral artery occlusion.
- *Weber syndrome*: unilateral oculomotor (CN 3) nerve palsy with contralateral hemiplegia due to midbrain infarction.
- *Avellis syndrome*: hemiparalysis of the larynx and soft palate on the same side due to infarction of the nucleus ambiguous in the medulla oblongata (central) or a mass lesion around the jugular foramen (peripheral) involves the glossopharyngeal and the vagus nerves (CN 9 + 10) (Fig. 2.2.11).
- *Foix–Chavany–Marie syndrome*: pseudobulbar palsy (CN 9–12) due to bilateral cortical infarction in the territory of the MCA.
- *Babinski–Nageotte syndrome*: ipsilateral Horner's syndrome, facial loss of pain and temperature, cerebellar hemiataxia, with paresis of the larynx and pharynx, and contralateral hemiparesis and loss of pain and temperature. The disease arises due to unilateral infarction of the medulla oblongata involving the spinal trigeminal tract and nucleus, nucleus ambiguous, lateral spinothalamic tract, sympathetic fibers, corticospinal tract, and afferent spinocerebellar tract (Fig. 2.2.11).
- *Cestan–Chenais syndrome*: has same clinical presentation as Babinski-Nageotte syndrome, and arises due to unilateral infarction of the medulla oblongata involving the spinal trigeminal tract and nucleus, nucleus ambiguous, lateral spinothalamic tract, sympathetic fibers, and corticospinal tract (Fig. 2.2.11).
- *Lateral (Wallenberg) syndrome*: ipsilateral Horner's syndrome, facial loss of pain and temperature, cerebellar hemiataxia, with paresis of the larynx and pharynx, and contralateral loss of body pain and temperature. It arises due to unilateral infarction of the medulla oblongata involving the spinal trigeminal tract and nucleus, nucleus ambiguous, lateral spinothalamic tract, sympathetic fibers, afferent spinocerebellar tracts, and vestibular nuclei (Figs. 2.2.11 and 2.2.12).
- *Dejerine syndrome*: ipsilateral tongue weakness with contralateral hemiparesis and face sparing hemihypesthesia. It arises due to unilateral infarction of the

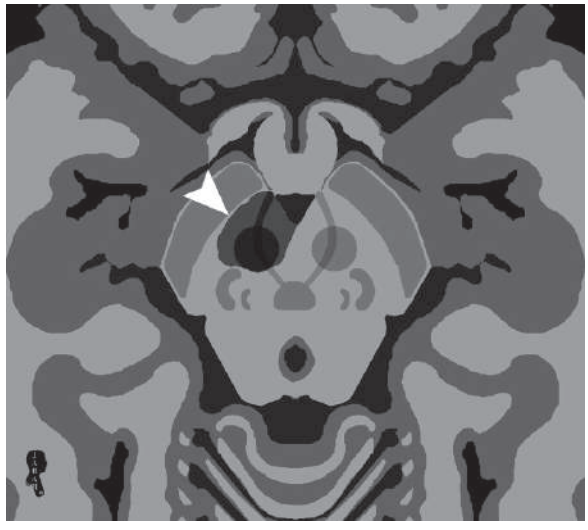

Fig. 2.2.10. Axial T1W brain stem MR-illustration at the level of the pone demonstrates the typical infarction region causing Claude syndrome (*arrowhead*)

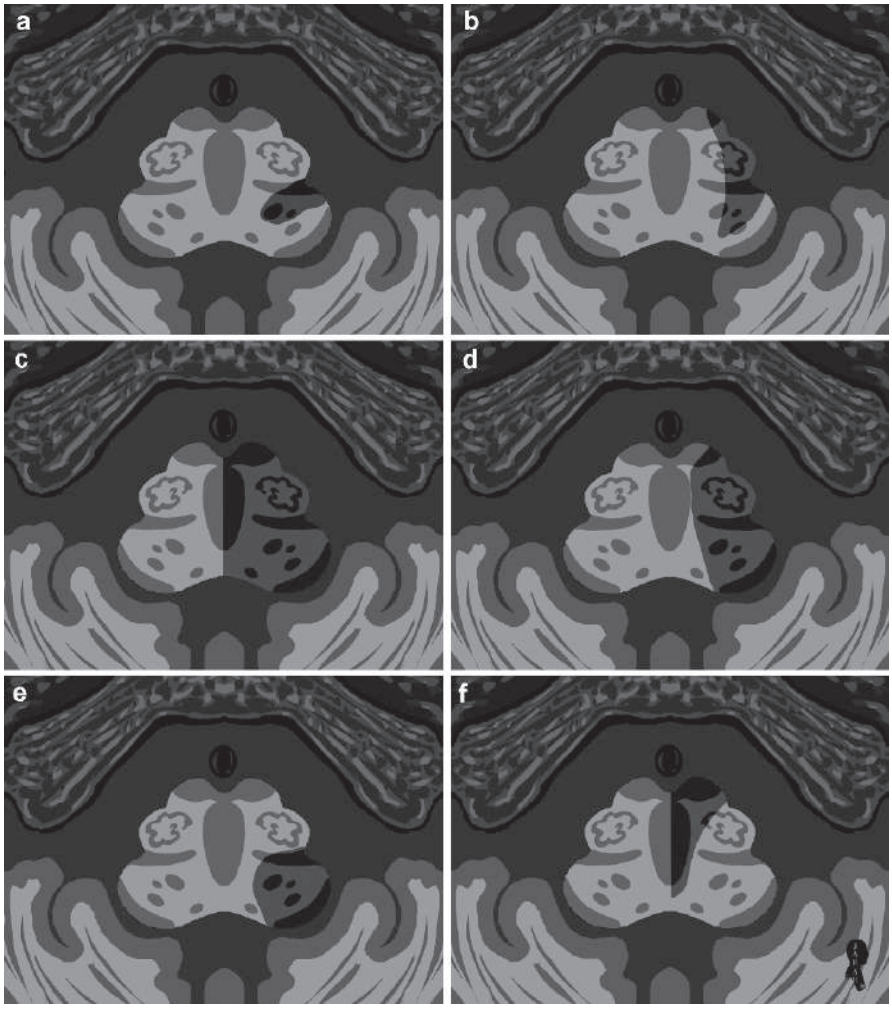

Fig. 2.2.11. Axial T1W brain stem MR-illustration at the level of the medulla demonstrates different kinds of diseases according to the area of medullary infarction: (**a**) Avellis syndrome, (**b**) Cestan–Chenais syndrome, (**c**) Reinhold (hemimedullary) syndrome, (**d**) Babinski–Nageotte syndrome, (**e**) Wallenberg syndrome, and (**f**) Dejerine syndrome

medulla oblongata involving the hypoglossal nucleus or fibers, corticospinal tract, and spinal medial lemniscus (Fig. 2.2.11).

- *Reinhold (hemimedullary) syndrome*: ipsilateral Horner's syndrome, facial loss of pain and temperature, cerebellar hemiataxia, with paresis of the larynx and pharynx, and contralateral hemiparesis and face sparing hemihypesthesia. It arises due to unilateral infarction of the medulla oblongata involving the spinal trigeminal tract and nucleus, nucleus ambiguous, afferent spinocerebellar tracts, sympathetic fibers, hypoglossal nucleus or fibers, corticospinal tract, and spinal medial lemniscus (Fig. 2.2.11).

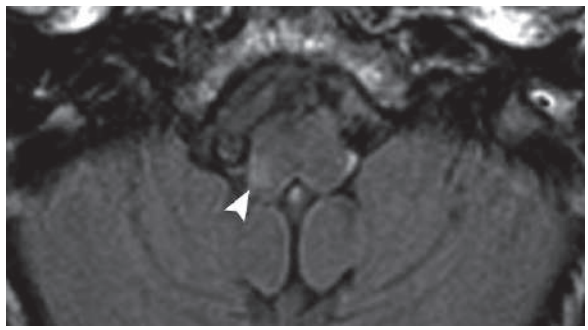

Fig. 2.2.12. Axial FLAIR image in the region of the medulla in a patient with Wallenberg syndrome (*arrowhead*) shows hyperintense signal intensity lesion in the lateral portion of the right medulla oblongata (*arrowhead*)

Subclavian Steal Syndrome

Subclavian steal syndrome (SSS) is a disease characterized by subclavian stenosis or occlusion at the segment between its origin from the aortic arch and the origin of the vertebral artery. This stenosis or occlusion causes reverse blood diversion (stealing) from the basivertebral arteries through the vertebral artery at the same side of subclavian occlusion to supply the ipsilateral arm (blood flow from the head and neck to supply the arm, rather than flow normally from the aortic arch toward the head via the vertebral artery).

Most patients with SSS are asymptomatic. However, symptomatic patients present with brain stem ischemia or stroke at rest or after exercise due to increased arm blood demand. Also, patients often complain from dizziness, cerebral dysfunction, and drop attacks when the disease is severe. Symptoms in the affected arm ranged between decrease pulses, coldness to claudications.

SSS doesn't appear when the stenosed subclavian artery is accompanied by vertebral artery arising separately from the aortic arch (6% of population). Angiography is the gold standard to establish the diagnosis of SSS.

Coronary-subclavian steal syndrome (*CSS*) is a disease seen in patients with previous history of coronary artery bypass graft surgery (CABG). The internal thoracic (mammary) artery, which is a branch of the subclavian artery, is commonly used as a graft for the left anterior descending artery (LAD). Severe stenosis of the subclavian artery that compromised the arm blood supply causes the blood flow to reverse in direction. The blood is withdrawn (stolen) from the coronary arteries via the internal thoracic artery graft to supply the arm. Patients typically present with exertional angina precipitated or exacerbated by arm exercise. Diagnostic keys of CSS include: history of CABG (mandatory), difference in blood pressure between the two arms >20 mmHg, and angina produced by activity of the affected arm, while activity of the contralateral normal arm produces no symptoms.

Signs on Angiography

Stenosis of the subclavian artery is seen in arch aortography. After injecting the contrast within the normal vertebral artery, the contrast is seen flowing within the contralateral vertebral artery via the vertebrobasilar system in a retrograde pattern to supply the arm when the patient is asked to exercise his arm (Fig. 2.2.13).

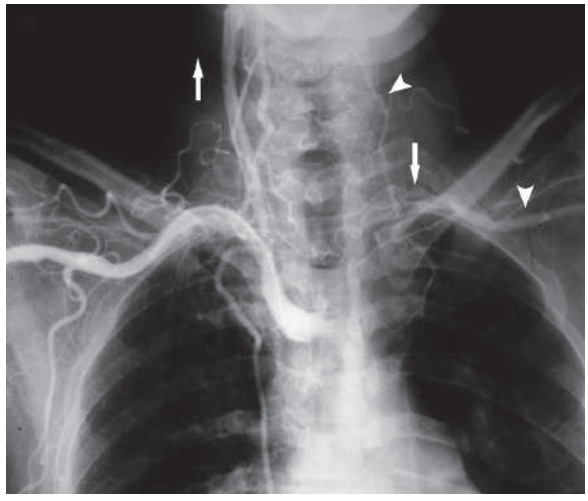

Fig. 2.2.13. Selective right subclavian artery angiogram shows retrograde flow in the left vertebral artery to supply the left arm via the brachial artery (*arrowheads*). The direction of the contrast flow is demonstrated by the *arrows*

Signs on Doppler sonography

- The earliest manifestation of stealing phenomenon is a transient sharp deceleration of blood flow after the first systolic peak. This deceleration is observed as a systolic peak with a median notch, creating two systolic peaks of the vertebral artery with stealing phenomenon. The nadir of the notch becomes progressively lower until it reaches and crosses the baseline.
- On rest, the vertebral artery flow shows double peak systolic waveform with a median notch. The waveform is classified according to the velocity of the nadir into: a nadir velocity greater than that of end diastole (type 1); a nadir velocity equal to the level of end diastole (type 2); a nadir velocity that reaches the baseline (type 3); and a nadir velocity that crosses the baseline (type 4).
- After asking the patient to exercise his ipsilateral arm, or applying brachial artery blood pressure cuff then deflating it to induce the stealing phenomenon, the arterial flow waveform of the vertebral artery is reversed and it is seen below the baseline, confirming the reversal blood flow.

Signs on MRI

In axial sections of 2D time-to-flight sequence, the vertebral artery with stealing phenomenon shows flow void signal compared to the contralateral vertebral artery and both internal carotid arteries (*localizer sign*), which indicates reversal of flow.

For Further Reading

1. Kim I-O et al Mitochondrial myopathy-encephalopathy-lactic acidosis and strokelike episodes (MELAS) syndrome: CT and MR findings in seven children. AJR. 1996;166: 641–5
2. Prasad BKD et al Cerebral amyloid angiopathy. Ind J Radiol Imag. 2006;16:745–747
3. Krasnianski M et al Between Wallenberg syndrome and hemimedullary lesion. Cestan-Chenais and Babinski-Nageotte syndromes in medullary infarctions. J Neurol. 2006;253:1442–6
4. Krasnianski M et al Babinski-Nageotte's syndrome and Hemimedullary (Reinhold's) syndrome are clinically and morphologically distinct conditions. J Neurol. 2003;250: 938–42
5. Hoffmann HJ. Moyamoya disease and syndrome. Clin Neurol Neurosurg. 1997;99 Suppl 2:S39–44
6. Hsu C-Y et al Moyamoya disease: the clue from computer tomography. J Emerg Med. 2004;26:339–42
7. Holz A et al Moyamoya disease in a patient with hereditary spherocytosis. Pediatr Radiol. 1998;28:95–7
8. Yamada I et al Moyamoya disease: diagnostic accuracy of MRI. Neuroradiology. 1995;37:356–61
9. Komiyama M et al Serial MR observation of cortical laminar necrosis caused by brain infarction. Neuroradiology. 1998; 40:771–7
10. Kinoshita T et al Reye's syndrome with cortical laminar necrosis: MRI. Neuroradiology. 1996;38:269–72
11. Hurwitz ES et al A cluster of cases of Reye syndrome associated with chickenpox. Pediatrics. 1982;70:901–6
12. Girija AS et al Neurological complications of chickenpox. Ann Indian Acad Neurol. 2007;10:240–6
13. Benito-Leon J et al "Man-in-the-barrel" syndrome: MRI and SPECT imaging. Euro J Radiol. 1997;24:260–2
14. Deleu D et al "Man-in-the-barrel" syndrome as delayed manifestation of extrapontine and central pontine myelinolysis: Beneficial effect of intravenous immunoglobulin. J Neurol Sci. 2005;237:103–106
15. Elting JW et al Predicting outcome drome coma: Man-in-the-barrel syndrome as potential pitfall. Clin Neurol Neurosurg. 2000;102:23–5
16. Ferrari G et al Foix-Chavany-Marie syndrome: CT study and clinical report of three cases. Neuroradiology. 1979;18: 41–2
17. Luxenberg EL et al Locked-in syndrome from rosto-caudal herniation. J Clin Neurosci. 2009;16:333–4
18. Masuzawa H et al Pontine gliomas causing Locked-in syndrome. Child's Nerv Syst. 1993;9:256–9
19. Zakaria T et al Locked-in syndrome resulting from bilateral cerebral peduncles infarctions. Neurology. 2006;67:1889
20. Van Son JAM et al Diagnosis and management of the coronary-subclavian steal syndrome. Euro J Cardio-thoracic Surg. 1998;3:565–7
21. Marquardt F et al The coronary-subclavian-vertebral steal syndrome (CSVSS). Clin Res Cardiol. 2006;95:48–53
22. Roldan-Valadez E et al Imaging diagnosis of subclavian steal syndrome secondary to Takayasu arteritis affecting a left-side subclavian artery. Arch Med Res. 2003;34:433–8
23. Kaneko A et al Color-coded Doppler imaging of the subclavian steal syndrome. Intern Med. 1998;37:259–64
24. Cuisset T et al Coronary-subclavian steal syndrome: an usual cause of refractory unstable angina. Int J Cardiol. 2008; 127:e181–e182
25. Sheehy N et al Contrast-enhanced MR angiography of subclavian steal syndrome: value of the 2D time-to-flight "localizer" sign. AJR. 2005;185:1069–73
26. Trattnig S et al Colour Doppler imaging of partial subclavian steal syndrome. Neuroradiology. 1993;35:293–5
27. Kliewer MA et al Vertebral artery Doppler waveform changes indicating subclavian steal physiology. AJR. 2000; 174:815–9

2.3 Intracranial Hemorrhage

Intracranial hemorrhage is a condition characterized by the presence of free blood within the cranium. The free blood can be collected in the epidural space, subdural space, subarachnoid space, intrabrain parenchyma, or intraventricular spaces.

Intracranial hemorrhage can be caused by head trauma, anticoagulants use, ruptured aneurysms, vascular malformations, and hypertension. The most common areas of intracranial hemorrhage are the temporo-parietal region and the cerebellum. Native, nonenhanced CT is the diagnostic modality of choice as an initial diagnostic modality to detect intracranial bleeding.

Blood exhibits different densities on CT or signal intensities on MRI according to the age of the hemorrhage (acute, subacute, or chronic) (Fig. 2.3.1).

Epidural Hematoma

Epidural hematoma is a free blood collection located between the inner skull table and the dura matter. It is a life-threatening emergency that usually results from trauma to the middle meningial artery (85% of cases).

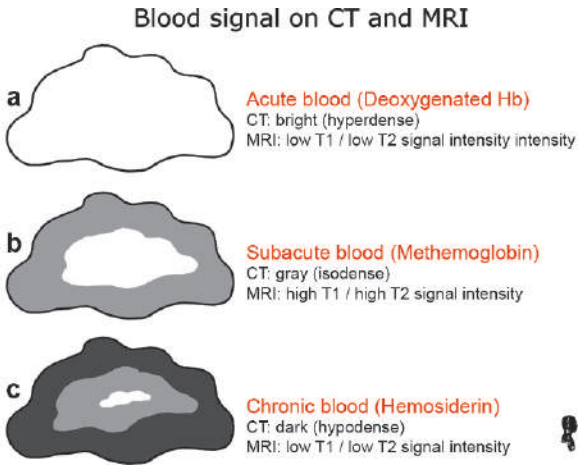

Fig. 2.3.1. Illustration demonstrates the different hematoma ages and manifestations on CT

Patients usually present with nausea, vomiting, and altered consciousness.

Signs on CT

- The CT typically shows semi-convex shaped, hyperdense blood collection usually located in the parieto-temporal area (Fig. 2.3.2).
- The collected blood does not cross suture lines as the dura matter is firmly attached to the clavaria.
- There is significant mass effect over the ventricles and the brain parenchyma in the acute phase.
- It is almost always acute. However, acute on top of chronic epidural hematoma can occur uncommonly, and it is seen as a semi-convex blood collection with hypodense and hyperdense component (Fig. 2.3.2).

Q: When can you find a black (hypodense) hematoma although the bleeding is acute?

This is a rare condition that is seen when the hemoglobin level in the blood is less than 4 mg/dL, because the hyperdense density that reflects the X-ray photons absorption by the iron in the blood is inadequate.

Subdural Hematoma

Subdural hematoma is a free blood collection located between the dura matter and the arachnoid. Subdural hematoma usually arises due to emissary veins tear from a minor trauma, or due to uncontrolled anticoagulants therapy. Acute subdural hematoma is a clinical emergency, where patients present with signs similar to epidural hematoma. In contrast, chronic subdural hematomas present with less severe symptoms, such as headache, nausea, and vomiting.

Differential Diagnoses and Related Diseases

Subdural hygroma: is a collection of cerebrospinal fluid or serum in the subdural space (Fig. 2.3.4). It is believed to be caused by chronic subdural hematoma in the elderly, or due to intracranial infections in

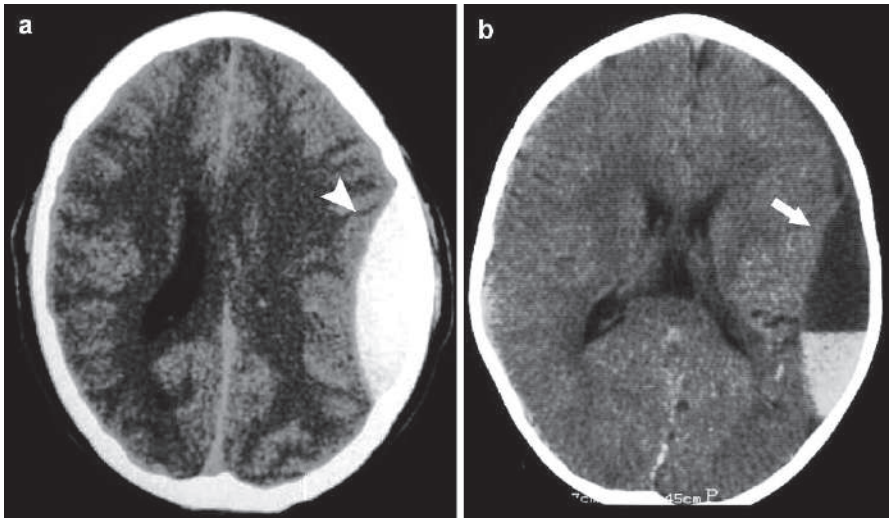

Fig. 2.3.2. Axial CT images of two different patients show acute epidural hematoma (**a**, *arrowhead*) and acute on top of chronic hematoma (**b**, *arrow*). Notice the mass effect on the left lateral ventricle in (**a**) when the hematoma is acute, and lack of the pressure effect on the lateral ventricles in (**b**) when the hematoma is chronic

children. Up to 30% of cases arise after head trauma. The condition is self-limited, and is thought to be caused by a tear in the arachnoid that functions as a one-way valve allowing cerebrospinal fluid to enter the subdural space to be trapped in little or no absorption. The most common symptom is headache with or without nausea and vomiting; in the acute phase, subdural hygroma behaves like an enlarged intracranial hemorrhage, and in the chronic phase it behaves like a space occupying lesion. After traumatic head injury, development of subdural hygroma is noted 6–46 days after the initial trauma.

Signs on CT

- Crescent-shaped, hyperdense blood collection usually located in the fronto-parietal region (Fig. 2.3.3). It can be bilateral in 15% of cases.
- The bleeding is not bounded by the sutures.
- There is significant mass effect over the ventricles and the cisterns.
- Subdural hematoma can be acute (hyperdense), subacute (isodense), and chronic (hypodense) (Fig. 2.3.3). Acute on top of chronic subdural hematoma can occur, and it seen as crescent-shaped blood collection with hypodense and hyperdense components (sedimentation subacute subdural hematoma).
- Subdural hygroma is seen as a cerebrospinal fluid collection in the subdural space (Fig. 2.3.4).

Subarachnoid Hemorrhage

Subarachnoid hemorrhage is characterized by the presence of free blood within the subarachnoid space and the arachnoid cisterns. It most commonly occurs as a complication of ruptured arterial aneurysms and trauma to the head. Patients typically present with sudden severe headache, nausea, vomiting with neck stiffness.

Signs on CT

- The cerebrospinal fluid spaces and cistern will be seen hyperdense (white) due to blood mixed with cerebrospinal fluid (Fig. 2.3.5).
- There is no midline displacement.

Intra-Cerebral/Intraparenchymal Hemorrhage

Intracerebral hemorrhage is the presence of free blood within the gray or the white brain matter. It commonly arises due to stroke, embolic vascular occlusion, tumors or after vascular rupture due to head trauma. Hypertension causes bleeding into the basal ganglia in 60% of cases.

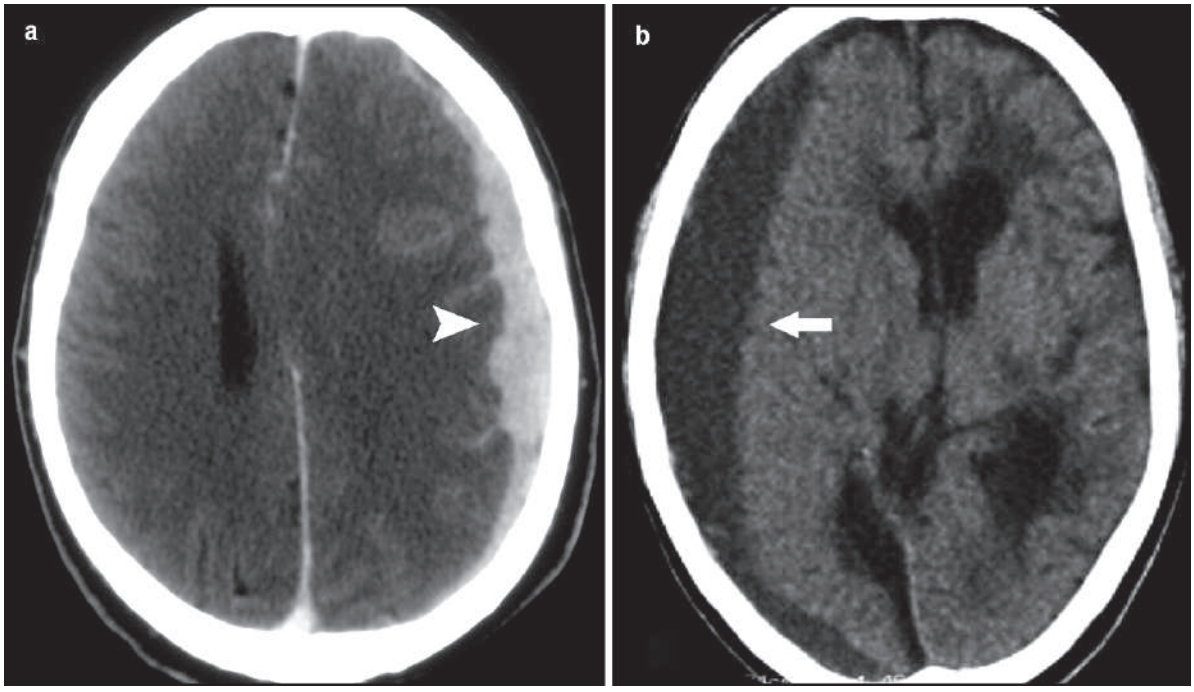

Fig. 2.3.3. Axial CT images of two different patients show acute subdural hematoma (**a**, *arrowhead*) and chronic subdural hematoma (**b**, *arrow*). Again notice the pressure effect over the lateral ventricles in the acute subdural hemaotoma (**a**) compared to the chronic subdural hematoma (**b**)

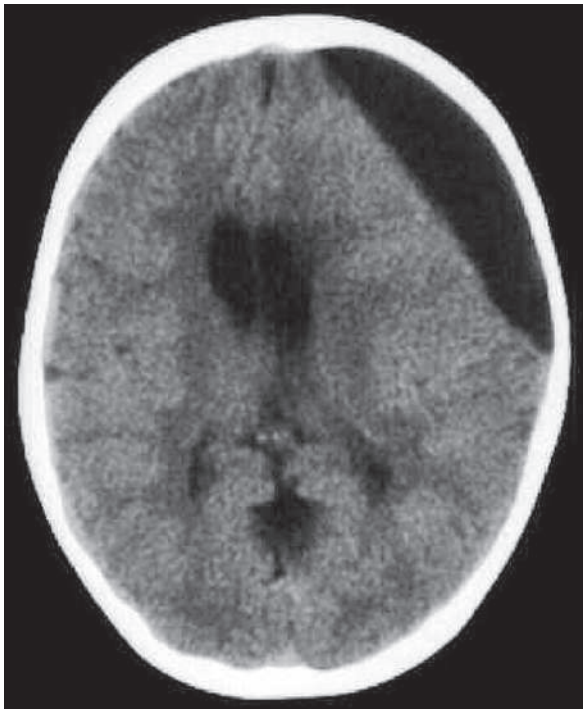

Fig. 2.3.4. Axial brain CT of a patient with a history of posttraumatic brain injury shows large left frontal subdural hygroma

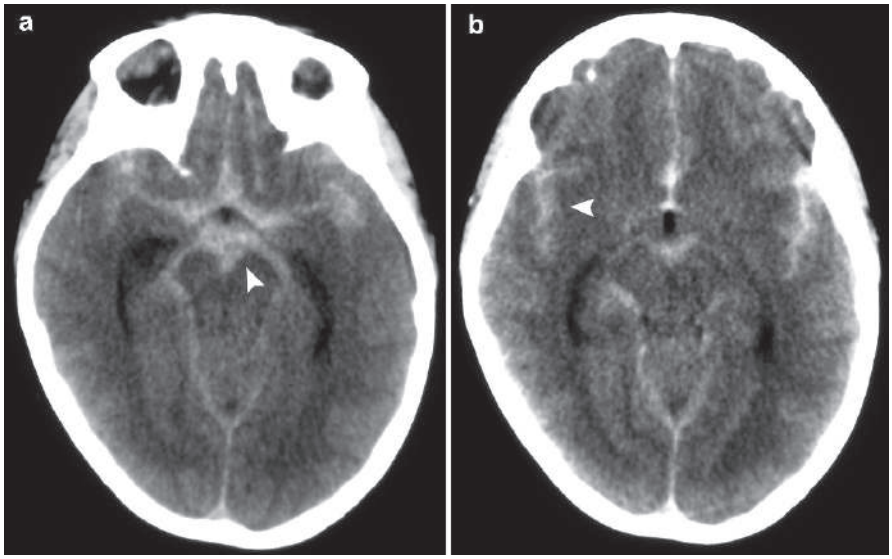

Fig. 2.3.5. Sequential axial CT images of a patient with subarachnoid hemorrhage show hyperdense suprasellar cistern and sylvian fissures (*arrowheads*) due to subarachnoid bleeding

Signs on CT

- There is hyperdense blood collection within the brain parenchyma that usually follows a vascular territory (Fig. 2.3.6).
- When the bleeding is due to stroke, it is surrounded by a halo-like edema (cytotoxic edema), while when it is due to a tumor, a finger-like edema is seen surrounding the blood collection (vasogenic edema).

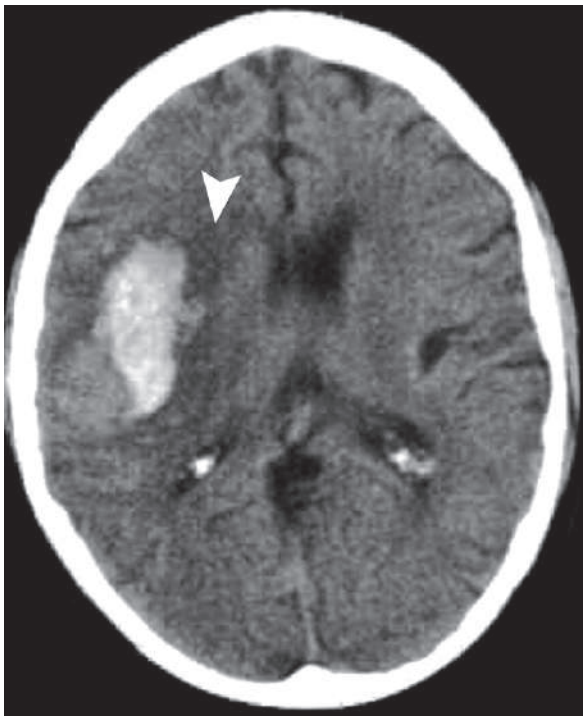

Fig. 2.3.6. Axial brain CT of a patient with intraparenchymal bleeding in the region of the right middle cerebral artery shows large area of intraparenchymal bleeding surrounded by cytotoxic edema exerting mass effect over the right anterior and posterior horns of the right lateral ventricle (*arrowhead*)

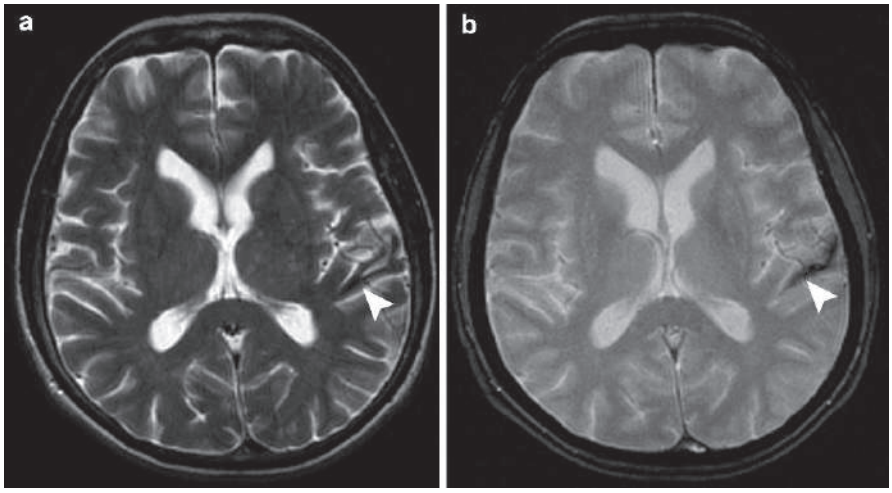

Fig. 2.3.7. Axial T2W (**a**) and T2* MRI of a patient with previous intraparenchymal bleeding in the left temporal lobe shows area of focal hypointense signal intensity on (**b**) due to hemosiderin. Notice the same area is visible on (**a**) but not as clearly seen as in the T2* image

Intraventricular Hemorrhage

Intraventricular hemorrhage is bleeding into the ventricles. Commonly, it occurs secondary to parenchymal or subarachnoid hemorrhage, and associated with diffuse axonal injury of the corpus callosum. Arteriovenous malformation is the most common cause for spontaneous intraventricular hemorrhage in adults. There are two types of intraventricular hemorrhage:

- *Ependymal intraventricular bleeding*: the blood is seen fixed to the ventricular walls.
- *Free intraventricular blood*: the blood is seen located in the posterior horns (gravity dependent).

Signs on CT

There is hyperdense blood within the ventricles, either in a free form lying in the posterior horns, or encapsulated within the ependymal ventricular wall (Fig. 2.3.8).

Signs on MRI

Chronic bleeding can be detected on T2* images as hypointense intraparenchymal areas (Fig. 2.3.7).

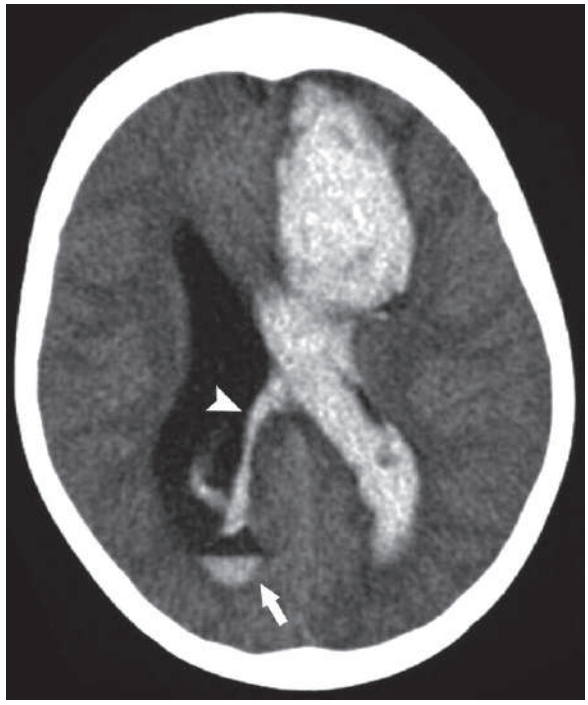

Fig. 2.3.8. Axial brain CT of a patient with severe intraventricular hemorrhage shows dilated both ventricles due to bleeding, with subependymal (*arrowhead*) and free (*arrow*) intraventricular bleedings also seen

Hemorrhage into Malignancy

2.3

Hemorrhage into neoplasms accounts for 10% of spontaneous intracranial hemorrhage. It can be seen in 14% of metastases from melanoma and bronchogenic carcinoma, and in 5% of cases of gliomas. Bleeding occurs because abnormal tumor vascularity usually occurs in higher grade malignancies.

Signs on CT

- Atypical location for bleeding in a patient with known primary or secondary brain malignancy.
- The signal intensity of the blood is more heterogeneous than that of nonneoplastic hemorrhage. This heterogeneous texture is attributed to the multiple episodes of bleeding with different ages (mixed hypodense and hyperdense pattern).

For Further Reading

1. Xi G et al Intracerebral hemorrhage, pathophysiology and therapy. Neurocrit Care. 2004;1:5–18
2. Schellinger PD et al Intracranial hemorrhage, the role of magnetic resonance imaging. Neurocrit Care. 2004;1: 31–45
3. Laguna P et al Intracranial hemorrhage in a boy with severe haemophilia A and factor VIII inhibitor. Child's Nerv Syst. 2006;22:432–5
4. Dincsoy MY et al Intracranial hemorrhage in hypothalamic low-birth-weight neonates. Child's Nerv Syst. 1990;6: 245–9
5. Heros RC et al Cerebral vasospasm after subarachnoid hemorrhage: an update. Ann Neurol. 1983;14:599–608
6. Koc RK et al Acute subdural hematoma: outcome and outcome prediction. Neurosurg Rev. 1997;20:239–44
7. Gross A et al Intraventricular hemorrhage originating from choroids plexues angioma in a road accident victim. Z Rechtsmed. 1989;102:409–13
8. Schwartz DT. Sensitivity of computed tomography for subarachnoid hemorrhage. doi:10.1016/j.annemergmed. 2008. 06. 471
9. Moster ML et al Chronic subdural hematoma with transient neurological deficits: a review of 15 cases. Ann Neurol. 1983; 14:539–42
10. Masuzawa T et al Computed tomographic evolution of post-traumatic subdural hygroma in young adults. Neuroradiology. 1948;26:245–8
11. Park CK et al Spontaneous evolution of post-traumatic subdural hygroma into chronic subdural hematoma. Acta Neurochir (Wien). 1994;127:41–7
12. Masuzawa T et al Computed tomography evolution of post-traumatic subdural hygroma in young adults. Neuroradiology. 1984;26:245–8

2.4 Meningitis

Meningitis is a disease characterized by inflammation of the meninges due to infections or inflammatory disease (e.g., sarcoidosis). Infectious meningitis can be bacterial (e.g., *Pneumococcus*) or viral (e.g., *Hemophilus influenza*).

Patients with meningitis classically present with fever, neck stiffness, and neurological symptoms. Rarely, meningitis may lead to suprarenal gland suppression, causing patient death due to adrenal gland insufficiency. Infection of the meninges occurs due to hematogenous spread (e.g., bacteremia), or from direct extension from local infectious pathology (e.g., otitis media). Imaging in meningitis is mainly performed to evaluate complications.

Signs on CT and MRI

- Meningitis is detected typically as thickened meningies with contrast enhancement. Meningeal enhancement is divided into pachymeningeal and leptomeningeal enhancement. The pachymeninges are the dura matter, with its thick inner meningeal component, and its inner table of the skull (periosteum) component. The leptomeninges are the pia and the arachnoid matters. Pachymeningeal enhancement is seen as enhancement of the inner skull table and meningeal reflections (e.g., falx cerebri) (Fig. 2.4.1). In contrast, leptomeningeal enhancement is seen as thin linear enhancement that follows the pial surfaces, the cortical gyri, and fills the subarachnoid spaces (Fig. 2.4.2).
- *Ventriculitis* is seen as an enhancement of the subependymal surface of the ventricles after contrast injection.
- *Subdural pus collection (empyema)*: is an extra-axial pus collection that usually results from untreated or chronic meningitis (crescent sign).
- *Abscess* is seen as an area of low density on CT or low T1 and high T2 signal intensities on MRI with uniform rim-enhancement after contrast injection (Fig. 2.4.3). The abscess is commonly surrounded by vasogenic edema.
- *Subdural Hygroma*: is a sterile collection of fluid located in the subdural space usually as a sequela of meningitis in children.
- *Hydrocephalus* may arise due to inflammation of the basal meningies blocking the 4th ventricle. It is seen in advanced stages of meningitis. Dilatation of the temporal horns is a definite sign of hydrocephalus.
- *Post meningio-encephalic sequela*: is a severe advanced stage of meningitis characterized by loss of brain tissue (encephalomalacia) and parenchymal calcification with hydrocephalus (Fig. 2.4.4).
- Superior sagittal sinus thrombosis may be seen as a triangular filling defect on axial images (*delta sign*).

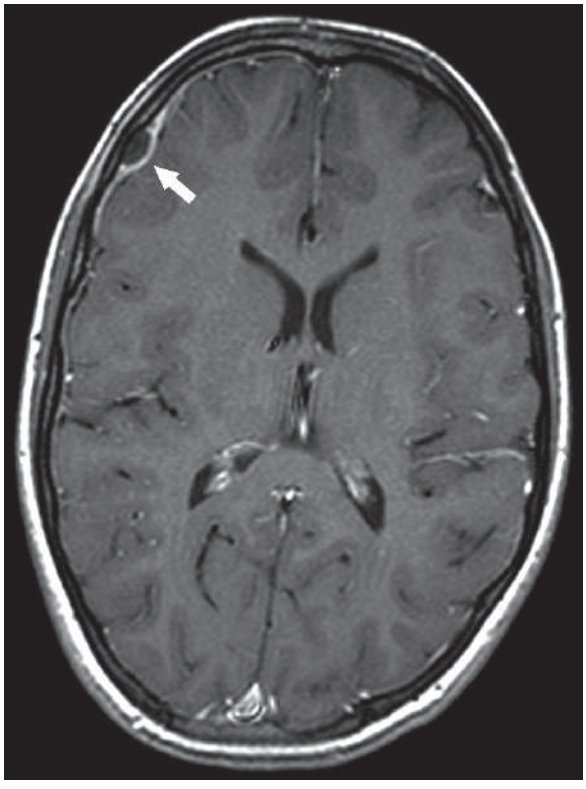

Fig. 2.4.1. Axial T1W postcontrast brain MRI shows right frontal pachymeningeal enhancement with epidural abscess formation (*arrow*)

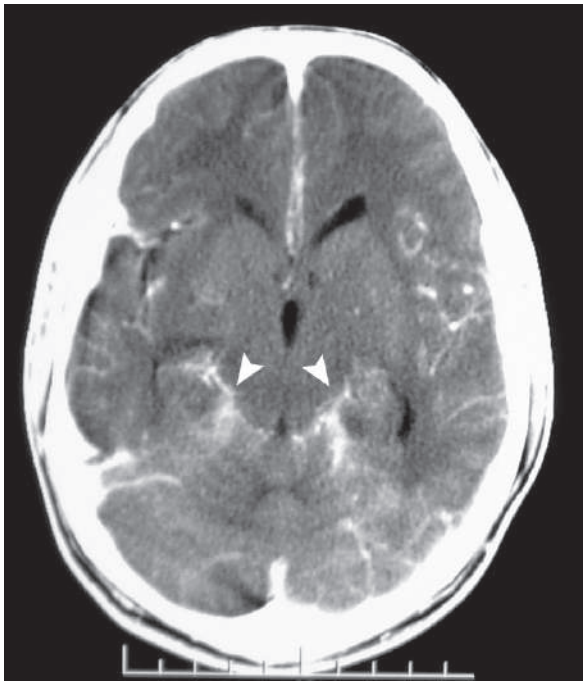

Fig. 2.4.2. Axial postcontrast brain CT shows enhancement of the leptomeningies around the ambient cisterns (*arrowheads*)

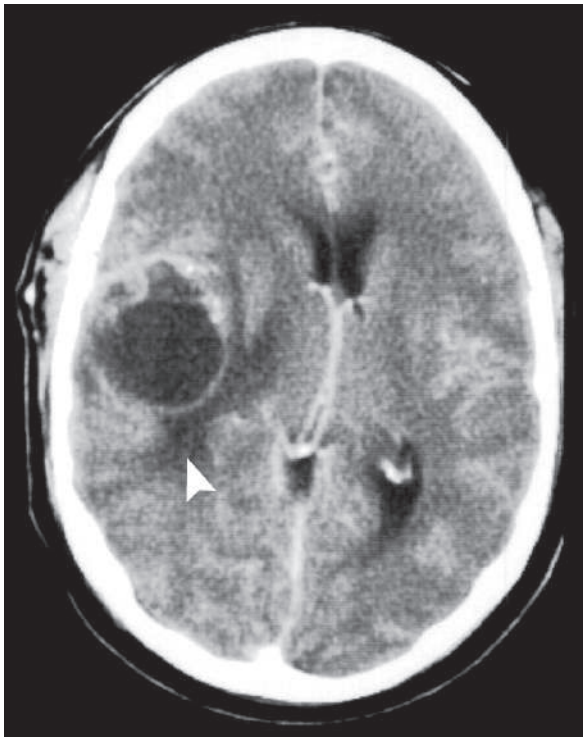

Fig. 2.4.3. Axial postcontrast brain CT shows right temporal abscess with thin rim enhancement and vasogenic edema (*arrowhead*) that exerts mass effect over the anterior horns of the lateral ventricles

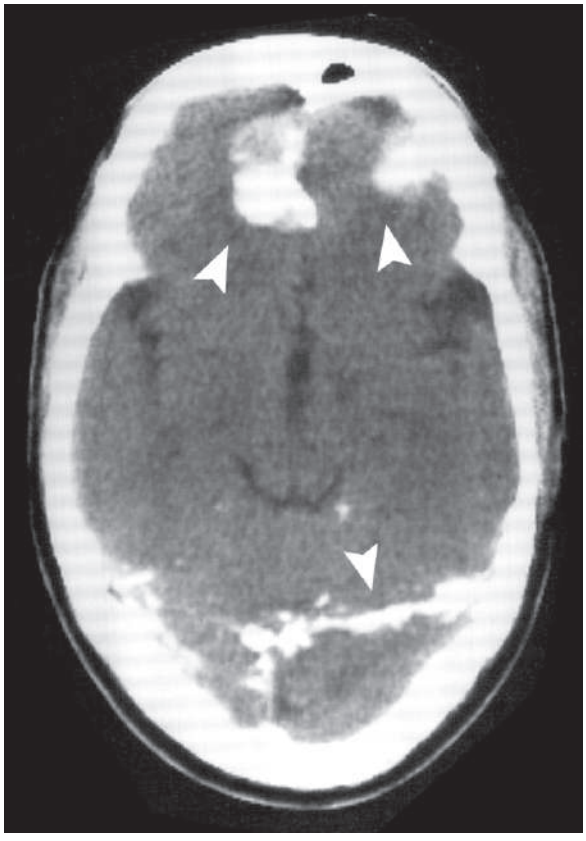

Fig. 2.4.4. Axial nonenhanced brain CT shows postmeningoencephalic parenchymal and meningeal (falx) calcification (*arrowheads*)

Differential Diagnoses and Related Diseases

- *Multiloculated hydrocephalus*: is a clinicopathological condition characterized by enlarged, loculated ventricles with paraventricular porencephalic cavities. The condition is seen in neonates, commonly as a sequel of ventriculitis complicating neonatal meningitis. Neonates presents with hydrocephalus, neurological deterioration, and seizures. Mortality rate is high (>70%). CT and MRI typically show multiloculated ventricles with irregular boarders and internal septae (Fig. 2.4.5).
- *Canalis basilaris medianus*: is a congenital anomaly characterized by a well-defined channel seen in the midline of the basiocciput, very close to the anterior rim of the foramen magnum. It is seen on CT or MRI as a linear defect in the midportion of the clivus (Fig. 2.4.6). Although it is an asymptomatic anomaly, it can be the source of recurrent meningitis in

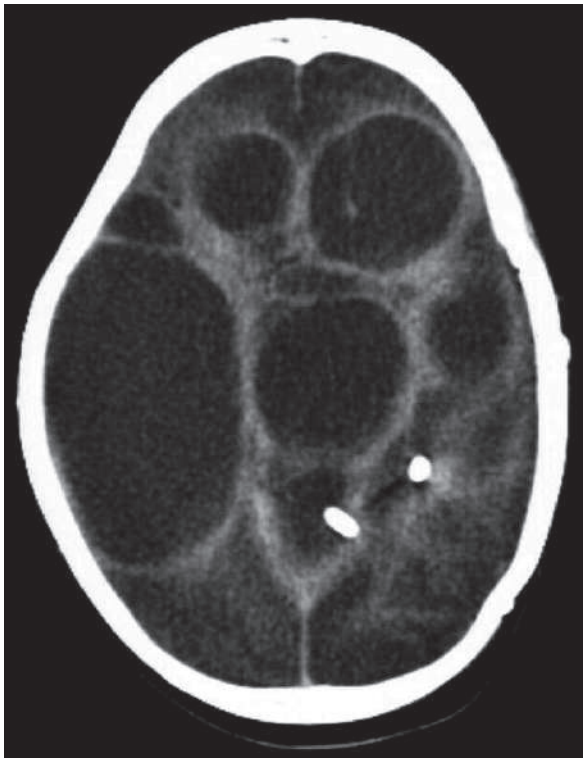

Fig. 2.4.5. Axial nonenhanced brain CT of a neonate shows multiloculated hydrocephalus

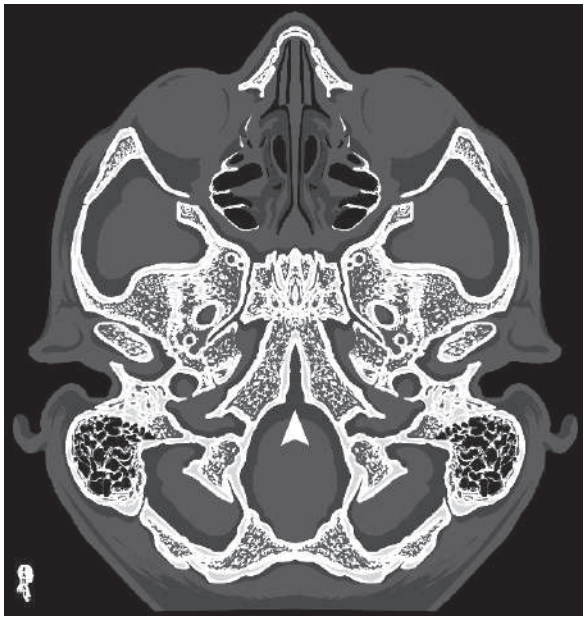

Fig. 2.4.6. Axial CT illustration of the base of the skull shows a linear median bony defect of the clivus (canalis basilaris medianus)

children due to transmission of bacteria from the superior nasopharynx into the central nervous system through this basiocciput defect.

- *Vogt–Koyanagi–Harada syndrome*: is a rare, sporadic, and systemic disorder mostly seen in adults and characterized by acute panuveitis, meningitis, and cutaneous manifestations. The disease arises due to a widespread pathology affecting the melanin-forming cells in different organs, typically in dark skinned people. Uveitis is inflammation of the uvea, which supplies nutrition to the globe and is composed of the iris, ciliary body, and choroid. Any part of the uvea can be involved in the inflammation (e.g., iritis), and patients typically present with a painful eye, with pain in the distribution of the trigeminal nerve (because the ciliary body is supplied by the ophthalmic division of the trigeminal nerve). The disease has three phases: a prodormal phase characterized by fever, severe headache, and tinnitus; an ophthalmic phase characterized by bilateral uveitis and optic disc hyperemia; and convalescent phase seen weeks after the ophthalmic phase, characterized by premature graying of hair (poliosis), vitiligo, alopecia, painful hearing (dysacousia), tinnitus, and vertigo. Diagnostic criteria include absence of ocular trauma with four of the following: (a) bilateral chronic iridocyclitis, (b) posterior uveitis including retinal detachment, (c) neurological signs with signs of meningitis (e.g., neck stiffness), and (d) cutaneous findings of alopecia, vitiligo, or poliosis. Signs on orbital CT or MRI may show choroidal and scleral thickening due to chronic inflammation on postcontrast images, or retinal detachment with typical (V-shaped sign) on severe cases (Fig. 2.4.7). Uncommonly, the disease can present with optic neuritis, seen as enhanced optic nerve on postcontrast images on both CT and MRI.

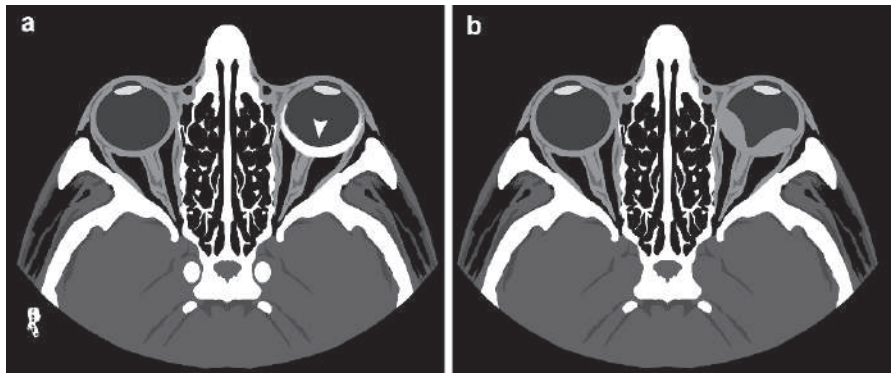

Fig. 2.4.7. Orbital CT postcontrast (**a**) and nonenhanced (**b**) illustrations of a patient show left eye choroidal/scleral thickening and enhancement due to uveitis in (**a**) (*arrowhead*), with V-shaped sign of retinal detachment in the left eye in (**b**)

For Further Reading

1. Bilaniuk LT et al Computed tomography in meningitis. Neuroradiology. 1978;16:13–4
2. Splendiani A et al Contrast-enhanced FLAIR in the early diagnosis of infectious meningitis. Neuroradiology. 2005; 47:591–8
3. Smirniotopoulos JG et al Patterns of contrast enhancement in the brain and meninges. RadioGraph. 2007;27:525–51
4. Albanese V et al Neuroradiological findings in multiloculated hydrocephalus. Acta Neurochir. 1982;60:297–311
5. Kamra P et al Infectious meningitis: prospective evaluation with magnetization transfer MRI. Brit J Radiol. 2004;77: 387–94
6. Jacquemin C et al Canalis basilaris medianus: MRI. Neuroradiology. 2000;42:121–3
7. Gilbert JA et al Vogt-Koyanagi-Harada syndrome: case report and review. J Emerg Med. 1994;12:615–9
8. Rao NA et al Vogt-Koyanagi-Harada disease diagnostic criteria. Int Opthalmol. 2007;27:195–9
9. McGehee BE et al Bilateral retinal detachment in a patient with Vogt-Koyanagi-Harada syndrome. Emerg Radiol. 2005; 11:366–71

2.5 Encephalitis

Encephalitis means inflammation of the brain parenchyma. Brain inflammation can result from different etiologies, most commonly viruses and autoimmune inflammation.

Patients with encephalitis typically present in early stages with headache or flue-like illness, followed by alteration in consciousness, drowsiness, confusion, fever, and seizures. Coma may result in severe cases.

This topic discusses the different kinds of encephalitis with their characteristic radiological features.

Limbic Encephalitis

The brain can be divided into regions according to functions. The first part is the brain stem, which plays a role in the basic attention, consciousness, arousal, heart and respiration adjustment, temperature control, and sleep–wake cycle control. The second part is the limbic system, which controls the behavior related to food, hormones and sex, jealousy, sadness and love, pleasure, and flight or fight responses. The limbic system is composed of the hippocampus, thalamus, hypothalamus, and amygdale. The third part is the rational brain (neocortex), which controls logic, thoughts, speaking, planning, and writing.

Limbic encephalitis (LE) involves inflammation of one structure or more related to the limbic system. LE can be caused by infections (e.g., herpes simplex virus), or auto-immune response.

Herpes encephalitis (*HSE*) is caused by herpes simplex virus type 1 or type 2. HSE type 1 is often seen in children and young adults. It starts as an orofacial infection (gingivostomatitis), which lasts for 1–2 weeks, followed by flu-like symptoms. Patients present with fever, headache, and change in mental status. The virus spreads in retrograde fashion along the trigeminal nerve course or the olfactory bulb into the brain. In the brain, the virus has affinity to infect the meningies, temporal lobes, and the inferior frontal lobe. HSE type 1 is the most common cause of encephalitis (95%). HSV type 2 is a genital form of HSE that affects neonates delivered by mothers, with herpes infection in the birth canal. It is an uncommon type of encephalitis (15%), and clinical diagnosis is usually confirmed by cerebrospinal fluid (CSF) analysis that reveals high leucocytes and protein content, and detection of the herpes virus DNA by serology.

Autoimmune LE has two forms. The first form is called *paraneoplastic limbic encephalitis* (*PLE*), which is seen in patients with particular cancers with paraneoplastic manifestations, such as thymus, lung, breast, and testes cancers. PLE is confirmed by detecting paraneoplastic antibodies in the patient blood like immunoglobulin G antibodies, ANNA 1, PCA 1, CV2, MA 2, and ANNA 2 antibodies.

The other form of autoimmune LE is nonPLE, which has the same picture as PLE in the absence of the serum paraneoplastic antibodies. The most common subsyndrome of the nonPLE is *voltage-gated potassium channel* (*VGKC*) *antibody-associated encephalitis*. This syndrome is commonly undiagnosed due to the lack of awareness about its existence. The diagnosis of autoimmune LE is important because it responds well to immunosuppressive drugs.

Signs on CT

- Initially, the scan may be normal, or shows hypodense lesions affecting the medial temporal lobes mainly in a bilateral asymmetrical pattern with mass effect and edema (Fig. 2.5.1). Areas of necrosis and hemorrhage may be seen on nonenhanced contrast images. Postcontrast images show patchy enhancement. The explanation for the temporal lobes affection lies in the reactivation of the virus from the trigeminal ganglia within Meckle's cave.
- Postencephalitic sequel includes parenchymal calcification and dilatation of ventricles.
- In HSE, the basal ganglia are often spared.

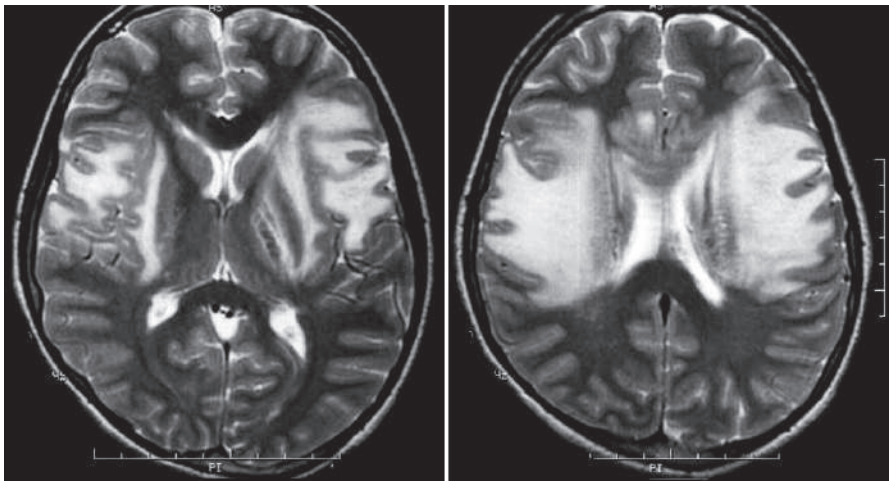

Fig. 2.5.1. Axial sequential T2W MR-Images show bilateral symmetrical hyperintense signal intensities affecting the region of the temporal lobes (both white and gray matters) in a patient with herpes encephalitis (HSE)

Signs on MRI

- In HSE, hyperintense, ill-defined cortical and white matter areas on T2W sequences with edema, mass effect, and gyral enhancement (Fig. 2.5.1) are seen. Later in the course of the disease, meningeal enhancement after contrast may be seen due to spread of the virus to the meningies.
- Autoimmune LE shows the same picture like HSE. Bilateral temporal and hippocampal lesions are typically seen. The main difference is based on the CSF analysis detecting the virus antibodies, or the autoimmune antibodies. Also, the history of cancer favors the autoimmune encephalitis.

Acute Demyelinating Encephalomyelitis (ADEM)

ADEM is an autoimmune demyelinating encephalitis that arises typically as an immune reaction 2 weeks after viral infection with MMR (measles, mumps, rubella), whooping cough infection (pertussis), or after immunization with MMR vaccine.

In ADEM, there is a hypersensitivity reaction affecting myelin and brain vessels (vasculitis). Patients classically present with sudden onset of neurological symptoms reflecting a wide central nervous system disturbance 2 weeks after viral infection or immunization.

ADEM has the same MRI picture as multiple sclerosis (MS). Unlike MS, which has multiple relapsing episodes, ADEM occurs once in life (monophasic course).

Acute hemorrhagic leukoencephalitis (*AHL*) is a severe form of ADEM characterized by intraparenchymal hemorrhage. AHL often arises after an upper respiratory tract infection or allergic reaction. The patient will show features of encephalitis, fever, and impaired consciousness.

Signs on MRI

- Large multifocal periventricular lesions with mild mass effect giving high signals in T2 (demyelinating areas) exactly like MS plaques, with asymmetric involvement of cerebral hemispheres (Fig. 2.5.2). MS plaques are often found bilaterally. The demyelinating plaques show ring enhancement after gadolinium injection in a similar fashion like acute MS plaques.
- Involvement of spinal cord and the cortical gray matter is common.
- Contrast enhancement is not always a feature.
- Typically, ADEM does not involve the corpus callosum.
- Bilateral optic neuritis may occur.
- In AHL, signs of hemorrhagic plaques are found on nongadolinium enhanced images.

How can you differentiate between MS and ADEM?

- MS has an acute and chronic phase, while ADEM has only one acute stage.
- MS affects white matter only, while ADEM affects white and gray matters.

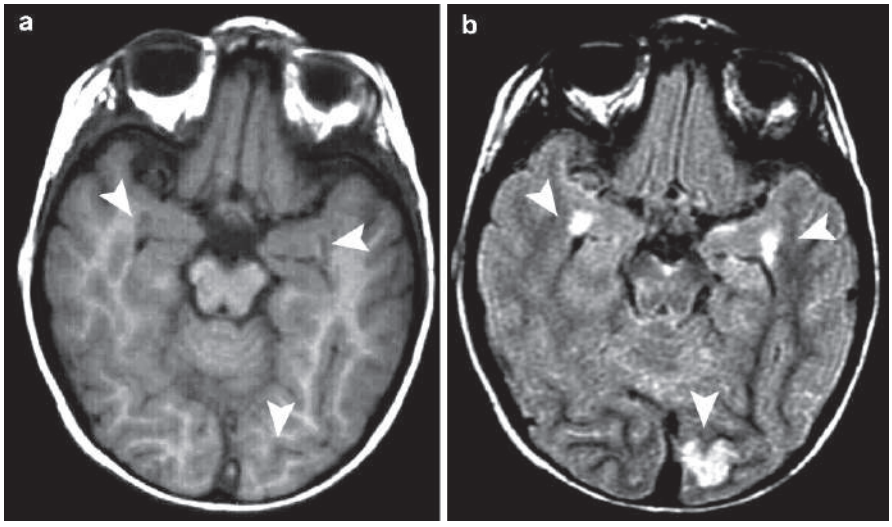

Fig. 2.5.2. Axial T1W (**a**) and FLAIR (**b**) images in a patient with acute demyelinating encephalomyelitis (ADEM) after measles, mumps, rubella (MMR) vaccination shows multifocal hyperintense areas in (**b**) affecting the posterior lobe and the area around the temporal horns of the lateral ventricles (*arrowheads*). The areas are patchy and asymmetrically distributed

- Clinical history of infection or immunization with ADEM.
- Corpus callosum is typically not affected in ADEM, while it is commonly affected in MS.
- ADEM causes bilateral optic neuritis, while MS typically causes unilateral optic neuritis.

Signs on MRI

The signs on MRI in HE are nonspecific. The MRI can be normal, or show nonspecific features of subcortical white matter changes (not the normal changes seen in a patient with epilepsy) (Fig. 2.5.3).

Hashimoto's Encephalitis

Hashimoto's encephalopathy (HE) is defined as a syndrome of persistent or relapsing neurological or neuropsychiatric symptoms, even though the thyroid levels are usually normal.

HE usually affects children in school age, with an incidence of 1.2% of population. Asymptomatic thyroid goiter can be seen in 85% of patients.

Patients with HE typically present with different unexplained neurological symptoms like epilepsy, behavioral changes, ataxia, hallucinations, or dementia. Diagnosis needs high level of suspicion. The characteristic feature that confirms HE in a patient with unexplained encephalitis is to find high levels of thyroid antibodies in the serum, which is always abnormally high. In contrast, the thyroid function levels usually are within normal or lower than normal range. The disease responds well to steroid therapy.

Rasmussen's Encephalitis (Rasmussen's Syndrome)

Rasmussen encephalitis (RE) is a rare, pediatric disease of chronic encephalitis usually effecting one hemisphere. The disease is characterized by partial motor seizures and progressive cognitive deterioration.

RE has an unknown cause, although viral and immunological causes have been suggested. Patients may show high titers of Epstein-Barr virus and cytomegalovirus in the CSF, with high serum GluR3 antibodies supporting the autoimmune and the viral theories.

RE is mostly seen in children (mainly pediatric disease), although few rare adult cases have been reported. RE has three stages, initial, acute, and residual. In the initial stage, the patient suffers from few partial motor seizures. Later in the acute stage, there is increased frequency of the seizures attack. The residual stage is characterized

2.5

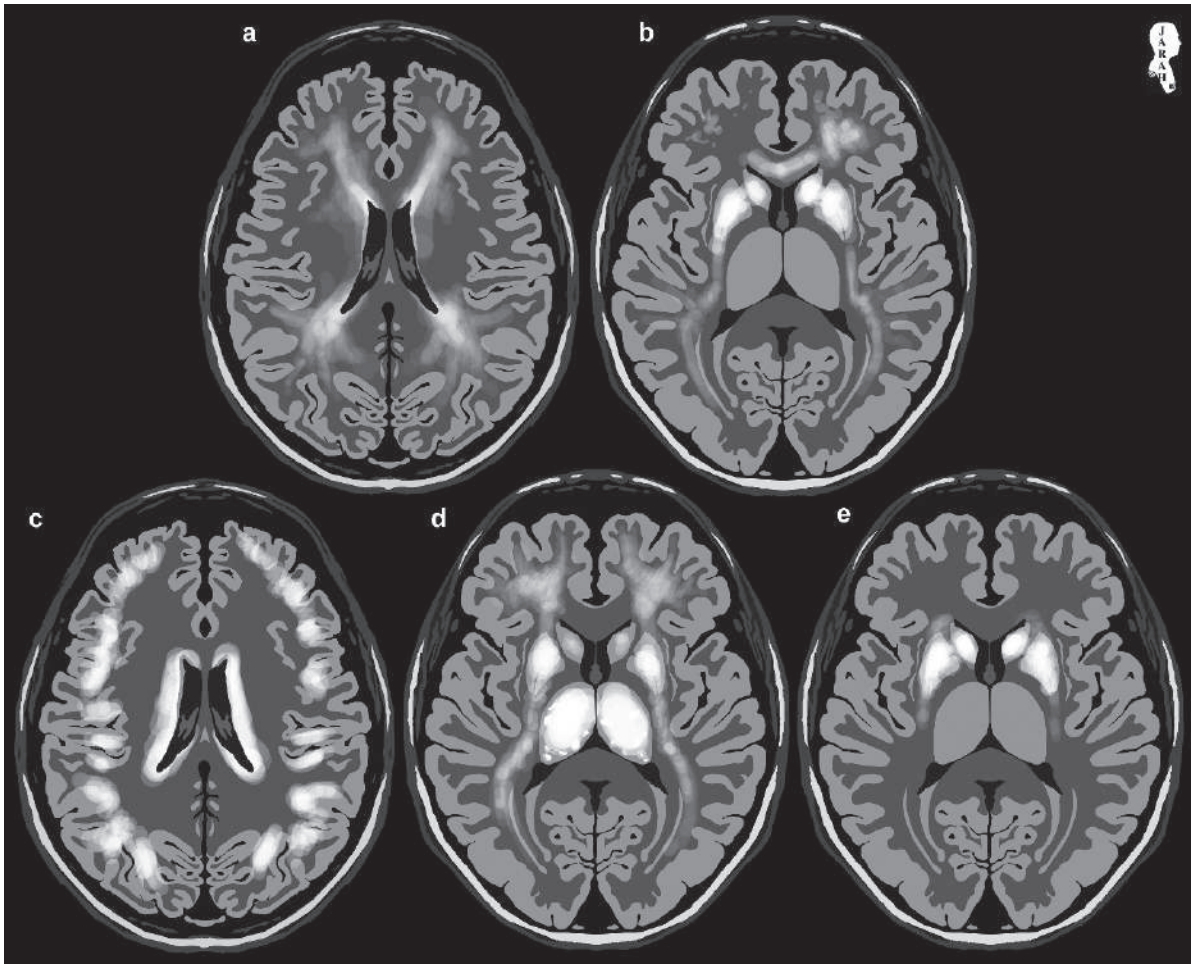

Fig. 2.5.3. Axial FLAIR MR-illustrations demonstrate different brain affection pattern in different types of encephalitis disorders: (**a**) Hashimoto encephalitis, (**b**) measles encephalitis (ME) (**c**) subacute sclerosing panencephalitis (SSPE), (**d**) Japanese encephalitis (JE), and (**e**) encephalitis lethargica

by cortical atrophy and permanent neurological deficits. Histopathology features include gliosis and perivascular cuffing in both the white and the gray matters.

The key to suspect and diagnose RE is to have a pediatric patient with multiple attacks of epilepsy, increasing in frequency, with serial MRI examinations showing changes and atrophy in one cerebral hemisphere only. Brain biopsy may be needed to confirm the diagnosis in atypical cases. Treatment ranges between antiepileptics, antiviral medications, corticosteroids and immunosuppressive agents.

Criteria to Diagnose Rasmussen Encephalitis

- Previously healthy child between 14 months and 14 years.
- Patients present with drug-resistant seizure, usually tonic-clonic or partial seizure.
- There are progressive unilateral neurological deficits that might lead to paresis (bilateral involvement occasionally).

Signs on MRI

- Hyperintense cortex is seen on T2W or FLAIR images on noncontrast enhanced images affecting the parieto-frontal or the temporal lobes in acute stages (Fig. 2.5.4). The MRI may be normal initially, and then shows signs of unilateral cortical atrophy. Classically, the contralateral hemisphere, basal ganglia, and the posterior fossa are unaffected. However, head of the caudate nucleus may be affected.
- In the residual stage, cortical atrophy, ventricular enlargement of the affected side (Evaccu dilatation), and caudate nucleus atrophy can be seen with atrophy of the whole cerebral hemisphere. Atrophic changes are predominantly seen in the peri-sylvian area and the caudate nucleus.

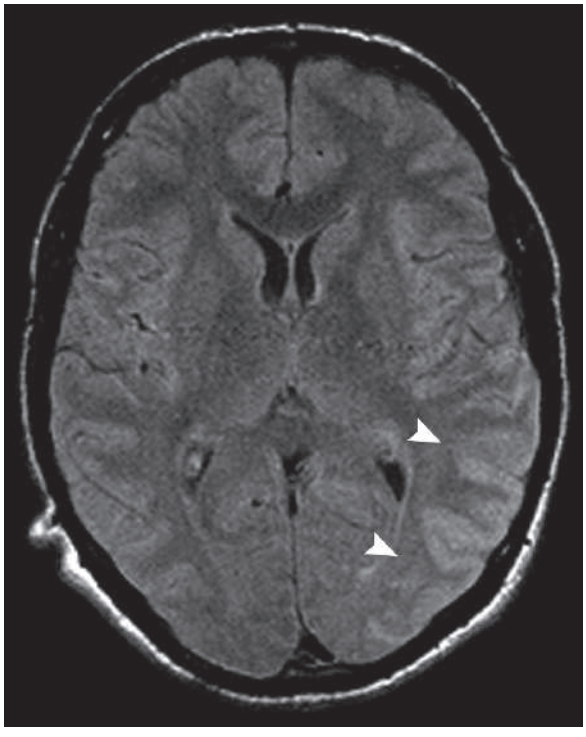

Fig. 2.5.4. Axial FLAIR image in a child with recurrent epilepsy shows moderate hyperintense cortices in the left temporo-occipital region in a unilateral pattern (*arrowheads*). The patient was diagnosed later as a case of Rasmussen encephalitis (RE)

Measles Encephalitis

Measles encephalitis (ME) is a brain inflammation due to an acute infection with measles virus. ME is considered rare due to the worldwide spread of MMR vaccine (0.05–0.4%), yet few sporadic cases are reported in the literature occasionally.

ME starts on the second to sixth day after development of the rash, but it may precede the rash. Patients present with the usual clinical picture of encephalitis. Diagnosis is made on the basis of identifying high antimeasles antibodies titers in the CSF.

Signs on MRI

- MRI often shows bilateral T1/T2 hyperintense signal intensities in the basal ganglia and the white matter (Fig. 2.5.3).
- The fronto-temporal areas may be affected in an asymmetric pattern bilaterally.

Subacute Sclerosing Panencephalitis (SSPE)

SSPE is a well-recognized chronic complication of measles virus, developing 6–12 years after initial measles infection.

SSPE is a rare disease, with an incidence of 1:1,000,000, and high mortality rate. The majority of patients with SSPE are known to have a previous attack of classical measles years before. Fifty percent of SSPE cases occur after 2 years from the initial measles infection, and patients are between 5 and 15 years of age.

Patients with SSPE often present behavioral changes with jerking movements know as myoclonic seizures. The myoclonic jerking is exacerbated on excitement. Later, grand-mal (tonic-clonic) seizure develops, with problems in swallowing, speech, and vision. Some patients may develop pyramidal signs with cerebellar signs (e.g., ataxia). Cortical blindness due to occipital lobe involvement or optic nerve edema may occur. The diagnosis of SSPE should be considered in patients with cortical blindness even when other classical findings of SSPE are absent. The duration of the illness can be short (e.g., 6 weeks), or very long (e.g., 10 years).

Diagnosis of SSPE is based on the high serum and CSF antimeasles antibody titers detection. Imaging is helpful in establishing differential diagnosis.

2.5

Signs on MRI

- Commonly, the periventricular and subcortical white matter are affected in SSPE (Fig. 2.5.3), with bilateral high T2W and FLAIR signal intensities seen on MRI.
- The basal ganglia, cerebellum, spinal cord, and corpus callosum are less frequently affected.

Japanese Encephalitis

Japanese encephalitis (JE) is acute viral encephalitis, caused due to infection with JE virus. JE virus belongs to the *Flaviviridae* family (Flavivirus). The virus is transmitted to humans from its hosts via its carrier, the *Culex tritaeniorhunchus* mosquito. The natural hosts of the JE virus are pigs, birds, dogs, and horses.

Following bite on the human body from an infected mosquito, the virus proliferates in the lymphatic system. From there, it enters the blood stream and crosses the blood-brain barrier (BBB) to start brain parenchymal inflammation. Patients with JE present with loss of appetite (anorexia), fatigue, headache, and vomiting. The initial stage of the disease is characterized by rapidly progressing fever and nonspecific central nervous system symptoms. The neurological symptoms include rigidity, Parkinson-like symptoms, altered mental status, and seizures. The fever and the systemic symptoms improve gradually after 7–8 days. In 10% of patients, long-term sequelae may occur, including psychiatric symptoms, motor impairment, and epilepsy.

Diagnosis is confirmed by detection of JE virus antibodies, or isolation of the virus from the CSF.

Signs on MRI

- The classical findings in JE include bilateral symmetrical high signal intensity lesions on T2W and FLAIR images located in both thalami (Fig. 2.5.3). Similar lesions may be found in the basal ganglia, substantia nigra, hippocampus, pons, and cerebral white matter.
- Hemorrhagic lesions in the thalami may be found occasionally.

West Nile Encephalitis

West Nile encephalitis (WNE) is encephalitis caused by acute infection with the West Nile virus (WNV). WNW is a positive-strand RNA virus belonging to the *Flaviviridae* family.

WNE is observed in the Middle East and African countries. The virus is transmitted to humans from the *C. tritaeniorhunchus* mosquito from its original hosts; the hosts of the WNV are crows and pigeons. WNV is an "arbovirus." Arboviruses are viruses that are transmitted from one animal host to the next by insects (anthropods). WNV is not transmitted from person to person.

Patients with WNE present with nonspecific febrile illness, lymphadenopathy, skin rash, headache, and body ache. Encephalitis symptoms start when the virus crosses the BBB, resulting in seizures, confusion, paralysis, and behavioral changes that may be mistaken with hysteria.

Diagnosis is based on detecting high titers of WNV antibodies in the CSF.

Signs on MRI

The scan shows bilateral symmetrical lesions in both thalami, with hemorrhagic tendency. The MRI picture is similar to the JE picture.

Tick-Borne Encephalitis (Spring-Summer Encephalitis)

Tick-borne encephalitis (TBE) is encephalitis caused by TBE virus, a virus that belongs to the *Flaviviridae* family.

Patients with TBE commonly present with meningitis (49%), followed by meningoencephalitis (41%), and meningoencephalomyelitis (10%). Patients may present with polio-like symptoms with polyradiculitis course. The virus has an affinity to the anterior horn cells in the spinal nerve roots.

Diagnosis is based on confirming the virus antibodies in the CSF.

Signs on MRI

- The brain MRI shows same picture like JE and WNE.
- Polyradiculitis is seen as marked contrast enhancement of the spinal nerve roots on contrast-enhanced images (Fig. 2.5.5).

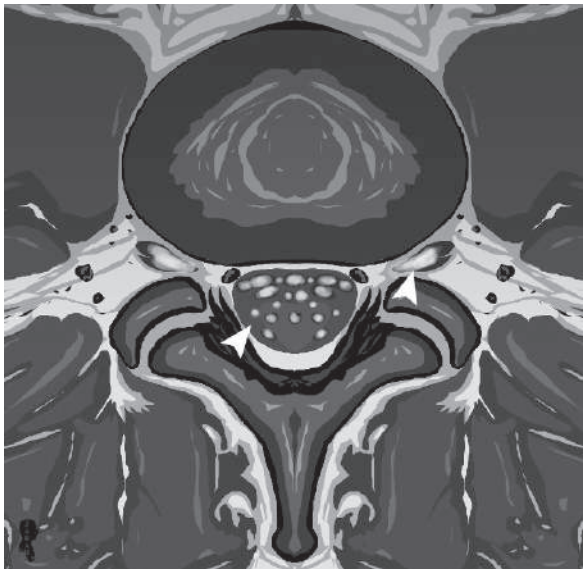

Fig. 2.5.5. Axial postcontrast spinal MR-illustration at the level of L3/L4 shows enhanced cauda equine roots and spinal roots representing polyradiculitis (*arrowheads*)

Murray Valley Encephalitis

Murray valley encephalitis (MVE) is encephalitis caused by MVE virus, another virus that belongs to the *Flaviviridae* family.

Majority of patients with MV virus are asymptomatic, with only 1:1,000 infected persons developing encephalitis. The symptoms are nonspecific, with neurological residua in 40% of survivors. Diagnosis is based on detecting the virus antibodies in the CSF.

Signs on MRI

The brain MRI shows same picture like JE, TBE, and WNE.

St. Luis Encephalitis

St. Luis encephalitis is a disease caused by the St. Luis virus, another virus that belongs to the *Flaviviridae* family. The virus was named after it was isolated from the human brain tissue in 1933 during a large epidemic in St. Luis city, USA.

The disease ranges between flue-like illnesses to a life-threatening central nervous system disease. Diagnosis is based on CSF serology.

Signs on MRI

- The brain MRI shows same picture like JE, TBE, MVE, and WNE.
- The substantia nigra is commonly involved in St. Luis encephalitis.

Encephalitis Lethargica

Encephalitis lethargica (EL) is a rare, mysterious form of encephalitis that was responsible for epidemic disease that killed 500,000 people from about 1917 until 1940. Many investigators link EL with the notorious Spanish flue influenza virus, which is responsible for the influenza epidemic at the end of the First World War. Although the disease is considered historical, few sporadic cases are reported from time to time.

EL typically has three forms: irritable, lethargic, and lethargic with paralysis. The irritable form is characterized by marked restlessness and excitability. The lethargic stage is characterized by a drowsy state, and expressionless, mask-like face, resembling Parkinson's disease. The third stage is characterized by drowsiness with some form of motor paralysis in the lower extremities, and frequent convulsions.

Patients with EL present with characteristic gradual onset of headache, lethargy and asthenia, low grade fever, cranial nerve palsies, and vomiting, especially in children. Other neuro-psychiatric symptoms include Parkinsonian mask-face, catatonia, choreiform movements, insomnia, delirium, and profound sweating.

Children with EL present with a wide variety of behaviors that can be regarded as psychopathic. These include personality change, emotional instability,

nervousness, restlessness, and destructive and impulsive mood.

EL is one of the causes of juvenile Parkinsonism, mainly the rigid-akinetic form. This can be explained by the fact that the basal ganglia are classically affected in EL.

2.5

Criteria to diagnose EL include encephalitis with three of the following major criteria, assuming all the known causes of encephalitis have been excluded

- Neuro-psychiatric symptoms.
- Sleep disturbance (e.g., insomnia)
- Signs of basal ganglia involvement (e.g., Parkinson-like symptoms).
- Ophthalmic symptoms.
- Obsessive compulsive behavior.
- Respiratory irregularity.

Signs on MRI

MRI of EL patients show bilateral basal ganglia lesions with high signal intensities on T2W and FLAIR images (Fig. 2.5.3).

For Further Reading

1. Urbach H et al Serial MRI of limbic encephalitis. Neuroradiology. 2006;48:380–6
2. Collison K et al Asymmetric cerebellar ataxia and limbic encephalitis as a presenting feature of primary Sjögren's syndrome. J Neurol. 2007;254:1609–11
3. Vilensky JA et al Children and encephalitis lethargica: a historical review. Pediatr Neurol. 2007;37:79–84
4. Beleza P et al From juvenile Parkinsonism to encephalitis lethargica, a new phenotype of post-streptococcal disorders: case report. Euro J Paediatr Neurol. 2008;12:505–7
5. Benneis C et al Encephalitis lethargica following Bartonella henselae infection. J Neurol. 2007;254:546–7
6. Alfaresi M et al West Nile virus in the blood donors in UAE. Indian J Med Microbiol. 2008;26:92–3
7. Bosanko CM et al West Nile virus encephalitis involving the substantia nigra. Neuroimaging and pathologic findings with literature review. Arch Neurol. 2003;60:1448–52
8. Bender A et al Sever tick borne encephalitis with simultaneous brain stem, bithalamic, and spinal cord involvement documented by MRI. J Neurol Neurosurg Psychiatry. 2005; 76:135–7
9. Pfefferkorn T et al Tick-borne encephalitis with polyradiculitis documented by MRI. Neuroradiology. 2007;68: 1232–3
10. Grubbauer HM et al Tick-borne encephalitis in a 3-month-old child. Eur J Pediatr. 1992;151:743–4
11. De Tiège X et al The spectrum of herpes simplex encephalitis in children. Euro J Paediatr Neurol. 2008;12:72–81
12. Senol U et al Subacute sclerosing panencephalitis: brain stem involvement in a peculiar pattern. Neuroradiology. 2000;42:913–6
13. Pedersen H et al Computed tomographic findings of early subacute sclerosing panencephalitis. Neuroradiology. 1982; 23:31–2
14. van der Meyden CH et al Gadolinium ring enhancement and mass effect in acute disseminated encephalomyelitis. Neuroradiology. 1994;36:221–3
15. Garg RK. Subacute sclerosing panencephalitis. J Neurol. doi:10.1007/s00415-008-9932-6
16. Feydy A et al Brain and spinal cord MR imaging in a case of acute disseminated encephalomyelitis. Eur Radiol. 1997;7: 415–7
17. Bermejo PE et al Hemorrhagic acute disseminated encephalomyelitis as first manifestation of systemic lupus erythematosus. J Neurol. 2008;255:1256–8
18. Lacroix C et al Acute necrotizing measles encephalitis in a child with AIDS. J Neurol. 1995;242:249–56
19. Baba Y et al Acute measles encephalitis in adults. J Neurol. 2006;253:121–4
20. Parmar RC et al Measles encephalitis: a case report of two cases with variable manifestations. Pediatr Int. 2002;44: 90–2
21. Lury KM et al Eastern equine encephalitis: CT and MRI findings in one case. Emerg Radiol. 2004;11:46–8
22. Wong SH et al Murray Valley encephalitis mimicking herpes simplex encephalitis. J Clin Neurosci. 2005;12:822–4
23. Kroeger MA et al Murray Valley encephalitis virus recombinant subviral particles protect mice from lethal challenge with virulent wild-type virus. Arch Virol. 2002;147: 1155–72
24. Parquet MC et al St. Louis encephalitis virus induced pathology in cultured cells. Arch Virol. 2002;147:1105–19
25. Abe T et al Japanese encephalitis. JMRI. 1998;8:755–61
26. Paprocka J et al Difficulties in differentiation of Parry-Romberg syndrome, unilateral facial scleroderma, and Rasmussen syndrome. Childs Nerv Syst. 2006;22:409–15
27. Granata T. Rasmussen's syndrome. Neurol Sci. 2003;24: S239–43
28. Rajesh B et al Putaminal involvement in Rasmussen encephalitis. Pediatr Radiol. 2006;36:816–22
29. Heo SH et al A case of unilateral hemispheric encephalitis. Neurol Sci. 2007;28:185–7
30. Deb P et al Neuropathological spectrum of Rasmussen encephalitis. Neurol India. 2005;53:156–61
31. Bertoni M et al Encephalopathy associated with Hashimoto's thyroiditis: an additional case. Euro J Intern Med. 2003;14: 434–47
32. Vasconcellos E et al Pediatric manifestations of Hashimoto's encephalopathy. Pediatr Neurol. 1999;20:394–8
33. Arain A et al Hashimoto's encephalopathy: documentation of temporal seizure origin by ictal EEG. Seizure. 2001; 10: 438–41

2.6 Epilepsy

Epilepsy is a chronic neurologic disease characterized by recurrent, spontaneous episodes of seizures, which are defined as excessive abnormal neuronal activity of the cortical neurons. Seizures originate either from a localized area within the brain (partial/focal), or arise from both hemispheres simultaneously (generalized).

Partial seizures can be associated with loss of consciousness (complex), or occur without loss of consciousness (simple/Jacksonian). Partial seizures can spread from one area to another, ending up in initiating secondary generalized seizure. Patients with partial simple seizures experience mental events like: confusion, mild hallucinations, jerking movements, or emotional events (déjà vu phenomenon). In contrast, partial complex seizure patients experience uncontrolled behavior, loss of judgment, and loss of consciousness. Also, patients with partial complex seizures often experience a warning sign such as aura, odd odor, or visual or auditory hallucinations. Partial seizures are resistant to antiepileptic drugs in up to 30% of cases.

Generalized seizures are divided into two types: one type is characterized by episodes of rigidity (tonic) followed by repetitive involuntary movements (clonic), and it is called "Grand mal seizure." The other type is characterized by absence of seizure with sudden, brief (seconds) episode of loss of physical movement, and it is called "Petit mal seizure."

Status epilepticus is a condition characterized by continuous seizure attack that lasts more for than 5 min, and can extend up to 30 min. Status epilepticus can occur as a withdrawal symptom of antiepileptic medications. *Todd's paralysis* is a form of temporary motor weakness experienced by the patient after an episode of seizure.

Epilepsy can be caused by a variety of clinical conditions. Any condition that insults the brain cortex is capable of initiating seizure attacks and epilepsy. Moreover, seizure attacks can be initiated by metabolic abnormalities (e.g., hypercalcemia). The role of brain imaging in epilepsy is to detect anatomical structural abnormalities. It is practical to divide the common causes of epilepsy into five simplified main groups:

- *Mesial hippocampal (temporal) sclerosis*: is a disease characterized by atrophy and sclerosis of the hippocampus. Most patients have a history of brain injury before the age of 5 years in the form of febrile convulsion or status epilepticus. Mesial temporal sclerosis is the most common cause of epileptic seizures in adults (40–60% of cases).
- *Congenital cortical anomalies*: constitute up to 50% of epilepsy cases in children, and up to 25% of adult cases. Anomalies that fall into this group include lissencephaly, pachygyria, polymicrogyria, gray matter heterotopia, and phakomatosis. The frontal lobe is commonly involved in congenital cortical anomalies.
- *Neoplasms*: constitute up to 4% of epilepsy cases, and they are mostly cortical neoplasms like astrocytoma, ganglioglioma, desmoplastic neuroepithelial tumor, and oligodendroglioma. The temporal lobe is commonly involved in cortical neoplasms.
- *Vascular abnormalities*: constitute up to 5% of epilepsy cases, and commonly include arteriovenous malformations and cavernous angiomas.
- *Gliosis*: is the result of the previous insult to the cortex like postinfarction, postinfection, and posttrauma.

Differential Diagnoses and Related Diseases

- *Lafora disease*: is a very rare, autosomal recessive disease characterized by myoclonic jerks, generalized tonic-clonic seizures, and multisystemic manifestation. *Myoclonus jerks* are brief involuntary contractions of a group of muscles (e.g., hiccups are myoclonus jerks of the diaphragm). The disease is caused by abnormal deposition of polyglucosan in the central nervous system, liver, myocardium, skin, and muscles. Diagnosis is confirmed by skin biopsy that identifies polyglucosan inclusions (*Lafora bodies*) by positive periodic acid Schiff (PAS) stain. Patients present typically before 20 years of age, complaining of multiple attacks of myoclonic, generalized tonic-clonic seizures, intellectual disturbance, and severe progressive motor and coordination disturbance. Patients often show abnormal liver profile due to liver failure. The disease is frequently seen in countries where consanguineous marriages are common, like the Middle East, India, and Pakistan.

Death occurs almost 6–10 years after the first manifestation of the disease.

- *Ulegyria*: is a disease characterized by destruction and gliosis of the gray matter in the depth of the sulci with relative preservation of the gyral surfaces, giving the gyri a "mushroom shaped-appearance." Ulegyria commonly arises as a late effect of perinatal and postnatal hypoxia. It tends to occur in a symmetrical fashion in the perisylvian areas.
- *Schinzel-Giedion syndrome*: is a rare, autosomal recessive disease characterized by seizures, mental retardation, and spasticity. Other manifestations include characteristic facial features, bitemporal narrowing giving the skull "figure of 8 shape," choanal atresia, congenital heart defects, wide occipital synchondrosis, distal phalangeal hypoplasia, and hypospadia.

Signs on CT and MRI

- In *mesial temporal sclerosis*, there is increased T2 signal intensity of the hippocampus, ipsilateral atrophy of the temporal lobe with dilatation of the temporal horn (Fig. 2.6.1). The key diagnosis is atrophy and high T2 signal intensity of the hippocampus.
- In *oligodendroglioma*, there is a brain mass with calcifications and minimal brain edema. The lesion is seen predominantly located in the frontal lobe, and shows heterogenous contrast enhancement (Fig. 2.6.2).
- In *ganglioglioma*, there is a lesion that arises from the frontal or the temporal lobes cortices. Usually, the patient has a history of epilepsy. The lesion can be cystic, solid, or mix. It may show heterogeneous contrast enhancement, and rarely shows calcification.
- In desmoplastic neuroepithelial tumor, there is a hypodense lesion located in the temporal lobe cortex on CT, with no specific signal on MRI. Usually, the patient has a history of epilepsy. The tumor shows no contrast enhancement (Fig. 2.6.3).
- In *gliosis*, the cortex shows an area of low signal intensity on T1W and T2W images due to parenchymal fibrosis (Fig. 2.6.4).
- In *cavernous angioma*, there is a honeycomb-like lesion that appears with no edema or mass effect (except in cases of fresh bleeding). The lesion has an isointense signal on T1W and T2W images, with mixed hyperintense (blood) and hypointense (calcium/hemosiderin) signals within it, and surrounded by a hypointense rim of hemosiderin (pathognomonic sign, Fig. 2.6.5). MR-angiography shows no vascular malformation, usually because most of the lesion is thrombosed.
- In *Lafora disease*, brain infarction in the frontal and parietal subcortical white matter areas may be seen after severe seizure attack. On MR-Spectroscopy, there is a characteristic decrease in *N*-acetylaspartate (NAA)/Creatine ratio in the frontal lobe and the basal ganglia.
- In *ulegyria*, the MRI scan shows thin gyri in the perisylvian area with abnormal high T2 signal in a bilateral, symmetrical fashion (Fig. 2.6.6). Unilateral lesions can occur.
- In *status epilepticus*, the hippocampus shows unilateral or bilateral high signal intensity signal on both T2W and FLAIR images (Fig. 2.6.7). This sign is usually seen in the acute phase, and can extend up to months after the initial attack.

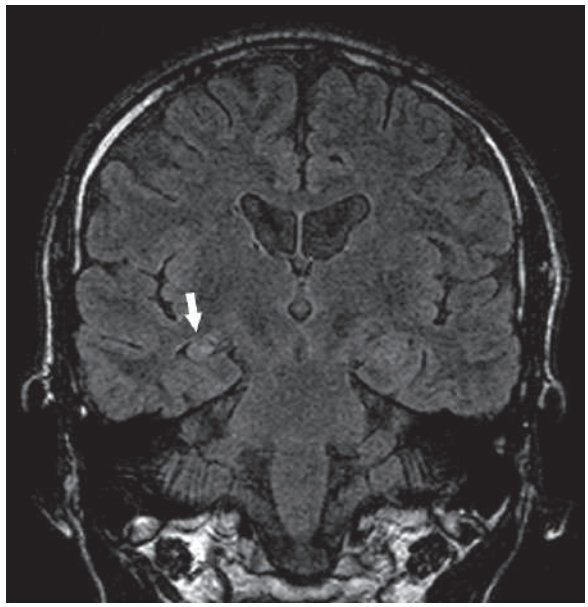

Fig. 2.6.1. Coronal T2W brain MRI of a patient with recurrent epilepsy shows mild atrophy of the right hippocampus with higher T2 signal intensity (*arrow*) compared to the left side (mesial temporal sclerosis)

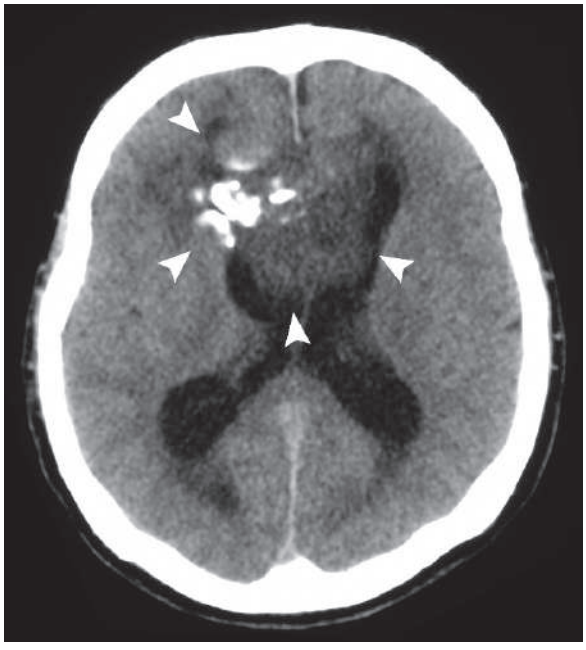

Fig. 2.6.2. Axial nonenhanced brain CT shows a right frontal lobe tumor that abuts the lateral ventricles (*arrowheads*) and shows areas of dense calcifications (oligodendroglioma)

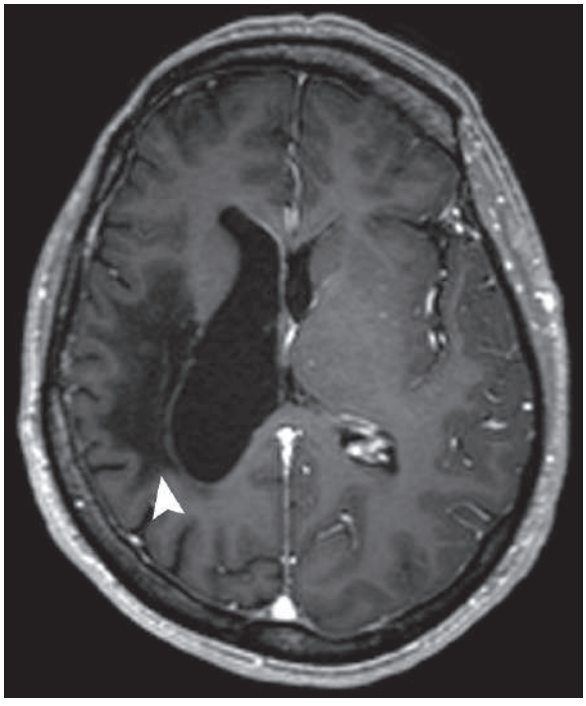

Fig. 2.6.4. Axial T1W postcontrast MRI of a patient with previous brain infarction shows area (*arrowhead*) of hypointensity, with dilatation of the right occipital horn of the lateral ventricle adjacent to it (gliosis)

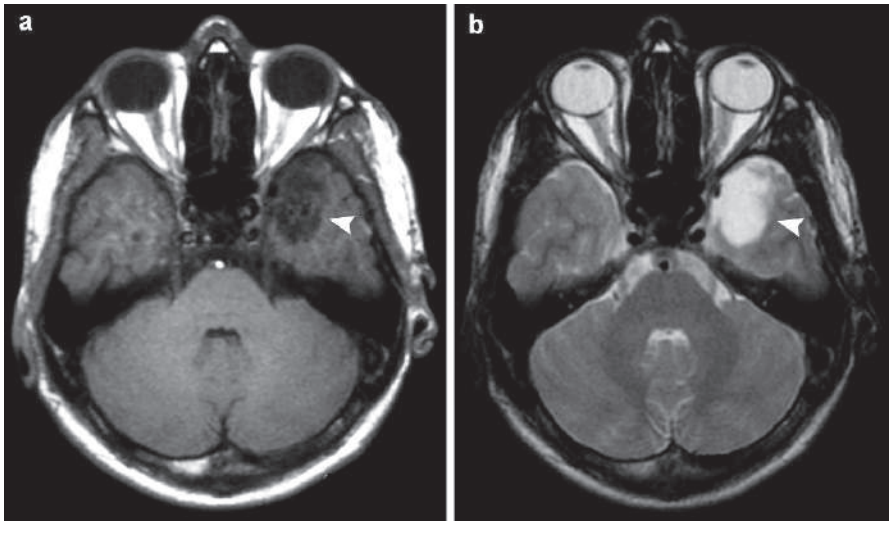

Fig. 2.6.3. Axial T1W postcontrast (**a**) and T2W (**b**) brain MRI in a patient with epilepsy show temporal cortical hypointense lesion with high T2 signal intensity and no contrast enhancement (desmoplastic neuroepithelial tumor)

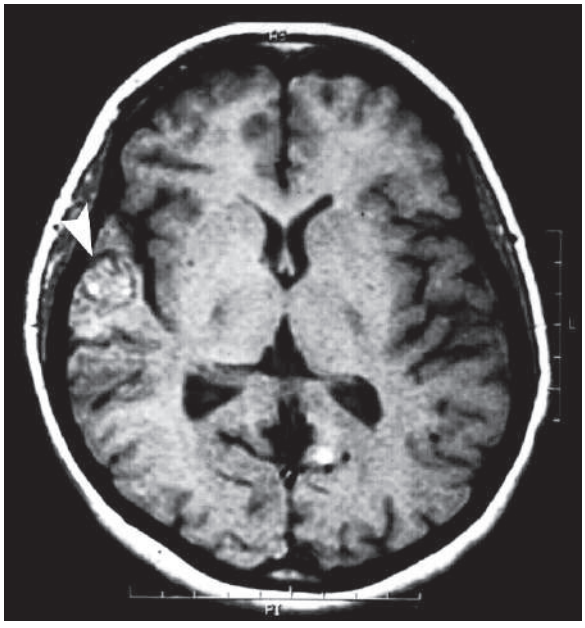

Fig. 2.6.5. Axial T1W brain image shows a hypointense signal intensity ring with multiple areas of different MR intensities (*arrowhead*) located within the right temporal lobe (cavernous angioma)

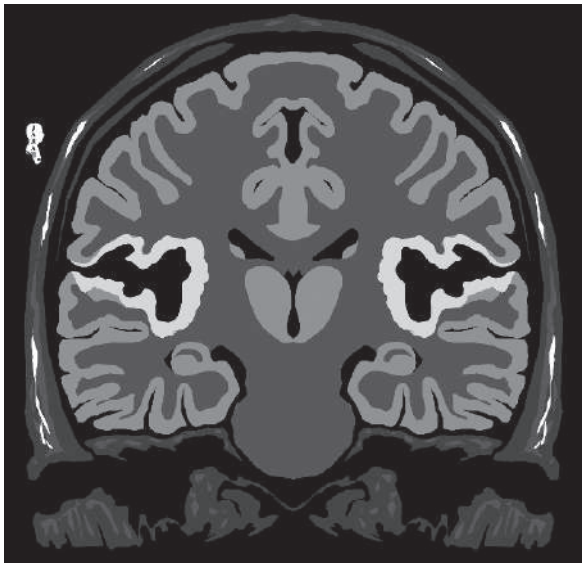

Fig. 2.6.6. Coronal FLAIR brain MR-illustration demonstrates the radiological findings in ulegyria

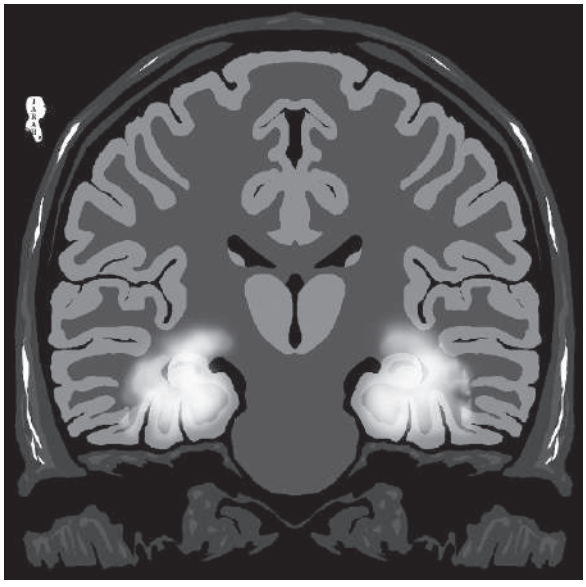

Fig. 2.6.7. Coronal FLAIR brain MR-illustration demonstrates the radiological findings in status epilepticus

For Further Reading

1. Deblaere K et al Structural magnetic resonance imaging in epilepsy. Eur Radiol. 2008;18:119–29
2. Urbach H. Imaging of epilepsy. Eur Radiol. 2005;15: 494–500
3. Ramos A et al Uncommon epileptogenic lesions affecting the temporal lobe. Semin Ultrasound CT MRI. 2008;29: 47–59
4. Urbach H et al MRI of long-term epilepsy-associated tumors. Semin Ultrasound CT MRI. 2008;29:40–6
5. Vazquez E et al Developmental abnormalities of temporal lobe in children. Semin Ultrasound CT MRI. 2007;29: 15–39
6. Paesschen WV et al Qualitative and quantitative imaging of the hippocampus in mesial temporal lobe epilepsy with hippocampal sclerosis. Neuroimag Clin N Am. 2004;14: 373–400
7. Vattipally VR et al MR imaging of epilepsy: strategies for successful interpretation. Neuroimag Clin N Am. 2004;14: 349–72
8. Villanueva V et al MRI volumetry and proton MR spectroscopy of the brain in Lafora disease. Epilepsia. 2006;47: 788–92
9. Gómez-Garre P et al Hepatic disease as the first manifestation of progressive myoclonus epilepsy of Lafora. Neurology. 2007;68:1369–73
10. Sirven JI et al MRI changes in status epilepticus. Neurology. 2003;60:1866
11. Al-Mudaffer M et al Clinical and radiological findings in Schinzel-Giedion syndrome. Eur J Pediatr. 2008;167: 1399–1407

2.7 Headache

Headache is the most common neurological complaint worldwide. There are over 300 different types and causes of headache, including teeth pain, frontal sinusitis, vision problems (e.g., myopia), hypertension, otitis media, intracranial tumors, and much more.
Radiological imaging for headache investigation is often indicated in cases of new-onset headaches, headaches with progressive course, headaches that never alternate sides and headaches associated with neurological deficits of seizures.

In this topic, some of the common causes of headache with well-defined radiological signs are discussed.

Migraine

Headache is divided into primary and secondary headaches. Primary headaches include migraine, tension-type headache, cluster-headache, and others. Secondary headaches in contrast, are attributed to a variety of causes that include vascular, sinusoidal, infectious, inflammatory causes.

Migraine headache is divided into two main types: migraine with or without aura. Migraine aura consists of neurological manifestations that precedes migraine, or can occur without it. Typically, the aura develops over 5 min and lasts no more than 60 min. Aura manifestations may include auditory and visual symptoms, numbness, paraesthesia, and tingling sensation.

Uncommon manifestations of migraine include cyclical vomiting (2.5%), which is characterized by unexplained nausea and vomiting. It often occurs in children and lasts for 1–5 h in the absence of gastrointestinal disease. Benign paroxysmal vertigo is characterized by recurrent attacks of vertigo (e.g., 5 episodes) that last from minutes to hours. Lastly, recurrent attacks of abdominal pain that are accompanied by anorexia, nausea, and some vomiting may be seen in children with migraine, and it is called "*abdominal migraine*."

Migrainous infarction can occur when one or more aural symptoms persist beyond 1 h. *Status migrainous* refers to an attack of migraine with headache that last >72 h.

Signs on CT

- In acute migraine, hypodense areas may be seen within the brain parenchyma commonly in the occipito-temporal areas (Fig. 2.7.1). These areas enhance after contrast injection. The hypodense areas are thought to represent brain edema and ischemia. Contrast enhancement supports the theory of ischemia. Migraine is thought to be caused by changes in the blood perfusion within the cerebral parenchyma.
- Cerebral vessels angiography is typically normal.
- Infarction is seen as an area of hypodense parenchyma surrounded by cytotoxic edema.

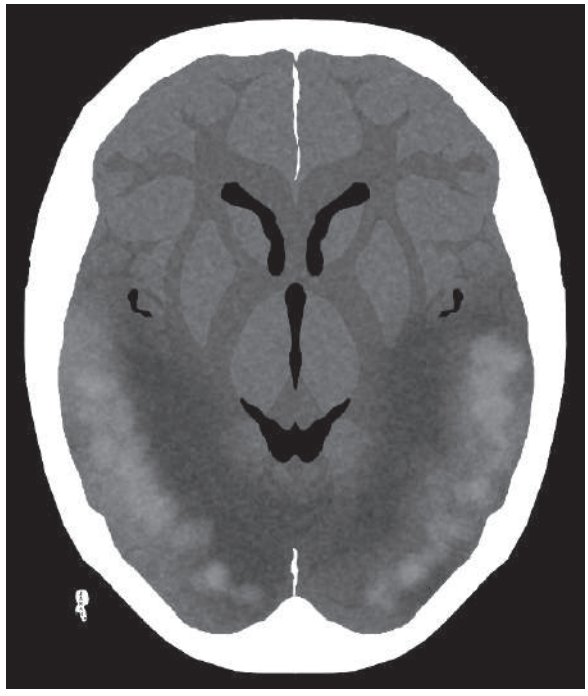

Fig. 2.7.1. Axial brain CT illustration shows bilateral occipital hypodensities, a sign that can be encountered in acute attack of migraine headache due to vasogenic edema

Signs on MRI

In majority of the cases, T2W and FLAIR hyperintense areas are noticed in the midpontine and cerebellar parenchyma (Fig. 2.7.2).

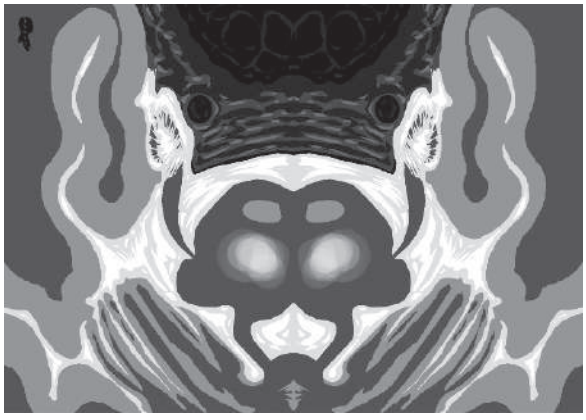

Fig. 2.7.2. Axial brain T2W MR-illustration at the level of the pons demonstrates bilateral hyperintense areas, a sign that can be seen in patients with migraine

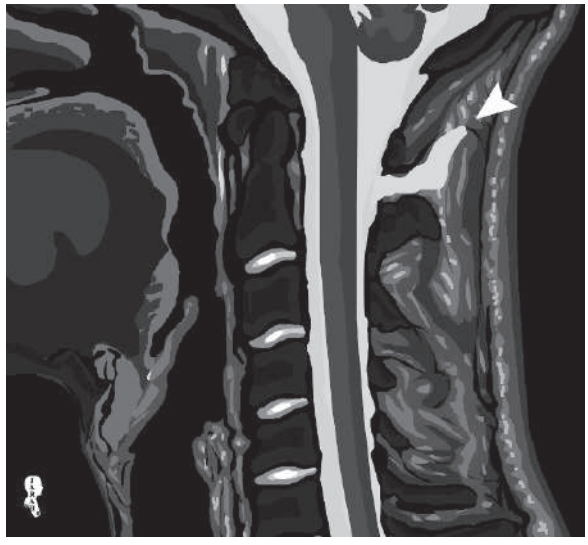

Fig. 2.7.3. Sagittal T2W cervical MR-illustration demonstrates cerebrospinal fluid (CSF) leak between the posterior elements of C2 and C3 (*arrowhead*)

Spontaneous Intracranial Hypotension (Schaltenbrand Syndrome)

Spontaneous intracranial hypotension (SIH) is a disease characterized by a typical headache that is evoked by changing body position from supine to standing position (orthostatic headache). The headache pain lasts for few minutes and improves or disappears after acquiring recumbent or supine position.

Causes of SIH can be due to cervical disc herniation, vigorous activity, sexual activity, minor head trauma, or a violent sneeze or cough.

Other features of SIH include: nausea and vomiting, hearing disturbance, and diplopia. SIH headache is either frontal or occipital in location, and typically is not relieved by analgesics.

Signs on MRI

- Meningeal thickening with diffuse gadolinium enhancement (most constant, typical finding).
- Signs of cerebrospinal fluid (CSF) leak on sagittal images of the cervical spines (Fig. 2.7.3).
- Subdural CSF collections with no mass effect (subdural hygromas).
- Downward displacement of the cranial content (medulla and cerebellar tonsils) into the foramen magnum, mimicking Arnold-Chiari malformation type I (*Sagering brain*).
- Displacement of the iter (the opening of the third ventricle into the aqueduct of sylvius).

Idiopathic Intracranial Hypertension (Pseudotumor Cerebri)

Idiopathic intracranial hypertension or pseudotumor cerebri (PTC) is a disease with unknown cause, characterized by papilledema with raised intracranial pressure in the absence of space-occupying lesions, normal CSF composition, and normal neuroimaging findings.

PTC can be seen in patients with particular medical disorders like obesity, hypervitaminosis, venous sinus thrombosis, iron deficiency anemia, typhoid fever, brucellosis, and oral contraceptive use. In children, the most common cause of PTC is otitis media.

Patients with PTC commonly present with headache, visual disturbance, diplopia, and pulsatile tinnitus or ear noise. The most serious condition in PTC is sudden visual loss. Fundoscopic examination typically reveals optic disc edema (papilledema). PTC can be associated uncommonly with *Parinaud's syndrome* (*Dorsal midbrain syndrome*), a disease characterized by upward gaze paralysis, convergence-retraction nystagmus, and light-near dissociation.

Signs on MRI

- The normal neuroimaging diagnostic criteria of PTC reflect the absence of a definite cause for the intracranial pressure (e.g., no space occupying lesion). However, neuro-radiological signs that reflect increased intracranial pressure do exist and have been reported.
- *Empty sella*: is a condition characterized by is flattened and pressed pituitary gland against the sellar floor. Empty sella is one of the radiological signs frequently seen in PTC. The infundibular stalk is seen dipping in the sella beyond the level of the posterior clinoid process (normally, the pituitary gland is connected to the infundibulum at the level of the posterior clinoid process) (Fig. 2.7.4). Most of the sellar space is occupied by CSF.
- Dilated optic nerve sheath due to increased CSF with its perineural subarachnoid space. The optic nerve can be clearly differentiated from the sheath.
- Bilateral, nonsymmetrical intraocular protrusion of the optic nerve, with tortuosity of the orbital optic nerve (due to the increased intracranial CSF pressure) (Fig. 2.7.5).
- Normal size ventricles with no signs of hydrocephalus.

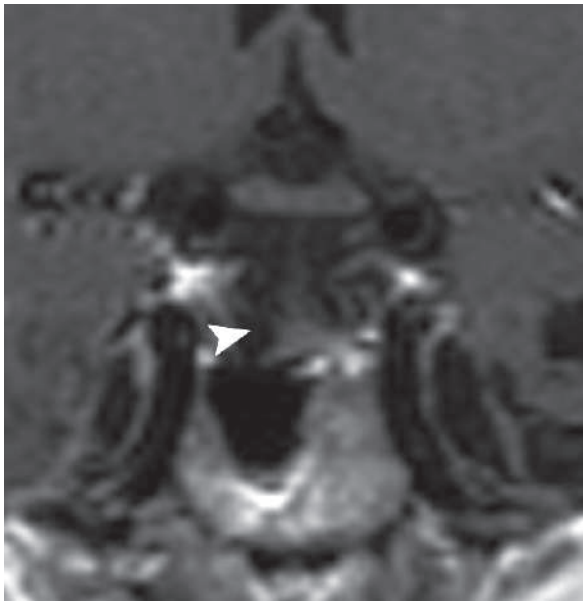

Fig. 2.7.4. Coronal nonenhanced MRI of the sella shows marked reduction of the sellar mass (*arrowhead*), with the pituitary stalk seen dipping in the sella beyond the level of the posterior clinoid process (empty sella)

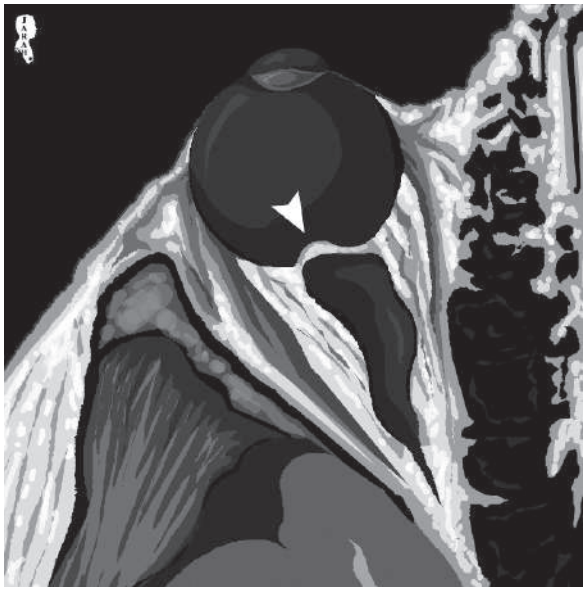

Fig. 2.7.5. Axial orbital T1W MR-illustration demonstrates bulging of the optic disc due to increased intracranial pressure in a patient with pseudotumor cerebri (PTC) (*arrowhead*)

Temporal (Giant) Cell Arteritis

Temporal (giant) cell arteritis is a chronic disease of large and medium-sized vasculitis characterized by granulomatous inflammation of the temporal vessels.

Giant cell arteritis (GCA) is characterized clinically by fever, weakness, anorexia, and headache localized over the area of temporal artery branches. Typically, the area is swollen and the arteries are tender on palpation. The disease is not only confined to the temporal vessels, as the occipital arteries may be affected also. Moreover, vasculitis may affect the central retinal arteries, resulting in partial or complete visual loss (20% of cases).

Up to 30% of patients present with mononeuropathies and peripheral polyneuropathies in the arms or legs. Transient ischemic attack or strokes may rarely occur. Aortic or subclavian stenosis with limb claudication may occur in up to 10–15% of cases. There is unexplained relationship between GCA and polymyalgia rheumatica (PMR). Up to 20% of patients with PMR develop GCA, while more than 50% of patients with GCA have PMR.

Laboratory investigations often show high erythrocytes sedimentation rate and C-reactive proteins reflecting

active inflammatory process. Moderate to severe anemia is characteristically found due to "toxic" suppression of the bone marrow. Biopsy of the temporal artery classically shows vasculitis characterized by predominance of mononuclear-cell infiltrates or granulomatous inflammation, usually with multinucleated giant cells (hence the name).

Signs on Doppler Sonography

- By placing the ultrasound probe over the dilated temporal vessels, the scan typically shows hypoechoic dark halo surrounding the arterial lumen, reflecting edema of the vessel wall.
- The Doppler signal within the artery may show small systolic peak that indicates arterial occlusion or pseudo-occlusion.
- Reduced or missing vessel wall pulsation.

Signs on MRI

Brain MR postgadolinium injection images show characteristic mural enhancement of the temporal arteries with or without the occipital arteries, indicating inflammation (Fig. 2.7.6). In normal situations, the arterial walls show no or mild mural enhancement.

For Further Reading

1. La Mantia L et al Headache and inflammatory disorders of the central nervous system. Neurol Sci. 2004;25:S148–53
2. Alvarez-Cermeno J-C et al Cranial computer tomography in pediatric migraine. Pediatr Radiol. 1984;14:195–7
3. Bousser MG et al Ischemic strokes and migraine. Neuroradiology. 1985;27:583–7
4. Mukhopadhyay S et al Evaluation of headache in children. Paediatr Child Health. 2008;18:1–6
5. Andrew J. Larner. Late onset migraine with aura: how old is too old. J Headache Pain. 2007;8:251–2
6. Haritanti A et al Spontaneous intracranial hypotension. Clinical and neuroimaging findings in six cases with literature review. Eur J Radiol. 2008. doi:10.1016/j.ejrad.2007.10.013
7. Firat AK et al Spontaneous intracranial hypotension with pituitary adenoma. J Headache Pain. 2006;7:47–50
8. Atalar MH et al Spontaneous intracranial hypotension: clinical and magnetic resonance imaging findings. Eur J Radiol Extra. 2004;51:57–60
9. Chiapparini L et al Headache and intracranial hypotension: neurological findings. Neurol Sci. 2004;25:S138–41
10. Christoforidis GA et al Spontaneous intracranial hypotension: report of four cases and review of the literature. Neuroradiology. 1998;40:636–43
11. Lipoton RB et al Classification of primary headaches. Neurology. 2004;63:427–35
12. Güngör K et al Pseudotumor cerebri complicating brucellosis. Ann Opthalmol. 2002;34:67–9
13. Chansoria M et al Pseudotumor cerebri with transient oculomotor palsy. Indian J Pediatr. 2005;72:1047–8
14. Mandelstam S et al MRI of optic disc edema in a childhood idiopathic intracranial hypertension. Pediatr Radiol. 2004;34:362

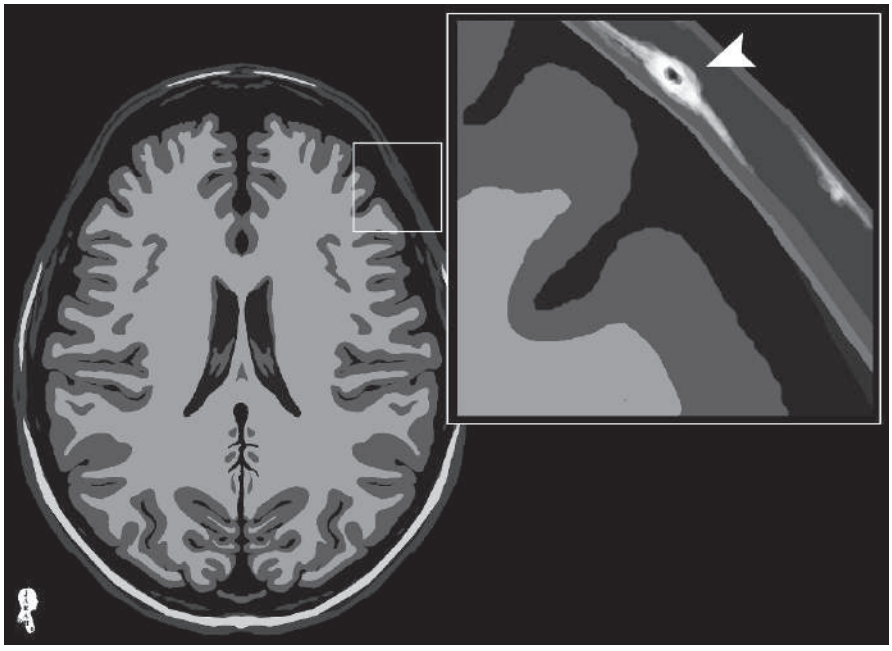

Fig. 2.7.6. Axial brain T1W postcontrast MR-illustration demonstrates mural enhancement of the temporal arteries due to inflammation (giant cell arteritis (GCA))

15. Lewis DW. Headaches in children and adolescents. Curr Probl Pediatr Adolesc Health Care. 2007;37:207–46
16. Seiden AM et al Headache and the frontal sinus. Otolaryngol Clin North Am. 2001;34:227–41
17. Salvarani C et al Polymyalgia rheumatica and giant-cell arteritis. N Engl J Med. 2002;347:261–70
18. Laldinpuii J et al Giant cell arteritis (temporal arteritis): a report of four cases from north east India. Ann Indian Acad Neurol. 2008;11:185–9
19. Reinhard M et al Color-coded sonography in suspected temporal arteritis—experience after 83 cases. Rheumatol Int. 2004;24:340–6
20. Bley TA et al High-resolution MRI in giant cell arteritis: imaging of the wall of the superficial temporal artery. AJR. 2005;184:283–7
21. Kruit MC et al Brain stem and cerebellar hyperintense lesions in migraine. Stroke. 2006;37:1109–12

2.8 Multiple Sclerosis and Other Demyelinating Diseases

Demyelinating disorders are a group of diseases characterized by myelin loss. Normally, the white matter before the myelination process is *hydrophilic* (contains a lot of water), which is detected as high T2 signal intensity and low T1 signal intensity on MRI at birth. After axonal myelination, the white matter becomes *hydrophobic* (contains a lot of fat), producing normal MRI signal as high T1 and relatively low T2 signal intensities. In demyelinating diseases, the normal myelin is lost, making the affected parts of the white matter to be hydrophilic again, producing high signal intensity on T2W images (signal of water).

Multiple Sclerosis

Multiple sclerosis (MS) is a disease of unknown origin characterized by progressive inflammatory demyelinating destruction of the brain and the spinal cord white matter (central nervous system demyelination).

MS is characterized by a remission/regression course, with "dissemination in time and space." The latter sentence means that MS lesions are changing and growing in space as time passes by (in a better or worse clinical course).

MS lesions (plaques) often start around the small venules that penetrate the ependymal layer of the ventricles. These venules are located perpendicular (90°) over the ventricles, making MS plaques classically seen as oval plaques perpendicular to the ventricles because they start around the venules and spread laterally. MS plaques are typically seen in the periventricular white matter, corpus callosum, cerebral peduncles, and spinal cord.

The typical age of incidence is from 10 to 50 years of age. MS usually is not diagnosed before or after this range. Up to 10% of MS case patients have isolated spinal cord injury. Patients present with neurological symptoms according to the area involved. The classical MS patient triad (of Charcot) is scanning speech, intention tremor, and nystagmus (Jerky, back-and-forth movements of the eyes). Internuclear ophthalmoplegia, also known as *medial longitudinal fasciculus syndrome*, is specific eye disease of MS characterized by medial rectus muscle palsy in attempted lateral gaze and monocular nystagmus in the abducting eye with convergence. Internuclear ophthalmoplegia results from demyelination of the medial longitudinal fasciculus. *Uhthoff's phenomenon* is a term used to describe worsening of MS symptoms after an episode of exercise or increased body temperature (e.g., during hot bath).

Criteria for radiological diagnosis of MS (at least three out of the four criteria)

- At least one contrast enhancement plaque, or nine hyperintense lesions on T2W or FLAIR images.
- At least one infratentorial lesion (including spinal cord).
- At least three periventricular lesions
- At least one subcortical lesion

Signs on CT

Multiple hypodense periventricular plaques that enhance after contrast administration (in acute phase only).

Signs on MRI

- Multiple hyperintense T2 signal plaques in the white matter seen classically at the periventricular area along the lateral ventricles and the occipital horns, the internal capsule, the corpus callosum, the pons, and the middle cerebral peduncles (Fig. 2.8.1).
- Contrast ring enhancement occurs in acute stage (remission) of the disease only. Contrast study is not recommended after therapy with intravenous steroid administration as active plaques will usually not enhance.
- Minimal surrounding edema.
- *Gliomatous/Tumefactive MS*: is a MS plaque with a mass effect. The plaque has a mass effect and is enhanced in a ring fashion (ring within a ring), which will be mistaken for a neoplasm or an abscess. Also, the enhanced ring is irregular and the thickness is increased in the side opposite to the ventricle.
- *Dawson's fingers*: they are focal hyperintensities seen on the inferior aspect of the corpus callosum in T2W or FLAIR images (Fig. 2.8.2).
- *Hyperintense dentate nucleus sign*: this sign describes hyperintense dentate nucleus of the cerebellum, usually in a bilateral fashion on T1W nonenhanced images. This sign is described with secondary progressive MS subtype. *Secondary progressive MS subtype* is a term used to describe an MS patient with gradually progressive worsening clinical course without recovery; it is seen in 10% of MS patients.

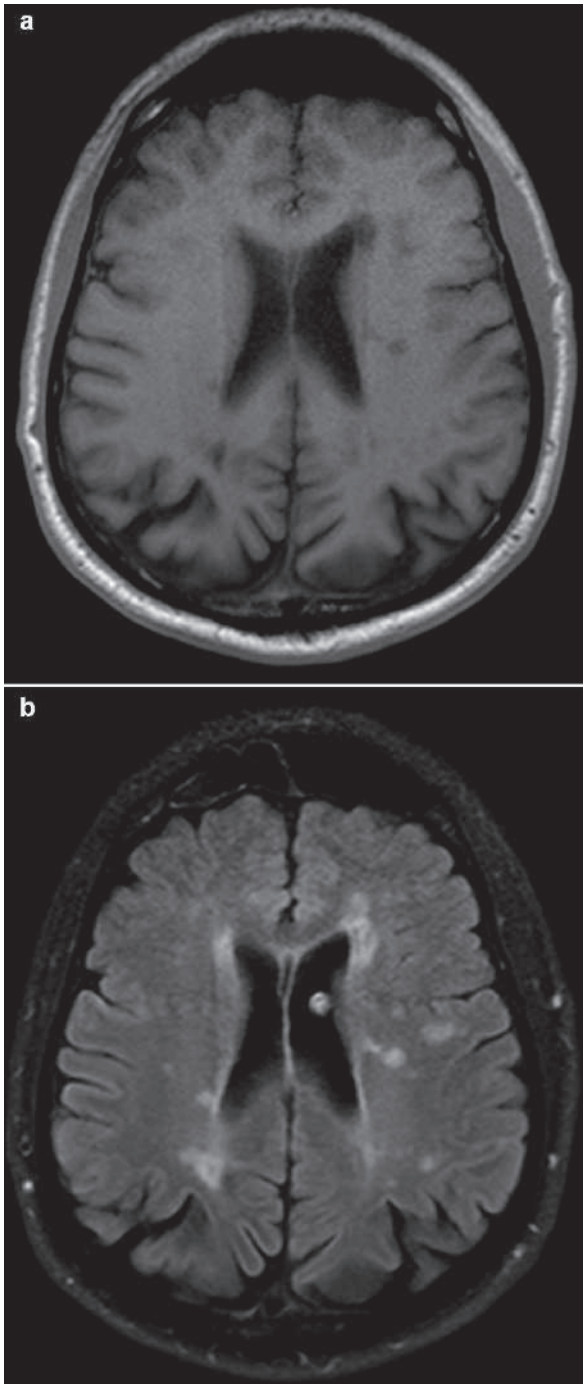

Fig. 2.8.1. Axial T1W (**a**) and FLAIR (**b**) brain MRI in a patient with MS shows classical periventricular white matter lesions (plaques)

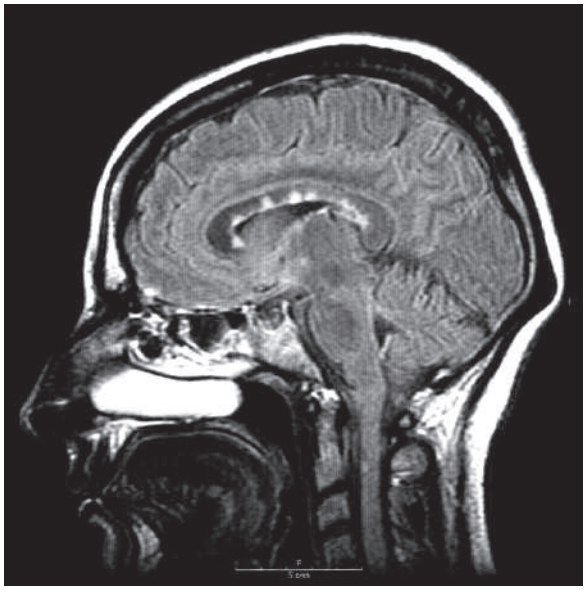

Fig. 2.8.2. Sagittal FLAIR brain MRI shows multiple hyperintense lesions within the corpus callosum starts from the inferior peripheral surface toward the center (Dawson's fingers)

The Concept of Diffusion Tensor MR Imaging

Diffusion tensor imaging (DTI), also known as MR-tractography, is a highly sophisticated MR method to image white matter tracts and fibers. Diffusion is defined as random translational molecular motion (*Brownian motion*) that results from the thermal energy carried by these molecules. Diffusion can be random (isotropic) or directional (anisotropic) depending on the characteristic of the tissue. The routine diffusion-weight imaging (DWI) provides a measure of the water molecules displacement in one direction. Since the white matter fibers are multidirectional, multidirectional DWI is needed. This multidirectional diffusion imaging is expressed by a *diffusion tensor*, which expresses the measurement of water diffusion in different directions.

Diffusivity is a term used to describe water diffusion per unit time. Pathological conditions alter both the diffusivity and the anisotropic diffusion characteristics of water and metabolites. Tissue anisotropy is measured by fractional anisotropy (FA), which represents the directionality of the white matter tracts. DTI results in diffusion-encoded FA map that shows the white matter fibers and tracts. In these maps, bright voxels

2.8

represent high diffusion anisotropy, whereas dark voxels represent low diffusion anisotropy. A color-coded FA map provides the direction of the white matter fibers. Most MRI machines represent *x*-direction (right to left) in red, *y*-direction (anterior-posterior) in green, and *z*-direction (superior-inferior) in blue.

The white matter fibers can be localized anatomically based on their color-coded FA map. The white matter fibers are classified anatomically into:

- *Commissural fibers*: fibers, which connect region of one hemisphere to the other hemisphere (e.g., corpus callosum). These fibers are encoded in red.
- *Association fibers*: fibers, which connect different regions of the cerebral cortex in the same hemisphere (e.g., optic radiation). These fibers are encoded in green.
- *Projection fibers*: fibers, which connect the cerebral cortex to the subcortical structures (e.g., corticospinal tract). These fibers are encoded in blue.

DTI can be used to localize the affected white matter tracts from the nonaffected white matter tracts in a pathological process, information that is so valuable for the neurosurgeon to plan his surgery, so he can avoid removing healthy functioning tracts in cases of brain tumor resection planning. Also, DTI can be used to monitor the therapy and disease progression in diseases with white matter tracts lesions like MS (Fig. 2.8.3) and amyotrophic lateral sclerosis, which mainly affects the corticospinal tract.

Neuromyelitis Optica (Devic's Syndrome)

Neuromyelitis optica (NMO) is an unusual acute fulminant variant of MS characterized by unilateral or bilateral optic neuritis with transverse myelitis. The lesions in NMO affect both gray and white matters (unlike typical MS).

Criteria for NMO diagnosis include:

- *Absolute*: optic neuritis, acute myelitis, with no evidence of clinical disease outside the optic nerve or spinal cord.
- *Major*: negative brain MRI at onset and spinal cord lesions that extend >3 vertebral segments.
- *Minor*: bilateral optic neuritis.

Patients may present initially with paroxysmal tonic spasms that typically last 10–30s due to the transverse myelitis. They are characterized by painful spasm, and usually mistaken with partial seizures. Prognosis is poor, with more than 50% of patients developing severe visual loss within 5 years of disease onset.

Signs on MRI

- Brain MRI is typically normal.
- Extensive spinal cord lesion with high T2 signal intensity and enhancement postcontrast that extends >3 vertebral segments.
- Unilateral or bilateral optic nerve enhancement after contrast administration reflecting optic neuritis.

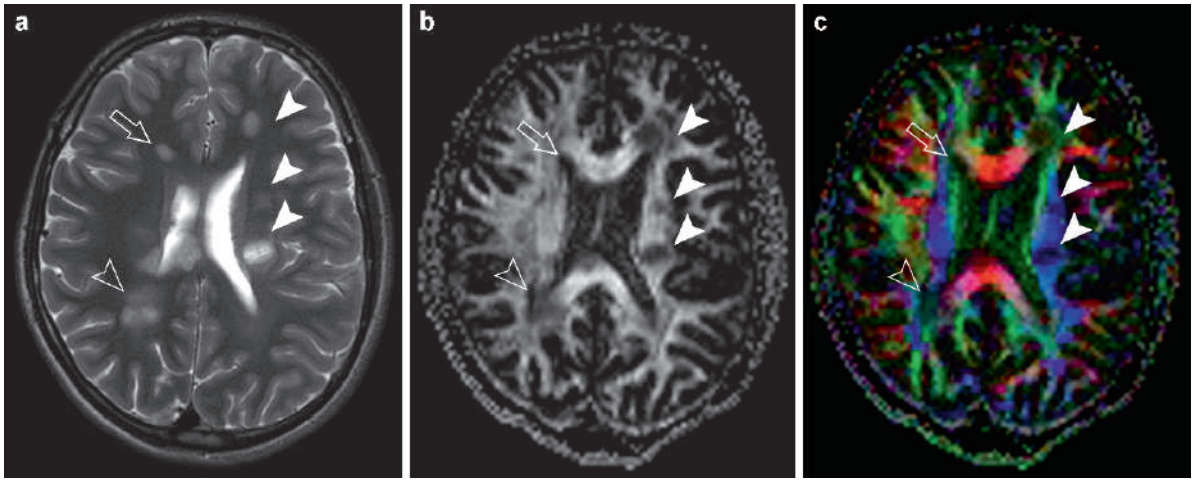

Fig. 2.8.3. Axial T2W brain MRI (**a**), diffusion-encoded FA map (**b**), and color-coded FA map (**c**) of a 16-year-old patient with MS. By comparing (**a**) with (**b**) and (**c**), the MS plaques can be assessed according to the white matter tract affected: the left superior region of corona radiata (*solid arrowheads*), the right forceps minor of corpus callosum (*hollow arrow*), and the right superior region of corona radiata plus the right forceps major of corpus callosum (*hollow arrowhead*)

Marburg's Type MS

Marburg's type MS is an acute, malignant, rapidly deteriorating form of MS that can be lethal within 4 weeks of onset if not treated.

Patients with Marburg's MS usually present with hyperacute onset of multifocal neurological deficits and altered consciousness status in different degrees. Death usually occurs when the disease destroys the brain stem.

The disease is characterized by *monophasic* demyelinating encephalopathy (like ADEM), with fulminant progression if not treated. History of infection or recent vaccination may help to differentiate it from acute disseminated encephalomyelitis (ADEM).

Signs on MRI

Marburg's MS usually is characterized by MS plaques with pressure effect and extensive demyelination (Fig. 2.8.4). Marburg's plaques mimic the tumefactive MS plaques. ADEM plaques in contrast usually are small and located in the periventricular areas.

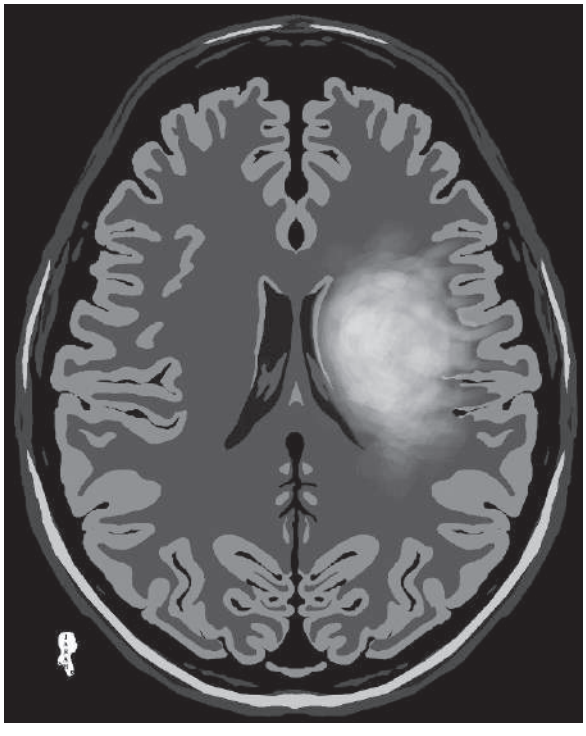

Fig. 2.8.4. Axial FLAIR brain MR-illustration demonstrates large left MS plaque with pressure effect over the lateral ventricle (Marburg's type MS)

Baló Concentric Sclerosis

Baló concentric sclerosis (BCS) is another MS variant characterized by demyelinating plaques like MS, but the main distinctive feature is that these plaques are arranged in concentric layers.

A BCS demyelinating plaque occurs first, and then this plaque is surrounded by a layer of preconditioning proteins at the periphery of the plaque. Later, another demyelinating plaque occurs at the periphery of the protein ring. Then, another protein ring is formed peripheral to the new demyelinating ring as an attempt to contain the demyelination, and so on.

Signs on MRI

The unique pathology sequence of BCS can be clearly appreciated on MRI as a demyelinating plaque with multiple concentric hyperintense and isointense signal intensities on T2W and FLAIR images (Fig. 2.8.5).

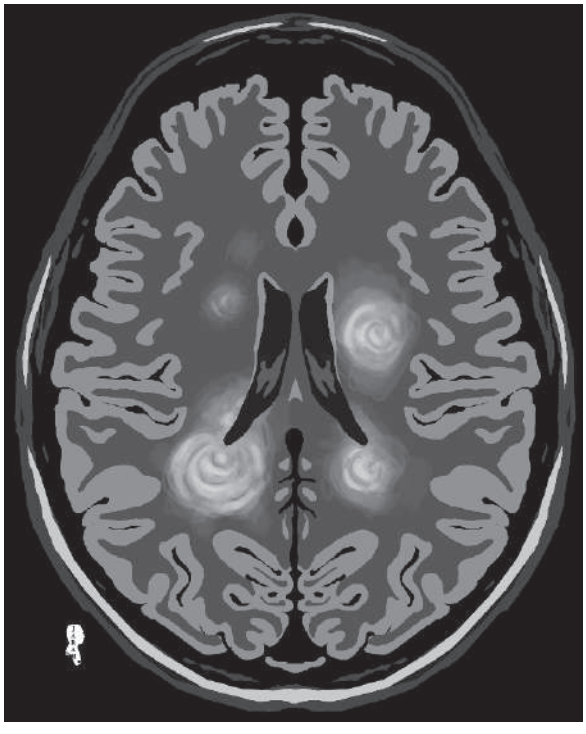

Fig. 2.8.5. Axial FLAIR brain MR-illustration demonstrates the concentric MS plaques of Baló concentric sclerosis (BCS)

2.8

Schilder's Disease (Diffuse Myelinoclastic Sclerosis)

Schilder's disease (SD) is a disease presenting in childhood with progressive, diffuse cerebral demyelination similar to MS.

SD diagnosis is very difficult, because it can be mistaken with other leukodystrophies. Diagnosis of SD can be suggested after exclusion of adrenoleukodystrophy. The typical patient is young female; with MRI picture resembling that of MS. The disease has two types, a self-limiting monophasic type, and a progressive relapsing type.

Signs on MRI

Typically, the lesions of SD are located in the central semiovale, bilaterally, with minimal edema and mass effect (Fig. 2.8.6). After contrast injection, the enhancement is limited to one side of the lesion. The lesions can be solitary or multiple.

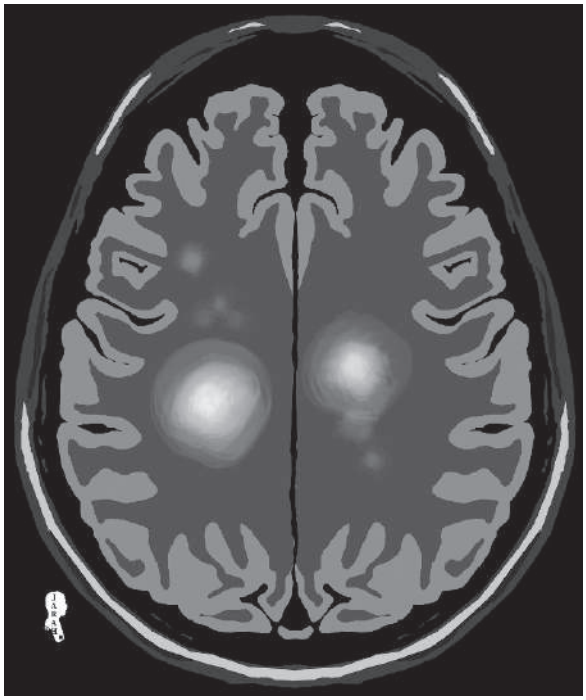

Fig. 2.8.6. Axial FLAIR brain MR-illustration demonstrates the MS plaques of Schilder's disease (SD) located in the centrum semi-ovale bilaterally

Susac's Syndrome

Susac's syndrome is an uncommon disorder characterized by microvascular angiopathy causing encephalopathy, and retinal artery branch occlusion that causes sudden blindness and cochlear hearing loss.

Susac's syndrome is of unknown origin, but autoimmune endotheliopathy theory was suggested to explain its manifestations because it responds to steroid therapy and immunosuppressive therapy. The disease predominantly affects females between 30 and 40 years of age.

Susac's syndrome manifestations usually do not present until advanced stages of the disease. Patients commonly present with the encephalopathy, which include predominantly severe migrainous headache with or without an aura.

The MRI shows multiple lesions that mimic MS and ADEM, leading to it being mistaken for and misdiagnosed with these two common conditions.

Signs on MRI

- Multiple lesions affecting the gray and white matters seen as high signal intensity lesions on T2W and FLAIR images. The lesions enhance after contrast injection (mimicking MS and ADEM).
- The corpus callosum is affected in its central portion by linear or cystic lesions (characteristic and pathognomonic finding) (Fig. 2.8.7).
- Leptomeningeal enhancement is seen in up to 33% of cases.

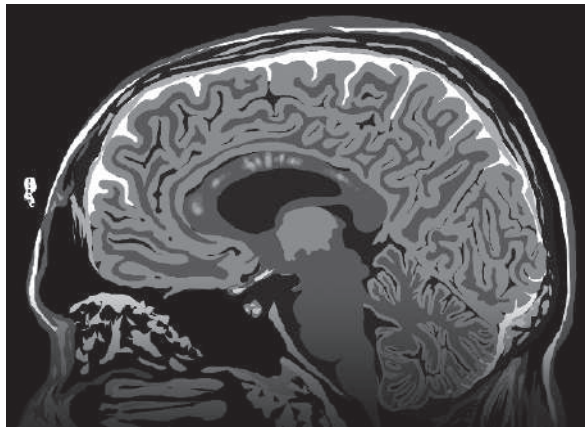

Fig. 2.8.7. Sagittal FLAIR brain MR-illustration demonstrates the characteristic central lesions of the corpus callosum seen in Susac's syndrome

How to differentiate between Susac's syndrome, MS and ADEM?

- Susac's corpus callosum lesions are in the center of the corpus callosum, while the lesions of the corpus callosum in MS (Dawson's fingers) are usually affecting the inferior edges. MS lesions start from the edges toward the center.
- Susac's syndrome affects both gray and white matter, like ADEM, while MS only affects white matter.
- The hearing loss differentiates Susac's syndrome from both ADEM and MS. Both clinical diseases do not present with hearing loss.

Gullian-Barré Syndrome

Gullian-Barré syndrome (GBS) is a disease characterized by acute inflammatory demyelination of the peripheral nervous system, commonly affecting the nerve roots in the conus medullaris and cauda equine.

Patients with GBS classically present with acute areflexic lower limbs flaccid paralysis preceded by respiratory or gastrointestinal infections (e.g., 6 weeks before the onset of symptoms). Infections known to be associated with GBS include *Epstein-Barr virus*, *Mycoplasma pneumoniae*, *cytomegalovirus*, and *Campylobacter jejuni*, GBS has been reported after vaccination, surgery, and head trauma. The paralysis is mainly motor, symmetric, with or without sensory and autonomic disturbances. Up to 50% of patients experience pain, which is described as severe, and occurring with even the slightest of movement.

The disease is caused by autoantibodies-mediated reaction against gangliosides and glycosphingolipids. The diagnosis of GBS is determined mainly by the clinical picture and the cerebrospinal fluid (CSF) findings, which classically show high protein counts in 80% of cases with normal cell count (albuminocytologic dissociation). The role of contrast-enhanced spinal MRI is to exclude other differential diagnosis, or to monitor the treatment response.

GBS weakness reaches a nadir at 2 weeks to 4 weeks after symptom onset. Recovery can be expected within 6–12 months. Some patients have residual paraesthesia or persistent minor weakness. Approximately 7–15% of patients have permanent neurological sequelae. Although GBS is a monophasic disease, about 7–16% of patients suffer recurrent episodes.

GBS have different variants. An example of GBS variant is "*Miller-Fischer syndrome*," which is characterized by ophthalmoplegia, areflexia, and cerebellar ataxia. Another example of GBS variants is "*polyneuritis cranialis*," which is characterized by acute multiple cranial nerves demyelination without spinal cord involvement or involvement of the cranial nerves I and II. Diagnosis of polyneuritis cranialis requires exclusion of other causes of multiple cranial nerves palsies (e.g., Garcin's syndrome).

Differential Diagnoses and Related Diseases

Garcin's syndrome (Hemibase syndrome): is a very rare syndrome characterized by progressive, unilateral, almost complete paralysis of the cranial nerves due to nasopharyngeal tumor, which invade the skull base and do not affect the brain itself. This disease is seen with cases of tonsillar carcinoma, nasopharyngeal carcinoma, and carcinoma of the base of the skull. Also, it can be caused by invasive infections (e.g., mucormycosis), and paraneoplastic syndromes. MRI typically reveals invasive carcinoma of the skull base or infection that affects the cranial nerves and invades their foramina.

Signs on Brain and Spinal MRI

- Classically, GBS shows thickened nerve roots in the conus medullaris and cauda equine with marked enhancement after contrast injection (Fig. 2.8.8). Normally, the nerve roots ganglia in the cauda equine and the conus medullaris do not enhance with gadolinium due to the intact blood–brain barrier. Abnormal enhancement of the nerve roots ganglia after gadolinium injection is a pathological process that is seen in GBS, arachnoiditis, sarcoidosis, lymphoma, and AIDS-related polyradiculopathy. Due to the previous fact, GBS is essentially diagnosed by the clinical picture and the CSF analysis. The spinal MRI supports the diagnosis.
- Miller Fisher syndrome classically shows a lesion affecting the brain stem (e.g., glioma).
- Polyneuritis cranialis cerebral MRI shows enhancement of multiple cranial nerves except the cranial nerves I and II.

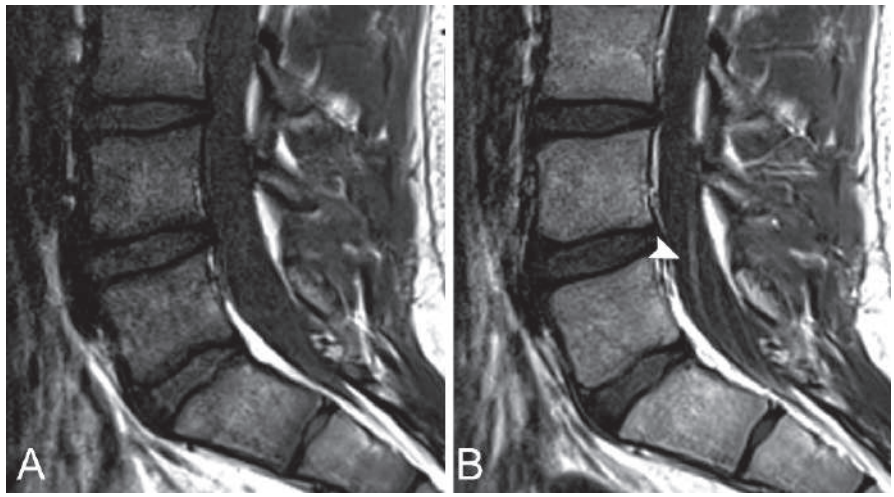

Fig. 2.8.8. Sagittal T1W (**a**) and T1W postcontrast (**b**) spinal MRI in a 10-year-old boy with flaccid lower limbs and motor deficits shows enhancement of the nerve roots of the cauda equina after contrast injection due to polyneuritis (*arrowhead*)

For Further Reading

1. Bielekova B, Kadom N et al MRI as a marker for disease heterogeneity in multiple sclerosis. Neurology. 2005;65: 1071–6
2. Houtchens MK et al Thalamic atrophy and cognitive in multiple sclerosis. Neurology. 2007;69:1213–23
3. González Sánchez JJ et al A case of malignant monophasic multiple sclerosis (Marburg's disease type) successfully treated with decompressive hemicraniectomy. J Neurol Neurosurg Psychiatry. 2008. doi:10.1136/jnnp.2007. 142133
4. Johnson MD et al Fulminant monophasic multiple sclerosis, Marburg's type. J Neurol Neurosurg Psychiatry. 1990;53: 918–21
5. Schwarz U et al Marburg's encephalitis in a young woman. Eur Neurol 2002;48:42–4
6. Capello E et al Marburg type and Baló concentric sclerosis: rare and acute variants of multiple sclerosis. Neurol Sci. 2004;25:S361–63
7. Hanemann CO et al Baló concentric sclerosis followed by MRI and positron emission tomography. Neuroradiology. 1993.;35:578–80
8. Hulcombe JE et al Baló concentric sclerosis. J Clin Neurosci. 1999;6:46–8
9. Fitzgerald MJ et al Recurrent myelinoclastic diffuse sclerosis: a case report of a child with Schilder's variant of multiple sclerosis. Pediatr Radiol. 2000;30:861–5
10. Barbareschi M et al Schilder disease (1912): report of a case. Ital J Neurol Sci. 1988;9:157–60
11. Kastrup O et al Balo's concentric sclerosis demonstrated by MRI. Neurology. 2001;57:1610
12. Erer S et al The first Susac's syndrome case in Turkey. J Neurol Sci 2006;251:134–7
13. Murata Y et al Susac syndrome. Am J Opthalmol. 2000; 129:682–4
14. Maddestra M et al Encephalopathy, hearing loss and retinal occlusions (Susac's syndrome): a new case. Ital J Neurol Sci. 1998;19:225–7
15. Eluvathingal Muttikkal TJ et al Susac syndrome in a young child. Pediatr Radiol. 2007;37:710–3
16. Jacob A et al Neuromyelitis optica. Ann Indian Acad Neurol. 2007;10:231–9
17. Wingerchuk DM et al Neuromyelitis optica: clinical predictors of a relapsing course and survival. Neurology. 2003; 60:848–53
18. Wingerchuk DM et al The clinical course of neuromyelitis optica (Devic's syndrome). Neurology. 1999;53:1107–14
19. Hahn CD et al MRI criteria for multiple sclerosis: evaluation in a pediatric cohort. Neurology. 2004;62:806–8
20. Li DKB et al MRI T2 lesion burden in multiple sclerosis: a plateauing relationship with clinical disability. Neurology. 2006;66:1384–9
21. Humm AM et al Quantification of Uhthoff's phenomenon in multiple sclerosis: a magnetic stimulation study. Clin Neurophysiol. 2004;115:2493–501
22. Iwata E et al MR imaging in Gullian-Barré syndrome. Pediatr Radiol. 1997;27:36–8
23. Alkan O et al Spinal MR findings of Gullian-Barré syndrome. Radiol Case. Mar 2009; 3:25–8
24. Vucic S et al Gullian-Barré syndrome: an update. J Clin Neurosci. 2009. doi:10.1016/j.jocn.2008.08.033
25. Morosini A et al Polyneuritis cranialis with contrast enhancement of cranial nerves on magnetic resonance imaging. J Paediatr Child Health. 2003;39:69–72
26. Gupta SS et al Pictorial essay: neurological application and physics of diffusion tensor imaging with 3D fiber tractography. Indian J Radiol Imaging. 2008;18:37–44
27. Bougias C et al Theory of diffusion tensor imaging and fiber tractography analysis. Eur J Radiogr. 2009;1:37–41
28. Filippi M et al Diffusion tensor magnetic resonance imaging in multiple sclerosis. Neurology. 2001;56:304–11
29. Roccatagliata L et al Multiple sclerosis: hyperintense dentate nucleus on unenhanced T1-weighted MR images is associated with the secondary progressive subtype. Radiology. 2009;251:503–10

2.9 Parkinsonism

Parkinsonism, previously known as "*paralysis agitans*," is a motor disease characterized essentially by resting tremor, rigidity, and poverty of spontaneous movements (bradykinesia).

Parkinsonism essentially arises due to nerve cell degeneration affecting the pigmented cells in the substantia nigra (release dopamine), and the cells within the caudate nucleus and putamen (striatum). Neurofilaments eosinophilic inclusions within the neurons in patients with Parkinsonism are called (Lewy bodies).

Causes of Parkinsonism can be: idiopathic (Parkinson's disease), postencephalitic (e.g., encephalitis lethargica), or drug-induced (e.g., metoclopramide). *Pseudoparkinsonism* is a term used to describe Parkinsonism that arises due to arteriosclerosis of the vessels supplying the striatum with perivascular hemorrhages and glial proliferation. It is usually found to affect the older population more than other Parkinsonisms (>60 years). *Hemiparkinsonism* is a term used to describe Parkinsonism features of progressive space occupying lesion. Other causes of Parkinsonism include brain trauma (e.g., boxers), and Wilson's disease (excess deposition of copper within the liver due to deficiency in its carrier ceruloplasmin).

As previously mentioned, the cardinal clinical manifestations of Parkinsonism include: resting tremor, rigidity, and bradykinesia. Resting tremor initially starts unilaterally as a relatively rhythmic alteration contraction of opposing groups of muscles. Tremor initially starts in the distal muscles, affecting the fingers and the hand. *Pill-rolling movement* is a term used to describe characteristic tremor movement, where the thumb repetitively moves on the first two fingers with wrist motion. This tremor characteristically is seen from 2 to 6 seconds. Other areas that may be affected by tremor include the jaw, tongue, and lips. Parkinsonism tremor is characteristically visualized at rest. It disappears as the patient starts to do a voluntary movement, or during sleep.

Rigidity is a term that describes a state of steady muscular tension equal in degree in the opposing muscle groups. This muscular tension is constant whether the limb is moved slowly or rapidly, this phenomenon is described as "*lead pipe resistance*." Sometimes when the rigid limb is moved passively, the examiner can feel a jerky intermittent resistance and the muscles seem to give way in a series of steps, a phenomenon known as "*cogwheel rigidity*."

Bradykinesia can be observed in many aspects along the disease progression. There is loss of the normal swinging of the arms while walking, reduced facial movements (masked-face), loss of eye blinking, difficulty in initiating smile, narrow-steps shuffling gait, and cervical and lumbar flexion in the standing position. The writing is shaky and tremulous, and characteristically gets smaller as the patient continues to write (micrographia). The speech articulation is disturbed and slurred, with monotone soft voice. Involuntary repetition of words or phrases (palilalia) may be seen. Sensory and deep reflexes are characteristically preserved in Parkinsonism. However, exaggerated orbicularis oris (snout) and orbicularis oculi (glabellar) reflexes are often exaggerated. Tapping on the glabella (forehead) may initiate repetitive eye blinking due to exaggerated reflexes (Myerson's sign).

Camptocormia is a rare postural involuntary posture of the trunk characterized by an extreme forward flexion of the thoracolumbar spine induced by walking, standing, or sitting that disappears while the patient is lying supine. Camptocormia can be seen in patients with Parkinsonism, and it is caused by severe paraspinal muscles atrophy.

Mental status changes in Parkinsonism may include depression (30%), slowness of memory, and global dementia in advanced stages of the disease (20%).

Postencephalitis Parkinsonism shows the same clinical features as Parkinson's disease (idiopathic form). However, postencephalitis Parkinsonism is characterized by some features that are not usually seen in Parkinson's disease. The cogwheel phenomenon is markedly observed in postencephalitis Parkinsonism. Autonomic nervous system disturbance with drooling of saliva (sialorrhea) and excessive sweating (hyperhidrosis) are commonly associated with postencephalitis Parkinsonism. Hypothalamic disturbance with increased appetite, with development of diabetes mellitus and diabetes insipidus are more observed with postencephalitis Parkinsonism. Moreover, two important ocular manifestations are observed in postencephalitis Parkinsonism that are not usually seen in Parkinson's disease: oculogyric crises and blepharospasm. *Oculogyric crises* are attacks of involuntary

conjugate upward deviation of the eyeballs, whereas *blepharospasm* is a period in which the eyes go nearly or completely shut, causing the patient to be virtually blind during this episode.

2.9

Differential Diagnoses and Related Diseases

Stiff man syndrome: is a rare disorder characterized by truncal and proximal limbs rigidity, sporadic spasm, and continuous motor unit activity (CMUA) even at rest. The disease is rare with an incidence of <1 per million in the general population. Stiff man syndrome diagnostic criteria include: stiffness and rigidity in the axial muscles, abnormal axial posture (exaggerated lumbar lordosis), and spasm precipitated by voluntary movement or emotions, CMUA in at least one group of muscles, and absence of brain stem, pyramidal, extrapyramidal, or lower motor neurons signs. The stiff man syndrome can be seen in cases of syringomyelia, tetanus, diabetes mellitus type 1, and Hashimoto's thyroiditis. Up to 5% of cancers may precipitate stiff man syndrome (e.g., small cell carcinoma of the lung).

Signs on MRI

- Generalized brain atrophy with prominent subarachnoid spaces.
- T2W hypointense areas in the putamen and the substantia nigra may be seen due to iron deposition (siderosis). (Fig. 2.9.1).
- Atrophy of the midbrain, cerebellum, and medulla can occur.
- In Camptocormia patients, sever paraspinal muscles atrophy with fatty changes in the thoracolumbar region can be seen.

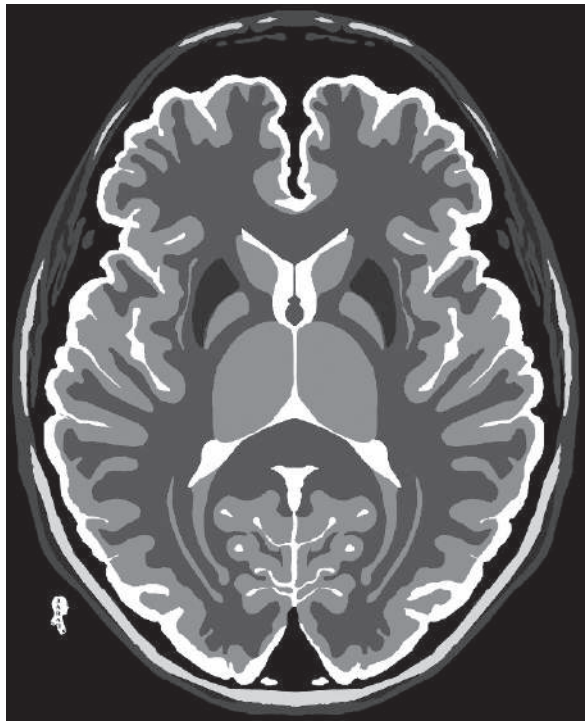

Fig. 2.9.1. Axial T2W brain MR-illustration demonstrates low signal intensity of the putamen bilaterally, a sign of Parkinson disease

For Further Reading

1. Bonneville F et al Camptocormia and Parkinson's disease: MR imaging. Eur Radiol. 2008;18:1710–1719
2. Fowler CJ. Update on the neurology of Parkinson's disease. Neurol Urodyn. 2007;26:103–9
3. Benabid AL et al Deep brain stimulation of subthalamic nucleus for the treatment of Parkinson's disease. Lancet Neurol. 2009;8:67–81
4. Agid Y et al Biochemistry of Parkinson's disease 28 years later: a critical review. Mov Disord. 1989;4:S126–44
5. DeJong RN. Parkinsonism. Dis Mon. 1961;7:1–39
6. Brown P et al The stiff man and stiff man plus syndromes. J Neurol. 1999;246:648–52
7. Andereadou E et al Stiff person syndrome: avoiding misdiagnosis. Neurol Sci. 2007;28:35–7
8. Gupta P et al Akinetic rigid syndrome: an overview. Ann Indian Acad Neurol. 2007;10:21–30

2.10 Dementia

Dementia is a multifactorial disease characterized by deterioration of the cognitive brain functions. Memory is the most common cognitive brain function lost in dementia. Each brain lobe or region processes different neurological and psychological functions, which can be affected according to the disease causing dementia. The occipital lobe is responsible for the visual activities and processing; the parietal lobe is responsible for spatial navigation; the temporal lobe is responsible for language and memory functions; whereas the frontal lobe is responsible for strategic planning, logic, planning, and social judgment.

The hippocampus is a critical structure for long-term memory storage. Emotions have a powerful influence on learning and memory, and they are controlled by the limbic system.

The limbic system is a complex brain network that controls emotions. It was first described by James Papez in 1937 (Papez circuit), and later was completed by Yakovlev in 1948 (Yakovlev circuit). The limbic system is generally composed of five main structures:

- *Limbic cortex*: include the cingulated gyrus and the parahippocampal gyrus. The cingulated gyrus in Latin means "belt bridge."
- *Hippocampal formation*: include the dentate gyrus, the hippocampus, and the subocular complex.
- *Amygdala*: it is an almond-shaped structure located deep within the temporal lobe beneath the uncus. It controls fear emotions. Amygdala, in conjunction with prefrontal cortex, is involved in retrieval of emotional memories.
- *Septal area*: is a gray matter structure that lies immediately above the anterior commissure of the corpus callosum, with extensive reciprocal connections with the hippocampus via the fornix.
- *Hypothalamus*: is subdivided into three regions form anterior to posterior: the supraoptic region, the tuberal region (tuber cinereum), and the mammillary bodies.

Alzheimer's Disease

Alzheimer's disease (AD) is a disease characterized by diffuse cortical brain atrophy with enlargement of the ventricular system.

AD is the most common cause of dementia, and is found in up to 10% of all persons >70 years of age with significant memory loss. The disease is caused by deposition of A amyloid in the neuronal cytoplasm and the cerebral vascular walls. The most important risk factors for AD are old age and a positive family history. *Presenile Alzheimer's disease* is a term used to describe AD that develops in patients <65 years old.

AD starts with memory loss that progress into language and visual-spatial deficits. Memory loss can interfere with the daily activities such as following job instructions or driving. In later stages, loss of judgment and reason often develop. Delusions are common in the later stages of the disease, with 10% of patients likely to develop Capgras syndrome. *Capgras syndrome* is a form of delusion where the patient believes that a person has been replaced by one or more imposers. The delusion is specific to one person, usually the patient's closest relative.

Signs on CT and MRI

- In AD, there is generalized brain atrophy, with bilateral atrophy of the medial temporal lobe and parietal lobe, which are the hallmark signs of AD (Fig. 2.10.1). Usually, there is enlargement of the temporal horns of the lateral ventricles due to parenchymal loss of volume (Fig. 2.10.1).
- In presenile AD, there is striking parietal lobe atrophy with mild medial temporal lobe atrophy. In contrast, in the classical AD, medial temporal lobe atrophy is the hallmark pathology.

2.10

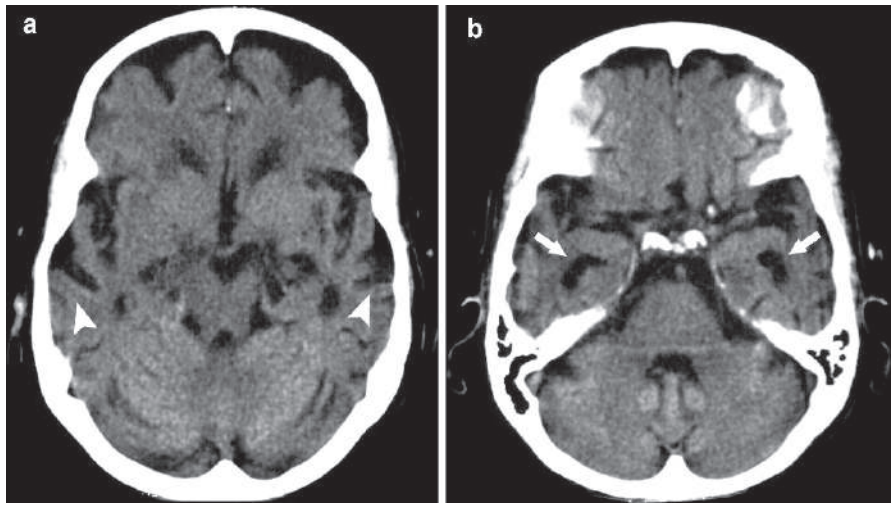

Fig. 2.10.1. Axial sequential brain CT images of a patient with Alzheimer's disease show generalized brain atrophy, medial temporal lobe atrophy bilaterally in (**a**) (*arrowheads*), bilateral frontal lobe atrophy in (**a**), dilatation of the temporal horns of the lateral ventricles in (**b**) (*arrows*), and dilated pre-pontine cistern in (**b**)

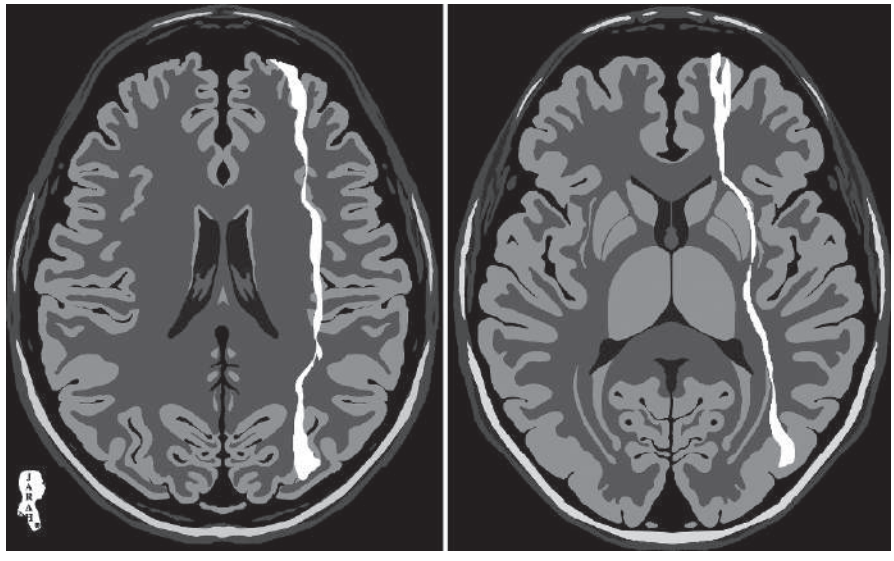

Fig. 2.10.2. Axial FLAIR brains MR-illustrations demonstrate the watershed zones (*white lines*)

Vascular Dementia

Vascular dementia (VaD) is a term used to describe dementia that develops due to vascular lesions involving Papez circuit. *Papez circuit* fibers include the fornix, mammillary bodies, mammillothalamic tracts, cingulated cortex, and anterior thalami. Lesions involving Papez circuit projections result in memory disturbance.

VaD is the second most common cause of dementia after AD, and is differentiated from AD by its sudden onset, usually after vascular insult. Stroke is the most common cause of VaD. Two types of strokes are often linked to VaD: watershed infarctions, and strategic infarctions.

Watershed infarctions occur between two or three vascular territories (Fig. 2.10.2). Anterior watershed infarction is located between the anterior cerebral artery (ACA) and the middle cerebral artery (MCA) territories. Posterior watershed infarction is located between MCA and the posterior cerebral artery (PCA) territories. Internal watershed infarction is located between ACA, MCA, and PCA territories. Watershed infarctions are caused by severe occlusion or stenosis

of the internal carotid artery, microemboli, or hypotension. Bilateral watersheds infarctions are typically caused by severe brain hypovolemia.

Strategic infarctions occur in areas important for normal cognitive function of the brain. Examples of strategic infarctions include:

- Angular gyrus and parieto-temporal area (MCA) infarction.
- Paramedian thalamic area (PCA) infarction.
- Superior frontal or parietal area infarction.
- Bilateral thalamic area infarction.

Frontotemporal Lobar Degeneration (Pick's Disease)

Frontotemporal dementia (FTD) is a group of progressive neurodegenerative diseases that include three syndromes: frontal variant FTD, progressive nonfluent aphasia, and semantic dementia.

FTD is the third most common cause of dementia after AD and dementia with Lewy bodies (DLB). It constitutes 5–15% of all cases of dementia.

Interestingly, studying FTD patients with artistic painting skills revealed development of new visual artistic skills during their illness. In FTD, the posterior parietal and temporal cortices are not frequently affected. These areas mediate the visuospatial and visuoconstructive skills important for drawing, painting, and copying. These new enhanced artistic skills are believed to be attributed to loss of inhibitory activity over the posterior parieto-temporal regions involved in visuospatial and visuoconstructive processes.

Signs on MRI

- There is marked atrophy of the frontal and/or the temporal lobes. Frontal lobe atrophy is the hallmark FTD (Fig. 2.10.3).
- Another characteristic finding is asymmetric atrophy of the temporal lobe in one hemisphere, resulting in temporal gyri that appear as sharp as knifes "knife blade atrophy" (Fig. 2.10.4). Areas of high signal intensity on FLAIR images might be found, presumed to be gliotic changes.

Dementia with Lewy Bodies

DLB is a rare neurodegenerative disorder with features of Parkinsonism (e.g., motor dysfunction) and AD (e.g., dementia).

Current diagnostic criteria of DLB include cognitive impairment with predominant visuospatial dysfunction, recurrent visual hallucinations, and Parkinsonism. Visual hallucinations differentiate DLB from classical Parkinson's disease.

DLB accounts for 25% of cases of dementia. Pathologically, the disease is characterized by deposition

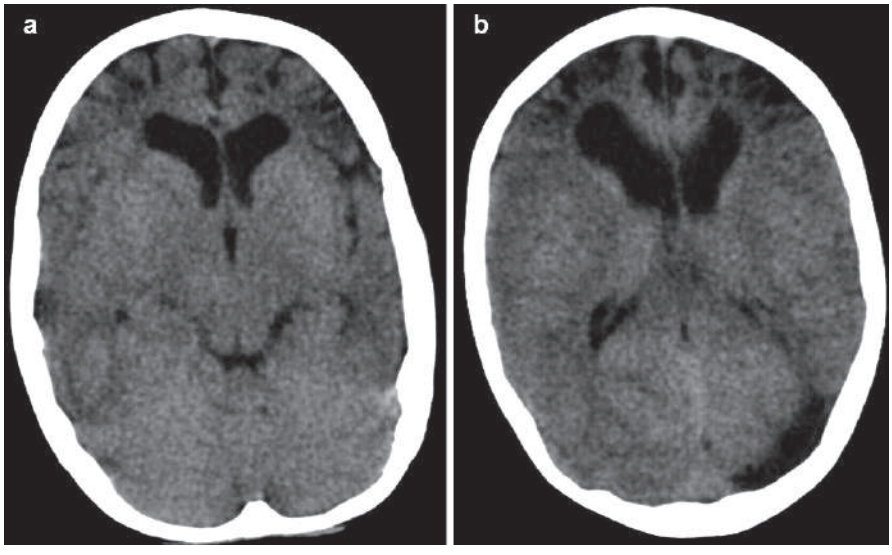

Fig. 2.10.3. Axial sequential brain CT images of a patient with frontotemporal dementia (FTD) show bilateral frontal lobes atrophy with dilatation of the anterior horns of the lateral ventricles

2.10

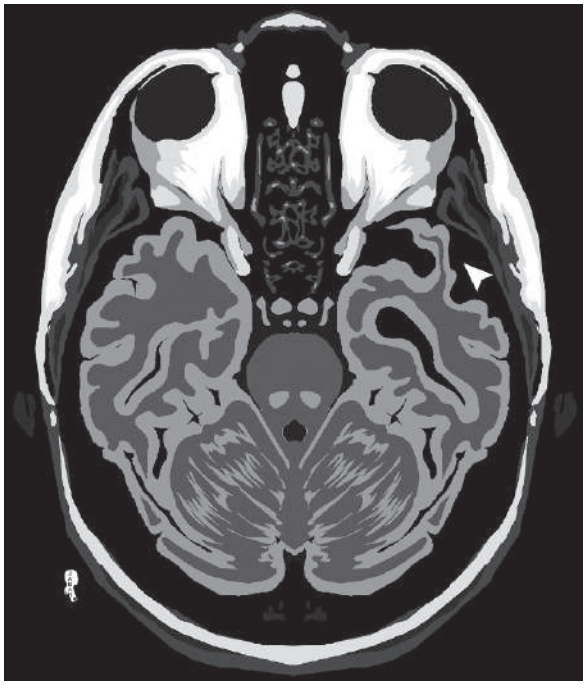

Fig. 2.10.4. Axial FLAIR brains MR-illustrations demonstrate left knife blade temporal atrophy commonly seen in FTD (*arrowhead*)

of Lewy bodies in the hippocampus and subcortical nuclei.

Progressive Supranuclear Palsy (Steele-Richardson-Olszewski Syndrome)

Progressive supranuclear palsy (PSP) is a neurodegenerative, Parkinsonian syndrome characterized by supranuclear vertical gaze palsy, balance disturbance, and limited response to L-dopa.

Early stages of SPS are not usually distinguishable from the classical Parkinson's disease. However, PSP neural deterioration occurs much faster than Parkinson's disease, with many patients dying within 6–7 years from the onset of symptoms. Death is often due to pneumonia, with dysphagia arising in the early stages of PSP. Vertical gaze palsy distinguishes PSP from DLB. Also, DLB is characterized by visual hallucinations, which are not part of the diagnostic criteria of PSP.

In PSP, patients typically present with truncal or neck rigidity, with absence or with only mild limb involvement and impaired postural reflexes leading to backward falls. Moreover, limb rigidity and bradykinesia develop in a symmetrical fashion. Resting tremor is uncommon. A patient with the past clinical picture with vertical gaze palsy should assist establishing the PSP diagnosis from Parkinson's disease.

Signs on MRI

The MRI shows three characteristic changes: atrophy of the anterior cingulated gyrus, atrophy of the corpus callosum trunk, and atrophy of the midbrain tegmentum resulting in convexity of its border referred to as "humming bird sign" (Fig. 2.10.5).

Multiple System Atrophy (Shy-Drager Syndrome)

Multiple system atrophy (MSA) is a rare disease characterized by Parkinson-like syndrome, and degeneration of three systems (autonomic, cerebellar, and extrapyramidal). When atrophy affects the autonomic nervous system mainly, the disease is called *Shy-Drager syndrome*.

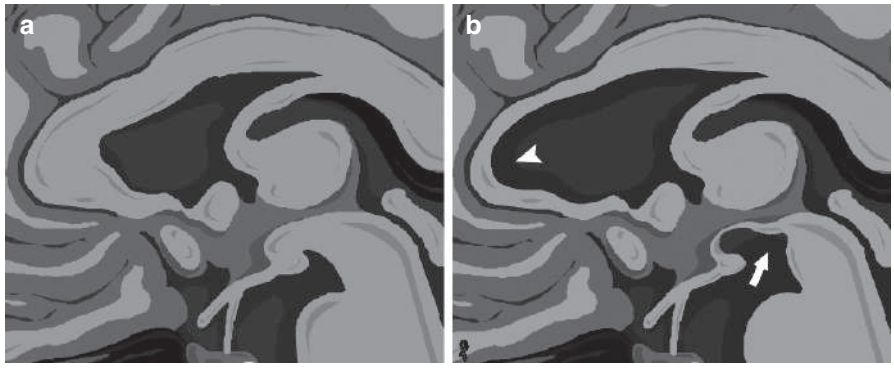

Fig. 2.10.5. Sagittal T1W brain MR-illustrations demonstrate normal brain stem with corpus callosum (**a**) and atrophied anterior part of the corpus callosum in (**b**) (*arrowhead*) with atrophied brain stem tegmentum in the form of the classical humming bird sign (*arrow*)

MSA arises typically due to olivo-ponto-cerebellar atrophy and striato-nigral degeneration. Postmortem findings in MSA reveal gliosis and/or neuronal loss in substantia nigra, putamen, caudate nuclei, cerebellar cortex, pontine nuclei, and inferior olive.

Patients with MSA first show signs of Parkinson's disease in their forties, do not respond to antiparkinsonian medications, and usually succumb to the disease 7–10 years after symptoms onset.

Signs on MRI

- There is characteristic atrophy of three regions: putamen, pons, and cerebellum (the three systems).
- characteristic pontine hyperintensity in a cross pattern referred to as "*hot cross bun sign*" may be seen, and it is characteristic of this disease (Fig. 2.10.6).
- Abnormal decreased signal in the putamen on T1W and T2W images can be found.

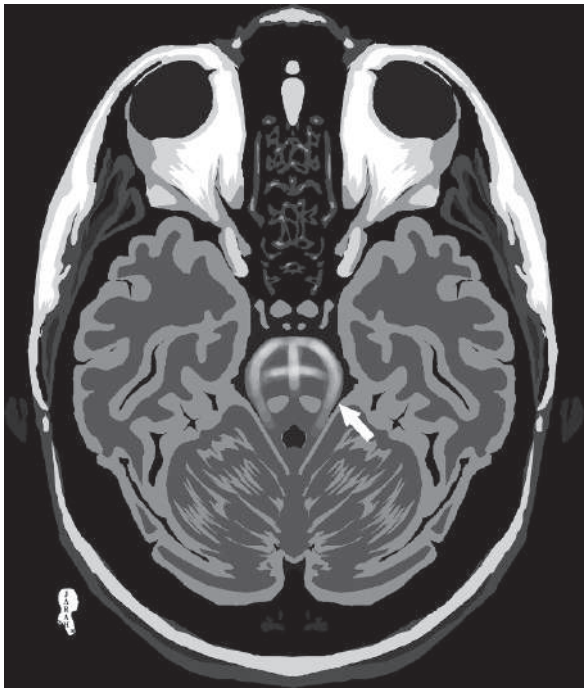

Fig. 2.10.6. Axial FLAIR brains MR-illustrations demonstrate the characteristic "hot cross bun" sign of the multiple system atrophy (MSA) disorder (*arrow*)

Subcortical Arteriosclerotic Encephalopathy (Binswanger Disease)

Subcortical arteriosclerotic encephalopathy (SAE) is a disease characterized by dementia due to arteriosclerosis and occlusion of the deep perforating cerebral arteries and their branches.

SAE is characterized by multiple, microinfarctions, focal or diffuses demyelination and gliosis of the periventricular area. Patient usually presents between 40 and 60 years of age with a history of chronic hypertension and multiple strokes episodes. Lack of interest, alteration in mood and personality with loss of appetite for social conducts are among the psychiatric symptoms of the disease. It may be difficult to distinguish Binswanger's disease from AD and other vascular dementias.

Signs on MRI

- Diffuse periventricular white matter T2 hyperintense signal, ventricular dilatation, and signs of anterior brain atrophy (Fig. 2.10.7). The white matter lesions can be mistaken for multiple sclerosis. However, these lesions characteristically fall in the border between two different vascular supplying systems.
- There may be T2 hyperintense signal in the basal ganglia, centrum semi-ovale, and brain stem representing old lacunar (micro) infarctions and Virchow-Robin spaces dilatation surrounding the perforating arteries (etat-crible). *Virchow-Robin (VR) spaces* are perivascular spaces surrounding the walls of vessels as they course from the subarachnoid space through the brain parenchyma. VR spaces surround the walls of arteries, arterioles, and venules. Cerebral veins are not surrounded by VR spaces. VR spaces <2 mm are found normally in all age groups. As age advances, larges VR spaces >2 mm in diameter can be found. VR spaces can be seen as normal variants, or part of pathologies (e.g., CADASIL). They are typically seen in the basal ganglia, parallel to the ventricles, and in the midbrain. VR spaces show cerebrospinal fluid signal on MR images (Fig. 2.10.8). Rarely, VR spaces can present with bizarre cystic lesion with pressure over the adjacent structures, which maybe mistaken for cystic tumors (e.g., pilocystic astrocytoma).

2.10

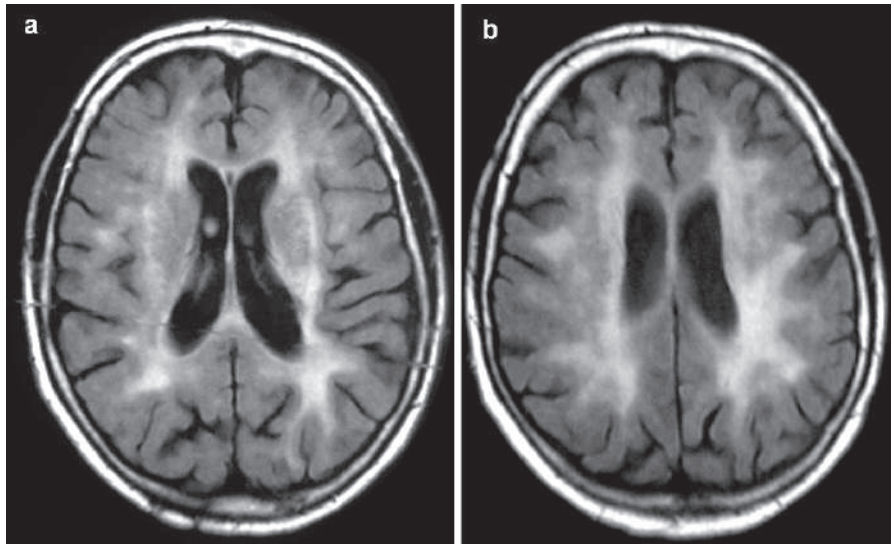

Fig. 2.10.7. Axila sequential FLAIR brain MRI of a patient with chronic hypertension and dementia shows bilateral symmetrical periventricular white matter diffuse hyperintense signal intensities with mild ventricular dilatation bilaterally without signs of brain atrophy (subcortical arteriosclerotic encephalopathy (SAE))

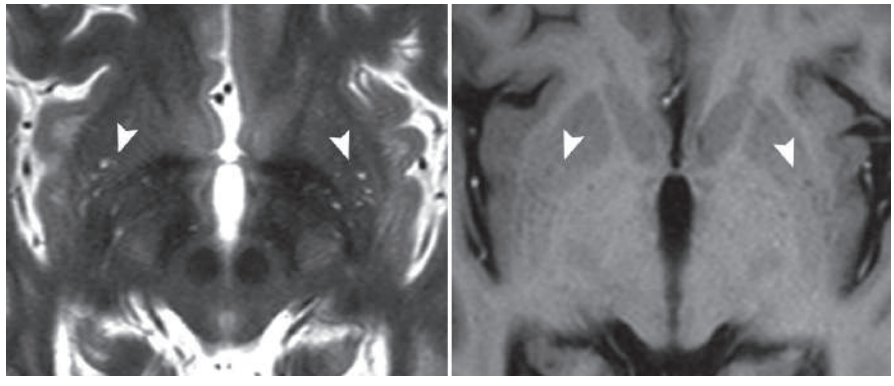

Fig. 2.10.8. Coronal T2W (**a**) and T1W (**b**) MRI shows Virchow-Robin spaces dilatation surrounding the perforating arteries (état criblé) (*arrowheads*)

Prion Disease

Prion disease, also known as transmissible spongiform encephalopathy, is a group of rare diseases characterized by cognitive dysfunction (dementia), psychiatric symptoms, and variable central nervous system manifestations.

Prion diseases can be found in both animals and human beings. In animals, major prion diseases include chronic wasting disease in deer and elks, scrapie in sheep and goats, and bovine spongiform encephalopathy (BSE) in cattle, notoriously known as "mad-cow disease." In human beings, prion diseases include Creutzfeldt-Jakob disease (CJD), Gerstmann-Sträussler-Scheinker disease (GSS), fatal familial insomnia (FFI), and Kuru. Human prion diseases are divided into three main categories according to their etiology:

- *Sporadic (most common)*: sCDJ.
- *Inherited*: fCDJ, GSS, FFI.
- *Acquired by infections*: vCDJ.

Gerstmann-Sträussler-Scheinker disease is an autosomal dominant, rare prion disease characterized by progressive spinocerebellar dysfunction, ataxia, spastic paraparesis, and dementia.

FFI is an autosomal dominant prion disease characterized by progressive untreatable insomnia, dysautonomia, and motor signs. MRI in patients with FFI typically shows hypothalamic lesions, which is the hallmark of this disease.

Kuru is a disease confined to the Fore linguistic group, a tribe in Papua-New Guinea. Kuru is a prion disease linked to ritual tribal cannibalism. The word Kuru in Fore language means "to tremble or to shake." The disease is also known as "laughing disease"

because the patients present with headache, ataxia, trembling limbs, and laughing or crying episodes without a prior reason.

CJD is a neurodegenerative prion disease with four main forms:

- *Sporadic CJD (sCJD)*: this is the most common form, with an incidence of 1–1.5 per million of population.
- *Familial CJD (fCJD)*: this is a rare form due to mutation in the PrP gene.
- *Iatrogenic CJD (iCJD)*: this form is related to neurosurgeries with cadaveric-derived dura matter or corneal grafts.
- *New variant CJD (vCJD)*: this form is related to consumption of meat infected with BSE. It is generally seen in younger patients than the classical CJD.

sCJD is characterized by rapidly progressing dementia, with 50% chance of death within 5 months of symptom onset. It is typically seen in patients 60–75-years old. Other neurological features include cerebellar ataxia, pyramidal and extrapyramidal signs, and cortical blindness. Death in sCJD patients is most commonly due to pneumonia.

vCJD is linked to consumption of infected cattle meat with BSE. vCJD is seen in younger age than sCJD, and the neurological symptoms are nonspecific, with patients often showing psychiatric and behavioral changes. Incubation period of the disease is approximately 10 years. MRI plays an important role in establishing the diagnosis, since definite diagnosis of prion diseases requires pathological sample examination.

Signs on MRI

- In sCJD, brain shows hyperintense signal changes in the caudate head and the putamen on T2W images (Fig. 2.10.9). This sign can be observed in other diseases like carbon monoxide poisoning, hypoglycemia, hemolytic-uremic syndrome, and Wilson's disease.
- In vCJD, there are bilateral, almost symmetrical T2 hyperintense lesions found in the pulvinar, the most posterior thalamic nucleus (*positive pulvinar sign*) (Fig. 2.10.10). Normally, the pulvinar is the most hypointense nuclei of the deep gray matter on T2W images. Positive pulvinar sign is a highly sensitive sign of vCJD (Fig. 2.10.10).

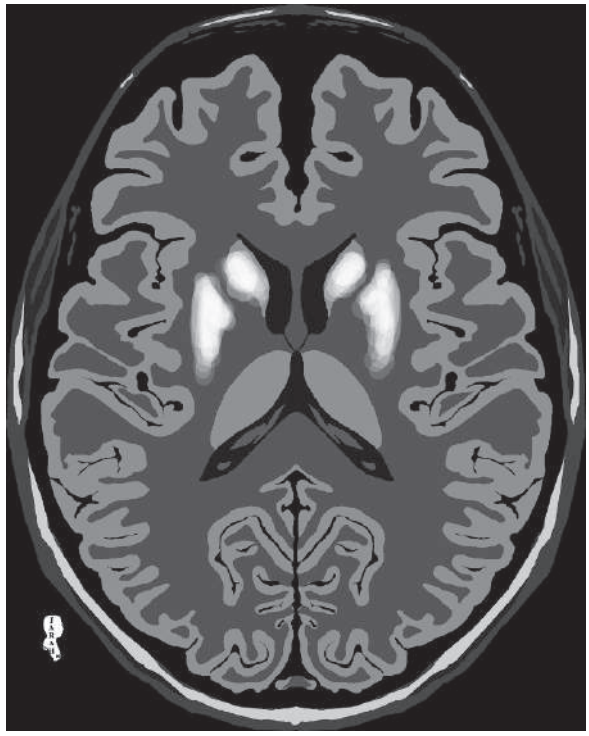

Fig. 2.10.9. Axial FLAIR brains MR-illustration demonstrates the MR signs of sCJD

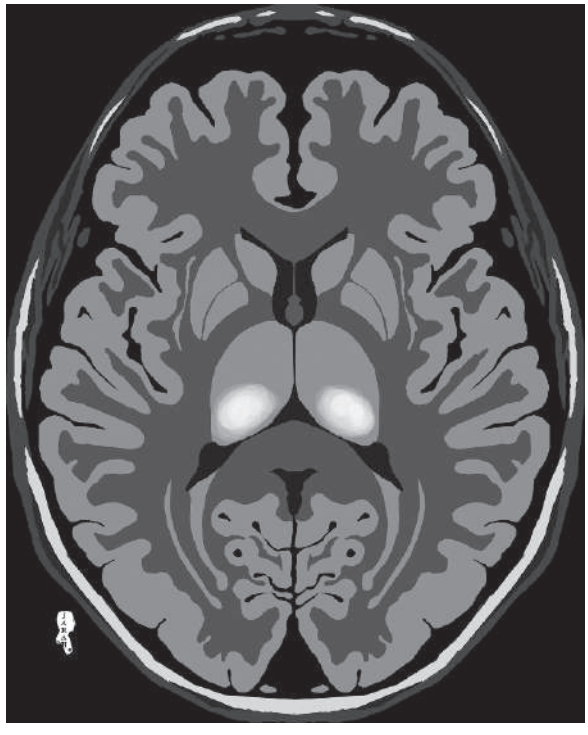

Fig. 2.10.10. Axial FLAIR brains MR-illustration demonstrates the bilateral posterior thalamic (pulvinar) hyperintense lesions in vCJD (positive pulvinar sign)

For Further Reading

1. Guermazi A et al Neuroradiological findings in vascular dementia. Neuroradiology. 2007;49:1–22
2. Arai K. MRI of progressive supranuclear palsy, corticobasal degeneration and multiple system atrophy. J Neurol. 2006;253 Suppl 3:III/25–III/29
3. RajMohan V et al The limbic system. Indian J Psychiatry. 2007;49:132–9
4. Sy M-S et al Human prion diseases. Med Clin N Am. 2002; 86:551–71
5. Almer G et al Fatal familial insomnia: a new Austrian family. Brain. 1999;122:5–16
6. Wang Y et al Report on the first Chinese family with Gerstmann-Str?sler-Scheinker disease manifesting the codon 102 mutation in the prion protein gene. Neuropathology. 2006;26:429–32
7. Collie DA et al MRI of Creutzfeldt-Jakob disease: imaging features and recommended MRI protocol. Clin Radiol. 2001;56:726–39
8. Lucchelli F et al The case of lost Wilma: a clinical report of Capgras delusion. Neurol Sci. 2007;28:188–95
9. Uhlenbrock D et al The value of T1-weighted images in the differentiation between MS, white matter lesions, and subcortical arteriosclerotic encephalopathy. Neuroradiology. 1989;31:203–12
10. Wodarz R. Watershed infarctions and computed tomography. A topographical study in cases with stenosis or occlusion of the carotid artery. Neuroradiology. 1980;19: 245–8
11. Bastos Leite AJ et al Thalamic lesions in vascular dementia: low sensitivity of fluid-attenuated inversion recovery (FLAIR) imaging. Stroke. 2004;35:415–9
12. Drago V et al What's inside the art? The influence of frontotemporal dementia in art production. Neurology. 2006;67: 1285–7
13. Clerici F et al Dementia with Lewy bodies with supranuclear gaze palsy: a matter of diagnosis. Neurol Sci. 2005; 26: 358–61
14. Massano J et al Teaching neuroimage: MRI in multiple system atrophy: "hot cross bun" sign and hyperintense rim bordering the putamina. Neurology. 2008;71:e38
15. Kwee RM et al Virchow-Robin spaces at MR imaging. RadioGraph. 2007;27:1071–86

2.11 Huntington's Disease

Huntington's disease (HD) is a chronic, progressive, autosomal dominant, degenerative disease of the brain characterized by motor, cognitive, and behavioral abnormalities.

Patients with HD initially present between 30 and 50 years of age with chorea. Chorea is an involuntary, jerking, dancing like movement of the distal limbs (Huntington's chorea). Chorea increases in severity in the first few years of life but eventually fades away again to be replaced by bradykinesia and hypokinesia, which are the real causes of motor disability in HD. In advanced stages, patients develop dysarthria, dysphagia, and impairment of gait and balance.

Psychiatric symptoms can be seen in HD, including depression, personality change, and anxiety. The suicide rate is high, especially in the early stage of the disease.

There is no treatment for HD, and death usually occurs 10–15 years after manifestations of the symptoms.

Signs on CT and MRI

- Both scans typically show bilateral symmetrical or asymmetrical caudate nuclei atrophy causing ballooning of the frontal horns (Boxcar-shaped frontal horns) (Fig. 2.11.1).
- Brain cortical and white matter atrophy, especially the frontal lobes, can be seen in advanced stages of the disease.

Differential Diagnoses and Related Diseases

Sydenham Chorea (rheumatic encephalitis): is a manifestation of a severe form of rheumatic fever. Sydenham chorea (SyC) is characterized clinically by involuntary and uncoordinated movements, frequent falls, dysarthria, and multiple weaknesses. There is female gender predominance, and mean age of 11.7 years at the onset of SyC. The duration of SyC ranges from a week to 2 years with average duration of 4 months. In rheumatic fever patients, female gender and the presence of carditis can be the risk factors for a longer duration of SyC. Interestingly, patients with previous history of SyC develop psychiatric manifestations later in life, such as obsessive–compulsive disorder, major depressive disorders, or attention deficits. On

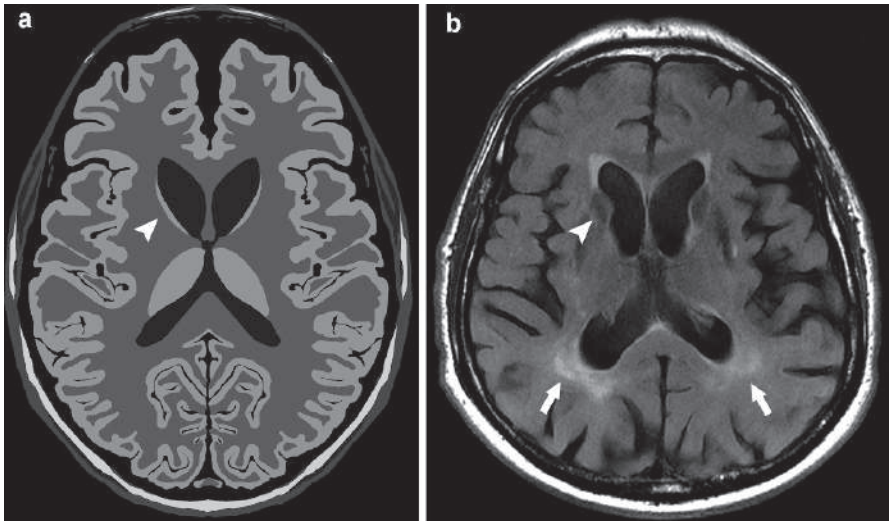

Fig. 2.11.1. Axial FLAIR MR-illustration (**a**) and FLAIR MRI (**b**) of patients with Huntington's disease (HD) show bilateral caudate nucleus head atrophy and the characteristic boxcar-shaped frontal horns (*arrowheads*)

MRI, basal ganglia hyperintense lesions may be found in patients with SyC.

2.11 For Further Reading

1. Terrence CF et al Computed tomography in Huntington's disease. Neuroradiology. 1977;13:173–5
2. Angelini L et al Tourettism as clinical presentation of Huntington's disease with onset in childhood. Ital J Neurol Sci. 1998;19:383–5
3. Craufurd D. Huntington's disease. Prenat Diagn. 1996;16: 1237–45
4. Faustino PC et al Clinical, laboratory, psychiatric and magnetic resonance findings in patients with Sydenham chorea. Neuroradiology. 2003;45:456–62

2.12

Heat Stroke (Pancerebellar Syndrome)

Heat stroke is a medical emergency characterized by a core body temperature >40°C or more, hot dry skin, and neurological disturbance.

Heat stroke may be environmental due to prolonged exposure to sun heat with hydration, endogenous as in runners during heavy military exercises (exertional heat stroke), or a combination of both. Heat stroke may also develop in other pathological conditions such as infections, and neuroleptic malignant syndrome (NMS). NMS is a rare complication of neuroleptic medication therapy (e.g., haloperidol) characterized clinically by hyperpyrexia, muscular rigidity, autonomic dysfunction, altered mental status, and elevation of serum creatine phosphokinase (CK) levels. Patients with NMS typically present with fever and muscle rigidity 24–72 h after the start of treatment with neuroleptic medications; however, NMS may develop weeks to months later. Cerebellar atrophy can be rarely caused by NMS.

The most dramatic effect of heat stroke is observed in the central nervous system, especially the cerebellum. Confusion, delirium, convulsions, myoglobinuria, stupor, or coma are seen in most cases. Downbeat nystagmus, which is defined as a primary position nystagmus with rapid downward phase and slow upward drift, may be seen with heat stroke cerebellar atrophy. Direct thermal insult to the brain may lead to intraparenchymal hemorrhage or stroke.

The most common permanent neurological sequela of heat stroke is *pancerebellar syndrome*, which is characterized by cerebellar atrophy causing dysarthria, irritability, ataxic gait, and poor concentrations. Classically, the patient presents with cerebellar atrophy symptoms weeks to months after the initial heat stroke attack. Cerebellar atrophy is caused by marked degeneration of Purkinje cells with pyknotic nuclei, chemolytic changes, and swollen dendrites. The cerebellar atrophy is indistinguishable from that seen in various degenerative diseases affecting the cerebellum (e.g., alcoholism), so history is very important.

Signs on Brain CT and MRI

- The initial CT scan may be normal. Follow-up scans after weeks or months may show bilateral cerebellar atrophy with dilatation of the cerebellopontine angles cisterns and the fourth ventricle. No changes in the cerebral hemispheres or the brain stem are noticed classically.
- Stroke or intraparenchymal hemorrhage may be seen in cases of direct thermal insult.
- Absence of increased intracranial pressure signs.
- On postcontrast MRI, patchy enhancement of the cerebellum hemispheres may be seen bilaterally.
- *Neuroleptic malignant syndrome*: may show hyperintense T2 white matter lesions affecting the parieto-occipital area. Rarely, cerebellar atrophy may be seen.

For Further Reading

1. Yaqub BA et al Pancerebellar syndrome in heat stroke: clinical course and CT scan findings. Neuroradiology. 1987; 29:294–6
2. McLaughlin CT et al MR imaging of heat stroke: external capsule and thalamic T1 shortening and cerebellar injury. AJNR Am J Neuroradiol. 2003;24:1372–5
3. Deleu D et al Downbeat nystagmus following classical heat stroke. Clin Neurol Neurosurg. 2005;108:102–4
4. Manto M et al Cerebellar gait ataxia following neuroleptic malignant syndrome. J Neurol. 1996;243:101–6
5. Becker T et al MRI white matter hyperintensity in neuroleptic malignant syndrome (NMS) - a clue to pathogenesis? J Neurol Transm [GenSect]. 1992;90:151–9

Chapter 3

Pulmonology

CONTENTS

J. A. Al-Tubaikh: *Internal Medicine* – An Illustrated Radiological Guide
DOI: 10.1007/978-3-642-03709-2_3, © Springer-Verlag Berlin Heidelberg 2010

3.1 Pleural Diseases

The pleura are composed of two layers: parietal and visceral layers, separated by a pleural space. The parietal pleuron is supplied by systemic vessels and drains into the right atrium via the azygos, hemiazygos, and internal mammary veins. The visceral pleuron is supplied by bronchial and pulmonary vessels and drains into the pulmonary veins.

The pleural space normally contains interstitial fluid (1–5 mL) that is cleared by the parietal pleural lymphatic vessels. There is no direct communication between the visceral pleura lymphatics and the pleural space.

The Pleura appear normally on radiographs only when the X-ray beam is tangentially set on the film. On radiographs, the pleura appear as fissures and junctional lines. Fissures are made up of two layers of visceral pleura. The normal parietal pleuron is never visualized on posteroanterior (PA) radiographs.

Different pathological conditions affecting the pleura can be diagnosed with confidence by PA chest radiographs alone. This topic discusses the main pathological pleural conditions with their typical radiologic manifestations.

Pleural Effusion

Pleural effusion is a condition characterized by abnormal fluid collection between the parietal and visceral pleura (excess pleural space fluid). The pleural fluid can be *water* (edematous effusion), *blood* (hemothorax), *pus* (empyema), *tumor cells* (malignant pleural effusion), or *lymph* (chylothorx).

Pathologically, pleural effusion is divided into serous or exudative according to the protein content after lab analysis. *Serous plural effusion* contains little protein content (<2.5 g/dL) and usually arises due to systemic disease like cardiac failure, nephrotic syndrome, or liver failure. *Exudative pleural effusion* contains high protein count (>2.5 g/dL) and usually arises due to inflammatory or infectious process like tuberculosis, malignancy, and acute pancreatitis.

Disruption of the thoracic duct due to lymphoma or a tumor can cause lymphatic blockage and leakage into the pleural space causing chylothorax. Malignant effusion typically results from metastasizing of the malignant cells into the pleural cavity via the parietal pleura lymphatics, and it is often massive.

Bronchopleural fistula is a condition characterized by opening of a bronchus into the pleural space. It can develop occasionally following thoracic surgery, infection, medical intervention, or malignancy. Bronchopleural fistula is seen in 2–3% of postpneumonectomy cases.

Signs on Chest Radiographs

- Obliteration of the lateral costophrenic angle with a meniscus like arc at the interface between the fluid and the chest wall in PA radiographs (Meniscus sign). (Fig. 3.1.1)
- Obliteration of the posterior costophrenic angle in lateral radiographs (Fig. 3.1.1). This angle is more sensitive to plural effusion collection due to gravity effect. Up to 50 mL of fluid is necessary to obliterate the posterior costophrenic angle, and 200 mL is necessary to obliterate the lateral costophrenic angle.
- *Subpulmonic pleural effusion* (*SPE*) is a pleural effusion that occurs below the lungs at the diaphragmatic surface. SPE does not obliterate the costophrenic angle, but it distorts the shape of the diaphragmatic dome giving the impression of raised hemidiaphragm. You can suspect SPE in the left lung when the space between the gastric bubble and the lower lung margins increases up to 3 cm instead of usual few millimeters. Beside the raised hemidiaphragm, the lung appears to end early on PA radiographs (Fig. 3.1.2).
- *Encysted* (*loculated*) *pleural effusion* is a localized encysted fluid at the fissures between lobes of the lung. It occurs usually at the right lung's minor fissure, and it has biconvex contour mimicking a mass (Fig. 3.1.3). Very rarely, a benign form of mesothelioma can grow along the major or minor fissures mimicking encysted pleural effusion, a condition known as "*pseudotumor*."
- *Para-pneumonic effusion* is an effusion that develops adjacent to pneumonias (empyema). Almost 30% of patients with pneumonia develop pleural effusion, and usually resolves with antibiotic therapy.
- *Mediastinal pleural effusion* is a fluid collection around the mediastinum. It is an unusual condition, and when it occurs, it forms silhouette sign along the mediastinal borders causing mediastinal widening. *Silhouette sign* is a term used to describe any opacity within the chest radiograph that obliterates a mediastinal border.

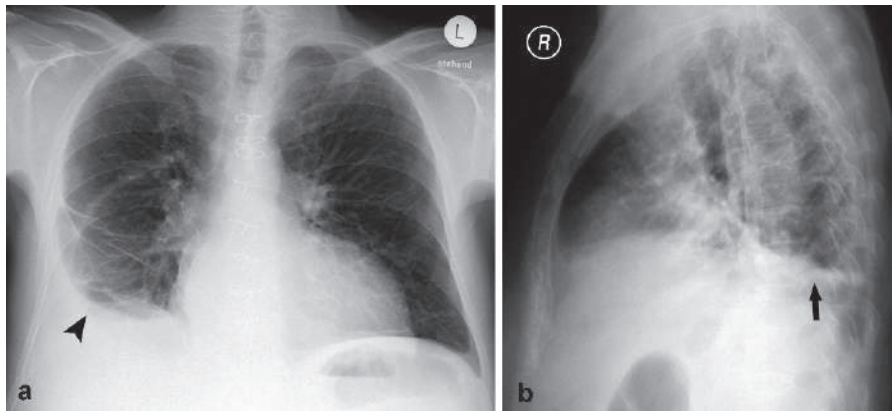

Fig. 3.1.1. Posteroanterior (**a**) and lateral (**b**) chest radiographs in two different patients with pleural effusion show meniscus sign with right pleural effusion obliterating the lateral costo-phrenic angle (*arrowhead*) in (**a**), and pleural effusion obliterating the posterior costo-phrenic angle in (**b**) (*arrow*)

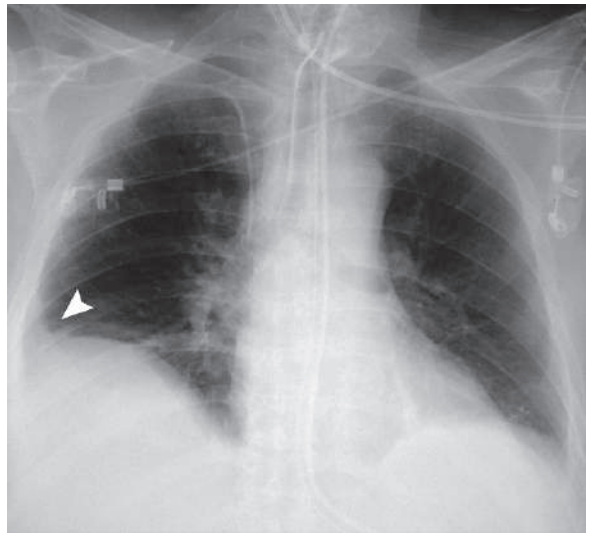

Fig. 3.1.2. Posteroanterior chest radiograph of a patient with right subpulmonic pleural effusion (SPE) shows raised hemidiaphragm, and the lung seems to end early (*arrowhead*)

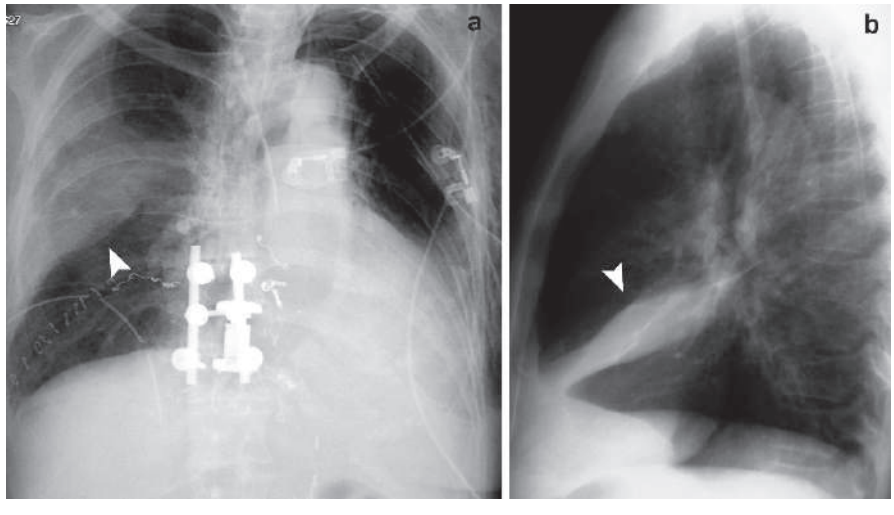

Fig. 3.1.3. Posteroanterior (**a**) and lateral (**b**) chest radiographs show right-sided encysted pleural effusion (*arrowheads*)

3.1

Signs on US

Pleura effusion appears as anechoic or hypoechoic collection that lies between the echogenic line of the visceral pleura and lung (Fig. 3.1.4).

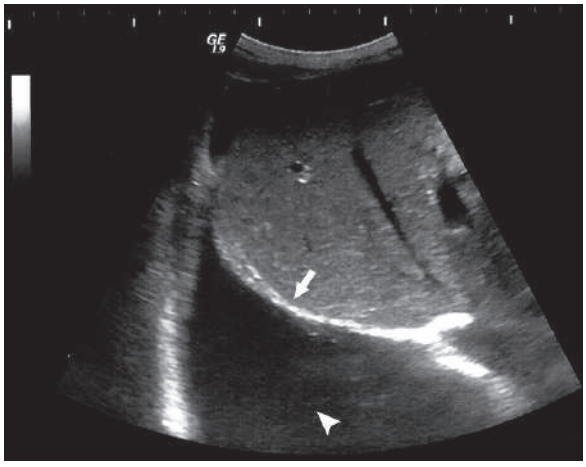

Fig. 3.1.4. Transverse ultrasound image shows right-sided pleural effusion (*arrowhead*). The diaphragm can be visualized as a hyperechoic line separating the right lung base from the liver (*arrow*)

Signs on CT

- Serous pleural effusion is visualized as a crescent peripheral area with CT water-density. Exodative effusion can be hyperdense.
- Empyema characteristically demonstrates thickened parietal/visceral pleura (e.g., > 2 mm) with effusion in between (split-pleura sign) (Fig. 3.1.5). Enhancement of the both pleura occurs in 80–100% cases after contrast injection. Multiple gas pockets within the empyema may be seen.
- Bronchopleural fistula: this condition occurs when a bronchus opens into the pleural space due to lung parenchymal destruction (e.g., pneumonia with empyema formation). It is seen as pleural effusion with air–fluid level on radiographs or HRCT (Fig. 3.1.6).

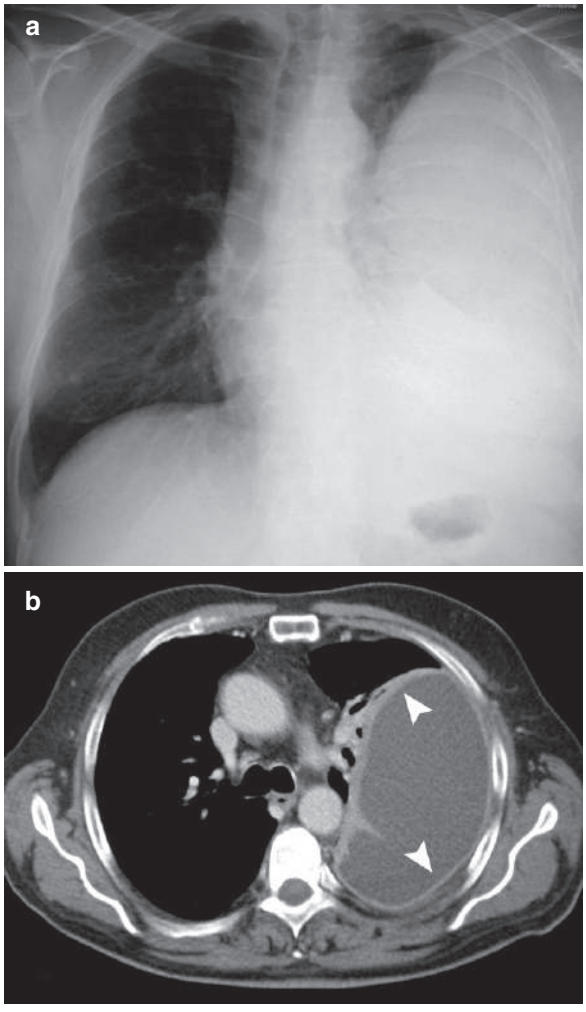

Fig. 3.1.5. Posteroanterior chest radiograph (**a**) and axial chest CT (**b**) of a patient with huge left-sided empyema show split-pleura sign in (**b**), with thickened, enhanced pleura with effusion in between (*arrowheads*)

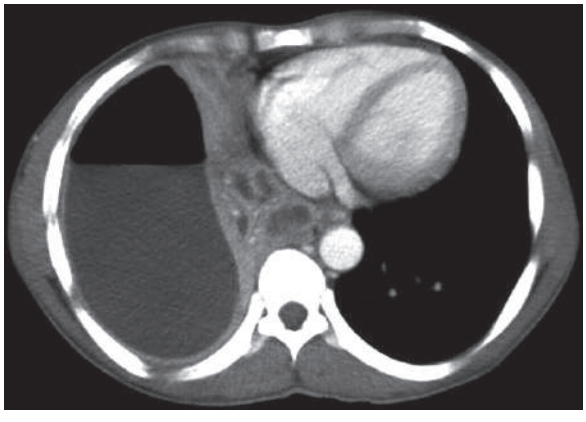

Fig. 3.1.6. Axial chest CT shows huge right bronchopulmonary fistula

Differential Diagnoses and Related Diseases

- *Meigs' syndrome* is a disease characterized by ascites, pleural effusion, and one of the following ovarian tumors (fibroma, thecoma, granulose cell tumor, or Brenner's tumor). In contrast, *Pseudo-Meigs' syndrome* is defined as ascites, pleural effusion, and ovarian tumor other than the ones mentioned previously. Absence of malignant cells from the ascites or the pleural effusion is mandatory for the diagnosis of Meigs' syndrome. Typically, the ascites and the pleural effusions resolve after tumor resection. Meigs' syndrome often occurs in postmenopausal women.
- *Yellow nail syndrome* is a rare disease characterized by extremities lymphadema and thickened, slowly-growing, yellowish-green nails that are excessively curved from side to side (Fig. 3.1.7). The disease is commonly accompanied by idiopathic pleural effusion, chronic bronchiectasis, chronic sinusitis, and lymphadema of the face. Yellow nail syndrome may be accompanied by rheumatoid arthritis or thyroid disease. The disease is believed to be caused by hypoplasia, atresia, or varicosity of the lymphatics.

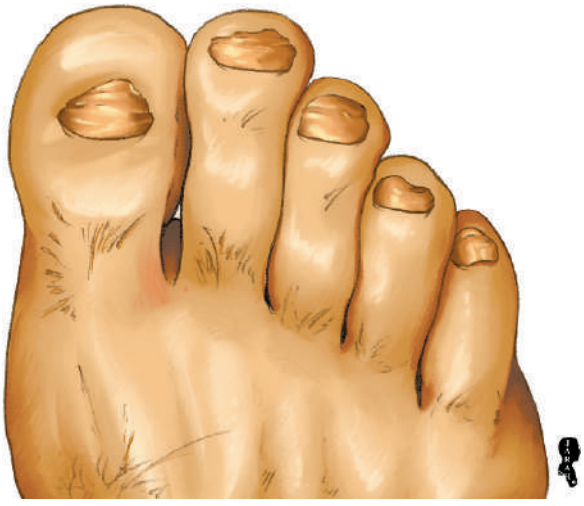

Fig. 3.1.7. An illustration demonstrates the yellowish-green nails of the yellow nail syndrome

Pneumothorax

Pneumothorax is a condition characterized by presence of air between the parietal and visceral pleura. There are three types of pneumothoraces:

- *Primary (spontaneous) pneumothorax*: this type occurs without a defined cause, and mainly seen in young males who are tall, thin, and smokers. Primary pneumothorax is attributed to rupture of subpleuritic blebs at lung apices according to some investigators.
- *Secondary pneumothorax*: this type occurs usually after penetrating trauma, ruptured bulla, or an interventional thoracic procedure (e.g., lung mass biopsy).
- *Tension Pneumothorax*: this type occurs when the air collection within the subpleural space is large enough to push the mediastinum to the other side, interfering with blood circulation within the major vessels.

Up to 40% of pneumothoraces may not be detected by chest radiographs. CT is 100% sensitive for detection of pneumothoraces. When pneumothorax opens into the mediastinum, a pneumomediastium develops. Pneumomediastinum is characterized by the presence of air around the mediastinal structures.

Sign on Radiograph

- A thin visceral pleural line is visible on radiographs. The line is outlined by air with absence of the peripheral vasculature laterally, and lung tissue with possible increased density due to collapse, medially (Fig. 3.1.8). Lung apices are the best sites checked for early detection of pneumothorax.
- Deep sulcus sign: the costophrenic angle deepens at the site of the pneumothorax (Fig. 3.1.9). It is seen in pneumothorax with large air collection.
- Tension pneumothorax is seen as complete collapse of the lung and shift of the trachea and mediastinum to the contralateral (other side) collapsed lung (Fig. 3.1.10).
- Pitfall: a skin fold and underlying clothing can mimic a pneumothorax (Fig. 3.1.11). Always correlate the radiological findings with the patient history and current status.
- Pneumomediatinum is detected when the medistinual structures are surrounded by dark radiolucent line of air (Fig. 3.1.12).

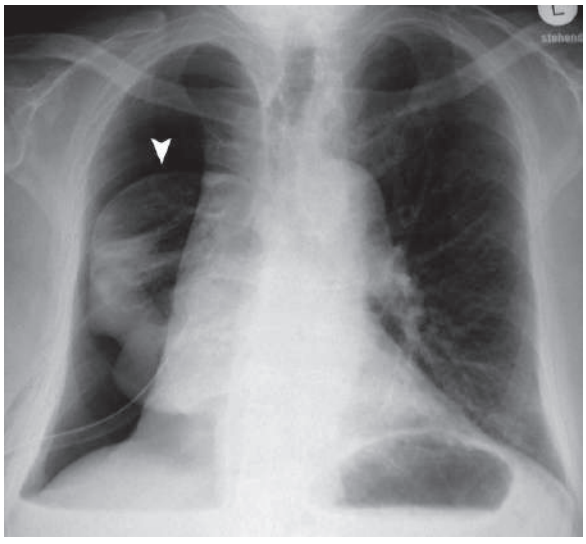

Fig. 3.1.8. Posteroanterior chest radiograph shows right pneumothorax with lung collapse (*arrowhead*)

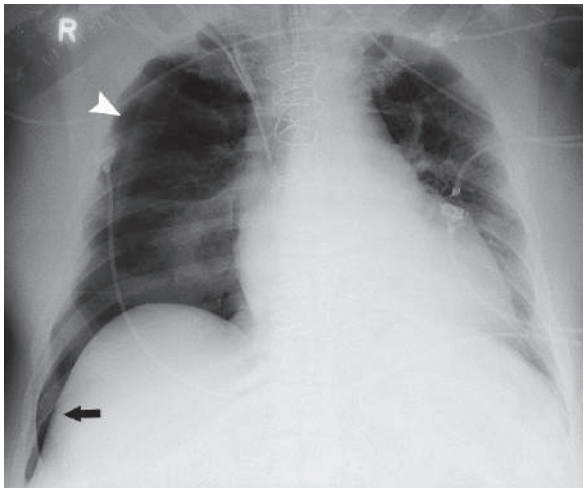

Fig. 3.1.9. Posteroanterior chest radiograph shows right-sided pneumothorax (*arrowhead*) with right deep sulcus sign (*arrow*)

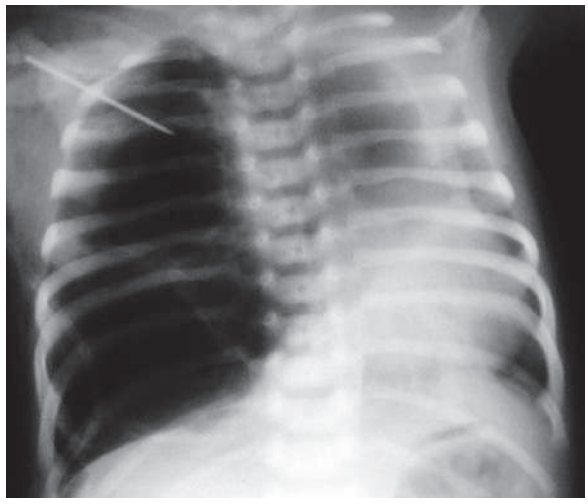

Fig. 3.1.10. Posteroanterior chest radiograph of a child with right tension pneumothorax shows mediastinal shift toward the left side

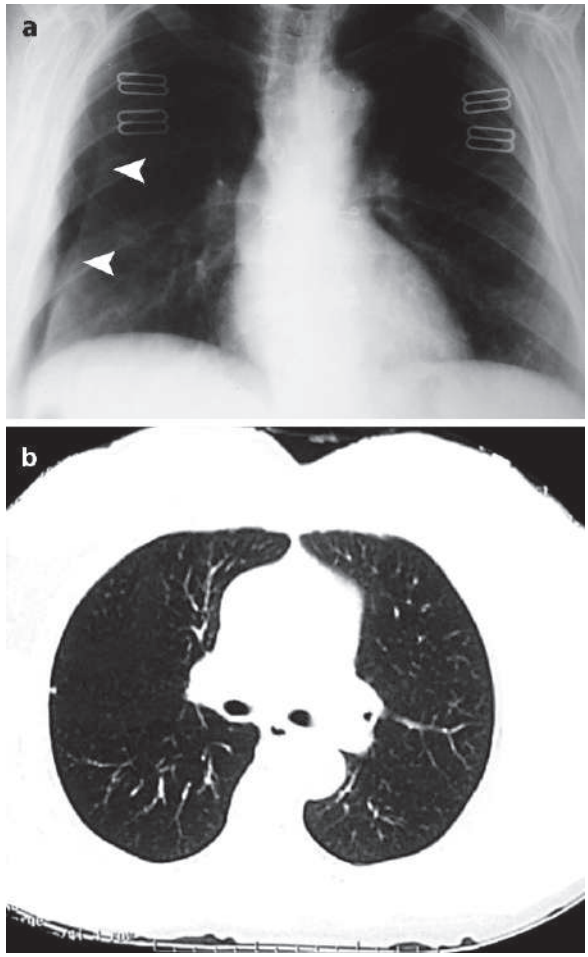

Fig. 3.1.11. Posteroanterior chest radiograph (**a**) and axial chest CT (**b**) of a patient with skin flap that appears as right-sided pneumothorax on chest radiograph (*arrowheads*), while on the HRCT, no pneumothorax is detected

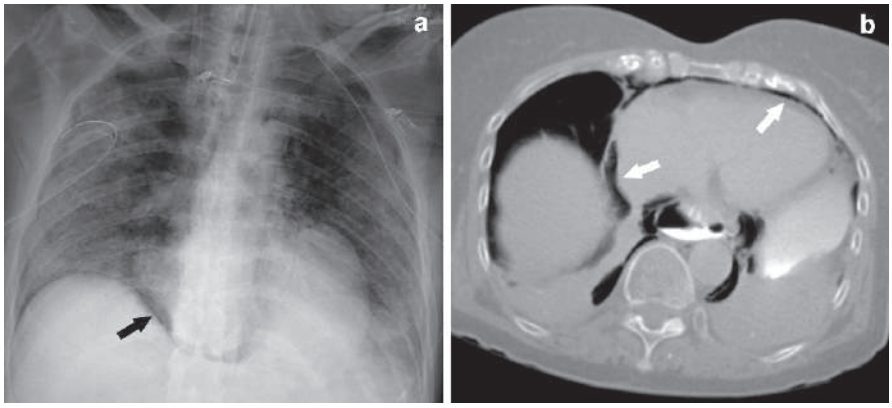

Fig. 3.1.12. Posteroanterior chest radiograph (**a**) and axial chest CT (**b**) of a patient with pneumomediastinum show air around the heart and the mediastinal structures (*arrows*)

Pleural Calcification

Pleural calcification can be seen following chronic pleural damage. Pleural calcification can be unilateral or bilateral. Unilateral pleural calcification occurs usually as a late complication of empyema, hemothorax, fungal infection, or tuberculosis. Bilateral pleural calcification is commonly caused by asbestosis

Asbestosis is a pathological condition that results from previous exposure to asbestos. Pleural plaques are the commonest manifestation of asbestosis, and they usually develop 20–30 years after the exposure to asbestosis. They are composed of focal areas of parietal pleura thickening with dense hyaline collagen. *Mesothelioma* is an uncommon primary tumor of the serosal lining of the pleura or peritoneum. Only 5–7% of patients with asbestosis develop mesothelioma. Mesothelioma has poor prognosis, with survival rate of 12 months. Bronchogenic carcinoma develops in 25% of cases of asbestosis, and it is the main cause of death.

Signs on Chest Radiographs

- Pleural plaques are seen as smoothly-demarcated, well-defined opacities (in-profile), or faint, ill-defined plaques (en-face), in a bilateral fashion. Unilateral pleural plaques may be seen in 25% of cases, and usually located on the left side. The plaques usually are <1 cm in thickness, and seen parallel to the chest wall.
- Pleural calcification is seen in 15–25% of cases after a latency period of 30–40 years (Fig. 3.1.13). Diaphragmatic calcification is pathognomonic finding of asbestosis.
- Asbestos-related diffuse pleural thickening is a bilateral thickening involving at least 25% of the chest or 50% if unilateral; plus pleural thickness >5 mm at any site. The diffuse pleura thickening can affect the visceral layer and the parenchyma below causing "fluffy fibrous strands".
- Round atelectasis: it is seen as a pleural mass (3–5 cm) that abuts over pleura with a curvilinear tails entering the mass (comet tail sign). The curvilinear densities are composed of fibrosed vessels, and the mass is commonly visualized at the base of the lungs (Fig. 3.1.14). Air bronchograms within the mass are common.
- Malignant mesothelioma is visualized as visceral or parietal pleural nodules that are indistinguishable from pleural metastases. The most common manifestation of malignant mesothelioma is a unilateral massive pleural effusion.

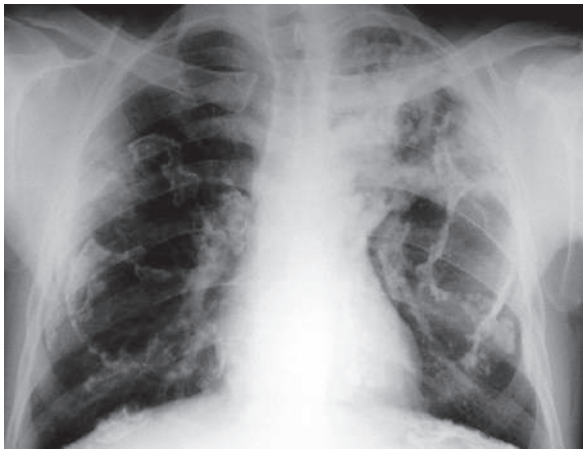

Fig. 3.1.13. Posteroanterior chest radiograph of a patient with asbestosis shows bilateral calcified pleural plaques

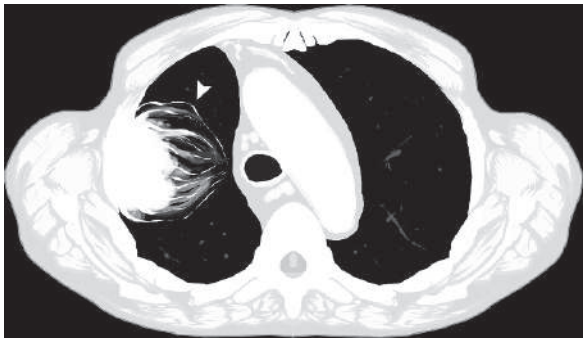

Fig. 3.1.14. Axial chest HRCT illustration demonstrates round atelectasis with comet tail sign (*arrowhead*)

Signs on HRCT

- Pleural plaques appear as well-circumscribed areas of pleural thickening separated from the underlying ribs by thin layer of fat. The edges of the pleural plaque are typically thicker than its center.
- Malignant mesothelioma is visualized as nodular pleural thickening (94%) that commonly involves the lung bases (50%) (Fig. 3.1.15). Diaphragmatic involvement (80%), pleural calcification (20%), and pleural effusion (80%) are other common features.

For Further Reading

1. Qureshi NR et al Imaging in pleural disease. Clin Chest Med. 2006;27:193–213
2. Gallardo X et al Benign pleural diseases. Eur J Radiol. 2000; 34:87–97
3. DeCoste SD et al Yellow nail syndrome. J Am Acad Dermatol. 1990;22:608–11
4. Sacco O et al Yellow nail Syndrome and bilateral cystic lung disease. Pediatr Pulmonol. 1998;26:429–33
5. Nicholas G et al Asbestosis and malignancy. AJR. 1967;100: 597–602
6. Akira M et al Asbestosis: high-resolution CT-pathologic correlation. Radiology. 1990;176:389–94
7. Goyal M et al Malignant pleural mesothelioma in a 13-year-old girl. Pediatr Radiol. 2000;30:776–78
8. O'Lone E et al Spontaneous pneumothorax in children: when is invasive treatment indicated? Pediatr Pulmonol. 2008; 43:41–6
9. Váuez JL et al Pneumomediastinum and pneumothorax as presenting signs in severe *Mycoplasma pneumoniae* pneumonia. Pediatr Radiol. 2007;37:1286–88
10. Nimkin K et al Localized pneumothorax with lobar collapse and diffuse obstructive airway disease. Pediatr Radiol. 1995;25:449–51

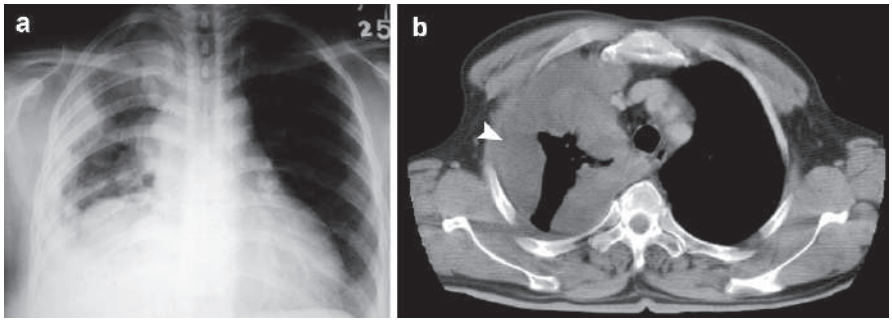

Fig. 3.1.15. Posteroanterior chest radiograph (**a**) and axial chest CT (**b**) of a patient with malignant pleural mesothelioma show nodular thickening of the pleura in the right lung field with extension toward the apex in (**a**) and (**b**). Notice the nodular mass that follows the pleural distribution in (**b**) (*arrowhead*)

3.2 Alveolar Lung Diseases

Alveolar lung diseases (ALD) are group of disorders characterized by pathological insult involving mainly the alveoli. The alveoli can be imagined as an empty cup, and alveolar diseases are classified according to the content of this cup. Alveolar diseases are characterized by filling of the alveoli with materials that impede its normal physiological function (ventilation). Alveolar diseases can be localized (focal) or diffuse. Names of the conditions depend upon the content of the material filling the alveoli.

Types of Alveolar Lung Diseases

- Alveoli filled with *serous fluid*: cardiogenic and noncardiogenic edema.
- Alveoli filled with *blood*: pulmonary hemorrhage, commonly due to vasculitis (e.g., Churge-Strauss syndrome).
- Alveoli filled with *pus*: pneumonia.
- Alveoli filled with *proteins*: alveolar protienosis and amyloidosis.
- Alveoli filled with *malignant cells*: bronchoalveolar carcinoma.
- Alveoli filled with *calcium*: alveolar microlithiasis.

Pulmonary Edema

The alveoli are the main units for respiratory-blood ventilation and oxygenation and normally are full of air on inspiration. You can think of the alveoli as an empty cup, and any pathological condition that fills this cup will form a pathological condition according to the cup content. Pulmonary edema arises due to alveolar filling with serous fluid (water).

Pulmonary edema can be either due to cardiac disease (cardiogenic), or other conditions (noncardiogenic). Most cases of noncardiogenic pulmonary edema are due to acute respiratory distress syndrome (ARDS).

Cardiogenic pulmonary edema is commonly seen with heart failure. It starts as an interstitial edema before it turns into alveolar edema, because the pulmonary veins lie in the interstitium. As the hydrostatic pressure within the veins rises, they leak into the interstitium first, and then progress to fill the alveoli. This process is rapid, and only very early edema can be seen as a pure interstitial linear pattern in chest radiographs.

Noncardiogenic Pulmonary edema has the same radiographic features as the cardiogenic pulmonary edema, but the causes are different: ARDS, chemical pneumonitis, drug-induced pulmonary edema, and transfusion-reaction are the most common causes for noncardiogenic pulmonary edema. ARDS is a situation where an alveolar capillary injury occurs as a result of variety of causes (e.g., sepsis). *Chemical pneumonitis* is a pulmonary edema that occurs due to inhalation of noxious chemical substance such as ammonia, smoking inhalation, near drowning situations, and gastric acid aspiration. The mechanism of pulmonary edema is the result of one of three mechanisms: irritation of the tracheo–bronchial tree that leads to inflammation and pulmonary edema formation; absorption of the noxious material from the respiratory tract, which can affect the lungs directly by its metabolites; and asphyxiation due to inhalation of high concentration of the noxious material that will displace oxygen from the blood and cause tissue hypoxia. *Drug-induced and transfusion reactions pulmonary edema* arise due to anaphylactic lupus-like reaction formation. The radiographic picture cannot be differentiated from ARDS unless you have history of drug ingestion or recent transfusion reaction. Classic examples of drugs causing pulmonary edema are heroin, aspirin, and penicillin. *Negative pressure pulmonary edema* is a term used to describe noncardiogenic edema that arises due to acute airway obstruction (type 1), or after the relief of chronic airway obstruction (type 2).

3.2

Signs on Radiograph

- There is a centrally-located, bilateral, symmetrical diffuse alveolar opacities emitting from the heilum and spares the periphery (butterfly or bat-wings sign) (Fig. 3.2.1). Usually, pulmonary edema causes homogenous opacities, but sometimes they can cause nodular or blotchy opacities.
- Cardiomegaly and signs of congestive heart failure (e.g., congested pulmonary vessels).
- Kerley lines: they represent thickening of the interlobar septae. Lung lymphatics and veins run in the interstitum, leakage of the veins (edema) or tumor infiltration of the lymphatics (lymphangitis carcinomatosis) can result in thickening of the interlobar septa, which are called Kerley lines. Kerley A lines are long lines located near the lung hilum and extend obliquely near the bronchoarterial bundle into the peripheries. Kerley B lines are short white lines seen perpendicular to the pleural surface at the lung bases, commonly near the costophrenic angles (Fig. 3.2.2). Kerley C lines are a mixture between the two lines resulting in a reticular pattern.
- Air-bronchogram sign: this is a sign seen when the alveoli are filled with fluid and the terminal bronchioles and bronchi are devoid of fluid (filled with air). The bronchioles appear as radiolucent lines within whitish radio-opaque opacities (Fig. 3.2.3). This sign is specific for alveolar disease, but nonspecific for the cause. Pulmonary edema, pulmonary hemorrhage, pneumonia, and alveolar carcinoma all looks the same on radiographs. All appears as ALD with air-bronchogram. The medical history plays a very important role in differentiating these conditions because the radiographic signs can be nonspecific.
- Blood diversion: normally, the upper lobe vessels are not visualized on radiographs, and the lower lobes vessels are mildly dilated and visible due to the gravity effect in upright posteroanterior (PA) radiographs. In cases of cardiac diseases and pulmonary hypertension, the upper lobe vessels will be as wide as the lower lobe vessels in upright radiographs. Note that the upper lobe vessels can be seen dilated normally in supine (lying) chest radiographs (e.g., in intensive care unit radiographs).
- Silhouette sign: this sign refers to a patchy, ill-defined radio-opaque shadow that obscures part of the normal mediastinal configuration.

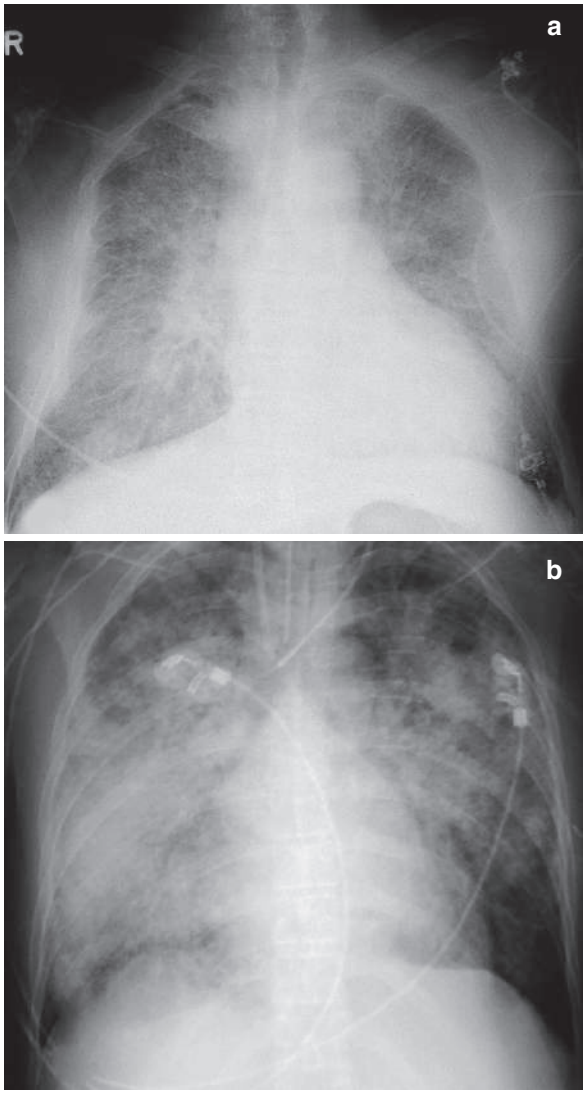

Fig. 3.2.1. Anteroposterior plain chest radiographs in two different patients show bilateral symmetrical pulmonary edema with bat wings appearance in (**a**), and bilateral, almost symmetrical pulmonary hemorrhage in (**b**). Notice that without history, you cannot differentiate pulmonary hemorrhage from pulmonary edema based on radiographic presentation alone

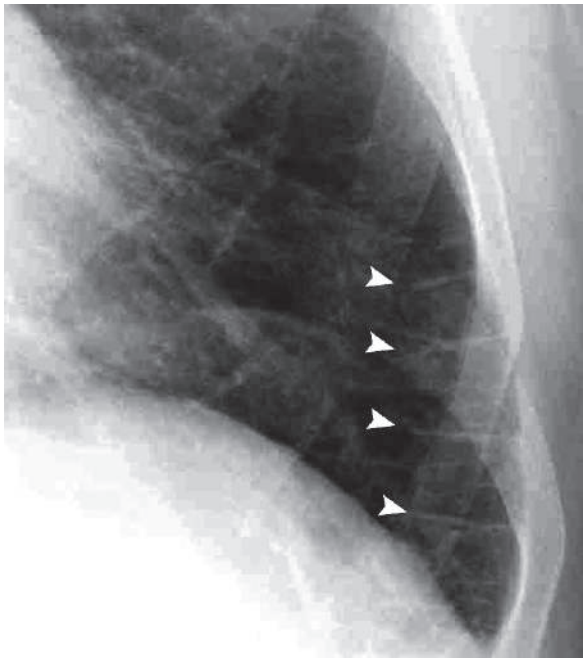

Fig. 3.2.2. Posteroanterior plain chest radiograph shows Kerley B lines (*arrowheads*)

How to differentiate between cardiogenic edema from ARDS on plain chest radiographs?

- ARDS usually has a normal heart size, while cardiogenic pulmonary edema shows signs of heart failure.
- ARDS usually affects peripheral lung field more than central, whereas cardiogenic edema typically starts from the center to the periphery.
- ARDS usually has no Kerley B lines.

Pneumonia

Pneumonia is a condition characterized by an infectious inflammation of the lung parenchyma and deposition of pus within the alveoli. Pneumonia can be caused by bacteria (e.g., Methicillin-resistant Staphylococcus aureus (MRSA)), fungi (e.g., *pneumocystic cainii*), and viruses (e.g., cytomegalovirus (CMV)).

Patients with pneumonia present with dyspnea, purulent sputum, fever, tachycardia, and maybe hemoptysis (e.g., tuberculosis). Complications of pneumonia include lung abscess formation, septicemia, and empyema. Rarely, arthritis and neurological symptoms may be encountered in atypical pneumonias (e.g., *Mycoplasma* pneumonia).

Pneumonias are divided into "typical pneumonia," which is caused by *Streptococcus pneumoniae (pneumococcus)*, and "atypical pneumonia," which is caused by any pathogen that is not *pneumococcus*. Typical pneumonia is clinically dominated by respiratory symptoms, whereas atypical pneumonia clinically is dominated by symptoms of fever and malaise more than the respiratory symptoms.

Types of Pneumonias

- *Air-space pneumonia* (*lobar pneumonia*): in this type, the infection is confined to a single lobe. There is usually one patch filling the whole affected lobe. This type is seen with *pneumococcus*, *Legionella*, *pseudomonas*, and primary tuberculosis infection. Lobar pneumonia is characterized by an "air-bronchogram sign".
- *Bronchopneumonia*: this type is characterized by an infection that starts in the bronchioles and small bronchi walls and then spread to the alveoli. This type is seen with *Staphylococcus aureus*, *Hemophilus influenza*, and *Mycoplasma* pneumonias.
- *Interstitial pneumonia*: this type is characterized by an infection that involves the interstitial septa and giving reticular interstitial pattern on chest radiograph. This type can be seen with viral infections like influenza virus and Varicella-zoster virus (VZV), and *Mycoplasma* infections (30% of cases).

MRSA is a serious infection with antibiotic-resistant staphylococci. MRSA is categorized as: community-acquired, nosocomial, and health care-associated infection. MRSA is the leading cause of nosocomial and health care-associated blood stream infection, globally. Also, it is responsible for 30–50% of ventilator-associated pneumonia. MRSA causes metastatic foci of infections in 30% of cases into the lungs, liver, kidneys, heart valves, and joints. Most community-associated MRSA strains carry the Panton-Valentine Leukocidin (PVL) gene, which is rarely found in the hospital-acquired MRSA or the normal strain of *S. aureus*. PVL toxin is a potent lethal factor to neutrophils, which causes tissue necrosis and severe necrotizing pneumonia. MRSA pneumonia is more frequently associated with sepsis, high-grade fever, hemoptysis, pleural

effusion, and death compared to PVL-negative *S. aureus*. MRSA pneumonia can result in the formation of pulmonary cavitary infiltration due to the development of necrotizing pneumonia. The development of MRSA necrotizing pneumonia should be suspected in a young patient presenting with hypoxia, hemoptysis, and single or multiple cavitary lung lesions.

Viral pneumonias are characterized by several pathologies that include bronchiolitis, tracheobronchitis, and classical pneumonia. Viruses that attack immunocompetent patients include influenza viruses, Epstein–Barr virus, and adenoviruses. Viruses that attack immuno-compromised patients include measles virus, VZV, and CMV. Measles virus attack usually children due to immunosuppression or vaccine failure. VZV pneumonia is a common complication of VZV septicemia in children with a mortality rate of 9–50%. Up to 90% of VZV pneumonia cases are seen in patients with lymphoma or immunosuppression. CMV pneumonia is commonly seen in transplant patients and immunocompromised patients. Patients may develop severe necrotizing pneumonia in spite of antiviral therapy.

Differential Diagnoses and Related Diseases

Hyperimmunoglobulinemia E syndrome (*Job's syndrome*): is a rare condition characterized by marked elevation of serum IgE levels against *S. aureus* resulting in decreased production of anti-staphylococcus IgG. The patient with this syndrome presents with frequent attacks of *S. aureus* pneumonia, pustular dermatitis, eczema, and sinusitis. Formation of chronic lung abscesses is a common feature on radiographs.

Signs on Radiograph

- Radio-opaque patches with an air-bronchogram sign (Fig. 3.2.3).
- Bulging -fissure sign: some infections will increase the volume of the lobe involved causing the adjacent fissure to bulge (commonly the transverse fissure) (Fig. 3.2.4). This sign is classically seen in Klebsella pneumonia.
- Bronchopneumonia: there is multiple patchy infiltration of the lung with or without segmental lobe atelectasis (if the bronchus is totally obstructed). (Fig. 3.2.3)
- Interstitial Pneumonia: shows nonspecific linear or reticular interstitial lung pattern. Correlation with history and laboratory findings is essential to establish the diagnosis.
- Viral pneumonias can appear as poorly-defined nodules (4–10 mm in diameter), with lung hyperinflation due to bronciolitis.
- Measles pneumonia show mix pattern of reticular interstitial pattern with patchy pneumonia (Fig. 3.2.5). Hilar lymphadenopathy may be associated.
- VZV pneumonia appears as multiple, ill-defined micronodules (5–10 mm) (Fig. 3.2.6). The lesions may calcify persisting as well-defined, randomly scattered, dense pulmonary calcification.
- CMV pneumonia is commonly seen as a mixed nodular interstitial pattern with ill-defined patchy lung infiltration. The patchy filling is caused pathologically by hemorrhage, neutrophilic and fibrinous exudates, and hyaline memebrane formation (Fig. 3.2.7).
- Chronic pneumonia can lead to fibrosis, traction bronchiectasis, and paracicatricial emphysema (Fig. 3.2.8).
- In MRSA necrotizing pneumonia, a pneumonic patch or a pulmonary mass with central cavitary lesion can be found. The lesion can be single, or multi-focal. The same manifestations are observed in HRCT. Differential diagnoses of cavitary lung infiltrations include lung abscess, metastases, pulmonary lymphoma, and Wegner's granulomatosis.

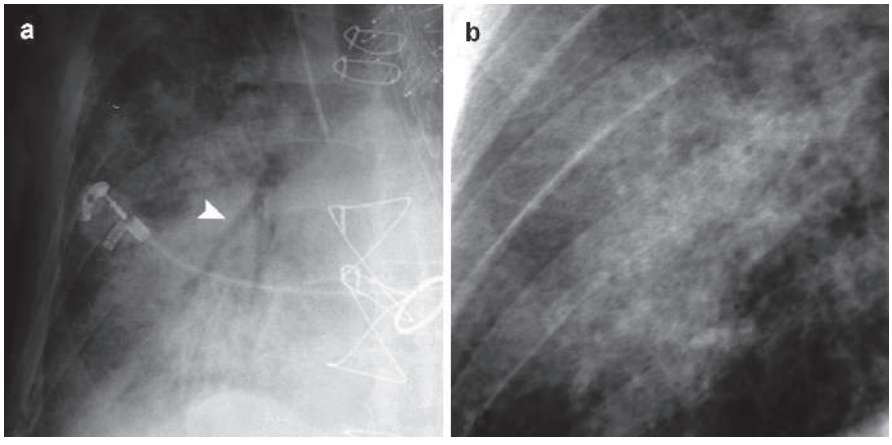

Fig. 3.2.3. Posteroanterior plain chest radiographs in two different patients with pneumonia show pneumonic lung patch with air columns within the patchy due to unaffected bronchi in (**a**) (*arrowhead*), and pneumonic lung patch with no air-bronchogram sign in (**b**). Patient (**a**) presents with air-space pneumonia, whereas patient (**b**) presents with bronchopneumonia

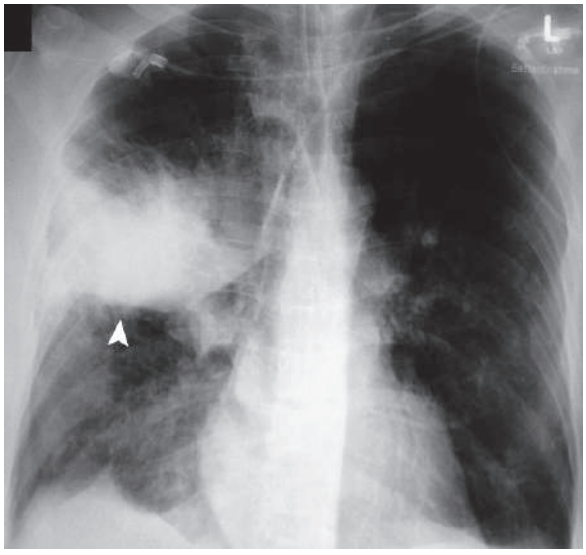

Fig. 3.2.4. Anteroposterior plain chest radiograph of a bedridden patient shows right upper lobe pneumonia with bulging of the transverse fissure (*arrowhead*)

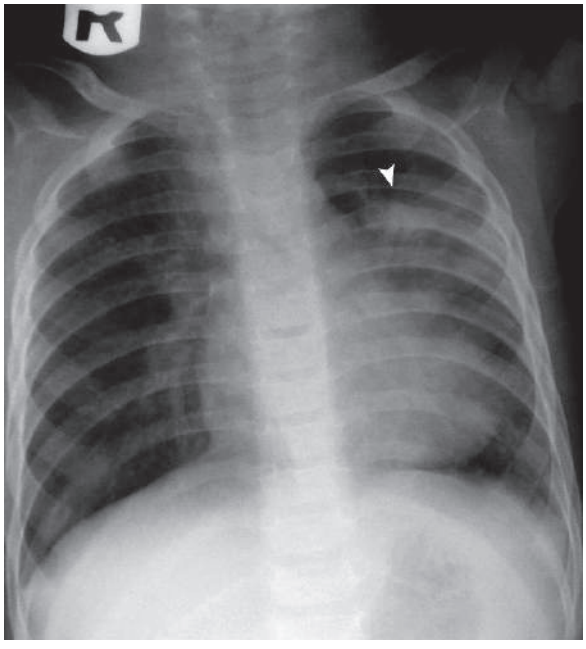

Fig. 3.2.5. Posteroanterior plain chest radiograph of a 5-year-old child with measles presenting with dyspnea shows ill-defined patchy pneumonia in the upper zone of the left lung (*arrowhead*)

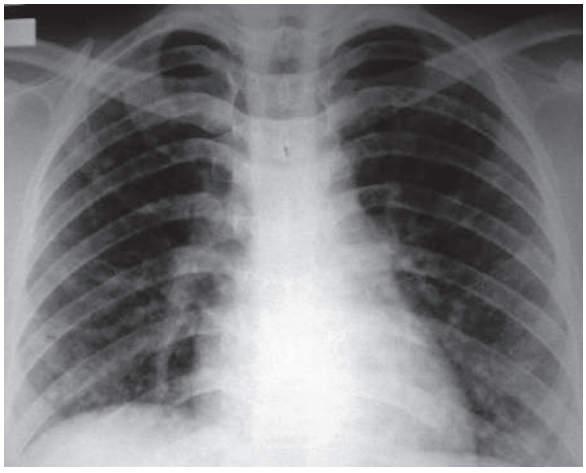

Fig. 3.2.6. Posteroanterior plain chest radiograph of a patient with Varicella-zoster virus (VZV) pneumonia shows diffuse micronodular interstitial lung pattern bilaterally

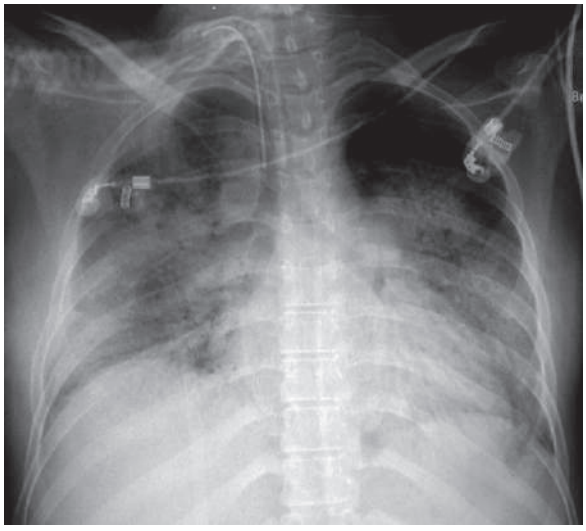

Fig. 3.2.7. Posteroanterior plain chest radiograph of a patient with cytomegalovirus (CMV) pneumonia after heart transplant shows mixed patchy lung infiltration with micronodular interstitial lung pattern

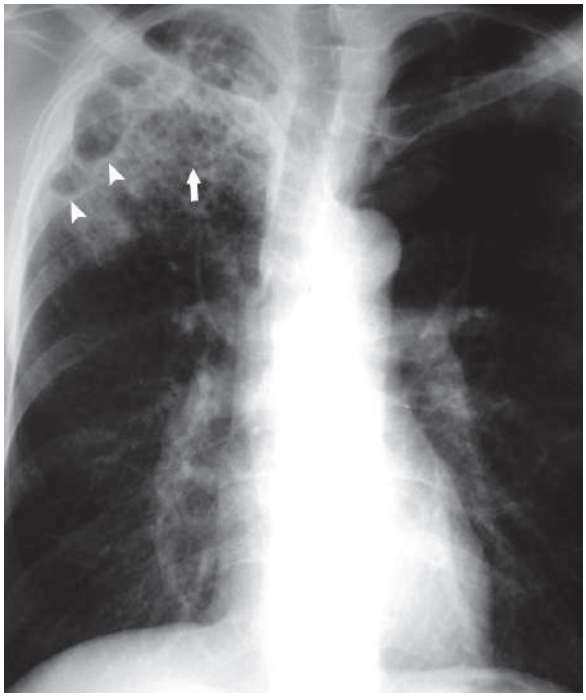

Fig. 3.2.8. Posteroanterior plain chest radiograph of a patient with mycoplasma pneumonia shows right upper lobe fibrosis with honeycombing due to traction bronchiectasis (*arrow*) and paracicatricial emphysema (*arrowheads*)

For Further Reading

1. Gattinoni L et al The role of CT-scan studies for the diagnosis and therapy of acute respiratory distress syndrome. Clin Chest Med. 2006;27:559–70
2. Fujinaga S et al Pulmonary edema in a boy with biopsy-proven poststreptococcal glomerulonephritis without urinary abnormalities. Pediatr Nephrol. 2007;22:154–55
3. Kawamata M et al Acute pulmonary edema associated with transfusion of packed red blood cells. Intensive Care Med. 1995;21:443–46
4. Chuang YC et al Negative pressure pulmonary edema: report of three cases and review of the literature. Eur Arch Otorhinolaryngol. 2007;264:1113–16
5. Kim EA et al Viral pneumonias in adults: radiologic and pathologic findings. RadioGraphics. 2002;22:S137–S149
6. Anuradha G. Methicillin-resistant *staphylococcus aureus* bacteremia and pneumonia. Dis Mon. 2008;54:787–92
7. Corriere MD et al MRSA: an evolving pathogen. Dis Mon. 2008;54:751–55
8. Decker CF. Pathogenesis of MRSA infection. Dis Mon. 2008;54:774–79
9. Ebert MD et al Necrotizing pneumonia caused by community-acquired methicillin-resistant Staphylococcus aureus: an increasing cause of "mayhem in the lung". Emerg Radiol. 2009;16:159–62
10. Connolly B et al Bronchial artery aneurysm in hyperimmunoglobulinemia E syndrome. Pediatr Radiol. 1994;24:592–93

3.3 Atelectasis (Lung Collapse)

Atelectasis is a condition characterized by lung collapse, which can be subtotal (25–50% collapse) or total (100% collapse).

Atelectasis can result due air resorption (*resorptive atelectasis*), lung compression (*compression atelectasis*), or loss of the surfactant in *acute respiratory distress syndrome (ARDS) and hyaline membrane disease (respiratory distress syndrome)* in preterm infants (microatelectases). Pulmonary atelectasis is a recognized complication of general anesthesia.

Pulmonary surfactant is secreted by pneumocytes type II, which is composed of phospholipids and proteins. The surfactant stabilizes the lung by reducing the surface tension at the air-liquid interface in the alveoli. Therefore, deficiency of pulmonary surfactant could result in collapse of the alveolar spaces.

Patients with atelectasis commonly present with dyspnea, tachypnea, cough, and pleuritic chest pain on inspiration. Hypoxemia may result from atelectasis due to reduced ventilation-perfusion equilibrium.

Types of Pulmonary Atelecteses

- *Resoptive atelectasis*: this type can arise due to intrinsic obstruction (e.g., mucus plug), or extrinsic obstruction (e.g., hilar lymphadenopathy). *Brock's syndrome* is a term used to describe right middle lobe (RML) atelectasis by enlarged hilar lymphadenopathy compressing the right main bronchi.
- *Passive atelectasis* results when the natural tendency of lung tissue to collapse due to elastic recoil goes unstopped. This condition can be seen in atelectasis due to pneumothorax.
- *Compressive atelectasis* is a variant of passive atelectasis and occurs when a space occupying lesion abuts the lung causing atelectasis (e.g., massive pleural effusion).
- *Cicatrization atelectasis*: this type is seen with fibrosis, where the scar tissue contracts and collapses the alveoli.
- *Adhesion atelectasis*: this type occurs due to surfactant deficiency, which is classically seen in hyaline membrane disease in infants and ARDS and pulmonary embolism in adults.
- *Plate atelectasis*: this type of atelectasis is composed of sheets of horizontal tissue collapse, which is commonly located 1–3 cm above the diaphragm. This type is commonly seen in conditions, which impede normal respiration (e.g., inflammatory conditions in the chest or abdomen).
- *Congenital atelectasis*: this type is seen in newborn infants due to failure to aerate the lung after pregnancy.
- *Round atelectasis*: this type of atelectasis is seen in asbestosis, and it is characterized by atelectasis of parenchymal tissues near the pleura. It is best diagnosed by CT, which will show bronchovascular marks entering the mass (comet tail sign).
- *Segmental atelectasis*: it is an uncommon type of atelectasis characterized by an entire lung segment collapse. It is highly suggestive of a tumor blocking the bronchial feeding of that segment.

Signs on Chest Radiograph

- Diaphragmatic elevation due to reduced lung volume.
- Shift of the right horizontal fissure upward due to upper lobe collapse (Fig. 3.3.1).
- RML and left lower lobe (LLL) atelectases are located behind the heart. They can be seen as dense radio-opaque triangles overlying the heart shadow (Figs. 3.3.2 and 3.3.3). They can be easily missed if the atelectasis is examined in posteroanterior view only; lateral views are advised if RML or LLL atelectases are suspected.
- Left upper lobe (LUL) atelectasis is generally seen as increased in lung density on posteroanterior (PA) view. This is explained by the fact that the LUL collapses anteriorly. Lateral view is shown clearly as an anterior mediastinal radio-opaque shadow representing the collapsed lobe (Fig. 3.3.4).
- Right upper lobe (RUL) atelectasis is seen as homogenous opacity located at the right upper lung zone and bounded inferiorly by the transverse fissure (Fig. 3.3.5).
- Shift of the trachea and the mediastinum toward the collapse.
- Spine sign: normally the lower vertebrae on lateral view are less dense than the upper vertebra. The upper vertebrae

appear denser due to the arm and axilla shadow overlying them. With progressive atelectasis of the lower lobes, the lobes will move more posteromedially, making the lower vertebra appears as dense as the upper vertebrae (Fig. 3.3.3).

- Golden S sign: this sign is seen when the RUL is collapsed due to hilar mass blocking the right main bronchus (e.g., in Brock's syndrome).
- Plate atelectasis is detected on radiographs as linear horizontal radio-opaque lines commonly located 1–3 cm above the diaphragm (Fig. 3.3.6).

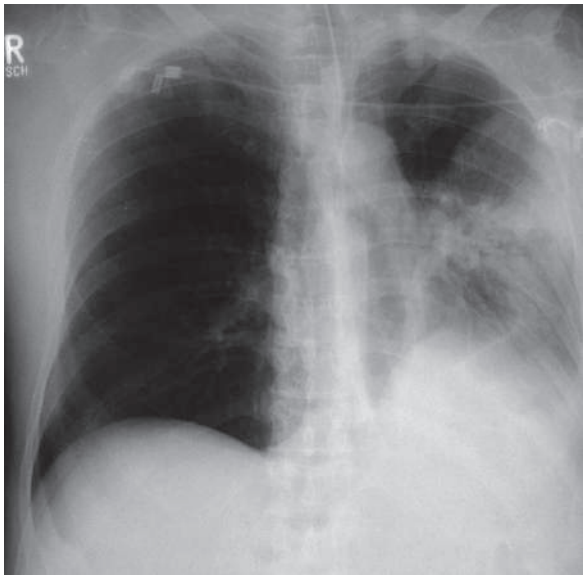

Fig. 3.3.1. Anteroposterior plain chest radiograph of a bedridden patient shows mediastinal shift toward the left side due to collapse of the left lung

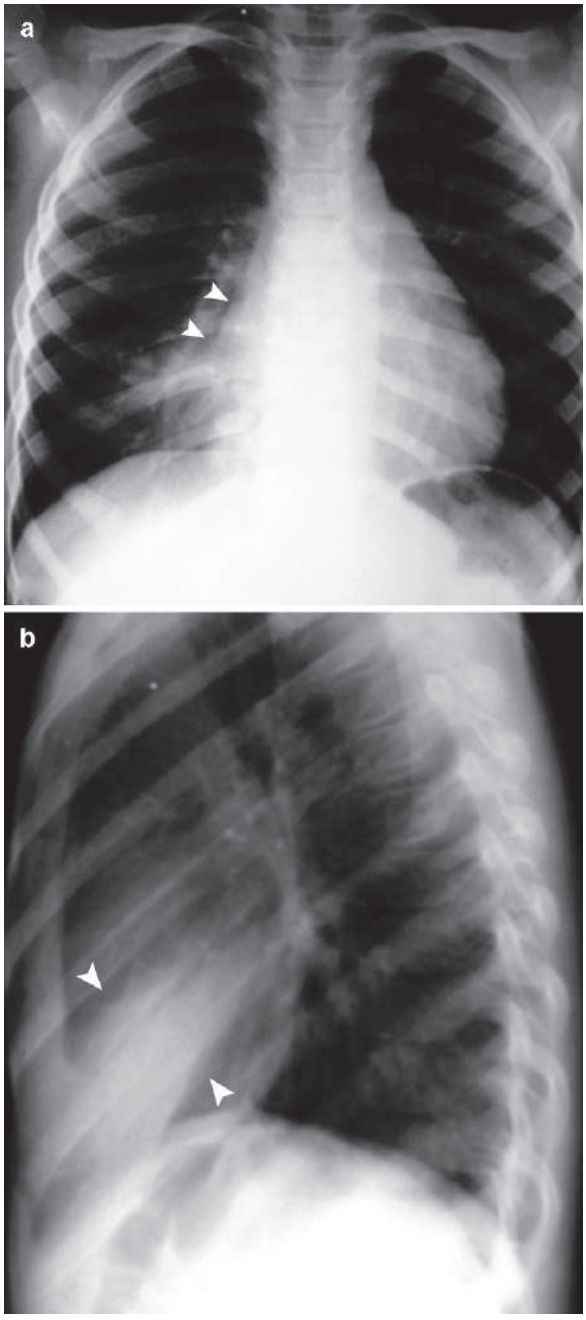

Fig. 3.3.2. Posteroanterior (**a**) and lateral (**b**) plain chest radiographs show right middle lobe (RML) atelectasis (*arrowheads*)

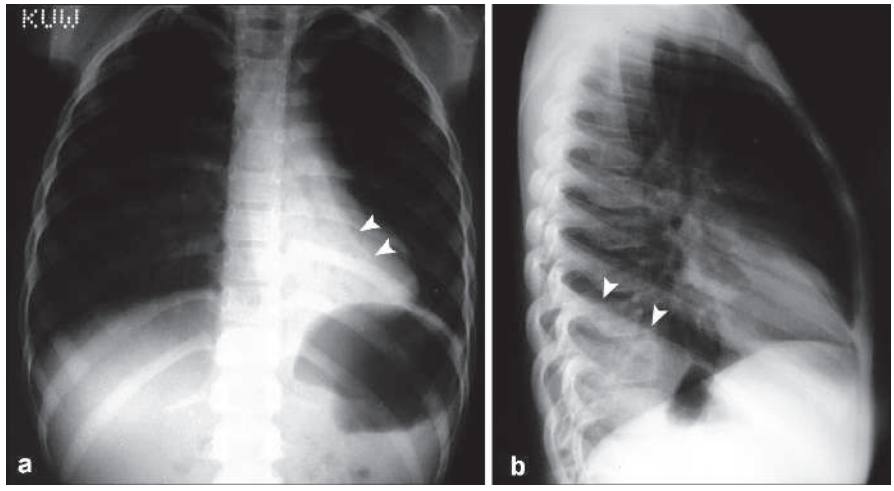

Fig. 3.3.3. Posteroanterior (**a**) and lateral (**b**) plain chest radiographs show left lower lobe (LLL) atelectasis (*arrowheads*). Notice that the lower thoracic vertebrae appear denser than the upper thoracic vertebrae due to the shadow of the atelectatic lobe overlying them (*spine sign*)

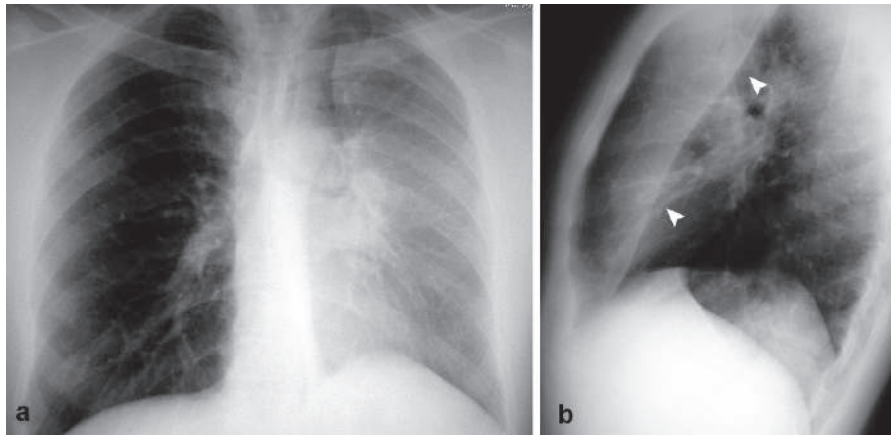

Fig. 3.3.4. Posteroanterior (**a**) and lateral (**b**) plain chest radiographs show left upper lobe (LUL) atelectasis. Notice the high density left lung field in (**a**), which is explained by atelectasis of the LUL anteriorly in (**b**) (*arrowheads*)

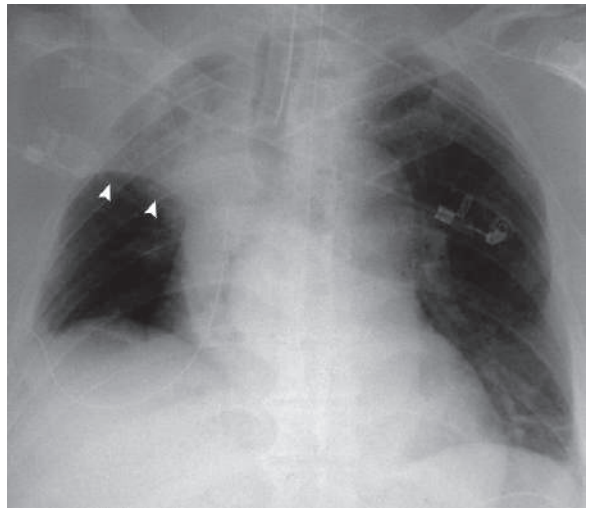

Fig. 3.3.5. Posteroanterior plain chest radiographs show right upper lobe (RUL) atelectasis bounded inferiorly by the transverse fissure (*arrowheads*)

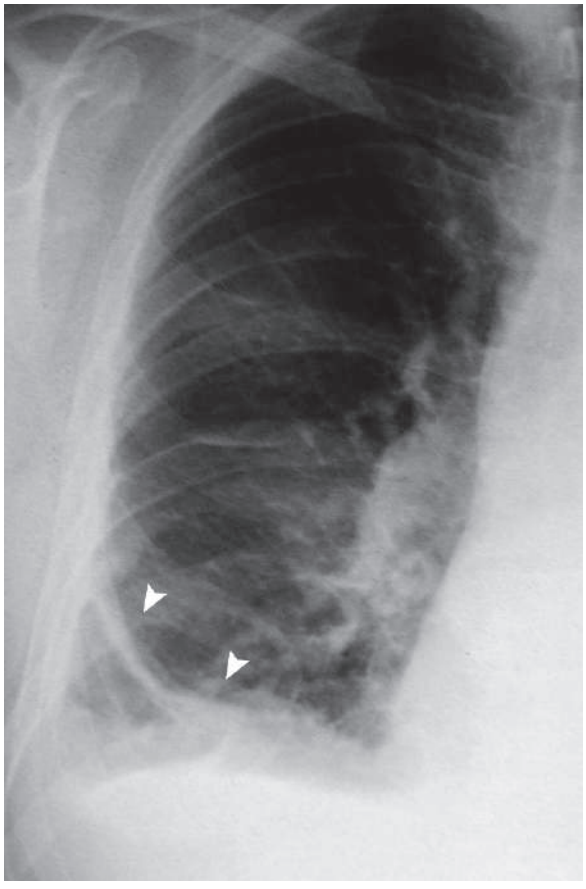

Fig. 3.3.6. Posteroanterior plain chest radiograph shows plate atelectasis as thick radio-opaque shadow at the right costophrenic angle

For Further Reading

1. Tsai KL et al Pulmonary atelectasis: a frequent alternative diagnosis in patients undergoing CT-PA for suspected pulmonary embolism. Emerg Radiol. 2004;10:282–86
2. Sargent MA et al Atelectasis on pediatric chest CT: comparison of sedation techniques. Pediatr Radiol. 1999;29: 509–13
3. Glay J et al Unusual pattern of left lower lobe atelectasis. Radiology. 1981;141:331–33
4. Zhao Y et al Atelectasis – an unusual and late complication of lung transplant. Clin Transplant. 2002;16:233–39
5. Westcott JL et al Plate atelectasis. Radiology. 1985;155:1–9

3.4 Sarcoidosis

Sarcoidosis, also known as *Boeck's sarcoid*, is a multisystemic granulomatous disorder characterized by the formation of multiple epithelioid granulomas within more than one system. Sarcoidosis belongs to a large family of granulomatous disorders, which includes tuberculosis, leprosy, Langerhans cell histocytosis, and more. All members of the granulomatous disease are characterized by the formation of granulomas within the body system.

Granuloma is a specific kind of chronic inflammation, and it is a term used to describe a nodular chronic inflammation that occurs in foci (granules), with collection of macrophages called epithelioid cells. *Epithelioid cells* are macrophages with abundant cytoplasm that is similar to the cytoplasm of epithelial cells. When multiple epithelioid cells fuse together, they form a bigger macrophage known as "*giant cell*." Epithelioid cells define granulomatous inflammation. On histological specimens, granulomas show endartritis obliterance, fibrosis, and chronic inflammatory cells (epithelioid cells). Granuloma can be due to an infection (e.g., tuberculosis), or due to an inorganic foreign body (e.g., silicosis).

Langerhans's cells are characteristically found within the sarcoid granuloma, which develops by the fusion of epithelioid cells, resulting in a modified macrophage with nuclei arranged in an arc-like pattern. Langerhans cells secrete lysozyme, collagenase, calcitriol, angiotensin-converting enzyme (ACE), and varied cytokines.

No body tissue is spared from sarcoidosis. There are two forms of the disease, an acute form and chronic form. *Acute sarcoidosis* responds well to steroids with frequent spontaneous recovery. Moreover, it is characterized by serum elevation of ACE in two thirds of patients and abnormal calcium metabolism (high serum calcium levels). In contrast, the *chronic sarcoidosis* is persistent, and the serum levels of calcium and ACE are often normal.

Sarcoidosis is often seen between 20 and 40 years of age. However, juvenile form (pediatric sarcoidosis) with a smaller age peak at 13–15 years has been reported to occur rarely.

Sarcoidosis manifestations are seen in almost any part of the body. The definite diagnosis is based on histopathology examination. Radiological investigations play an important role in monitoring the therapy and the disease progression.

Pulmonary Sarcoidosis

The pulmonary system is involved in up to 90% of patients with sarcoidosis. Patients with sarcoidosis are classically young females presenting with nonspecific symptoms of a systemic disease (e.g., malaise). In pulmonary sarcoidosis, dyspnea and cough are common, whereas hemoptysis (coughing blood) is rare.

Sarcoidosis Has Five Radiological Grades on Plain Chest Radiograph

Grade 0: Normal chest radiograph.
Grade 1: There are clear lung fields with bilateral hilar lymphadenopathy (85% of cases). It is usually identified by accident, and the patient is asymptomatic (Fig. 3.4.1).
Grade 2: There is reticulo-nodular interstitial pattern with hilar lymphadenopathy. The areas affected are usually located in the upper lobes.

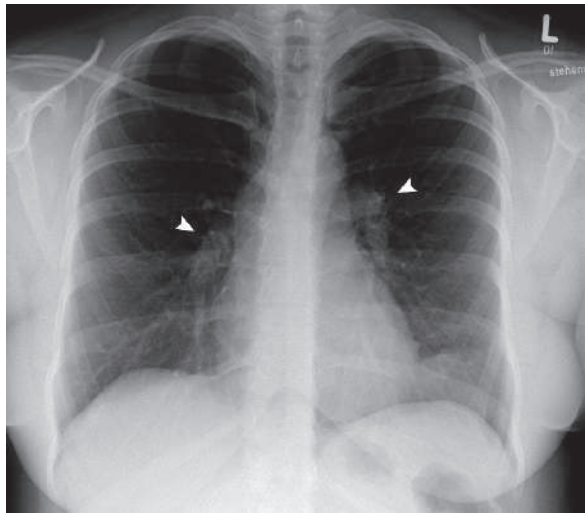

Fig. 3.4.1. Posteroanterior chest radiograph of a female patient with grade 2 pulmonary sarcoidosis shows bilateral hilar lymphadenpathy (*arrowheads*) with clear lung fields

Grade 3: There is reticulo-nodular interstitial pattern without hilar lymphadenopathy (Fig. 3.4.2).
Grade 4: There is pulmonary parenchymal scarring and fibrosis (Fig. 3.4.3).

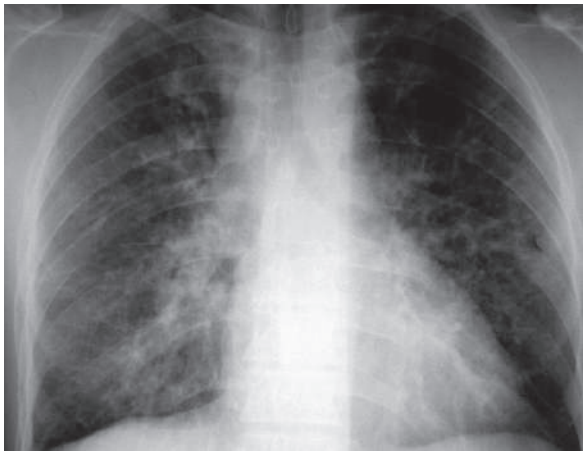

Fig. 3.4.2. Posteroanterior chest radiograph of a patient with grade 3 pulmonary sarcoidosis shows bilateral diffuse reticular interstitial pattern due to lung fibrosis

Signs on HRCT

- Sarcoid granulomas are typically distributed along the lymphatic vessels within the interstitium. Due to this fact, miliary nodules plus linear thickening of the interlobar septa can be found in a similar fashion to the interstitial disease seen in lymphangitis carcinomatosis and lymphoproliferative diseases.
- Bilateral hilar lymphadenopathy observed in grade 2 and 4. Punctuate, stippled, or egg shell calcification patterns may be seen.
- Occasionally, multiple granulomas may aggregate to form a mass-like nodule within the lungs that mimics metastasis (Fig. 3.4.4). Lung nodule is a lesion <3 cm in diameter, whereas lung mass is a lesion >3 cm in diameter.
- Necrotizing sarcoid granulomatosis: is a rare variant of sarcoid characterized by the formation of cavitating granulomas.
- Hilar lymphadenopathy with egg-shell calcification and bilateral upper lobes fibrosis are typical findings in pulmonary silicosis. Sarcoidosis may mimic silicosis when it produces the same set of radiographic manifestations on plain chest radiograph.

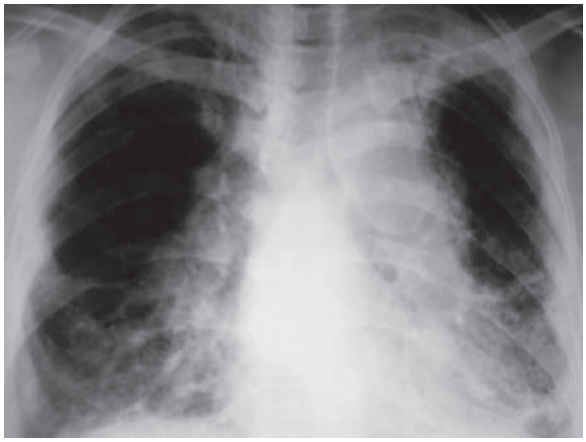

Fig. 3.4.3. Posteroanterior chest radiograph of a patient with chronic grade 4 pulmonary sarcoidosis shows bilateral lung fibrosis distorting the heart silhouette (shaggy heart appearance)

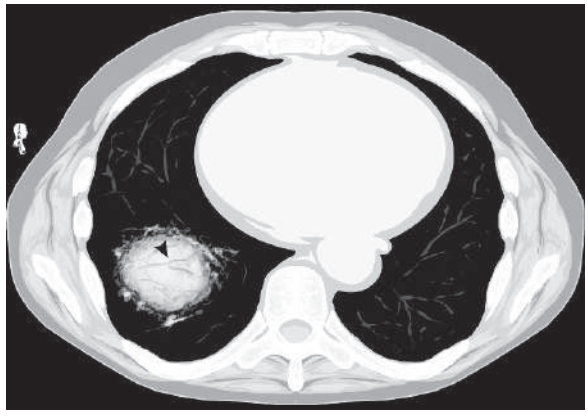

Fig. 3.4.4. Axial thoracic lung-window HRCT illustration demonstrates a pulmonary mass that is composed of multiple aggregated sarcoid granulomas. Although it is a difficult diagnosis to confirm without biopsy, the presence of air bronchogram or areas of normal tissue lines within the mass (*arrowhead*) can differentiate this rare lesion from bronchogenic carcinoma

Hepatic, Splenic and Gastric Sarcoidosis

Hepatic sarcoidosis is seen in 5–15% of patients with high ACE levels (acute disease). There are multiple hepatic granulomas that can be easily mistaken on CT and MRI for metastasis or lymphoma. Simultaneous involvement of the spleen favors the diagnosis of sarcoidosis and lymphoma.

Splenic sarcoidosis classically affects the white bulb and the arterial circulation. The spleen is affected in 5–14% of patients with sarcoidosis. Patients may suffer from symptoms of hypersplenism, anemia, thrombocytopenia, and leucopenia.

Gastric sarcoidosis is the most common feature of gastrointestinal involvement of sarcoidosis. It often involves the antrum. Massive retroperitoneal lymphadenopathy may be rarely encountered in sarcoidosis.

Signs on CT

- Hepatic sarcoidosis is seen as multiple hypodense lesions with irregular shapes on liver contrast-enhanced images.
- Splenic sarcoidosis is seen on contrast-enhanced images as multiple, irregularly diffuse, hypodense lesions within the spleen representing granulomas (Fig. 3.4.5). Hepatic lesions may be noticed in the same scan (50% of cases). The same lesions are seen hypoechoic on US and hypointense on T1W and T2W images on MRI compared to the background.
- Gastric sarcoidosis features ranges from ulceration mimicking peptic ulcer, to mucosal thickening mimicking Menetrier disease. Diagnosis requires endoscopic biopsy to confirm the epithelioid granuloma.

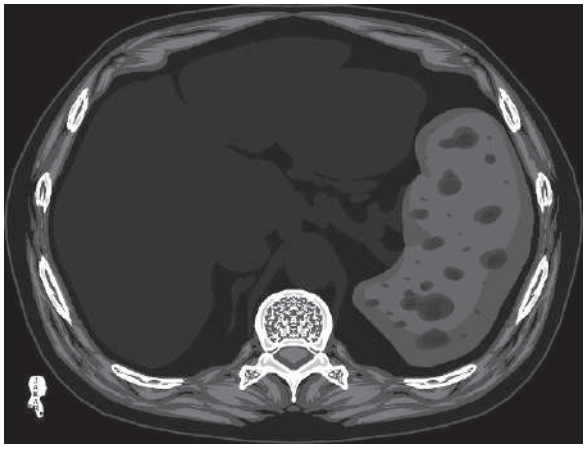

Fig. 3.4.5. Abdominal nonenhanced CT illustration demonstrates multiple hypodense lesions within the spleen representing splenic sarcoid granulomas

Dermatological Sarcoidosis

Skin lesions are seen in up to 25% of patients with sarcoidosis. Skin lesions in sarcoidosis are divided into: reactive and specific lesions. Reactive sarcoidosis skin lesions do not contain granuloma formation histologically (e.g., erythema nodosum). In contrast, specific sarcoidosis skin lesions are characterized by noncaseating granuloma formation (e.g., Drier-Roussy nodules).

In the acute reactive sarcoidosis, *erythema nodosum* is the most common finding, and it is seen as multiple patchy red lesions found over the shin, often in a bilateral fashion. Systemic manifestations like fever, malaise, and polyartheralgia occur in about 50% of patients with erythema nodosum.

The chronic reactive sarcoidosis, on the other hand, is characterized by a specific lesion called "lupus pernio." *Lupus pernio* is a specific skin lesion in sarcoidosis characterized by dusky-red plaques formation on the nose, ears, lips, and face. Lupus pernio is classically seen in women with chronic sarcoidosis and extensive pulmonary infiltration, anterior uveitis, and bone lesions. The nose lesion is typically red to purple in color, and seen on the tip of the nose causing bulbous appearance (Fig. 3.4.6). The nose lesion infiltrates the mucosa, and may destroy the underlying nasal bone.

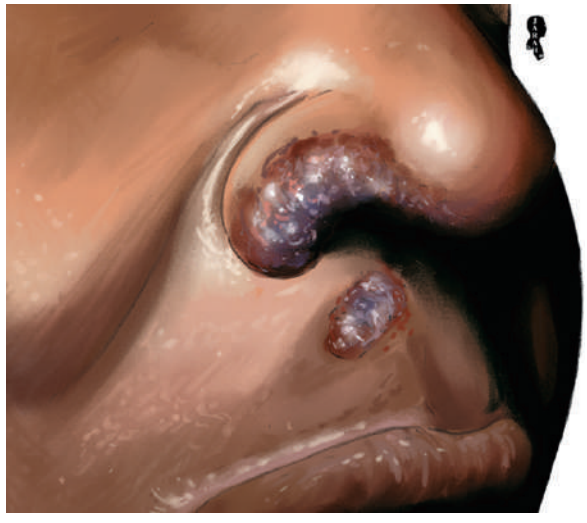

Fig. 3.4.6. An illustration demonstrates lupus pernio on the ala of the nose

3.4

In black patients, maculopapular eruptions are the most common skin manifestations of sarcoidosis. *Darier–Roussy nodules* are small painless subcutaneous nodules that arise within the dermis and the epidermis. They represent noncaseating granulomas.

Differential Diagnoses and Related Diseases

Löfgren syndrome: is a disease characterized by the combination of arthralgia, bilateral hilar lymphadenopathy, and erythema nodosum in a patient with sarcoidosis.

Cardiac Sarcoidosis

Sarcoidosis affects the heart in the form of patchy infiltration of the myocardium by granulomas causing fibrosis and scarring. Patients with cardiac sarcoidosis are at risk of sudden cardiac death due to ventricular arrhythmias or conduction block. Most patients are asymptomatic; with only 5% of cardiac sarcoidosis patients being symptomatic. Cor pulmonale may arise secondary to pulmonary hypertension as a consequence of pulmonary fibrosis.

Signs on Cardiac MRI

- The protocol of cardiac sarcoidosis should include T1W pre- and postcontrast images (there are multiple areas of contrast enhancement due to noncaseating granulomas), T2-STIR (to show edema or scar formation as low intensity areas), and CE-IR images to assess global function.
- Inflammatory changes show myocardial high T2 signal intensity lesions (Fig. 3.4.7), with postcontrast enhancement and myocardial thickening. Postinflammatory changes include myocardial high T2 signal intensity lesions, with no contrast enhancement.

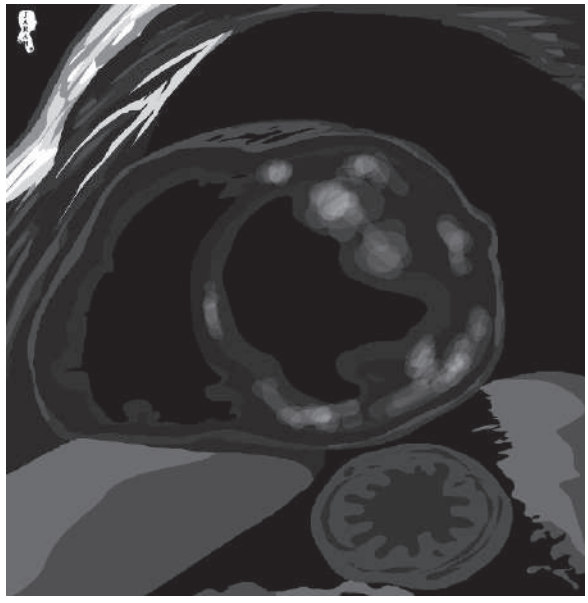

Fig. 3.4.7. Short-axis dark-blood cardiac T2W MR-illustration demonstrates multiple high signal intensity lesions within the myocardium due to granuloma formation in a patient with sarcoidosis

Neurosarcoid

Involvement of the central nervous system by sarcoidosis (neurosarcoid) is noticed in <10% of patients. There are three patterns of involvement: meningial, parenchymal, and vascular.

In the brain, neurosarcoid has an affinity to involve base of the brain and the cranial nerves. It commonly affects the hypothalamus, pons, meningies, spinal cord, basal ganglia, and cranial nerves (optic, facial, and vestibulococchlear). Neurosarcoid is the commonest cause of bilateral facial nerve paralysis. Leptomeningeal thickening in the form of aseptic meningitis is commonly seen in neurosarcoid. When the lesion affects the hypothalamus, it leads to abnormal water balance and disturbance of thirst mechanism (sarcoid diabetes insipidus). Neurosarcoid can present in the absence of systemic sarcoidosis in 3% of cases.

Differential Diagnoses and Related Diseases

Klein–Levin syndrome: is a disease that arises due to hypothalamic or medial thalamic lesions characterized by episodes of compulsive eating (bulimia), hypersexuality in adolescent males, and hypersomnolence. Patients with hypersomnolence sleep an excessive amount of time at night, take long naps during the day, and generally feel drowsy and distracted when awake. Each episode lasts days to weeks with a symptom-free interval of 3–6 months between attacks. Klein-Levin syndrome is reported to occur rarely due to neurosarcoidosis.

- Cranial nerve neuritis is seen as enhancement of the nerves like the facial or the vestibulococchlear within the internal auditory canal on T1W postcontrast images (Fig. 3.4.9).
- When diabetes inspidus is present, thickening of the infundibulum and the optic chiasm with isointense T1/high T2 signal intensities and homogenous contrast enhancement is typically observed.
- Intramedullary spinal cord lesions on T2W images with enhancement after contrast injection may be found representing neurosarcoid granuloma.
- In Klein–Levin syndrome, Hypothalamic T2 high signal lesions with leptomeningeal enhancement on postcontrast injection images may be seen.

Signs on MRI

- Within the brain parenchyma, multiple or solitary brain lesions with a ring-like appearance may be seen on T2W and FLAIR images.
- Thickening and enhancement of the meningies of postcontrast images is a classic finding in neurosarcoid in the area of the sellar diaphragm and the spinal cord (Fig. 3.4.8). Inflammation of basal meningies can lead to interference with cerebrospinal fluid (CSF) flow or aqueduct involvement leading to obstructive hydrocephalus.

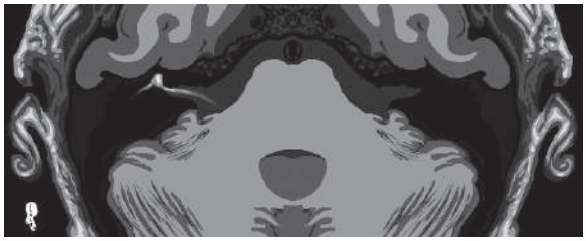

Fig. 3.4.9. Axial cerebellopontine angle T1W postcontrast MR-illustration demonstrates enhancement of the right facial nerve due to neuritis (the labyrinthine segment, the geniculate gangelion, and the proximal tympanic segment)

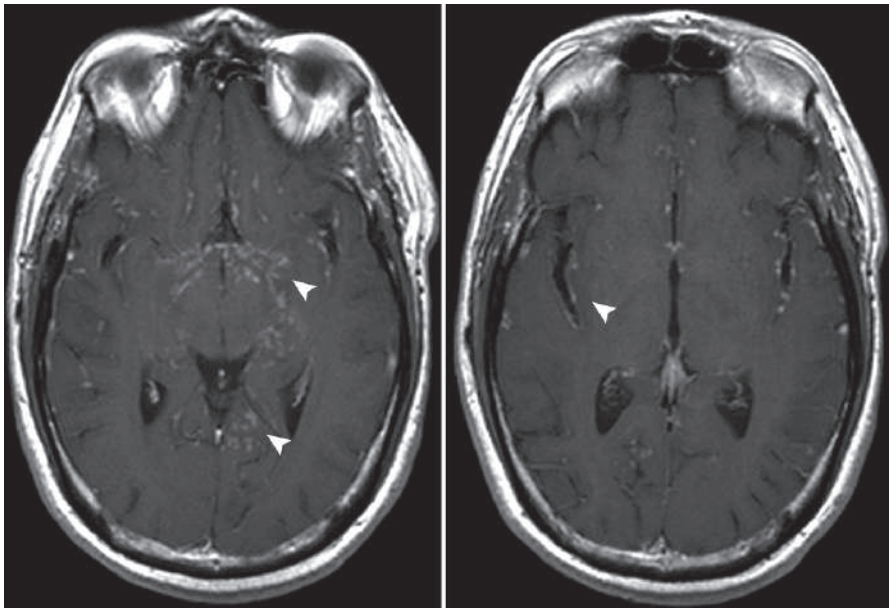

Fig. 3.4.8. Sequential axial T1W postcontrast brain images show nodular thickening and enhancement of the leptomeningies (*arrowheads*) in a patient with sarcoidosis (neurosarcoid)

Musculoskeletal Sarcoidosis

3.4

The musculoskeletal system in sarcoidosis present in the form of arthritis (40%), bony lesions, and muscular lesions. The musculoskeletal manifestations are commonly seen in chronic sarcoidosis, not in the acute form.

Sarcoid arthritis is migratory polyarthritis that involves usually the ankles and the knees, followed by the wrists and the interphalangeal joints. Early sarcoid arthropathy occurs in the first 6 months of symptoms, and it involves migratory polyarthritis (>4 joints). The second form occurs after 6 months or more and is characterized by oligoarthritis (2–3 joints) and inflammation of fingers or toes (dactylitis). Tenosynovitis may occur occasionally, causing a sausage-like finger similar to that seen in psoriatic arthritis.

Bony lesions in sarcoidosis are seen in 5–10% of patients. They present as extensive bony erosions or cystic-like osteolytic lesions typically seen in the phalanges in the hands and feet (*osteitis multiplex cystica*). The same type of lesions can be seen in tuberculosis and classically known as "*osteitis tuberculosa multiplex cystica*." Uncommonly, clavarial sarcoidosis may manifest as an expansile bony lesion.

Muscular sarcoidosis often presents as a nodular mass within the muscle due to granuloma formation.

Signs on Plain Radiographs

- In the phalanges, a sharply-demarcated cystic-like lesion is often found in skeletal sarcoidosis (osteitis multiplex cystica) (Fig. 3.4.10). Swelling of the affected finger with soft-tissue mass found around the lesion is characteristic.
- Sarcoid arthritis involving the hands often shows periarticular soft-tissue swelling plus punched-out lesions of the phalanges.

Signs on MRI

Muscular sarcoidosis presents as a muscular heterogenous mass with hypointense center in all sequences representing fibrosis. Peripheral enhancement may be seen due to active disease process.

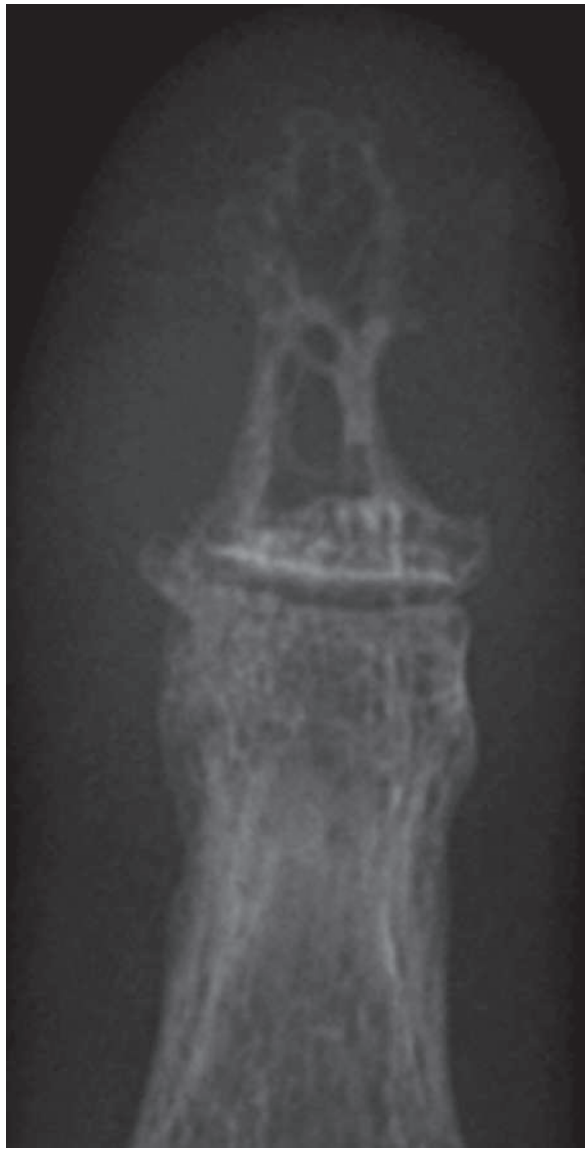

Fig. 3.4.10. Plain radiograph of the index finger of a patient with chronic sarcoidosis shows multiple osteolytic cystic lesions located within the terminal phalanges (osteitis multiplex cystica)

Head and Neck Sarcoidosis

Ocular manifestations of sarcoidosis occur in up to 80% of patients in the form of bilateral uveitis, and lacrimal duct inflammation. However, any structure of the eye may be involved. Conjunctival lesions are the second most common lesions seen in ophthalmic sarcoidosis after

anterior uveitis. Keratoconjunctivitis sicca may occur in 5% of cases when lacrimal gland infiltration occurs.

Parotid gland involvement in a bilateral fashion can be seen in up to 6% of patients. The features resemble the parotid symptoms observed in Sjögren's syndrome and lymphoma.

In up to 30% of cases, patients with sarcoidosis present with cervical, nonender, movable lymphadenopathy commonly located in the posterior triangle.

Hoarseness of voice may rarely arise in patients with sarcoidosis due to vocal cord thickening and granulomas formation. It is a rare manifestation affecting 1–3% of patients.

Paranasal sarcoidosis may occur, especially with lupus pernio. It has an affinity to involve the mucosa of the inferior turbinate and the nasal septum, causing mucosal thickening and nasal septal destruction.

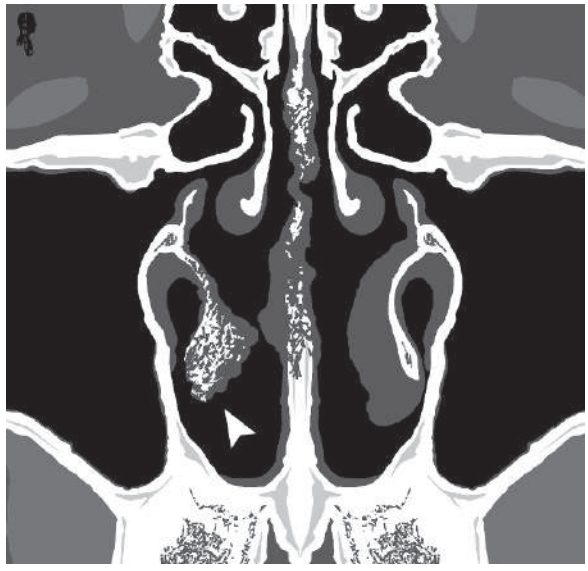

Fig. 3.4.11. Coronal paranasal sinuses CT illustration demonstrates right inferior turbinate destruction (*arrowhead*) with nasal septum erosions due to sarcoidosis

Differential Diagnoses and Related Diseases

Heerfordt syndrome: is a disease that occurs in a patient with sarcoidosis characterized by the triad of fever and anterior uveitis, bilateral parotid enlargement, and facial nerve palsy.

Signs on CT and MRI

- Bilateral enlargement of the lacrimal glands with contrast enhancement is commonly seen in ophthalmic sarcoidosis.
- Bilateral parotid enlargement, with high signal T2 intensity, and enhancement on postcontrast images is seen in cases of parotid involvement.
- Inferior turbinate destruction with nasal septum erosion is seen in paranasal sinus CT (Fig. 3.4.11).

Signs on Scrotal US

Epididmyitis is seen as enlarged heterogeneous epididydmis with marked increased signal flow on color Doppler and Power Doppler due to hyperemia.

Signs on CT

- Interstitial nephritis is seen on postcontrast images as striated nephrogram, usually on both kidneys.
- Rarely, renal sarcoidosis may present with bilateral hypodense tumor-like nodules on contrast-enhanced images that may be mistaken for lymphoma.

Genitourinary Sarcoidosis

Renal sarcoidosis manifestations are related to nephrocalcinosis due to hypercalcemia, or granuloma formation within the cortex and the medulla (interstitial nephritis). Scrotal sarcoidosis is uncommon but can present in the form of bilateral epididymitis.

Signs on MRI

Epididmyitis is seen as bilaterally enlarged epididydmis with high signal intensity on T2W images, with contrast enhancement in postgadolinium injection.

For Further Reading

1. Cummings MM et al Sarcoidosis. Dis Mon. 1960;6:1–40
2. Geraint JD et al Descriptive definition and historic aspects of sarcoidosis. Clin Chest Med. 1997;18:663–79
3. Sharma OP. Sarcoidosis. Dis. Mon. 1990;36:474–535
4. Turkish M et al Osteitis tuberculosa multiplex cystica: its treatment with streptomycin and promizole. J Pediatr. 1949; 35:625–29
5. Koyama T et al Radiologic manifestations of sarcoidosis in various organs. RadioGraphics. 2004;24:87–104
6. Geraint JD et al Descriptive definition and historic aspects of sarcoidosis. Clin Chest Med. 1997;18:663–79
7. Moore SL et al Musculoskeletal sarcoidosis: spectrum of appearances at MR imaging. RadioGraphics. 2003;23: 1389–99
8. Rosell A et al Lupus pernio with involvement of nasal cavity and maxillary sinus. ORL 1998;60:236–39
9. Yanardağ H et al Bone cysts in sarcoidosis: what is their clinical significance? Rheumatol Int. 2004;24:294–96
10. Fodor D et al Dactylitis and bone lesions at the onset of sarcoidosis: a case report. Pol Arch Med Wewn. 2008;118: 774–77
11. Spilberg I et al The arthritis in sarcoidosis. Artheritis Rheum. 1969;12:126–36
12. Warshauer DM. Splenic sarcoidosis. Semin Ultrasound CT MRI. 2007;28:21–27
13. Farman J et al Gastric sarcoidosis. Abdom Imaging. 1997; 22:248–52
14. Henry DA et al Multiple imaging evaluation of sarcoidosis. RadioGraphics 1986;6:75–95
15. Kuhlman JE et al The computed tomographic spectrum of thoracic sarcoidosis. RadioGraphics 1989;9:449–66
16. Pattishall EN et al Sarcoidosis in children. Pediatr Pulmonol. 1996;22:195–203
17. Poyanli A et al Vertebral sarcoidosis: imaging findings. Eur. Radiol. 2000;10:92–94
18. Tamme T et al Sarcoidosis (Heerfordt syndrome): a case report. Stomatologija, Baltic Dental Maxillofacial J. 2007;9: 61–64
19. Afshar A et al Sarcoidosis: a rare cause of Kleine-Levine-Critchley syndrome. Sarcoidosis Vasc Diffuse Lung Dis. 2008;25:60–63
20. Burov EA et al Morpheaform sarcoidosis: report of three cases. J Am Acad Dermatol. 1998;39:345–8

3.5

Emphysema

Emphysema is a chronic obstructive airway disease characterized by an abnormal, irreversible, permanent enlargement of the air spaces distal to the terminal bronchioles, associated with destruction of the alveolar walls, and without obvious fibrosis.

The mechanism of emphysema is mainly mediated by the proteolytic enzymes (proteases) of the neutrophils and macrophages. The proteolytic enzymes dissolve the alveolar walls creating holes that facilitate air leak from one alveolus to another, compromising gas exchange and trapping air within the acini. Normally, there are few small physiological holes between the alveoli that connect two adjacent alveoli together (pores of Khon). In emphysema, the holes between the alveoli are numerous and much bigger than the normal Khon's pores, resulting in reducing the surface area for gas exchange.

The enzyme α-1 antitrypsin is a proteinase inhibitor that counteracts the effect of the proteolytic enzymes produced by neutrophils and macrophages. Emphysema results from imbalance between the proteolytic enzymes (proteases) production and α-1 antitrypsin (antiproteases).

The first emphysema mechanism arises due to increased alveolar infiltration by neutrophils and macrophages, with increased proteolytic enzymes' production that exceeds the capacity of the normal circulating α-1 antitrypsin levels to counteract. This scenario is classically seen in emphysema due to cigarette smoking. The other mechanism of emphysema is seen due to congenital α-1 antitrypsin deficiency disease, where emphysema is produced with normal quantities of proteolytic enzymes.

Pathologically, emphysema is divided according to the level of alveolar destruction and the air trapping pattern within the secondary lobule (e.g., central or peripheral). Four major types of emphysema are described:

- *Centrilobular emphysema*: this type starts at the center of the secondary lobule (centri-lobular), and it results from the destruction of the alveoli around the proximal respiratory lobule. This type is typically seen in chronic cigarette smokers, and it affects predominantly the upper lung lobes. The emphysematous spaces may coalesce into a lager *bulla*, which is defined as sharply demarcated area of air collection > 1 cm in diameter and with a wall less than 1 mm in thickness (Fig. 3.5.1).
- *Panlobular* (*panacinar*) *emphysema*: this type of emphysema is diffuse and involves the whole secondary lobule. This type is classically seen in nonsmoker patients with congenital α-1 antitrypsin deficiency disease and in *Swyer–James syndrome* (unilateral hyperinflated lung with pulmonary vasculature atresia, and it may be accompanied by bronchiectasis). Panlobular emphysema can be seen in conjunction with centrilobular emphysema in chronic smokers. Panlobular emphysema involves mainly the lower lung lobes.
- *Paraseptal* (*distal lobular*) *emphysema*: this type is seen as air trapping at the periphery of the secondary lobule, especially adjacent to connective tissue septa. This type is typically seen at the periphery, at the subpleural spaces, and along the fissures and pleural reflections. It plays an important role in the development of spontaneous pneumothoraces.
- *Irregular* (*paracicatricial*) *emphysema*: this type is an air collection that occurs in an area of massive fibrosis (scar tissue). It is commonly found in the upper lobes in an area of old tuberculosis fibrosis.

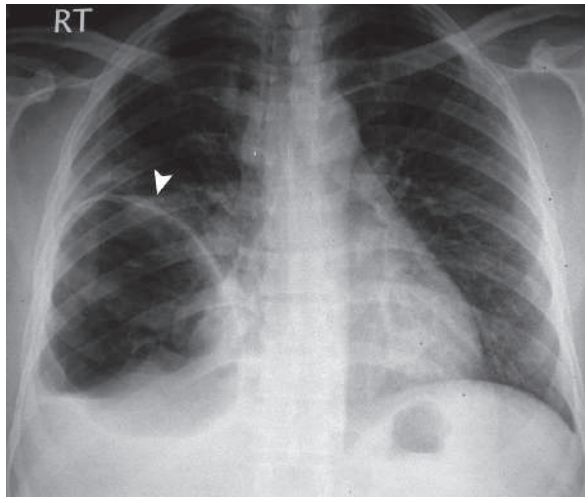

Fig. 3.5.1. Posteroanterior plain chest radiograph shows large right lower zone bulla (*arrowhead*)

Other types of emphysema include:

- *Emphysema due to old age*: it occurs due to the loss of lung volume (atrophy). It is panacinal type without airways obstruction.

3.5

- *Compensatory emphysema* (*Postpneumonectomy syndrome*): this type occurs when a lung lobe collapses or has been removed. The other lung will expand to occupy the space of lung deficiency. There is no airways obstruction with this type.
- *Giant bullous emphysema* (*Vanishing lung syndrome*): it is airways destruction due to extensive alveolar atrophy due to avascular necrosis of the lung parenchyma, resulting in hyperinflation of the affected lung. It is most commonly seen in young men with bilateral upper lobes bullae. It is panlobular type affecting the upper lobes mainly, and commonly present in individuals in their 40s. Up to 20% of patients have congenital α-1 antitrypsin deficiency disease.
- *Bronchial atresia emphysema*: this type arises due to developmental bronchial atresia. The segment with the atrophic bronchus receives its aeration by the "collateral air-drift mechanism" via "pores of Kohn" and "canals of Lambert." It is panacinar type and usually affects the left upper lobe.
- *Foreign body emphysema*: It is lung hyperinflation due to an obstructed bronchus. It's reversible airways obstruction.
- *Subcutaneous* (*surgical*) *emphysema*: it is defined as collection of air at the level of subcutaneous tissues superficial to the deep fascia that covers the skeletal muscle plane. This type is commonly seen after trauma to the trachea or the esophagus in car accidents, stab wounds, or gunshot wounds. It can also be seen in intensive patients on a positive airway-pressure ventilator. *Air-leak syndrome* is a term used to describe generalized thoracic air leak that includes subcutaneous emphysema, pneumomediastinum, pneumopericardium, with or without pneumothorax.

Signs on Chest Radiographs

- Lung hyperinflation, which is detected as posterior rib counts >10 ribs, anterior rib count >7 ribs, and increased intercostals spaces distance.
- Prominent hilar vessels with disappearance of the peripheral vessels
- Increase in the retrosternal trans-radiant area size on lateral radiographs, which is the area behind the sternum where the two lungs come in contact. This space is usually up to 3 cm deep. An increase in this area above 3 cm might indicate emphysema (Fig. 3.5.2).
- Deep sulcus sign: the costophrenic angle deepens due to lung hyperinflation (Fig. 3.5.3).
- Flattening of the diaphragm with barrel (funnel-shaped) chest configuration (Fig. 3.5.4).
- Bulla is visualized as a hypelucent area surrounded by thin wall.
- Compensatory emphysema: a hyper inflated lung with a part herniating into the other side of the chest to compensate an area of lung deficiency or atelectasis (Fig. 3.5.3).
- Vanishing lung syndrome: bilateral upper zones giant bullae (Fig. 3.5.5).
- Foreign body emphysema: unilateral hyperinflated lung usually with radio-opaque structure located at the areas of the main bronchi or trachea.
- Subcutaneous emphysema: radiolucent air is visualized under the skin and around the muscles (Fig. 3.5.6).

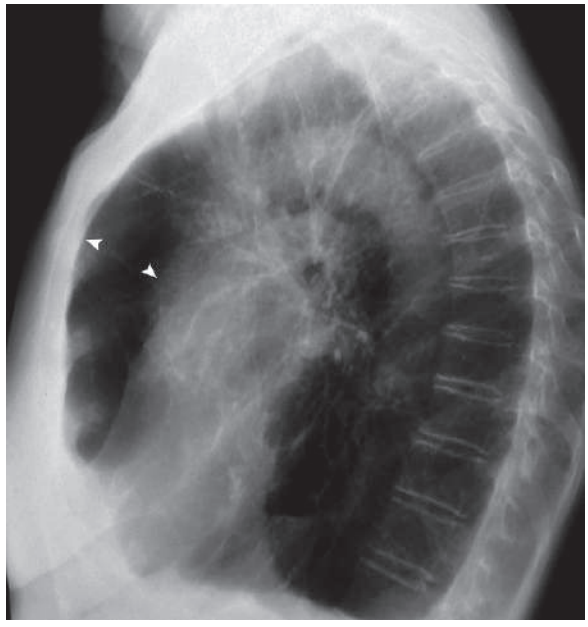

Fig. 3.5.2. Lateral plain chest radiograph of a patient with congenital α-1 antitrypsin deficiency disease shows increased retrosternal space due to emphysema (*arrowheads*)

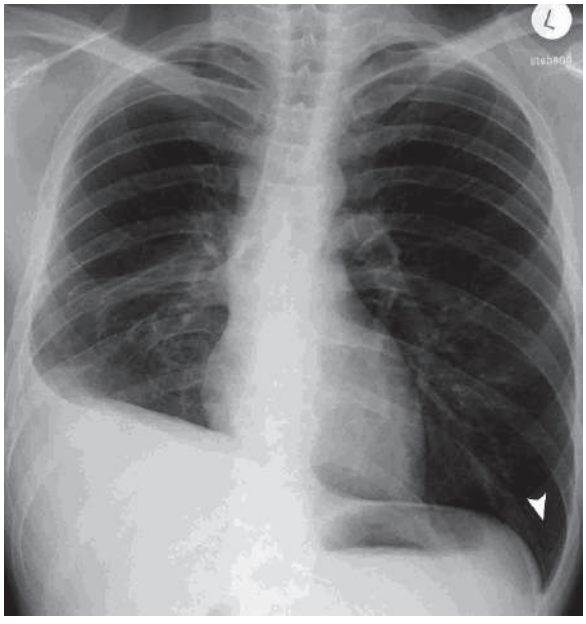

Fig. 3.5.3. Posteroanterior plain chest radiograph of a patient with postpneumonectomy of the right lower lung lobe shows compensatory emphysema of the left lung with deep sulcus sign (*arrowhead*)

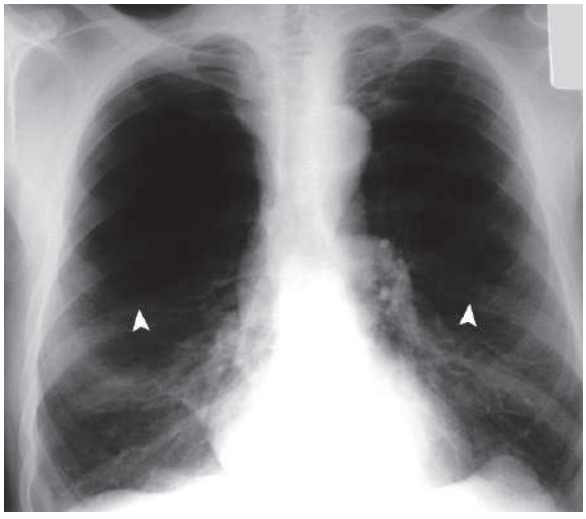

Fig. 3.5.5. Posteroanterior plain chest radiograph of a patient with vanishing lung syndrome shows bilateral giant upper lobes bullae (*arrowheads*)

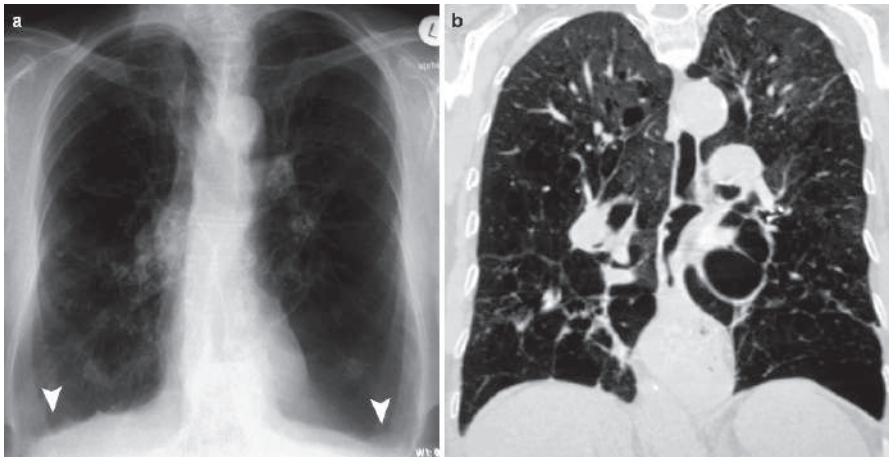

Fig. 3.5.4. Posteroanterior plain chest radiograph (**a**) and coronal chest HRCT (**b**) of two patients with congenital α-1 antitrypsin deficiency disease shows flattened diaphragm in (**a**) (*arrowheads*), and bilateral panlobular and centrilobular emphysema in (**b**)

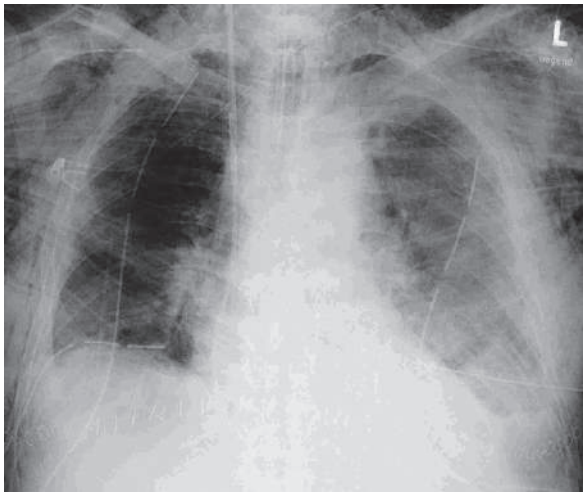

Fig. 3.5.6. Anteroposterior plain chest radiograph of a patient with subcutaneous emphysema shows air that surrounds the pectoralis muscle fibers bilaterally

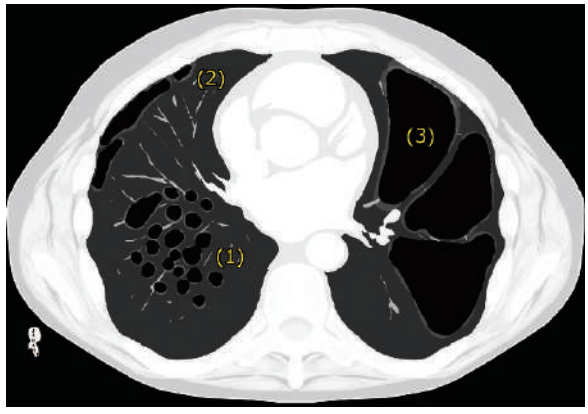

Fig. 3.5.7. Axial thoracic HRCT illustration demonstrates types of emphysema on HRCT: (**1**) centrilobular, (**2**) paraseptal, and (**3**) panlobular

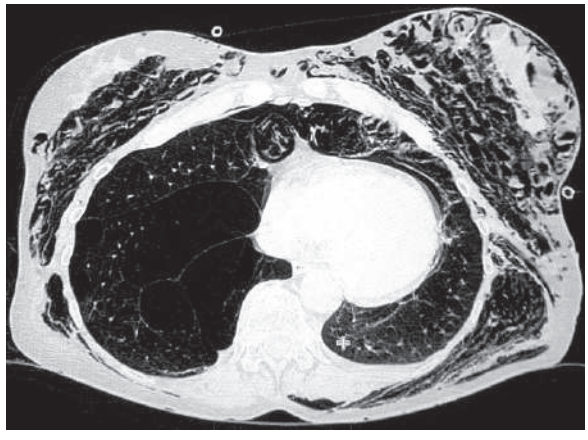

Fig. 3.5.8. Axial thoracic HRCT of a female patient with air-leak syndrome shows right panlobular emphysema, subcutaneous emphysema affecting the thoracic wall and breasts bilaterally, and mild pneumopericardium

Signs on HRCT and Conventional CT

- Centrilobular emphysema: appears as focal, oval, or round areas of low attenuation up to 1 cm in diameter, within a homogenous background of lung parenchyma (Fig. 3.5.7), and not associated with fibrosis. It has a characteristic upper lung zones predominance.
- Panlobular emphysema: appears as large, uniform low attenuation areas with characteristic lower lung zones predominance (Fig. 3.5.7).
- Paraseptal emphysema: appears as multiple small areas of low attenuation located typically at lung peripheries with subpleural location (Fig. 3.5.7). It has thin walls, and should not be confused with honeycombing, which is characterized by thick wall bronchiectasis, with signs of fibrosis and architectural distortion.
- Irregular emphysema: appears as air bullae trapped within areas of fibrosis.
- Congenital α-1 antitrypsin deficiency disease is typically associated with signs of liver cirrhosis, with risks of developing hepatocellular carcinoma. Patients are typically in their 40s presenting with dyspnea with signs of hepatic dysfunction.
- Air leak syndrome is detected as generalized subcutaneous emphysema, pneumomedistinum, parenchymal emphysema, pneumopericardium, with or without pneumothorax (Fig. 3.5.8).

For Further Reading

1. Stern EJ et al CT of the lung in patients with pulmonary emphysema: diagnosis, quantification, and correlation with pathologic and physiologic findings. AJR Am J Roentgenol. 1994;162:791–98
2. Thurlbeck WM et al Emphysema: definition, imaging, and quantification. AJR Am J Roentgenol. 1994;163:1017–25
3. Thurlbeck WM et al Radiographic appearance of chest in emphysema. AJR Am J Roentgenol. 1978;130:429–40
4. Kazerooni EA et al Imaging of emphysema and lung volume reduction surgery. RadioGraphics 1997;17:1023–36
5. Marti de Gracia M et al Subcutaneous emphysema: diagnostic clue in the emergency room. Emerg Radiol. 2009;16:343–48. DOI 10.1007/s10140–009–0794-x
6. Yamanoha A et al Air-leak syndrome associated with bronchiolitis obliterans after allogeneic peripheral blood stem cell transplantation. Int J Hematol. 2007;85:95–96
7. Bergin C et al The secondary pulmonary lobule: Normal and abnormal CT appearance. AJR Am J Roentgenol. 1988; 151:21–25

3.6 Idiopathic Interstitial Pneumonias

Idiopathic interstitial pneumonias (IIPs) are a group of diseases characterized by parenchymal lung fibrosis. IIPs are classified by the American Thoracic Society (ATS) and the European Respiratory Society (ERS) into seven disease entities: idiopathic pulmonary fibrosis, nonspecific interstitial pneumonia (NSIP), cryptogenic organizing pneumonia (COP), respiratory bronchiolitis-associated interstitial lung disease (RB-ILD), desquamative interstitial pneumonia (DIP), lymphoid interstitial pneumonia (LIP), and acute interstitial pneumonia (AIP).

Although the ATS-ERS classification differentiates between the subtypes of IIPs based on histopathology findings, radiology can help in the diagnosis assessment based on the computed tomography findings of each disease. Lung extension can be characteristic for some IIP subtypes.

Patients with IIPs generally present with progressive dyspnea, cough, and other nonspecific respiratory symptoms.

Idiopathic Pulmonary Fibrosis

Idiopathic pulmonary fibrosis (IPF), also known "*usual pulmonary fibrosis*," is a disease characterized by lung fibrosis with unknown cause.

Patient with IPF is typically a 50-year-old patient presenting with progressive dyspnea and nonproductive cough. Clinical examination may show signs of chronic cyanosis, finger clubbing, and basal lung crepitation on auscultation. Diagnosis of IPF by histology is very important because IPF patients usually do not respond to high corticosteroid therapy, with a median survival time ranging from 2 to 4 years after starting symptoms.

History of smoking can be a risk factor for IPF. However, it does not affect the course of the disease.

Signs on Radiographs and HRCT

- Typically, patients with IPF present with reticular interstitial pattern with reduced lung volume, subpleural reticular opacities, and macrocytic honeycombing (bronchiectatic changes). The distribution of the lung fibrosis characteristically involves the lung bases and decrease toward lung apices (apicobasal gradient) (Figs. 3.6.1 and 3.6.2).
- Shaggy heart appearance: it is a term used to describe fibrosis silhouetting the heart borders (Fig. 3.6.2).

Nonspecific Interstitial Pneumonia

NSIP is a disease with lung fibrosis that is usually difficult to differentiate from IPF. However, differentiating IPF from NSIP is important, since the latter has a better response to high corticosteroid therapy.

Patients with NSIP are typically seen in their 40s with signs and symptoms similar to IPF. NSIP has no obvious relation with cigarette smoking. NSIP may be encountered with other systemic disorders (e.g., connective tissue disorders).

Signs on Radiographs and HRCT

Patients with NSIP show patchy subpleural reticulonodular pattern, bilateral almost homogenous lung involvement, and microcytic honeycombing (Fig. 3.6.1). The main differences between IPF and NSIP are the lack of the apicobasal gradient involvement (seen in IPF) and the macrocytic honeycombing (also seen in IPF).

Cryptogenic Organizing Pneumonia

COP, formerly known as "*bronchiolitis obliterans with organizing pneumonia*" (BOOP), is chronic pulmonary disease characterized by bronchiolar inflammation (bronchiolitis) and obstruction by a polypoid plug of

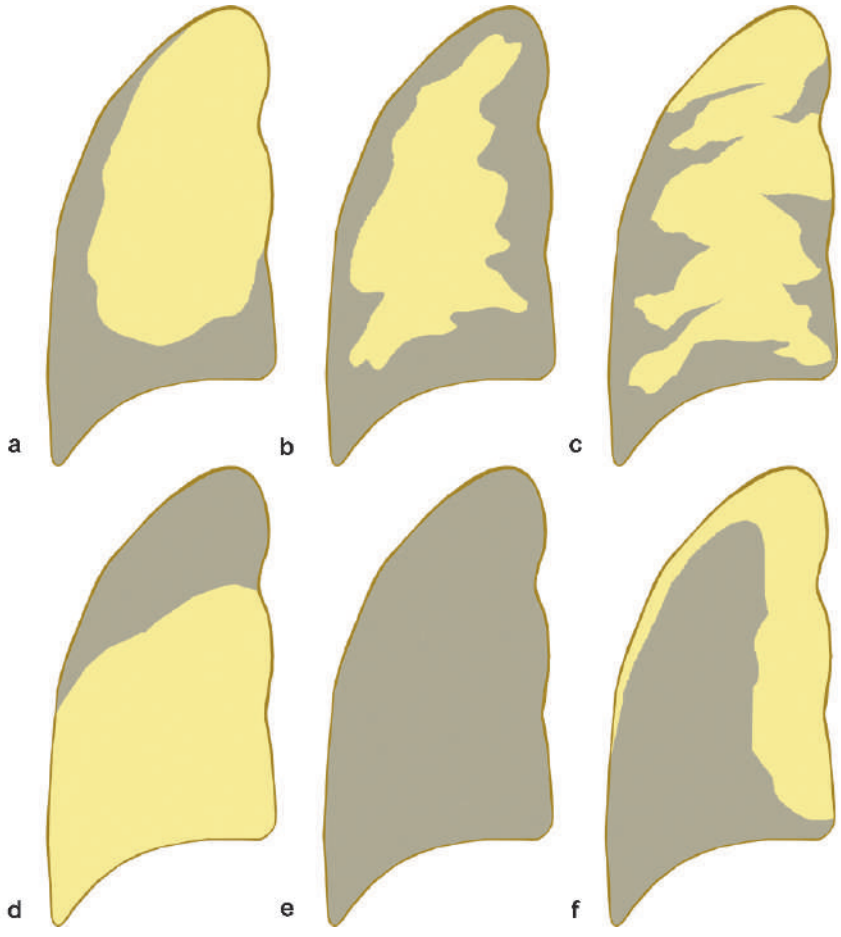

Fig. 3.6.1. An illustration demonstrates the different types of Idiopathic interstitial pneumonias (IIPs) and their pathological distribution patterns: (**a**) idiopathic pulmonary fibrosis, (**b**) nonspecific interstitial pneumonia (NSIP), (**c**) cryptogenic organizing pneumonia (COP), (**d**) Respiratory bronchiolitis-associated interstitial lung disease (RB-ILD), (**e**) lymphoid interstitial pneumonia (LIP), and (**f**) acute interstitial pneumonia (AIP)

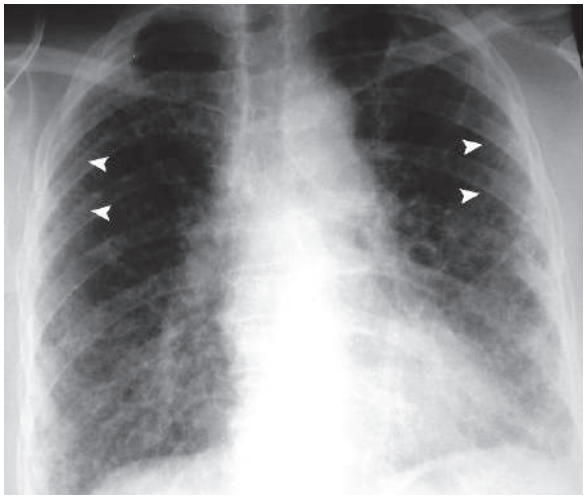

Fig. 3.6.2. Posteroanterior chest radiograph of a patient with Idiopathic pulmonary fibrosis (IPF) shows bilateral reticular interstitial lung pattern located mainly at the base with gradient crawling toward the apices (*arrowheads*). Notice the shaggy heart appearance

granulation tissue formation (obliterance). The granulation tissue blocks the small airways proximal to the alveoli resulting in patchy parenchymal disease. Pneumonia often develops in bronchiolitis obliterance due to inflammation of the surrounding parenchyma as a consequence to the bronchiolitis (organizing pneumonia).

The bronchioles are classified into terminal bronchioles and respiratory bronchioles. A disease involving the terminal bronchioles will result in a clinical picture that resembles a conductive airways disease. In contrast, when the respiratory bronchioles are affected by a disease, a clinical picture resembles restrictive airways disease that arises because the adjacent alveoli are affected too. COP is a disease of the respiratory bronchioles.

Most cases of COP are unknown, and seen in patients between 40 and 60 years of age. COP in adults can arise secondary to variety of causes such as chronic aspiration pneumonia, radiation therapy, bone marrow transplant, medications (e.g., amiodarone), and connective tissue

disorders (e.g., rheumatoid arthritis). Most patients with COP are nonsmokers, or ex-smokers.

Patients usually present with persistent nonproductive dry cough that resists antibiotics for duration that can last up to months. Dyspnea, low-grade fever, malaise, and weight loss are other common features. Lab results usually show elevated erythrocyte sedimentation rate (ESR) and C-reactive proteins, with restrictive pattern on pulmonary function tests.

Signs on Radiographs

- Chest radiographs show peripheral lung field patchy infiltration that can be unilateral or bilateral, often with basilar predominance (Figs. 3.6.1 and 3.6.3).
- Bilateral interstitial, reticulo-nodular pattern may be seen.

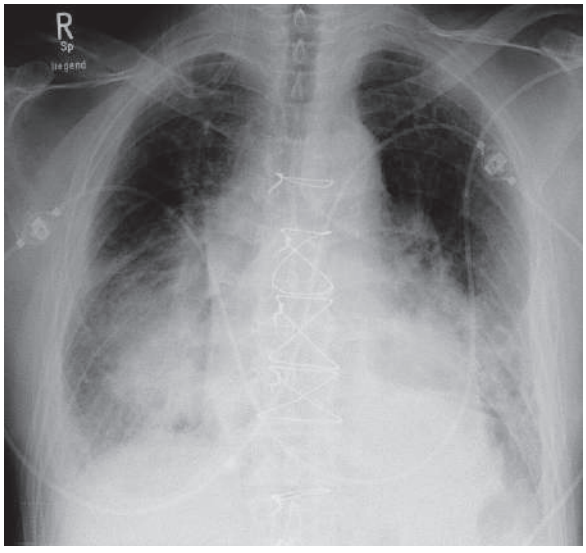

Fig. 3.6.3. Anteroposterior chest radiograph of a patient with bone marrow transplant due to leukemia who developed COP shows bilateral patchy infiltrations located at the lung bases with peripheral patchy infiltration

Signs on HRCT

- The typical HRCT picture of COP is bilateral, patchy, triangular areas of consolidation located in the peripheral subpleural areas (60–90% of cases) (Fig. 3.6.4). Also, peribronchial patchy consolidations located in the lower lobes are also a common presentation.
- Bilateral, scattered ground-glass appearance opacities with thickened interlobular septa can be seen in up to 60% of cases (Fig. 3.6.4). These areas are hyperdens in cases of amiodarone toxicity due to the presence of iodine in the drug.
- Another uncommon presentation of COP is a focal parenchymal mass often located in the upper lobes in contact with the pleura and fissures (30% of cases). This presentation cannot be differentiated from cancer by imaging alone; biopsy is needed to confirm the diagnosis.
- COP also can present as multiple, mass-like parenchymal lesions with speculated margins, another presentation that may mimic metastasis, infections, or lymphoma. Biopsy is needed to confirm the diagnosis. This pattern can be produced by therapy with bleomycin in cancer patients.
- Bronchocentric COP: this form of COP appears as areas of parenchymal consolidation around the bronchovascular bundle (33% of cases). This pattern resembles the HRCT picture of patients with vasculitis (e.g., Churge-Strauss syndrome) (Fig. 3.6.4).
- Atoll sign: it is seen as an area with ground glass opacity surrounded by a ring of increased density parenchyma. This sign is typical of COP (Fig. 3.6.4).
- Band-like opacities: these are thread-like opacities that run from the bronchi toward the pleura; they may show air-bronchogram sign.

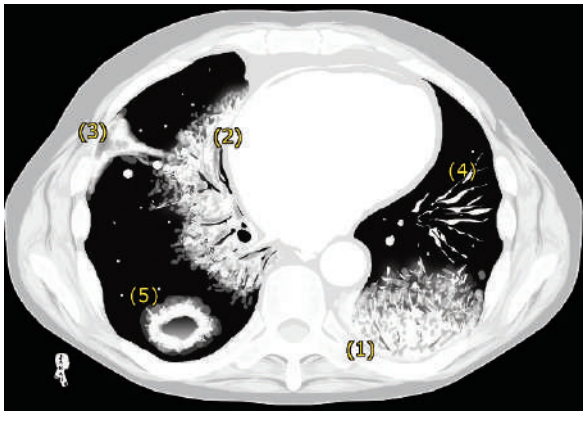

Fig. 3.6.4. Axial thoracic ling-window HRCT demonstrates the different manifestations of COP: (**1**) peripheral classical patchy infiltration of COP, (**2**) bronchogenic COP, (**3**) bronchocentric COP, (**4**) thickened interlobar septae, and (**5**) Atoll sign

3.6

Respiratory Bronchiolitis-Associated Interstitial Lung Disease

RB-ILD is a disease that is considered as an exaggerated form of respiratory bronchiolitis, and it is a smoking-related condition. Also, RB-ILD is considered as the early stage of DIP.

Patients with RB-ILD are commonly males in their 30s or 40s with history of chronic smoking. Smoking cessation is an important element in the medical management of RB-ILD.

Signs on Radiographs and HRCT

- Chest radiograph can be normal.
- On HRCT, the key findings in RB-ILD are centrilobular nodules in combination with ground-glass opacities and bronchial wall thickening predominantly located in the upper lung zones (Fig. 3.6.1).

Desquamative Interstitial Pneumonia

DIP is a condition that is considered as severe form of RB-ILD, and it is strongly associated with cigarette smoking. However, it can arise in nonsmokers due to variety of conditions (e.g., exposure to organic dust). Patients with DIP are often between 30 and 40-years old.

Signs on Radiographs and HRCT

- Radiographic findings are nonspecific.
- CT finding shows diffuse ground-glass opacity that is predominantly located peripherally and in the lower lobes. However, features overlapped with RB-ILD may be seen.

Lymphoid Interstitial Pneumonia

LIP is a disease characterized by lymphoid tissue proliferation and infiltration of the pulmonary interstitium by lymphocytes.

The normal lymphoid system of the lung is composed of four components:

- *Bronchus-associated lymphoid tissue* (*BALT*): it consists of submucosal lymphoid follicles distributed along distal bronchi and bronchioles, usually at the bifurcation. This complex is analogous to other mucosa-associated lymphoid tissue (MALT) such as Peyer's patches in the intestine.
- *Hilar lymph nodes*: these are seen along the trachea and at the lung helium.
- *Intrapulmonary lymph nodes*: they are composed of noncapsulated lymphocytes clusters, usually located in the subpleural parenchyma.
- *Interstitial lymphocytes*: they are seen within the lung interstitium with the pulmonary venules.

LIP is a disease characterized by interstitial lymphocytes proliferation, resulting in an interstitial lung disease. It arises commonly secondary to systemic autoimmune disease (e.g., Sjögren's syndrome), and rarely as idiopathic disease. Most patients are middle-aged, who often present with systemic symptoms, dyspnea, and cough. Almost all patients have dysprotienaemia, usually polyclonal hyper- or hypogammaglobulinaemia.

Signs on Radiographs and HRCT

- Radiographic signs are nonspecific reticulonodular interstitial pattern that is commonly diffuse.
- On CT, LIP shows ground-glass opacities plus multiple fine lung cysts located mainly at the center of mid- and lower lung zones (Fig. 3.6.1). The combination of systemic disease, ground-glass opacities, and small lung cysts at the mid- and lower zones are suggestive criteria of LIP.

Acute Interstitial Pneumonia (Hamman–Reich Syndrome)

AIP is a rare fulminant form of lung disease that occurs in previously healthy individuals. Patients present with signs of acute respiratory distress syndrome (ARDS), fever, and cough with rapid deterioration suggesting pneumonia-like illness.

Patients with AIP are usually lung-disease free, and are over 40 years old. Most patients develop severe

dyspnea that requires mechanical ventilation. The condition is treated with corticosteroid, with a mortality rate that reaches >50% of cases.

Signs on Radiographs and HRCT

Patients show the radiographic signs of ARDS with lower zones predominance bilaterally, and may show spared costophrenic angles (Fig. 3.6.1).

If you were given one investigation to detect lung fibrosis cause, what would you choose?
Invasive test: open lung biopsy.
Noninvasive: HRCT.

For Further Reading

1. Mueller-Mang C et al What every radiologist should know about idiopathic interstitial pneumonias. RadioGraphics 2007;27:595–615
2. Katzenstein AA et al Diagnosis of usual intestitial pneumonia and distinction from other fibrosing interstitial lung diseases. Human Pathol. 2008;39:1275–94
3. Fellrath JM et al Idiopathic pulmonary fibrosis/cryptogenic fibrosing alveolitis. Clin Exp Med. 2003;3:65–83
4. Desai SR et al Traction bronchiectasis is cryptogenic fibrosing alveolitis: associated computed tomographic features and physiological significance Eur Radiol. 2003;13: 1801–08
5. Gibson M et al Lymphocytic disorders of the chest: pathology and imaging. Clin Radiol. 1998;53:469–80
6. Sharief N et al Fibrosing alveolitis and desquanative interstitial pneumonitis. Pediatr Pulmonol. 1994;17:359–65
7. Arakawa H et al Bronchiolitis obliterance with organizing pneumonia versus chronic esinophilic pneumonia: high resolution CT findings in 81 patients. AJR 2001;176: 1053–58
8. Polverosi R et al Organizing pneumonia: Typical and atypical HRCT patterns. Radiol Med. 2006;111:202–12
9. Ghanei M et al Bronchiolitis obliterance following exposure to sulfur mustard: Chest high resolution computed tomography. Eur J Radiol. 2004;52:164–69
10. Tempone V et al Bronchiolitis obliterance organizing pneumonia secondary to chronic aspiration of pharmaceutical tablets: Radiologic-pathologic correlation. Eur J Radiol. (Extra) 2008;67:e99–e101
11. Gibson M et al Lymphocytic disorders of the chest: Pathology and imaging. Clin Radiol. 1998;53:469–80

3.7 Histiocytoses

Histiocytoses are a group of diseases characterized by abnormal proliferation and multiorgan infiltration by histiocytes. Different diseases and clinical presentations fall under the umbrella of histiocytoses.

Histiocytes are bone marrow-derived cells, and they fall into two main groups: the mononuclear phagocytes (macrophages) and dendritic cells. Macrophages are part of the immune system, and their main function is to engulf bacteria and damaged tissues (phagocytosis). They are found in all body organs like the liver (Kupffer cells), brain (microglial cells), etc. In contrast, dendritic cells are a cell family that includes Langerhans cells, interdigitating reticulum cells, and follicular dendritic cells. They are found in the reticuloendothelial system, and their main function is to activate the major histocompatibility complex (MHC)-restricted T-cells by expressing high levels of MHC class II molecules. The reticuloendothelial system includes the liver, spleen, and lymph nodes.

Histiocytoses are classified into three main classes:

Class 1 histiocytoses: Langerhans cell histiocytosis (LCH).
Class 2 histiocytoses: Infection-associated hemophagocytic syndrome, Rosai-Dorfman's syndrome, and Omenn syndrome (OS).
Class 3 histiocytoses: True malignant proliferation, and include acute monoblastic leukemia and true histiocytic lymphoma.

There are other diseases classified as non-LCH and include: Erdheim-Chester disease (ECD) and xanthoma disseminatum (Montgomery syndrome).

Langerhans Cell Histiocytosis

LCH is a disease of unknown origin characterized by proliferation and body infiltration by nonmalignant histiocytes (macrophages and dendrites cells).

The basic lesion in LCH is a granuloma composed of Langerhans cells and lymphocytes (proliferative stage). Next, the granuloma becomes necrotic, with admixture of eosinophis and sometimes multinucleated giant cells (granulomatous stage). Finally, fibrosis of the granuloma occurs with deposition of lipid-laden histiocytes (xanthogranulomatous stage). Electron microscopy reveals characteristic rod-shaped bodies in the cytoplasm of the cells (Birbeck granules).

LCH is a broad spectrum of overlapped syndromes with multiple systemic manifestations. Characteristic bone manifestations include sharply-defined, punched-out lytic bony lesions and vertebra plana. Lung involvement is common and shows diffuse reticulonodular interstitial pattern of involvement, cystic bronchiectasis, and pneumothorax. Central nervous system (CNS) involvements mainly affect the hypothalamic-pituitary axis resulting in diabetes insipidus. Other CNS involvements include white matter lesions that are often seen in the cerebellum and the pyramidal tracts causing ataxia in advanced stage of the disease. Skin involvement is characterized by reddish-brown thoracic and pelvic purperic papules. When these purperic papules are found in a new born, the condition is called "*blueberry muffin baby*," which is commonly seen in neonates with congenital infection (TORCH) and congenital leukemia (Fig. 3.7.1).

The disease can be seen in pediatric and adult patients in a localized or diffuse form. In pediatrics, the disease presents in three main forms: eosinophilic granuloma (EG) (local form), Hand–Schüller–Christian's disease (HSCD, chronic form), and Lettere-Siwe's disease (LSD, acute form). In adults, the most severe presentation is pulmonary LHC.

Eosinophilic granuloma (*EG*) is a solitary localized lytic lesion of the bone, which is typically seen in children <15 years of age. Children EG can be asymptomatic, or present with pain, swelling, and fracture at the site of the lesion. The bony lesions are classically

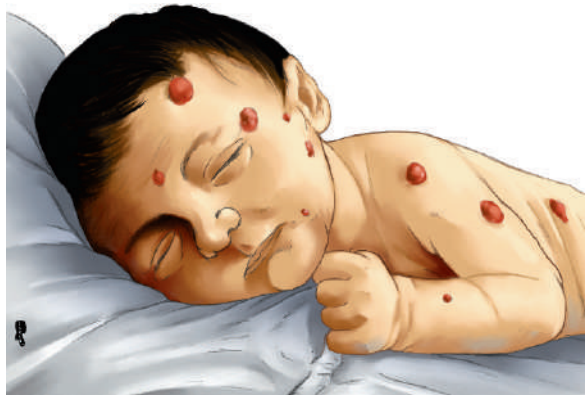

Fig. 3.7.1. An illustration demonstrates the purperic papules in a neonate with blueberry muffin baby condition

found in flat bones, such as the skull, mandible, and pelvis. When EG affects long bones, the lytic lesions are typically seen in the diaphyses, and maybe the metaphyses. ES affecting the epiphyses is rare.

Hand–Schüller–Christian's disease (*HSCD*) is a disease that is seen in children <10 years of age and characterized by a triad of exophthalmos, diabetes insipidus, and hepatosplenomegaly. Cases of HSCD may occur between 20 and 30 years of age. Other manifestations of HSCD include anemia, scaly seborrheic skin rash, restrictive lung diseases (fibrosis), and cerebellar ataxia. Osteolytic bony lesions like EG can be seen.

Lettere–Siwe's disease (*LSD*) is a disease seen in children <2 years old and characterized by hepatosplenomegaly, lymphadenopathy, and sclerosing cholangitis. In LSD, the child grows normally from birth until two years of age, where the disease starts to manifest. LSD is the most aggressive form of LCH. Mental retardation, multiple bony fractures, hemorrhagic rash, anemia, and thrombocytopenia may be seen.

Adult pulmonary Langerhans' cell histocytosis (*PLCH*) affects 1–2 cases per million, and it is often seen in young smokers. There is a strong association between PLCH and cigarette smoking. Cigarette smoking was found to increase the number and accumulation of dendritic cells and Langerhans' cells within the alveolar epithelium in smokers. Most patients with PLCH are asymptomatic. Symptomatic PLCH patients present with dyspnea (35–87%), pleuritic chest pain (9–18%), nonproductive cough (50–70%), pneumothorax (25%), and fever (15%).

Signs on Plain Skeletal Radiographs

- In the clavarium, EG classically presents as osteolytic lesion with geographic, punched-out, sharply-defined border measuring 1–4 cm in diameter (Fig. 3.7.2). The lytic lesion may contain bony sequestrum or bony fragments resembling osteomyelitis. Other lesions show osteolytic lesion with bony sequestrum and include: bone lymphoma and fibrosarcoma.
- EG of the long bone is classically present as punched-out lytic lesion in the diaphysis or the metaphysis. Cortical tunneling, permeative cortical destruction, and periostitis may be seen occasionally, giving the lesion a malignant feature. In the vertebrae, a pucned-out lytic lesion is commonly observed (Fig. 3.7.3).
- Vertebra plana (Pancake vertebra): is a term that describes a vertebra with severe flattening. In a young patient, the most common causes are langerhans' cell histiocytosis (eosionphilic granuloma) or trauma. In an old patient, the most common causes are multiple myeloma or trauma. Typically, there is vertebral body flattening with normal adjacent vertebral discs and sparing of the posterior elements.
- Jaw lesions in EG or HSCD (20%) can present as radicular cysts, periodontal disease, osteomyelitis, and sharply, expansile, punched-out alveolar lesions that spare the roots making the teeth appear as if they are "floating in air".

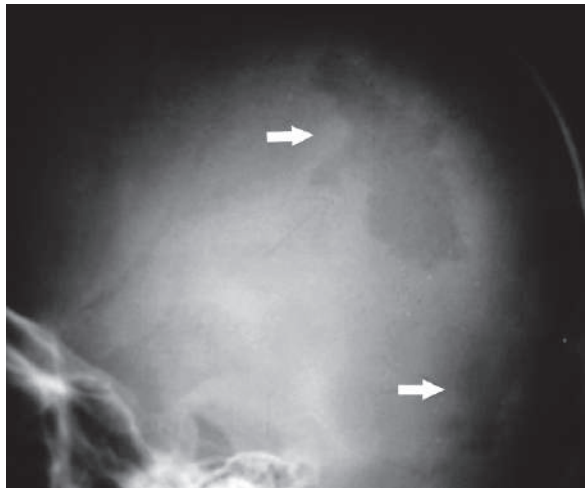

Fig. 3.7.2. Lateral plain skull radiograph shows two sharply lytic, punched-out lesions with geographic edges (*arrows*) in a child with eosinophilc granuloma

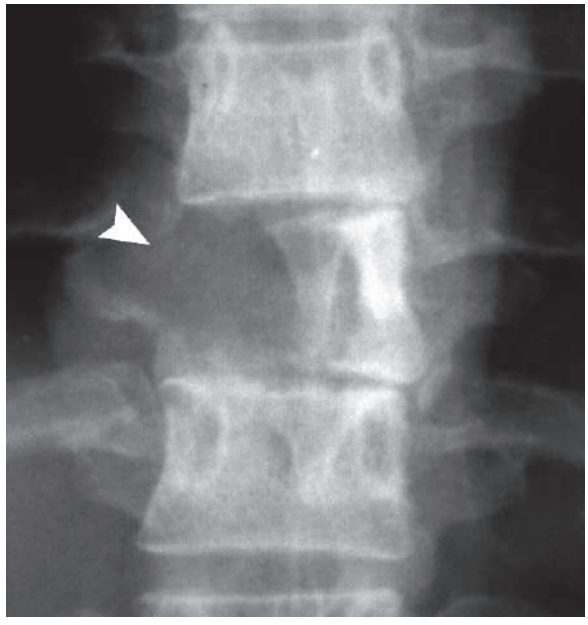

Fig. 3.7.3. Anteroposterior thoracic vertebral plain radiograph shows punched-out lytic lesion affecting the vertebral body in a patient with Langerhans cell histocytosis (LHC) (*arrowhead*)

3.7

Signs on Chest Radiographs and HRCT

- In early PLCH, lung fields show small nodules (1–10 mm in diameter) with irregular borders. The nodules are predominantly seen in the upper and mid-lung zones, sparing the lung bases (Fig. 3.7.4).
- Advanced PLCH shows reticulonodular interstitial pattern and cystic bronchiectasis. The cystic interstitial patterns mimic that of bullous emphysema or lymphangiomyomatosis; the latter is typically seen in tuberous sclerosis. The cysts usually measure 2–3 cm in diameter (Fig. 3.7.5).
- Pneumothorax can be seen in 25% of cases (Fig. 3.7.5).
- Hilar lymphadenopathy can be seen in rare cases.

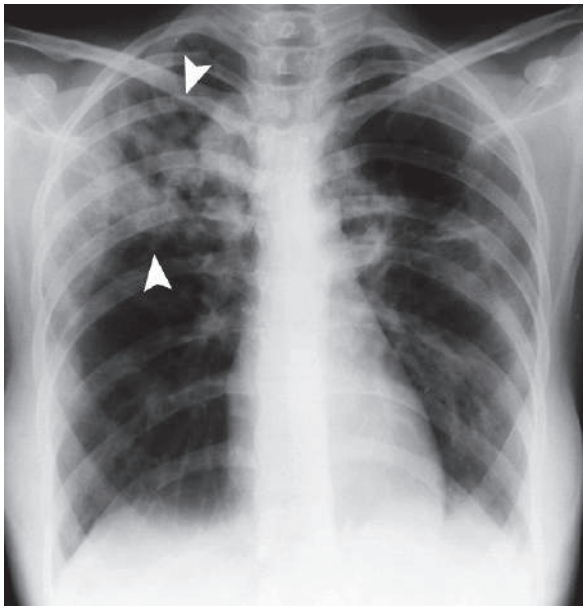

Fig. 3.7.4. Posteroanterior chest radiograph of a patient with adult pulmonary Langerhans' cell histocytosis (PLCH) shows multiple pulmonary nodules with different sizes located at the right upper lung zone (*arrowheads*)

Signs on MRI

- In the sella, the pituitary stalk is typically thickened and shows contrast enhancement in cases of diabetes mellitus (HSCD).
- On MRCP, sclerosing choalngitis in LSD shows absence of the peripheral biliary radicals with intra-hepatic biliary tree stenosis. Notice that these findings are seen in a child.
- Vertebra plana is seen as severely flattened vertebral body (Fig. 3.7.6).

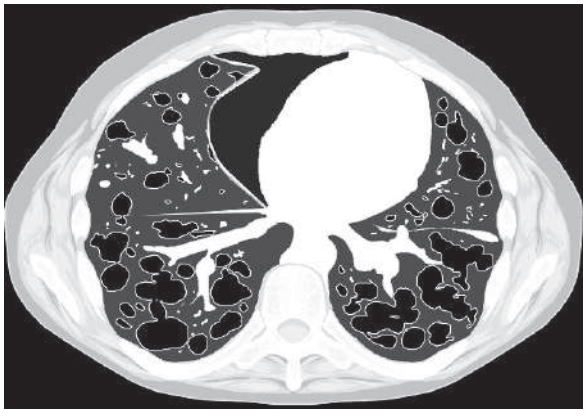

Fig. 3.7.5. Axial HRCT illustration of a patient with PLCH shows diffusely bronchiectatic, cystic changes of the lung parenchyma in a bilateral pattern with right pneumothorax

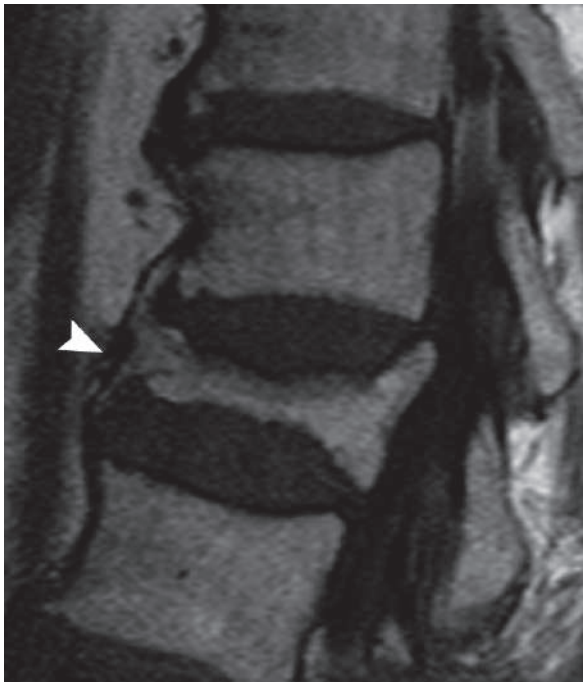

Fig. 3.7.6. Sagittal thoracic vertebral MRI shows vertebra plana (*arrowhead*)

Infection-Associated Hemophagocytic Syndrome

Infection-associated hemophagocytic syndrome is a disease characterized by histiocytes hyperplasia (increased numbers), often due to viral infection (e.g., human immunodeficiency virus).

Patients present with high spiking fever, jaundice, lethargy, and generalized lymphadenopathy and hepatomegaly. Laboratory investigations show hemophagocytosis, hypertriglyceridemia, pancytopenia, and consumptive coagulopathy.

Omenn Syndrome

Omenn syndrome (OS) is a rare, autosomal recessive, non-Langerhans' cell histiocytosis disorder characterized by severe combined immunodeficiency (SCID), erythroderma, hepatosplenomegaly, lymphadenopathy, and alopecia.

Infants with OS typically present in the first few years of life with generalized cutaneous lesions composed of red, exfoliative dermatitis that involves almost the whole body (erythroderma) (Fig. 3.7.7). Erythroderma in infants combined with splenomegaly or lymphadenopathy is diagnostic of OS.

Laboratory investigations may show high serum levels of IgE, and hypogammaglobulinemia.

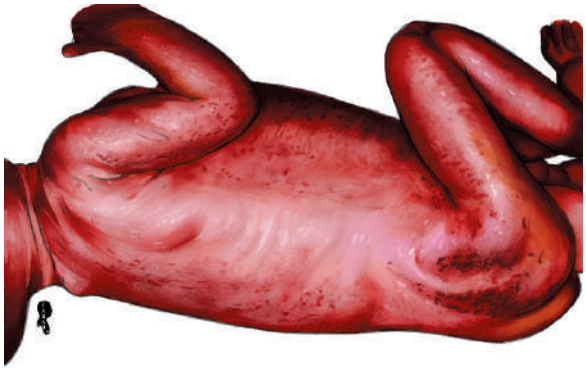

Fig. 3.7.7. An illustration demonstrates the features of Omenn syndrome in a neonate

Chédiak–Higashi Disease

Chédiak–Higashi disease (CHD) is an autosomal recessive, rare disorder characterized by oculocutaneous albinism, increased susceptibility to infections due to immunodeficiency, silvery gray hair, photophobia, neurological impairment, and abnormal giant lysosomes in the leucocytes. Most patients with CHD develop lymphoma-like phase characterized by widespread lymphohistiocytic infiltrates in the lymphoreticular organs (85%).

CHD presents in two main forms: childhood and adult forms. The childhood form is characterized by recurrent pyogenic infections and hepatosplenomegaly. In contrast, the adult form presents in early adulthood with various neurological manifestations that include: Parkinsonism, dementia, spinocerebellar degeneration, and peripheral neuropathy.

Skin hyperpigmentation after exposure to sun light is a characteristic initial feature of CHD. Increased susceptibility to infections in CHD patients is attributed to the defective function of neurtophils. Parental consanguinity is a common feature of CHD.

Differential Diagnoses and Related Diseases

- *Griscelli disease*: is a rare condition characterized by abnormal transfer of melanin granules resulting in light skin and silver hair (Fig. 3.7.8). Griscelli syndrome may be accompanied by neurological abnormalities (type 1), immunodeficiency and neutropenia (type 2), or no other abnormalities (type 3). Patients with Griscelli disease are typically children presenting with characteristic silver hair in addition to febrile episodes, lymphadenopathy, hepatosplenomegaly, anemia, and pancytopenia. Patients may develop seizures and hemiparesis. Brain CT may show brain atrophy. Griscelli disease can be initially mistaken with CHD.
- *Elejalde syndrome* (*Neuroectodermal melanolysosomal syndrome*): is a very rare disease characterized by slivery gray hair, bronze-colored skin, profound

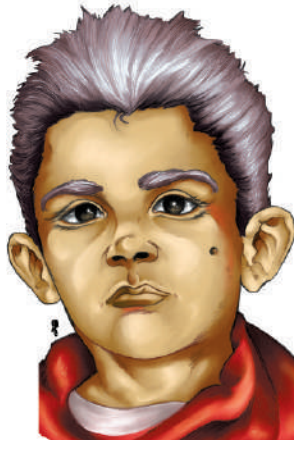

Fig. 3.7.8. An illustration demonstrates the features of Griscelli disease

CNS dysfunction, and a normal immune system. Neurological abnormalities in Elejalde syndrome include sever hypotonia or hyperreflexia, spastic hemi-or quadriplegia, ataxia, seizures, and profound developmental delay. Some investigators believe that Elejalde syndrome and Griscelli syndrome type one are the same disease. However, Elejalde syndrome lacks the immunological abnormalities commonly seen in patients with Griscelli and Chédiak-Higashi syndromes.

Rosai–Dorfman's Disease (Sinus Histiocytosis)

Rosai–Dorfman's disease (RDD) is a rare benign disease characterized by idiopathic proliferation of the phagocytes within the lymph nodes sinuses.

Patients with RDD are typically male children presenting with bilateral massive cervical lymphadenopathy (Fig. 3.7.9), low-grade fever, with or without exophthalmus. Extranodal manifestation like any other histiocytosis disease can involve any part of the body.

Pathologically, the enlarged lymph nodes show infiltration of the sinuses by large histiocytes. The histiocytes contain engulfed lymphocytes and plasma cells (empeiopolesis), which is the hallmark of this disease. Laboratory investigations show leucocytosis, high erythrocytes sedimentation rate, and hypergammaglobulinemia. Burkitt's lymphoma should be ruled out before establishing the diagnosis of RDD. RDD generally resolves without treatment after several months. However, RDD transformation into true malignant lymphoma may occur.

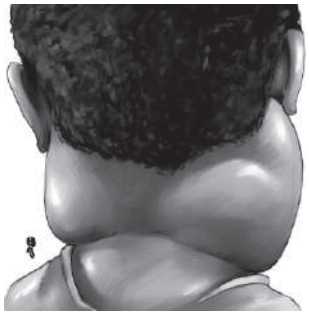

Fig. 3.7.9. An illustration demonstrates the features of Rosai–Dorfman's disease (RDD)

Xanthoma Disseminatum (Montgomery Syndrome)

Xanthoma disseminatum (XD) is a rare, nonmalignant form of non-Langerhans cells histiocytosis characterized by body xanthomata formation that include the skin, trachea, and the larynx in a normal lipid profile patient. Other manifestations include hypopituitarisum, diabetes insipidus (40% of patients), multiple osteolytic lesions seen on plain radiographs, and expansile cystic lesions in the bones of the hands. Patient's brain MRI may show nongliotic brain mass with heterogenous contrast enhancement. Moreover, multiple spinal cord lesions with heterogeneous high T2 signal intensities and intense contrast enhancement may be found. CT of the neck and the thorax may show laryngeal and treacheal wall thickening.

Erdheim–Chester Disease (Lipogranulomatosis)

ECD is a rare, non-Langerhans' cell histiocytosis characterized by almost constant bone lesions and extraosseus manifestations.

ECD affects patients with wide age range (7–78 years). Patients often present with painless bilateral exophthalmos, progressive cerebellar ataxia, diabetes insipidus, and bone pain. Bone involvement is found in 60% of patients, and it is a diagnostic criteria. Diagnosis of ECD is based on: presence of characteristic bony lesions, visceral involvement (especially the retroperitoneal structures), and pathological findings.

ECD is characterized by the formation of lipid granulomas. The cerebral manifestations of ECD are similar to other histiocytoses. Laboratory findings are usually unremarkable, and cerebrospinal fluid analysis is usually normal.

Signs on Plain Radiographs

- Bilateral symmetrical osteosclerotic lesions affecting the metaphyses (83%) and the diaphyses of long bones (98%), with relative sparing of the epiphyses. The corticomedullary junction is blurred, and the bone marrow is obliterated by dense bone. These lesions classically spare the axial skeleton, hands, and feet.
- Radiolucent bands separating the sclerotic metaphysis from the sclerotic diaphysis can be found.
- In <10% of ECD cases, the bony lesions can be purely lytic with no osteosclerosis.

Signs on MRI

- The affected long bones diaphyses and metaphyses exhibit low T1 and T2 signal intensities due to osteosclerosis. Periostitis may be seen in some cases. After contrast injection, enhancement of the periosteum is seen as a white line along the bone margin.
- In CNS, multiple contrast-enhanced lesions on T1W images affecting the meningies, eye, and pituitary are typically found (This combination is very characteristic of ECD).
- Orbital involvement in ECD is seen in the form of retro-orbital masses or diffuses infiltration of the retro-orbital fat (causing exophthalmos).

How can you differentiate ECD from HSCD?

- ECD presents with osteosclerotic lesions, whereas HSCD presents with osteolytic lesions.
- ECD affects patients in the range of 7–78 years, whereas HSCD affects children < 10 years old.
- Retroperitoneal lesions are almost a characteristic finding in ECD.
- On pathology, ECD shows lipid-laden histiocytes.

For Further Reading

1. Stéphan JL. Histiocytoses. Eur J Pediatr. 1995;154:600–09
2. Hoover KB et al Langerhans cell histiocytosis. Skeletal Radiol. 2007;36:95–104
3. Shaffer MP et al Langerhans cell histiocytosis presenting as blueberry muffin baby. J Am Acad Dermatol. 2005;53: S143–6
4. Tamura T et al Congenital Letterer-Siwe disease associated with protein losing enteropathy. Eur J Pediatr. 1980;135: 77–80
5. Young PM et al Rosai-Dorfman disease presenting as multiple soft tissue masses. Skeletal Radiol. 2005;34:665–69
6. Jurić G et al Extranodal sinus histiocytosis (Rosai-Dorfman disease) of the brain parenchyma. Acta Neurochir. 2003;145: 145–49
7. Dion E et al Bone involvement in Erdheim-Chester disease: Imaging findings, including periostitis and partial epiphyseal involvement. Radiology 2006;238:632–39
8. Kumar P et al Chediak-Higashi syndrome. Indian J Pediatr. 2000;67:595–97
9. Hauser RA et al Adult Chediak-Higashi parkinsonian syndrome with dystonia. Mov Disord. 2000;15:705–08
10. Hurvitz H et al A kindred with Griscelli disease: Spectrum of neurological involvement. Eur J Pediatr. 1993;152:402–05
11. Haraldsson Á et al Griscelli disease with cerebral involvement. Eur J Pediatr. 1991;150:419–22
12. Abbott GF et al Pulmonary Langerhans cell histocytosis. RadioGraphics 2004;24:821–41
13. Leatherwood DL et al Pulmonary Langerhans cell histocytosis. RadioGraphics 2007;27:265–68
14. Meyer JS et al Langerhans cell histocytosis: Presentation and evolution of radiologic findings with clinical correlation. Radiographics 1995;15:1135–46
15. Doyle DJ et al Imaging of multisystem Langerhans cell histocytosis in an adult. Eur J Radiol. (Extra) 2007;61:109–117
16. Pupo RA et al Omenn's syndrome and related combined immunodeficiency syndrome: Diagnostic considerations in infants with persistent erythroderma and failure to thrive. J Am Acad Dermatol. 1991;25:442–6
17. Simanski C et al The Langerhans' cell histocytosis (eosinophilic granuloma) of the cervical spine: A rare diagnosis of cervical pain. Magn Reson Imaging 2004;22:589–94
18. Kashihara-Sawami M et al Letterer-Siwe disease: Immunopathologic study with a new monoclonal antibody. J Am Acad Dermatol. 1988;18:464–54
19. Scolozzi P et al Multisystem Langerhans' cell histocytosis (Hand-Schüller-Christian disease) in an adult: A case report and review of the literature. Eur Arch Otorhinolaryngol. 2004;261:326–30
20. Weidauer S et al Cerebral Erdheim-Chester disease: Case report and review of the literature. Neuroradiology 2003;45: 241–45
21. Caparros-Lefebvre D et al Neuroradiologic aspects of Chester-Erdheim disease. AJNR 1995;16:735–740
22. Albayram S et al Spinal dural involvement in Erdheim-Chester disease: MRI findings. Neuroradiology 2002;44:1004–07
23. Alexander AS et al Xanthoma disseminatum: A case report and literature review. Br J Radiol. 2005;78:153–57
24. Baron J et al Xanthoma disseminatum: A rare cause of upper airway narrowing. AJR 2003;180:1180–81
25. Odell WD et al Xanthoma disseminatum: A rare cause of diabetes insipidus. J Clin Endocrinol Metab. 1993;76:777–80
26. Kaneda T et al Langerhans cell histiocytosis in the mandible: Computed tomography and magnetic resonance imaging. Oral Radiol. 1997;13:109–14
27. Burihan J et al Elejalde syndrome: Report of a case and review of the literature. Pediatr Dermatol. 2004;21:479–482
28. Ivanovich J et al 12-year-old male with Elejalde syndrome (neuroectodermal melanolysosomal disease). Am J Med Genet 2001;98:313–16
29. Malhotra AK et al Griscelli syndrome. J Am Acad Dermatol. 2006;55:337–40

3.8 Hemoptysis

Hemoptysis is a term used to describe the pathological condition of coughing blood, typically due to lower respiratory tract disease. Hemoptysis can be a life-threatening condition, and the condition needs urgent evaluation.

The normal lung is supplied by pulmonary arterial system, and bronchial arterial system. *The pulmonary arteries* supply the lungs and take part in gas exchange. In contrast, *the bronchial arteries* are small arteries (2 mm or less in diameter) that arise from the descending thoracic aorta and supply the trachea, the bronchial tree, the visceral pleura, the esophagus, and part of the mediastinal lymph nodes. Histologically, the two systems are connected by thin-walled capillary anastomoses.

The right bronchial artery arises at the level of the fifth or sixth thoracic vertebra posteriorly and usually forms a common trunk with the intercostals artery. The left bronchial artery arises from the descending thoracic aorta anteriorly, with a second left bronchial artery found in up to 70% of population. On CT angiography scan, the right bronchial artery is seen as dots or lines of increased density located in the retrotracheal, retrobronchial, and retroesophageal, regions (Fig. 3.8.1). The left bronchial artery is identified typically as a linear or nodular hyperdensity in the space below the aortic arch above the pulmonary artery (within the aortopulmonary window) (Fig. 3.8.1). Both bronchial arteries normally have highly tortuous course.

The differential diagnosis of hemoptysis is diverse and can occur due to pulmonary infection (e.g., tuberculosis), malignancy (e.g., bronchogenic carcinoma), vascular event (e.g., pulmonary embolism), and vascular anomaly (e.g., arteriovenous malformation). *Cryptogenic hemoptysis* is a term used to describe hemoptysis with no identifiable cause, and it is responsible for up to 42% of hemoptysis episodes, especially in smokers. Cryptogenic hemoptysis is a diagnosis of exclusion, and patients are often recommended to perform another CT several months later to exclude small occult neoplasms formation.

This topic discusses some of the causes of hemoptysis, in which radiology plays an important role in establishing their diagnosis.

Bronchopulmonary Sequestration

Bronchopulmonary sequestration (BPS) is a rare condition characterized by nonfunctioning lung parenchyma mass that is not in continuity with the tracheobronchial tree and is supplied by an anomalous systemic arterial vessel, typically arising from the abdominal aorta and ascending to the mass through the pulmonary ligament. The term sequestration describes disconnected lung tissue with its own anomalous systemic artery.

The primitive lung tissue mass of BPS has its own anomalous systemic vascular supply, usually from the aorta (not bronchial pulmonary circulation). Most cases are diagnosed before the age of 10 years, where the child presents with chronic cough, hemoptysis, and

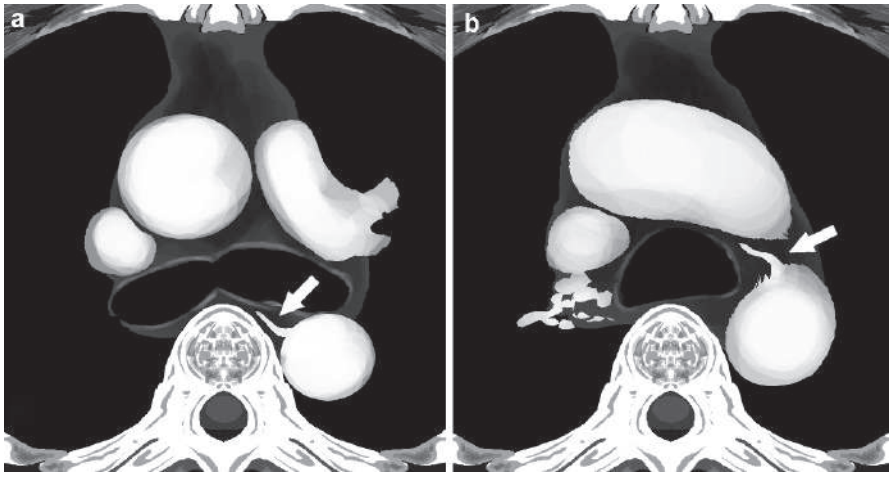

Fig. 3.8.1. Sequential axial CTA illustration demonstrates the normal anatomy of the right bronchial artery (*arrow in* **a**) and the left bronchial artery (*arrow in* **b**)

recurrent pneumonias. *Hybrid lesion* is a term used to describe a lesion, where the sequesterd lung mass has a congenital cystic adenomatous malformation lesion within it. The definite diagnosis of hybrid lesion is by histopathology. BPS is divided into intralobar and extralobar forms.

In *intralobar BPS*, the mass is located inside the lung, surrounded by normal lung parenchyma and shares the visceral pleura with the normal lung tissue. It accounts for 75% of the sequestration cases. The mass is located on the left side in the posterior basal segment in 98% of cases. The mass has its arterial supply from the descending aorta, and its venous drainage from the azygos or systemic veins. In *extralobar BPS*, the mass usually lies within the pleura and has its own pleural layer, and has the same radiological features as the interlobar sequestration. It accounts for 1–6% of the sequestration cases. The mass receives its arterial supply from the thoracic or the abdominal aorta in 80% of cases and is usually found between the lower lobes and the diaphragm. Most cases present within the first 6 months of life with dyspnea, cyanosis, and feeding difficulties.

Signs on CT

The scan shows a hyperdense pulmonary mass that may contain cystic changes or air-fluid level. The mass may appear as a consolidation or atelectatic mass. After contrast injection, an anomalous vessel arises from the abdominal aorta, or the descending thoracic aorta is seen penetrating the mass, which is a pathognomonic finding (Fig. 3.8.2). The sequestred mass may show homogenous or inhomogeneous contrast enhancement.

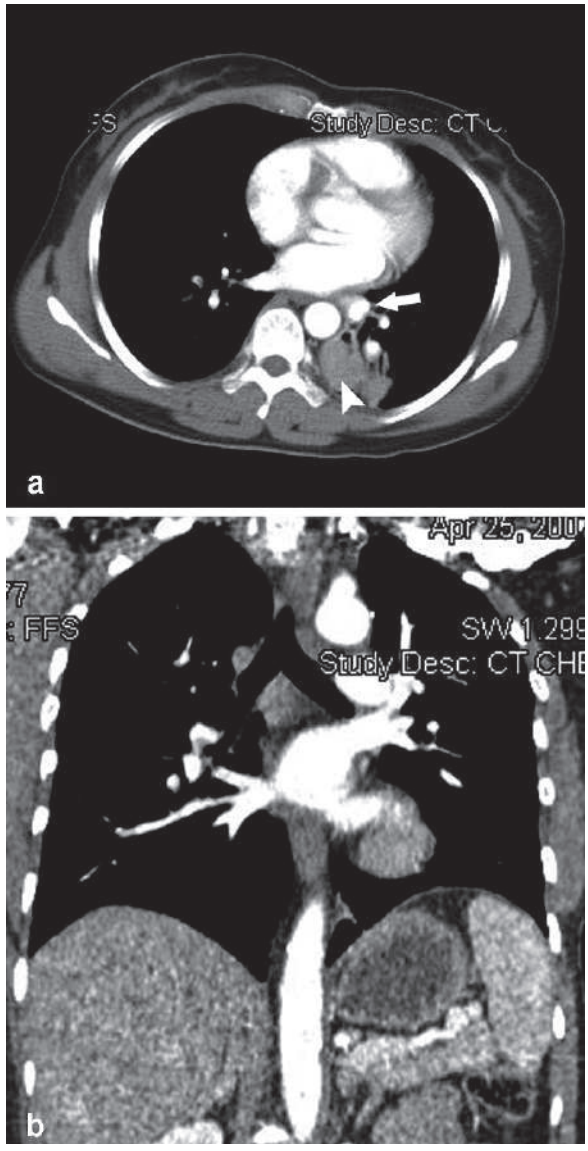

Fig. 3.8.2. Axial (**a**) and coronal (**b**) chest CT shows left lower lobe intralobar bronchopulmonary sequestration mass (*arrowheads*) with its abnormal arterial supply arising form the descending thoracic aorta (*arrows*)

Anomalous Systemic Artery Supplying Normal Lung Parenchyma

3.8

Anomalous systemic artery supplying normal lung parenchyma is a condition characterized by a normal lung parenchyma supplied by anomalous artery in the absence of congenital heart or lung disease. Unlike bronchopulmonary sequestration, there is no abnormal tissue mass, and the vessel is not typically arising from the abdominal aorta. The condition is sometimes referred to as "*pseudosequestration*."

Adult patients with the anomalous systemic artery can be asymptomatic, or present with recurrent hemoptysis. In contrast, pediatric patients with this condition often present with cardiac murmur.

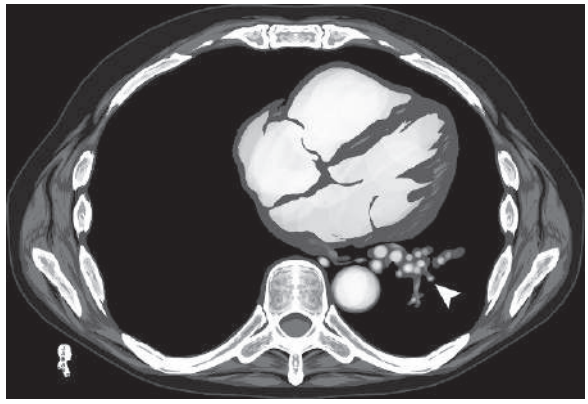

Fig. 3.8.3. Axial CTA illustration demonstrates left pseudosequestration seen as multiple dilated vascular nodules surrounded by normal lung parenchyma (*arrowhead*)

Signs on CTA

- The normal bronchial arteries are <2 mm in diameter, and arise directly from the descending thoracic aorta between the levels of T5 and T6 thoracic vertebrae (orthotopic origin). Anomalous bronchial arteries are defined as arteries that originate outside the range of T5 and T6 thoracic vertebrae (ectopic origin). Hypertrophies bronchial arteries are visualized as nodular or linear mediastinal or retro-bronchial dilated vessels (>2 mm in size) with early enhancement and density similar to the aorta. The hypertrophied bronchial arteries are classically detected in the retro-tracheal area, retro-esophageal area, aortopulmonary window, or the posterior wall of the main bronchus.
- In anomalous systemic artery supplying normal lung parenchyma, a hypertrophies vessel is often identified in an area of normal lung parenchyma in the absence of signs of intra- or extrathoracix abnormal lung mass (differentiate it from bronchopulmonary sequestration) (Fig. 3.8.3). The anomalous systemic arteries usually are very tortuous, and are not parallel to the bronchi (differentiate them from normal bronchial arteries).
- Nonbronchial systemic arteries enter the lung parenchyma through the pulmonary ligament, or the adherent pleura. Identification of dilated vessels within extrapleural fat associated with pleural thickening (> 3 mm) and lung parenchymal abnormalities may be regarded as nonbronchial systemic arteries responsible for hemoptysis.

Pulmonary Vasculitis

Pulmonary vasculitis are group of disorders characterized by inflammation of the pulmonary vessels with granulomas formation. Patients are typically middle-aged presenting with recurrent attacks of fever, dyspnea, and hemoptysis.

The most recognized pulmonary vasculitis diseases are: Wegner's granulomatosis (WG), Churg–Strauss syndrome (CSS) (allergic vasculitis and granulomatosis), and lymphomatoid granulomatosis.

Wegner's granulomatosis (*WG*) is a disease characterized by the triad of febrile sinusitis, glomeulonephritis, and pulmonary vasculitis. Patients often present with dyspnea, rhinitis, otitis media, pleurtic chest pain, and hemoptysis. The presence of cytoplasmic pattern of antineutrophil cytoplasmic autoantibody (c-ANCA) in the patient's serum is a high indicator of WG (96% sensitive for active WG). The serum level of c-ANCA can be used to monitor the disease activity. Histopathologically, WG is characterized by chronic inflammation of the medium-sized and small pulmonary arteries, veins, and capillaries.

CSS is a disease characterized by the triad of asthma or allergic rhinitis, marked peripheral eosinophilia, and systemic vasculitis involving two or more extrapulmonary organs. *Asthma* is a disease characterized by reversible airways obstruction. Patients with CSS are presenting with pulmonary distress, hemoptysis, fever, gastrointestinal symptoms, and arthralgia occasionally.

The typical laboratory findings include marked eosinophilia in the absence of parasitic disease, and high levels of serum rheumatoid factor in 52% of cases. Extrapulmonary vasculitis may be seen in the form of coronary vasculitis, renal-induced hypertension, glomerulonephritis, cerebral hemorrhage, and purpuric skin lesions. CSS can be differentiated from WG by the characteristic association with asthma (rarely encountered in WG), cardiac involvement (up to 47% of CSS cases), and less severe paranasal sinus involvement in CSS. Moreover, patients with CSS show serological positivity of perinuclear antineutrophil cytoplasmic autoantibody (p-ANCA), while WG shows serological positivity of c-ANCA.

Lymphomatoid granulomatosis (*LG*) is a multisystemic disease characterized by lung manifestations (100% of cases), skin and nervous system manifestations (up to 53%), and renal disease (up to 40%). It is characterized pathologically by angiocentric infiltration of the lymphoid tissues and the vessels by atypical lymphocytes, and a mixture of plasma cells and histiocytes, causing tissue destruction and necrosis. Patients typically present with severe generalized symptoms that can be confusing. There is no specific serological marker, and erythrocytes sedimentation rate can be normal in spite of active disease. The main diagnostic method is biopsy of the lesions.

Signs on Radiographs and HRCT

- In *WG*, the early stages of the disease show reticular or nodular interstitial lung pattern mainly located at the lung basis. As the disease progresses, diffuse alveolar lung disease may be seen bilaterally due to pulmonary hemorrhage (Fig. 3.8.4).WG may cause areas of consolidation or nodules with a cavity formation in the center.
- In *CSS*, the plain radiographs may be normal in 25% of cases. The pathological signs are similar to WG, with the formation of multiple granulomatous nodules with or without central cavity likely to be seen (Fig. 3.8.5).
- In *LG*, there are typically large lung mass-like opacities located within the lung parenchyma (due to pulmonary infarcts). Up to 80% of cases present as multiple, bilateral nodules located within the middle and the lower lung lobes (Fig. 3.8.6). Unilateral involvement is unusual (21% of cases). Subpleural nodules may be seen, with pleural effusion likely to be found in 40% of cases. Mediastinal lymphadenopathy is unusual.

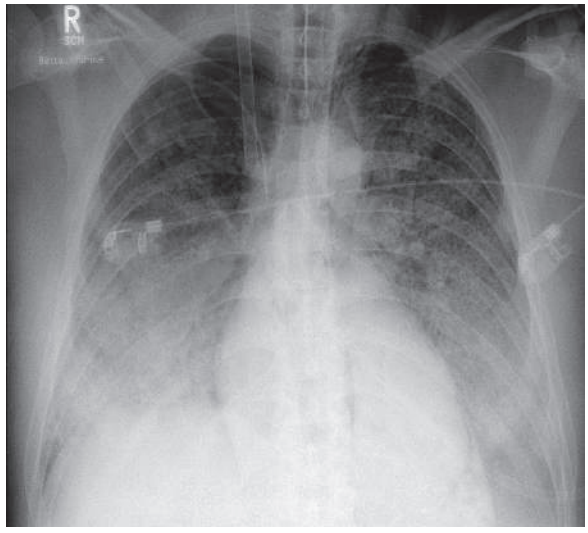

Fig. 3.8.4. Anteroposterior plain chest radiograph of a Wegner's granulomatosis (WG) patient in the intensive care unit shows bilateral diffuse alveolar lung disease due to pulmonary hemorrhage

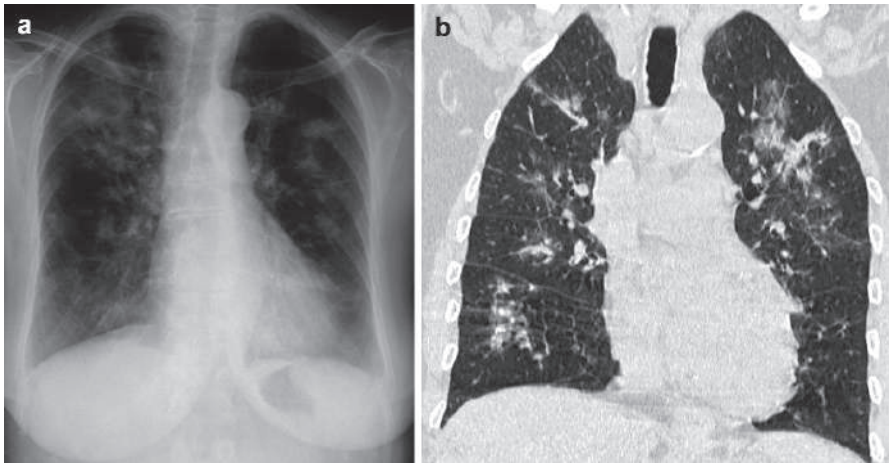

Fig. 3.8.5. Posteroanterior plain chest radiograph (**a**) and coronal HRCT (**b**) of a patient with Churg-Strauss syndrome (CSS) shows bilateral nodular patchy lung infiltration due to vasculitis and granulomatosis

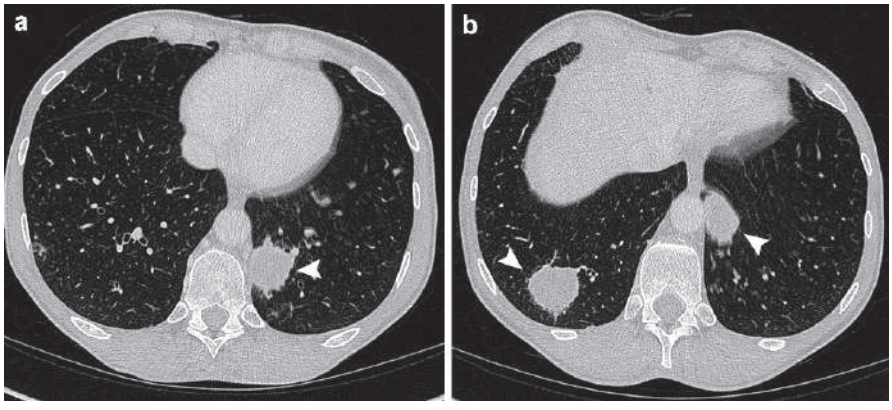

Fig. 3.8.6. Sequential axial HRCT of a patient with lymphomatoid granulomatosis (LG) shows multiple lung masses located at the lung bases in the left lung in (**a**) and bilaterally in (**b**) (*arrowheads*)

Cardiac Bronchus

Cardiac bronchus is a rare congenital anomaly in which there is accessory bronchus that arises from the medial wall of the intermediate bronchus at its proximal third, but occasionally from the right main bronchus. The accessory bronchus runs medially and caudally toward the heart, hence the cardiac appellation.

Cardiac bronchus is not identified on plain chest radiographs, and usually incidentally found on CT scans. The anomaly is asymptomatic; however, it may result in hemoptysis when it is infected.

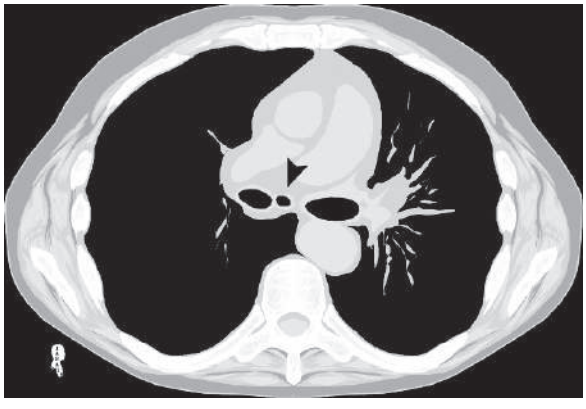

Fig. 3.8.7. Axial HRCT illustration demonstrates the typical radiographic sign and location of the cardiac bronchus on CT (*arrowhead*)

Signs on CT

The cardiac bronchus is typically identified as a small accessory bronchus medial to the intermediate bronchus on the right lung (Fig. 3.8.7).

Dieulafoy Disease

Dieulafoy disease is a very rare condition characterized by abnormally dilated submucosal vessels that are prone to bleed, and classically described in the colon, small intestine, and the bronchi.

Dieulafoy disease can be seen with cases of chronic bronchitis. On bronchoscopy, the visualization of dilated submucosal blood vessels in the presence of mucosal dilatation should alert the bronchoscopist of the possibility of Dieulafoy disease. Dieulafoy disease can be the case of massive upper gastrointestinal bleeding in 1–2% of cases.

For Further Reading

1. Furuse M et al Bronchial arteries: CT demonstration with arteriographic correlation. Radiology. 1987;162:393–8
2. Cooper C et al CT appearance of the normal inferior pulmonary ligament. AJR Am J Roentgenol. 1983;141:237–40
3. Khalil A et al Role of MDCT in identification of the bleeding site and the vessels causing hemoptysis. AJR Am J Roentgenol. 2007;188:W117–25
4. van der Werf TS et al Fatal hemorrhage from Dieulafoy's disease of the bronchus. Thorax. 1999;54:184–5
5. Löschhorn C et al Dieulafoy's disease of the lung: a potential disaster for the bronchoscopist. Respiration. 2006;73: 562–5
6. Son JS et al Anomalous systemic arterial supply to the basal segments of the right lower lobe in neonate. Pediatr Cardiol. 2008;29:1009–10
7. Temes E et al Young patient with recurrent hemoptysis. Resp Med (Extra). 2006;2:64–6
8. Wilson SR et al CT visualization of mediastinal bronchial artery aneurysm. AJR Am J Roentgenol. 2006;187:W544–5
9. Ahmed M et al Multislice CT and CT angiography for non-invasive evaluation of bronchopulmonary sequestration. Eur Radiol. 2004;14:2141–3
10. Yoon YC et al Hemoptysis: bronchial and non-bronchial systemic arteries at 16-detector row CT. Radiology. 2005; 234:292–8
11. Bentala M et al Cardiac bronchus: a rare cause of hemoptysis. Eur J Cardiothoracic Surg. 2002;22:643–5
12. Katayama K et al Adult case of accessory cardiac bronchus presenting with bloody sputum. Jpn J Thorac Cardiovasc Surg. 2005;53:641–4
13. Chung MJ et al Bronchial and non-bronchial systemic arteries in patients with hemoptysis: Depiction on MDCT angiography. AJR Am J Roentgenol 2006;186:649–55
14. Bruzzi JF et al Multi-detector row CT of hemoptysis. RadioGraphics. 2006;26:3–22
15. Frazier AA et al Pulmonary angiitis and granulomatosis: Radiologic-pathologic correlation. RadioGraphics. 1998;18: 687–710
16. Do KH et al Systemic arterial supply to the lung in adults: Spiral CT findings. RadioGraphics. 2001;21:387–402
17. Bolca N et al Bronchopulmonary sequestration: Radiological findings. Eur J Radiol. 2004;52:185–91

Chapter 4

Cardiology

CONTENTS

J. A. Al-Tubaikh: *Internal Medicine* – An Illustrated Radiological Guide
DOI: 10.1007/978-3-642-03709-2_4, © Springer-Verlag Berlin Heidelberg 2010

4.1 Acute Chest Pain

Acute chest pain is one of the most common complaints encountered in medical emergency departments. Chest pain is divided into cardiac and noncardiac chest pain. Causes of cardiac chest pain include angina pectoris (stable and unstable), myocardial infarction (MI) (ST-segment elevation and non-ST-segment elevation), myocarditis, etc. Noncardiac chest pain includes diseases of the great vessels, esophagitis, pneumonia, etc.

This topic discusses the use of radiology in detecting acute chest pain and how the radiologist can contribute in assessing causes of acute chest pain in emergency departments.

Acute Coronary Syndrome

Acute coronary syndrome (CAS) is a term used to describe symptoms and manifestations of myocardial ischemia induced by coronary artery disease.

The most important components of CAS are angina pectoris and its severe complication MI. *Angina pectoris* is a term used to describe transient myocardial ischemia in the absence of myocardial cell death. In contrast, *MI* is a term used to describe myocardial cell death and necrosis due to ischemia.

Patients with angina pectoris classically present with retrosternal chest pain, which radiates to the neck and the left shoulder, accompanied by a sensation of numbness in the fingers. Associated symptoms include tachycardia, dyspnea, and possibly arrhythmia. The chest pain in angina pectoris typically lasts <10 min in duration. Patients with MI classically present with the symptoms of angina pectoris in a severe fashion. The retrosternal chest pain is severe and associated with autonomic nervous system hyperactivity, causing profound sweating and at times loss of consciousness. The chest pain typically may last up to 30 min in duration.

MI can be transmural involving the whole thickness of the myocardial wall due to complete occlusion of the coronary artery. MI can also be subendocardial, which is classically seen in coronary arterial spasm and hypertension due to hypoperfusion. The vascular supply of the endocardium is the part of the heart wall that is most sensitive to hypoperfusion.

Cardiac CT is used in patients with acute chest pain to rule out three main conditions (triple rule-out): acute MI, pulmonary embolism (PE), and aortic dissection. Cardiac CT can also be used to detect calcium plaques within the coronary arteries in a technique known as "calcium scoring."

Calcium scoring is a method that quantifies the atherosclerotic plaques within the coronary vessels. The calcium score is used to assess the risk of heart events, not to detect coronary stenosis. The basic idea of calcium scoring is to perform a noncontrast CT of the heart to detect calcified plaques (Fig. 4.1.1). Once a calcified plaque is identified in the coronary arteries, the examiner encircles the plaque by a cursor and a special program will measure the plaque attenuation and express it as a number in Hounsfield units as a score (Agatston score). Each coronary branch is measured separately, and then the numbers added to give a total calcium burden score. The score predicts the probability of heart attacks in the next 5–10 years on the current status of the patient without treatment modifications.

Uncalcified atherosclerotic plaques take up to 15 years before they are calcified and visualized in a calcium scoring study or noncontrast CT study. The uncalcified (vulnerable) plaque appears inhomogeneous or with low density on CT scan (25 ± 15 HU). Uncalcified and

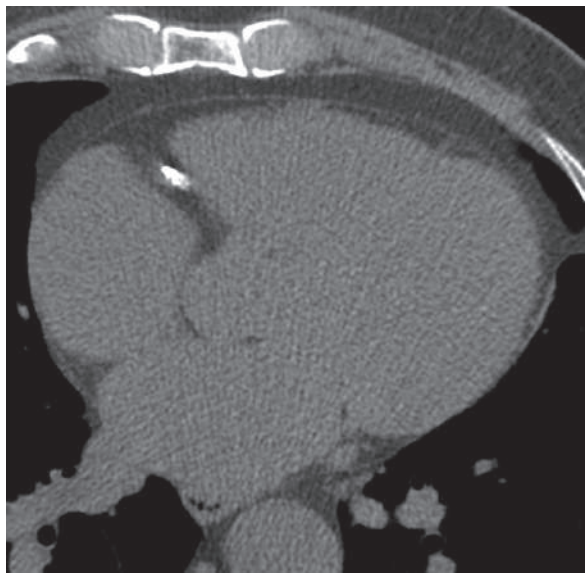

Fig. 4.1.1 Axial non-enhanced cardiac CT examination for calcium scoring shows calcified plaque in the right coronary artery

partially calcified plaques are more associated with ACS than are calcified plaques, because they are unstable and can be dislodged, initiating a coronary embolic attack.

Cardiac MRI in CAS patients is mainly used to study myocardial wall motion (*myocardial function study*), perfusion (same as the *thallium perfusion study*), viability, and ejection fraction measurement like cardiac Doppler study (*phase-contrast flow quantification*). The role of cardiac MRI postinfarction is to identify viable (salvageable) myocardium, which is mainly detected by the (*myocardial viability study*).

The basic concept of the myocardial viability study is to detect how much viable (alive and contractile) myocardium is left after MI. The technique depends upon the fact that gadolinium diffuses into the myocardial interstitial spaces after its injection into the body. As long as the myocardial membrane (sarcolemma) is intact, the gadolinium is pumped out of the intracellular compartment and concentrated in the extracellular compartment until it is washed out 10 min after its injection. This scenario occurs with normal and viable myocardium. If the myocardium is diseased or infarcted, the gadolinium will diffuse inside the extra- and intracellular compartments, which makes its clearance take longer time than 10 min. Myocardial contrast enhancement that exceeds 10 min from gadolinium injection is called "late gadolinium enhancement," which is considered pathological and the test is considered positive for nonviable myocardium.

Loss of cardiac wall motion, which is assessed in the myocardial function study, is another important sign of nonviable myocardium. However, there are two situations where the myocardium is viable but is not contracting: myocardial stunning and hibernating myocardium. *Myocardial stunning* is a situation where the cardiac muscles are viable but they do not contract as a transient phenomenon after MI (like penumbra after stroke). *Hibernating myocardium* is a situation where the cardiac muscles are viable but are not contracting after reestablishing coronary perfusion due to a long period of chronic perfusion abnormalities. This situation is typically seen in patients with long-standing, compromised coronary perfusion who have undergone coronary artery bypass surgery (CABG). Although the perfusion is normally established after a long period of hypoperfusion, the muscles are not contracting due to a long period of cardiac muscle ischemia and hypofunction.

Signs on Chest Radiographs

- Indirect signs of CAS include aortic calcification of aorta or coronary arteries calcification.
- If the MI is complicated by heart failure, signs of pulmonary edema may be detected such as upper lobe vessel cephalization and enlarged cardiac silhouette (Fig. 4.1.2).

Signs on Cardiac CT

- In a patient with acute chest pain, detection of calcified plaques on the nonenhanced coronary vessels with absence of signs of aortic dissection or embolism confirms the diagnosis of CAS. However, absence of the coronary calcified plaques does not rule out CAS because uncalcified plaques can be present. Up to 50% of patients with sudden cardiac arrests show calcified lesions in their coronary arteries (Fig. 4.1.1).
- MI may be seen as a subendocardial ventricular hypodense area depending upon the blocked coronary artery and its vascular territory.
- Post myocardial infarction calcification and ventricular dilatation may occur (Fig. 4.1.3).

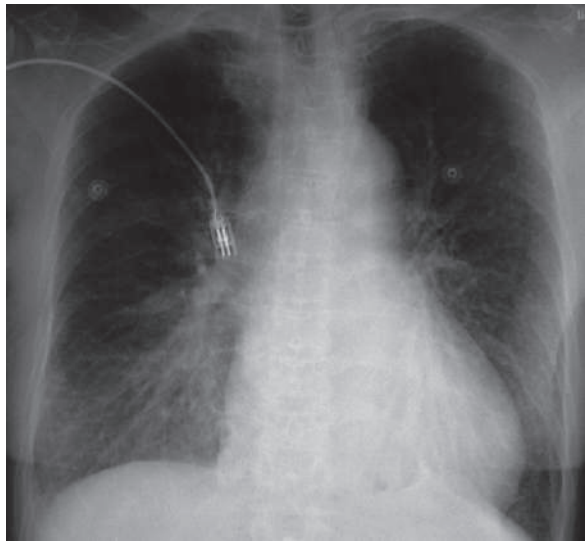

Fig. 4.1.2 Anteroposterior chest radiograph of a bedridden patient with myocardial infarction (MI) shows congested hilar vessels and beginning of pulmonary edema

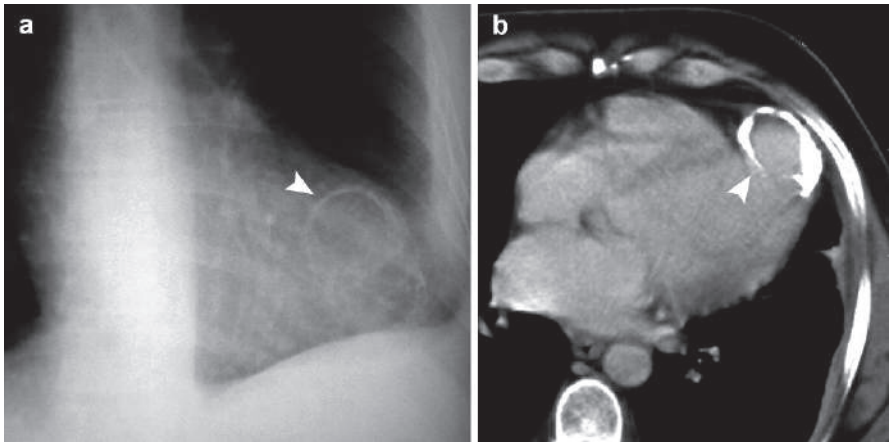

Fig. 4.1.3 Posteroanterior chest radiograph (**a**) and thorax CT (**b**) shows focal apical left ventricular dilatation with calcified rim due to old MI of this region (*arrowheads*)

Signs of MI on MRI

- Wall motion abnormalities (akinesia or hypokinesia) on Cine-MRI.
- Contrast enhancement on delayed images (>10 min). There are four patterns of late contrast enhancement of MI: *First pattern* is subendocardial enhancement with sparing of the subepicardial region (Fig. 4.1.4a). *Second pattern* is full thickness myocardial wall enhancement (Fig. 4.1.4b). *Third pattern* is full thickness myocardial wall enhancement, with subendocardial hypointense area, representing a severe edema compressing the intramural vessels (Fig. 4.1.4c). *Fourth pattern* is seen as a dark hypointense area that represents the infracted area surrounded by a rim enhancement (Fig. 4.1.4d). The fourth pattern is seen in extensive MI with less viable myocardium.
- Stunned and hibernating myocardium is visualized as wall motion abnormalities (akinesia or hypokinesia) in Cine-MRI with no contrast enhancement on delayed images (>10 min).

Why does atherosclerosis not develop in the veins and is only seen in the arteries, although the cholesterol circulates in the blood in both veins and arteries?

This occurs because the arterial pulsation assists in the deposition of the cholesterol molecules within the intima. Normally, the pulmonary arteries do not pulsate, but when pulmonary hypertension develops, the high pressure blood within the arteries evokes the arterial wall to pulsate, resulting in developing atherosclerosis within the pulmonary arteries.

Acute Pulmonary Embolism

Acute pulmonary embolism (PE) is an emergency situation characterized by closure of a pulmonary artery by an embolus causing pulmonary ventilation-perfusion mismatch, or in a worse scenario, pulmonary infarction.

The bronchial circulation only supplies nutrients and does not participate in gas exchange in normal situations. However, in PE, the bronchial circulation responds with enlargement and hypertrophy, and participates in blood oxygenation due to decreased pulmonary flow and ischemia.

PE is categorized according to severity into two main types: acute sub-massive and acute massive PE. Acute sub-massive PE is characterized by <50% occlusion of the pulmonary vascular bed, whereas acute massive PE is characterized by >50% occlusion of the pulmonary vascular bed.

Patients with acute PE often describe acute sudden chest "gunshot-like" pain with progressive dyspnea, tachycardia, and cyanosis. Many patients have a history of deep venous thrombosis (DVT), varicose veins, immobilization, or recent pelvic surgery. A dislodged part of the initial thrombus, mostly from the lower limbs, travel through the venous circulation until it blocks an arterial pulmonary vessel in the chest as an

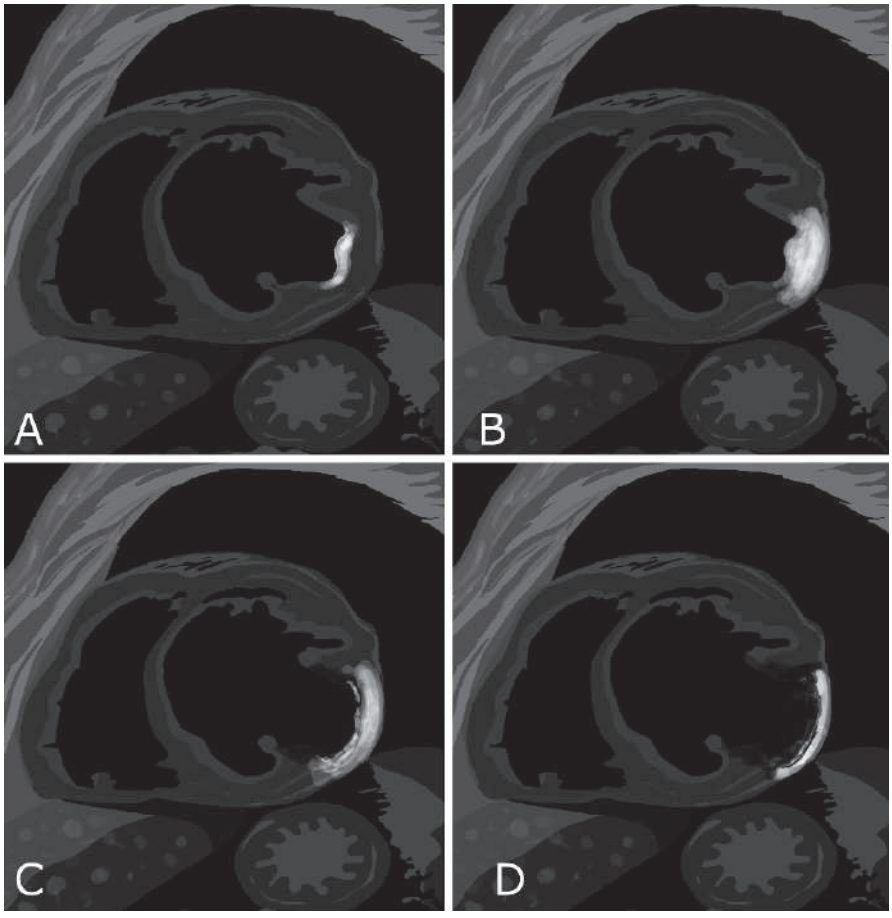

Fig. 4.1.4 Short-axis dark-blood T1W postcontrast cardiac MR illustrations show different pattern of myocardial enhancement after MI: (**a**) subendocardial enhancement with sparing of the subepicardial region, (**b**) full-thickness myocardial wall enhancement, (**c**) full-thickness myocardial wall enhancement, with subendocardial hypointense area, and (**d**) dark hypointense area represents the infarction surrounded by a rim enhancement

embolus, causing pulmonary vascular congestion. If this congestion persists, pulmonary infarction occurs.

In small percentage of patients, the unresolved thrombus after treatment can be incorporated into the vessel wall and covered by a layer of epithelium. This thrombus organization causes intravascular stenosis of the affected lumen, resulting in the development of pulmonary hypertension and cor pulmonale.

Acute PE is best diagnosed by V/Q scan (ventilation/perfusion nuclear scan study) in circulatory stabilized patient. The scan typically shows pulmonary ventilation-perfusion mismatch. In unstable acute PE patients, CT pulmonary angiography is the initial examination of choice.

Signs on Chest Radiograph

- Radiographs are normal in 12% of cases.
- Pulmonary infarction can appear as a patchy radio-opaque shadow on chest radiograph, which cannot be differentiated from patchy pneumonia or pulmonary contusions. Therefore, the radiographic signs have to be correlated with the history and the clinical data.
- *Hampton's Hump*: is a wedge-shaped radio-opaque patch that is round-shaped, located at the lung periphery, and directed from peripheral toward the hilum (Fig. 4.1.5). This patch represents wedge-shaped infarction of the peripheral lung parenchyma.
- PE can be accompanied by Hemorrhagic pleural effusion.

4.1

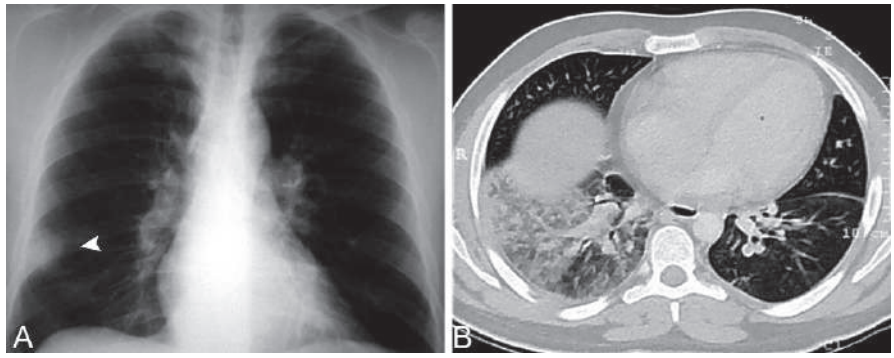

Fig. 4.1.5 Posteroanterior chest radiograph (**a**) and chest HRCT in two different patients with pulmonary infarction show Hampton's hump in (**a**) (*arrowhead*), and basal area of pulmonary parenchymal consolidation due to infarction in (**b**)

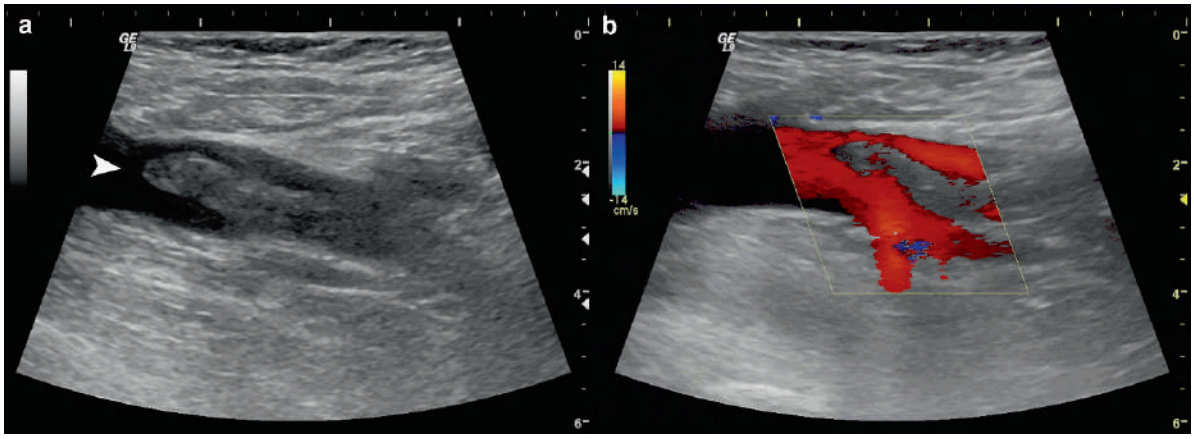

Fig. 4.1.6 Sagittal, Doppler sonography (**a**) and Duplex (**b**) images of a patient with DVT show hypoechoic material within the external iliac vein with free labile edge

Signs on Doppler Sonography

- Doppler sonography should be performed for patients with PE or patients with high risk of DVT who show signs of respiratory distress (e.g., bedridden patients).
- DVT is diagnosed on Doppler sonography when an intravenous echogenic material is detected (e.g., thrombus), the vein is distended and noncompressible (most specific and diagnostic sign), and there is loss of color duplex signal within the vein. The thrombus should be followed by the probe to detect its free edge, and an observation of labile, freely-moving edge on real-time sonography should be reported. A labile, free edge thrombus has a high risk of embolization (Fig. 4.1.6).

Signs on CTA

- PE is detected as complete filling defect with failure to enhance the entire lumen (complete thrombosis). The thrombosed vessel may be enlarged, and the thrombus may appear hyperdense on non contrast-enhanced images.
- Partial filling defect of a pulmonary vessel surrounded by areas of contrast material enhancement (Fig. 4.1.7) may be seen.
- Pulmonary infarction is visualized as a wedge-shaped area of lung parenchyma with high density located in the periphery of the lung, with the base lying along the pleura (Fig. 4.1.5).
- Areas of lobar atelectasis in PE may show contrast enhancement.

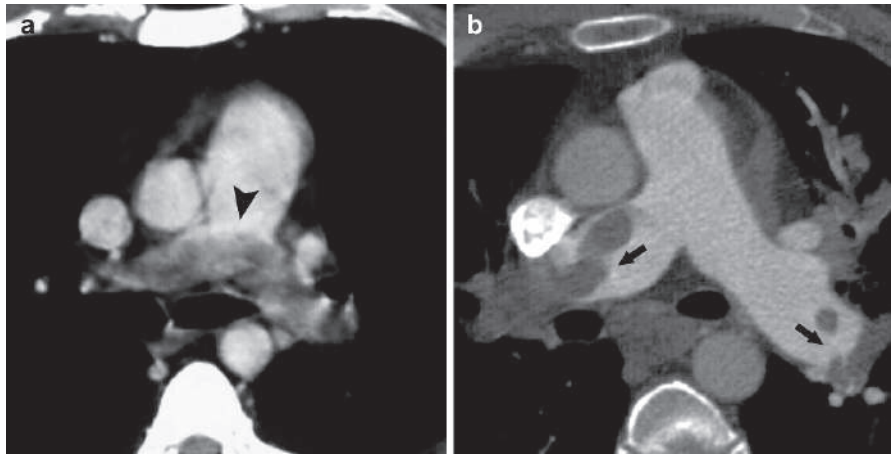

Fig. 4.1.7 Axial pulmonary CTA of two different patients with pulmonary embolism (PE) shows saddle thrombus in (**a**) (*arrowhead*), and distal complete thrombosis of the right pulmonary artery with partial thrombosis of the distal part of the left pulmonary artery (*arrows*)

- Chronic PE is visualized as a peripheral intra-arterial wall filling defect. Calcification of the organized thrombus may be seen.
- *Saddle thrombus*: is a term used to describe a big thrombus that abuts over the bifurcation of the main pulmonary arteries (Fig. 4.1.7).
- Signs of right ventricular enlargement might be seen in CT with displacement of the ventricular septum toward the left ventricle, as a sign pulmonary hypertension.
- Areas of mosaic lung parenchyma pattern with pruning of the pulmonary vessels may be seen (Fig. 4.1.8).

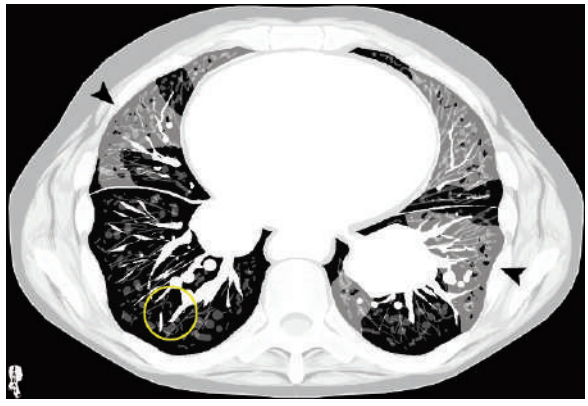

Fig. 4.1.8 Axial chest HRCT lung-window illustration shows mosaic pulmonary parenchymal pattern (*arrowheads*) and pruning of the pulmonary arteries (*yellow circle*)

Aortic Dissection

The term "*acute aortic syndrome*" is applied to multiple acute chest pain presentations that are caused by thoracic aortic diseases, including aortic dissection, aortic intramural hematoma (IMH), and penetrating atherosclerotic ulcer.

Aortic dissection is a condition characterized by separation of the aortic intima with presence of blood in a false lumen between the intima and the medial layers of the aortic wall.

The intima is the innermost layer of the aortic wall. Aortic wall intimal tear starts typically at sites of highest intramural pressure and wall tension. After intimal tear, the blood flow inside the tear dissects its way between the intima and the media layer, creating a false lumen. The structure between the true and the false lumen is called "intimal flap," which is the key diagnosis of aortic dissection on radiological examinations.

The most common predisposing factors of aortic dissection are systemic hypertension, bicuspid aortic valve, aortic coarctation, and Marfan's syndrome. Patients typically present with sudden acute chest pain that is described as "tearing" sensation, and classically radiation to the back.

Aortic Dissection Is Classified According to the Stanford and Debakey Classifications

Stanford Classification

Type A: this type involves the ascending aorta, and it is managed surgically. This type carries the risk of spontaneous rupture into the pericardium resulting in pericardial tamponade, or it can continue dissection to involve the coronary arteries (right coronary more than

4.1

the left). Patients with this type can also develop aortic regurgitation (50% of cases).
Type B: this type involves the descending aorta only. The site of dissection is typically just distal to the subclavian artery, near the insertion of the ligamentum arteriosum. When the dissection involves both the descending and the ascending aorta, it is classified as type A. This type is managed medically; however, in the current era, even type B is managed with endovascular stent across the origin of the dissection.

Debakey Classification

Type I: involves ascending aorta only
Type II: involves the ascending and the descending aorta.
Type III: involves the descending aorta only.

Differential Diagnoses and Related Diseases

Vascular Ehlers-Danlos syndrome is a disease characterized by joint hypermobility, skin abnormalities (e.g., easy bruising), fragility of intestinal and genitourinary organs, and vascular fragility leading to dissection or rupture of medium to large muscular arteries. The disease has an autosomal dominant mode of inheritance, and caused by mutation in collagen type 3 gene (COL3A1). The dissection arises in vascular Ehlers-Danlos syndrome that occurs typically without preceding aneurysm.

Signs on Radiographs

There is mediastinal widening with obliteration of the aortic knuckle on plain radiographs.

Signs on CTA

- The key diagnostic finding in aortic dissection is identification of the intimal flap, which appears as a thin "line" of soft tissue within the aortic lumen separating the false lumen from the true lumen (Fig 4.1.9).
- The true lumen shows higher enhancement than the false lumen, because filling of the false lumen is slower than the true lumen. Moreover, the false lumen may show signs of intravascular thrombosis.
- In the ascending aorta, the false lumen is typically the more anterior lumen, while in the descending aorta, it is typically the more posterior lumen.
- Coronary artery dissection can be suspected when the intimal flap is detected at or near the site of a coronary ostium. When this sign is identified, coronary CTA should be performed to detect the extension of the dissection.
- Pericardial hemorrhagic effusion may be detected as highly attenuated fluid within the pericardial space (40–50 HU).

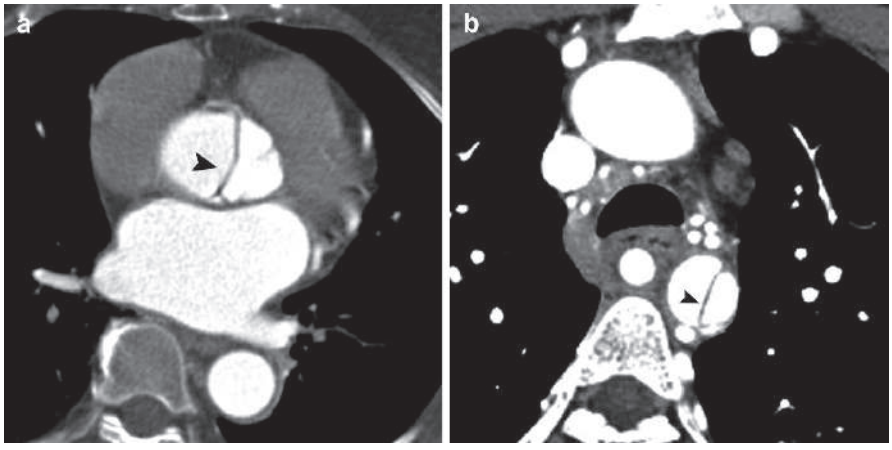

Fig. 4.1.9 Axial cardiac CTA of two different patients with aortic dissection Stanford type A (**a**) and Stanford type B (**b**) shows the classic intimal flap (*arrowheads*) separating the true from the false lumen

Aortic Intramural Hematoma

IMH is a condition characterized by rupture of the vasa vasorum, the network of vessels that supply the aorta itself, resulting in bleeding within the aortic wall, mostly within the media layer.

IMH is clinically indistinguishable from aortic dissection. Patients present with signs of acute aortic syndrome consisting of sudden chest pain that is radiating to the back or chest depending on which part of the aorta is affected. IMH accounts for 10–30% of cases of acute aortic syndrome, and it may be caused by hypertension, blunt trauma, or penetrating atherosclerotic ulcer. In contrast to aortic dissection, no intimal tear flap is identified in this condition. However, the hematoma can progress into a true dissection if the aortic wall continues to enlarge in thickness by the hematoma >5 cm.

Signs on CTA

On contrast-enhanced scan, the aortic wall show a crescentic area of wall thickening that may show high attenuation if the bleeding is fresh. There is no intimal flap (Fig. 4.1.10).

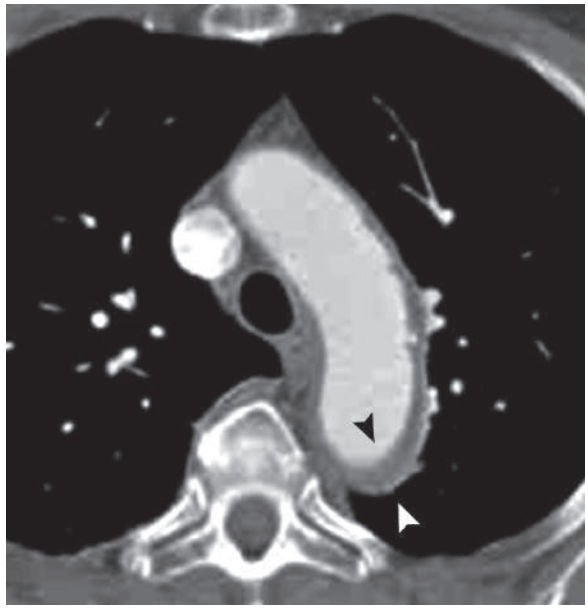

Fig. 4.1.10 Axial cardiac CTA shows posterior aortic arch focal area of aortic wall thickening due to intramural hematoma (*arrowheads*)

Penetrating Atherosclerotic Ulcer

Penetrating atherosclerotic ulcer is a condition that results from ulceration and break of an aortic atherosclerotic plaque resulting in an intimal defect. This defect causes bleeding within the aortic wall surrounding the ulcer, which will result in IMH formation or pseudoaortic aneurysm formation.

Signs on CTA

The scan will show an area of intimal defect within the aorta with the formation of saccular pseudoaneurysm, IMH, or periaortic mediastinal hematoma (Fig. 4.1.11).

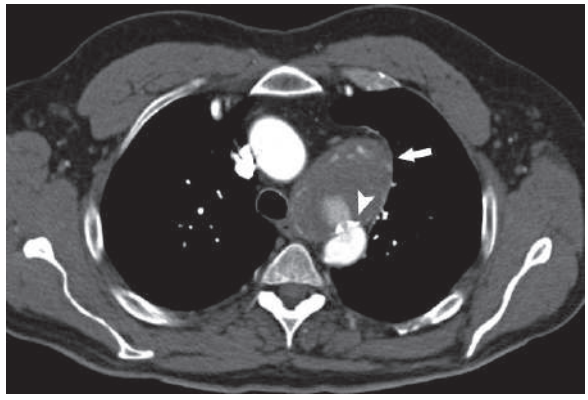

Fig. 4.1.11 Axial cardiac CTA shows an area of aortic wall ulceration of the descending thoracic aorta (*arrowhead*) with a jet of bleeding into the aortic wall creating a periaortic mediastinal hematoma (*arrowhead*)

For Further Reading

1. Hoffmann U et al Cardiac CT in emergency department patients with acute chest pain. RadioGraphics. 2006;26: 963–80
2. Oliver TB et al Spiral CT in acute non-cardiac chest pain. Clin Radiol. 1999;54:38–45
3. Jeudy J et al Nontraumatic thoracic injuries. Radiol Clin N Am. 2006;44:273–93
4. Birchard KR. Acute aortic syndrome and acute traumatic aortic injury. Semin Roentgenol. 2009. doi:10.1053/j.ro.2008.10.002
5. Choe YH et al. Comparison of MDCT and MRI in the detection and sizing of acute and chronic myocardial infarcts. Eur J Radiol. 2008;66:292–9
6. Winter-Muram HT et al Suspected acute pulmonary embolism: evaluation with multi-detector row CT versus digital subtraction pulmonary arteriography. Radiology. 2004; 233:806–15
7. Castañer E et al Congenital and acquired pulmonary anomalies in the adult: radiologic overview. RadioGraphics. 2006;26:349–71
8. De Becker J et al Marfan and Marfan-like syndromes. Artery Res. 2009;3:9–16

4.2 Diseases of the Great Vessels

The great vessels include the aorta, the superior and inferior vena cava, the pulmonary artery, and the pulmonary veins. There are multiple medical conditions affecting the great vessels that require imaging to asses their complications, establish their diagnosis, or monitor their therapy response. This topic discusses some of the common medical conditions where radiology plays an important role in their diagnosis and assessment.

Thoracic Aortic Aneurysm

Thoracic aortic aneurysm (TAA) is a disease characterized by dilatation of the wall of the aorta affecting its three layers (intima, media, and adventitia). In contrast, pseudo-aortic aneurysm is a condition characterized by saccular dilatation of the outer most layers of the aortic wall (media and/or adventitia) with an intact inner wall layer (intima).

The most common cause of TAA is atherosclerosis, while the most common cause of pseudo-aortic aneurysm is aortic trauma violating the wall integrity. TAA originates in the ascending aorta (50%), descending aorta (40%), and the aortic arch (10%). In contrast, pseudo-aortic aneurysm usually arises at three basic levels: the aortic root, the aortic isthmus, and the aortic diaphragm.

Patients with TAA are typically in their 50s and 70s, and usually are asymptomatic. Up to 30% of patients present with complications due to TAA rupture. Pain or dysphagia due to mass effect over the adjacent mediastinal structure may be seen uncommonly.

TAA expands at a rate of 0.5 cm per year, with an increased risk of rupture when it is >5 cm in diameter. Patients with TAA >6 mm may present with spontaneous bleeding resulting in hemomediastinum or periaortic hematoma formation.

Differential Diagnoses and Related Diseases

- *Marfan syndrome* is a disease characterized by ocular, musculoskeletal, central nervous system, and cardiovascular complications. Marfan syndrome patients are known to suffer from aortic root dilatation in up to 80% of cases. Patients may suffer also from mitral valve prolapse, or dissection of the aorta.
- *Loeys-Dietz syndrome* is a disease characterized by aortic aneurysm and dissection, with widespread arterial tortuosity/aneurysms (seen in the thoracic aorta and neck vessels mainly). The disease has an autosomal dominant mode of inheritance. The disease is divided into two types: type I Loeys-Dietz syndrome is characterized by craniosynostosis, hypertelorism, bifid uvula, cleft palate, and/or arterial aneurysms and tortuosity; type II lacks the hypertelorism, craniosynostosis, and cleft palate.
- *Aortoduodenal syndrome* is a very rare disease characterized by obstruction of the duodenum by aneurysmal dilatation of the abdominal aorta. Patients classically present with abdominal pain, bilious vomiting, and pulsatile abdominal mass.

Signs on Radiographs

- Aortic aneurysm is detected as a marked dilatation of the aortic knuckle and mediastinal widening (Fig. 4.2.1).
- Bronchial compression or erosion of the thoracic vertebrae due to mass effect and chronic pressure causing anterior scalloping may be seen on lateral views.
- Aortic wall calcification may be seen.

4.2

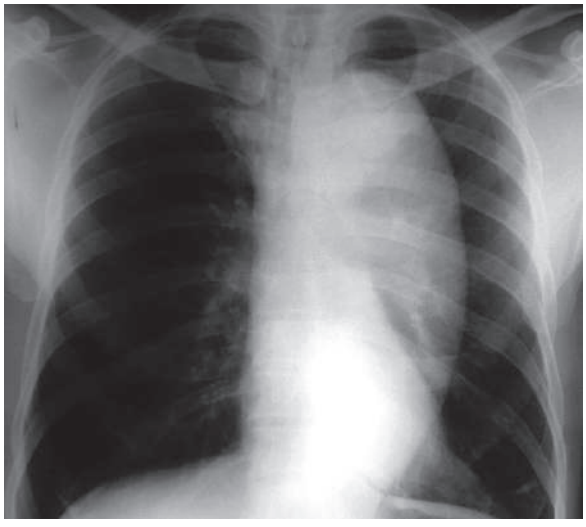

Fig. 4.2.1. Posteroanterior chest radiograph of a patient with thoracic aortic aneurysm (TAA) shows marked dilatation of the aortic knuckle and the descending thoracis aorta

Signs on CTA

- The thoracic aorta is considered dilated when its diameter is >4 cm (Fig. 4.2.2).
- Periaortic hematoma is detected as a hypodense mass located in the mediastinum surrounding the aorta. If the bleeding is fresh, the hematoma may show high density (Fig. 4.2.3).
- Aortic wall calcification may be seen.

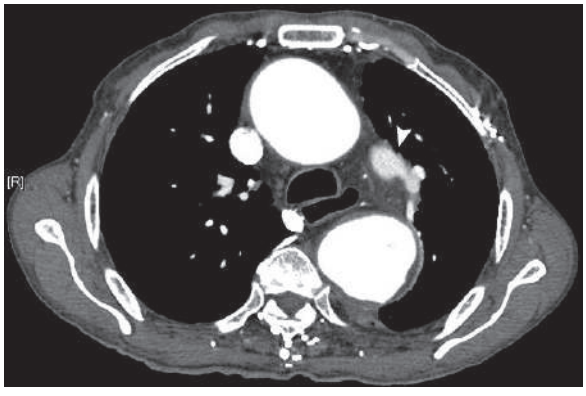

Fig. 4.2.2. Axial thoracic CTA demonstrates TAA with fresh blood leak into the mediastinum (*arrowhead*)

Pulmonary Hypertension

Pulmonary hypertension (PHT) is a disease characterized hemodynamically by a mean pulmonary artery pressure >25 mmHg at rest (normal level, 10 mmHg) or >30 mmHg during exercise (normal level, 15 mmHg) with increased pulmonary vascular resistance.

Causes of PHT can be divided into two main groups: a group with pathology is confined to the arterial side of the pulmonary circulation (*precapillary PHT*), and a second group with pathology confined to the venous circulation, between the capillary bed and the left atrium (*postcapillary PHT*). When the cause of the PHT is unknown, it is called "idiopathic or primary" PHT, and when the cause of the PHT is known, it called "secondary" PHT.

Causes of PHT

- *Precapillary PHT*: primary PHT, congenital heart defects with left-to-right shunt, pulmonary embolism, parasites (e.g., schistosomiasis), and talcosis (lung disease due to talc crystals inhalation).
- *Postcapillary PHT*: primary veno-occlusive disease, mitral stenosis, and mediastinal fibrosis.

Primary PHT is an idiopathic condition characterized by precapillary PHT in the absence of an identifiable cause. Patients typically present with dyspnea (60%), fatigue, angina, cor pulmonale, and Raynaud's phenomenon. Typically, the patient is a young or middle-aged female. Risk factors associated with primary PHT include: portal hypertension, collagen vascular disease, pregnancy, and women who use contraceptive pills.

Congenital heart defects associated with left-to-right shunts predispose to PHT. Common defects with PHT include: atrial septal defects, ventricular septal defects, and truncus arteriosus. *Eisenmenger syndrome* is an advanced stage of PHT associated with congenital heart defects. The disease is characterized by dyspnea, cyanosis, generalized fatigue, and syncope. Patients with Eisenmenger syndrome may die at a young age due to cardiac arrhythmias, which are

common features of this disease. Patients may also develop paradoxical embolus passing from the right side of the heart to the left through a heart defect.

Pulmonary veno-occlusive disease (*PVOD*) is a rare idiopathic disease characterized by postcapillary PHT, in the presence of normal left atrial and left ventricular pressures. PVOD is characterized by PHT, congestive heart failure, and interstitial pulmonary edema with a normal wedge pressure on cardiac catheterization. The pathological findings in PVOD show extensive and diffuse occlusion of pulmonary veins by fibrous tissue, which may be loose edematous or dense and sclerotic. Patients present with dyspnea, flue-like symptoms, and hemoptysis. It commonly affects children (30% of cases), transplant patients, and pregnant women. The disease may be misdiagnosed initially as interstitial lung disease (Fig. 4.2.3).

Signs on Chest Radiograph

- The pulmonary vasculature diminishes in caliber as it extends from the center toward the periphery (pruning), with a mean width of the right descending pulmonary artery >24 mm (normal <17 mm in width).
- Dilatation of the right and left main pulmonary arteries (Fig. 4.2.4).
- Signs of right ventricular enlargement, right atrial enlargement, or left atrial enlargement (mitral stenosis).
- POVD is suggested radiographically when the radiograph shows signs of pulmonary PHT associated with pulmonary interstitial edema, and normal-size left atrium. The interstitial edema is visualized as a diffuse linear interstitial pattern. Mediastinal hilar lymphadenopathy may be present.

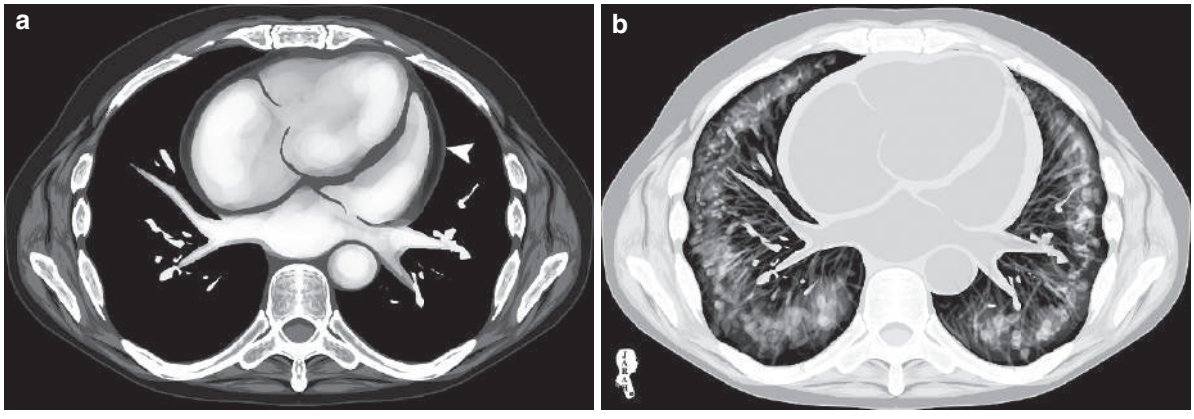

Fig. 4.2.3. Axial mediastinal-window (**a**) and lung-window (**b**) HRCT illustrations of a patient with pulmonary veno-occlusive disease (PVOD) show right-sided heart chambers dilatation with normal left heart chambers size. In (**b**), the lung parenchyma shows bilateral diffuse linear interstitial lung pattern. Notice also the small pericardial effusion in (**a**) (*arrowhead*)

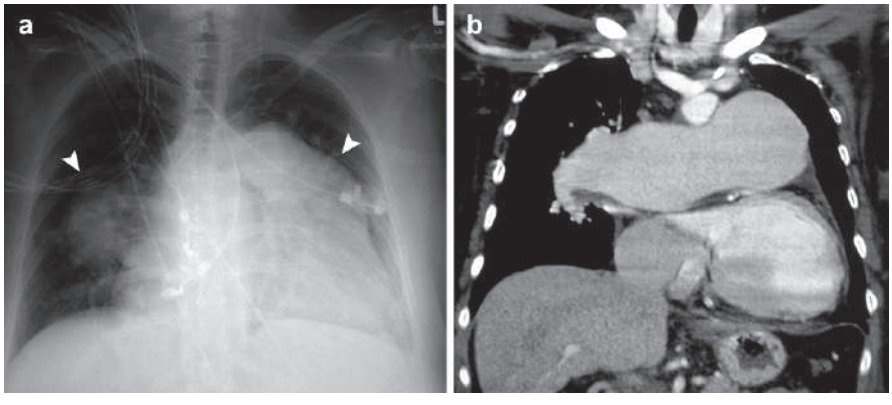

Fig. 4.2.4. Antero-posterior chest radiograph (**a**) and coronal CTA (**b**) of a patient with primary pulmonary hypertension (PHT) shows massively dilated pulmonary arteries (*arrowheads*)

4.2

Signs on HRCT and CTA

- PHT is diagnosed when the mean diameter of the pulmonary artery is >29 mm, with a segmental artery-to-bronchus ration >1:1 in three or four pulmonary lobes (Fig. 4.2.4).
- The lung parenchyma shows mosaic pattern of lung attenuation due to variation in parenchymal perfusion.
- Arteriography shows symmetric enlargement of the central arteries with tapering subsegmental vessels toward the peripheries (pruning).
- The right ventricle is considered dilated when the ratio of its diameter to the diameter of the left ventricle is greater than 1:1, with bowing of the interventricular septum toward the left ventricle.
- Right ventricular hypertrophy is confirmed when the myocardial wall thickness is >5 mm (normally <4 mm).
- Signs of pericardial thickness with small pericardial effusion can be seen in a percentage of patients with PHT without an obvious reason.
- In *PVOD*, classical CT finding show the combination of diffuse linear interstitial lung pattern with or without mosaic ground glass opacities, dilated pulmonary arteries, right-sided heart chambers dilatation, mediastinal lymphadenopathy, pericardial or pleural effusion, with normal-sized left atrium and pulmonary veins (Fig. 4.2.3).

Coral Reef Aorta

Coral reef aorta is a rare condition characterized by excessive calcification of the suprarenal and juxtarenal aorta resembling the growth of hyperplastic bone, in the absence of abnormalities in serum calcium levels.

Coral reef aorta can cause malignant hypertension due to significant abdominal aortic lumen stenosis, or renal artery stenosis when it involves the renal arteries. Other complications include blue toe syndrome due to dislodged ulcerated atherosclerotic plaques.

Signs on CT

On non-enhanced images, the aorta shows hard, irregular, and gritty intra-aortic mass of calcification. In contrast to the typical appearance of atherosclerosis of the great vessels, which follows the curve of the vessel wall, the calcification in coral reef aorta is irregular and protrudes into the lumen (Fig. 4.2.5).

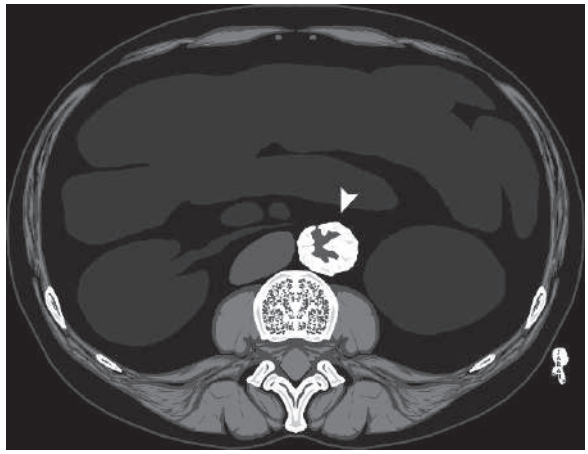

Fig. 4.2.5. Axial abdominal CT illustration demonstrates coral reef aorta seen as diffusely calcified arterial wall with projection of the calcified plaques into the aortic lumen (*arrowhead*)

Superior Vena Cava Syndrome

Superior vena cava syndrome (SVCS) is a disease characterized by a triad of edema of the upper torso, venous distension of the neck, and chylothorax. SVCS arises due to extrinsic or intrinsic SVC obstruction, causing disturbance of the venous backflow from the head and neck region and formation of venous collaterals.

Extrinsic causes of SVCS include bronchogenic carcinoma or lymphoma compressing the SVC (80% of cases). Intrinsic causes of SVCS are mostly due to thrombosis, most commonly due to intravenous catheters use. Other causes of intrinsic SVCS include thrombus propagation from the subclavian veins to the SVC due to thoracic outlet syndrome.

Patients with SVCS typically present with marked cyanosis and swelling involving the head and neck region and the upper extremities, with development of superficial collateral circulation. Complications include pulmonary embolism (5–35% of cases), thrombophlebitis, sepsis, and thrombus propagation into intracranial sinuses or veins. In some patients, blood may be "sucked" into the thorax during inspiration, but because of the limited ventricular filling, the neck veins may become further distended (Kussmaul's sign).

In infants, SVCS has been linked with the formation of hydrocephalus, called "*extraventricular obstructive hydrocephalus*" (EVOH). The mechanism of hydrocephalus is believed to be caused by decrease in cerebrospinal fluid absorption at the level of the arachnoid

granulation secondary to the elevated venous pressure. EVOH can be seen in up to 91% in infants with SVCS. Complications of EVOH include hemorrhagic infarction and seizures.

Signs on Chest Radiographs

- Pleura effusion (chylothorax).
- The chest may show the cause of SVCS if the reason was obstruction from a mediastinal tumor.
- Rib notching may present with long-standing SVC obstruction.

Signs on Superior Vena Cavography

There is partial or complete SVC filling defect with formation of numerous venous collaterals (Fig. 4.2.6).

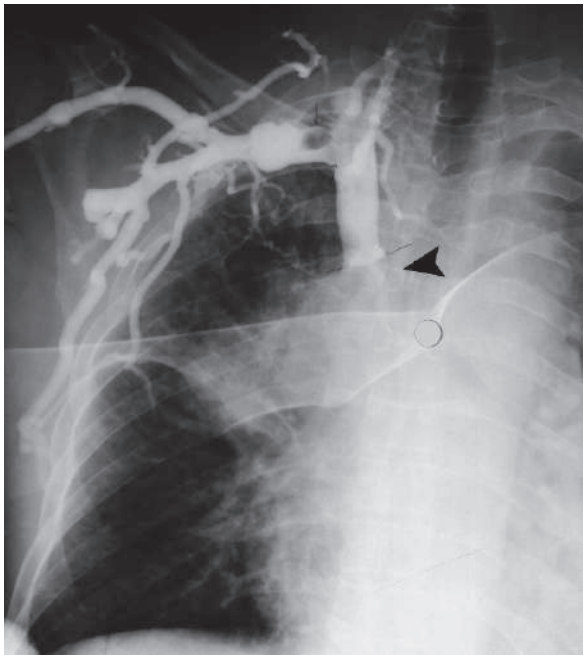

Fig. 4.2.6. Superior vena cava venography shows occlusion of the superior vena cava (SVC) due to thrombosis (*arrowhead*)

Signs on Chest CT

- Mediastinal masses (e.g., bronchogenic carcinoma) can be found in cases of extrinsic SVC obstruction.
- After contrast injection, partial or complete filling defects representing SVC thrombosis can be seen in cases of intrinsic SVC obstruction.

Signs on Brain CT

In infants with EVOH, brain CT may be normal in early stages, or show signs of ventricular dilatation due to hydrocephalus.

For Further Reading

1. Gotway MB et al Thoracic aorta imaging with multislice CT. Radiol Clin N Am. 2003;41:521–43
2. Schulte K-M et al Coral reef aorta: a long-term study of 21 patients. Ann Vasc Surg. 2000;14:626–33
3. Rosenberg GD et al Blue toe syndrome from a "coral reef" aorta. Ann Vasc Surg. 1995;9:561–4
4. Rosenberger A et al Superior vena cava syndrome: a new radiologic approach to diagnosis. Cardiovasc Intervent Radiol. 1980;3:127–30
5. Karmazyn N et al Neuroimaging findings in neonates and infants from superior vena cava obstruction after cardiac operation. Pediatr Radiol. 2002;32:806–10
6. Frazier AA et al Pulmonary vasculature: hypertension and infarction. RadioGraphics. 2000;20:491–524
7. Beghetti M et al Eisenmenger syndrome. A clinical perspective in a new therapeutic era of pulmonary arterial hypertension. JACC. 2009;53:733–40
8. Akpinar E et al PVOD suggested by MDCT and clinical findings in a pregnant woman. Emerg Radiol. 2008;15:193–5
9. Johnson PT et al Loeyz-Dietz syndrome: MDCT angiography findings. AJR. 2007;189:W29–35
10. Deitch JS et al Abdominal aortic aneurysm causing duodenal obstruction: two case reports and review of the literature. J Vasc Surg. 2004;40:543–7
11. Takagi H et al Aortoduodenal syndrome. J Vasc Surg. 2006;43:851

4.3 Myocardial Diseases (Cardiomyopathies)

Cardiomyopathies are a group of diseases with different etiologies, all characterized by cardiac muscles dysfunction. Cardiomyopathies are an important cause of arrhythmias and sudden cardiac death in young patients. Three types of cardiomyopathies have been described by the World Health Organization (WHO):

- *Hypertrophic cardiomyopathy* (*HCM*) is characterized by inappropriate left ventricular hypertrophy, with preservation of the myocardium contractility.
- *Dilated cardiomyopathy* (*DCM*) is characterized by ventricular dilatation with contractility dysfunction. Most secondary causes of cardiomyopathies are related to this type.
- *Restrictive cardiomyopathy* (*RCM*) is characterized by diastolic dysfunction and restricted contractility.

Other uncommon forms of cardiomyopathies include: athlete's heart, arrhythmogenic right ventricular dysplasia (ARVD), noncompaction cardiomyopathy (NCCM), and peripartum cardiomyopathy. Each of the classic three forms and the uncommon forms of cardiomyopathies are discussed below.

Hypertrophic Cardiomyopathy

Primary HCM is a disease characterized by inappropriate myocardial hypertrophy in the absence of a cause (e.g., hypertension). In contrast, secondary HCM can be seen due to diseases of protein deposition (e.g., amyloidosis).

Cardiac muscles hypertrophy in HCM is described as "concentric" or "eccentric." *Concentric heart hypertrophy* means increased heart muscle bulk and wall thickness, and it is best assessed on cardiac MRI by looking at the heart thickness in the short axis view. *Eccentric heart hypertrophy* means general increase in the heart muscles with preservation of the normal cardiac wall thickness (isometric).

Patients with HCM often present with symptoms that include ischemic cardiac pain and arrhythmias, although most patients may be asymptomatic. HCM is the most common cause of sudden cardiac death in athletes. Up to 25% of HCM patients have left ventricle outflow tract (LVOT) obstruction due to the thickened interventricular septum. "*Venturi effect*" is a term used to describe LVOT obstruction by hypertrophic interventricular septum during systole, which causes retrograde jet flow toward the mitral valve, causing anterior mitral valve leaflet regurgitation.

Athlete's heart is a physiological cardiac hypertrophy. Sports are divided into endurance sports (e.g., weight lifting) and dynamic sports (e.g., running). Endurance sports cause concentric cardiac hypertrophy (<12 mm) thickness, while dynamic sports cause eccentric cardiac hypertrophy that may reach (13 mm) in thickness.

Differentiation between athlete heart and HCM can be difficult by imaging alone. However, evidence of bizarre electrocardiogram (ECG) patterns, female sex, abnormal left ventricular filling, and marked left ventricular enlargement, all favor HCM. Moreover, athlete heart shows reduction in the heart muscle wall thickness from 2 to 5 mm after a 3-month period of athletic abstaining, a feature that is not seen in true HCM.

Differential Diagnoses and Related Diseases

- *Yamaguchi syndrome*, also known as *apical HCM*, is a disease characterized by HCM that is confined to, or located primarily in, the left ventricle (LV) apical region. Up to 40% of patients are asymptomatic. ECG leads show characteristic deeply inverted T wave, which might be mistaken for coronary ischemic disease.
- *Barth syndrome* is an x-linked recessive disorder characterized by HCM, neutropenia, skeletal myopathy, growth delay, hypocholesterolemia, and urinary excretion of 3-methylglutarate, 3-methylglutaconate, and 2-ethyldracrylate.
- *Romano-Ward syndrome* is an autosomal dominant disease characterized by long ECG QT interval, cardiac arrhythmia, and occasional incidence of HCM.
- *Jervell and Lange-Nielsen syndrome* is an autosomal recessive disease characterized by long ECG QT interval, cardiac arrhythmia, sensorineural hearing loss, syncopal attacks evoked by emotional stress, and occasional HCM.

Signs on Chest Radiographs

The heart size can be enlarged with signs of left ventricular dilatation.

Signs on MRI

- Normal LV end-diastolic septal wall thickness is 8.5–9.0 mm. In athletes, the LV end-diastolic septal wall thickness should not exceed >13 mm in males, and >11 mm in females. LV end-diastolic septal wall thickness >15 mm is definitely abnormal.
- Disproportional ventricular wall hypertrophy with end-diastolic septal wall thickness >15 mm. The interventricular septum is affected in >70% of patients (Fig. 4.3.1).
- Abnormal, late (>10 min) patchy contrast enhancement of the hypertrophic muscles is found in 79% of patients of HCM, probably due to small-vessel disease and ischemia.
- Venturi effect is seen as an area of signal void and mitral valve regurgitation with LVOT obstruction on Cine-images during systole.
- *Yamaguchi syndrome* shows hypertrophic left ventricular apex, causing the left ventricular cavity to exhibit characteristic "spade-like" configuration.
- *Athlete heart* is visualized as mild increase in the left ventricular myocardial wall thickness that does not exceed 13 mm in thickness on short-axis views. There is no abnormal wall enhancement after contrast injection.

Dilated Cardiomyopathy

DCM is characterized by left ventricular or biventricular dilatation with impaired systolic function.

The most common presentation of DCM is left-sided heart failure. Causes can be due to alcoholism (50% of cases), cocaine abuse, and hyper- and hypothyroidism. Contrast-enhanced MRI for DCM study is mainly indicated to differentiate primary DCM (e.g., without a cause) from secondary (e.g., postmyocardial infarction) DCM.

Signs on Chest Radiographs

The cardiac heart is markedly enlarged with increased cardio-thoracic ratio due to cardiac muscles dilatation (Fig. 4.3.2).

Signs on MRI

- There is marked dilatation of the heart ventricles, often with global wall motion abnormalities on Cine MR images. Focal wall motion abnormalities are more commonly seen in DCM due to ischemic heart disease (e.g., postmyocardial infarction) (Fig. 4.3.3).
- Secondary DCM usually shows late contrast enhancement, depending on its primary cause (e.g., myocardial infarction): the contrast uptake reflecting areas of degeneration, necrosis, and fibrosis. In contrast, primary DCM shows no late contrast enhancement. The contrast enhancement can be subendocardial or transmural.
- Intraventricular thrombus may be found.

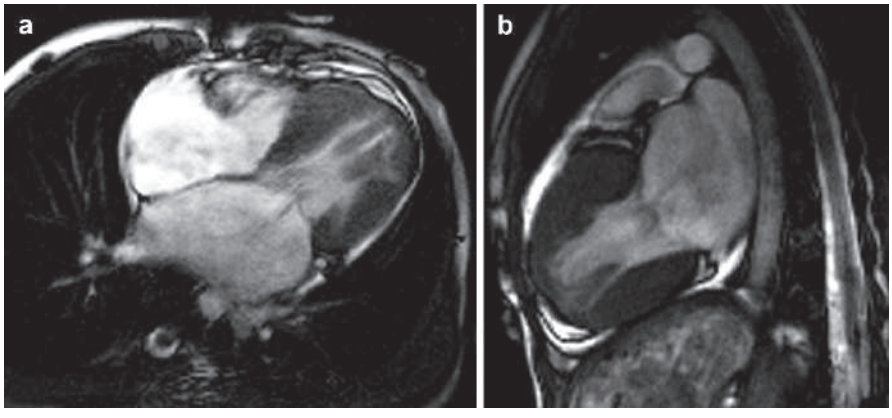

Fig. 4.3.1 Four-chamber white-blood cardiac MRI (**a**) and two-chamber view (**b**) show concentric hypertrophic cardiomyopathy (HCM). Notice the thickened chorda tendinae in (**a**)

4.3

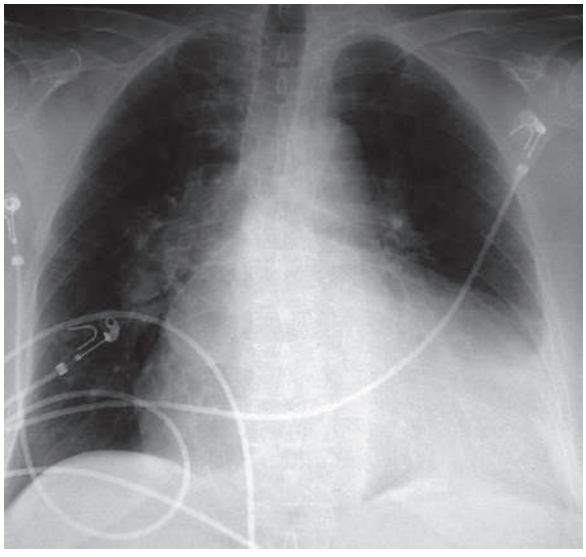

Fig. 4.3.2 Anteroposterior chest radiograph of a bedridden patient shows massively dilated heart due to dilated cardiomyopathy (DCM)

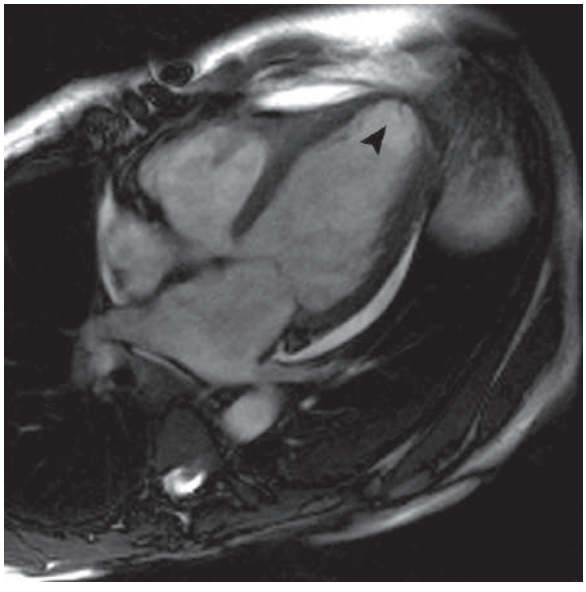

Fig. 4.3.3 Four-chamber white-blood cardiac MRI shows left ventricular apical dilatation due to previous myocardial infarction (*arrowhead*)

Restrictive Cardiomyopathy

RCM is a disease characterized by ventricular filling defect. RCM can be caused by diseases that disturb the myocardial integrity such as: amyloidosis, sarcoidosis, metastasis, and glycogen storage diseases.

Patients may present with signs of congestive heart failure because of ventricular contractility restriction in a similar fashion to constrictive pericarditis. Cardiac MRI in RCM is used to differentiate restrictive pericarditis from RCM.

Signs on Chest Radiographs

The heart size is generally enlarged due to atrial dilatation or due to the development of congestive heart failure.

Signs on MRI

The ventricular chamber dimensions and thickness are within normal range, with both atria enlarged as a direct sign of right ventricular and left ventricular filling resistance.

Arrhythmogenic Right Ventricular Dysplasia

ARVD is a rare, progressive disease characterized by infiltration and replacement of the right ventricle free wall myocardium with fibro-fatty tissue, which causes contractility dysfunction and right ventricular dilatation.

ARVD is one of the causes of arrhythmias and sudden cardiac deaths because this fibro-fatty tissue causes electrical instability of the right ventricular wall. ARVD is familial in up to 50% of cases, with an autosomal dominant mode of inheritance. The disease has a male predominance. Patient is typically a young male (30 years) complaining from arrhythmias initiated by exercise.

Signs on MRI

- There is right ventricular bulging and dilatation, thinning of the right ventricle free wall (2–6 mm in thickness), and high signal intensity seen within the myocardium on T1W images representing fat infiltration within the myocardium (diagnostic key) (Fig. 4.3.4). If fatty infiltration cannot be demonstrated, right ventricular trabeculation also fulfills the criteria of ARVD, presuming the clinical picture also suggests it.
- Abnormal wall motion is demonstrated on Cine images.

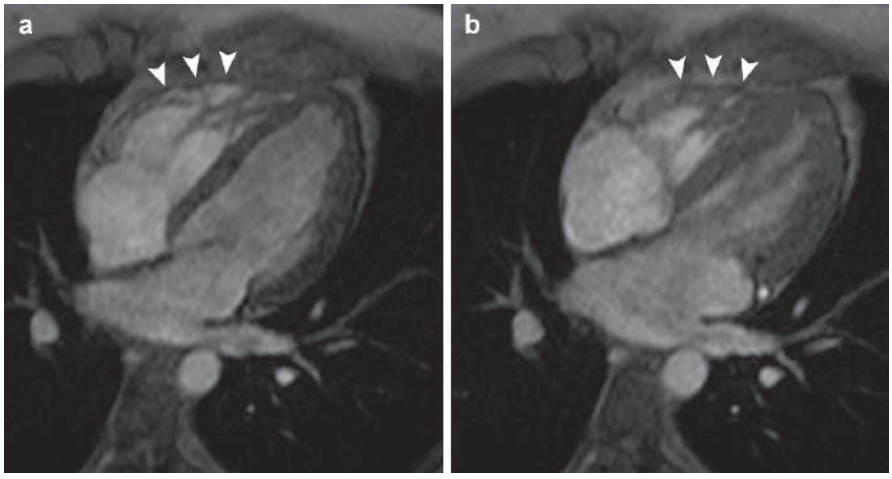

Fig. 4.3.4 Four-chamber white-blood cardiac MRI during diastole (**a**) and systole (**b**) of a patient with arrhythmogenic right ventricular dysplasia (ARVD) show thinning of the left ventricle (LV) wall with hyperintense signal within the wall representing fibro-fatty changes (*arrows*)

Noncompaction Cardiomyopathy (Spongy Myocardium)

NCCM is a rare, distinct cardiomyopathy characterized by arrest of the left ventricular muscle compaction during embryonal development, causing left ventricular myocardial trabeculation with deep intertrabecular recesses that makes the left ventricular myocardium looks like sponge.

NCCM commonly affects the LV; however, the right ventricle can be involved occasionally. The disease has an incidence of 0.05% in the general population, and can occur as an isolated case or associated with other cardiac anomalies. The clinical picture is variable. Patients may show no symptoms, while others may show signs of severe heart failure and arrhythmias.

Signs on MRI

The left ventricular walls look thickened with prominent ventricular trabeculations within them (diagnostic feature) (Fig. 4.3.5).

Peripartum Cardiomyopathy (Cardiomyopathy of Pregnancy)

Peripartum cardiomyopathy is defined as heart failure that occurs during the last 4 weeks of a term pregnancy, or the first 5 months after delivery.

Peripartum cardiomyopathy is a rare condition with an incidence of 1:15,000 postpartum women. Exclusion

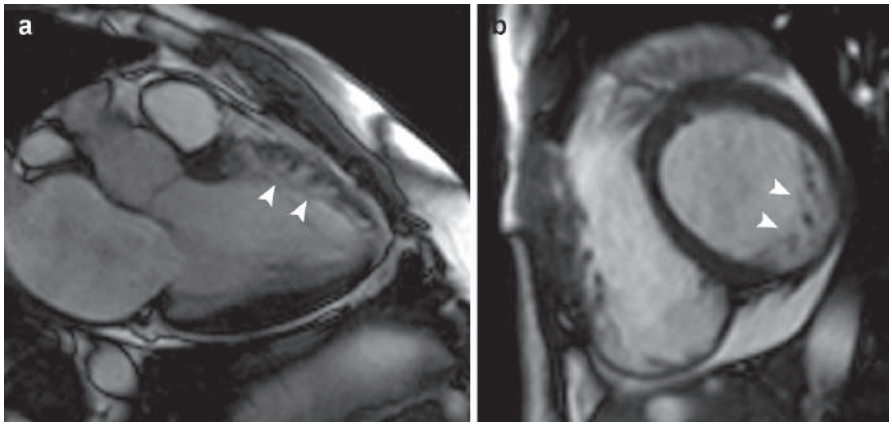

Fig. 4.3.5 Three-chamber white-blood cardiac MRI (**a**) and short-axis view (**b**) show LV trabeculation in a patient with noncompaction cardiomyopathy (NCCM) (*arrowheads*)

of previous heart disease is essential before making the diagnosis of peripartum cardiomyopathy. There is a 50% risk of thromboembolic complications associated with peripartum cardiomyopathy.

4.3

For Further Reading

1. Leon MB et al Hypertrophic cardiomyopathy. Dis Mon. 1981;28:1–87
2. Burch GE et al Heart muscle disease. Dis Mon. 1968; 14:1–68
3. Zenovich AG et al Hypertrophic cardiomyopathy with apical aneurysm. Circulations. 2004;110:e450
4. Isbell DC et al The evolving role of cardiovascular magnetic resonance imaging in nonischemic cardiomyopathy. Semin Ultrasound CT MRI. 2006;27:20–31
5. Alhabshan F et al Extent of myocardial noncompaction: comparison between MRI and echocardiographic evaluation. Pediatr Radiol. 2005;35:1147–51
6. Oduncu V et al Images in cardio-thoracic surgery. Biventricular noncompaction presenting with stroke. Eur J Cardiothorac Surg. 2008;33:737
7. Hamamichi Y et al Isolated noncompaction of the ventricular myocardium: Ultrafast computed tomography and magnetic resonance imaging. Int J Cardiothorac Imaging. 2001;17:305–14
8. Hedrich O et al Sudden cardiac death in athletes. Curr Cardiol Rep. 2006;8:316–22
9. Rochitte CE et al The emerging role of MRI in the diagnosis and management of cardiomyopathies. Curr Cardiol Rep. 2006;8:44–52
10. Sparrow P et al Cardiac MRI and CT features of inheritable and congenital conditions associated with sudden cardiac death. Eur Radiol. 2008. doi:10.1007/s00330-008-1169-5
11. Duygu H et al Apical hypertrophic cardiomyopathy might lead to misdiagnosis of ischemic heart disease. Int J Cardiovasc Imaging. 2008;24:675–81
12. Bachou T et al A novel mutation in the G4.5 in a Greek patient with Barth syndrome. Blood Cells Mol Dis. 2009; 42:262–4
13. Reardon W et al Consanguinity, cardiac arrest, hearing impairment, and ECG abnormalities: counselling pitfalls in the Romano-Ward syndrome. J Med Genet. 1993;30:325–7
14. Schwartz PJ et al The Jervell and Lange-Nielsen syndrome: natural history, molecular basis, and clinical outcome. Circulation. 2006;113;783–90
15. Malouf J et al Apical hypertrophic cardiomyopathy in a father and a daughter. Am J Med Genet. 1985;22:75–80
16. Zandrino F et al Magnetic resonance imaging of athlete's heart: myocardial mass, left ventricular function, and cross-sectional area of the coronary arteries. Eur Radiol. 2000;10: 319–25

4.4 Endocarditis

Endocarditis is a term used to describe acute or chronic inflammation of the cardiac chamber's interior. Although the most common cause of endocarditis is infectious agents, other rare causes of endocarditis can be encountered uncommonly.

Infective Endocarditis

Infective endocarditis (IE) is a disease that results from bacterial colonization of the platelet fibrin vegetation on the surface of the heart endothelium by circulating microorganisms.

IE can be acute or subacute. Acute IE is caused by highly virulent bacteria infecting even a healthy valve, whereas subacute IE occurs in a patient with prosthetic or defective heart valve with low virulent bacteria. The bacteria in the acute IE are present in the blood as septicemia, while in the subacute IE, a bacteremia is sufficient to initiate the disease.

The acute IE embolus initiates abscess and pyemia in the tissue in which it is deposited because of the high virulent bacteria within it. In contrast, subacute emboli cause localized effect within the vessels or the organs such as mycotic aneurysms and infarction due to vascular occlusion.

Classically, patients with IE are patients with known previous injury to their heart valves (e.g., patients with past history of rheumatic fever) who present with signs of fever and night sweat, typically weeks after dental or surgical procedures. Nowadays, intravenous drug abusers (IVDAs) are the most common population at risk of developing IE.

The most common infectious organisms causing IE include: *staphylococci*, *streptococci*, *Candida albicans*, *Coxiella burnetii* (Q fever), and the HACEK organisms (*Hemophilus parainfluenza*, *Hemophilus aphrophilus*, *Actinobacillus [Hemophilus] actinomycetemcomitans*, *Cardiobacterium hominis*, *Eikenella* species, and *Kingella* species).

Patients with IE typically present with fever, anorexia, weight loss, malaise, night sweat, bacteremia, evidence of active vasculitis, septic emboli, and immunologic vascular phenomenon. However, the previous typical stigmata are not always present and the symptoms may be nonspecific, especially among IVDA patients.

The modified Duke criteria for IE diagnosis: Diagnosis of IE must fulfill two major criteria, 1 major plus 3 minor, or 5 minor criteria.

Major Criteria

- Positive blood culture.
- Two separated blood cultures consistent with IE organisms (e.g., *Staphylococcus aureus*) in the absence of the primary focus.
- Evidence of endocardial involvement.
- Positive echocardiogram for heart valves vegetations.
- New partial dehiscence of prosthetic valve.
- New valvular regurgitation.

Minor Criteria

- Predisposing heart condition (e.g., congenital heart disease)
- Fever.
- Vascular phenomenon (septic arterial emboli, intracranial or conjunctival hemorrhage, Janeway's lesions).
- Immunologic phenomenon (glomerulonephritis, Osler's nodes, Roth's spots, or rheumatoid factor).
- Positive blood culture that does not meet major criteria or serological evidence of infection.

The cardiac complications of IE include valvular heart defect, mostly affecting the mitral valve followed by the aortic valve. The valvular disease in the subacute form is due to stenosis and long-term fibrosis, whereas in the acute form, the valvular disease or insufficiency arises due to acute valvular destruction. The most common valves involved are the left-side heart valves, except in IVDAs, where infection in the right-side valves is as common as in the left side. Left-sided heart failure is the end product of mitral or aortic valves insufficiency when the tricuspid or the pulmonary valves are also involved. Extra-cardiac manifestations of IE are mostly related to septic vascular emboli, vascular phenomenon, and immunological phenomenon.

4.4

The organs most commonly affected are the central nervous system, the thorax, the vascular system, the spleen, the kidneys, and the skin.

Neurological manifestations of IE are the most common complications, and they involve embolic strokes (15–20% of cases). The septic embolic stroke may precede the diagnosis of IE in up to 75% of IE complicated by strokes. Septic embolic strokes rate increases in patients with IE when the vegetation is >10 mm in diameter. Rarely, the septic emboli may result in the formation of brain abscess, or meningitis. *S. aureus* is the most common organism causing embolic strokes. Mycotic arterial aneurysm involving the cerebral vessels with intracranial hemorrhage is seen in 2–10% of IE cases. Mycotic aneurysm is formed secondary to septic emboli injuring the vascular endothelium intima of the vasa vasorum and implanting infectious focus, or due to vasculitis. Patients with mycotic aneurysms may present with headaches and neurological deficits. Mortality can reach up to 80% if the mycotic aneurysm is ruptured. Streptococci are the most common organisms causing mycotic aneurysms.

Thoracic IE complications are seen when IE affects the right side of the heart. Complications include septic emboli (65–75% of cases) and pulmonary infarction, pneumonia, empyema, abscess formation, and mycotic aneurysm of the pulmonary arteries. IVDA patients are affected by pulmonary septic emboli in up to 75% of cases.

Splenic abscesses are the most common abdominal extra-cardiac manifestations of IE (55% of cases), and occur due to septic emboli dissemination. The abscess formation can be single or multiple. Renal involvement may occur in up to 66% of patients in the form of glomerulonephritis or renal infarction due to septic emboli.

Musculoskeletal complications of IE include spondylodiscitis (1.8–5% of cases), sacroiliitis, septic arthritis, and osteomyelitis; all which are explained by septic emboli dissemination. However, aseptic, self-limiting arthralgia with low back pain may occur in up to 44% of cases.

Skin manifestations of IE are explained by vasculitis that results from deposition of circulating immune complexes on various endothelial locations. The most common skin lesions in IE are Osler's nodes and Janeway's lesions. *Osler's node* is a tender, erythematous, non-hemorrhagic lesion with white center located at the fingers pads (Fig. 4.4.1), whereas *Janeway's lesions* are non-tender, small hemorrhagic,

Fig. 4.4.1. A hand illustration of a patient with IE shows Osler's nodes, Janeway's lesion, and splinter hemorrhage

and slightly nodular lesions located at the palms and soles (Fig. 4.4.1). *Splinter hemorrhage* is another lesion found in IE, which is characterized by extravasation of blood from the longitudinally located vessels of the nail bed (Fig. 4.4.1). Splinter hemorrhage is seen as small areas of bleeding under the nails, commonly affecting the fingernails more than the toes. *Roth's spots* are areas of retinal bleeding within the globe, which is seen on fundoscopy (Fig. 4.4.2). Clubbing of fingers occurs due to chronic toxemia in the subacute form.

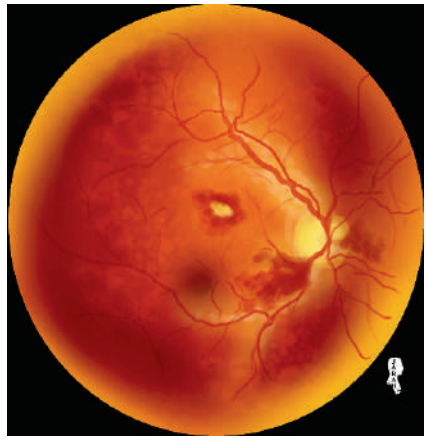

Fig. 4.4.2. A Fundoscopic illustration demonstrating Roth's spots as multiple hemorrhages within the vitreous humor

Signs on Chest Radiographs

- Signs of heart failure with enlarged cardio-thoracic ratio (>55%), and pulmonary edema is seen in up to 65% of cases in patients with clinical signs of heart failure.
- Empyema is detected as a pleural effusion with thick irregular meniscus sign that is immobile on decubitus views.

Signs on CT and CTA

- On cardiac CT, vegetations are seen as round lesions located at the heart valves (Fig. 4.4.3). Lesions >10 mm in diameter have a high risk of embolization.
- In the brain, embolic strokes are often multiple, and typically are located at the corticomedullary junction extending to the gray matter. Up to 90% of septic embolic strokes are in the middle cerebral artery (MCA) vascular territory.
- Cerebral mycotic aneurysms are most commonly seen at the distal branches of the MCA, and multiple in 29% of cases.
- Single or multiple splenic abscesses are seen as hypodense lesions within the spleen on non-enhanced scan. The lesions typically show rim-enhancement after contrast injection.
- Renal infarction is detected as a peripheral wedge-shaped area that fails to enhance after contrast injection. The "cortical rim sign" can be seen in 50% of cases.

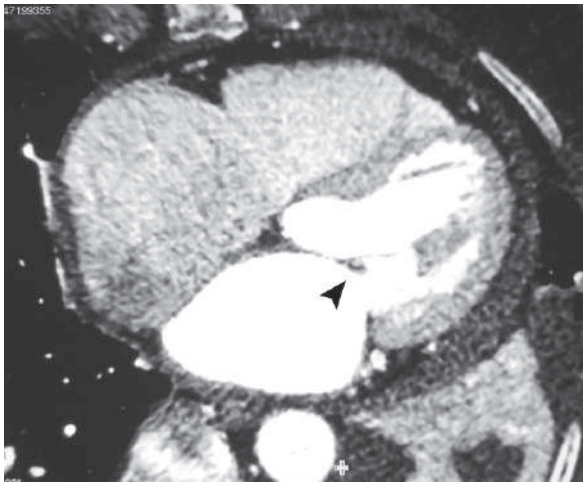

Fig. 4.4.3. Axial cardiac CTA of a patient with IE shows mitral valve vegetation (*arrowhead*)

Löffler Endocarditis (Eosinophilic Endomyocardial Disease)

Löffler's endocarditis (LE) is a rare disease characterized by eosinophilic vasculitis, inflammation, and fibrosis of the myocardium associated with peripheral systemic eosinophilia. It can be primary (idiopathic hypereosinophilia) or secondary to some types of malignancies (e.g., leukemia).

Infiltration of the myocardium by eosinophils causes myocarditis, which is transformed later into myocardial fibrosis and can be superimposed by thrombus formation within the myocardium (mural thrombus). The myocardial fibrosis later on results in restrictive myocardial normal movement similar to the mechanism of restriction encounter in restrictive cardiomyopathy, which results in heart failure. When the fibrosis extends to the papillary muscles and chordae tendineae, disruption of the atrioventricular valves occurs (mitral or tricuspid valves insufficiency).

LE has poor prognosis with high mortality due to heart failure, sudden death, or thromboembolism. Systemic eosinophilic vasculitis can cause multiple infarctions in the brain, kidney, and lungs.

The most characteristic finding in LE which should be indicative is the presence of high eosinophilia in the routine white blood count (CBC), associated with fever and signs of cardiac failure.

The eosinophilia can be absent in chronic cases of LE, where the clinical picture shows the picture of restrictive endocarditis instead of the acute picture of the disease, which is characterized by eosinophilia and cardiac enlargement due to inflammation.

Signs on CT

- Thickening of the myocardium, commonly seen at the apex with areas of hypodensity within the myocardium representing edema and inflammation (Fig. 4.4.4).
- Localized hypodense mass within the myocardium can be seen occasionally representing intramyocardial thrombus.

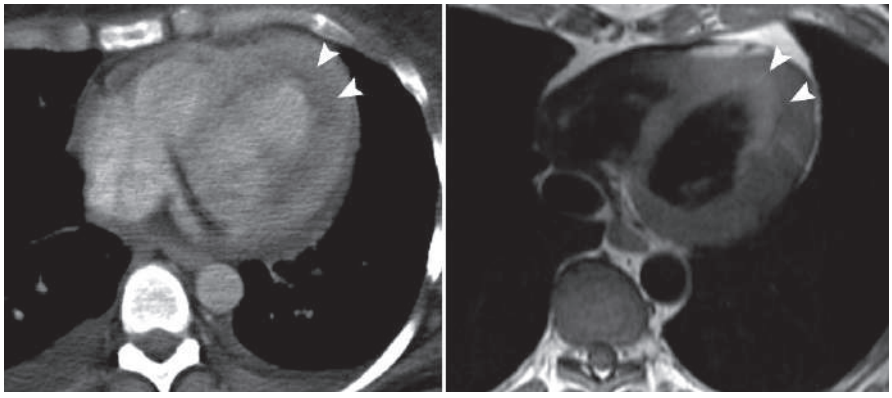

Fig. 4.4.4. Axial cardiac CT (**a**) and dark-blood MRI (**b**) of a patient with Löffler's endocarditis (LE) showing hypertrophic left ventricle myocardium with subendocardial hypodensities in (**a**) (*arrowheads*), and hypertrophic left ventricle myocardium with subendocardial hyperintensities in (**b**) due to myocardial inflammation and edema

Signs on MRI

- Ventricular wall thickening with hypointense signal in T1W and T2W images representing fibrosis
- High signal within the myocardium in T2W images can be seen representing edema and active myocardial inflammation (Fig. 4.4.4).
- Enhancement of the myocardium after gadolinium injection.

Marantic Endocarditis (Non-Bacterial Thrombotic Endocarditis)

Non-bacterial thrombotic endocarditis (NBTE) is a condition characterized by non-bacterial heart valves vegetation composed of sterile masses of platelets and fibrin fibers. The term is partly a misnomer, because myocardial inflammation is absent.

NBTE is most commonly associated with end-stage malignancies like those of the breast, lung, and colon. Also, NBTE can be seen uncommonly with autoimmune diseases like systemic lupus erythematosus (SLE) (*Libman-Sacks endocarditis*).

Libman-Sacks vegetations are noninfective verrucous vegetations that develop mainly on the mitral valves, and maybe the aortic valve. Libman-Sacks vegetations are found in approximately 1 of 10 patients with SLE. Libman-Sacks endocarditis may be differentiated from IE by measuring the white blood count (high in IE, and expected to be low during lupus flare), the C-reactive protein (high in IE, and possibly suppressed in SLE), and the antiphospholipid antibody level (moderate to high levels in SLE, and unlikely to be high in IE).

The vegetation is believed to be caused by the state of hypercoagubility secondary to malignancies or autoimmune diseases. The vegetations are usually <3 mm in diameter, and can present with multiple systemic embolic attacks involving the cerebral nervous system or the vascular system (e.g., blue toe syndrome). The vegetations rarely alter valve function or produce murmurs. *Blue toe syndrome* is a condition characterized by sudden onset of acute pain and cyanosis in one or more toes due to embolic event (Fig. 4.4.5).

A blood culture is considered negative after three or more sets of blood cultures incubated for a week fail to demonstrate growth. The most common causes of culture negative endocarditis are antibiotic therapy prior to the blood cultures and infection due to fastidious organisms. NBTE should be considered when a patient with suspected IE fails to demonstrate positive blood culture and fails to respond to antibiotic therapy, or in a patient with multiple cerebral strokes due to unknown cause. Early recognition of NBTE will lead to early detection of occult malignancy or autoimmune disease.

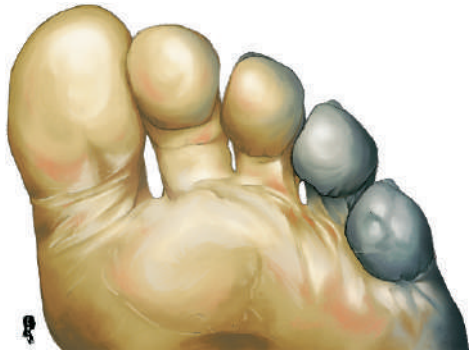

Fig. 4.4.5. An illustration demonstrating the gross appearance of blue toe syndrome

For Further Reading

1. Colen TW et al Radiologic manifestations of extra-cardiac complications of infective endocarditis. Eur Radiol. 2008;18:2433–45
2. Bayer AS et al Diagnosis and management of infective endocarditis and its complications. Circulation. 1998;98: 2936–48
3. Friday BB et al Systemic complications of infective endocarditis. Circulation. 2005;112:e324
4. Fellah L et al Combined assessment of tricuspid valve endocarditis and pulmonary septic embolism with ECG-gated 40-MDCT of the whole chest. AJR. 2007;189:W228–30
5. Mahlab K et al Diagnosis of Candida endocarditis by computed tomography scanning. IMAJ. 2006;8:442–4
6. Lawrence R. Freedman. Endocarditis updated. Dis Mon. 1979;26:1–51
7. Farrior JB et al A consideration of the difference between a Janeway's lesion and an Osler's node in infectious endocarditis. Chest. 1976;70:239–43
8. Saladi RN et al Idiopathic splinter hemorrhages. J Am Acad Dermatol. 2004;50:289–92
9. Hirschmann JV et al Blue (or purple) toe syndrome. J Am Acad Dermatol. 2009;60:1–20
10. Kleinfeldt T et al Hypereosinophilic syndrome: a rare case of Loeffler's endocarditis documented in cardiac MRI. Int J Cardiol. 2009. doi:10.1016/j.ijxard.2009.03.059
11. Files MD et al A child with eosinophilia, Loeffler endocarditis, and acute lymphoblastic leukemia. Pediatr Cardiol. 2009. 30:530–532
13. Lofiego C et al Ventricular remodeling in Loeffler endocarditis: implications for therapeutic decision making. Eur J Heart Fail. 2005;7:1023–6
14. Yalonetsky S et al Mitral valve destruction by Hodgkin's lymphoma-associated Loefler endocarditis. Pediatr Cardiol. 2008. doi:10.1007/s00246-007-9135-6
15. Joshi SB et al Marantic endocarditis presenting as recurrent arterial embolization. Int J Cardiol. 2009;132:e14–16
16. Fanale MA et al Some unusual complications of malignancies. Case 2. Marantic endocarditis in advanced cancer. J Clin Oncol. 2002;20:4108–14
17. Singh V et al Marantic endocarditis (NBTE) with systemic emboli and paraneoplastic cerebellar degeneration: uncommon presentation of ovarian cancer. J Neurooncol. 2007;83:81–3
18. Moyssakis I et al Libman-Sacks endocarditis in systemic lupus erythematosus: prevalence, associations, and evolution. Am J Med. 2007;120:636–42

4.5

Pericardial Diseases

The pericardium is a double-walled sac that encloses the heart. The outer sac is called the "fibrous pericardium," and the inner sac is called the "serous pericardium." The serous pericardium is composed of an outer (parietal) layer, and an inner (visceral) layer separated by potential space (pericardial cavity). Both the fibrous and the serous layers are continuous with the adventitia of the great vessels.

The anterior aspect of the fibrous pericardium is attached to the left half of the sternum and to the fourth, fifth, and sixth left costal cartilages. Inferiorly, it is attached to the central tendon of the diaphragm. Only the fibrous pericardium below the fifth or sixth intercostal space is sensitive to pain, while the remaining fibrous and entire serous pericardium is insensitive. When this pain-sensitive area is stimulated by a disease, pericardial pain is perceived as pain in the neck and trapezius muscle via the phrenic nerve, which enters the spinal cord at the fourth and fifth cervical segments.

The pericardial cavity contains normally 20–50 mL of serous fluid, although the sac has a potential space of 80–100 mL. The pericardial fluid is absorbed by the lymphatics found near the base of the heart. The blood supply of the pericardium comes from the internal thoracic artery via the pericardiophrenic artery.

Pericardial effusion is a disease characterized by excess fluid within the pericardial cavity that exceeds 50 mL. Like pleural effusion, this fluid can be classified into transudative or exudative based on the protein content. The pericardial fluid can be edematous (e.g., in uremia), hemorrhagic (e.g., in trauma), contain pus (e.g., infective endocarditis), or contain lymph (e.g., due to rupture of the thoracic duct). When the pericardial fluid is severe enough to compromise the heart contractility, the condition is called "*pericardial tamponade*," and it is a medical emergency. Between 150 and 250 mL of fluid must be present within the pericardial cavity to cause a cardiac tamponade.

Pericarditis is a condition characterized by inflammation of the pericardium, which can be acute or chronic. Pericarditis can arise due to infections, autoimmune diseases, and granulomatous diseases. Patients with pericarditis often present with symptoms due to inflammation, pericardial effusion or tamponade, or constriction and/or restriction due to fibrosis.

Symptoms of pericarditis include acute sudden neck or upper arm pain that is exaggerated by body movements, respiration, swallowing, and rarely by heart beat. The pain may be relieved by leaning forward, which will stabilize the pericardial sac and reduce the movement of the pain-sensitive area. When the peripheral diaphragmatic pleura are inflamed, epigastric pain is felt, which can be seen in up to 50% of patients with acute idiopathic pericarditis. Moreover, dull abdominal pain in the right upper quadrant may be felt due to congestion of the abdominal viscera in cases of tamponade and pericardial constriction. Other symptoms include fever, dyspnea, and paroxysmal nocturnal dyspnea in complicated cases. *Paradoxical pulse* is a normal pulse variation representing the fact that the systolic pressure is less during inspiration than during expiration in a normal person. An accentuation of this normal respiratory variation may be found in patients with pericarditis with tamponade. Also, in patients with tamponade, an alternation of a weak pulse and a strong pulse in the presence of a regular rhythm may be found (*pulsus alternans*).

A pleural effusion may accompany pericarditis in all stages of the disease (>50% of cases). In patients with large pericardial effusion, an area of dullness of variable size can be found in the region of the inferior angle of the scapula where there is normally bronchial breathing (Ewart's sign). This sign is explained by the fact that large pericardial effusion forces the heart and the great vessels backward, thereby compressing the lung and the bronchi.

Chronic pericarditis, like any chronic inflammation, is characterized by calcification and fibrosis. Pericardial fibrosis due to chronic inflammation with pericardial space limitation is called "*constrictive pericarditis*." Constrictive pericarditis can occur due to tuberculosis, radiation, previous pericardiotomy, and up to 49% are idiopathic. Patients with constrictive pericarditis often present with signs of right-sided heart failure, and atrial fibrillation in up to 40% of cases. Clinical signs of liver enlargement, ascites, and peripheral edema may be seen in patients with constrictive pericarditis due to congestive heart failure. On auscultation, patients with acute and constrictive pericarditis have pericardial friction rub, in which a sound is heard

during heart beat cycle due to friction of the fibrous pericardium layers. Pericardial rub is a diagnostic clinical sign of pericarditis.

Pneumopericardium is a rare condition characterized by the presence of air within the pericardial cavity. Pneumopericardium can occur as a complication of pneumomediastinum, pneumothorax, or pericardial fluid aspiration.

Differential Diagnoses and Related Diseases

- *Dressler's syndrome*, also known as "*post-myocardial infarction syndrome*," is a disease seen as early as 10 days and as late as 2 years following myocardial infarction characterized by fever, pericarditis or pleuritis with hemorrhagic effusion, and pneumonia with gross hemoptysis. The disease has a tendency for recurrence.
- *CACP syndrome* is an uncommon disease characterized by *C*amptodactyly, noninflammatory *A*rthropathy, *C*oxa vara, and *P*ericarditis. The disease is related to a group of diseases known as "*familial arthropathy diseases*." The disease arises due to hypertrophies synovium in the absence of synovitis (in contrast to rheumatoid arthritis or its juvenile form), which is typically detected by synovial biopsy. Patients affected present with arthropathy usually since childhood. Camptodactyly is a congenital or acquired nontraumatic flexion deformity of the proximal interphalangeal (PIP) joint of one or several fingers, which is usually bilateral in CACP syndrome. Noninflammatory arthropathy involves large joints such as elbows, knees, and ankles. Coxa vara is a horizontally oriented femoral neck. Mild noninflammatory pericarditis with pericardial effusion occurs in 30% of cases. The condition may be mild or self-limited. MRI studies classically show hypertrophied synovium with rim-like enhancement of the fluid-filled bursae, a feature that distinguishes CACP syndrome from rheumatoid arthritis, which shows synovial hypertrophy, signs of soft tissue hyperemia, and diffuse contrast enhancement.

Signs on Chest Radiographs

- Pericardial effusion is detected as increased heart enlargement on serial radiographs. The pericardial effusion starts to show radiographic abnormalities when the pericardial fluid exceeds 250 mL in adults (Fig. 4.5.1).
- Constrictive pericarditis can be detected when calcification of the pericardium occurs (Fig. 4.5.2). Calcified pericardium is visualized as a wide area of calcification that follows the heart silhouette.
- Pneumopericardium is visualized as an air surrounding the heart contour (Fig. 4.5.3).

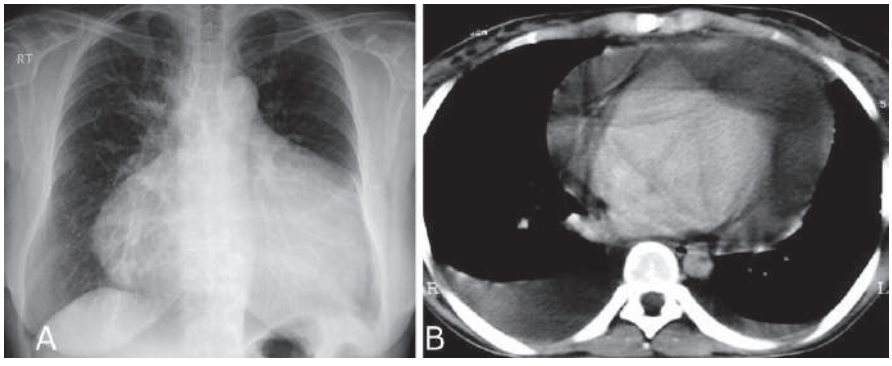

Fig. 4.5.1 Posteroanterior chest radiograph (**a**) and axial chest CT of two different patients with pericardial tamponade show massive heart enlargement in (**a**) due to pericardial effusion, and hypodense material is seen surrounding the heart due to marked pericardial effusion in (**b**). Also, bilateral pleural effusion can be seen in (**b**)

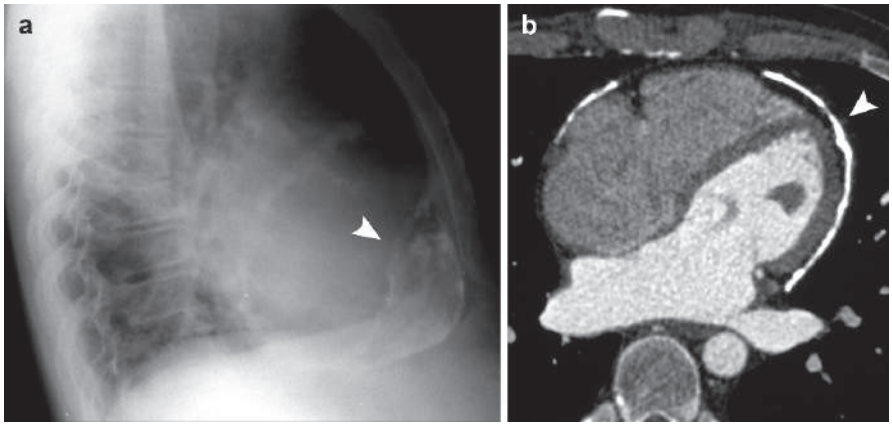

Fig. 4.5.2 Lateral chest radiograph (**a**) and axial chest CT of two different patients with constrictive pericarditis show calcified pericardium (*arrowheads*)

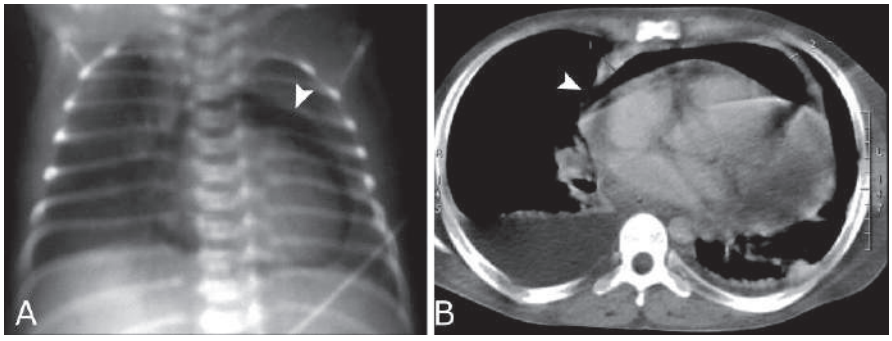

Fig. 4.5.3 Posteroanterior chest radiograph (**a**) and axial chest CT of two different patients with pneumopericardium show air surrounding the heart in (**a**) and (**b**) (*arrowheads*)

Signs on CT and MRI

- Pericardial effusion and tamponade are seen as fluid signal intensity material located within the pericardial space (Fig. 4.5.1). The normal pericardial space should not exceed 4 mm in width. On CT, the fluid can have high density if it is hemorrhagic (e.g., >80 HU). On MRI, the signal intensity of the fluid is variable according to the content of the fluid (e.g., high T1 and T2 signal intensities if it is hemorrhagic).
- The normal pericardium is visualized on MRI as a thin hypointense line surrounding the heart outlined by the high-intensity pericardial fat, which normally should not exceed 3 mm in thickness. Acute pericarditis on CT and MRI is diagnosed when the pericardium is >3 mm in thickness and enhances after contrast injection (Fig. 4.5.4).
- Constrictive pericarditis shows diffuse thickening and irregularities of the pericardium with or without calcification. Pericardial calcification is a diagnostic sign of constrictive pericarditis (Fig. 4.5.2). Normal or near normal thickening of the pericardium does not rule out constrictive pericarditis.
- Pneumopericardium is seen as an air that surrounds the heart within the pericardial space (Fig. 4.5.3).

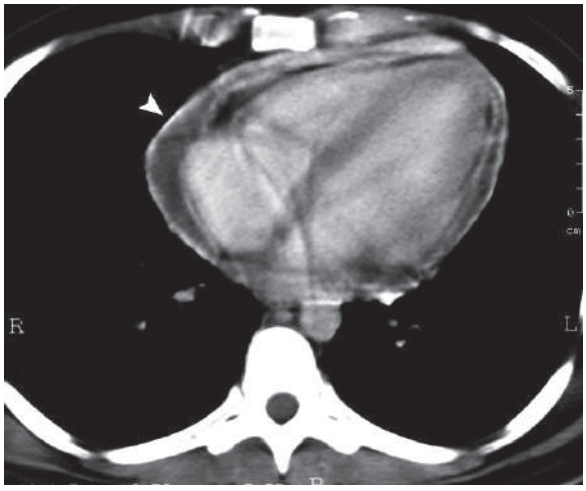

Fig. 4.5.4 Axial postcontrast cardiac CT with contrast shows pericardial enhancement (*arrowhead*) with moderate pericardial effusion in a patient with acute pericarditis

For Further Reading

1. McIntosh HD. Pericarditis. Dis Mon. 1964;10:1–39
2. Glockner JF. Imaging of pericardial diseases. Magn Reson Imaging Clin N Am. 2003;11:149–62
3. Weiser NJ et al The postmyocardial infarction syndrome: the nonspecificity of the pulmonary manifestations. Circulation. 1962;25:643–50
4. Oberholzer K et al Pneumomediastinum and pneumopericardium due to malignant subcarinal lymphadenopathy: CT demonstration. Eur Radiol. 1997;7:583–5
5. Talreja DR et al Constrictive pericarditis in 26 patients with histologically normal pericardial thickness. Circulation. 2003;108:1852–7
6. Yousefzadeh DK et al The triad of pneumonitis, pleuritis, and pericarditis in juvenile rheumatoid arthritis. Pediatr Radiol. 1979;8:147–50
7. Spiegel R et al Eosinophilic pericarditis: a rare complication of idiopathic hypereosinophilic syndrome. Pediatr Cardiol. 2004;25:690–2
8. Choi B-R et al Camptodactyly, arthropathy, coax vara, pericarditis (CACP) syndrome: a case report. J Korean Med Sci. 2004;19:907–10
9. Al-Mayouf SM. Familial arthropathy in Saudi Arabian children: demographic, clinical, and biochemical features. Semin Arthritis Rheum. 2007;36:256–61

Chapter 5

Nephrology

CONTENTS

J. A. Al-Tubaikh: *Internal Medicine* – An Illustrated Radiological Guide
DOI: 10.1007/978-3-642-03709-2_5, © Springer-Verlag Berlin Heidelberg 2010

5.1 Hypertension

Hypertension is a disease characterized by an increase in systolic blood pressure >140 mmHg, and in diastolic blood pressure >100 mmHg. Hypertension is 90% primary (without a cause), and 10% secondary to an organic cause. Radiological modalities are mainly used to detect secondary causes of hypertension.

Secondary causes of hypertension include the following:

- *Renovascular diseases*: atherosclerosis (adults), fibromuscular dysplasia (children), vasculitis (polyarteritis nodosa (PAN) and Takayasu arteritis (TA)), and renal artery aneurysm.
- *Adrenal causes*: pheochromocytoma, primary hyperaldosteronism, and Cushing's syndrome.
- *Renal parenchymal diseases*: chronic glomerulonephritis, diabetic nephropathy, lupus nephritis, polycystic kidney disease, and page kidney.
- *Aortic diseases*: coarctation of the aorta and mid-aortic syndrome.
- *Other causes*: brain tumors, congenital AVM, carcinoid tumors, acromegaly, and hypercalcemia.

Renal Artery Stenosis

Renal artery stenosis (RAS) constitutes 1–5% of patients with hypertension. Atherosclerosis is the commonest cause of renovascular hypertension in adults, while renal artery fibromuscular dysplasia is the most common cause of renovascular hypertension in children. Atherosclerosis RAS often affects the proximal part of the artery, while fibromuscular dysplasia often involves the middle and the distal part in a form of small stenotic and aneurysmal dilatation, giving the so-called "beaded appearance" on angiography.

RAS is suspected as a cause of hypertension in the following situations:

- Hypertension in a patient <30 years of age, or a patient >50 years.
- Hypertension that is resistant to three antihypertensive regimens.
- Sudden renal functions worsening in a hypertensive patient.
- Sudden development or worsening of hypertension in any age.
- Unilateral small kidney.
- Renal impairment after treatment with angiotensin-converting enzymes (ACE) inhibitors.

RAS is commonly diagnosed by color-coded duplex scanning by two methods: direct and indirect. The direct method involves measuring the blood velocity directly within the renal artery (Fig. 5.1.1). In contrast, the indirect method involves measuring the blood velocity within the segmental and interlobar intra-renal vessels (Fig. 5.1.2). The indirect method is insensitive for less than 60% RAS.

The resistance index (RI) is the maximal systolic velocity minus the end diastolic velocity divided by the maximal velocity. Increase in renal artery RI is seen in RAS, transplant rejection, acute tubular necrosis, graft infections, and obstructive hydronephrosis. The RI tends to be high in patients with chronic renal disease.

Goldblatt kidney is a condition where the kidney starts to release rennin to overcome RAS, leading to renovascular hypertension. *Page kidney*, on the other hand, is a condition where the kidney is compressed from an adjacent pathology that causes cortical ischemia. The kidney releases rennin to overcome the ischemia, leading to renovascular hypertension.

The Normal Renal Artery Waveform Parameters

- The normal renal artery waveform shows low resistance, continuous profile through the cardiac cycle, with an RI <0.7. Also, the normal main renal artery waveform has an early systolic peak (ESP) (Fig. 5.1.3).
- *The renal-aortic ration* (*RAR*) is defined as the maximum peak systolic velocity (PSV) of the renal artery divided by the maximum PSV of the aorta at the level of the superior mesenteric artery (SMA). A high false RAR can be seen in cases of abdominal aortic aneurysm, and aortic PSV <40 cm/s, or aortic PSV >125 cm/s. Also, RAR should not be used in the assessment of renal artery aneurysm for young patients or patients with renal artery stents.
- The normal interlobar and segmental arteries display an ESP at the beginning of the systole. The ESP is

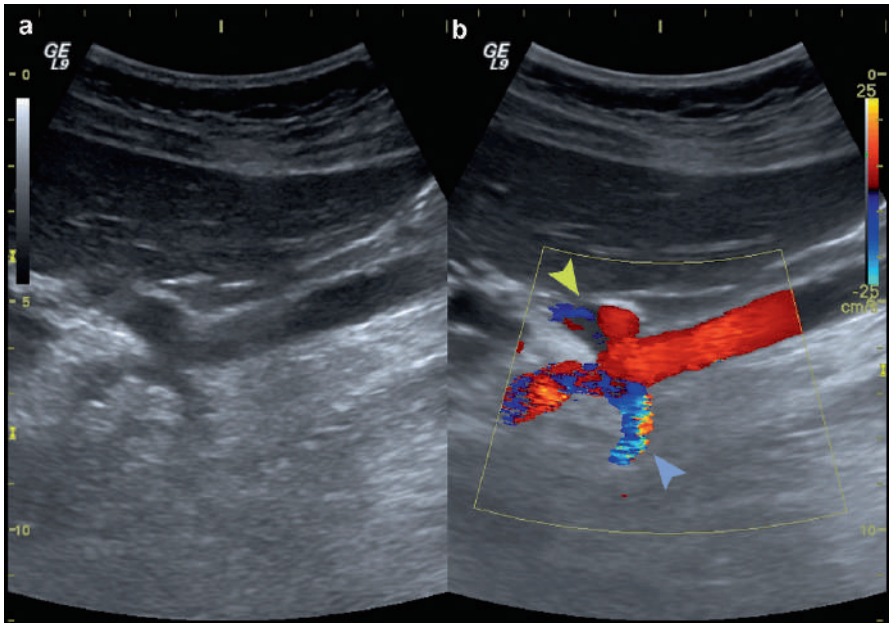

Fig. 5.1.1. Color Doppler sonogram of the aorta shows a normal anatomy of the renal arteries (Banana peel view) in gray-mode in (**a**) and Duplex colored mode in (**b**) taken while the patient is in the lateral decubitus position. The right renal artery is clearly detected in (**b**) (*yellow arrowhead*), and the left renal artery is also detected well in this position (*blue arrowhead*)

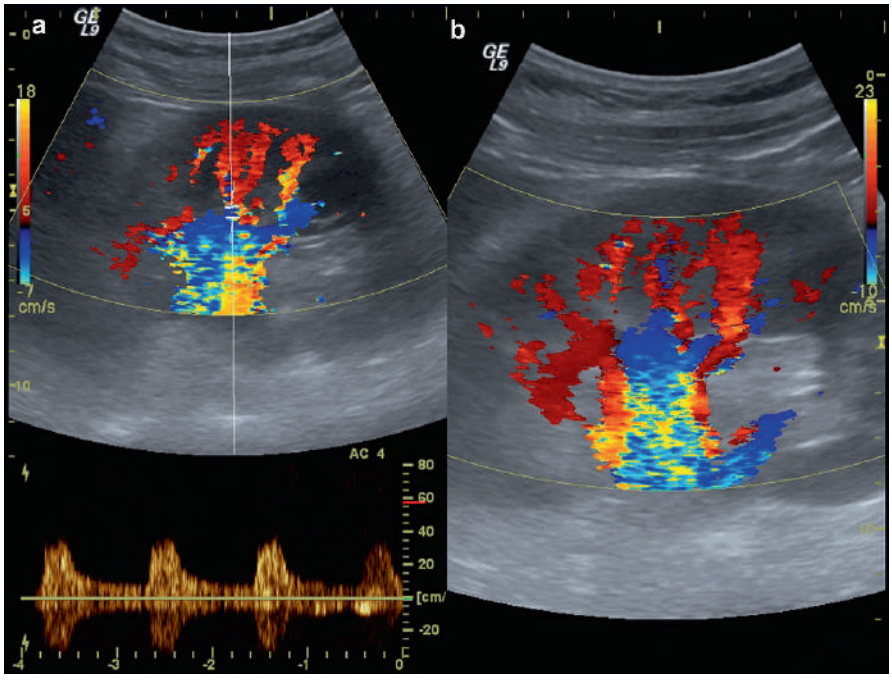

Fig. 5.1.2. Color Doppler sonogram of the left kidney demonstrates its vascular anatomy in (**b**) and arterial waveform detection in (**a**) to assess the arterial vascular supply as an indirect method for detecting RAS

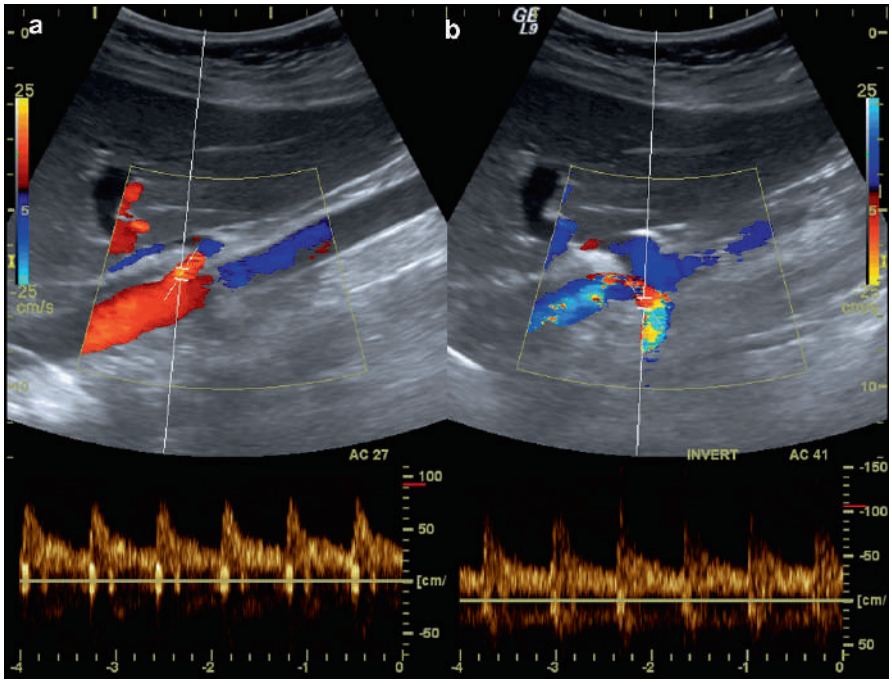

Fig. 5.1.3. Color Doppler sonogram of the renal arteries demonstrates normal arterial waveform of the right renal artery (**a**) and the left renal artery (**b**)

absent when the arterial stenosis is >60%. The Doppler angle should be <30°; otherwise the peak will not be demonstrated.

- *The systolic acceleration time* (*SAT*) is defined as the time measured from the start of the systolic upstroke to the first ESP. Normally it is <0.07.

Signs of Direct RAS on Doppler Sonography

- High renal parenchymal echogenicity that may reach or exceed the liver echogenicity (signs of renal parenchymal damage). A kidney disease can cause renal artery resistant waveform, which may be mistaken with RAS.
- Normal RAR (<3.5) and the normal renal PSV (<180 cm/s). Sixty percent RAS shows RAR <3.5, with PSV between 180 and 200 cm/s. There is no poststenotic turbulence (mosaic pattern/ aliasing artifact) with RAS <60%. A 60–99% RAS shows RAR >3.5, PSV >200 cm/s, and poststenotic turbulence.

Signs on Indirect RAS on Doppler Sonography

- Absence of the ESP.
- An accelerated time peak >100 ms is consistent with >60% stenosis.
- *Tadus parvus waveform*: this waveform consists of slow, damped systolic acceleration (tardus) and rounding and flattening of the systolic peak (parvus).
- More than (−5) difference between the two kidneys RI.
- Kidney size <9 cm, or the difference in size between the two kidneys >2 cm in diameter (normal kidney size = 9–12 cm in diameter).

Signs on CT

- *Arterial cut-off sign*: the course of the renal artery is seen interrupted on contrast- enhanced images. It is a sign of renal artery obstruction (Fig. 5.1.4).
- *Rim sign of vascular compromise*: the kidney fails to enhance on contrast-enhanced images, with a thin rim of subcapsular enhancement seen paralleling the renal margin (Fig. 5.1.4). This sign is caused by renal medullary arterial perfusion interruption in cases of renal artery obstruction, with preserved perfusion of the renal cortex by the capsular perforating vessels. This sign can be seen in cases of renal vein thrombosis, renal arterial occlusion, and acute tubular necrosis.
- *Reverse rim sign*: this sign is seen as hypodense renal cortex against a contrast-enhanced background of intact meullary arterial perfusion (Fig. 5.1.4). This sign is seen in cases of compromised renal arterial perfusion in cases of cortical necrosis.

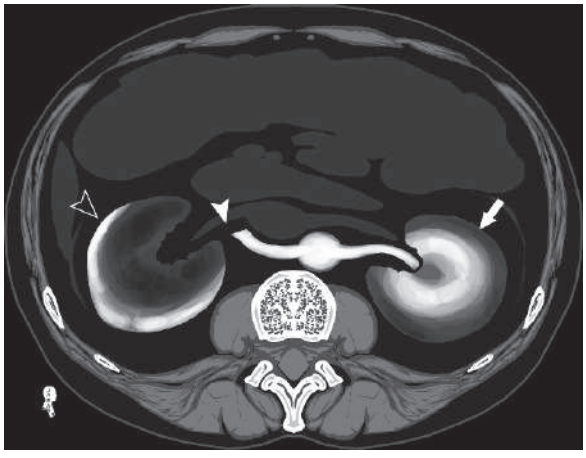

Fig. 5.1.4. Axial postcontrast-enhanced CT illustration shows the arterial cut-off sign (*solid arrowhead*), rim sign of vascular compromise (*open arrowhead*), and reverse rim sign (*arrow*)

Signs on MRA

- Magnetic resonance angiography (MRA) demonstrates the aortic vessels clearly and it is mostly used after detection of RAS on Doppler sonography for surgical planning (Fig. 5.1.5).

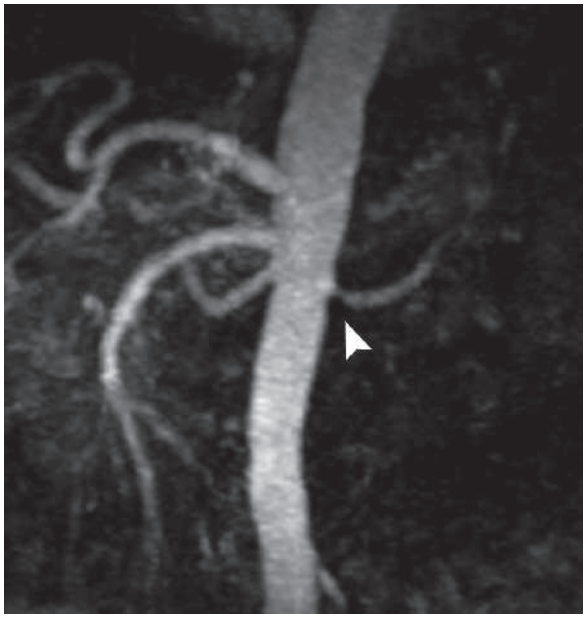

Fig. 5.1.5. MRA image shows >50% stenosis of the left renal artery (*arrowhead*) in a patient with peripheral vascular disease

Coarctation of the Aorta

Coarctation of the aorta is a condition characterized by aortic lumen narrowing, most commonly located below the origin of the left subclavian artery (the aortic isthmus near the ligamentum arteriosum), causing hypertension below the level of the narrowing.

Patients with aortic coarctation often present with severe hypertension that does not respond to antihypertensive medication and chest pain that radiates to the back. Patients with aortic coarctation carry the risk of aortic dissection, which is characterized by aortic wall intimal tear and leaking of the blood in between the aortic wall layers.

When it is chronic, aortic coarctation causes dilatation of the internal mammary and intercostals arteries. Chronic high-pressure pulsation of the intercostals arteries over the inferior aspect of the ribs may result in rib notching. Coarctation of the aorta can be seen in up to 30% in patients with bicuspid aortic valve.

Pseudo-coarctation of the aorta is a relatively rare condition characterized by kinking of the aorta at its

isthmus near the ligamentum arteriosum without lumen narrowing. Pseudocoarctation resembles true coarctation; differentiation is possible by looking for changes of the collateral circulation, where there will be no enlarged peripheral vessels, signs of pressure gradients, or rib notching. The condition is symptomless, and can be associated with congenital bicuspid aortic valve.

Signs on Chest Radiograph

- In chronic cases of aortic coarctation, the ribs show irregular lower border representing rib notching (Fig. 5.1.6). This condition can be also seen in other conditions affecting the intercostals neurovascular bundle like superior vena cava obstruction syndrome and neurofibromatosis of the intercostals nerves.
- The aortic arch is often bulging with dilatation of the aortic knuckle (Fig. 5.1.7).
- Pseudocoarctation of the aorta is seen as elongated aortic knuckle appearing like a posterior mediastinal mass.

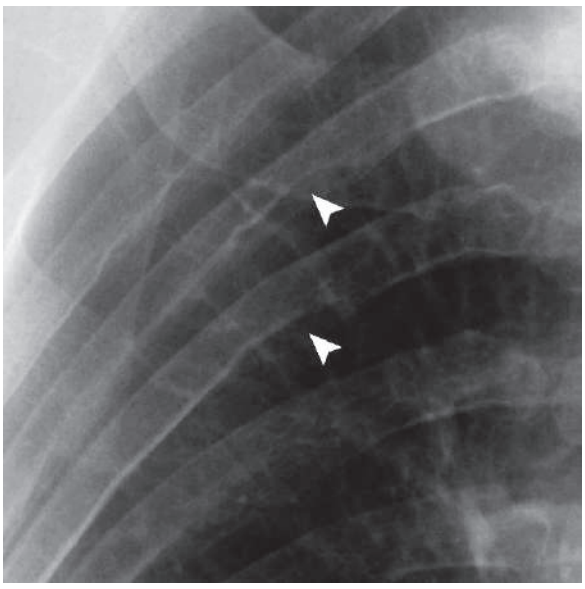

Fig. 5.1.6. Plain chest radiograph shows rib notching in a patient with severe aortic coarctation since 12 years (*arrowheads*)

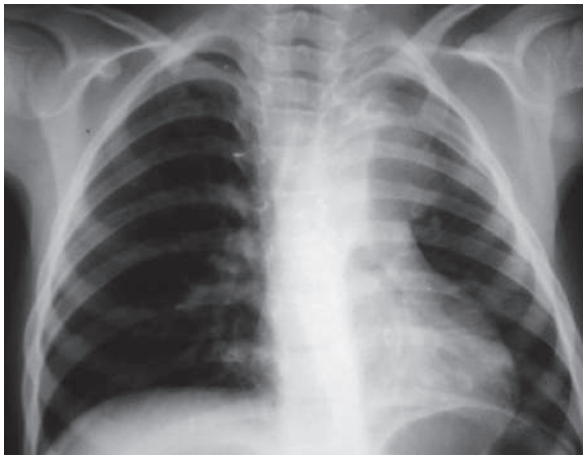

Fig. 5.1.7. Posteroanterior plain chest radiograph in a patient with coarctation of the aorta shows bulging of the aortic knuckle

Signs on CT and MRI

- Aortic coarctation classically is seen in sagittal reformatted images as a narrowing of the aortic lumen located at the area of the aortic isthmus, giving the classic "inverted shape of 3" (Fig. 5.1.8).
- Aortic dissection is seen as hypodense layer found within the aortic lumen on postcontrast-enhanced images representing the false lumen (Fig. 5.1.9). *Stanford type A* dissection involves dissection of the ascending aorta and the arch up to the origin of the left subclavian artery. *Stanford type B* dissection involves dissection of the descending aorta below the origin of the subclavian artery. Type A is managed surgically, while type B is managed medically, providing evidence of end-organ ischemia not being present.
- Aortic pseudocoarctation is seen on axial CT images as higher than normal located arch, with a well-defined enhancing vascular mass located near the aortic arch, representing the kinked portion of the arch.

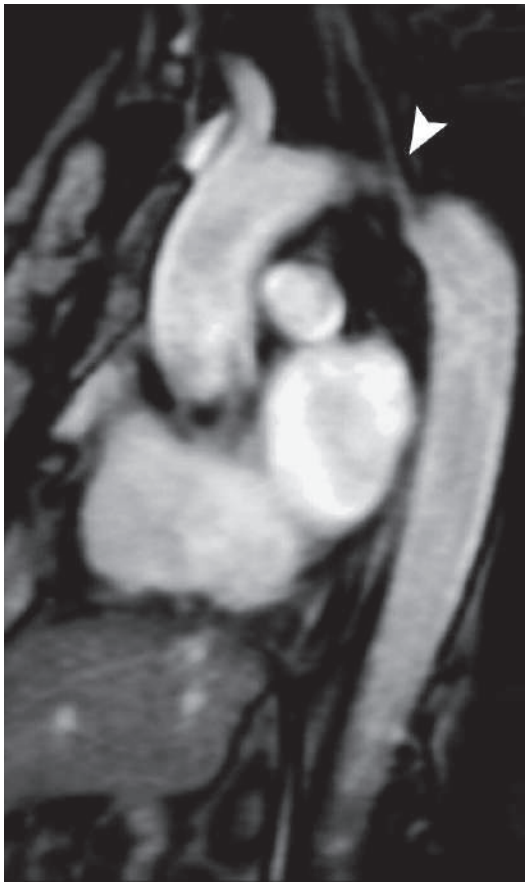

Fig. 5.1.8. Sagittal MRA of a patient with coarctation of the aorta shows the inverted shape of 3, which is characteristic of this condition (*arrowhead*)

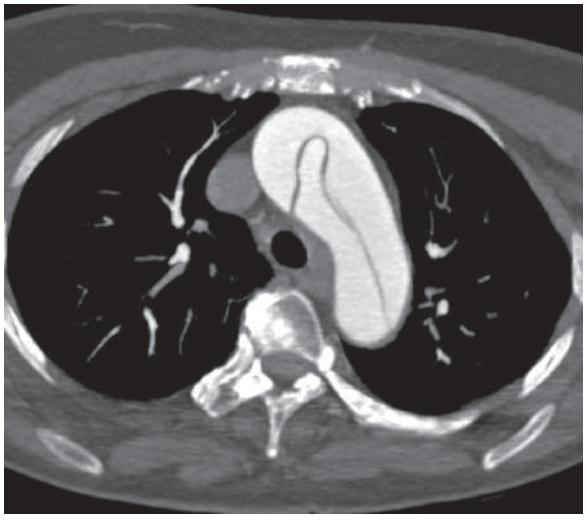

Fig. 5.1.9. Axial CT-angiography shows the classical intimal flap in a patient with aortic dissection Stanford type A

Polyarteritis Nodosa

Polyarteritis nodosa is a rare disease characterized by aneurismal, nodular lesions that affect the medium-sized and small-sized arteries due to fibrinoid necrotizing vasculitis.

Vasculitides are a diverse group of diseases characterized by inflammation and necrosis of all three coats of the vessels (intima, media, and adventitia). They are divided into large-vessels vasculitis (e.g., Takayasu and giant cell arteritis), medium-sized vessels vasculitis (e.g., polyarteritis nodosa and Kawasaki disease), and small-sized vessels (e.g., Wegener's granulomatosis and Henoch-Schönlein purpura).

Polyarteritis nodosa commonly causes multiple arterial aneurismal wall formation, plus fragmentation and degeneration of the adventitia layer. Necrosis starts in the media layer, and spreads to involve the entire width of the vascular wall. This inflammation and necrosis is associated with eosinophilic infiltration, fibrin deposition, and destruction of the elastic tissue and the intima layer. Vascular thrombosis or an aneurysm, mainly at the vessels bifurcation or the hilar region of viscera, may occur. Later, a granuloma is formed at the area of previous inflammation with fibroblasts proliferation. A healed stage is characterized by vascular recanalization, and formation of a nonvascularized fibrous mass that completely replaces a section of the vessel wall. The disease rapidly progresses once started, and death may result from strokes or myocardial infarctions within 2–3 months after onset.

Any organ can be affected by PAN, including the central and peripheral nervous system. The kidney is the most commonly involved (80–90%), followed by the gastrointestinal (GI) tract (50–70%). Clinically, patients present with vague signs and symptoms like fever, myalgia, headache, and malaise. Renal artery involvement, especially at the renal hilum, often results in rapidly progressing hypertension. Involvement of the GI tract may present with lower GI bleeding, abdominal pain, and vomiting (6% of cases). Peripheral nervous system involvement compromises the nervous tissue blood supply causing polyneuropathy. Other lesions involve pericarditis, myocardial infarction, and purpuric skin rash. Up to 30% of patients test positive to hepatitis B surface antigens, and up to 50% of patients have arthralgias.

Laboratory investigations usually show leucocytosis with eosinophilia (4%), anemia, uremia, and high erythrocyte sedimentation rate.

5.1

Signs on Angiography or MRA

Polyarteritis nodosa is suggested by detection of multiple aneurysms up to 1 cm in diameter within the renal, mesenteric, hepatic, or central venous vasculature. This finding is not pathognomonic since it can be seen in patients with necrotizing angiitis associated with drug-abuse. The history and the high suspicion of PAV with this angiographic picture help to differentiate the two entities.

Signs on CT

- The bowel walls are thickened and show white-attenuated target sign after contrast injection.
- CT-angiography shows multiple aortic aneurysms in the branches of the SMA or the celiac trunk.
- *Spotted nephrogram*: small vessels occlusion in cases of PAN may cause patchy perfusion of the kidney on IVU or contrast-enhanced CT due to multiple infarctions (Fig. 5.1.10). This sign can be also seen in scleroderma and hypertensive nephrocalcinosis.

Takayasu Arteritis

Takayasu arteritis is a rare, granulomatous disease characterized by inflammation of the large vessel walls, leading to progressive stenosis, aneurysms, or limb ischemia. The disease affects mainly the aorta and its major branches.

TA affects mainly young females between 20 and 30 years of age, who present with nonspecific systemic inflammatory symptoms like fever, night sweat, weight loss, myalgia, and arthralgia. TA has two main phases with different clinical presentations, an early and a late phase. The early phase is characterized by nonspecific inflammation in the blood vessels walls affecting the media and the adventitia layers. These nonspecific inflammatory changes are responsible for the nonspecific, systemic inflammatory symptoms. In contrast, the late phase is characterized by arterial symptoms with no systemic symptoms. The absence of the systemic symptoms in the late phase is attributed to the development of systemic collaterals; however, this is not seen in all patients. In the late phase, the coronary arteries might be affected. Hypertension, arterial stenosis, aneurysms, and dissection all can be seen in late phase of TA.

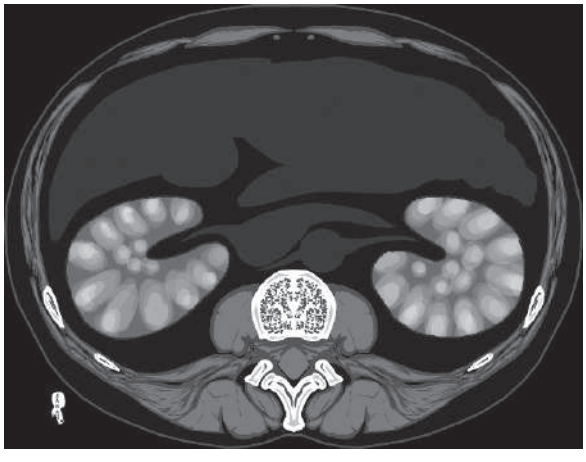

Fig. 5.1.10. Axial CT illustration demonstrates the spotted nephrogram that may be seen in patients with polyarteritis nodosa

Criteria for TA diagnosis (TA Diagnosis Requires At Least Three Criteria)

- Age of presentation <40 years.
- Limbs caludication.
- Decrease one or both brachial arteries pulse.
- Blood pressure difference of the extremities >10 mmHg.
- Bruit heard over the aorta or the subclavian arteries.
- Angiographic abnormalities include arterial occlusion, stenosis or aneurysms of the aorta or its main branches. Commonly, these abnormalities are observed bilaterally.

Signs on CT and CT-Angiography

- In the acute phase, there is thickening of the great vessels wall without signs of calcification due to inflammation and intramural hematomas (especially the aorta) (Fig. 5.1.11).
- The thickened vascular wall may show enhancement in early contrast-phase due to inflammatory hyperemia.
- Aneurysmal dilatation of the aortic root or its major branches is mainly observed in late chronic phase of the disease.
- Signs of dissection, stenosis or occlusion of the major vessels may be seen (Fig. 5.1.12).

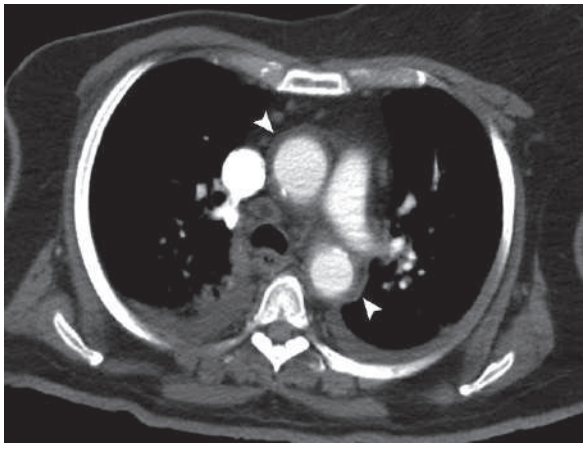

Fig. 5.1.11. Axial CT-angiography in a 50-year-old female patient presented with nonspecific systemic inflammatory symptoms with absent right arm pulsation and limb claudication. Patient was suspected to have Takayasu arteritis by the attending physician. CTA confirmed the acute thickening of the aortic wall (*arrowheads*), with occlusion of the right subclavian artery and multiple aneurysms affecting the carotid arteries (not shown)

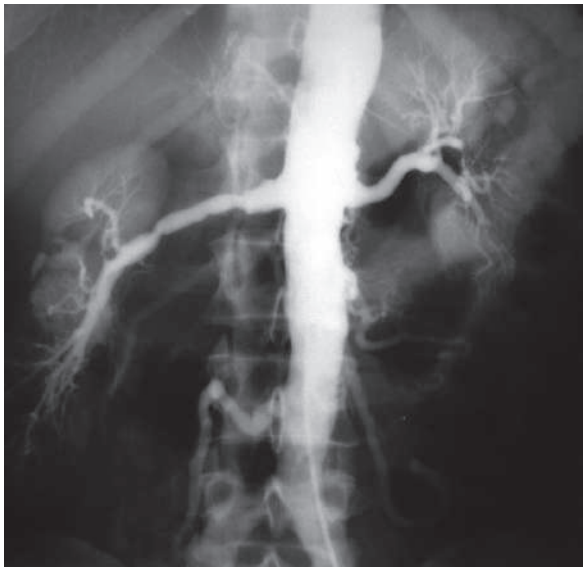

Fig. 5.1.12. Aortic-renal angiography in a patient with chronic Takayasu arteritis shows multiple small stenoses and dilatations affecting the right renal artery and the abdominal aorta in a milder degree

Midaortic Syndrome

Midaortic syndrome (MAS) is a nonspecific arteritis that affects the mid-portion of the abdominal aorta and its main branches.

MAS classically starts from the infra-renal part of the aorta and progresses proximally to involve the renal arteries (80%), SMA, and the celiac artery (25%). MAS mainly affects children and young adults who typically present with renovascular hypertension due to bilateral RAS. If untreated, the disease is fatal by the age of 30, with many patients experiencing intracranial bleeding due to malignant hypertension. The inferior mesenteric artery (IMA) and the common iliac arteries are almost never involved.

How can you differentiate between MAS and TA?

- Takayasu arteritis often present with systemic symptoms of fever, malaise, and weight loss. These features are not part of MAS.
- MAS affects mainly children and young adults, while Takayasu arteritis mainly affects females between 20 and 30 years of age.
- MAS exclusively affects the mid-abdominal aorta, while Takayasu arteritis involves any vessels and can even affect the pulmonary artery, causing pulmonary hypertension.

Signs on Doppler Sonographs

- Stenosis of the mid-abdominal aorta.
- Renal artery stenosis is often seen unilaterally or bilaterally.

Signs on CT-Angiography

- The aorta shows stenosis typically from the infrarenal portion, and extends proximally to involve the renal arteries, IMA, or the celiac.
- The IMA and the common iliac vessels are spared.

Preeclampsia

Preeclampsia is a pregnancy-related condition characterized by hypertension, lower leg edema, and protienuria. In contrast, eclampsia is a life-threatening condition characterized by the same symptoms as preeclampsia plus tonic-clonic seizures.

Hypertensive disorders occur in about 3–10% of all pregnancies, and the incidence of preeclampsia ranges

5.1

between 10 and 15% in primigravida (first birth) and 5.7–7.3% in multiparas (multiple pregnancies). Hypertension in preeclampsia is diagnosed after 20 weeks of gestation by a diastolic blood pressure >90 mmHg stable over 4 h, or one measurement of diastolic blood pressure >110 mmHg. Protienuria is defined as a concentration of protein of 0.1 g/L or more in at least two random urine samples collected 4 h or more apart; or as 0.3 g/L in a 24 h urine collection in the absence of urinary tract infection.

Patients with preeclampsia usually present with hypertension (hallmark of the disease), lower leg edema, protienuria, headache, visual symptoms, and epigastric pain. Absence of hypertension in the presence of edema and protienuria does not exclude the diagnosis of preeclampsia. The liver is uncommonly affected by preeclampsia (10% of cases). When liver dysfunction occurs, mild elevation of serum enzymes is common.

HELLP syndrome is a disease characterized by hemolytic anemia (Hb <11 g/dL), elevated liver enzymes, low platelets count that predispose to thrombocytopenia (<100,000/μL), and subcapsular liver hematoma. The incidence of HELLP syndrome is 2–12% of preeclampsia cases. Patients often present with epigastric pain (65%), nausea and vomiting (50%), and nonspecific symptoms. Severe hypertension is not a constant or a frequent finding in HELLP syndrome.

Signs on CT or MRI

- In patients with HELLP syndrome, the imaging findings include subcapsular hematoma, hepatomegaly with bulging of the left lobe, fatty liver, free abdominal ascitis, bilateral pleural effusions, or bilateral basal lobes atelectasis (Fig. 5.1.13).

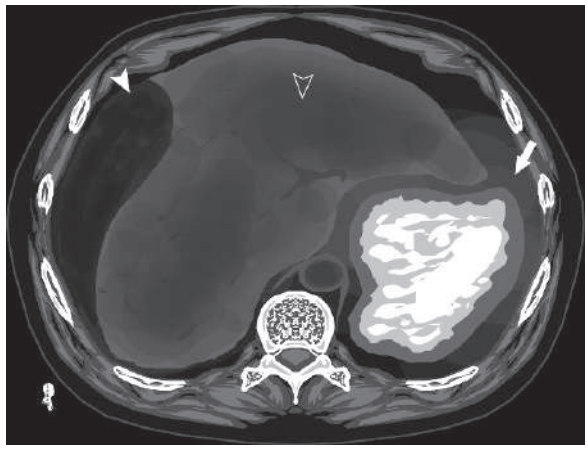

Fig. 5.1.13. Axial abdominal postcontrast CT illustration demonstrates signs of HELLP syndrome. There is hepatic subcapsular hematoma (*solid arrowhead*), fatty liver changes (*open arrowhead*), and ascites (*arrow*)

Reversible Posterior Leucoencephalopathy Syndrome (Hypertensive Encephalopathy)

Reversible posterior leucoencephalopathy syndrome (RPLES) is a disease with unknown cause characterized by cerebral demyelination in the posterior white matter areas of the brain (occipital lobes). PRLES is thought to be caused by increased permeability of the blood brain barrier in the posterior circulation.

PRLES is typically seen in patients with hypertension, eclampsia, and patients on immunosuppressive and cytotoxic drugs like cephalosporine and methotrexate. PRLES is a reversible condition once the cause is removed (e.g., control hypertension). If the cause persists, it will lead to cerebral infarction. Patients will present with headache, vertigo, vomiting, seizures, and altered mental status.

Signs on CT and MRI

- On CT, there are symmetrical, noncontrast-enhancing hypodensities located in the posterior region of the occipital and the parietal lobes.
- On MRI, symmetric low T1 signal intensity with high T2 and FLAIR signal intensities in the region of the occipital and the parietal lobes (Fig. 5.1.14).
- There is cytotoxic edema and restricted water diffusion (high DWI signal intensity) in cases of infarction.

Nephroptosis (Floating Kidney)

Nephroptosis, also known as floating or wandering kidney, is a condition characterized by renal descent of 5 cm or more (or two vertebral bodies) when the patient moves from supine to an upright position.

Nephroptosis occurs more commonly in slim women (ten times more common than in males), and affects the right kidney more than the left (20% of cases). Causes of nephroptosis include multiple pregnancies, rapid loss of retroperitoneal fat, variation in the shape of the spinal cord, shallow Gerota's fossa, and direct renal trauma.

Patients with nephroptosis are rarely symptomatic. Symptomatic patients typically present with history of flank pain in the upright position that reduces or is relieved by lying down. The pain is attributed to intermittent functional excretory obstruction, forceful traction of the renal artery causing renal ischemia, or traction of the perirenal nerves. The most severe manifestation of nephroptosis is "*Dietl's crisis.*" Dietl's crisis is a condition characterized by violent paroxysmal colicky flank pain, tachycardia, nausea, chills, oligouria, hypertension, and transient hematouria or protienuria. The condition is caused by acute hydronephrosis due to kinking or vascular obstruction of the ureters.

On physical examination, the lower pole of the kidney can be palpated on deep inspiration. The examiner's finger should reach over the upper pole of the kidney and push it down to the navel. On Dietl's crisis, the kidney is tender on palpation and may be enlarged.

Historically, nephroptosis is used to be corrected by *nephropexy*, a surgical procedure characterized by suturing part of the renal capsule to the surrounding abdominal wall and vertebral column.

Signs on IVU

- IVU is the classical diagnostic investigation for nephroptosis. The patient is injected with the contrast intravenously, and the kidney is imaged after opacification of the renal parenchyma and ureters while the patient is supine. The patient is then imaged while he is on erect position. The kidney is clearly seen descending caudally from its normal position between the two films (e.g., from the level of L2 to the level of L5). The normal kidney is located between the lumbar vertebral levels L1 to L4.

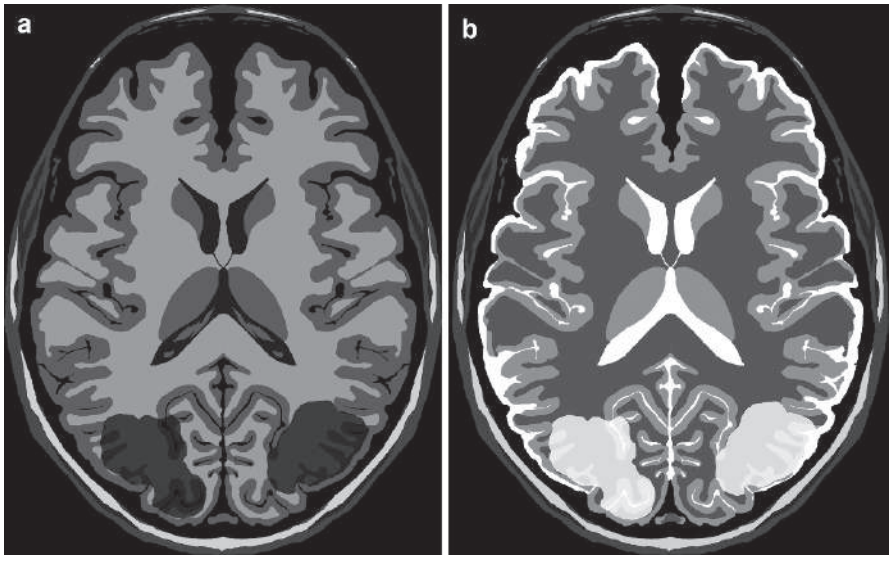

Fig. 5.1.14. Axial T1W (**a**) and T2W (**b**) MR-illustrations demonstrate bilateral almost symmetrical low T1 and high T2 signal intensity lesions located in the posterior lobes. This sign with a history of hypertension is diagnostic of RPLES

5.1

Signs on Doppler Sonography

- In suspected cases of nephroptosis, the resistive indexes (RIs) of the interlobar parenchyma renal arteries should be measured on both supine and erect positions. Both kidneys should be imaged for comparison. In the ptotic kidney, there is a change in the RI values >0.1 between the erect and supine examinations (e.g., on supine it is 0.5, and on erect it is 0.6). The other normal kidney shows no change in the RI values on both supine and erect examinations. These findings are explained by the renal artery tension occurring due to downward movement of the kidney.

Riley-Day Syndrome (Familial Dysautonomia)

Riley-Day syndrome (RDS) is a rare inherited disorder characterized by infantile hypertension, postural hypotension, and recurrent attacks of unexplained fever due to autonomic nervous system dysfunction.

As a rule, RDS manifests in infancy, which is important to assume the diagnosis. The major features are often seen in an infant or a child with recurrent attacks of unexplained fever, hypertension, and vomiting. Infants commonly have excessive drooling with swallowing difficulties, making them prone to recurrent aspiration pneumonia. Aspiration pneumonia is the main cause of death in patients with RDS.

Hypertension of RDS is characteristically associated with excitement. Intermittent attacks of hypertension with vomiting may cause RDS to be confused with infantile pheochromocytoma. Postural hypotension can be demonstrated in most patients beyond 2 years of age, and it can be so marked as to give raise to "blackout spells" when the patient stands.

Stafne's Bone Defect of the Mandible

Stafne's bone defect of the mandible is a rare cyst-like bony defect with cortical bone thickening with continuity from the base of the mandible around the gonial angle of the mandible, under the mandibular canal on panoramic radiography or cone-beam CT. Most cases are seen in hypertensive patients from 40 to 60 years old. The bony defect is symptomless.

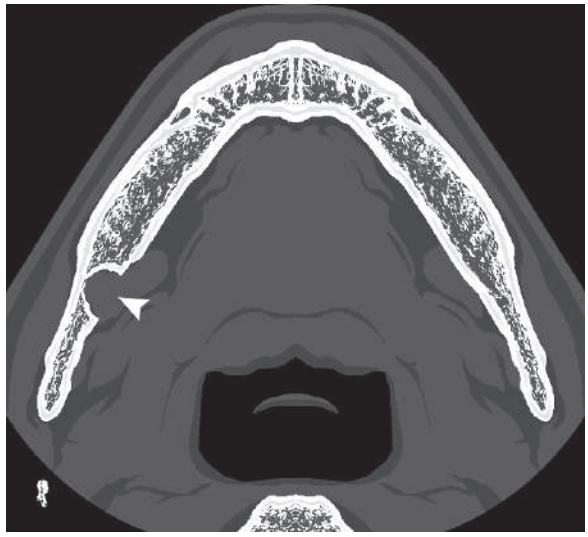

Fig. 5.1.15. Axial CT illustration of the mandible demo nstrates Stafne's bone defect of the mandible on the right side (*arrowhead*)

Stafne's mandibular bony defect is considered as a complication of long-standing hypertension, and thought to be caused by high pressure exertion by the facial artery over the mandible (Fig. 5.1.15).

Hypertensive Heart Disease

Patients with long-standing hypertension develop left ventricle hypertrophy due to raised left ventricular wall tension, which may lead to coronary microangiopathy of the mid-wall portion of the left ventricle wall. *Hypertensive heart disease* is a term used to describe a hypertensive patient with cardiac failure due to diastolic heart dysfunction with normal systolic heart function (normal ejection fraction).

Left ventricular hypertrophy can be generalized reducing the internal cavity (concentric hypertrophy), or localized to the interventricular septum (eccentric hypertrophy). Left ventricular hypertrophy in hypertensive patients is usually concentric, and typically found in moderate to severe hypertension in middle-aged and elderly patients. Left ventricular hypertrophy can cause atrial fibrillation and arrhythmias. Also, left ventricular hypertrophy in hypertensive patients is associated with three- to fourfold increase in the risk of stroke, a two- to threefold increase in coronary heart disease, and a threefold increase in peripheral arterial disease.

Signs on Cardiac MRI

- Patients with left ventricular hypertrophy due to hypertensive heart disease can show intra-mural, mid-wall, or subendocardial delayed contrast enhancement (e.g., >15 min), mostly due to myocardial ischemia, necrosis, or fibrosis (Fig. 5.1.16). Patients with delayed contrast enhancement on cardiac MRI may show ST-segment depression or T-wave inversion on electrocardiogram.

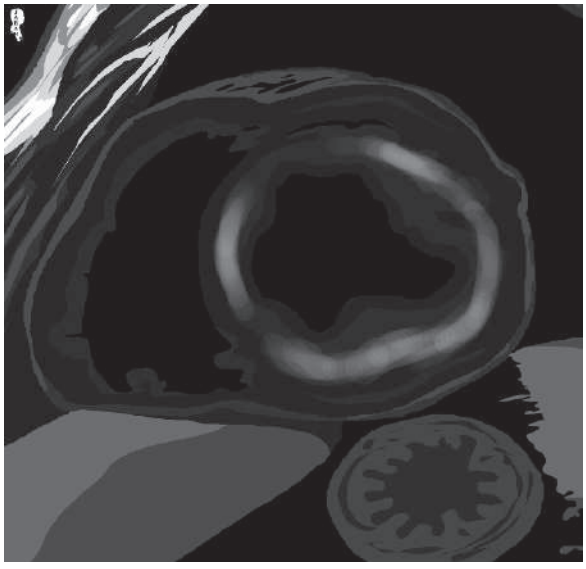

Fig. 5.1.16. Short-axis dark-blood postcontrast cardiac MR-illustration demonstrates left ventricular concentric hypertrophy with intramural enhancement representing MR findings in hypertensive heart disease

For Further Reading

1. Hartman RP et al Evaluation of renal causes of hypertension. Radiol Clin N Am. 2003;41:909–29
2. Chen Pet al Color and power Doppler imaging of the kidneys. World J Urol. 1998;16:41–5
3. Soulez G et al Imaging of renovascular hypertension: Respective values of renal Doppler US, and MR angiography. RadioGraphics. 2000;20:1355–68
4. Olivier H et al Renovascular disease: Doppler ultrasound. Semin Ultrasound CT MRI. 1997;18(2):136–46
5. Ha HK et al Radiologic features of vasculitis involving the gastrointestinal tract. RadioGraphics. 2000;20:779–94
6. Rooholamini SA et al Imaging of pregnancy-related complications. RadioGraphics. 1993;13:753–70
7. Dineen R et al Imaging of acute neurological conditions in pregnancy and the puerperium. Clin Radiol. 2005;60: 1156–70
8. Ferrazzani S. Hypertension in pregnancy. Saudi J Kidney Dis Transplant. 1999;10(3):298–312
9. Strohmeyer DM et al Changes of renal blood flow in nephroptosis: assessment by color Doppler imaging, isotope renography and correlation with clinical outcome after laparoscopic nephropexy. Eur Urol. 2004;45:790–93
10. Hoenig DM et al Nephroptosis: a "disparaged" condition revisited. Urology. 1999;54:590–96
11. Moss SW. Floating kidneys: a century of nephroptosis and nephropexy. J Urol. 1997;158:699–702
12. Barber NJ et al Nephroptosis and mephropexy - hang up on the past? Eur Urol. 2004;46:428–33
13. Taneja K et al Pseudocoarctation of the aorta: complementary findings on plain film radiography, CT, DSA, and MRA. Cardiovasc Intervent Radiol. 1998;21:439–41
14. Son JS et al Pseudocoarctation of the aorta associated with the anomalous origin of the left vertebral artery: a case report. Korean J Radiol. 2008;9:283–85
15. Applegate KE et al Spontaneous colonic ischemia in a patient with Riley-Day syndrome. Pediatr Radiol. 1995;25: 312–13
16. Akpunonu BE et al Secondary hypertension: evaluation and treatment. Dis Mon. 1996;42(10):609
17. Lewis VD III et al The midaortic syndrome: diagnosis and treatment. Radiology. 1988;167:111–13
18. Das BB et al Midaortic syndrome presenting as neonatal hypertension. Pediatr Cardiol. 2008;29:1000–1
19. Stadlmaier E et al Midaortic syndrome and celiac disease: a case of local vasculitis. Clin Rheumatol. 2005;24:301–4
20. Fujita T et al Takayasu arteritis evaluated by multi-slice computed tomography in old man. Int J Cardiol. 2008;125: 286–87
21. Canyigit M et al Imaging characteristics of Takayasu arteritis. Cardiovasc Intervent Radiol. 2007;30:711–18
22. Ando H et al Abnormal collateral arterial system in Takayasu's arteritis and Lariche's syndrome evaluated by whole body acquisition using multislice computed tomography. Int J Cardiol. 2007;121:306–8
23. Bulum J et al Takayasu's arteritis and chronic autoimmune thyroiditis in a patient with type 1 diabetes mellitus. Clin Rheumatol. 2005;24:169–71
24. Dyer RB et al Classic signs in uroradiology. RadioGraphics. 2004;24:S247–80
25. Shimizu M et al CT analysis of the Stafne's bone defects of the mandible. Dentomaxillofacial Radiol. 2006;35:95–102
26. Van Hoe L et al Liver involvement in HELLP syndrome: CT and MRI findings in two patients. Eur Radiol. 1995;5:331–34
27. Andersen K et al Myocardial delayed contrast enhancement in patients with arterial hypertension: initial results of cardiac MRI. Eur J Radiol. 2009;71:75–81
28. Lip GYH et al Hypertensive heart disease. A complex syndrome or a hypertensive 'cardiomyopathy'? Eur Heart J. 2000;21:1653–65

5.2 Polycystic Kidney Disease

Polycystic kidney disease (PKD) is a disease characterized by development of multiple cysts within the kidneys in bilateral fashion. A cyst is defined as a fluid-filled sac lined with a single layer of tubular epithelium. A cystic kidney is defined as a kidney that contains three or more cysts.

Simple renal cyst is the most common renal anomaly. Up to 22% of symptomless patients over 70 years old or older have at least one renal cyst. There are three types of PKD: autosomal dominant (adult) PKD, autosomal recessive (infantile) PKD, and acquired PKD.

Autosomal Dominant Polycystic Kidney Disease

Autosomal dominant polycystic kidney disease (ADPKD) is the fourth cause of chronic renal failure through the world. The disease has an autosomal dominant mode of inheritance as its name states, with a positive family history of ADPKD elicited in 60% of patients.

ADPKD is typically seen in adults, with both kidneys affected in a bilateral, almost symmetrical, fashion. The kidneys are enlarged in size as the disease progresses. In a patient <30 years old with a positive family history of ADPKD, the presence of two cysts, either unilateral or bilateral, is sufficient to make the diagnosis. In patients >30 years old with a positive family history of ADPKD, at least two cysts in each kidney are sufficient to make the diagnosis.

Patients with ADPKD present with bilateral renal cysts with enlarged kidneys (100%), renal pain (60%), hematuria (42%), hypertension (75%), colonic diverticuli (80%), and hepatic cysts (57%). Potential causes of hematuria in ADPKD include renal stones formation (20%), and golmerulonephritis.

Hypertension arises in 75% of ADPKD with normal renal functions. Cyst expansion is believed to alter blood flow by glomerular compression, which results in the release of rennin, leading to the formation of angiotensin II.

Hepatic cysts occur in 57% of patients with ADPKD, and they are rare before puberty. Hepatic cysts are believed to originate from cystic dilatation of the bile ducts. Patients may present with right upper quadrant pain due to liver capsule stretching and hepatomegaly.

Colonic diverticuli are seen in up to 80% of patients with ADPKD, usually with end-stage renal disease. Patients with ADPKD are at risk of cerebral aneurysm rupture, which has a prevalence of <5%. ADPKD patients with positive family history of cerebral arteries aneurysm have an increased incidence of developing cerebral aneurysm (22%) than ADPKD patients with no family history of cerebral aneurysm (5%). ADPKD patients with aneurismal rupture present with signs of intracranial bleeding or subarachnoid hemorrhage such as severe headache, neck stiffness, altered consciousness, with nausea and vomiting.

Rare manifestations of ADPKD include coronary arteries or abdominal aorta aneurysm, mitral valve prolapse, aortic regurgitation, pancreatic cysts (10%), splenic cysts (5%), and inguinal hernias. Patients with ADPKD may develop seminal vesicle cysts, which present clinically as painful ejaculation, prostatitis, urinary tract obstruction, or epididymitis.

Signs on US

- The kidneys show multiple echo-free parenchymal cysts with typical posterior shadowing.
- Liver, pancreatic, or splenic cysts may be seen (Fig. 5.2.1).

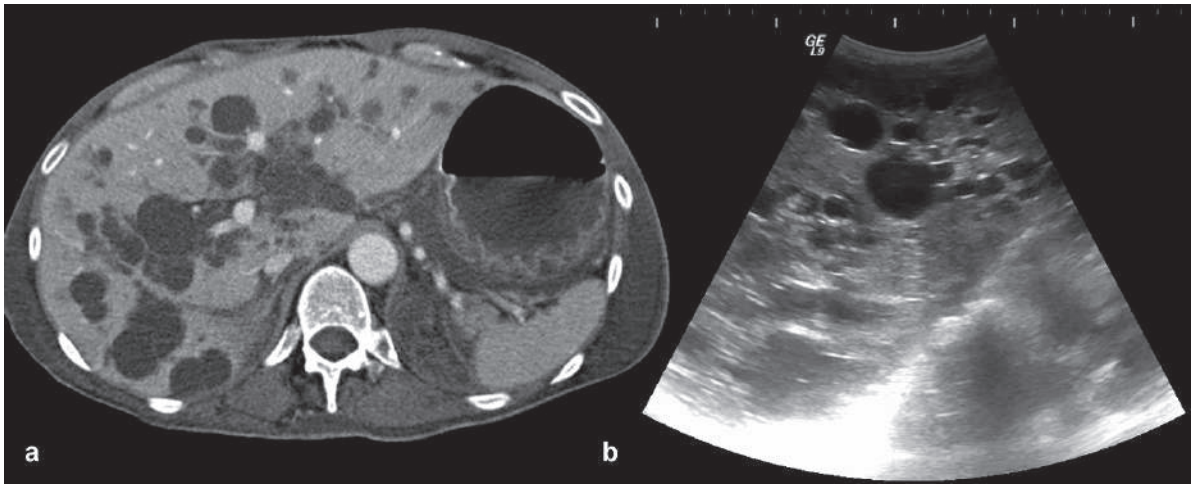

Fig. 5.2.1. Axial CT postcontrast (**a**) with liver ultrasound (**b**) images show multiple liver cysts in a patient with ADPKD

Signs on CT

- Typically, both kidneys are enlarged with multiple cysts of variable sizes (Fig. 5.2.2).
- Hyperdense calculi may be seen within the renal pelvis or the ureters.
- Hepatic, pancreatic, or splenic cysts may be seen (Fig. 5.2.1). Intrahepatic cystic bile duct dilatation (Caroli's disease) can be associated with PKD in up to 70% of cases.

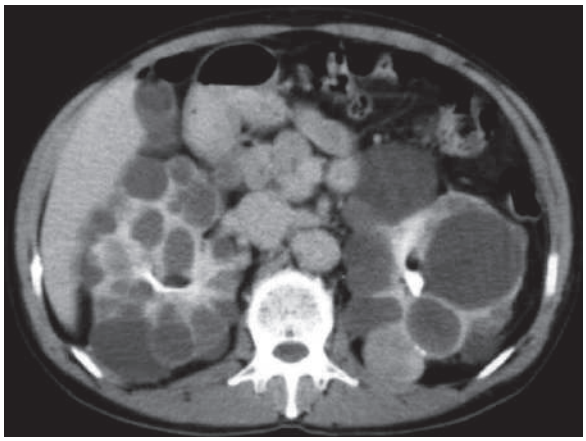

Fig. 5.2.2. Axial CT urography image in a patient with ADPKD shows bilateral mildly enlarged kidneys with multiple cysts

Signs on MRI

- Cerebral MR-angiography should be performed for ADPKD patients with positive family history of cerebral aneurysms as a screening examination. These aneurysms are classically saccular aneurysms that occur at the bifurcation of cerebral vessels, and resemble a berry in size and shape (*berry aneurysm*). Up to 80% of berry aneurysms arise from the circle of Willis, and 20% arise from the posterior fossa.
- Seminal vesicle cyst is detected as unilocular cyst with fluid-signal located at the posterolateral aspect of the urinary bladder. The cyst may be associated with ipsilateral ejaculatory duct dilatation that may protrude into the urinary bladder mimicking ectopic uretrocele.

Autosomal Recessive Polycystic Kidney Disease

Autosomal recessive polycystic kidney disease (ARPKD) is a rare genetic disease with prevalence of 1:20,000 live births. ARPKD typically starts in neonates and infants as early renal failure. Infant's death usually occurs within the first year of life, unless renal transplantation is considered.

The kidneys are massively enlarged with numerous cysts. Hepatic fibrosis is very common in ARPKD (60%). Hypertension occurs in almost all cases. Pregnant women with an infant with ARPKD typically display oligohydramnios.

5.2

Signs on CT

- Both kidneys are massively enlarged while maintaining a reniform shape (Fig. 5.2.3).

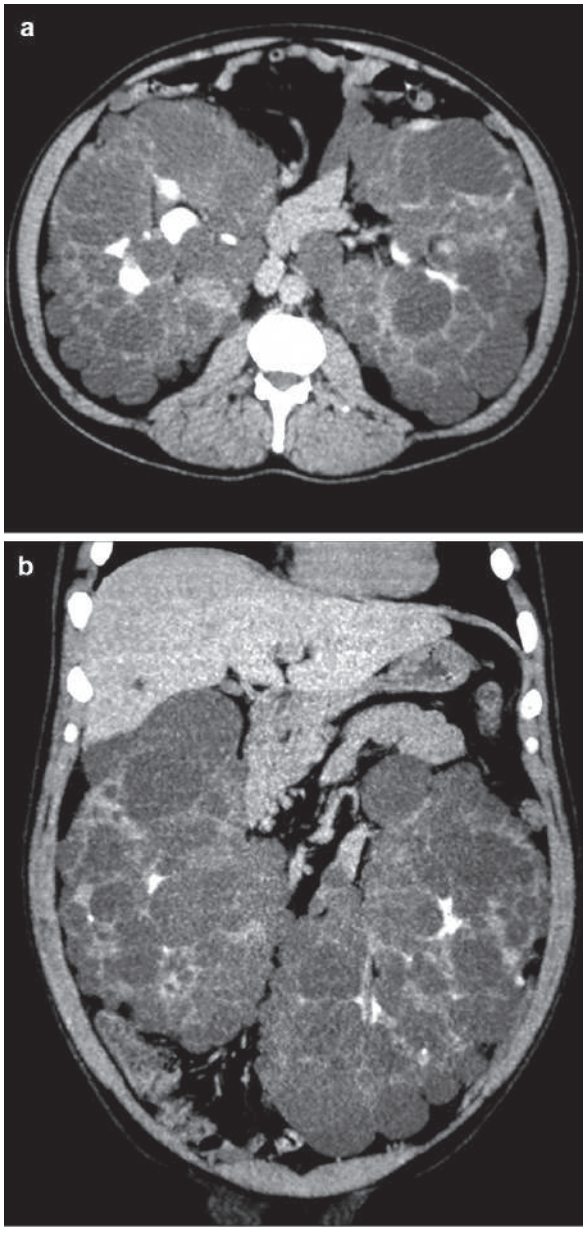

Fig. 5.2.3. Axial (**a**) and coronal (**b**) CT urography images in a child with ARPKD show massively enlarged kidneys with numerous small cysts bilaterally

Acquired Polycystic Kidney Disease

Acquired polycystic kidney disease (APKD) is typically seen in chronic renal failure and dialysis. Chronic potassium depletion in humans has been associated with the development of renal cysts (e.g., primary Hyperaldosteronism). Some investigators use the term "multiple cystic kidney disease" for this condition to differentiate it from the true congenital polycystic kidney disease.

In contrast to ADPKD and ARPKD, the kidney size is usually normal or smaller than normal. Also, the acquired polycystic kidney has a tendency for malignant transformation.

Signs on CT

- Bilateral normal size or shrunken kidneys with multiple cysts (Fig. 5.2.4).
- Signs of other complication of end-stage disease, or adrenal hyperplasia (hyperaldosteronism) may be seen.

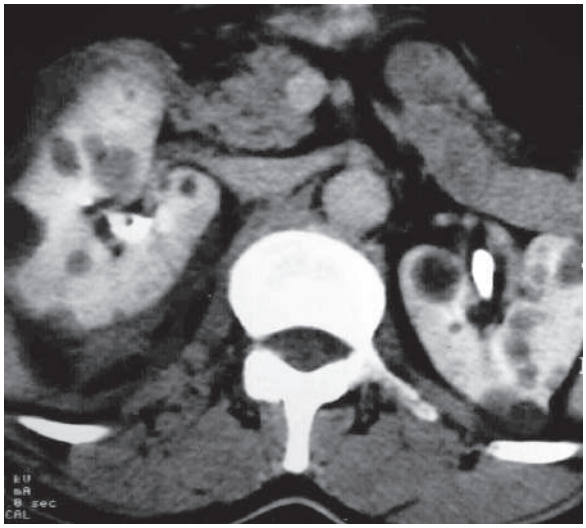

Fig. 5.2.4. Axial CT urography in a patient with acquired polycystic kidney disease shows bilateral normal-sized kidneys with small cysts

Differential Diagnoses and Related Diseases

Nephronophthisis is an uncommon autosomal dominant disorder characterized by a triad of anemia, salt-wasting, and abnormal levels of nitrogen-containing compounds like urea and creatinine (azotemia) due to tubulo-interstitial nephritis. Patients are usually young adults or children presenting with end-stage renal failure. Due to its nonspecific symptoms, definite diagnosis is usually established by kidney biopsy, which classically shows tubular basement membrane disintegration, tubular cyst formation, and tubulo-interstitial fibrosis. The disease has three forms: infantile, juvenile, and adolescent. Nephronophthiasis can be associated with retinitis pigmentosa (Senior-Løken syndrome), cerebellar ataxia and cerebellar vermis hypoplasia (Joubert's syndrome), oculomotor apraxia (Cogan's syndrome), hepatic fibrosis and biliary duct proliferation (Boichis syndrome), phalangeal cone-shaped epiphysis (Saldino-Mainzer disease/conorenal syndrome), hypopituitarism (RHYNS syndrome), ectodermal dysplasia (Sensenbrenner syndrome), and leber amaurosis (Arima-Dekaban syndrome). Brain MRI shows the characteristic "molar tooth sign" due to superior cerebellar vermis hypoplasia of Joubert's syndrome. On ultrasound, kidneys show multiple cysts up to 2 cm in size, characteristically located at the renal medulla, with hyperechoic cortex and loss of the cortico-medullary differentiation. Many researches consider the clinical presentation of nephronophthisis with ultrasound picture of medullary renal cysts as being characteristic and sufficient to establish the diagnosis without the need for renal biopsy. However, renal medullary cysts may be absent in 30% of cases, so the absence of medullary renal cysts does not rule out the diagnosis.

For Further Reading

1. Martinez JR et al Polycystic kidney disease: etiology, pathogenesis and treatment. Dis Mon. 1995;41(11):693–765
2. Capisonda R et al Autosomal recessive polycystic kidney disease: outcomes from a single-center experience. Pediatr Nephrol. 2003;18:119–26
3. Vauthey J-N et al Adult polycystic disease of the liver. Br J Surg. 1991;78:542–527
4. Roche CJ et al Selections from the buffet of food signs in radiology. RadioGraphics. 2002;22:1369–84
5. Salomon R et al Nephronophthisis. Pediatr Nephrol. (2009);24:2333–2344
6. Blowey DL et al Ultrasound findings in juvenile nephronophthisis. Pediatr Nephrol. 1996;10:22–4
7. Grossman H et al Sonographic diagnosis of renal cystic diseases. AJR. 1963;140:81–5

Chapter 6

Endocrinology and Metabolism

CONTENTS

J. A. Al-Tubaikh: *Internal Medicine* – An Illustrated Radiological Guide
DOI: 10.1007/978-3-642-03709-2_6

6.1 Grave's Disease (Hyperthyroidism)

Graves's disease (GD) is an autoimmune disorder characterized by hyperthyroidism, thyroid goiter, and ophthalmopathy. The disease arises due to the production of autoantibodies that auto-stimulates the thyrotropin receptors in the thyroid gland to secrete thyroid hormones.

GD clinical manifestations are mainly due to hyperthyroidism (thyrotoxicosis). Patients are commonly females between the third and fifth decades presenting with thyroid goiter. The thyroid is hypervascular, with venous humming that can be heard by stethoscope in some cases.

Systemic manifestations of hyperthyroidism include rapid weight loss (>10% of body weight in less than 6 months), profuse sweating and heat intolerance, increased appetite (85%), anorexia (15%), increased bowel motion and diarrhea, oligomenorrhea in females, gynecomastia in males due to increased sex-hormone binding proteins, and proximal muscle weakness and muscle wasting due to increased basal metabolic rate. Skin manifestations include skin moisture due to sweating, vitiligo, and pretibial skin thickening due to mucin deposition in the dermis (myxoedema).

Graves' ophthalmopathy is the most characteristic sign of this disease. GD is the most common cause of exophthalmos (abnormal prominent eye) and proptosis (protrusion) of globe in adults. It occurs in 35% of cases. The proptosis can precede the actual thyroid abnormalities or occur after the disease has been brought under control. Proptoses are commonly bilateral and symmetrical; unilateral proptosis is uncommon.

Proptosis in GD can be explained by:

- Infiltration and deposition of mucopolysaccharidosis (hyaluronic acid) into orbital muscles. The muscles' bellies are characteristically increased in size while their tendons are spared (fusiform enlargement). The inferior rectus and the medial rectus muscles are the most commonly involved. The lateral rectus is the last muscle to be involved. Hypertrophy of the lateral rectus only can be seen in orbital pseudotumor, and hypertrophy of the superior rectus only can be seen in orbital lymphoma.
- Increased volume of the retrobulbar fat which will push the globe anteriorly.

Clinical signs of Graves' ophthalmopathy include widened palpebral fissure (*Dalrymple's sign*), staring expression with infrequent blinking (*Stellwag's sign*), lid lag on downward gaze (*von Graefe's sign*), and poor convergence (*Möbius's sign)*. Up to 5% of patients with Graves' ophthalmopathy develop optic neuropathy due to compression of the nerve in its canal because of backward herniation of the retro-orbital fat through the optic canal, or from hypertrophied ocular muscle belly at the orbital apex.

Signs on US and Doppler Sonography

- The gland is diffusely hypoechoic and enlarged in size.
- On color Doppler scan, the gland shows bilateral diffuse increase duplex signal due to hypervascularity. This sign is characteristic for GD and is called "thyroid inferno" sign (Fig. 6.1.1).

Signs of Graves's Ophthalmopathy on CT and MRI

- Bilateral, symmetrical increase in orbital muscles bellies width with spares tendons causing the orbital muscles to have fusiform appearance. The inferior rectus and the medial rectus muscles are characteristically affected (Figs. 6.1.2 and 6.1.3).
- Increases in the retrobulbar fat size.
- CT evidence of proptosis is defined as globe protrusion exceeding the interzygomatic line by 21 mm or more on axial images at the level of the lens (Fig. 6.1.4).

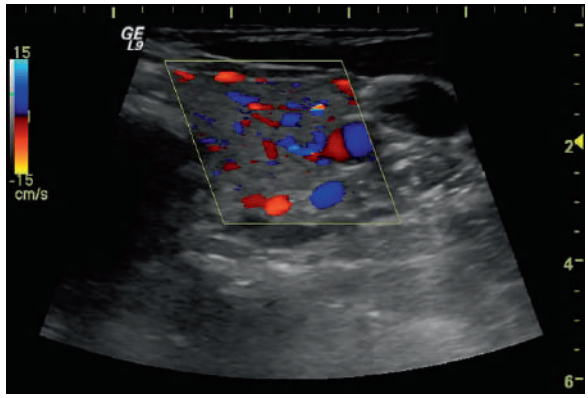

Fig. 6.1.1. Color Doppler (Duplex) scan of the thyroid in a patient with Grave's disease shows marked vascular signal due to bruit (thyroid inferno sign)

- GD optic neuropathy can be detected if retro-orbital fat is seen extending 4 mm beyond the boundary of the superior orbital fissure, or if the optic nerve is seen compressed by a hypertrophied ocular muscle belly at the orbital apex.
- Uncommonly, isolated dilatation of the superior ophthalmic vein may occur in patients with GD, and it can be easily mistaken for carotid-cavernous fistula. CT-angiography can confirm the absence of carotid-cavernous fistula.

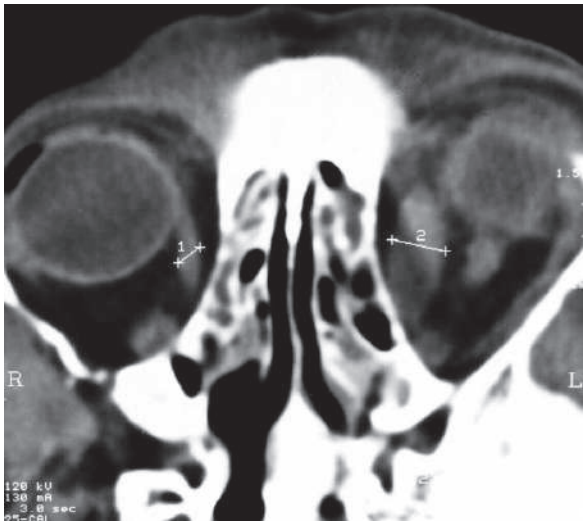

Fig. 6.1.2. Axial ophthalmic CT image of a patient with Grave's ophthalmopathy shows marked thickening of the medial rectus muscle of the left eye. Notice the difference in the medial rectus belly thickness (2) in comparison with the right eye (1)

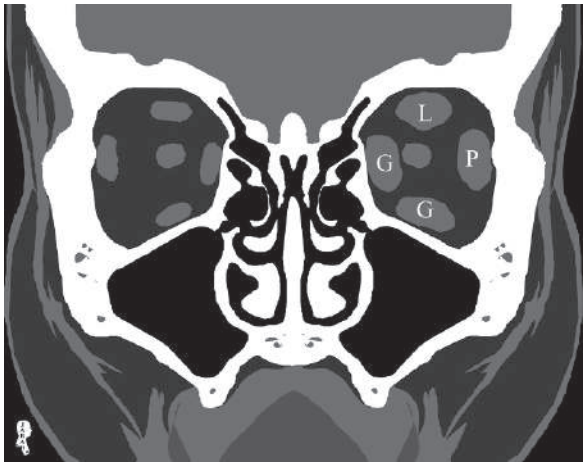

Fig. 6.1.3. Coronal sinuses and orbital CT illustration shows a differential diagnosis of recti muscles enlargement, the letter (G) stands for Grave's disease, (L) for lymphoma, and (P) for orbital pseudotumor

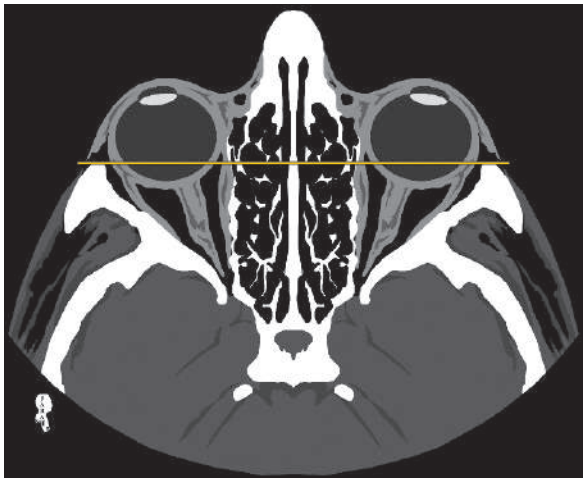

Fig. 6.1.4. Axial ophthalmic CT illustration demonstrates the interzygomatic line. A globe that protrudes >21 mm or more across this line is considered proptosis

For Further Reading

1. Reed Larsen P. Hyperthyroidism. Dis Mon. 1976;22:1–30
2. Greer MA et al Hyperthyroidism. Dis Mon. 1967;13:1–45
3. Rawson RW. Hyperthyroidism. Dis Mon. 1955;1:3–43
4. Babcock DS. Thyroid disease in pediatric patient: emphasizing imaging with sonography. Pediatr Radiol. 2006;36:299–308
5. Ralls PW et al Color-flow Doppler sonography in Graves disease: "thyroid inferno." AJR. 1988;150:781–4
6. Arslan H et al Power Doppler sonography in the diagnosis of Graves' disease. Eur J Ultrasound. 2000;11:117–22
7. Birchall D et al Graves ophthalmopathy: intracranial fat prolapse on CT images as an indicator of optic nerve compression. Radiology. 1996;200:123–7
8. Charkes ND et al MR imaging in thyroid disorders: correlation of signal intensity with Graves disease activity. Radiology. 1987;164:491–4
9. Nugent RA et al Graves orbitopathy: correlation of CT and clinical findings. Radiology. 1990;177:657–82

6.2 Hyperparathyroidism

Hyperparathyroidism is a metabolic disease characterized by the metabolic triad of high serum calcium level (hypercalcemia), low serum phosphorus level (hypophosphatemia), and increased calcium and phosphorus renal excretion (hypercalciuria).

Hyperparathyroidism can be caused by increased parathyroid hormone (PTH) release due to parathyroid adenoma or hyperplasia (primary type), chronic renal failure or parathyroid glands insensitivity to elevated serum calcium level (secondary type), or chronic renal failure with autonomous PTH release even after correction of the renal failure (tertiary type). Chronic renal failure causes reduction in serum calcium level, which induces hypersecretion of PTH to elevate serum calcium level. PTH increases serum calcium by increasing osteoclastic activity, promoting vitamin D renal hydroxylation, and promoting tubular renal absorption of calcium.

Hyperparathyroidism generally arises in those endocrine phases of life when endocrine glands are most active or rapidly changing like puberty, during the active phase of sexual life, or after menopause. Thus, hyperparathyroidism is rare before puberty and less commonly starts in later decades.

Symptoms and clinical presentation of hyperparathyroidism are related to its complications. Renal stones formation is one of the most common presentations of hyperparathyroidism. Increased renal excretion and serum calcium level promotes renal calculi formation. Peptic ulcers may occur in association with hyperparathyroidism for unknown reasons. It is speculated that changes in the calcium ion concentration may play a role in parasympathetic nervous system tone, which predisposes to increased secretions of gastric acids by increased vagal activity.

Episodes of acute pancreatitis are commonly associated with hyperparathyroidism for unknown reasons. Thirst and urinary frequency are common symptoms. Muscle fatigue and low back pain are also common complaints, and they are independent of bone changes.

The most common metabolic changes in hyperparathyroidism are observed in the skeletal system. Diffuse osteoporosis and bone resorption are commonly seen in primary hyperparathyroidism. In contrast, diffuse or focal osteosclerosis is observed in secondary hyperparathyroidism. Subperiosteal, subchondral, and subligamentous bone resorption are the commonest findings radiologically.

Brown tumor is an eccentrically located, expansile bony lesion uncommonly seen in secondary hyperparathyroidism. In severe hyperparathyroidism, large areas of bone marrow cavity are lost due to bone resorption. This bony resorption leads to microfractures and bleeding in the resorbed areas, which will create a mass-like effect within the trabecular bone. This mass-like structure has a brown pigment in gross section due to hemosiderin content. Gradually, this mass undergoes cystic changes. As the severity of the disease increases, these changes can progress to severe and diffuse type of bone expansion, cystic changes, and bone marrow fibrosis, a condition which is known as "*osteitis fibrosa cystica*." Brown tumor mimics giant cell tumor (*osteoclastoma*) radiologically and histologically. Differentiation between the two clinical conditions depends on the presence or absence of hyperparathyroidism manifestations. Osteitis fibrosa cystica is a rare complication of hyperparathyroidism that is seen in advanced stage disease. It is usually seen in young patients <20 years.

Nephrocalcinosis is a condition characterized by calcification and calcium deposition within the renal parenchyma, either in the cortex or in the medulla. *Cortical nephrocalcinosis* occurs due to prior insult to the renal cortex like in tuberculosis, ischemia, and glomerulonephritis. Usually it affects one kidney, and the affected kidney is small with global atrophy. *Medullary nephrocalcinosis*, on the other hand, arises due to calcification of the medullary pyramids due to deposition of calcium within the renal tubules. Medullary nephrocalcinosis is the most common type of nephrocalcinosis (95%), and is caused by systemic hypercalcemic states like in hyperparathyroidism, distal renal tubular acidosis, malignancy, and acute sarcoidosis. Typically, it affects both kidneys in a bilateral and symmetrical fashion, because the cause usually is a systemic disease.

Primary hyperparathyroidism can be a part of "*multiple endocrine neoplasia (MEN) syndrome*." MEN syndrome is characterized by the occurrence of tumors involving two or more endocrine glands within a single patient. There are two major types of MEN: MEN type 1 (MEN1, Wermer's syndrome) and MEN type 2 (MEN2, Sipple's syndrome). Both syndromes

are inherited as autosomal dominant. MEN1 is characterized by the combined occurrence of parathyroid tumors, pancreatic islet cells tumors (e.g., gastrinoma), and anterior pituitary tumors (e.g., prolactinoma). Associated tumors include adrenal tumors, carcinoid tumors, and lipoma. Although not part of the original description, meningioma has been reported to occur in patients with hyperparathyroidism due to MEN type 1. MEN type 2, on the other hand, is divided into three subtypes: MEN2a, MEN2b, and MTC-only. MEN2a describes the association of medullary thyroid carcinoma (MTC), pheochromocytoma, and parathyroid tumors. MEN2b describes the association of MTC, pheochromocytoma, Marfanoid body habitus, mucosal neuromas, and megacolon. Lastly, MTC-only is a variant in which MTC is the sole manifestation of this syndrome.

In up to 2% of normal people, an ectopic parathyroid tissue may be found within the mediastinum. The ectopic parathyroid tissue is commonly located within the anterior mediastinum. An ectopic parathyroid adenoma is rare, and should be suspected in a patient with hyperparathyroidism who was operated and the signs and symptoms of hyperparathyroidism persisted (5–10% of cases). Other areas where ectopic parathyroid tissue may be found include the neck (45%), upper cervical area (8%), or along the aortic arch (5%).

Differential Diagnoses and Related Diseases

- *Hyperparathyroidism-jaw tumor syndrome* is a rare, autosomal recessive disease characterized by hyperparathyroidism (90%), ossifying fibroma of the maxilla and/or mandible (30%), renal cysts and/or tumors (10%), and uterine tumors. Ossifying fibroma is a benign lesion that arises from cells in the periodontal ligament and is mainly restricted to the tooth-bearing areas of the jaw. The lesion is visualized as a well-demarcated bony lesion composed of fibrocellular tissue and mineralized material. The tumor is typically painless and located at the posterior region of the mandible. Patients are often >35 years old. However, a juvenile form (<20 years) may be seen.
- *Hungry bone syndrome* (*HBS*) is a rare complication of parathyroidectomy manifested by severe, prolonged, sometimes life-threatening hypocalcemia. The hypercalcemia in hyperparathyroidism is mainly due to increased bone turnover with predominant osteoclastic bone resorption and increased renal tubular absorption of calcium. After parathyroidectomy, the PTH-stimulus over the osteoclasts is suddenly removed, stopping the osteoclastic activity, but the osteoblastic activity continues at its high rate, resulting in marked increase in bone uptake of calcium to facilitate bone remodeling. The excessive osteoblastic bony remodeling causes severe hypocalcemia. HBS is seen in 12% of parathyroidectomy cases, and it is suspected in patients who had parathyroidectomy and presented with persistent hypocalcemia and hypophosphatemia. Predisposing factors for HBS include parathyroid adenoma >5 cm in diameter, high preoperative PTH, calcium, and alkaline phosphatase levels, advanced age, and osteitis fibrosa cystica.

Signs on Plain Radiographs

- On chest radiograph, tracheal shift due to enlarged parathyroid adenoma may be the first sign detected in an asymptomatic patient.
- On abdominal radiographs, urinary tract calcium calculi are seen as radio-opaque lesions in the renal area or the uretral course.
- Cortical nephrocalcinosis is often detected as a unilateral renal "eggshell calcification," while medullary nephrocalcinosis is detected as multiple, punctuated calcification seen within the kidney shadows in a bilateral symmetrical fashion (Fig. 6.2.1).

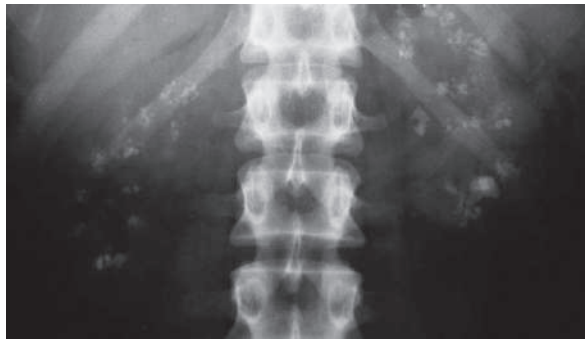

Fig. 6.2.1. A plain radiograph of the kidneys in a patient with medullary nephrocalcinosis shows bilateral, almost symmetrical, punctuated calcification within the renal shadow

6.2

Signs on Skeletal Radiographs

- Diffuse osteoporosis and lytic bony lesions are commonly found in primary hyperparathyroidism.
- Widening of sacroiliac joints due to subchondral bone resorption can be seen.
- *Salt and pepper skull appearance*: this occurs due to resorption of the trabecular bone in the skull and replacement of the resorbed bone by a newly formed connective tissue causing loss of integrity in the shape of the skull bones (Fig. 6.2.2).
- The vertebral bodies in secondary hyperparathyroidism show sclerosis of the endplates (Rugger-Jersey spines) (Fig. 6.2.3).
- *Subperiosteal cortical resorption* typically occurs in the hand, especially at the radial aspect of the middle phalanx, which is a specific sign seen in both primary and secondary hyperparathyroidism (Fig. 6.2.4).
- *Brown tumor* is seen as a well-circumscribed cystic bony lesion which can cause bone expansion. There are often multiple lytic lesions found together. When the hyperparathyroidism is treated, the brown tumor undertows ossification and will transform into a bone island (sclerotic lesion). The most common areas for brown tumors are the pelvis, rib, long bone diaphysis, clavicle, and mandible (Fig. 6.2.5).
- *Subligamentous bone resorption* at the sites of ligament insertion into bone can be seen. It is commonly observed at the elbows over the olecranon, plantar aspect of the calcaneus, and the superior pole of the dorsal aspect of the patella.
- *Chondrocalcinosis* occurs due to deposition of calcium pyrophosphate dehydrate into the cartilage of the joints (metastatic calcification). It is found in up to 40% of hyperparathyroidism cases.
- *Osteitis fibrosa cystica* presents as a lytic expansile bony lesion that mimics metastatic bone disease (Fig. 6.2.6).
- Diffuse osteosclerosis is commonly seen in patients with secondary hyperparathyroidism (Fig. 6.2.7).

Signs on US

- Thyroid ultrasound often shows oval or round hypoechoic mass in the posterior inferior poles of the thyroid (usually <3 cm in diameter) representing parathyroid adenomas. The mass has a well-defined echogenic line separating the adenoma from the thyroid gland representing the capsule. The mass shows internal cystic changes, mixed echogenicity, or calcification as the size exceeds 3 cm in diameter.
- Renal calculi are seen as hyperechoic lesions with posterior shadowing.
- Medullary nephrocalcinosis is detected as hyperechogenic renal pyramids.

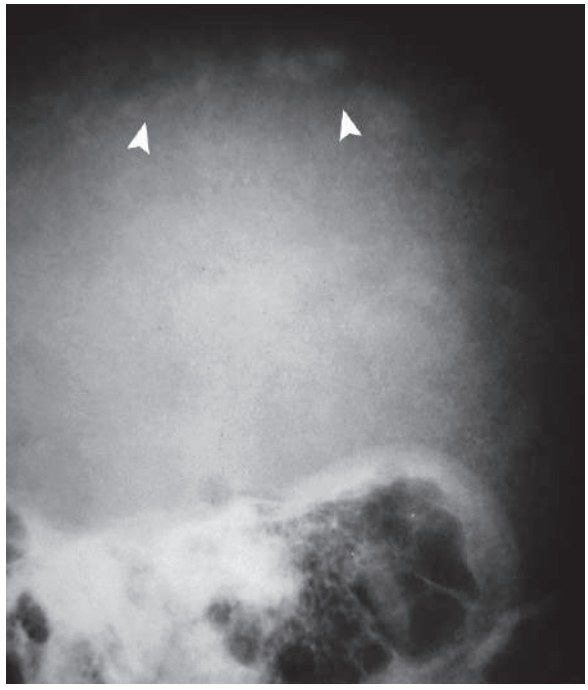

Fig. 6.2.2. A lateral plain radiograph of the skull shows mild salt and pepper skull lesions in a patient with primary hyperparathyroidism

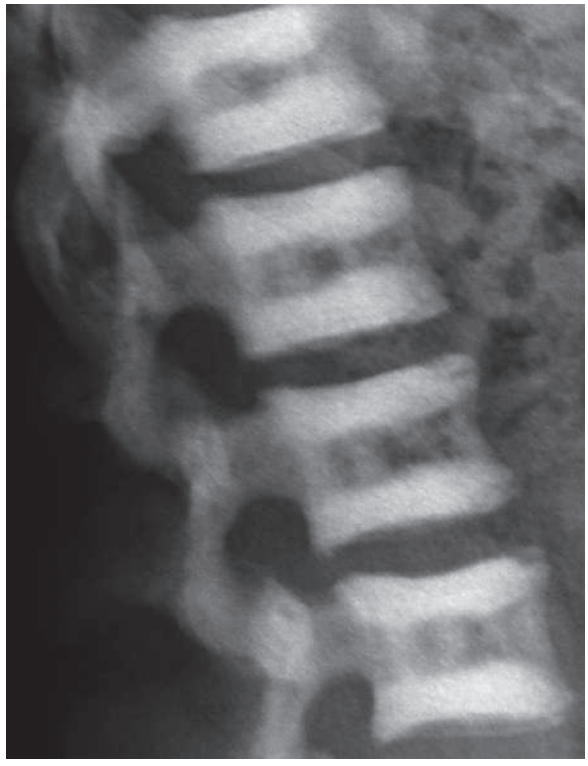

Fig. 6.2.3. A lateral spine radiograph of a patient with secondary hyperparathyroidism shows diffuse vertebral endplates sclerosis (Rugger-Jersey spines)

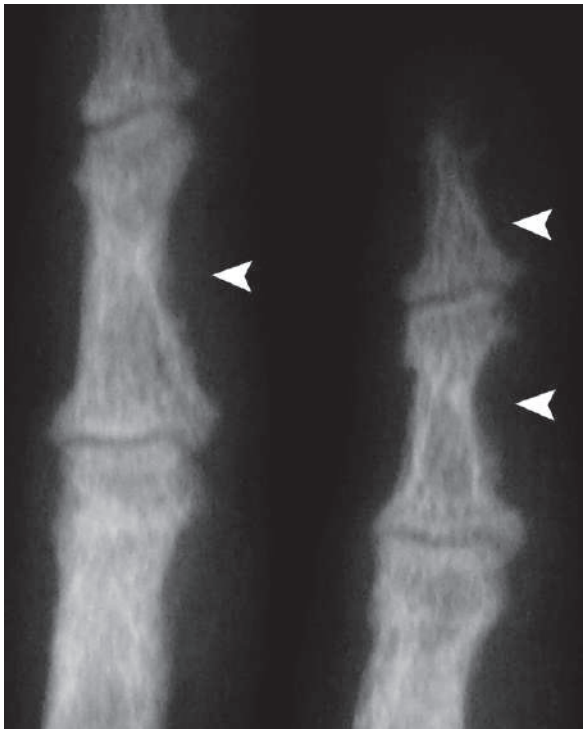

Fig. 6.2.4. A plain radiograph of the fingers shows radial side subperiosteal resorption of the middle and distal phalanges (*arrowheads*), a specific sign of prolonged hyperparathyroidism

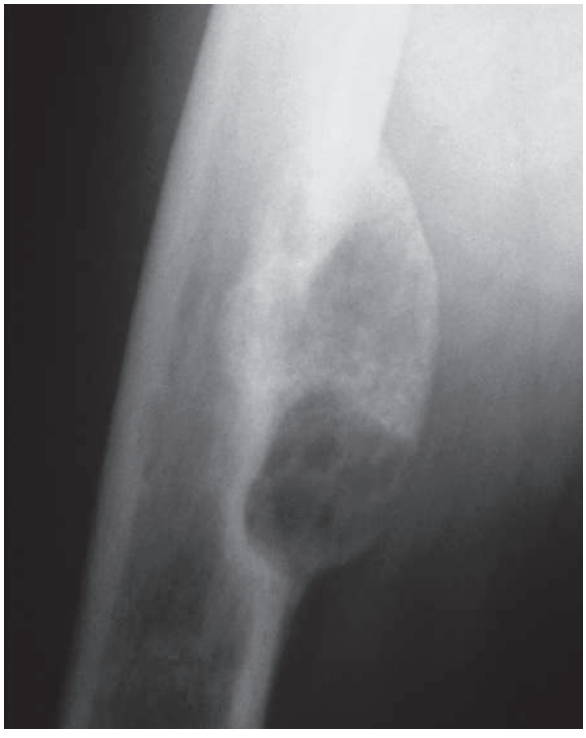

Fig. 6.2.5. A femoral diaphyseal lytic, expansile bony lesion in a patient with prolonged hyperparathyroidism. Pathological biopsy proved to be brown tumor

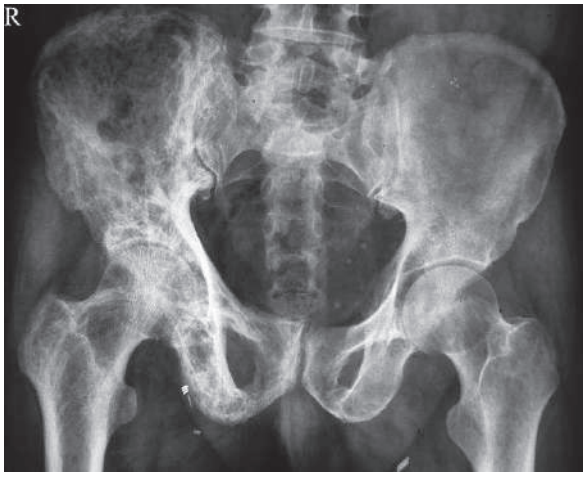

Fig. 6.2.6. A plain hip radiograph of a patient with prolonged undiagnosed hyperparathyroidism. The right side of the hip shows numerous bony lytic and sclerotic lesions with a semi-moth-eating appearance that was initially thought to be Paget's disease. Bone biopsy proved to be osteitis fibrosa cystica

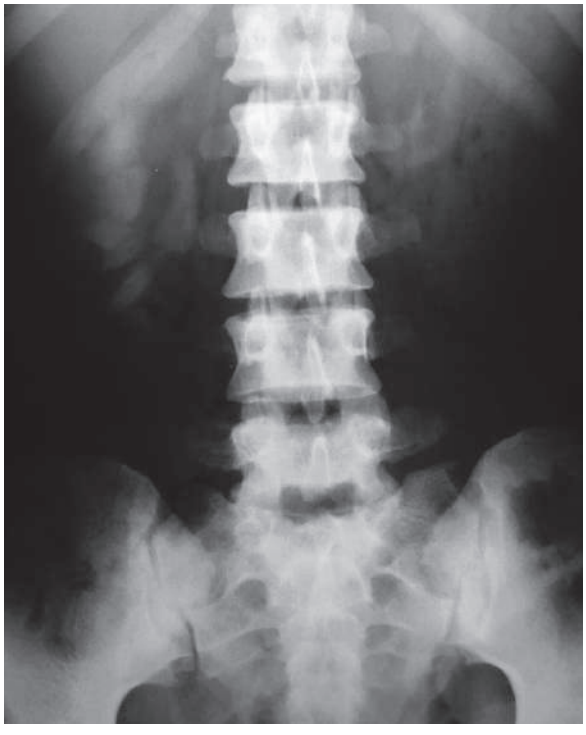

Fig. 6.2.7. A plain abdominal radiograph of a patient with secondary hyperparathyroidism shows diffuse osteosclerosis

Signs on Doppler Sonography and PD

The parathyroid adenoma typically shows high blood flow signal and perfusion, especially at the peripheral portion of the adenoma.

6.2

Signs on CT and MRI

- On CT, parathyroid adenoma is detected as a well-defined mass located in the posterior/inferior pole of the thyroid with intense enhancement after contrast administration. On MRI, the mass shows intermediate T1 and high T2 signal intensities with intense enhancement after contrast injection.
- Ectopic parathyroid adenoma is identified as an anterior mediastinal mass with high contrast enhancement (similar to the usual parathyroid adenomas). The ectopic parathyroid mediastinal adenoma is classically <2 cm in diameter.
- Brown tumors have characteristically low T2 signal intensity due to hemosiderin content. It shows early intense enhancement after contrast injection due to marked vascularity. Fluid–fluid levels may be observed within the tumors in some cases due to intramural bleeding.
- *Ossifying fibroma*: is seen on CT as a well-demarcated lytic lesion with mixed mineralized material (up to 50% are purely lytic lesions). The lytic lesion typically is expansile, and may mimic fibrous dysplasia with its ground-glass appearance if the matrix is extensively calcified (Fig. 6.2.8). On MRI, ossifying fibroma typically shows low to intermediate signal intensity on both T1W and T2W images with homogeneous contrast enhancement after contrast injection.
- The salt and pepper skull appearance seen in plain radiograph can be seen on MRI as bone resorption (Fig. 6.2.9).

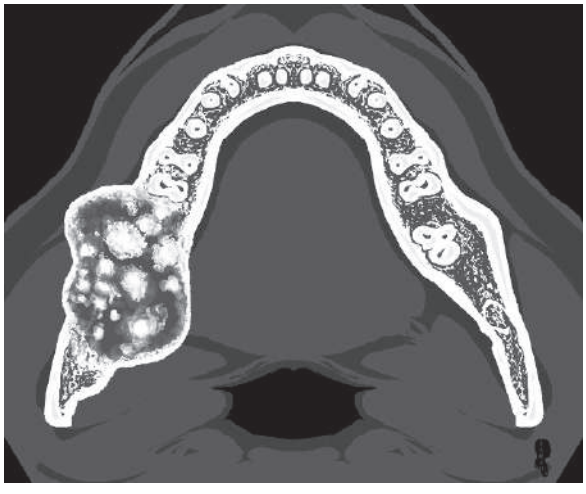

Fig. 6.2.8. A CBCT dental illustration shows ossifying fibroma as lytic expansile bony lesion with mixed calcified matrix

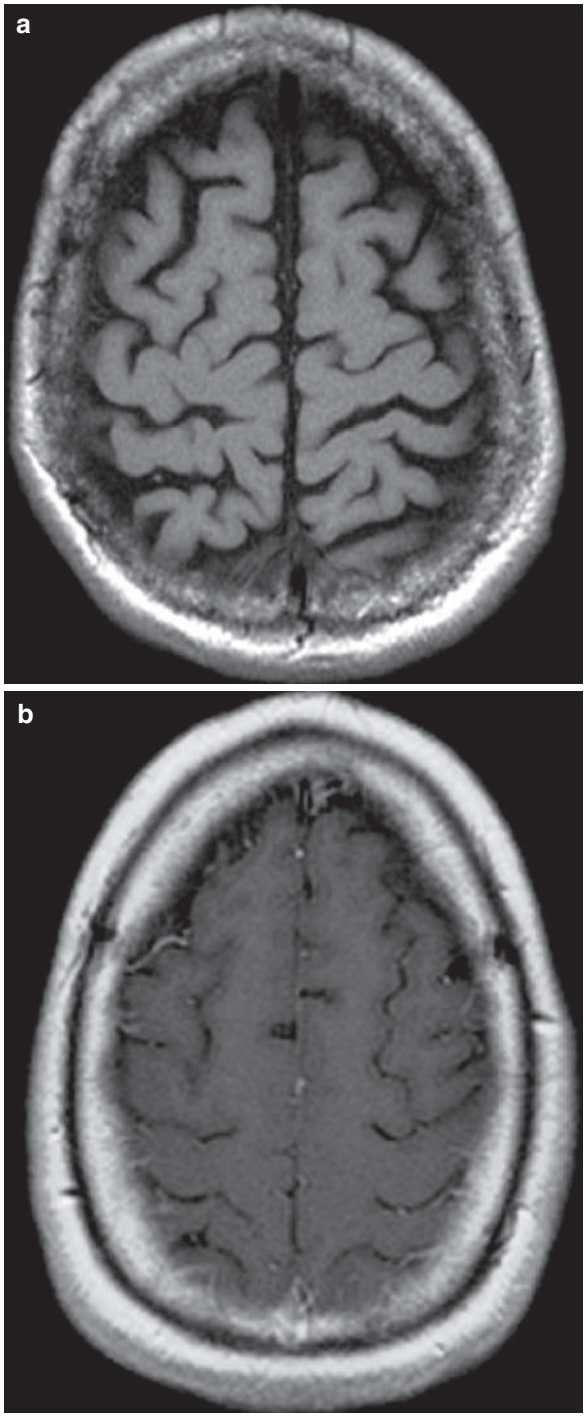

Fig. 6.2.9. Two different patients with T1W image MRI of the brain. In image (**a**), there is marked bone resorption of the inner surface of the skull in a patient with prolonged primary hyperparathyroidism (salt and pepper skull appearance). Compare the skull bones with the normal skull in image (**b**)

For Further Reading

1. McDonald DK et al Primary hyperparathyroidism due to parathyroid adenoma. RadioGraphics. 2005;25:829–34
2. Hsieh M-C et al Pathologic fracture of the distal femur in osteitis fibrosa cystica simulating metastatic disease. Arch Orthop Trauma Surg. 2004;124:489–501
3. Rypins EL. Osteitis fibrosa cystica at unusual age. J Bone Joint Surg Am. 1933;15:509–12
4. Kabala JE. Computed tomography and magnetic resonance imaging in diseases of the thyroid and the parathyroid. Eur J Radiol. 2008;66:480–92
5. Schmidt BP et al Hyperparathyroidism-jaw tumor syndrome: a case report. J Oral Maxillofac Surg. 2009;67:423–7
6. Takeshita T et al Brown tumor with fluid-fluid levels in a patient with primary hyperparathyroidism: radiological findings. Radiat Med. 2006;24:631–4
7. Reuter K et al Unsuspected medullary nephrocalcinosis from furosemide administration: sonographic evaluation. J Clin Ultrasound. 1985;13:357–9
8. Eggert P et al Nephrocalcinosis in three siblings with idiopathic hypercalciuria. Pediatr Nephrol. 1998;12:144–6
9. Ahuja AT et al Imaging of primary hyperparathyroidism – what beginners should know. Clin Radiol. 2004;59: 967–76
10. Wang Q et al Power Doppler imaging findings in multilocular giant parathyroid adenoma which caused hypercalcaemic crisis. J Laryngol Otol. 1998;112:769–99
11. Falchetti A et al Multiple endocrine neoplasia type I variants and phenotypes: more than nosological issue. J Clin Endocrinol Metab. 2009;94:1518–20
12. Bertolini F et al Multiple ossifying fibromas of the jaw: a case report. J Oral Maxillofac Surg. 2002;60:225–9
13. Ghanaat F et al Hungry bone syndrome: a case report and review of the literature. Nutr Res. 2004;24:633–8
14. Smith D et al Hungry bones without hypocalcemia following parathyroidectomy. J Bone Miner Metab. 2005;23: 514–5
15. Krudy AG et al The detection of mediastinal parathyroid glands by computed tomography, selective arteriography, and venous sampling. Radiology. 1981;140:739–44

6.3 Growth Hormone Diseases

The human growth hormone (GH) is a polypeptide consisting of 188 amino acids and having a molecular weight of 21,500. GH from other species shares partial sequences of amino acids in common with human GH (e.g., bovine GH). These partial sequences consist of active cores, which are pharmacologically active. Thus, it may be not necessary to synthesize the entire bovine GH molecule to yield an actively working substance in humans.

GH disorders result from either excess or reduction of its secretion within the body. The normal GH is secreted in two cyclic rhythms: one in the morning and the other in the evening.

Growth Hormone Insufficiency (Hypopituitarism)

GH insufficiency (hypopituitarism) can be idiopathic (primary), or due to pituitary gland tumor (secondary). Idiopathic GH insufficiency children exhibit growth retardation, delayed puberty, and hypothyroidism without elevated thyroid-stimulating hormone (TSH) level. Growth retardation is assumed if the child falls more than three standard deviations below the mean for his/her age, and also if the child's growth rate is <50% of the anticipated growth rate over a period of 1 year.

Pituitary stalk interruption syndrome (*PSIS*) is a form of GH insufficiency due to abnormal pituitary stalk. Children with PSIS have pronounced GH insufficiency, with or without other anterior pituitary hormonal deficiencies.

Signs on Skeletal Radiographs

- Plain skeletal radiographs can be used to accurately assess bone age according to the bone maturation. Each bone in the body starts to ossify at a certain age. By imaging certain bones within the body, assessing their ossification maturation, and comparing it to a standard reference of bone maturation of the patient's current age, the radiologist can easily assess the patient bone maturation rate. This method is a valuable tool that can detect GH abnormalities in a relatively short time with much accuracy.
- Both hands and elbows are often X-rayed, and the shapes of all epiphyses of the radius, ulna, carpals, metacarpals, and all the phalanges are assessed in comparison with a standard reference. Delayed bone maturation can be seen in GH insufficiency and hypothyroidism.
- The normal appearance of primary ossification centers of the wrist: capitate (2–3 months), hamate (3 months), triquetral (2–3 years), lunate (3 years), trapezium (3–4 years), trapezoid (4 years), scaphoid (4–5 years), pisiform (8–9 years), ulnar epiphysis (6–7 years), and radial epiphysis (1 year).
- The normal appearance of primary ossification centers of the elbow (CRITOE): capitulum (6 months), radial head (5 years), internal (ulnar) epicondyle (6–7 years), trochlea (9 years), olecranon (9–10 years), and external (radial) epicondyle (10–11 years).
- By applying the previous primary ossification centers age to a skeletal radiograph of a child, radiologists can estimate roughly the age of that child. However, precise age estimation should be assessed using a standard reference (Fig. 6.3.1).

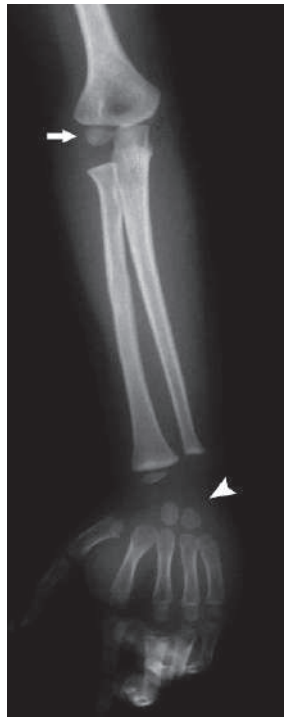

Fig. 6.3.1. A plain radiograph of the hand, wrist, and forearm in 4-year-old boy with growth retardation shows skeletal maturation retardation. Although the child's age is 4 years, only the capitate and hamate bones are ossified (*arrowhead*), which commonly start ossification at 2–3 months. At 4 years of age, we expect the scaphoid, lunate, and trapezium to be seen too. Moreover, the elbow shows only the ossification center of the capitulum (*arrow*), which starts to ossify at 6 months of age. It seems as if the patient's age has been stunted at 6–12 months old

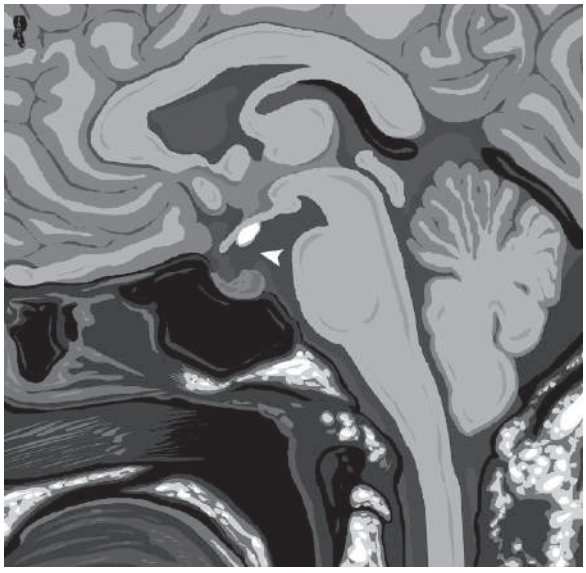

Fig. 6.3.2. Sagittal T1W sella MR-illustration demonstrates interruption of the pituitary stalk with ectopic high T2 signal intensity characteristic of ectopic neurohypophysis and pituitary stalk interruption syndrome (PSIS) (*arrowhead*)

Signs on MRI

The pituitary on MRI in patients with GH insufficiency shows absence or marked thinning of the pituitary stalk, reduced size of the anterior pituitary, lack of the normal posterior pituitary high signal, and presence of a high signal nodule in the region of the infundibular recess of the third ventricle representing ectopic posterior pituitary (Fig. 6.3.2).

Acromegaly and Gigantism

Excess GH pituitary release or GH abuse in bodybuilders results in two disorders named acromegaly and gigantism. The term acromegaly was used for the first time by "Pierre Marie" in France in 1886 describing patients with characteristic hands and feet (acro) hypertrophy (megaly). Acromegaly literally means hypertrophy of the extremities. The disease has been described in historical writings, especially in people whose body development is considerably greater than normal, and who are looked upon as giants. It is even described in the Jewish Talmud by the Biblical name *sarua* that refers to abnormal growth of a single limb, which rendered a priest unfit to serve in the Temple.

Acromegaly is an adult disease characterized by increased production of the GH resulting in characteristic body changes. When the excess GH release starts in adolescence with open epiphyses, the condition is called "gigantism." The common etiology in both cases is a pituitary adenoma that increases GH production. GH causes retention of nitrogen with an overall anabolic effect. It also increases the transport of amino acids in the tissues and their release into proteins, and mobilizes lipids from adipose tissue increasing their oxidation as a source of energy, and thus sparing muscle glycogen. Due to previous GH effects, an athlete who abuses GH may realize an improvement in performance and strength with the use of GH supplements. Amino acids supplements of arginine, ornithine, and lysine, in combination or alone, can stimulate the production of endogenous GH. GH release can be also stimulated by some medications like L-dopa, clonidine, and propranolol. Athletes with GH abuse may develop acromegaly or acromegalic-like state with complications similar to acromegaly.

Patients with acromegaly are characterized by overgrowth of the terminal parts of the skeleton (e.g., hands) and the soft tissue parts of the viscera. The earliest complaints include headache, visual defects in 30% of patients (bitemporal) fatigability, asthenia, and sweating. Later, the size of the head, hands, and feet starts to grow progressively.

Patients with acromegaly develop characteristic appearance. The facial features become coarse and thickened, with enlargement of the nose. Protrusion of the mandible (prognathism), tongue enlargement, widening of the teeth, vertebral kyphosis, skin thickening, and protrusion of the supra-orbital ridges are also characteristic features. The heart, spleen, liver, and kidneys may be enlarged. Patients with acromegaly show higher tendency toward gastrointestinal cancers (e.g., colon cancer).

Women with acromegaly show high incidence of intrauterine bleeding or amenorrhea. In both males and females, there is gradual loss of libido, and testicular or ovarian atrophy may develop later in life.

Other hormonal abnormalities may be found in patients with acromegaly. Thyroid enlargement usually occurs due to hypertrophy with increased thyroid function rate. Inappropriate lactation due to hyperprolactinemia may be found in some patients. Increased serum phosphorus level is a characteristic feature of acromegaly due to increased tubular reabsorption. Adrenal gland

6.3

hypertrophy without signs of cortical hyperfunction may occur. Lastly, large patients with acromegaly develop diabetes mellitus due to the diabetogenic effect of GH which increases the serum blood glucose level. Most of the hormones in the body increase the serum glucose blood level like glucagons, cortisol, and GH. Only insulin is capable of reducing the serum glucose blood level.

Patients with gigantism exhibit the same clinical and radiological features as acromegaly. The characteristic feature in gigantism is the tall height of the patients. Increased GH production delays the closure of the epiphyses, so patients will start to grow in height beyond the normal age of epiphyseal closure. This may result in patients reaching a height of up to 2.4 m according to the historical medical literature.

Differential Diagnoses and Related Diseases

Van Buchem disease is a rare hereditary disorder characterized by endosteal hyperostosis of the skull and the mandible due to excessive lamellar bone deposition with narrow Haversian canals. The disease has both autosomal dominant and recessive forms. Clinically, Van Buchem disease may resemble acromegaly, but not radiologically. Patients with Van Buchem disease present with thickening of the bridge of the nose, deafness due to petrous bone thickening, eye abnormalities due to stenosis of the optic canal, and cranial nerves palsies due to hyperostosis at the base of the skull (Fig. 6.3.3).

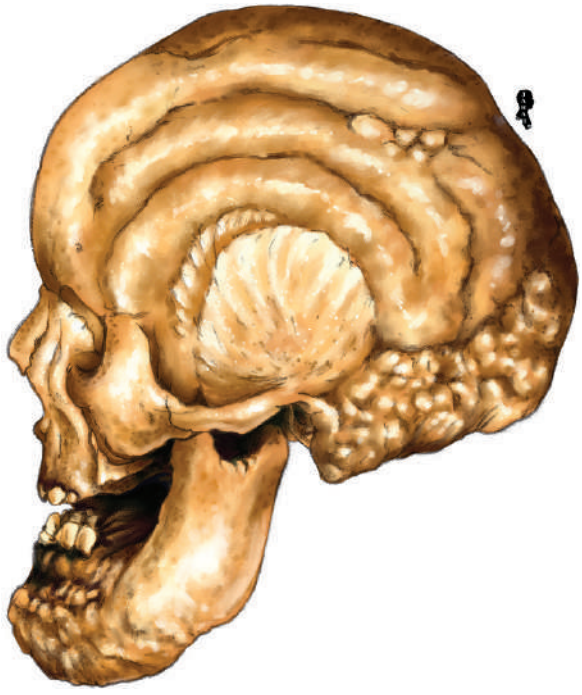

Fig. 6.3.3. An illustration of the skull in a lateral view shows the gross pathological changes seen in van Buchem disease. Notice the enlargement and thickening of the mandible, with sclerosis of the skull base and clavarium

Signs on Skeletal Radiographs

- Increased thickness of the flat bones of the skull (Fig. 6.3.4).
- Enlargement of the sinuses and mastoid air-cells (Fig. 6.3.4).
- Enlargement of the external occipital protuberance (Fig. 6.3.4).
- Enlargement of the sella turcica (due to adenoma). The posterior clinoid processes may show signs of erosions.
- Enlargement of the vertebrae, especially in their transverse diameter.
- Increased size and widening of the distal phalangeal tufts (spade-like appearance) (Fig. 6.3.5).

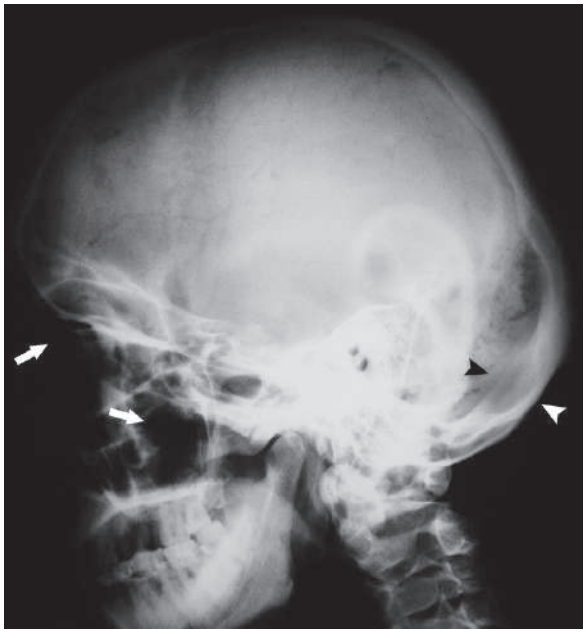

Fig. 6.3.4. A lateral skull radiograph of a patient with acromegaly shows thickened occipital bone (*arrowheads*), and enlargement of the frontal and maxillary sinuses (*arrows*)

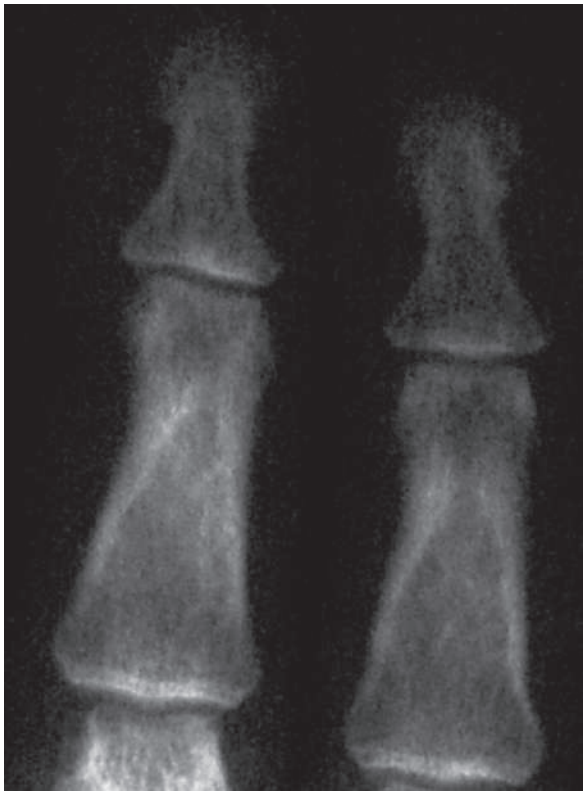

Fig. 6.3.5. Anteroposterior plain radiograph of the third and fourth fingers of a patient with acromegaly shows widening of the distal phalangeal tufts (spade-like appearance)

- Increased soft tissue thickening of the heel pad (normal up to 23 mm in men and 21 mm in women).
- Hypertrophic osteoarthritis of the joints.
- *Locking of the metacarpals* is a relatively rare condition that can be seen in patients with acromegaly. The condition is characterized by a hook-like osteophytes formation in the heads of the metacarpal bones. As the patient makes a fist or grasps something, the volar distal part of the proximal phalanx will be locked against the osteophyte in the metacarpal head, locking the finger in the grasping position.
- *Hyperostosis frontalis interna* is a condition where thickening of the inner surface of the frontal bone may be seen in some cases with acromegaly.
- In van Buchem disease, there is generalized skull hyperostosis, mandibular hyperostosis and enlargement, ribs and clavicular thickening, and diaphyseal endosteal sclerosis that spares the bone ends, especially in the phalanges. Unlike acromegaly, there is no dental widening or mandibular prognathism.

Signs on Brain MRI

- Pituitary adenoma is seen as a bulging lesion in the superior or inferior aspect of the pituitary gland with low T1/high T2 signal. The adenoma is hypointense compared to the normal pituitary tissue on postcontrast images (Fig. 6.3.6).

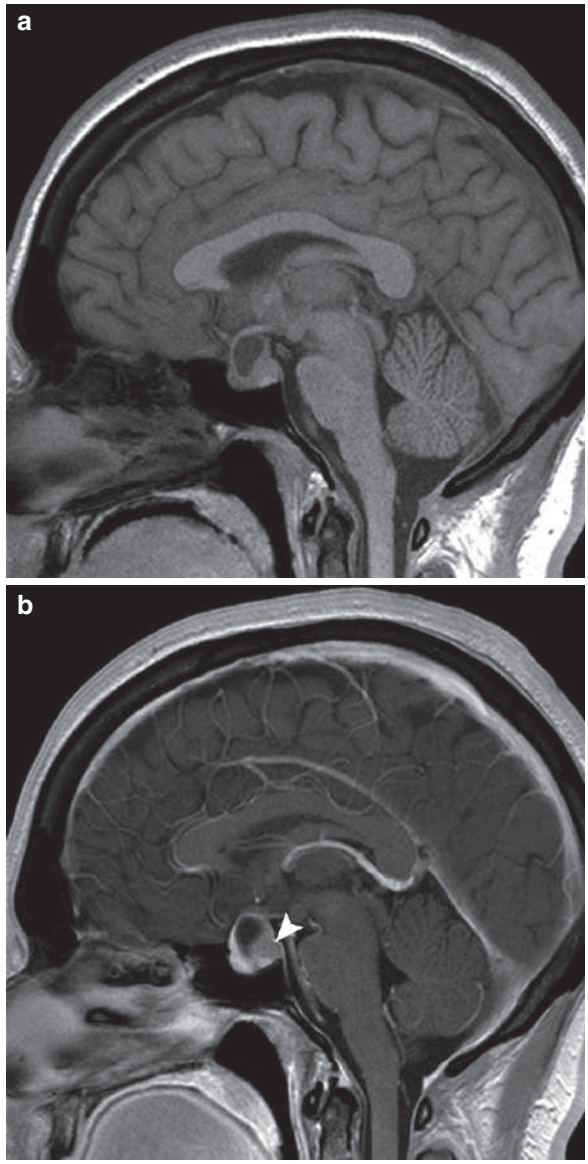

Fig. 6.3.6. Sagittal T1W (**a**) and T1Wpostcontrast (**b**) sella MRI in a patient presented with features of acromegaly. The MR examination showed macroadenoma with cystic changes. The adenoma is detected as a mass with low contrast enhancement (*arrowhead*) compared with the highly enhanced normal pituitary tissue due to its rich blood supply

- Indirect signs of pituitary adenoma include: convex upper border of the gland with shifted pituitary stalk. When the cavernous internal carotid artery is completely surrounded by the tumor, then the cavernous sinus is mostly invaded by the tumor.

6.3

Growth Hormone Insensitivity (Laron Syndrome)

Laron syndrome (LS) is a rare, autosomal recessive, congenital disease characterized by GH receptors gene defects, resulting in lack of body tissue response to GH.

Patients with LS present with dwarfism, severe growth retardation, and characteristic facial features. Most cases are reported from patients with Oriental Jewish origin, or patients originating in the Mediterranean area like Arab, Turkish, Iranian, and Pakistani origin.

Patients with LS typically have small chin (micrognathia), underdeveloped facial bones, smaller head circumference according to age, protruding forehead, and saddle nose deformity due to nasal bone underdevelopment. The teeth are defective and crowded due to micrognathia. The hair is silky and shows frontal and temporal thinning. Alopecia is often seen in males (Fig. 6.3.7).

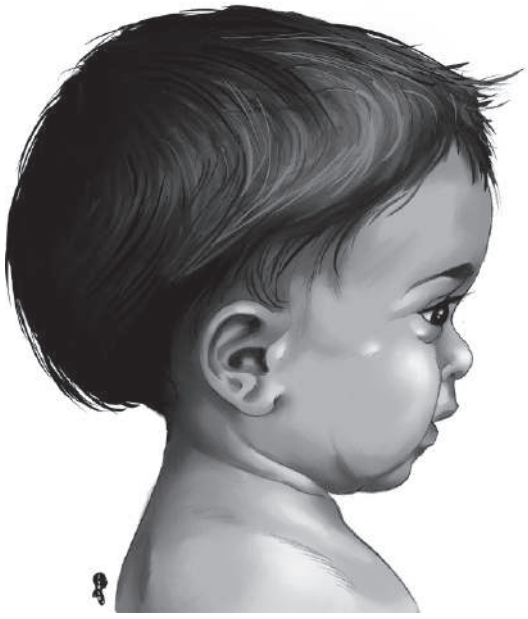

Fig. 6.3.7. An illustration of a child demonstrates the characteristic features of Laron syndrome (LS) like micrognathia, silky hair with temporal thinning, saddle nose deformity, and mildly protruding forehead

Patients are usually obese due to underdevelopment of bones and muscles. The children and even adults have very high-pitched voices due to narrow oropharynx. Hands and feet are small (acromicria). The genitalia and gonads are small since birth, and males show delayed puberty more than females. LS patients do not have real pubertal growth spur.

Laboratory investigations show severe hypoglycemia in neonates that improves with age, low serum alkaline phosphatase and creatinine, low serum cholesterol, and low density lipoproteins.

Hormonal investigations show increased serum GH levels with very low serum levels of insulin-like growth factor-I (IGF-I). IGF-I is the anabolic effector hormone of GH. Prolactin levels may be elevated due to a drift phenomenon to the GH secretion. Serum insulin level is usually high with hypoglycemia.

Signs on Radiographs

- Generalized bone maturation delay and osteoporosis.
- Epiphyseal closure occurs after age 16–18 in girls and 20–22 in boys.
- Underdeveloped facial bones, with thin diploe of the skull.
- Atlanto-axial joint degeneration and spinal stenosis is often observed.
- Os odontoideum may be seen. Os odontoideum is a situation where the axial den (odontoid process) is hypoplastic, absent or separated from the axis body as a congenital variant (not due to previous trauma). It is due to failure of the three dens ossification centers to fuse together with the axis body. It is seen as a round ossicle with smooth edges over the axis body in open mouth view (best view to evaluate the dens). It is may be impossible to differentiate os odontoideum from a previous old dens fracture without history.

Carney's Complex

Carney's complex (CNC) is a rare disease characterized by the formation of multiple endocrine and non-endocrine tumors, spotty skin pigmentation, myxomas, and endocrine overactivity. The disease is also known as *NAME syndrome* (naevi, atrial myxoma, myxoid neurofibromata, and freckles), and *LAMB syndrome* (lentigines, atrial myxoma, mucocutaneous myxomas, and blue naevi).

CNC condition has an autosomal dominant mode of inheritance. *Carney's syndrome* is a different clinical condition characterized by a triad of several neoplasms including gastric epithelioid leiomyosarcoma, pulmonary chondroma, and extra-adrenal paraganglioma. Patients with CNC are diagnosed by fulfilling two or more of the CNC diagnostic criteria.

Carney's Complex Major Diagnostic Criteria

- *Lentiginosis and blue naevi*: Lentigo is a brownish-black flat macule that is typically found in the lips, around the inner canthus of the eye, axilla, or genitals (Fig. 6.3.8). When the macules are found diffusely in the body, the condition is called "lentiginosis." The other characteristic skin lesion found in CNC is blue skin naevi.

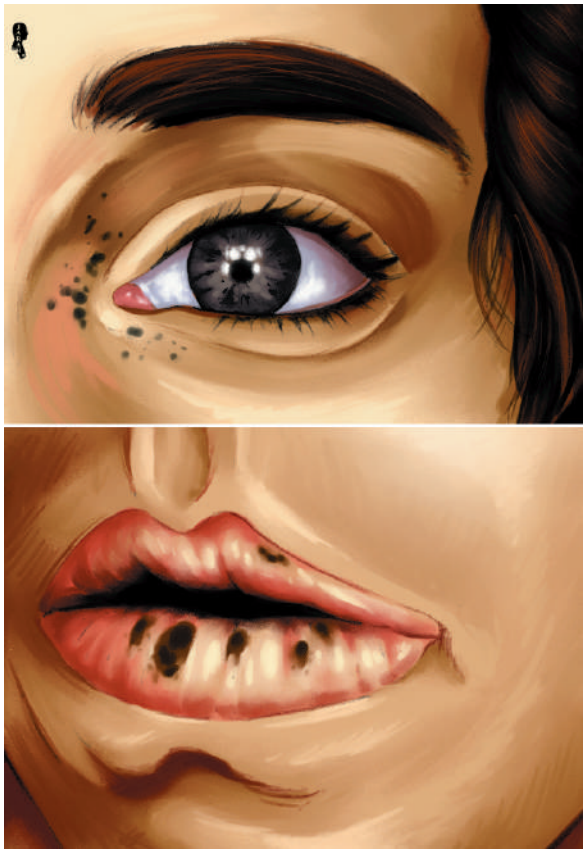

Fig. 6.3.8. An eye and lip illustrations demonstrates the lentigo pigmented lesions found in the inner canthus and the lips in a patient with Carney's complex (CNS)

- *Cutaneous myxomas*: are seen on the trunk as small red papules.
- *Cardiac myxoma*: it is the most common component of CNC. Cardiac myxoma is a gelatinous tumor, and it is the most common primary cardiac neoplasm in adults (50% of cardiac neoplasms). Ninety percent of cases are seen in adult women between 30 and 60 years of age. Most cases are sporadic. Patients usually present with CNS symptoms, fatigue, arthralgia, fever, anemia, and weight loss. Twenty percent of myxomas are asymptomatic. Patients with CNC cardiac myxoma are younger than patients with sporadic myxoma (an average age of 24 years).
- *Acromegaly*: CNC patients can develop acromegaly due to GH-releasing pituitary micro-/macroadenoma.
- *Primary pigmented nodular adrenocortical disease* (*PPNAD*): It is a rare disease of children and young adults below 20 years of age. It can be the first manifestation of CNC. Pathologically, the adrenal shows small black, brown, red, or yellow nodules separated by atrophic adrenal cortex. Diagnosis is essentially based on histological findings. PPNAD is one of the common causes of ACTH-independent Cushing's syndrome.
- *Large-cell calcifying Sertoli cell tumor* (*LCCSCT*): bilateral germ cell tumors of the testes are the initial presentation of CNC in 20% of cases. Diagnosis is strengthened by the detection of high serum levels of estrogen or androgen.
- One or more of the following cancers: breast fibromyxomas (25% of cases), osteochondromyxoma, follicular thyroid carcinoma, psammomatous melanotic schwannoma.

Signs on US

In LCCSCT, the testes show multiple, round, well-defined, large (5–10 mm) echogenic calcification with acoustic shadowing representing the stromal tumors.

Signs on MRI

- *Cardiac myxoma*: myxoma typically appears as a heterogeneous mass on T2W images with a narrow base attachment located in the interatrial septum at the area of fossa ovalis (90% of cases). Eighty percent of myxomas arise in the left atrium, and 10% in the right atrium. Calcification is frequently

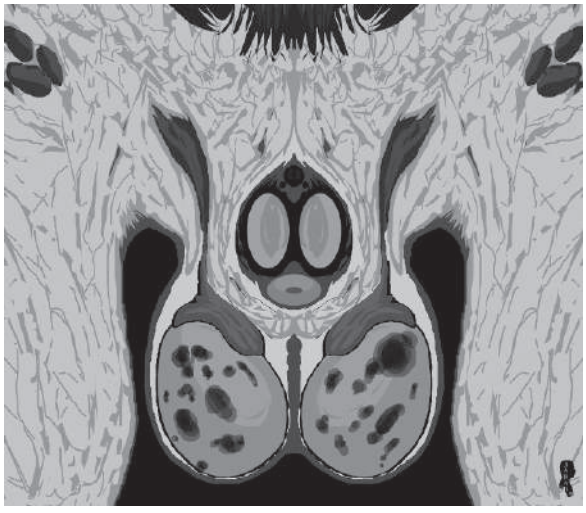

Fig. 6.3.9. Coronal T2W testicular MR-illustration shows bilateral hypointense T2 signal intensity lesions in the testes bilaterally representing large-cell calcifying Sertoli cell tumor (LCCSCT)

seen, and the mass shows heterogeneous contrast enhancement. The location of the tumors is very characteristic.

- *LCCSCT*: are detected as multiple high T2 intratesticular masses with hypointense areas representing calcifications (Fig. 6.3.9).
- Sella MRI may show pituitary adenoma especially in patients with signs of acromegaly.
- *PPNAD*: the adrenal glands may be normal, or show limbs macronodularity (>5 mm in size).

For Further Reading

1. Daughaday WH et al The pituitary in disorders of growth. Dis Mon. 1962;8:1–47
2. Kaplan SA. Human growth hormone. Dis Mon. 1968;14: 1–33
3. Frohman LA. Diseases of hypothalamic releasing factors. Dis Mon. 1976;22:1–37
4. Ron E et al Acromegaly and gastrointestinal cancer. Cancer. 1991;68:1673–77
5. Tani Y et al Locking of the metacarpophalangeal joints in a patient with acromegaly. Skelet Radiol. 1999;28:655–7
6. Fisher MS. An unusual bone change in acromegaly. Skelet Radiol. 1978;3:177–8
7. Doppman JL et al Cushing syndrome due to primary pigmented nodular adrenocortical disease: findings at CT and MR imaging. Radiology. 1989;172:415–20
8. Elster AD. Imaging of the sella: anatomy and pathology. Semin Ultrasound CT MRI. 1993;14:182–94
9. Wyszynski DF. Dysmorphology in the Bible and the Talmud. Teratology. 2001;64:221–5
10. Laron Z. Growth hormone insensitivity (Laron syndrome). Rev Endocr Metab Disord. 2002;3:347–55
11. Laron Z. Laron syndrome (primary growth hormone resistance or insensitivity): the personal experience 1958–2003. J Clin Endocrinol Metab. 2004;89:1031–44
12. Kornerich L et al Laron syndrome abnormalities: spinal stenosis, Os odontoideum, degenerative changes of the atlanto-odontoid joint, and small oropharynx. AJNR Am J Neuroradiol. 2002;23:625–31
13. Chakraborty PP et al Laron's syndrome in two siblings. Indian J Pediatr. 2007;74:870–1
14. Jacobs P. Van Buchem disease. Postgrad Med J. 1977;53: 497–506
15. Boikos SA et al Pituitary pathology in patients with carney complex: growth-hormone producing hyperplasia or tumors and their association with other abnormalities. Pituitary. 2006;9:203–9
16. Vandersteen A et al Cutaneous signs are important in the diagnosis of rare neoplasia syndrome Carney complex. Eur J Pediatr (2009);168:1401–1404
17. Mateus C et al Heterogeneity of skin manifestations in Patients with Carney syndrome. J Am Acad Dermatol. 2008;59:801–10
18. Cazabat L et al PRKAR1A mutations in primary pigmented nodular adrenocortical disease. Pituitary. 2006;9:211–9
19. Haupt HA. Anabolic steroids and growth hormones. Am J Sport Med. 1993;21:468

6.4 Osteoporosis

Osteoporosis is a group of disorders characterized by reduced bone mass or density in the absence of defect in bone mineralization. Osteoporosis can arise due to unknown reasons (primary) or due to pathological conditions (secondary).

Bones reach their peak density in the third decade of life and then decrease gradually at the rate of 0.25–1% per year. This percentage is higher in women at the menopause, which may reach up to 8% per year. Osteoporosis affects the axial skeleton more than the perpendicular skeleton, while osteomalacia (excess un-mineralized bone matrix) affects the perpendicular skeleton more than the axial skeleton. Osteoporosis starts to show itself on radiographs when 30–60% of bone mass is lost.

Primary Osteoporosis

Primary osteoporosis is a term used to describe reduction in bone density in the absence of a specific clinical condition that explains this bone density reduction. It is divided into juvenile, idiopathic, and postmenopausal types.

Idiopathic juvenile osteoporosis is osteoporosis that affects children and young adults and is typically seen before puberty. Patients present with difficulties and gait abnormalities, and multiple fractures that typically involve the metaphyses of distal tibias and the vertebral bodies. Pain in the heels and the lower back is a common complaint. Diagnosis of this condition is established after exclusion of all cases that may present with similar manifestations (e.g., osteogenesis imperfecta and homocysteinuria).

Idiopathic osteoporosis is a term used to define osteoporosis seen in patients between 20 and 45 years of age with the same clinical features as the juvenile form. *Postmenopausal osteoporosis* is seen in women who have undergone natural menopause, or after oophorectomy. Primary osteoporosis affects mainly the hip more than any other area in the skeleton.

Vacuum phenomenon, also known as "intervertebral cleft sign," is a term used to describe a condition characterized by accumulation of gas, mostly nitrogen (95%), within the vertebral bodies, intervertebral discs, and synovial joints. The gas is produced from the surrounding soft tissues, and its accumulation mechanism is poorly understood. The main hypothesis of vacuum phenomenon suggests ischemic origin. Osteonecrosis of the vertebral endplates with negative pressure between the bone fragments is mandatory to release gas from the surrounding tissue, a situation that can be classically seen in osteoporotic vertebral fractures and collapse. Vacuum phenomenon is also seen in osteonecrosis due to long-term corticosteroid therapy, diabetes mellitus, arteriosclerosis, multiple myeloma, and alcoholism.

The main differential diagnosis of the intravertebral vacuum phenomenon is gas produced by osteomyelitis and malignancies. In infectious gaseous production, the gas has high pressure and tends to accumulate in small collections, plus extends into the adjacent soft tissues, which is not seen in vacuum phenomenon where gas is limited to the bony or intra-discal areas.

Kümmell disease is a term used to describe vacuum phenomenon within a vertebra that arises from vertebral endplates osteonecrosis and vertebral collapse. Kümmel's disease represents healing failure of an osteoporotic vertebral fracture with the formation of pseudoarthrosis (false-joint).

Signs on Plain Radiograph and CT

- Thinning of the cortex (compact bone) is the main radiographic feature of osteoporosis (Fig. 6.4.1). It is best seen in the second metacarpal bone diaphysis. Normally, the cortex in the mid-shaft of the second metacarpal should be almost one-third the thickness of the metacarpal width. This sign is seen in up to 50% of cases.
- *Dowager's Hump*: osteoporotic multiple thoracic vertebrae causing wedge deformities (Fig. 6.4.2).
- *Pathologic fractures* mostly occur at the neck of the femur, distal radius, and humeral neck.
- *Intracortical tunneling* is a sign of rapid bone loss. It is typically seen as long lucent lines parallel to the long axis of the bone (Fig. 6.4.3). When the tunneling is severe, a double cortical line is seen.
- *Diffuse bone resorption* occurs in 50% of cases and is characterized by loss of the trabecular bone.
- *Linear translucent bands* of 4–8 mm thickness are seen within the bone in radiograph. They are commonly seen with disuse osteoporosis and leukemic patients.

6.4

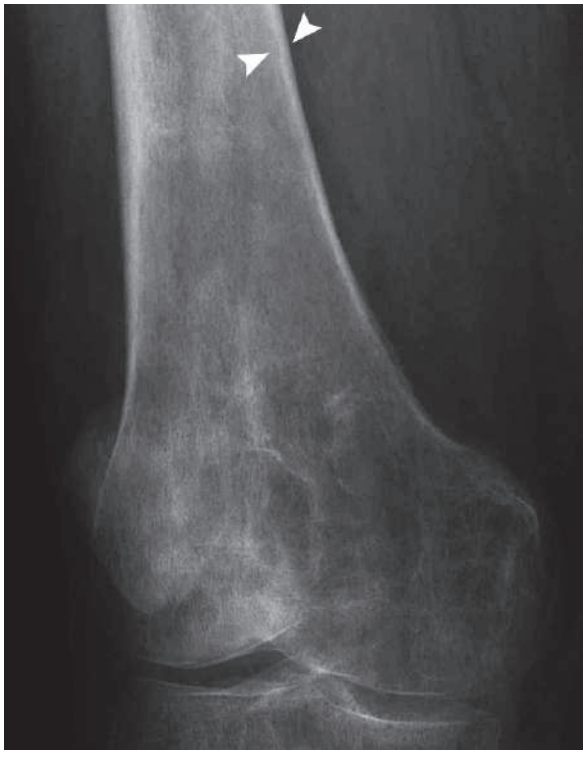

Fig. 6.4.1. A plain radiograph of the knee shows diminished bone mineral density (BMD) with thinning of the cortex (*arrowheads*)

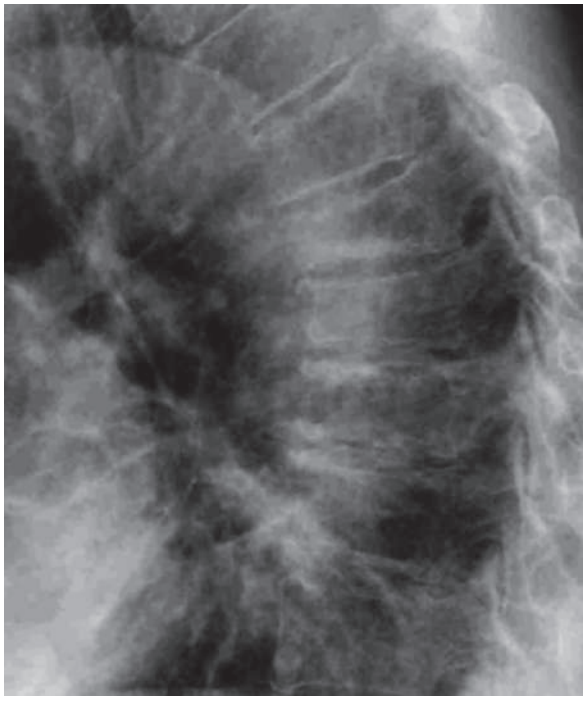

Fig. 6.4.2. A lateral thoracic vertebrae radiograph shows kyphosis of the thoracic vertebrae due to osteoporosis (Dowager's Hump)

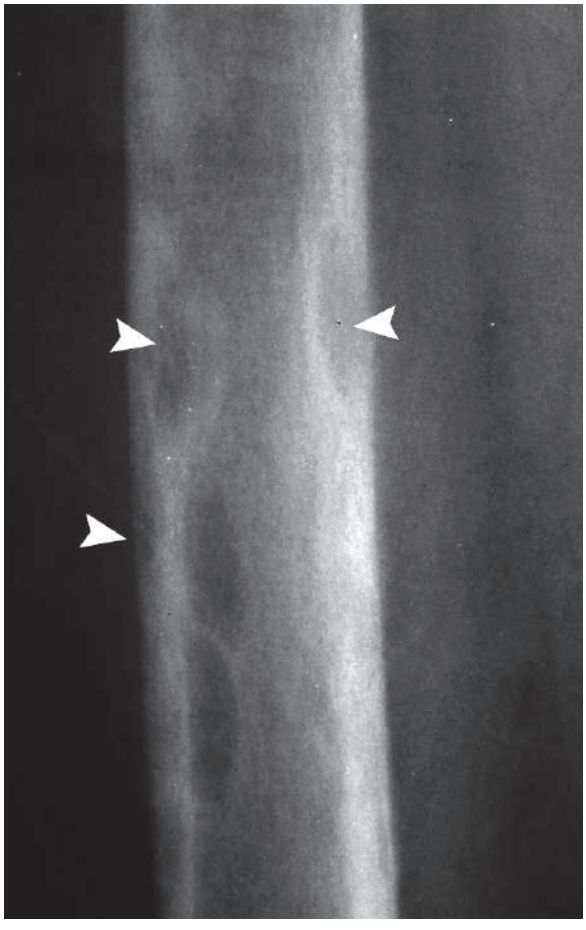

Fig. 6.4.3. A plain radiograph of osteoporosis of the femoral shaft demonstrates clearly the intra-cortical tunneling sign (*arrowheads*)

- *Patchy bone resorption*: seen as multiple lucent patches usually in the carpal or tarsal bones. It can be mistaken with lytic lesions of Ewing's sarcoma and multiple myeloma (Fig. 6.4.4).
- Vacuum phenomenon is seen as a gas collection in a collapsed vertebra or in intervertebral disc space (Fig. 6.4.5).
- *Singh index* is a simple method to estimate the level bone mineral density (BMD) on radiograph by analyzing the changes in the trabecular pattern of the proximal femur. A scale of six grades is classically described, with the first grade showing only basic trabecular structures (low BMD, severe osteoporosis), and the sixth grade showing trabecular structures in all areas of the proximal femur (high BMD, normal bone).

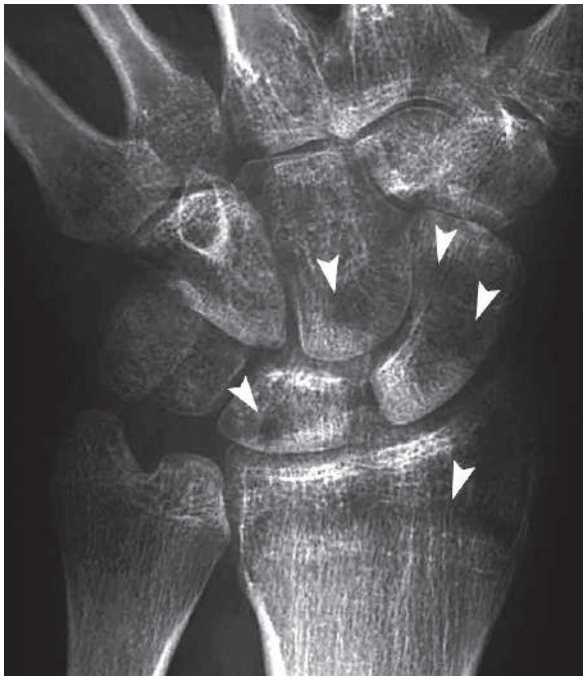

Fig. 6.4.4. Anteroposterior plain wrist radiograph in a patient with osteoporosis shows patchy areas of radiolucent opacities representing patchy osteoporosis (*arrowheads*)

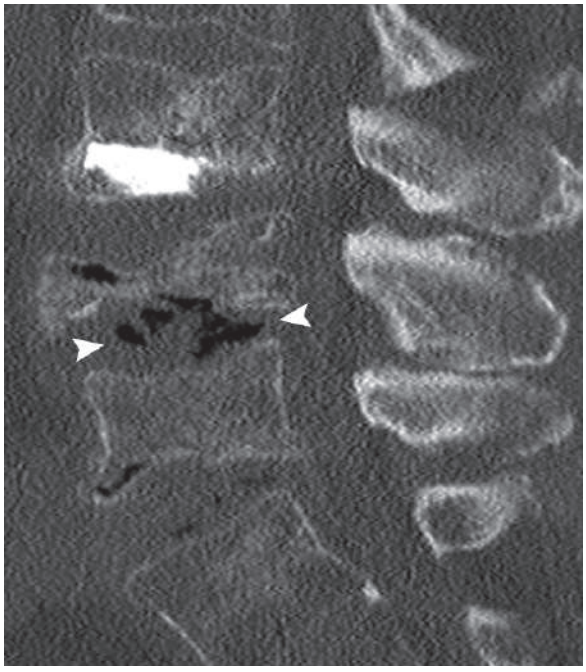

Fig. 6.4.5. Sagittal lumbar CT image in a patient with osteoporosis shows severe osteopenia, collapse of L4 vertebra (vertebra plana), vertebroplasty of L3, with gas formation located in the intervertebral disc space between L4 and L5 (*arrows*)

Signs on MRI

- The area of vacuum phenomenon may appear as an area of fluid signal intensity on T2W images. This finding is explained by the fact that fluid replacement tends to fill the area of vacuum gas on long supine position. This T2 flow signal depends on the time of scanning. In the first 10 min of the scan, the vacuum area is seen as a hypointense area on T2W images. The signal turns into T2 hyperintense signal between 20 and 40 min after positioning.
- In *Kümmel's disease*, the vertebral end plates are seen compressing over the fractured area in flexion. In extension, the gap between the fractured end plates open. Intervertebral air can be seen on CT and MRI, with no signs of inflammation on T2W images.

Dual Emery X-Ray Absorptiometry (DEXA) Scan

DEXA scan is a quantitative method for measuring bone mass by using low energy X-ray beam. The bone mass is measured in units of gram per cubic centimeter of bone. The World Health Organization (WHO) defines the *T*-scores as follows: between +1 and −1 indicates normal bone; between −1 and −2.5 indicates osteopenia; and osteoporosis is diagnosed when the *T*-score is less than −2.5.

Pitfall: sclerosis and osteophytes in the vertebral column can increase the values of the DEXA scan giving a false impression of a good bone density. For this reason, DEXA report should always be written after comparison of the results with plain frontal and lateral radiographs of the vertebral column to avoid misinterpretation.

Secondary Osteoporosis

Secondary osteoporosis is seen in association with other clinical conditions such as endocrine diseases (e.g., Cushing's syndrome), nutritional diseases (e.g., scurvy), drug-induced (e.g., heparine), neoplasms (e.g., multiple myeloma), metabolic diseases (e.g., diabetes mellitus), and chronic inflammatory conditions (e.g., rheumatoid arthritis). Radiological manifestations are same as primary osteoporosis.

Regional Migratory Osteoporosis of the Hip (Bone Marrow Edema Syndrome)

6.4

Regional migratory osteoporosis (RMO) is a rare condition characterized by migrating arthralgia of weight-bearing joints in the lower limbs (hips, knees, and ankles).

RMO typically affects males between 50 and 60 years of age presenting with pain confined to a single joint. Patients experience progressive pain in one joint that can last from weeks to months. Peak intensity of the pain is experienced usually in the second and third months after the initial presentation. There is no history of trauma or signs suggesting joint infection (e.g., septic arthritis). The symptoms resolve spontaneously often between 4 and 11 months after presentation.

Signs on Radiographs

Typically, there is osteopenia of the affected joint compared to the other joint which normally shows no osteopenia (unless the patient is generally osteoporotic). Unfortunately, this sign is seen after 3–6 weeks from the start of symptoms. Remineralization of the affected area may take up to 2 years to complete after the symptoms are resolved.

Signs on MRI (Four Morphological Criteria at T1W Images Are Needed to Indicate RMO of the Hip)

- The bone marrow edema must involve the femoral head, and often spares the subchondral bone resulting in a thin rim of unaffected subchondral marrow. The edema may extend to the femoral neck.
- The bone marrow lacks the definite margins or transitional zone between the lesion and the adjacent marrow.
- The signal is homogeneous with areas of high- or low-intensity foci.
- The signal intensity of the marrow is moderately reduced. All the above four criteria must be evaluated on T1W images.
- Joint effusion is seen in 75% of patients.
- *RMO of the knee* has the same diagnostic criteria as the RMO of the hip, and typically involves the lateral femoral condyle, although it can affect any part of the knee (Fig. 6.4.6).

RMO Differential Diagnoses

- *Avascular necrosis*: usually with history of trauma, steroid use, chemotherapy, or renal disease. No such history is associated with RMO. Risk factors for RMO include low dietary calcium and tobacco smoking.

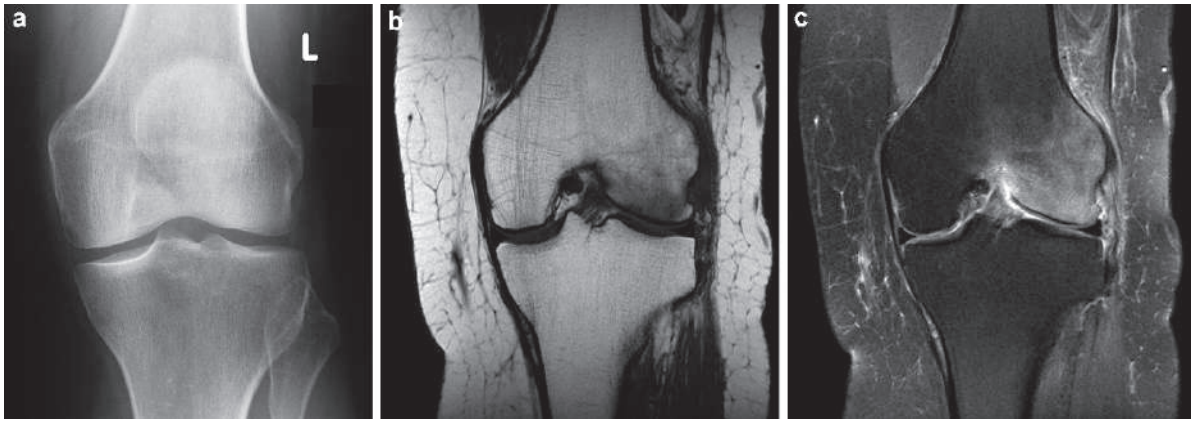

Fig. 6.4.6. Anteroposterior plain radiograph of the left knee (**a**), with coronal T1W image (**b**), and coronal PD image (**c**) of a 57-year-old lady who presented with nonspecific knee pain for 3 weeks' duration. The plain radiograph shows no signs of obvious pathology or diminished bone density. On the MR images, the lateral femoral condyle showed bone marrow edema signal with no sign of a fracture of cortical destruction. The knee showed no signs of abnormalities that explain the knee pain. The diagnosis was regional migratory osteoporosis (RMO) of the knee and the patient was advised a 3-month MRI follow-up examination

- *Reflex sympathetic dystrophy*: there are atrophic skin changes and history of neurological disease, which are not seen in RMO.
- *Chronic recurrent multifocal osteomyelitis*: has the same picture as RMO on MRI, but plain radiographs show both lytic and sclerotic lesions, which is not characteristic of RMO.

For Further Reading

1. Goldring SR et al Metabolic bone disease: osteoporosis and osteomalacia. Dis Mon. 1981;27:1–103
2. Lutwak L et al Osteoporosis. Dis Mon. 1963;9:1–39
3. Freedman BA et al Kummel disease: a not-so-rare complication of osteoporotic vertebral compression fracture. J Am Board Fam Med. 2009;22:75–8
4. Lorenc RS. Idiopathic juvenile osteoporosis. Calcif Tissue Int. 2002;70:395–7
5. Williamson MR et al Osteoporosis: diagnosis by plain chest film versus dual photon bone densitometry. Skelet Radiol. 1990;19:27–30
6. Aloia JF et al Risk for osteoporosis in black women. Calcif Tissue Int. 1996;59:415–23
7. Karantanas AH. Acute bone marrow edema of the hip: role of MR imaging. Eur Radiol. 2007;17:2225–36
8. Cahir JG et al Regional migratory osteoporosis. Eur J Radiol. 2008;67:2–10
9. Vande Berg BC et al Bone marrow edema of the femoral head and transient osteoporosis of the hip. Eur J Radiol. 2008;67:68–77
10. Akpinar E et al The intravertebral vacuum phenomenon. Eur J Radiol Extra. 2008;66:e55–7
11. Sarli M et al The vacuum cleft sign: an uncommon radiological sign. Osteoporos Int. 2005;16:1210–14
12. Kumpan W et al The intravertebral vacuum phenomenon. Skelet Radiol. 1986;15:444–7
13. Libicher M et al The intravertebral vacuum phenomenon as a specific sign of osteonecrosis in vertebral compression fractures: results from a radiological and histological study. Eur Radiol. 2007;17:2248–52
14. Hauschild O et al Evaluation of Singh index for assessment of osteoporosis using digital radiography. Eur J Radiol. 2009;71:152–8

6.5

Rickets and Osteomalacia

Rickets is a group of conditions characterized by accumulation of nonmineralized bony matrix (osteoid) within the skeleton in children, while osteomalacia is an accumulation of nonmineralized bony matrix in the mature skeleton of adults (the bone quantity is normal, but the bone quality is abnormal).

Understanding bone physiology and metabolism is crucial for understanding the pathology of rickets and osteomalacia. Bones are made up of bony cells surrounded by extra-cellular matrix. The extra-cellular matrix has organic and inorganic components. The *organic* component, also called "osteoid," is made of type I collagen fibers embedded in a ground substance composed of proteoglycans and other components. The osteoid is secreted by the osteoblasts, and it accounts for 35% of the bone mass. In contrast, the *inorganic* component is composed of osteoid plus calcium and pyrophosphate (mineral salts). The inorganic materials are what give bone its density, and account for 65% of the bone mass. Rickets and osteomalacia are diseases of matrix mineralization, while osteoporosis is a disease of bony matrix.

After osteoid mineralization, the mineralized collagens are arranged in either woven or lamellar pattern. *Woven bone* is immature bone with its fibers not arranged in any direction. Normally it presents in life as a transitional stage and then is replaced by lamellar bone. Woven bone is not found in mature skeleton normally; however, it is produced during healing of fractures or remodeling (callus formation). Its presence indicates abnormality when found in mature skeleton. *Lamellar bone*, on the other hand, is mature bone with its fibers arranged in a certain pattern to withstand mechanical pressure. The mature skeleton is made only of lamellar bone, and the fibers are arranged in vertical form in the cortical bone and arranged in transverse form in the trabecular bone. Some sheets of lamellar bone are circumferentially arranged around a bundle of blood vessels and lymphatics, forming what are known as "Haversian canals or osteons." These Haversian canals are found in the cortical bone and arranged along the long axis of the bone, and they communicate with each other through channels of interstitial lamellae.

The *physis* is the cartilaginous growth plate in immature skeleton which is responsible for adding length to bone. The growth plate functions as a one-way barrier to blood vessels, allowing the blood from epiphyseal capillaries to supply the metaphysis but not vice versa.

Hormones that affect bone metabolism and hemostasis include the parathyroid hormone (PTH) and the active form of vitamin D, 1,25-dihydroxyvitamin D ($1,25(HO)_2D$). PTH is secreted in response to low plasma calcium concentration. PTH promotes bone formation on the physiological level, but it causes bone resorption at high concentrations. Vitamin D undergoes two hydroxylation steps in the liver and the kidney before it becomes metabolically active, promoting calcium absorption from the intestines. Calcitonin is a hormone that opposes the action of both PTH and vitamin D.

From the latter explanation of the bone metabolism, any condition that can result in hormonal imbalance or matrix mineralization defects can result in the development of rickets or osteomalacia. Causes of rickets include:

- Acquired rickets due to vitamin D deficiency (most common form).
- Congenital rickets due to vitamin D enzyme hydroxylation deficiency.
- Congenital rickets due to vitamin D resistance and receptors mutation.
- Congenital rickets due hypophosphatemia (low phosphates). It can be X-linked, autosomal-dominant, or autosomal-recessive.
- Acquired rickets due to hypocalcemia.
- Acquired rickets due to renal failure. Reasons for developing rickets or osteomalacia are loss of the hydroxylation step of vitamin D and raised PTH levels.

Patients with rickets often present with bowing of the legs, swollen joints, bone pain, and muscle weakness. Patients with rickets due to vitamin D resistance may present with alopecia.

Differential Diagnoses and Related Diseases

Dent's disease is a rare disease characterized by X-linked recessive hypophosphatemic rickets, idiopathic low molecular weight proteinuria, and X-linked

recessive nephrolithiasis. Patients with this disorder commonly present with hypercalciuria, nephrocalcinosis, and renal failure at advanced stage of the disease. Radiological investigations in these patients include plain radiographs of the bone to show signs of rickets, and renal ultrasound to detect urinary stones and medullary calcinosis.

Signs of Rickets on Plain Radiograph

- Flaring of the epiphysis.
- Bending of the diaphysis of long bones, commonly the tibia (Fig. 6.5.1).
- Cupping deformity of the metaphysis due to herniation of the hypertrophied physis into the metaphysis (Fig. 6.5.2). The metaphyses may also show fine bony speculation (Fig. 6.5.3).
- *Looser's zone fracture* (*pseudofractures*) is a very distinctive feature of osteomalacia, which is characterized by a fracture through a large osteoid area within the bone. This type of fracture is rare and tends to occur in the scapula or the pelvis.
- *Rachitic rosary* is swelling of the costo-chondral junction of the middle ribs.
- Osteomalacia presents with signs of osteopenia on radiographs. It cannot be differentiated from osteoporosis with radiographs alone. History of chronic renal failure is a helpful clue.
- Rickets due to hypophosphatemia are usually associated with craniosynostosis (e.g., scaphocephaly).
- Skull radiographs in patients with rickets show soft skull bones (craniotabes), flattening of the skull, hot-cross-bun skull (caput quadratum), and delayed closure of the fontanelles.
- Hypocalcemic rickets characteristically show hypoplasia of the dental enamel, whereas abscesses of the teeth occur more often in rickets due to hypophosphatemia.

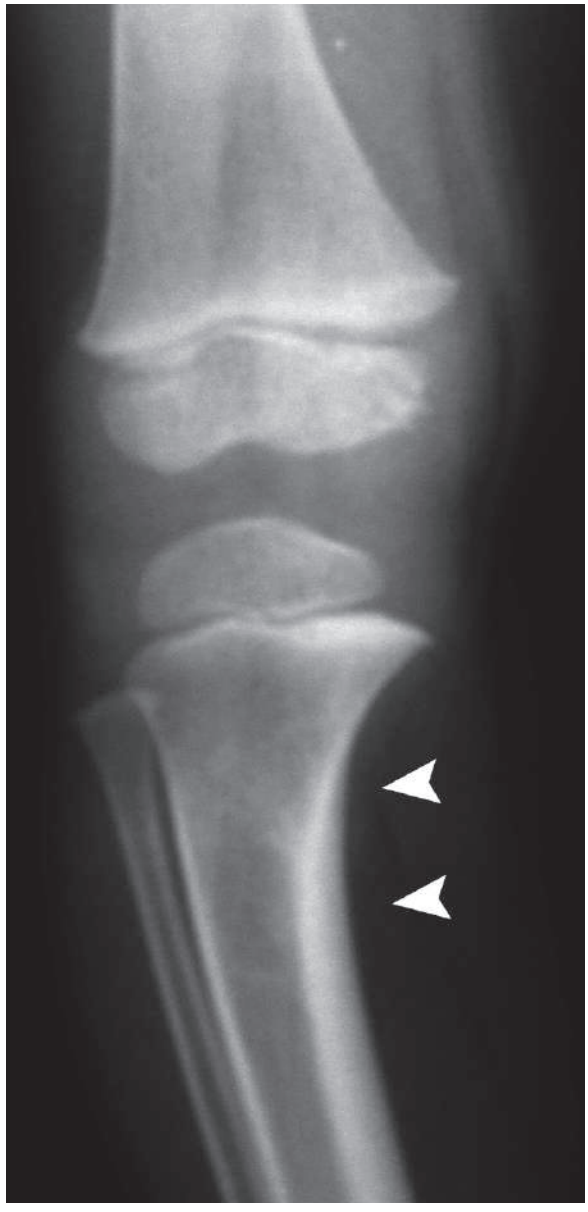

Fig. 6.5.1. Anteroposterior plain radiograph of the right knee in a child with rickets shows mild bowing of the proximal tibial metaphysis (*arrowheads*)

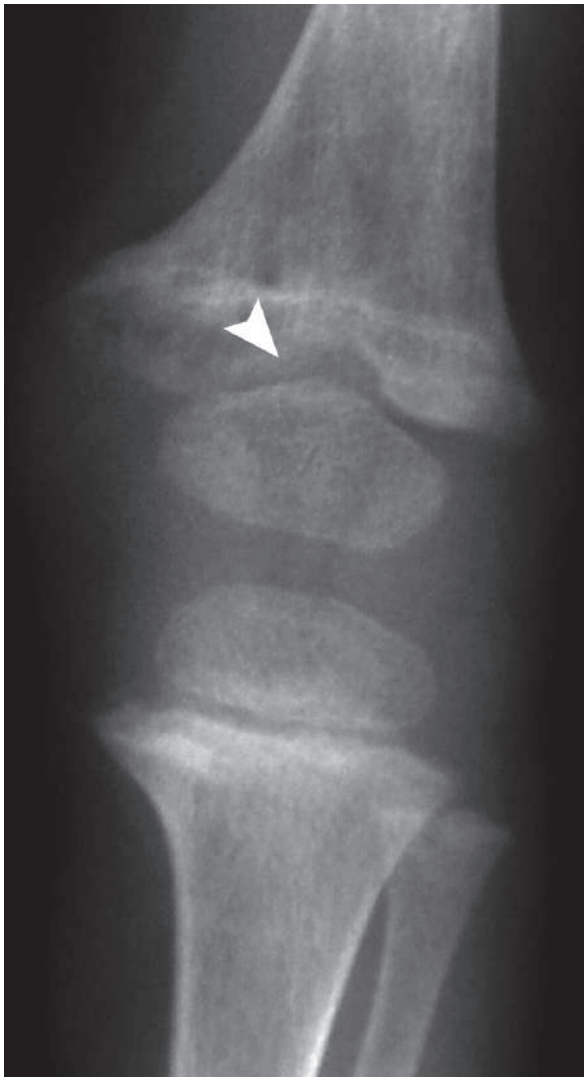

Fig. 6.5.2. Anteroposterior plain radiograph of the left knee in a child with rickets shows focal cupping of the distal femoral metaphysis (*arrowhead*)

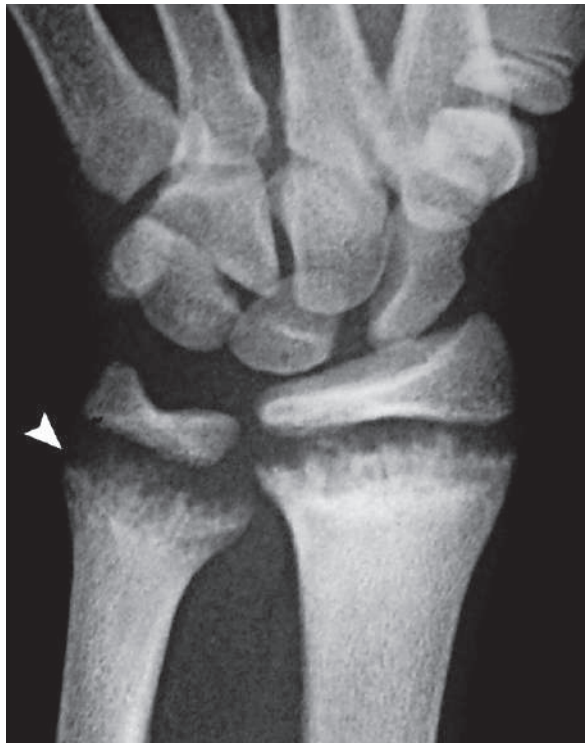

Fig. 6.5.3. A plain wrist radiograph of a patient with rickets shows metaphyseal bony speculations (*arrowhead*)

For Further Reading

1. Ramavat LG. Vitamin D deficiency rickets at birth in Kuwait. Indian J Pediatr. 1999;66:37–43
2. DeJong AR et al Pseudotumor cerebri and nutritional rickets. Eur J Pediatr. 1985;143:219–20
3. Currarino G. Sagittal synostosis in X-linked hypophosphatemic rickets and related diseases. Pediatr Radiol. 2007;37:805–12
4. McBride A et al Vitamin D-resistance rickets (X-linked hypophosphataemic rickets). Curr Orthop. 2007;21:369–99
5. Mays S et al Skeletal manifestations of rickets in infants and young children in a historic population from England. Am J Phys Anthropol. 2006;129:362–74
6. Brickley M et al Evaluation and rickets interpretation of residual rickets deformities in adults. Int J Osteoarchiol. 2008. doi:10.1002/oa.1007
7. Cheong HI et al Phenotype and genotype of Dent's disease in three Korean boys. Pediatr Nephrol. 2005;20:455–9
8. Tosetto E et al Dent's disease and prevalence of renal stones in dialysis patients in Northeastern Italy. J Hum Genet. 2006;51:25–30

6.6 Scurvy

Scurvy is disease that arises due to vitamin C deficiency. Most cases of scurvy arise due to severe malnutrition, alcoholism, and drug abuse.

Vitamin C (ascorbic acid) functions as a cofactor, enzyme complement, co-substrate, or a strong antioxidant in a variety of metabolic activities. It provides electrons needed to reduce molecular oxygen. It also works as a cofactor for collagen synthesis and norepinephrine synthesis. Vitamin C is present in marine fish, vegetables, and citrus fruits (in high concentrations).

Vitamin C absorption occurs in the small intestine, and is excreted by the kidneys. The maximum concentration of vitamin C is found in the pituitary gland, leukocytes, brain, adrenals, and the eye.

Patients with scurvy usually present with irritability, limb pain, and tenderness with pseudoparalysis. Unusual manifestations of scurvy include subdural and subarachnoid hemorrhage, hematuria, melena, pleural hemorrhage, and retro-orbital hemorrhage causing proptosis. Patients improve within 2 days to 1 week from starting vitamin C therapy. Scurvy is often found in children, and radiographic abnormalities are rare before 6 months of age.

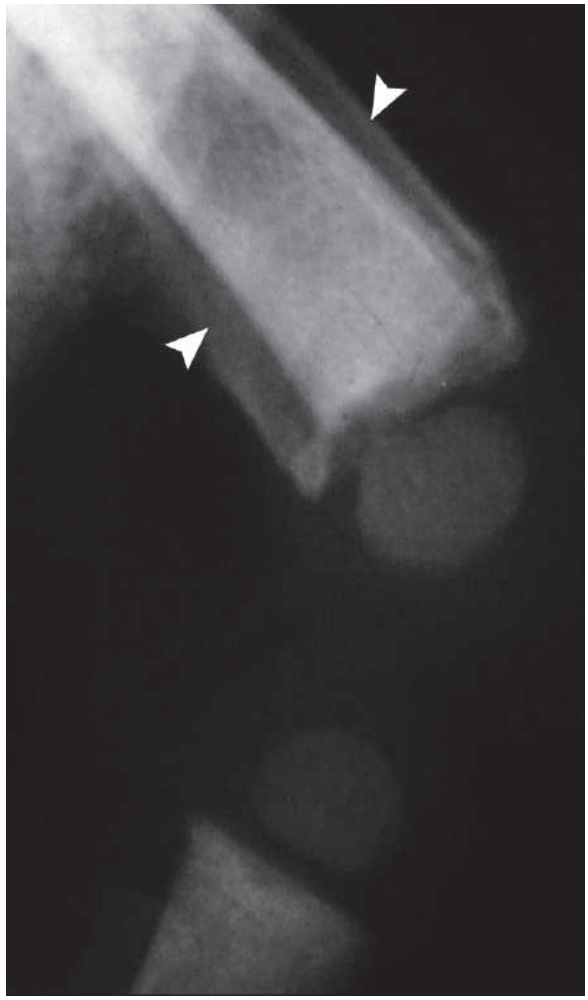

Fig. 6.6.1. Anteroposterior left femoral radiograph shows periosteal hemorrhage in a baby with scurvy seen as radiolucent shadow that surrounds the distal femur shaft (*arrowheads*)

Signs on Plain Radiograph

- *Subperiosteal hemorrhage* is seen as elevated periosteum from the bone (Fig. 6.6.1).
- *Wimburger's sign*: sclerotic rim surrounding the epiphysis in children.
- *White line of Frankel*: dense sclerotic metaphyseal line over the metaphysis (Fig. 6.6.2).
- *Pelkin's fracture*: metaphyseal avulsion fracture.
- Scurvy is a frequent cause of osteoporosis in children (Fig. 6.6.2), and it can predispose to slipped distal femoral epiphysis due to epiphyseolysis.

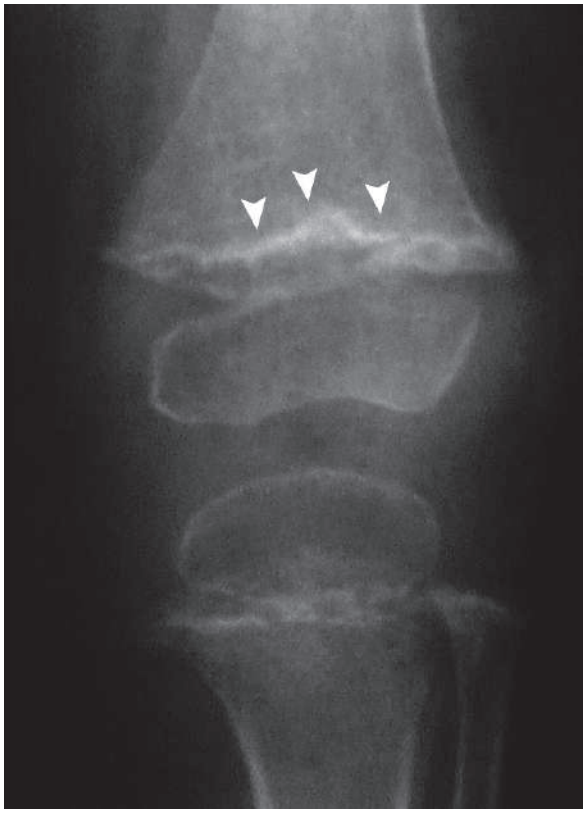

Fig. 6.6.2. Anteroposterior plain knee radiograph in another child with scurvy shows dense sclerotic metaphyseal line (*White line of Frankel*). Notice the diffuse osteoporosis affecting the entire knee joint

For Further Reading

1. Suvarna J et al Hemorrhagic pleural effusion: can it be scurvy? Indian J Pediatr. 2007;74:1050–1
2. Verma S et al Unilateral proptosis and extradural hematoma in a child with scurvy. Pediatr Radiol. 2007;37:937–9
3. Brickley M et al Skeletal manifestations of infantile scurvy. Am J Phys Anthropol. 2006;129:163–72
4. Ratageri VH et al Scurvy in infantile tremor syndrome. Indian J Pediatr. 2005;72:883–4
5. Akikusa JD et al Scurvy: forgotten but not gone. J Paediatr Child Health. 2003;39:75–7
6. Firth N et al Oral lesions in scurvy. Aust Dent J. 2001;46: 298–300

6.7 Fluorosis

Fluorosis is a clinical condition characterized by excessive ingestion of fluoride, which causes toxicity and systemic manifestations that can be disabling.

Fluoride is an element that is found in water, soil, and air. It results from the combination of the "fluorine" gas with different natural elements. Fluoride can be found in food, seawater, and tea. Each cup of tea may supply 0.3–0.5 mg of fluoride. The safe daily intake of fluoride for an adult is <4 mg/day. Skeletal fluorosis results from ingesting fluoride >10 mg/day for at least 10 years.

Fluorosis classically results from ingestion of water or food with high fluoride content in endemic areas. Fluorosis toxicity may also develop from chronic intake of sodium fluoride as a long-standing therapy for osteoporosis, using teflon-coated pots, chewing tobacco, and the overuse of niflumic acid (nonsteroidal anti-inflammatory drug).

Fluoride absorption in the body can be reduced by taking calcium or magnesium salts. In contrast, phosphate, sulfates and molybdenum increase gastrointestinal absorption of fluoride and lead to fluoride toxicity.

Up to 99% of the absorbed fluoride combines with the mineralized bones, mostly in the teeth, pelvis, and vertebrae. Dental fluorosis deposits mainly in the enamels and causes brown or black dental pigmentation (Fig. 6.7.1). Pitting, chipping, and mottling of the teeth may also occur.

Fig. 6.7.1. An illustration demonstrates the clinical appearance of dental fluorosis

Patients with fluorosis often complain from pain in the joints and back, which is often mistaken with rheumatic disorders like rheumatoid arthritis and ankylosing spondylitis. Back stiffness, limb paresthesia, and restricted spine movement are early signs of fluorosis. In severe form of back fluorosis, the vertebral column becomes one continuous column of bones due to calcification of the paravertebral ligaments, a condition known as "*poker back*" (Figs. 6.7.2 and 6.7.5). Development of genu varum, genu valgum, and kyphosis may occur. Involvement of the ribs by fluorosis results in a barrel-shaped chest with restricted respiratory breathing. Abdominal breathing becomes the main breathing mechanism is severe cases.

Fig. 6.7.2. An illustration demonstrates a patient with poker back due to fluorosis

6.7

Neurological manifestations of fluorosis usually are related to the spinal cord compression due to vertebral canal stenosis. Patients experience radiculopathy and difficulty in walking due to muscle weakness. Cranial nerve compression may occur when fluorosis affects the skull base foramina.

Some patients develop hyperparathyroidism for unknown reasons. It is thought that the resistance of the osteoclastic activity by the sclerotic bones causes parathyroid hormone over-activity.

Diagnosis is confirmed by detecting high level of fluoride in the urine (main path of fluoride excretion), serum, and bone. A 24-h sampling of urine is the most reliable method for confirming fluorosis. The serum alkaline phosphatase level is usually high.

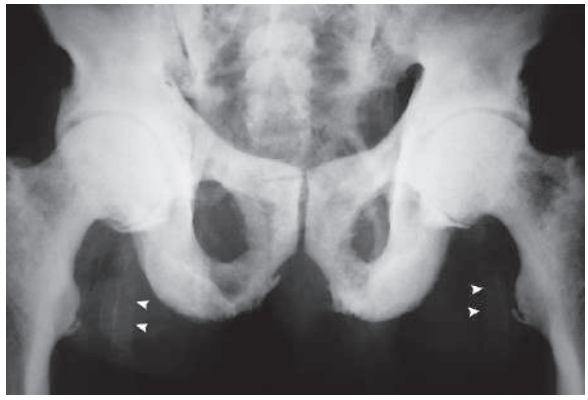

Fig. 6.7.3. Anteroposterior pelvis radiograph shows severe systemic fluorosis with diffuse skeletal sclerosis. Calcification can be seen affecting even the femoral vessels (*arrowheads*)

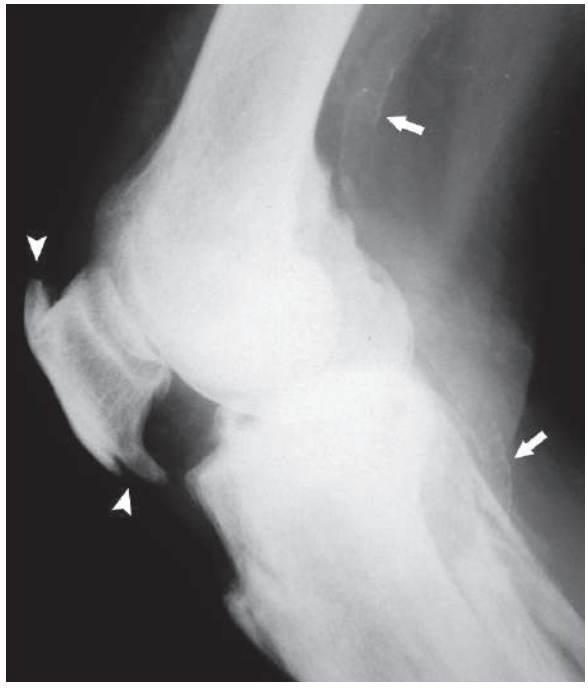

Fig. 6.7.4. Lateral knee radiograph of the same patient shows diffuse sclerosis with sclerosis and osteophytes formation of the quadriceps and patellar tendons insertion at the superior and the inferior poles of the patella (*arrowheads*). Sclerosis of the popliteal vessels can be observed too (*arrows*)

Signs on Radiographs

- The axial skeleton is mainly affected in the form of sclerosis of the trabecular bone and thinning of the cortical bone, mostly affecting the vertebrae and the iliac wings (Fig. 6.7.3). Although the pelvis shows sclerosis, the long bones may show osteopenia. A theory to explain this finding states that bones which accumulate fluoride are resistant to the osteoclastic activity of bone remodeling. The hyperparathyroidism resulting from fluorosis causes high resorption of the long bones which do not contain fluorosis, but not of the sclerotic axial bones. This may explain the mixed sclerotic–osteoporotic radiological picture seen in fluorosis.
- Subperiosteal new bone formation causes the long bones to become uneven (Fig. 6.7.4).
- Ligament calcification is a very characteristic sign of fluorosis, affecting commonly the sacro-tuberous and the petroclinoid ligaments. Paravertebral ligament calcification causes vertebral column restriction (Fig. 6.7.5).
- Prominence of the occipital protuberance with formation of exostosis occasionally is another minor manifestation.

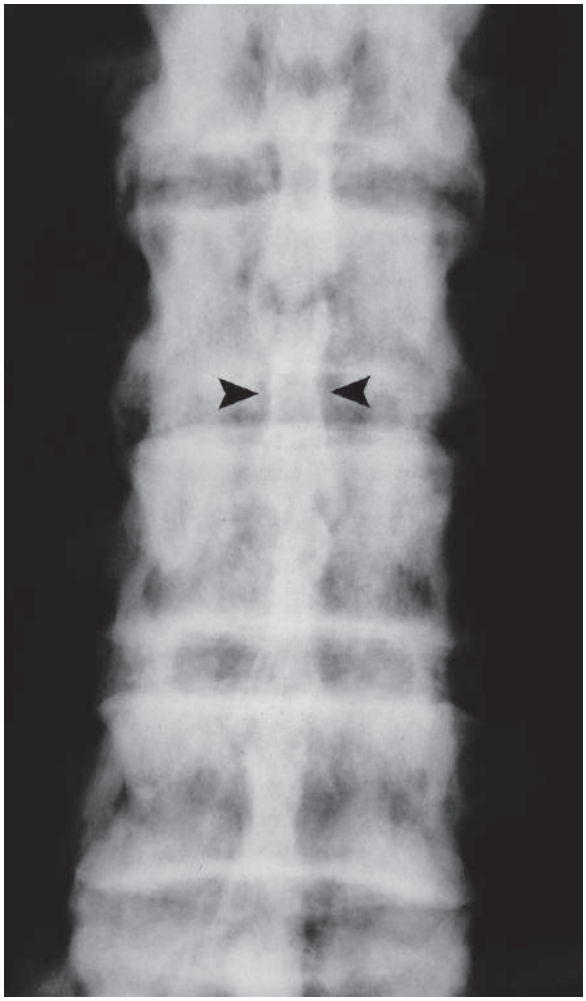

Fig. 6.7.5. Anteroposterior plain radiograph of the thoracic spines of the same patient shows severe vertebral and paravertebral ligaments sclerosis (poker back). Calcification of the supraspinous ligament results in the classical "dagger sign" that is usually seen in ankylosing spondylitis (*arrowheads*)

For Further Reading

1. Mithal A et al Radiological spectrum of endemic fluorosis: relationship with calcium intake. Skelet Radiol. 1993;22: 257–61
2. Lian Z-C et al Osteoporosis – an early radiographic sign of endemic fluorosis. Skelet Radiol. 1986;15:350–3
3. Whyte MP et al Skeletal fluorosis and instant tea. Am J Med. 2005;118:78–82
4. Boillat MA et al Radiological criteria of industrial fluorosis. Skelet Radiol. 1980;5:161–5
5. Gupta RK et al Compressive myelopathy in fluorosis: MRI. Neuroradiology. 1996;38:338–42
6. Tamer MN et al Osteosclerosis due to endemic fluorosis. Sci Total Environ. 2007;373:43–8

6.8

Lead Poisoning (Plumbism)

Lead poisoning is a clinical condition which arises either due to direct ingestion of the lead metal compounds (e.g., in water) or by inhalation of lead oxide fumes. Ingestion of lead compounds is often seen in children, whereas in adults it is often due to occupational lead inhalation. In children, lead toxicity can be also due to pica (e.g., dirt eating), inhalation of toxic fumes, or ingestion of lead-based paints.

The effect of lead poisoning is mainly noticed in the growing bone. When lead is ingested or inhaled, its ions deposit on the hydroxyapatite crystal preferentially in the zone of provisional calcification in the growth plate (physis). Lead mainly inhibits osteoclastic remodeling without affecting the osteoblasts, resulting in an increase in the thickness and the trabeculae at the metaphyses. This is seen on plain radiographs as a dense band of bones at the metaphyses of long bones (dense metaphyseal band sign).

Dense metaphyseal band sign may be seen as a normal variant in healthy children following prolonged exposure to sunlight. The cause of this phenomenon is unknown, but it may involve overproduction of endogenous vitamin D. Other causes of dense metaphyseal band sign include vitamin D toxicity, congenital hypothyroidism, and recovery from scurvy.

Signs on Radiograph

- Dense metaphyseal bands are seen as thick radiopaque bone at the metaphysis of long bones, especially at the wrists and knees. All of the other bone structures are normal (Fig. 6.8.1).
- The presence of a dense metaphyseal band at the proximal fibula is a strong indication of lead toxicity.

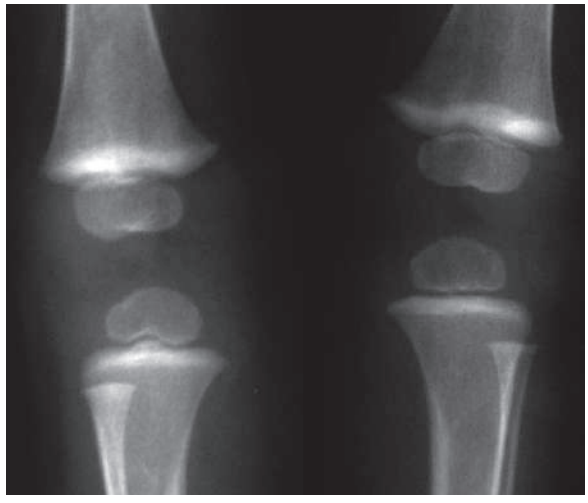

Fig. 6.8.1. Anteroposterior plain radiograph of both knees in a child with lead poisoning shows dense metaphyseal band sign in the distal femur and the proximal tibia of both knees. The right proximal fibular metaphysis shows also the dense metaphyseal band as a strong indication of lead poisoning

For Further Reading

1. Nagaraj BR et al A rare case of lead poisoning – a case report. Indian J Radiol Imaging. 2005;15:67–8
2. Raber SA. The dense metaphyseal band sign. Radiology. 1999;211:773–4
3. Blickman JG et al The radiologic "lead band" revisited. AJR. 1986;146:245–7
4. Wiwanitkit V et al Lead intoxication: a summary of the clinical presentation among Thai patients. BioMetals. 2006;19:345–8

6.9 Adrenal Glands Abnormalities

The adrenal glands are a pair of retroperitoneal endocrinal glands located above the kidneys. Each gland is composed of a cortex derived from the mesoderm, and a medulla derived from the neural crest.

The cortex is composed of three layers: *zona fasciculate* that secretes cortisol, *zona glomerulosa* that secretes aldosterone, and *zona reticularis* that secretes androgens. The medulla secretes epinephrine and norepinephrine. Adrenal masses are divided into functioning and nonfunctioning tumors depending on whether they secrete hormones or not.

Cortical bodies are islands of ectopic chromaffin tissues (adrenal cortical tissues) found in the broad ligament of the uterus, spermatic cord, or epididymis. A tumor of the ectopic adrenal tissues is called "*paraganglioma*." Paragangliomas can be found in the paraspinal region, pineal gland, and in the urinary bladder.

On MRI and CT, the thickness of the adrenal limbs can be compared with the thickness of the adjacent diaphragmatic crus. The normal glands width should not exceed that of the adjacent diaphragmatic crus (normally <5 mm). Both adrenals are found at the level of T12. The right gland is located posterior to the IVC, while the left gland is adherent to the left diaphragmatic crus.

Cushing's Syndrome

Cushing's syndrome (CS) is a disease characterized by multiple systemic manifestations due to chronic exposure to excess glucocorticoids, often due to adrenal hyperplasia. *Cushing disease* is a pathological condition with similar clinical manifestations as CS, but it arises due to increase glucocorticoid production secondary to an adrenocorticotropic hormone (ACTH)-secreting pituitary adenoma. *Pseudo-Cushing syndrome* is a term used to describe any condition that results in distortion of the hypothalamic–pituitary–adrenal axis.

The clinical manifestations of CS are attributed to the chronic exposure to glucocorticoids; however, none of these symptoms or signs is pathognomonic of the syndrome. Progressive central obesity is the most common sign of CS. Fat accumulation in the cheeks results in a "moon" face appearance. Enlarged fat pads that fill the supraclavicular fossae and obscure the clavicles making the neck appear shortened are characteristic signs of CS. Up to 5% of patients have increased retroorbital fat content that may cause exophthalmos.

Hypertension, menstrual abnormalities, oligomenorrhea, insomnia, and impaired short-term memory are well-known manifestations of CS. In obese persons and patients with CS, renal pelvis lipomatosis may develop. *Renal pelvis lipomatosis* is a condition characterized by excess proliferation of the encapsulated fat cells in the renal pelvis. The proliferated fat causes mass effect on the intrarenal collecting system, but rarely leads to symptoms. *Replacement lipomatosis of the kidney* is an uncommon extreme form of renal pelvis lipomatosis where the lipomatosis is accompanied by atrophied or destructed kidney.

Skin manifestations include skin atrophy, easy bruisability, and purple cutaneous striae due to skin stretching. Hyperpigmentation can be seen in CS due to increased ACTH release, which induces melanocytes pigment over-production. When CS is associated with excess androgens secretion, oily skin, acne, increased libido, female virilization, and temporal balding may be seen.

Differential Diagnoses and Related Diseases

Nelson's syndrome is a rare disease characterized by skin hyperpigmentation after bilateral CS adrenalectomy. The main mechanism of development of this condition can be explained by hyperactive pituitary function. The loss of the partial cortisol inhibition on the pituitary ACTH secretion after adrenalectomy causes the pituitary to secrete a very large amount of ACTH that may promote growth of an anterior pituitary adenoma. Serum ACTH levels are excessively high in patients with Nelson's syndrome. The prevalence of Nelson's syndrome after bilateral adrenalectomy ranges from 8 to 29%, with a time interval between the adrenalectomy and the development of the disease ranging from 6 months to 24 years.

6.9

Signs on Skeletal Radiographs

Osteoporosis and pathological bone fractures are commonly seen in chronic cases of CS due to the osteolytic effect of glucocorticoids on the bones.

Signs on CT and MRI

- Adrenal hyperplasia is checked by detecting bilateral increased thickness of the adrenal limbs (>5 mm). The adrenal limbs appear thicker than the adjacent diaphragmatic crus, with the preservation of the gland's general shape (Fig. 6.9.1).
- In Cushing disease and Nelson's syndrome, anterior pituitary adenoma is often found (Fig. 6.9.2).
- Renal pelvis lipomatosis shows proliferation of hypodense fat at the renal pelvis. Replacement lipomatosis of the kidney is seen as a fatty mass at the renal pelvis with markedly atrophied renal parenchyma (Fig. 6.9.3).

Conn's Syndrome (Hyperaldosteronism)

Conn's syndrome is a clinical pathological condition characterized by hypertension and hypokalemia due to excess secretion of aldosterone. Conn's syndrome commonly arises due to adrenal adenoma (80%) or adrenal hyperplasia (20%).

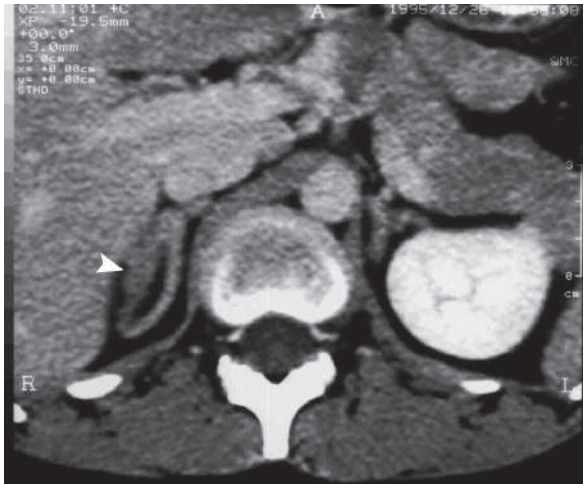

Fig. 6.9.1. Axial postcontrast CT image of a patient with adrenal hyperplasia shows enlargement of the lateral limb of the right adrenal gland (*arrowhead*)

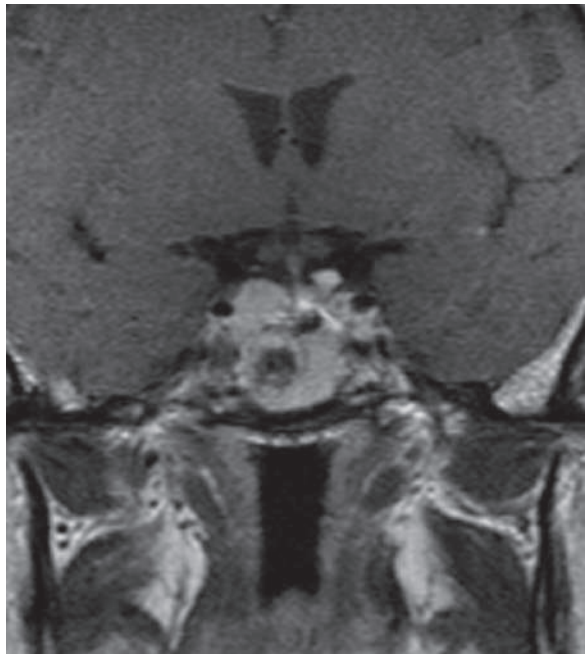

Fig. 6.9.2. Coronal T1W postcontrast MRI of the sellas shows large pituitary adenoma with inner cystic changes and infiltration of the left cavernous sinus in a patient with Nelson's syndrome. The patient had bilateral adrenalectomy in 1994, and he developed pituitary adenoma in 2006

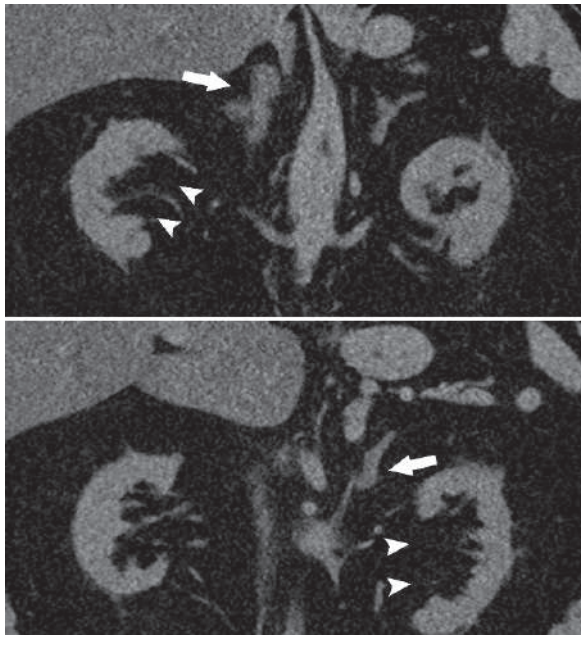

Fig. 6.9.3. Coronal sequential nonenhanced CT images of another patient with Cushing's syndrome (CS) show bilateral renal pelvis lipomatosis (*arrowheads*), and bilateral adrenal hyperplasia (*arrows*). Notice how the right adrenal gland is markedly thickened

Aldosterone secretion is mainly stimulated by plasma sodium depletion. Acute hemorrhage is a potent stimulus for aldosterone secretion. Aldosterone facilitates sodium absorption and facilitates potassium excretion in the kidney. Increased aldosterone secretion can occur in some conditions that are not related to a true pathology such as anxiety, adaptation to hot weather, high potassium intake, low sodium intake, and pregnancy (second and third trimesters).

Differential Diagnoses and Related Diseases

- *Liddle syndrome* is a rare autosomal dominant pediatric disorder characterized by failure to thrive, hypertension, metabolic alkalosis, hypokalemia, and an abnormally decreased rate of aldosterone and renin secretion. In this disease, the nephrone acts as if it were exposed to a large amount of aldosterone even when the aldosterone is absent. Children with Liddle syndrome present classically with a triad of hypertension, hypokalemia, and metabolic alkalosis.
- *Gordon syndrome* is a rare autosomal dominant disease characterized by hypertension, hyperkalemia, hyperchloremia, and normal renal glomerular function. Inconstant features include short stature and muscle weakness. The basic abnormality is related to excessive renal sodium retention, causing suppression of renin and aldosterone.
- *Bartter syndrome* is a disease characterized by hyperplasia of the juxta-glomerular apparatus and hyper-reninism leading to secondary hyperaldosteronism, metabolic alkalosis, severe hypokalemia, and normal blood pressure. Up to 80% of patients have peculiar facies, distinguished by triangular face, large eyes, and protruded ears. A milder form of Bartter syndrome associated with hypocalciuria and hypomagnesemia is called "*Gitelman syndrome*."

Signs on CT

- Adrenal hyperplasia: like CS.
- Adrenal carcinoma shows focal nodular enlargement of one or more adrenal limbs (>5 mm), with contrast enhancement after contrast injection. Regional lymphadenopathy may be found.

Addison's Disease

Addison's disease (AD) is a clinical condition that arises due to decreased or absent glucocorticoids.

AD typically results from adrenal hypofunction, usually when >90% of the gland cortex is destroyed. Patients with AD often present with hypotension, salt-craving, and hyperpigmentation due to increase ACTH secretion from the pituitary. The most common causes of AD are tuberculosis and autoimmune diseases. The disease is diagnosed by clinical picture and biochemistry, not by imaging. Imaging is often used to confirm the bilateral adrenal atrophy.

Differential Diagnoses and Related Diseases

- *Wolman's disease* is a rare neonatal, autosomal recessive, lysosomal storage disorder that manifests within the first week of life as striking hepatosplenomegaly, poor feeding, abdominal distension, and loose stool and vomiting. Liver cirrhosis and pulmonary failure may occur later in life due to lipid storage disease. Death usually occurs within the first year of life.
- *Allgrove's syndrome* (*Triple A syndrome*) is a rare disease characterized by *A*drenal hypoplasia and insufficiency, *A*chalasia, and *A*lacrimia (lacks of tear drops). The disease has an autosomal recessive mode of inheritance, and it is one of the ACTH insensitivity inherited diseases. Patients usually develop adrenal insufficiency (AD) in the first two decades of life. In contrast, symptoms of achalasia start from the early 6 months of age or early childhood.
- *Triple H syndrome* is a disease characterized by dysfunctional triad of the hypothalamic–pituitary axis (e.g., isolated ACTH deficiency), the hippocampus (e.g., impairment of anterograde memory), and hair follicles (e.g., alopecia universalis).

Signs on CT

- Whether the cause is tuberculosis or autoimmunity, both glands typically appear shrunken with calcifications due to chronic destruction and atrophy (Fig. 6.9.4).

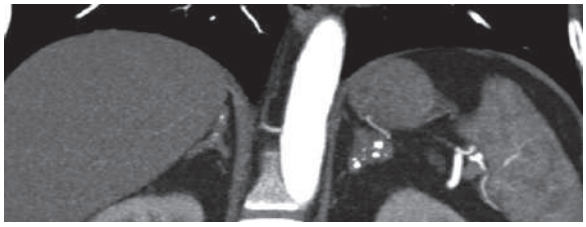

Fig. 6.9.4. Coronal postcontrast CT image of a patient with Addison's disease (AD) shows bilateral adrenal calcification (classical finding)

- In *Wolman's disease*, CT of the abdomen examination shows hepatosplenomegaly with bilateral adrenal calcifications. The clinical picture plus the CT findings are usually sufficient to confirm the diagnosis of Wolman's disease.
- In *Allgrove's syndrome*, CT usually shows bilateral adrenal hypoplasia like AD, but often in a child patient.

Pheochromocytoma

Pheochromocytoma is an adrenal medullary tumor that arises from chromaffin cells of the sympathetic system with increase secretion of catecholamine.

Pheochromocytoma is one of the most common causes of malignant hypertension. It is usually suspected in a young patient (<30 years) with history of hypertension. Classic pheochromocytoma symptoms are summarized by 5 Ps: high blood pressure, *p*ain (abdomen or heart), *p*erspiration, *p*alpitation, and *p*anic attacks.

Pheochromocytoma has a classical "rule of 10%": 10% bilateral, 10% inherited as autosomal dominant, 10% extra-adrenal (paragangliomas), and 10% occurring with von Hippel-Lindau syndrome.

Extra-adrenal intraabdominal pheochromocytoma is usually detected in the para-aortic area at the level of the celiac axis and the renal hilum, para-caval area at the level of the renal hilum, and the retrocaval area.

Rarely, paraganglioma may be found in the bladder wall. Patients present with signs of pheochromocytoma during micturition due to catecholamine release during micturition "*micturition attack*," and it is seen in 50% of cases. Although most cases of bladder paragangliomas are sporadic, they can be associated with Phakomatosis (e.g., von Hipple-Lindau syndrome).

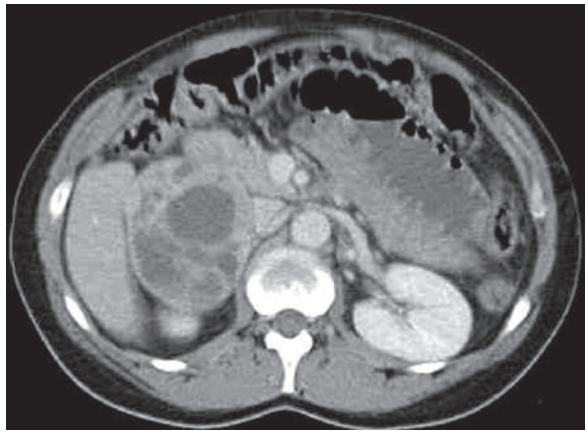

Fig. 6.9.5. Axial, delayed postcontrast CT image of a patient with pheochromocytoma shows large mass in the area of the adrenal gland with multiple cystic changes inside the mass

Signs on CT

- Pheochromocytoma is detected as round, homogeneous adrenal mass with intense contrast enhancement due to hypervascularity. The mass can show internal calcifications or cystic changes (Fig. 6.9.5). Rarely, pheochromocytoma can present like a cystic mass that mimics hydrated cyst (cystic pheochromocytoma).
- Bladder paraganglioma is detected usually as a single mass with well-defined or lobulated border that may show cystic necrosis, and circumferential ring calcification (highly suggestive).

Signs on MRI

Pheochromocytoma shows typically low T1 signal intensity and intense high T2 signal intensity, and marked contrast enhancement after contrast injection (Fig. 6.9.6). The fact that pheochromocytoma has intense T2 signal intensity is useful to detect ectopic paragangliomas, which shows the same MR signal characteristics.

Neuroblastoma

Neuroblastoma is a pediatric malignant tumor that arises from immature neuroblasts from the adrenal medulla, or the sympathetic chain. When the tumor histopathologically contains mature ganglion cells, it

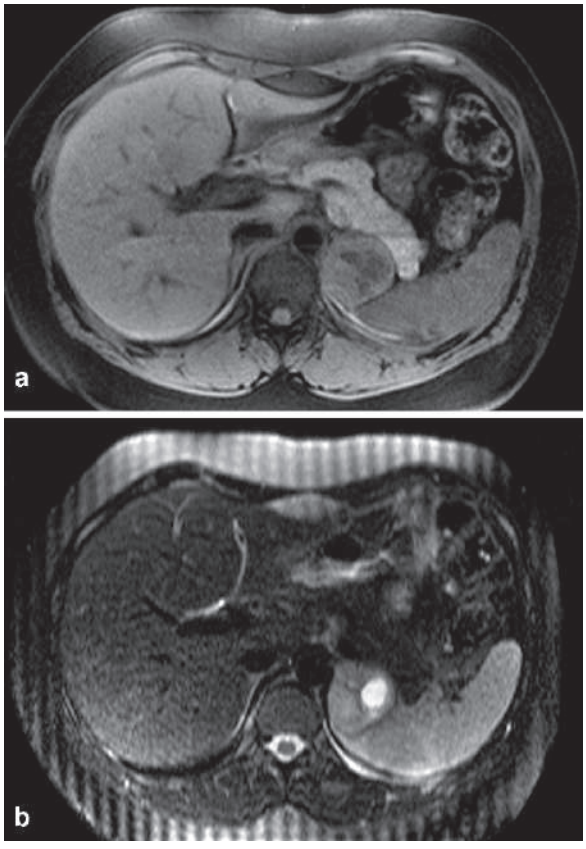

Fig. 6.9.6. Axial T1W (**a**) and T2W (**b**) nonenhanced MRI of a patient with left adrenal pheochromocytoma shows low signal intensity tumor in (**a**), and the intense T2 signal intensity of the tumor in (**b**)

is called "*ganglioneuroblastoma*." Both tumors are usually diagnosed <10 years of age.

Neuroblastoma constitutes for up to 15% of childhood cancer fatalities, and it is the second most common retroperitoneal mass in children after Wilm's tumor (nephroblastoma). The most common complain is pain, or abdominal fullness. Other uncommon symptoms include Horner's syndrome, limping, or irritability due to metastasis (Hutchinson's syndrome).

Differential Diagnoses and Related Diseases

- *Hutchinson's syndrome*: is characterized by neuroblastoma, extensive skeletal metastasis (especially skull), bone pain, and proptosis due to orbital metastasis.
- *Pepper syndrome*: is characterized by neuroblastoma and hepatomegaly due to extensive metastases.

Signs on CT and MRI

Neuroblastoma is detected as a large posterior mediastinal, pelvic, or retroperitoneal mass with calcification, cystic changes, or hemorrhage. A fluid–fluid level within the cystic changes indicates hemorrhage within the tumor. Rib or pedicular erosions can be seen in cases of mediastinal neuroblastoma. A full metastasis workup by scintigraphy, PET/CT, or whole-body MRI should be performed.

X-Linked Adrenoleukodystrophy

X-linked adrenoleukodystrophy (ALD) is X-linked recessive, peroxisomal disease characterized by accumulation of very long chain of fatty acids (called birefringent striations) within the brain, the adrenal cortex, and the testicular interstitial glands. Adrenal insufficiency (AD) occurs in 10% of cases.

ALD is both demyelinating and dysmyelinating disease. Demyelinating diseases are characterized by the formation of normal myelin, and then the myelin is destroyed. In contrast, dysmyelinating diseases are characterized by the formation of abnormal nonfunctioning myelin.

Pathologically, ALD is characterized by "three zone of demyelination": the outer zone is made of external actively demyelinating white matter; the middle zone is made of inflammatory demyelinating process in varying stages with inflammatory cell infiltration (sudanophilic macrophages); and the central inner zone is made up of burned-out axons with gliotic scar. Initially, ALD affects the parieto-occipital area. As the disease progresses, the temporal and frontal areas are affected too.

Male children with ALD often present between 4 and 8 years of age with progressive disturbance of gait, disturbance in vision and hearing, gradual deterioration in school work, behavioral changes, and dementia

Signs on CT

- Low-density white matter affecting mainly the occipital lobes and corpus callosum (almost always).
- Frontal and temporal lobes might be affected in advanced stages of the disease.

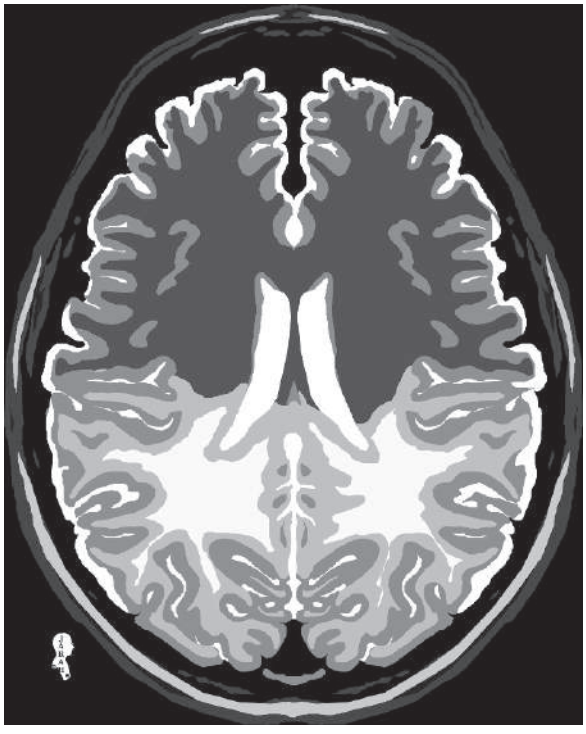

Fig. 6.9.7. Axial brain T2W MR-illustration shows the three areas of demyelination in bilateral parieto-occipital area typically seen in X-linked adrenoleukodystrophy (ALD)

Signs on MRI

- Variable high T2 signal intensities affecting the occipitoparietal lobes bilaterally and symmetrically representing the three zones of demyelination (almost pathognomonic appearance) (Fig. 6.9.7).
- Contrast enhancement occurs in the early acute phases along the outer margin of the demyelinating area (outer zones), while the center does not enhance (gliotic inner zone).
- MR spectroscopy shows low *N*-acetyl cystine concentration, and high cholin, glutamate, and glutamine concentrations.

Testicular Adrenal Rest Tumors

During embryogenesis, development of the primitive adrenal cortex occurs close to the gonads. Testicular adrenal rest tumors (TARTs) are tumors that arise from aberrant adrenal cortical tissues located in the testes from the primitive adrenal cortex residuals.

TARTs are usually felt as palpable testicular mass. The aberrant testicular adrenal rests may proliferate and grow in conditions with high ACTH levels like congenital adrenal hyperplasia, AD, Nelson's syndrome, and CS. In congenital adrenal hyperplasia, neonates present with bilateral testicular masses with or without salt wasting. TARTs can lead to precocious puberty and male infertility in patients with congenital adrenal hyperplasia.

Signs on US

TARTs are seen as multifocal, possibly bilateral hypoechoic masses within the testes. The masses may be mistaken for tumors or infarctions.

Signs on MRI

TARTS are detected as bilateral low T1 and T2 signal intensity lesions with marked contrast enhancement after contrast injection (Fig. 6.9.8).

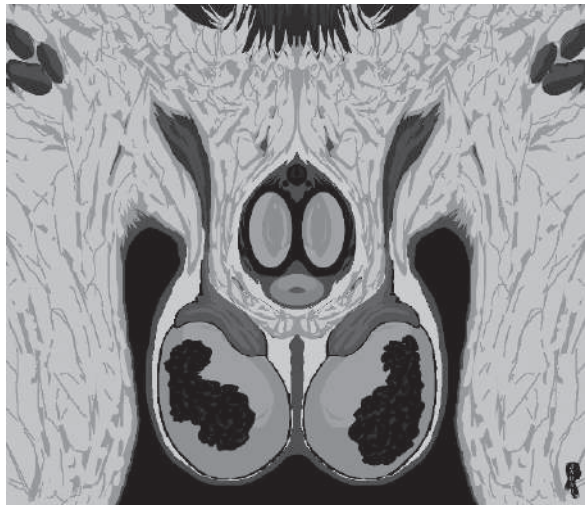

Fig. 6.9.8. Coronal T2W MR-illustration shows bilateral low T2 signal intensity lesions demonstrating testicular adrenal rests tumors

Selected References

1. A. J et al. Luetscher. Aldosteronism. Dis Mon. 1964;10(5):1–46.
2. Assadi FK et al. Liddle syndrome in a newborn infant. Pediatr Nephrol. 2002;17:609–11.
3. Assie G et al. The Nelson's syndrome…revisited. Pituitary 2004;7:209–15.
4. Dogra V et al. Sonographic appearance of testicular adrenal rest tissue in congenital adrenal hyperplasia. J Ultrasound Med. 2004;23:979–81.
5. Elsayes KM et al. Adrenal masses: MR imaging features with pathologic correlation. RadioGraphics 2004;24:S73–6.
6. Garel L et al. Nephrocalcinosis in Bartter's syndrome. Pediatr Nephrol. 1988;2:315–17.
7. Juan YH et al. Adrenal nodular hyperplasia with so called testicular tumor of adrenogenital syndrome (adrenal rests of both testes): a case report and review of the literature. Chin J Radiol. 2008;33:41–6
8. Kannan CR. Diseases of the adrenal cortex. Dis Mon. 1988;34:601
9. Kasar PA et al. Allgrove syndrome. Indian Journal of Pediatrics 2007;74:959–61.
10. Lockhart ME et al. Imaging of adrenal masses. Eur J Radiol. 2002;41:95–112.
11. Low G et al. Characteristic imaging findings in Wolman's disease. Clin Radiol Extra. 2004;59:106–8.
12. Ma ES et al. Tuberculous Addison's disease: morphological and quantitative evaluation with multidetector-row CT. Eur J Radiol. 2007;62:352–8.
13. Madrigal G et al. Bartter syndrome in Costa Rica: a description of 20 cases. Pediatr Nephrol. 1997;11:296–301.
14. Martinez-Aguayo A et al. Testicular adrenal rest tumors and Leydig and Sertoli cell function in boys with classical congenital adrenal hyperplasia. J Clin Endocrinol Metab. 2007;92:4583–9.
15. Mayo-Smith WW et al. From the RSNA refresher courses, state-of-the-art adrenal imaging. RadioGraphics 2001; 21:995–1012.
16. Otal P et al. Imaging features of uncommon adrenal masses with histopathologic correlation. RadioGraphics 1999; 19:569–81.
17. Puura A et al Gordon syndrome and succinylcholine. J Inherit Metab Dis. 2005;28:1157–8
18. Renken NS et al. Magnetic resonance imaging of the adrenal glands. Semin Ultrasound CT MRI 2005;26:162–71.
19. Rha SS et al. The renal sinus: pathologic spectrum and multimodality imaging approach. RadioGraphics 2004; 24:S117–31.
20. Shoaib SA et al. Primary hyperaldosteronism (Conne syndrome): MR imaging findings. Radiology 2000; 214:527–31.
21. Stikkelbroeck NMML et al. Testicular adrenal rest tumors. Eur Radiol. 2003;13:1597–603.
22. Waragi M et al MRI of adrenoleukodystrophy involving predominantly the cerebellum and brain stem. Neuroradiology. 1996;38:788–91

6.10

Sex Hormones Abnormalities

There are multiple pathological conditions that result in abnormalities in the estrogen–androgen levels in both males and females. Androgen is a term that refers to a compound, natural or synthetic, that controls or maintains the male masculine characteristics.

Radiology can help establish the diagnosis of many endocrinal pathological conditions that are related to abnormal levels of estrogen and androgen when combined with the clinical history, clinical examination, and laboratory investigations.

Polycystic Ovary Disease (Stein-Leventhal Syndrome)

Polycystic ovary disease (PCOD) results from inability of the mature follicular cyst to release its ova, resulting in formation of a follicular cyst.

Women with PCOD commonly present with amenorrhea, anovulation, infertility, and hirsutism; the latter symptom is due to increased levels of androgen. Criteria to diagnose PCO require two of the following features with exclusion of other causes:

- Presence of polycystic ovaries confirmed by ultrasound or MRI.
- Elevated levels of estrogen and androgen, with low levels of follicle-stimulating hormone (FSH) and luteinizing hormone (LH).
- Oligomenorrhea or amenorrhea. Up to 80% of women with oligomenorrhea have PCOD.

Signs on MRI

The typical feature of PCOD includes bilateral slightly enlarged ovaries with low-intensity central stroma accompanied by multiple, small (<1 cm) follicular cysts arranged at the peripheries (Fig. 6.10.1). Enlargement of the central stroma is an important sign differentiating this condition from other conditions with follicular cysts (e.g., ovarian hyperstimulating syndrome).

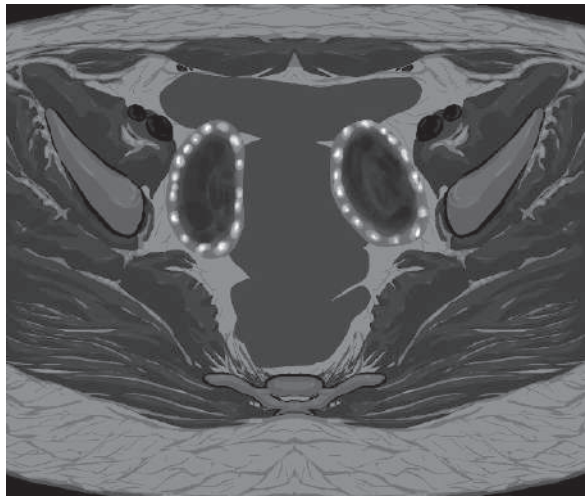

Fig. 6.10.1. Axial T2W fat-sat MR illustration demonstrates polycystic ovary disease (PCOD) seen as bilateral ovarian central hypointense stroma surrounded by peripheral multiple small cysts

Precocious Puberty

Precocious puberty is a condition characterized by premature development of secondary sexual characteristics before 8.5 years in girls, and 9.5 years in boys. Delayed female puberty is defined as a girl who shows no signs of secondary sexual characteristics by the age of 13 or absence of menstruation after age of 15. In contrast, delayed male puberty is defined as a male who shows no signs of secondary sexual characteristics by the age of 14.

Puberty is initiated by increasing the release of hypothalamic secretion of gonadotropin-releasing hormone (GnRH), which stimulates the release of anterior pituitary gonadotropins (LH and FSH). The gonadotropic hormones stimulate Leydig's cells in males to release testosterone, and ovarian follicles in females to release estrogen.

Precocious puberty is divided into isosexual and heterosexual from a clinical standpoint. *Isosexual precocious puberty* refers to physical sexual development that is appropriate to the individual (e.g., female with early feminine characteristics). In contrast, *heterosexual precocious puberty* refers to physical changes that are consistent with those of the opposite sex (e.g., female with early male characteristics).

Isosexual precocious puberty is further divided into two types: central or true (gonadotropin-dependent) and peripheral or incomplete (gonadotropin-independent).

Central precocious puberty (CPP) arises due to an increase in the release of gonadotropin and sex steroids due to premature activation of the hypothalamic–pituitary axis. In contrast, peripheral precocious puberty (PPP) arises due to excess release of gonadal sex steroids due to a peripheral cause (e.g., adrenal tumor).

CPP is characterized by true isosexual physical characteristics and gonads maturation. The girl exhibits all features of true puberty. In contrast, PPP is characterized by early secondary sexual characteristics without gonads maturation (incomplete). Maturation is incomplete with usually only one type of sexual characteristic developing early. In girls, if ovarian estrogen secretion predominates, breast development is the major manifestation of precocious puberty (premature thelarche). In contrast, if adrenal steroids secretion and early and rogenization predominates, pubic hair development in the absence of virilization is the major manifestation of precocious puberty (premature adrenarche). In summary, PPP indicates that the sexual development is not mediated by the pituitary gland.

In CPP, a disease, often a tumor, results in the early activation of the hypothalamic–pituitary axis. This early activation releases GnRH from the hypothalamus, which facilitates the release of FSH and LH from the adenohypophysis. The most common central lesion causing CPP is hypothalamic and tuber cinereum hamartomas. Hamartoma is defined as a group of normal cells in an abnormal configuration.

Radiological evaluation of a child with precocious puberty should include bone age assessment, ultrasound for the testes or the ovaries to exclude tumors, and MRI of the sella.

Differential Diagnoses and Related Diseases

McCuune-Albright syndrome is a rare disease which affects young females characterized by polyostotic fibrous dysplasia, precocious puberty, and skin hyperpigmentation (Café-au-laite spots).

Signs on Plain Radiographs

Bone age determination is an important step in evaluating a precocious puberty patient. Children with premature adrenarche or thelarche often show normal or slightly advanced bone age.

Signs on US

- In true precocious puberty, both testes are enlarged in males, and both ovaries are enlarged in females. In PPP, a tumor may be found in the testes or the ovaries.
- Patients with McCuune-Albright syndrome show large asymmetric ovaries bilaterally. The ovarian volume is the largest among all types of causes of precocious puberty (e.g., >4 cm^3). This large volume is often due to single or multiple cystic lesions with autonomous hormonal secretion.

Signs on MRI

Tuber cinereum hamartoma is seen as an isointense lesion, up to 2 cm in diameter, and is located at the region of the tuber cinereum, which lies between the pituitary stalk and the mamillary bodies. The lesion has low T1 and high T2 signal intensities, and does not enhance after contrast administration (because they are normal cells, but disorganized) (Fig. 6.10.2).

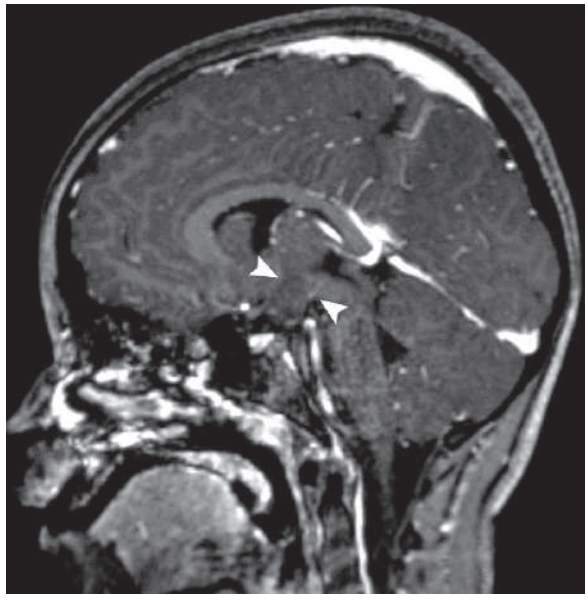

Fig. 6.10.2. Sagittal T1W postcontrast image of a patient with tuber cinereum hamartoma shows a lesion (*arrowheads*) located at the area of the tuber cinereum of the hypothalamus with no contrast enhancement

Van Wyk and Grumbach Syndrome

6.10

Van Wyk and Grumbach syndrome (VWGS) is a disease of young girls characterized by precocious puberty due to over-production of FSH and LH, and delayed bone maturation due to juvenile hypothyroidism.

The patient typically is a female child presenting with breast enlargement, enlarged labia minora, estrogenic changes in vaginal smear, with absence of pubic hair. Irregular vaginal bleeding and spontaneous ovarian hyperstimulation syndrome (*hyperraction luteinaris*) may be seen. Hyperraction luteinaris is a condition characterized by high serum levels of human chorionic gonadotropins (hCG) due to an intrinsic cause like normal pregnancy or gestational trophoblastic disease (e.g., hydatiform mole). The same condition is often produced in females receiving exogenous hCG to induce ovulation.

Patients with VWGS suffer from juvenile hypothyroidism with delayed bone maturation in the first place. The lower level of thyroid hormone may provoke the hypothalamus to secrete thyroid stimulating hormone (TSH). The excessive response by elevated TSH can cause pituitary hypertrophy, which in turn secretes higher levels of adenohypophysial hormones. The excess levels of adenohypophysial hormones are responsible for the precocious puberty and the other features of the disease.

Laboratory investigations in VWGS characteristically show low thyroxin (T_4 and T_3) levels, high TSH level, and high FSH and LH levels.

Signs on Plain Radiograph

Patients with VWGS typically show signs of osseous bone mineralization delay with bone age below their current age when radiographic bone age assessment is carried out. VWGS is the only form of precocious puberty in which the bone age is delayed.

Signs on US

- Thyroid US may be normal, or show signs of small atrophic thyroid gland.
- Abdominal US show bilateral or unilateral enlarged cystic ovarian mass due to hyperraction luteinaris

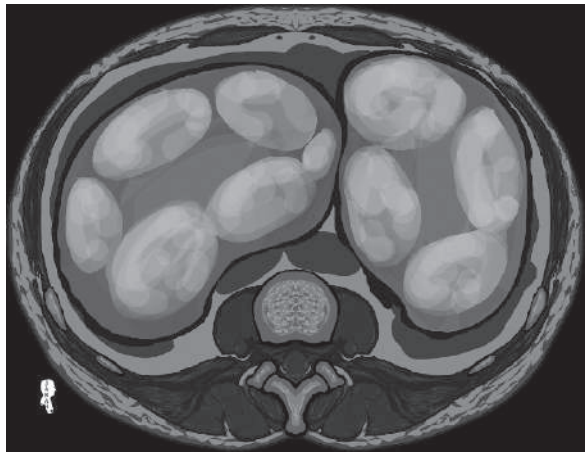

Fig. 6.10.3. Axial T2W MR illustration demonstrates bilateral enlarged ovaries with large cysts of almost uniform size within (hyperraction luteinaris)

Signs on MRI

- On abdominal MRI, hyperraction luteinaris is characterized by unilaterally or bilaterally enlarged ovaries with multiple, uniformly sized cysts that mimic cystic neoplastic disease (Fig. 6.10.3). In contrast, neoplastic cysts are seen as nonuniform cysts separated by septa. History and laboratory investigations are the key differential diagnostic tools.
- On MRI of the sella, anterior pituitary macro- or microadenoma is usually found.
- The anterior pituitary gland may show convex upper surface due to hypertrophy in the absence of neoplasm (normally it is concave).

Gynecomastia

Gynecomastia is defined as benign breast enlargement in males due to proliferation of the glandular breast tissue. In contrast, pseudo-gynecomastia is defined as increase in the breast size in males due to increased breast fatty content (e.g., like in obesity).

Physiological gynecomastia in males is seen in three age peaks. The first is in neonates due to transplacental passage of estrogen. The second is seen in mid-adolescent boys (10–14 years) due to imbalance between serum estrogen and androgen levels. The third is seen in patients aged 50–80 years old.

Pathological gynecomastia is related to increased serum level of estrogen in males, or reduced serum androgen level. Causes of pathological gynecomastia can be idiopathic (25%), drug-related in 15% of cases (e.g., cemetidin), Klinefelter's syndrome, and testicular tumors of the germ cell.

Testicular tumors are rare, and classically are divided into: germ cell tumors and stromal tumors. Stromal tumors make up approximately 5% of testicular tumors and may arise from Leydig, Sertoli, theca, granulosa, or lutein cells. When stromal elements coexist with germ cell elements, the tumor is called "gonadoblastoma." Leydig cells are cells that secrete testosterone, and are found within the testicular interstitium in males, while Sertoli cells are supporting cells and phagocytes. They form a junction with one another forming a blood–testis barrier. Sertoli cells are located within the seminiferous tubules in males.

Leydig cell tumors constitute approximately 2% of testicular tumors, and commonly seen in male children between 3 and 6 years old, as well as adults between 30 and 50 years of age. Patients present with painless scrotal swelling, and the tumors are hormonally active in up to 30% of cases. Serum androgen or estrogen levels are high causing precocious puberty, gynecomastia, or impotence.

Testicular sertoli cell tumors are rare, and they lead to feminization and gynecomastia in males. A distinct subtype of Sertoli cell tumors is called "large-cell calcifying Sertoli cell tumor," which is found in genetic syndromes like Peutz-Jeghers syndrome and tuberous sclerosis. Sertoli cell tumors may develop metastases in 10–15% of cases. In women, ovarian Sertoli-Leydig cell tumors are a common cause of virilization in young women.

Primary testicular germ cell tumors may regress spontaneously with formation of distant metastases, a phenomenon known as "burned-out germ cell tumor." The phenomenon is poorly understood, and is believed to be caused by high tumor metabolic rate that makes the tumor outgrow its blood supply. Patients present with normal size testes and widespread germ cell tumor metastases, making physicians look for the primary germ cell tumor in extragonadal regions like in the thoracic mediastinum, retroperitonium, or the pineal gland, which all return negative in the end.

The role of imaging in gynecomastia is reserved to search for tumors that may cause gynecomastia, assuming no other cause is found by history and clinical examination.

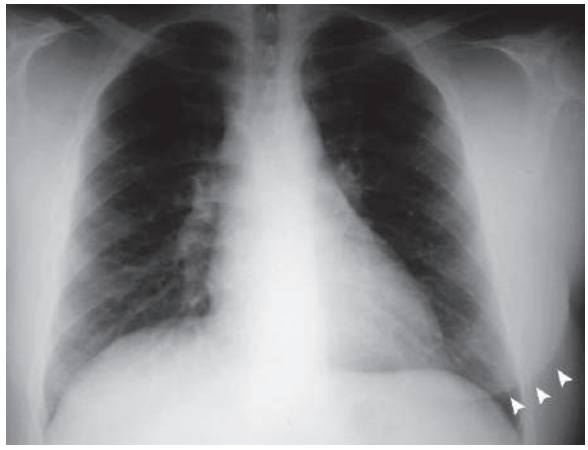

Fig. 6.10.4. A plain chest radiograph of a patient with gynecomastia demonstrates unilateral enlarged breast shadow

Signs on Plain Radiographs

Gynecomastia is detected as unilateral or bilateral breast shadow enlargement (Fig. 6.10.4)

Signs on US

- *Leydig cell tumors* are seen as hypoechoic lesions within the testes with peripheral vascularity on color Doppler sonography. Larger tumors show cystic changes and mixed echo-texture. Large-cell calcifying Leydig cell tumors are detected as multiple areas of high echogenicity with acoustic shadowing representing calcification.
- *Testicular Sertoli cell tumors* are seen usually as bilateral hypoechoic lesions with areas of dense echogenic foci due to calcified scars (burned-out appearance), or as multicystic lesion arranged in a "spoke wheel" configuration.

Signs on MRI

- *Testicular Sertoli cell tumors* show low T1 and high T2 signal intensity with marked contrast enhancement after contrast injection. History and elevated androgen or estrogen serum levels are important supportive tools for diagnosis.

6.10

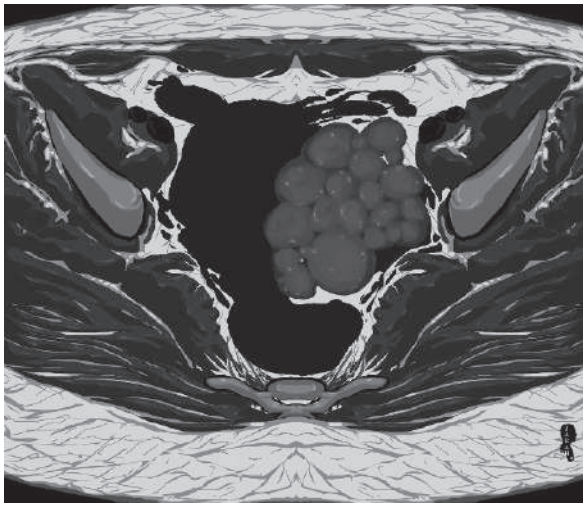

Fig. 6.10.5. Axial T1W nonenhanced MR illustration demonstrates left-sided multilobulated ovarian mass with internal small cystic lesions representing ovarian Sertoli cell tumor

- *Ovarian Sertoli cell tumor* is detected as unilateral, multilobulated mass with or without internal cysts. The mass can show low T2 signal depending on the extents of fibrous stroma. After contrast injection, the cells show intense heterogeneous contrast enhancement (Fig. 6.10.5).

Intersex Disorders

Intersex disorders are a group of diseases characterized by ambiguous genitalia and abnormalities in sexual differentiation. *Ambiguous genitalia* are defined as external genitalia that do not have a typical male or female anatomic appearance. A person's phenotypic sex results from the differentiation of the Müllerian ducts and external genitalia under the influence of hormones and transcription factors.

There are four main categories of intersex disorders: female pseudohermaphroditism, gonadal dysgenesis, true hermaphroditism, and male pseudohermaphroditism. Imaging plays a role in detecting abnormalities in the internal pelvic sex organs, and early detection of malignant masses formed within these organs. There is an increased prevalence of stromal and gonadal tumors in patients with intersex disorders. Image analysis included evaluation of the presence or absence of the uterus, ovaries, testes, penis, and clitoris.

Female Pseudohermaphroditism

Female pseudohermaphroditism is a female genetically (46, XX) with two ovaries for gonads, but their external genitalia show a variable degree of virilization due to exposure to excess androgens in utero. *Virilization* refers to male sexual characteristics due to androgen exposure.

Female pseudohermaphroditism most commonly arises due to *congenital adrenal hyperplasia* (*CAH*). In CAH, there are enzymatic defects in cortisol production pathway at certain key positions. These enzymatic defects cause excessive accumulation of the intermediate steroids compounds that are produced before the metabolic block. Some of these intermediate steroids are converted into androgenically active substances. This excess androgen exposure causes virilization of the external genitalia, which is manifested commonly as enlarged clitoris (clitoromegaly).

Signs on US

CAH is seen as enlarged adrenals located above the kidneys with a "cerebriform patten" (the adrenal glands have multiple coils that look like cerebral gyri). The adrenal gland limbs are commonly over 20 mm long, 4 mm wide, and with normal corticomedullary differentiation.

Signs on MRI

- MRI demonstrates masculinized external genitalia with normal ovaries, fallopian tubes, uterus, and vagina. The clitoris mimics a small penis due to prominent corpora cavernosa and corpus spongiosum (Fig. 6.10.6).
- The vagina and the uterus may be filled with urine due to urogenital sinus formation.

Male Pseudohermaphroditism

In male pseudohermaphroditism, patients are genetically male (46, XY) with two testes for gonads, but their external genitalia show a variable degree of feminization due to defect in the testes, or testosterone metabolism.

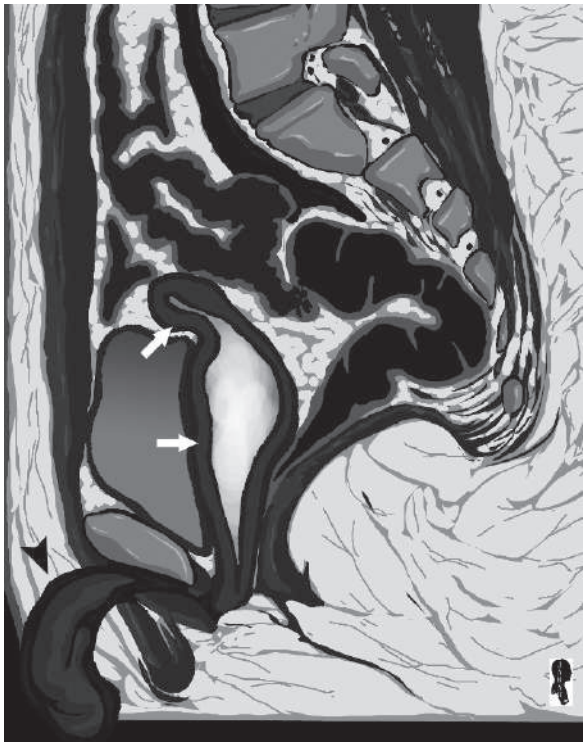

Fig. 6.10.6. Sagittal T1W pelvic MR illustration demonstrates enlarged clitoris with prominent corpora cavernosa and corpus spongiosum (*black arrowhead*) with normal vagina and uterus (*white arrows*) in a patient with female pseudohermaphroditism

The phenotype of the male pseudohermaphroditism ranges from completely female external genitalia to a mild male phenotype with hypospadia or cryptorchidism. *Cryptorchidism* is a condition characterized by both abnormal testicular development and failure of the intra-abdominal testes to descend into the scrotum. The testes may be located at any point along the normal descent route. This condition can be seen in up to 30% in premature infants, and up to 8.8% in full-term infants.

Male pseudohermaphroditism can be classified into eight groups according to the etiology:

- *Leydig cells failure*: Leydig cells are testicular cells that secrete testosterone in males. Failure of testosterone secretion results in male pseudohermaphroditism
- *Testosterone synthesis defects*: any cause of testosterone synthesis results in male pseudohermaphroditism.
- *Androgen insensitivity syndrome* (AIS) (*Morris syndrome*): this syndrome, also known as *testicular feminization syndrome*, arises due to insensitivity of the body cells to testosterone due to mutation of the steroid-binging receptors. Children with AIS exhibit a female external genitalia, although the karyotype is (46, XY), and testes are located internally. Most patients with AIS are not diagnosed until puberty, when they are investigated for amenorrhea.
- *5α-Reductase deficiency* is an autosomal recessive condition characterized by defect in conversion of testosterone to the active form dihydrotestosterone through the enzyme 5α-reductase.
- *Persistent Müllerian duct syndrome* (*PMDS*): as mentioned before, Sertoli cells are supporting cells and phagocytes. In the embryo, Sertoli cells secrete anti-Müllerian inhibitory substances that cause apoptosis and regression of the Müllerian ducts, facilitating the male phenotype development. Failure of Sertoli cells to secrete the Müllerian inhibitory substances results in male pseudohermaphroditism.
- *Testicular dysgenesis*: abnormal formation of the testes can result in male pseudohermaphroditism.
- *Congenital anorchia* (*vanishing testes syndrome*) is a disease where the testes are absent. Loss of the testes before8 weeks' gestation results in a male (46, XY) with female external and internal genitalia. A loss of testes function after the critical male differentiation period at 12–14 weeks' gestation results in a normal male phenotype externally with anorchia internally.
- *Exogenous source*: due to insult to the male development mechanism in utero, often due to maternal ingestion of progesterone or estrogen or various environmental hazards.

Differential Diagnoses and Related Diseases

- *PAGOD (Mecham) syndrome* is an extremely rare disease characterized by pulmo, and pulmonary artery hypoplasia, agonadism, omphalocele/diaphragm defect, and dextrocardia. Most infants die shortly after birth due to cardiopulmonary problems.
- *Denys-Drash syndrome* (*DDS*) is a disease characterized by male pseudohermaphrodism, progressive glomerulopathy, and urinary tract tumors (e.g., Wilm's tumor). Nephropathy starts in infancy as a diffuse mesangial sclerosis and rapidly progresses to end-stage renal failure by the age of 3 years. DDS have overlap manifestations with Mecham syndrome, which is characterized by congenital diaphragmatic

hernia, double vagina, sex reversal, and cardiac malformations. Unlike DDS, those with Mecham syndrome do not develop Wilm's tumor.

- *Fraiser syndrome* is a disease characterized by male pseudohermaphrodism, progressive glomerulopathy, and urinary tract tumors (e.g., Wilm's tumor). Unlike DDS, nephropathy is a steroid-resistant focal segmental sclerosis, and it starts in childhood and progresses to end-stage renal failure by the second or third decade of life. Both Fraiser and DDS may present with congenital diaphragmatic hernias.
- *Aarskog (facial–digital–genital) syndrome* is a disease characterized by characteristic short status and facial features (e.g., hypertelorism), digital abnormalities (e.g., short fingers), and genital abnormalities (e.g., cryptorchidism). Radiographic findings of Aaskorg syndrome show maxillary hypoplasia, hypoplasia of terminal phalanges of fingers, spina bifida occulta, and hypoplastic middle phalanges of the toes. Children with Aaskorg syndrome may show features of growth hormone deficiency.
- *LEOPARD syndrome* is a disease characterized by Lentigines (pathognomonic), electrocardiographic (ECG) conduction defects, ocular hypertelorism, pulmonary stenosis, abnormal genitalia, retardation of growth, and sensorineural deafness. To establish LEOPARD syndrome diagnosis, lentigines and two of the other characteristic features need to be fulfilled. The disease has an autosomal dominant mode of inheritance.

Signs on US

Cryptorchidism can be detected by US as an isoechoic or hypoechoic mass relative to the normal testes located in the inguinal canal (70% of cases), or the prescrotal region just beyond the external inguinal ring (20%).

Signs on CT and MRI

- Both testes are present either in the scrotum or in the inguinal canal (undescended testes). The external genitalia are incompletely masculinized, or frankly ambiguous. Prostatic tissue appears to be present.

- *AIS*: patients with AIS may show cystic lesions within the pelvis representing residual parts of the Müllerian system. It is important to screen patients with male pseudohermaphroditism radiologically because of the high risk of malignant transformation of the nonfunctioning Müllerian system residuals. Bilateral gonadectomy is recommended in patients with AIS because of the high incidence of seminomas.
- *PMDS*: patients with PMDS are males with uterus and fallopian tubes inside their pelvis. Two forms are present, the male and the female forms. The male form, also called *hernia uteri inguinale*, is characterized by a male with one testis descended in the scrotum and the other testis located at the contralateral ovary position in the pelvis. In the female form, the phenotype is of a female with a hypoplastic, blind-ended uterus located behind the bladder. The testes are bilaterally located in the "ovarian" position (not within the scrotum) (Fig. 6.10.7).

True Hermaphroditism

In true hermaphroditism, patients have both ovaries and testes for gonads, often due to chromosome mosaicism (*chimerism*).

There are three types of true hermaphroditism:

- *Lateral true hermaphroditism*: patients have a testis on one side and an ovary on the other side in the pelvis.
- *Unilateral true hermaphroditism*: patients have both a testis and an ovary on one side, and a testis or an ovary on the other side of the pelvis.
- *Bilateral true hermaphroditism*: patients have both a testis and an ovary on both sides of the pelvis.

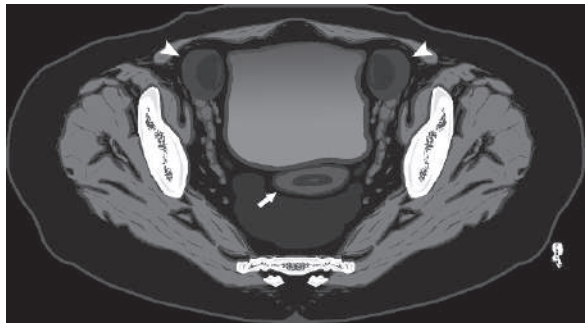

Fig. 6.10.7. Axial pelvic CT illustration demonstrates the female form of persistent Müllerian duct syndrome (PMDS). The uterus is detected behind the bladder (*arrowhead*), and the testes are located at the position of the ovaries bilaterally (*arrowheads*)

Patients with true hermaphroditism also show ambiguous genitalia, with hypospadias, cryptorchidism, and incomplete fusion of the labioscrotal folds.

Signs on MRI

- The external genitalia are ambiguous.
- There are both testes and ovaries found in the pelvis according to the type (lateral, unilateral, or bilateral).
- Hypoplastic uterus is found in almost all cases.

Gonadal Dysgenesis

Patients with gonadal dysgenesis are male pseudohermaphroditism with Müllerian duct structures. Gonadal dysgenesis disorders are a spectrum of anomalies that include pure gonadal dysgenesis, partial gonadal dysgenesis and mixed gonadal dysgenesis. In pure gonadal dysgenesis, patients have bilateral streak gonads (dysfunctional gonads without germ cells). In mixed and partial gonadal dysgenesis, there is one testis on one side, and a streak gonad on the other side.

Gonadal dysgenesis is characterized by defect in the sex-determination region on chromosome Y (SRY). The infant initially starts as a male karyotype (46, XY), but due to the failure in the SRY, the testes are not developed and the female development takes place (sex reversal), despite the presence of the Y chromosome. The patient is a female with XY karyotype and Müllerian derivatives including uterus, fallopian tubes, and cervix. Turner syndrome (45, XO) is an example of gonadal dysgenesis disorder.

Swyer syndrome is an uncommon form of pure gonadal dysgenesis. The male child with Swyer syndrome looks female externally, but the karyotype is (46, XY) with a nonfunctioning Y chromosome. Patients with Swyer syndrome may have *multiple pterygium syndrome*, which is characterized by multiple body contractures since birth with webbing of the neck, elbows, knees, and intracrural areas.

Streak gonads should be removed surgically because the risk of malignant transformation within the first two decades of life can reach up to 30% of cases.

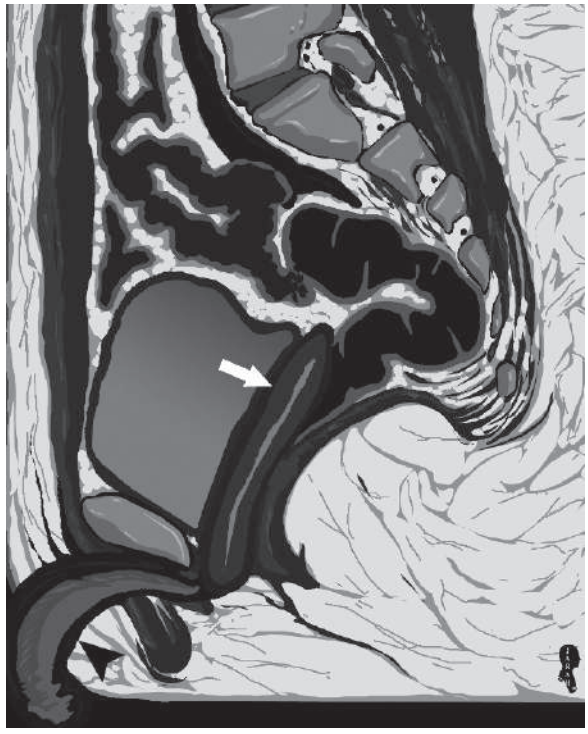

Fig. 6.10.8. Sagittal T1W pelvic MR illustration demonstrates findings in a patient with gonadal dysgenesis. There is vagina with absent uterus representing Müllerian duct derivatives (*white arrow*), in the presence of the penis (*black arrowhead*)

Signs on MRI

The patient shows both testes and Müllerian duct derivatives (e.g., uterus) (Fig. 6.10.8).
Streak gonads are difficult to detect and usually seen as low signal intensity stripes on T2W images. High signal intensity of streak gonads on T2W images could represent a sign of malignant transformation.

For Further Reading

1. Franceschi R et al Prevalence of polycystic ovary syndrome in young women who had idiopathic central precocious puberty. Fertil Steril. 2009. doi:10.1016/j.fertnstert.2008.11.016
2. Johnsen DE et al MR imaging of the sellar and juxtasellar regions. Radiographics. 1991;11:727–58
3. Browne LP et al Van Wyk and Grumbach syndrome revisited: imaging and clinical findings in pre- and postpubertal girls. Pediatr Radiol. 2008;38:538–42

4. Jagadhish LCTK. Van Wyk and Grumbach syndrome (a syndrome of incomplete isosexual precocity and juvenile hypothyroidism). MJAFI. 2002;58:343–5
5. Sharafuddin MJA et al MR imaging diagnosis of central precocious puberty: importance of changes in the shape and size of the pituitary gland. AJR. 1994;162:1167–73
6. Hyun G et al A practical approach to intersex in the newborn period. Urol Clin N Am. 2004;31:435–43
7. Yanai Y et al Androgen insensitivity syndrome with serous gonadal cyst. Fertil Steril. 2008;90:2018.e9–11
8. Karabulut N et al Stromal tumor of the sex cord in a woman with testicular feminization syndrome: imaging features. AJR. 2002;178:1496–8
9. Wu H-C et al Persistent Müllerian duct syndrome with seminoma: CT findings. AJR 2000;174:102–4.
10. Narlawar RS et al Persistent mullerian duct syndrome with teratoma in an ectopic testis: imaging features. Eur Radiol. 2001;11:955–8
11. Erdem CZ et al Polycystic ovary syndrome: dynamic contrast-enhanced ovary MR imaging. Eur J Radiol. 2004; 51:48–53
12. Wang Y-C et al Maternal and female fetal virilization caused by pregnancy luteoma. Fertil Steril. 2005;84:509.e15–7
13. Elon Gale M. Hermaphroditism demonstrated by computed tomography. AJR. 1983;141:99–100
14. Hernanz-Schulman M et al Sonographic findings in infants with congenital adrenal hyperplasia. Pediatr Radiol. 2002;32: 130–7
15. Chen H-Y et al Pure XY gonadal dysgenesis and agenesis in monozygotic twins. Fertil Steril. 2006;85:1059.e9–11
16. Angle B et al XY gonadal dysgenesis associated with a multiple pterygium syndrome phenotype. Am J Med Genet. 1997;68:7–11
17. Hedlund GL et al Disorders of puberty: a practical imaging approach. Semin Ultrasound CT MRI. 1994;15:49–77
18. Chavhan GB et al Imaging of ambiguous genitalia: classification and diagnostic approach. RadioGraphics. 2008;28: 1891–904
19. Choi HK et al MR imaging of intersexuality. RadioGraphics. 1998;18:83–96
20. Christensen JD et al The undescended testis. Semin Ultrasound CT MRI. 2007;28:307–16
21. Kim JB et al A case of PAGOD syndrome with hypoplastic left heart syndrome. Int J Cardiol. 2007;114:270–1
22. Cho HY et al Hydrothorax in a patient with Denys-Drash syndrome associated with diaphragmatic defect. Pediatr Nephrol. 2006;21:1909–12
23. Aso C et al Gray-scale and color Doppler sonography of scrotal disorders in children: an update. RadioGraphics. 2005;25:1197–214
24. Jung SE et al CT and MRI findings of sex-cord stromal tumor of the ovary. AJR. 2005;185:207–15
25. Woodward PJ et al Tumors and tumorlike lesions of the testes: radiologic-pathologic correlation. RadioGraphics. 2002; 22:189–216
26. Kodama M et al Aarskog syndrome with isolated growth hormone deficiency. Eur J Pediatr. 1981;135:273–6
27. Yagubyan M et al LEOPARD syndrome: a new polyaneurysm association and an update on the molecular genetics of the disease. J Vasc Surg. 2004;39:897–900

Chapter 7

Rheumatology

CONTENTS

J. A. Al-Tubaikh: *Internal Medicine* – An Illustrated Radiological Guide
DOI: 10.1007/978-3-642-03709-2_7, © Springer-Verlag Berlin Heidelberg 2010

7.1 Rheumatoid Arthritis

Rheumatoid arthritis (RA) is a chronic, multisystemic, nonspecific inflammatory disease with unknown etiology that primarily affects the joints and the skeletal muscles.

RA is diagnosed by qualifying certain criteria. Four of the following criteria should be present for more than 6 months to fulfill the diagnosis of RA:

- Morning stiffness that lasts at least an hour before maximal improvement.
- Soft-tissue swelling and arthritis in a bilateral symmetrical fashion of at least three joints (polyarthritis).
- Swelling of the metacarpophalangeal, proximal phalangeal, or wrist joints.
- Subcutaneous rheumatoid nodules.
- A positive test for rheumatoid factor.
- Radiographic signs of RA.

In joints, the main pathology of RA is related to synovial inflammation and proliferation. The normal synovium is attached to the inner joint capsule in synovial joints. The articulating surface of the joint is covered with cartilage except for a small region at the insertion of the joint capsule. This area is covered only by synovium, and it is called the "bare area." Synovial inflammation and bone erosions start from this area in RA. The granulation tissue (pannus) that results from the chronic synovial inflammation adheres and extends to the articular cartilage and the subchondral surface. This extension causes bone resorption and articular adhesions that may ossify, and leads to bony fusion. Intra-articular loose bodies may develop as a consequence of the inflammatory process. The loose intra-articular bodies are composed of destroyed cartilage or hypertrophied synovium.

RA affects mainly women between 30 and 40 years of age. Any joint in the body can be affected by RA, but the disease often affects the small joints of the hands excluding the terminal phalanges. Wrists, knees, and feet are also commonly affected by RA. Patients often present with morning stiffness, small joints swelling due to tenosynovitis, muscular pain, and stiffness commonly after a period of immobilization. Extra-articular manifestations of RA make the disease mixed in its early stage with systemic lupus erythematosus (SLE). SLE, however, may be seen in patients with chronic RA.

Nervous system manifestations in RA can be categorized into four groups: central nervous system rheumatoid nodules, cerebral vasculitis, cervical myelopathy due to atlantoaxial sublaxation, and peripheral neuropathy. The atlantoaxial sublaxation may lead to the development of "*double crush syndrome*." The double crush hypothesis refers to the concept that a single lesion in the course of a nerve predisposes that nerve to a second lesion further along its course. This phenomenon is often observed in patients with thoracic outlet syndrome, where compression of the brachial plexus can result in the development of carpal tunnel syndrome. Median nerve neuritis (carpal tunnel syndrome), Raynaud's phenomenon, and hyperemia of the palms (liver palms) may be seen in cases of rheumatoid peripheral neuropathy and sympathetic nervous system hyperactivity. Moreover, the cervical manifestations of RA can be seen as rheumatoid discitis, and myelopathy due to thickening of the dura. Rheumatoid discitis arises due to annulus fibrosis and replacement of the normal intravertebral disc by rheumatoid pannus.

Rheumatoid nodules (10–20%) are seen in juxta-articular surfaces or on the extensor surfaces of the arm and elbows, especially the olecranon surface. Rheumatoid nodules consist histologically of three zones: a central zone of necrotic tissue, a middle zone of histiocytes and monocytes, and an outer zone of chronic inflammatory granulation tissue. They can affect any part of the body including the heart, larynx, eye, Achilles' tendon, and lungs. The presence of rheumatoid nodules is indicative of severe disease. An uncommon complication of rheumatoid nodule includes breakdown of the overlying skin and discharge of the content (*fistulous rheumatism*). Rarely, rheumatoid nodules may present as linear, elongated, cord-like subcutaneous bands.

Moderate hypochromic normocytic anemia can be found in chronic RA due to anemia of chronic disease. Diseases that can be associated with RA are psoriasis (8%), ulcerative colitis, amyloidosis, and asthma. Lymphadenopathy can be seen in cases of RA.

Rheumatoid nodulosis (*RN*) is a rare, benign RA variant characterized by the presence of subcutaneous rheumatoid nodules with absence of synovitis, absence of systemic manifestations in benign course, and mild radiological findings. Classically, the presence of

rheumatoid nodule is a sign of advanced RA with poor prognosis. As a rule, the benign course of the disease and the mild radiological findings are what differentiate RA from RN. RN is found in up to 25% of classical RA cases, and presents between ages 30 and 50 years. RN has a male predominance (81%), whereas RA has a female predominance. The subcutaneous rheumatoid nodules in RN appear at the onset of clinical symptoms, and are usually observed over bony surfaces like the back of the hands and the olecranon (Fig. 7.1.1).

CNS Manifestations of RA include vasculitis, pachymeningitis, leptomeningitis, rheumatoid nodules formation, stroke, seizures, and encephalopathy. The diagnosis of cerebral manifestation of RA must be supported by high titres of RF and anticyclic citrullinated peptide (Anti-CCP), clinical symptoms of RA, and good response to immunosuppressive therapy. Classically, CNS manifestations of RA are associated with subcutaneous rheumatic nodules, cutaneous vasculitis, and peripheral neuropathy (advanced stage of the disease).

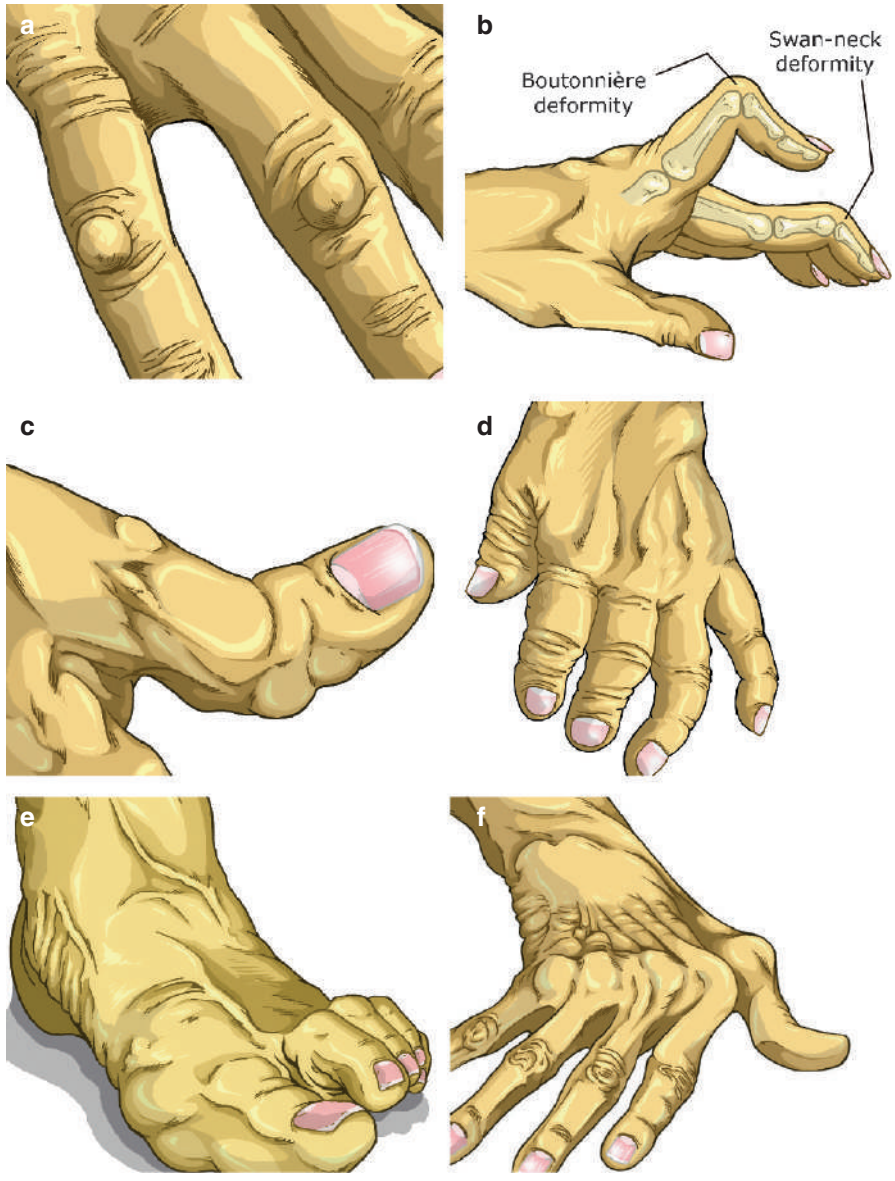

Fig. 7.1.1. An illustration demonstrates different manifestations of rheumatoid arthritis (RA) in the hand: (**a**) rheumatoid nodulosis, (**b**) Boutonnière and swan-neck deformities, (**c**) Hitchhiker thumb deformity, (**d**) Opera-glass hand, (**e**) Hammer toe deformity, and (**f**) ulnar deviation

Differential Diagnoses and Related Diseases

7.1

- *Juvenile rheumatoid arthritis* (*JRA*) is a form of RA that emerges before 16 years of age. It has similar manifestations like adult RA.
- *Still's disease* is a rare disease of unknown origin characterized by episodes of spiking fever, skin rash, hepatosplenomegaly, and JRA. It affects 20% of patients with JRA, and RF and antinuclear antibodies are negative. It is usually a disease of exclusion.
- *Caplan's syndrome* is a disease characterized by the association of RA with coal worker's lung (pneumoconiosis). On radiographs, the disease is characterized by multiple, well-defined, round opacities 0.5–5 cm in size that mimic pulmonary metastases, representing of necrobiotic rheumatoid lung nodules. Calcification of these opacities is common.
- *Felty's syndrome* is a disease characterized by the triad of RA, splenomegaly, and leucopenia. It is a rare extra-articular manifestation of RA and affects less than 1% of patients. Felty's syndrome patients are often women between 55 and 65 years of age, with long-standing RA (10–15 years). Hepatomegaly and abnormal liver profile are seen in up to 65% of cases, with hepatic nodular hyperplasia being the most common hepatic lesion found in these patients. Leg ulceration with hyperpigmentation occurs in 25% of cases.
- *Pseudo-Felty's syndrome* (*large granular lymphocyte syndrome*) is a disease characterized by RA and proliferation of large granular lymphocytes (LGL). LGLs are a distinct subset of peripheral blood mononuclear cells, with a natural killer activity. Patients present clinically with RA, splenomegaly, and leucopenia similar to classic Felt's syndrome. The only distinction is the laboratory detection of abnormal high levels of LGLs in the blood.
- *Progressive pseudorheumatoid dysplasia* (*PPsRD*) is a rare, autosomal recessive disease characterized by polyarthralgia, multiple joint contractures, prominent interphalangeal joints, and short stature. The disease starts to manifest between 3 and 4 years as progressive cartilage destruction in the absence of synovitis. Rheumatoid factor is typically negative, and genetic testing shows positive WISP3 gene. The disease can be mistaken for JRA and Scheuermann's disease. In contrast to JRA, PPsRD lacks the lymphadenopathy and fever that can be seen in Still's disease. The disease is diagnosed clinically by identifying enlarged carpometacarpal joint bilaterally (Fig. 7.1.2). The disease is essentially diagnosed radiologically due to its typical radiological features, with genetic and rheumatoid factor laboratory testing as supporting tests for final conformation.

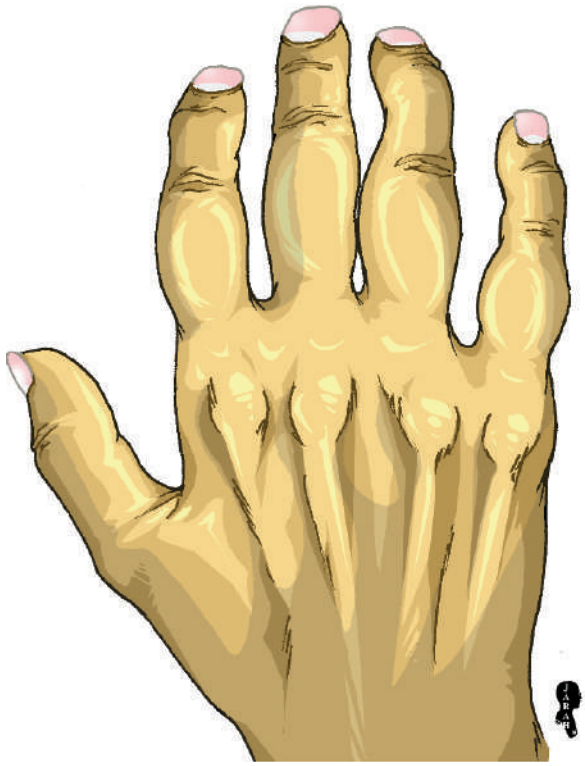

Fig. 7.1.2. An illustration demonstrates the enlarged carpometacarpal and proximal metacarpophalangeal joints in progressive pseudorheumatoid dysplasia (PPsRD)

- *Lupus polyarthritis* is one of the major manifestations of SLE Arthritis in SLE and is characterized by mild arthralgia, tenosynovitis, almost absent erosive changes on radiographs, and joint deformities without bone destruction. Concurrence of RA and SLE is termed "*rhupus*."
- *Remitting sero-negative symmetrical synovitis with pitting edema* (*RS_3PE syndrome*) is a disease characterized by sudden onset of symmetrical synovitis with pitting edema of the extremities. Although the etiology is unknown, RS_3PE syndrome is known to co-occur with diseases like RA, polymyalgia rheumatica, paraneoplastic syndromes, chronic gout, lymphoma, and *Mycoplasma* pneumonia. Constitutional symptoms like fever, fatigue, and weight loss are reported. Patients classically presents with symmetrical polyarthritis of both hands and feet particularly affecting the MCP and PIP joints, with pitting edema that can be mistaken with RA. Other joints can be affected like the wrists, shoulder, knees, and ankles. RS_3PE

syndrome is characteristically associated with high serum CRP and ESR levels, with sero-negative RF and ANA levels. Characteristically, the serum level of vascular endothelial growth factor (VGEF) is higher than any other rheumatic disorder, and it helps to establish the diagnosis with the radiological findings. The condition responds well to steroid therapy.

- *Jaccoud's arthropathy* is a nonerosive, chronic, progressive, almost painless arthropathy characterized by severe deformities and joint sublaxations of the hands and feet with well-preserved functions. In the hands, Jaccoud's arthropathy presents classically with painless ulnar deviation, swan-neck, and boutonnière deformities of the fingers and thumb, making the disease easily mistaken for RA. Jaccoud's arthropathy is classically seen in cases of long-standing rheumatic fever, SLE, scleroderma, sarcoidosis, dermatomyositis, and rarely psoriasis. However, the disease can present in the absence of other diseases (idiopathic Jaccoud's arthropathy).

Signs on Plain Radiographs

- Osteoporosis that can be generalized or focal (juxta-articular), due to hyperemia and disuse (Figs. 7.1.3 and 7.1.4).
- Joint space narrowing due to destruction of the articular surface (Figs. 7.1.3 and 7.1.4). Typically, the distal interphalangeal joint (DIP) is spared in RA.
- Marginal erosions and subchondral cysts formation (geodes) (Fig. 7.1.3). Up to 47% of patients develop erosions within 1 year after onset of RA.
- *Boutonnière deformity*: flexion at the proximal interphalangeal joint (PIP) and hyperextension at the DIP (Figs. 7.1.1 and 7.1.5).
- *Swan-neck deformity*: hyperextension at the PIP and flexion at the DIP (Fig. 7.1.1).
- *Mallet finger*: rare finding that is characterized by laxity at the insertion of the extensor tendon on the distal phalanx, thus causing the distal phalanx to drop.
- *Hitchhiker thumb deformity*: flexion at the proximal metacarpophalangeal joint of the thumb and hyperextension at the DIP joint (Figs. 7.1.1 and 7.1.6).
- *Mutlans deformity* (*Opera-glass hand*): a severe hand deformity seen in rapidly progressing RA characterized by severe osteoporosis and phalangeal resorption that causes shortening of the fingers. The carpal and metacarpal bones are commonly resorbed and crumbled due to intercarpal/metacarpal ligaments disruption (Figs. 7.1.1 and 7.1.7). Grossly, the fingers are shortened and the skin is wrinkled, giving the impression that the phalanges were retraced one into another like opera glass (Fig. 7.1.1).
- *Hammer toe deformity*: the toe is bent at the middle joint, so that it resembles a hammer (Fig. 7.1.1). It is commonly seen affecting the second, third, or fourth toes.
- Due to muscular atrophy, shifting deformities can arise in hands (ulnar deviation), or feet (fibular deviation) (Fig. 7.1.1).
- In the humerus, RA can cause "*high-riding shoulder*" due to rotator cuff tear.
- In the hip joint, RA causes migration of the femoral head in an axial fashion in the hip joint. In contrast, osteoarthritis causes migration of the femoral head in a superior fashion.
- Involvement of the foot may occur in up to 90% of cases. The first and the fifth metatarsophalangeal joints are affected in up to 50% of cases (Fig. 7.1.4).
- *Atlantoaxial sublaxation* is present when the distance between the posterior aspect of the anterior arch of the atlas and the odontoid process is >3 mm in adults or >5 mm in children on flexion radiographs. Atlantoaxial sublaxation arises in RA with an incidence of 16–36% of cases, presumably secondary to synovitis causing laxity or tearing of the transverse atlantoaxial ligament (Fig. 7.1.8). The atlantoaxial sublaxation can progress into atlantoaxial dissociation.
- *Atlantoaxial impaction*: occurs when both the facets of the atlas and axis collapse due to erosions. The atlas will articulate with the body of the axis instead of the odontoid process. On lateral radiographs, the odontoid process will be seen inside the foramen magnum.
- *In juvenile rheumatoid arthritis*, there is fusion between the carpometacarpal joint of the index and middle fingers, and enlargement of the epiphysis and the metaphysis end of long bones.
- In *Still's disease*, radiographic features in the hands are a mix between RA and psoriasis arthropathy with affection of the DIP joints in a similar fashion to psoriasis arthropathy erosions.
- Lung fibrosis can be seen in long-standing RA (Fig. 7.1.9).
- In *PPsRD*, patients are classically young presenting with widening of the metaphyses of long bones involving the proximal femur and the distal knee, epimetaphyseal enlargement of the metacarpal heads and the phalanges, mega os trigonum, and flattened vertebrae (platyspondyly) with narrowed disc spaces and irregular endplates mimicking Scheuermann's disease. The flattened vertebrae and irregular endplates are seen mainly in the thoracic region in Scheuermann's disease, whereas in PPsRD, the flattened vertebrae with irregular endplates involve the whole spine almost equally (key diagnostic feature).
- In *RS_3PE syndrome*, in contrast to RA, plain radiographs show absent joint erosions.
- Jaccoud's arthropathy, in contrast to RA, plain radiographs of the hands typically show joint deformities in the absence of bone erosions or cartilage destruction.

7.1

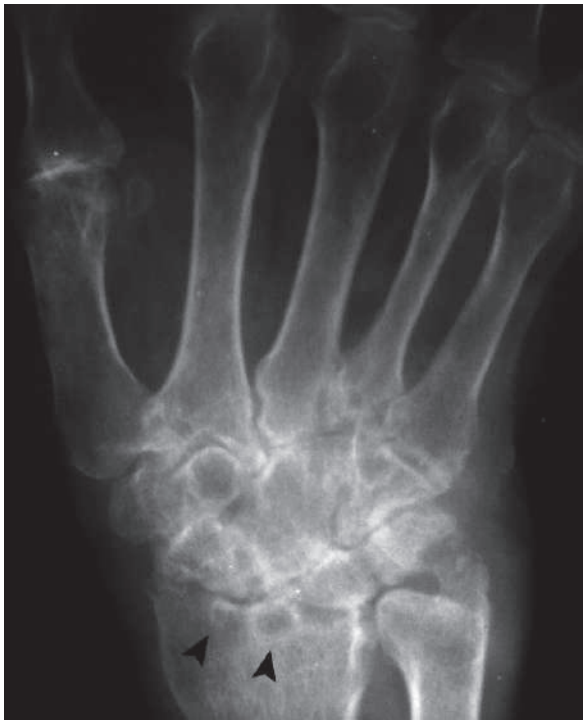

Fig. 7.1.3. Plain radiograph of the hand of a patient with RA shows diffuse osteoporosis and reduced space narrowing between the carpal bones, and between the carpal bones and the distal radioulnar joint with formation of geodes (*arrowhead*)

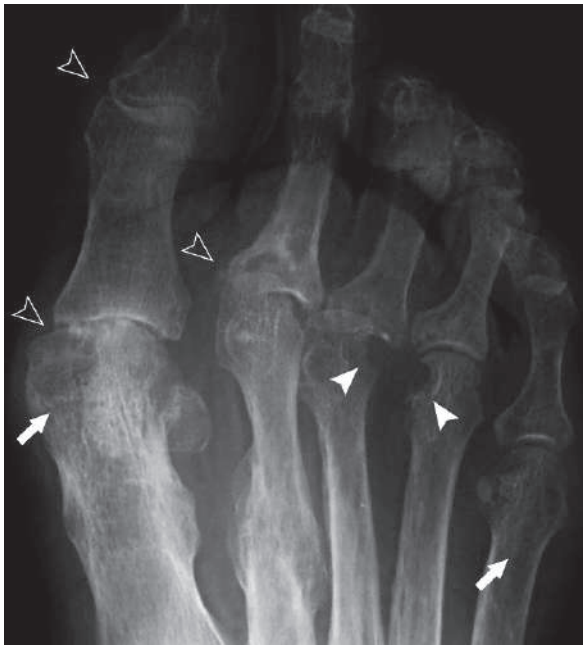

Fig. 7.1.4. A plain radiograph of a patient foot with RA shows marginal erosions of the metatarsals (*solid arrowheads*), joint space narrowing of the metatarsophalangeal and interphalangeal joints (*hollow arrowheads*), and patchy osteoporosis (*arrows*) There is old mid-diaphyseal fracture with callus formation of the 2nd metatarsal bone

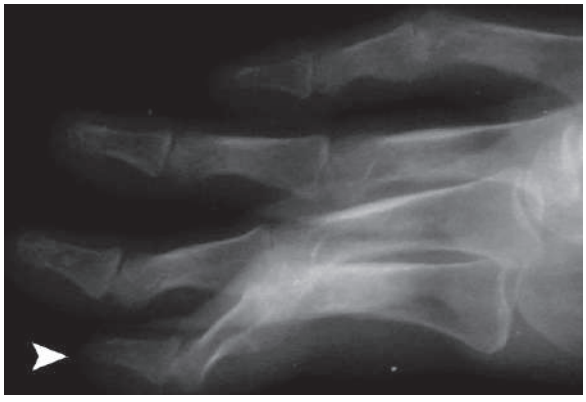

Fig. 7.1.5. Lateral plain radiograph of the fingers of a patient with RA shows Boutonnière deformity (*arrowhead*)

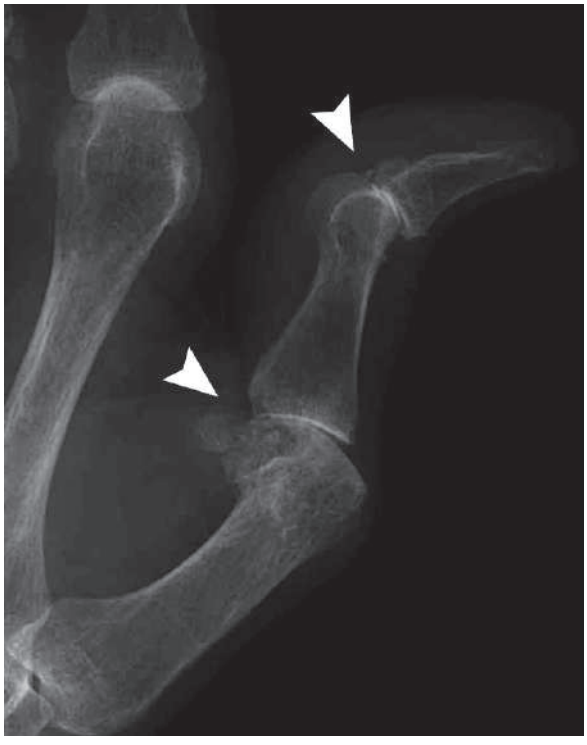

Fig. 7.1.6. Plain radiograph of the thumb shows flexion at the proximal metacarpophalangeal joint of the thumb and hyperextension at the DIP joint (*arrowheads*). (Hitchhiker thumb deformity)

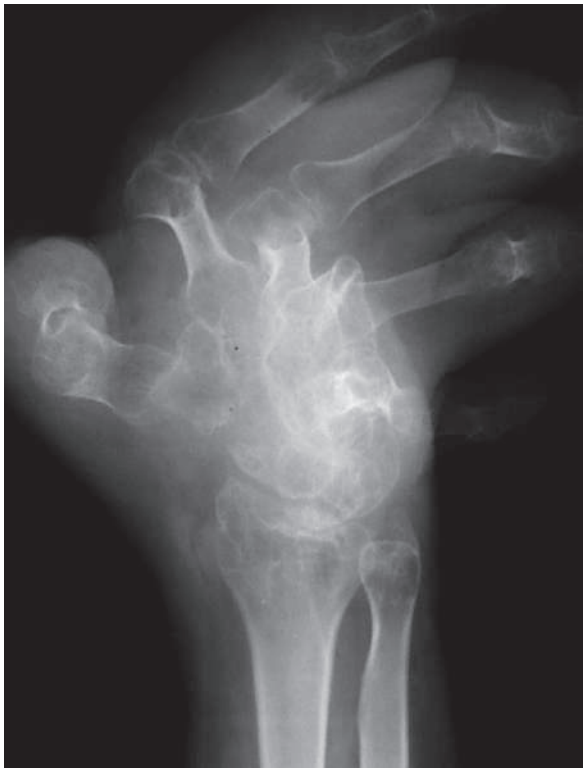

Fig. 7.1.7. Plain radiograph of the hand of a patient with RA shows crumbling of the carpal bones with severe deformity of the hand plus osteoporosis (Mutlans deformity)

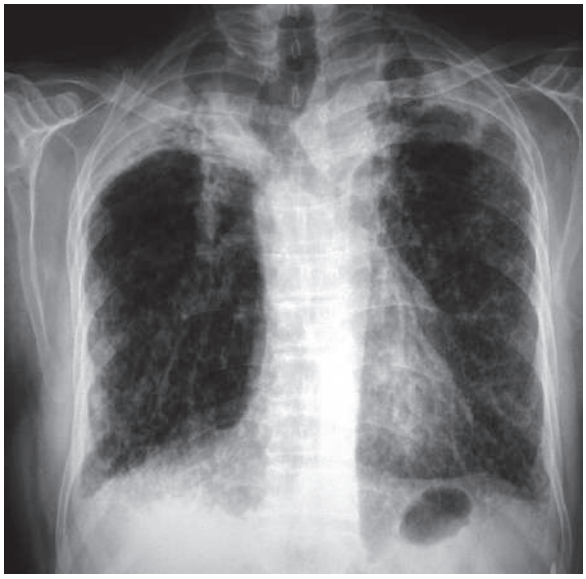

Fig. 7.1.9. Posteroanterior chest radiograph of a patient with RA shows diffuse reticulonodular interstitial pattern reflecting lung fibrosis

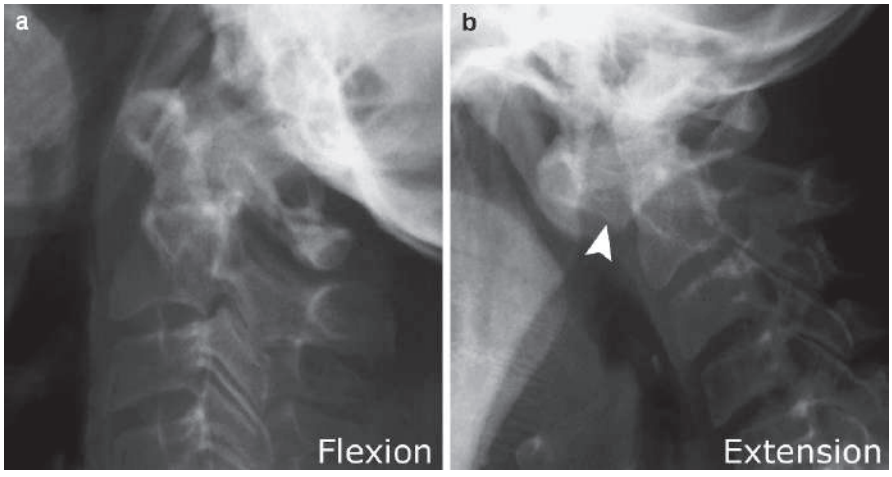

Fig. 7.1.8. Lateral plain radiograph of the atlantoaxial joint of a patient with atlantoaxial sublaxation due to RA shows a significant gap between the anterior arch of the atlas and the odontoid process (*arrowhead*) on extension radiograph

7.1

Signs on MRI

- Different manifestations of inflammation can be seen involving high signal intensity on T2W images of the muscles, bone marrow, tendons, and the articular surface due to effusion. After contrast injection, enhancement of the thickened synovium (pannus) can be seen, and it is a typical sign of RA.
- Extensor carpi ulnaris tendenitis is a typical finding in early RA. On T2W images, fluid signal is observed around the tendon sheath with change in the tendon signal intensity.
- *Popliteal* (*Baker*) *cyst* is a synovial juxta-articular cyst filled with fluid collection that is lined by synovial cells that may, or may not, communicate with the joint. Baker's cyst is a synovial cyst that is located in the posteromedial aspect of the knee, and represents a fluid extension through a slit-like communication between knee joint and the gastrocnemius-semimembranosus bursa. The cyst is typically seen as a fluid collection that passes between the gastrocnemius tendon and the semimembranosus tendon (Fig. 7.1.10). The cyst may show rim enhancement after contrast injection that mimics neoplasm. Rupture of the cyst may present with severe sudden pain that mimics thrombophlebitis or deep venous thrombosis. If the cyst is large enough to compress the popliteal artery, calf claudication arises rarely.
- *Rice bodies* are small, rice-like hypointense bodies seen inside large joints like knee and hip joints due to cartilage destruction or synovial proliferation (Fig. 7.1.11). Rice bodies are an uncommon feature, and very characteristic of RA.
- *Cerebral rheumatic nodules* are seen as focal parenchymal lesions with high signal intensities on T2W and FLAIR images, associated with adjacent leptomeningeal enhancement (Fig. 7.1.12). Rheumatoid pachymeningitis may occur rarely.
- In *PPsRD*, the whole vertebral column shows flattened vertebrae with irregular endplates and multiple intervertebral disc herniations along almost the whole spine. Remember that the MRI picture is seen in a child or a young man, not in a geriatric person with diffuse degenerative changes.
- In *RS_3PE syndrome*, MRI typically shows signs of tenosynovitis with synovium thickening and enhancement postcontrast injection.

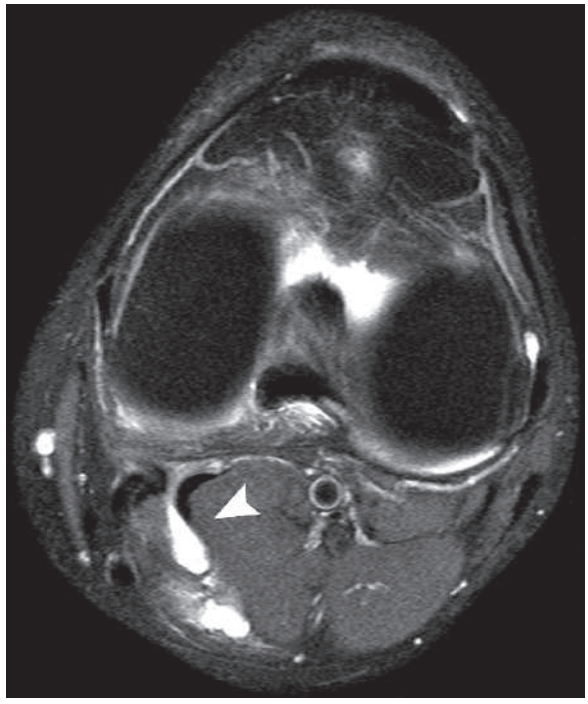

Fig. 7.1.10. Axial PD knee MRI shows popliteal (Baker) cyst seen as a fluid collection that passes between the gastrocnemius tendon and the semimembranosus tendon (*arrowhead*)

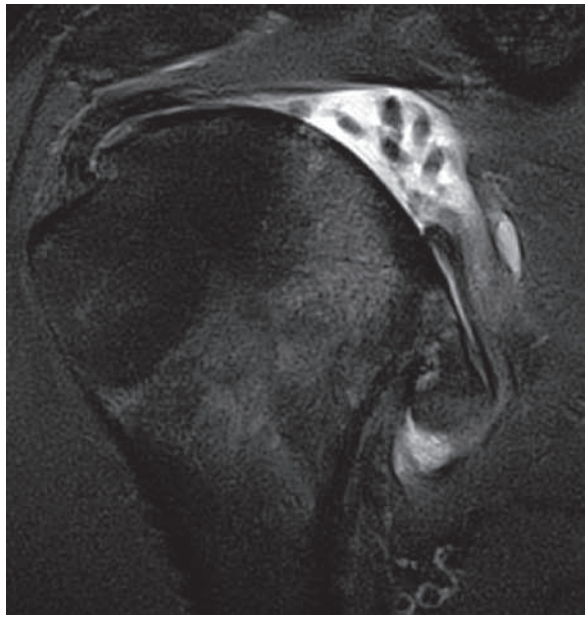

Fig. 7.1.11. Coronal STIR shoulder MRI shows right shoulder joint effusion with multiple intra-articular hypointense lesions (rice bodies). Differential diagnosis of such sign is synovial chondromatosis, which classically shows intra-articular calcification best demonstrated on plain shoulder radiograph

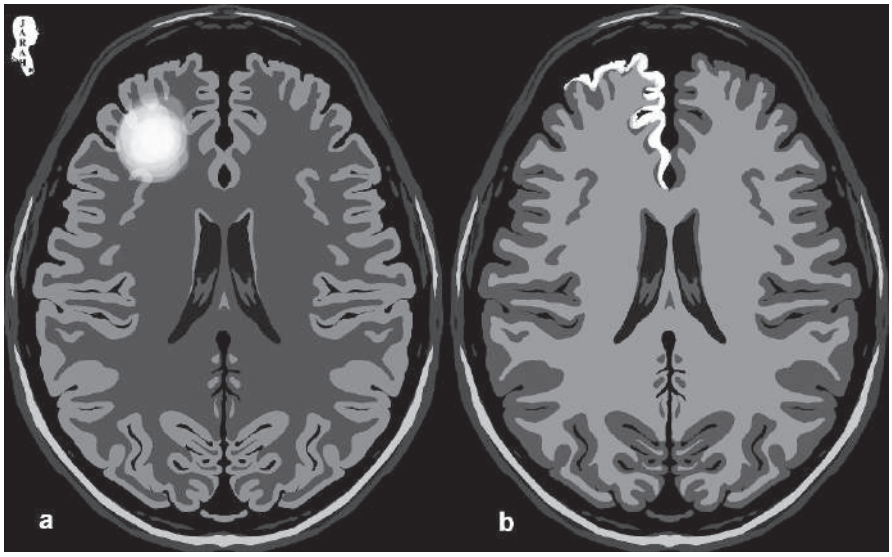

Fig. 7.1.12. Axial brain FLAIR (**a**) and T1W postcontrast (**b**) MR-illustrations demonstrate the classical findings of cerebral rheumatoid nodule. There is T2 hyperintense lesion on (**a**) associated with leptomeningeal enhancement of the adjacent meningies (**b**)

For Further Reading

1. Rosenstein ED et al Felty's and pseudo-Felty's syndromes. Semin Arthritis Rheum. 1991;21:129–42
2. Hurd ER. Extraarticular manifestations of rheumatoid arthritis. Semin Arthritis Rheum. 1979;8, 151–176
3. Tehranzadeh J et al Advanced imaging of early rheumatoid arthritis. Radiol Clin North Am. 2004;42:89–107
4. Sommer OJ et al Rheumatoid arthritis: a practical guide to the state-of-the-art imaging, image interpretation, and clinical implications. RadioGraphics. 2005; 25:381–98
5. Bancroft LW et al Cysts, geodes, and erosions. Radiol Clin North Am. 2004;42:73–87
6. Calatayud J et al Nodular pulmonary amyloidosis in a patient with rheumatoid arthritis. Clin Rheumatol. 2007;26: 1797–98
7. Bednařik J et al Median nerve mononeuropathy in spondylotic cervical myelopathy: double crush syndrome? J Neurol. 1999;246:544–51
8. Beaman FD et al MR imaging of cysts, ganglia, and bursae about the knee. Radiol Clin North Am. 2007;45:969–82
9. Ragan C et al Rheumatoid arthritis. Dis Mon. 1955;1:2–51
10. Zolcinski M et al Central nervous system involvement as a major manifestation of rheumatoid arthritis. Rheumatol Int. 2008;28:281–83
11. Goñi MA et al Rheumatoid nodulosis: a puzzling variant of rheumatoid arthritis. Clin Rheumatol. 1992;11:396–401
12. Bordel Gómez MT et al Rheumatoid nodulosis: report of two cases. JEADV 2003;17:695–8
13. Paci R et al Neuroradiological picture of cerebral vasculitis in rheumatoid arthritis. Neuroradiology. 1983;25:343–5
14. Cellerini M et al MRI of cerebral rheumatoid pachymeningitis: report of two cases with follow-up. Neuroradiology. 2001;43:147–50
15. Solomon WM et al Chronic absorptive arthritis or opera-glass hand: report of eight cases. Ann Rheum Dis. 1950;9: 209–20
16. Marik I et al Dominantly inherited progressive pseudorheumatoid dysplasia with hypoplastic toes. Skeletal Radiol. 2004;33:157–64
17. Ehl S et al Clinical, radiographic, and genetic diagnosis of progressive pseudorheumatoid dysplasia in a patient with sever polyarthropathy. Rheumatol Int. 2004;24:53–6
18. Kaya A et al Clinical and radiological diagnosis of progressive pseudorheumatoid dysplasia in two sisters with sever polyarthropathy. Clin Rheumatol. 2005;24:560–64
19. Mampaey S et al Progressive pseudorheumatoid dysplasia. Eur Radiol. 2000;10:1832–5
20. Weissman BNW et al Prognostic features of atlantoaxial sublaxation in rheumatoid arthritis patients. Radiology. 1982;144:745–51
21. Tada Y et al Flexor tenosynovitis of the ahnd as an initial manifestation of systemic lupus erythematosus. Mod Rheumatol. 2000;10:173–5
22. Sivas F et al Idiopathic Jaccoud's arthropathy. APLAR J Rheumatol. 2005;8:60–2
23. Wu Y et al Jaccoud's arthropathy and psoriatic arthritis, a rare association. Rheumatol Int. doi: 10.1007/s00296-009-1017-1
24. Galvão V et al Profile of autoantibodies in Jaccoud's arthropathy. Joint Bone Spine. 2009;76:356–60
25. Sugisaki K et al Remitting seronegative symmetrical synovitis with pitting edema (RS3PE) syndrome following spontaneous rupture of a gouty tophus. Mod Rheumatol. 2008;18:630–3
26. Manganelli P et al Remitting seronegative symmetrical synovitis with pitting edema in a patient with myelodysplastic syndrome and relapsing polychondritis. Clin Rheumatol. 2001;20:132–5
27. Unlu Z et al Magnetic resonance imaging findings in a case of remitting seronegative symmetrical synovitis with pitting edema. Clin Rheumatol. 2005;24: 648–51

7.2

Ankylosing Spondylitis (Marie–Strümpell Disease)

Ankylosing spondylitis (AS) is a chronic, progressive inflammatory disease of unknown origin that affects the axial skeleton (vertebral column plus the pelvis), and is characterized by bilateral sacroiliitis, stiffness of the axial joints (ankylosis), and syndesmophytes formation.

AS is a rheumatoid factor sero-negative arthritis that is positively associated with HLA-B27. HLA stands for human leucocyte antigen (HLA) system. In the body, there are two classes of HLA antigens. Class I HLA is expressed by the human cells for histocompatibility, so the body knows that these cells are its own cells. Class I HLA antigens have an important role in transplant rejection. Class II HLA antigens are expressed by the immunocompetent cells including macrophages, Langerhanse cells, B cells, and some T cells. HLA-B27 antigen is associated with AS in 90% of cases. However, only 5% of patients with positive HLA-B27 develop AS.

Patients with AS often present with back stiffness, low back ache, and discomfort in thighs and buttocks. Extra-skeletal manifestations include anterior uveitis, ascending aortitis and bronchiolitis obliterans with organizing pneumonia (cryptogenic organizing pneumonia).

Cauda equina syndrome is an uncommon complication of AS. Patients classically present with symptoms related to compression of the cauda equine such as low back and lower extremities pain, impotence, overflow incontinence, cutaneous sensory defects (paresthesia), and motor dysfunction. Up to 30% of patients describe severe burning or shooting pain in the lower limbs.

Signs on Radiograph

- *Sacroiliitis* involvement is almost always in a bilateral and symmetrical fashion in AS (90% of cases). However, unilateral involvement may occur in 10% of cases. Radiological findings include multiple small erosions (rat bite erosions) along the iliac side of the joint. In advanced stage of the disease, the erosions increase in size and widen the sacroiliac joint. Later, sclerosis of the sacroiliac joint occurs (Fig. 7.2.1).
- *Vertebral bodies squaring* is an early manifestation of AS that arises due to inflammation of the peripheral fibers of the annulus fibrosis at their attachment to the upper and lower corners of the vertebral bodies (enthesitis). Enthesitis means inflammation of the entheses, the location where a tendon or a ligament is inserted into a bone. Erosions of the vertebral body at these areas make the vertebral body look square in shape (Fig. 7.2.2).
- *Syndesmophytes* are para-vertebral ossifications that resemble osteophytes, except that they arise vertically from one vertebra to the other (Fig. 7.2.3), while osteophytes run in a horizontal fashion along the vertebral bodies. When the syndesmophytes are diffusely affecting the vertebral column, the vertebral column is said to have a "bamboo spines appearance" (Fig. 7.2.4). Syndesmophytes are ossifications of the annulus fibrosus–longitudinal ligament complex as a healing process after enthesitis.
- *Dagger sign* is longitudinal radiopaque line seen along the vertebral column representing calcification of the supraspinous ligament (Fig. 7.2.5).
- *Trolley track sign*: Three dense radiopaque lines are seen along the vertebral column representing calcification of the supraspinous and ankylosis of the facets joints.

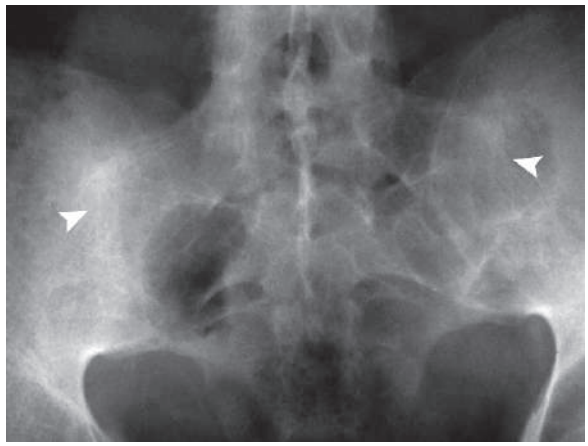

Fig. 7.2.1. Anteroposterior plain radiograph of the hip of a patient with advanced ankylosing spondylitis (AS) shows complete sclerosis of the sacroiliac joints bilaterally (*arrowheads*)

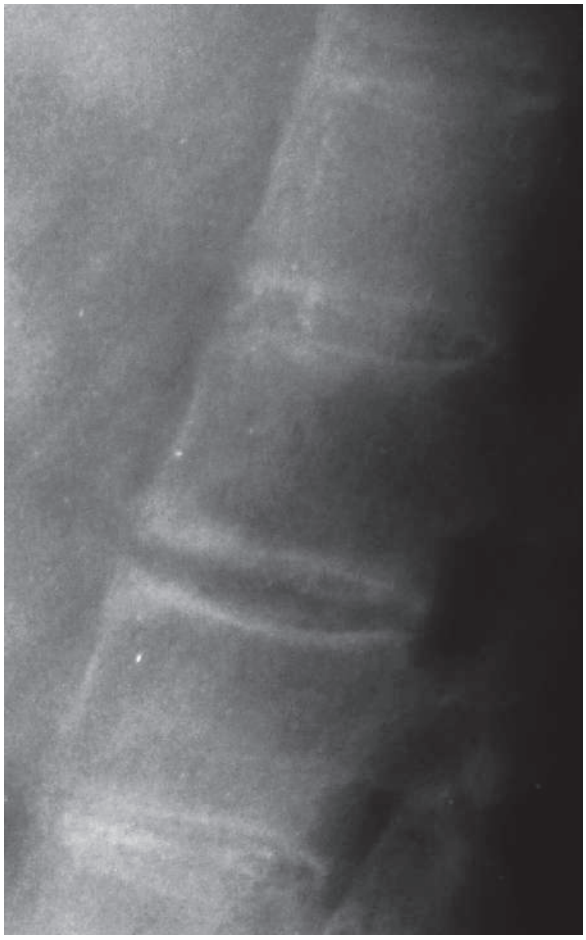

Fig. 7.2.2. Lateral plain radiograph of the thoracic vertebrae in advanced stage of AS shows squaring of the vertebrae

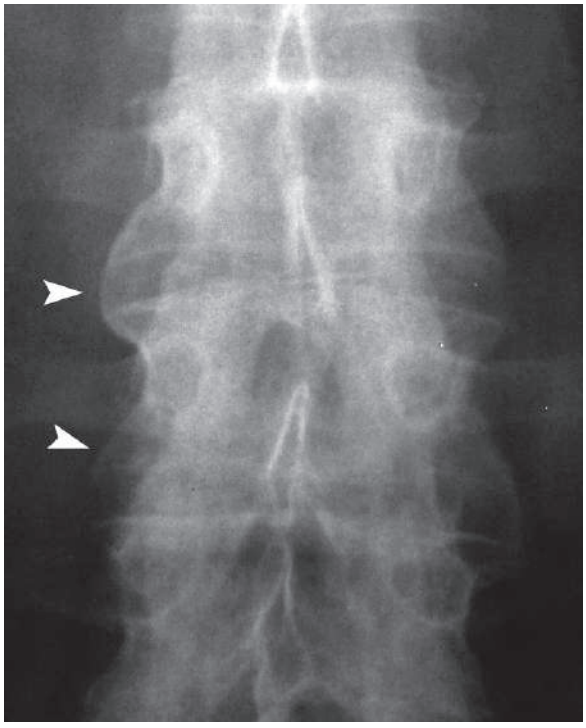

Fig. 7.2.3. Anteroposterior plain radiograph of the thoracic vertebrae shows syndesmophytes (*arrowheads*)

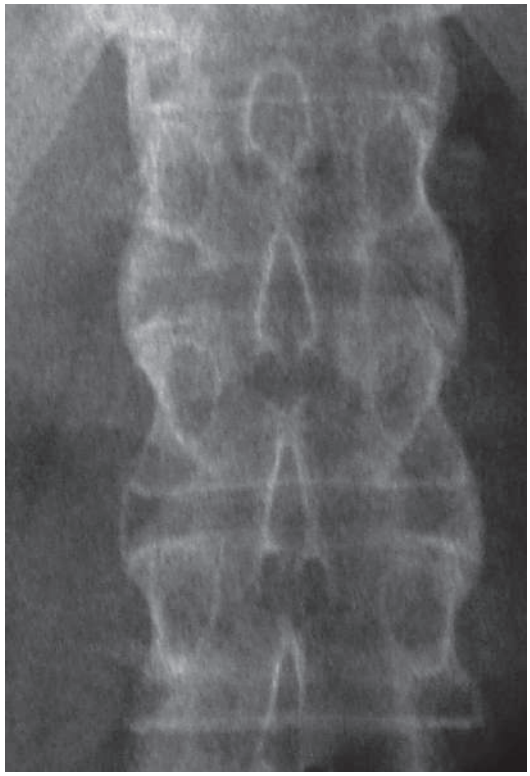

Fig. 7.2.4. Anteroposterior plain radiograph of the thoracic vertebrae shows the classic appearance of bamboo spines

7.2

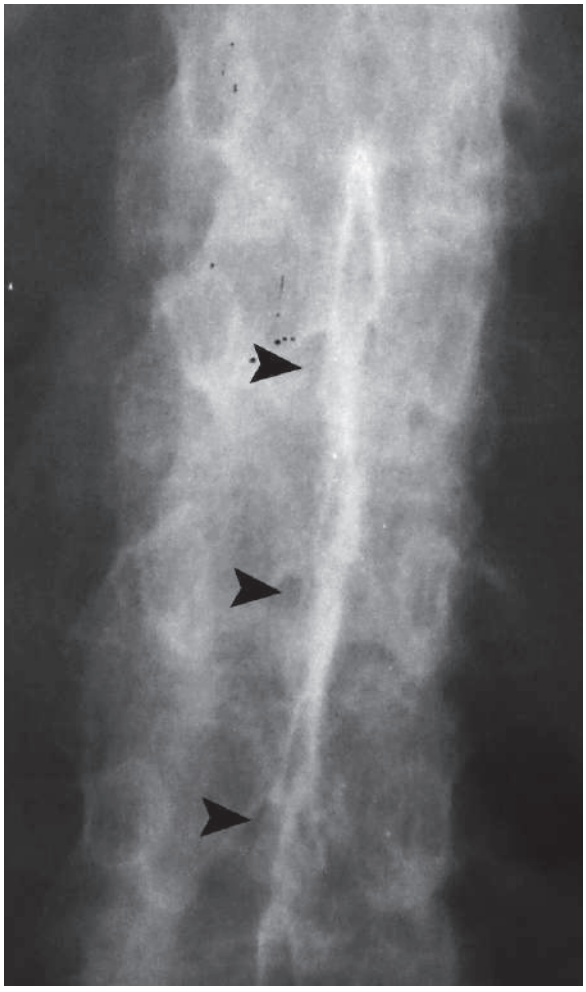

Fig. 7.2.5. Anteroposterior plain radiograph of the thoracic vertebrae shows the dagger sign

Signs on MRI

- *Cauda equina syndrome* typically presents as enlargement of the thecal sac, multiple dorsal diverticula, with asymmetric scalloped erosions of the bony canal.
- *Romanus lesion* is enthesitis at the insertion of the annulus fibrosus–longitudinal ligament complex. There is low T1 signal intensity, high T2 signal intensity, and marked contrast enhancement within the annulus fibrosus at the discovertebral junction, indicating active enthesitis (Fig. 7.2.6). When the active enthesitis starts to heal, it forms sendesmophytes.
- *Anderson lesion* is a focal erosive change in the vertebral endplate that resembles bacterial discitis (Fig. 7.2.7). Typical features of Anderson lesion include disc space narrowing, focal bone destruction at the vertebral endplate adjacent to the disc, surrounding sclerosis, and local kyphosis. Differentiation between bacterial discitis and Anderson disease can be difficult in patients with AS. However, the vertebral disc is typically involved in bacterial discitis, while in Anderson lesion the disc signal is generally preserved or shows degeneration. Moreover, perivertebral effusion and intradiscal effusion are commonly found with bacterial discitis, whereas they are rare with Anderson lesion. After contrast injection, both Anderson lesion and bacterial discitis show contrast enhancement. Bacterial discitis high T2 signal intensity is due to hyperemia and edema, while enhancement in Anderson lesion is due to granulation tissue formation.

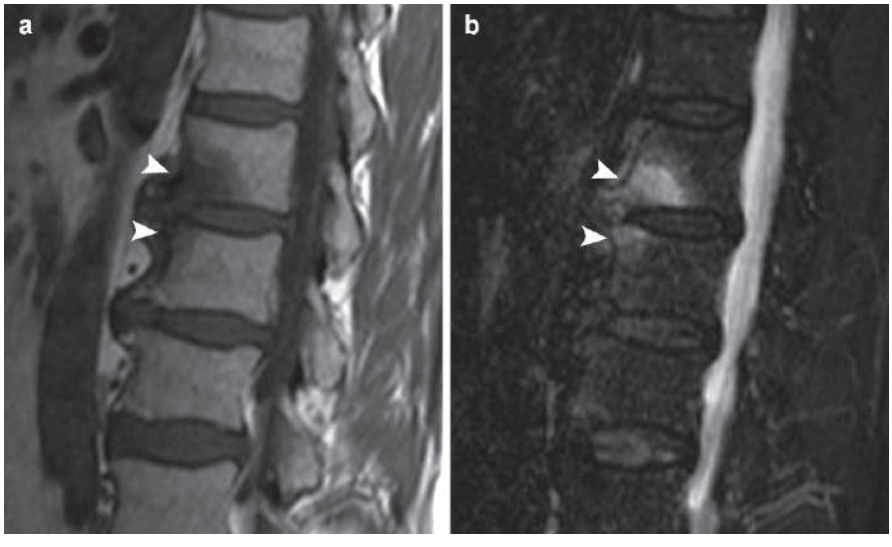

Fig. 7.2.6. Sagittal thoracic T1W (**a**) and STIR (**b**) MRI show enthesitis at the anterior superior and anterior inferior vertebral endplates of two adjacent vertebrae (Romanus lesion) (*arrowheads*)

Fig. 7.2.7. Sagittal lumbar T1W MR illustration demonstrates Anderson's lesions (*arrowheads*)

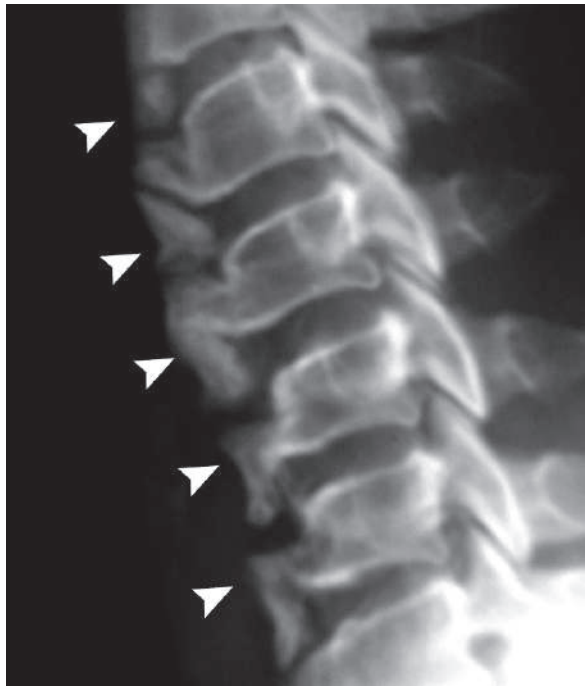

Fig. 7.2.8. Lateral plain radiograph of the cervical vertebrae shows multisegmental vertebral fusion due to ligamentous calcification and ossification due to diffuse idiopathic skeletal hyperostosis (DISH) (*arrowheads*)

Differential Diagnoses and Related Diseases

- *SAPHO syndrome* is a rare musculoskeletal disease of unknown origin characterized by *S*ynovitis, *A*cne, *P*ustulosis of the palmar and plantrar skin surfaces, *H*yperostosis of the bones, and *O*steitis. Patients with the adult form of SAPHO syndrome usually present with unilateral Sacroiliitis and syndesmophytosis that may mimic the radiographic picture of AS.
- *Diffuse idiopathic skeletal hyperostosis* (*DISH*) is a disease characterized by multisegmental vertebral fusion due to ligamentous calcification and ossification. The disease is commonly seen in the cervical and the thoracic vertebrae. Patients are usually above 70 years of age presenting with neck pain and stiffness. DISH can be mistaken with AS. Characteristic radiological signs of DISH include flowing vertebral ossification of at least four contiguous vertebral bodies, broad band of ossification along the anterolateral aspect of each vertebra (Fig. 7.2.8), absence of degenerative disc disease, and absence of sacroiliac joints disease.

For Further Reading

1. Uppal SS et al Ankylosing spondylitis and undifferentiated spondyloarthropathies in Kuwait: a comparison between Arabs and South Asians. Clin Rheumatol. 2006;25:219–24
2. Pham T. Pathophysiology of ankylosing spondylitis: what's new ? Joint Bone Spine. 2008;75:656–60
3. Sant SM et al Cauda equina syndrome in ankylosing spondylitis: a case report and review of the literature. Clinical rheumatol. 1995;14:224–6
4. Soeur M et al Cauda equina syndrome in ankylosing spondylitis. Anatomical, diagnostic, and therapeutic considerations. Acta Neurochirurgica. 1981;55:303–15
5. Lee Bennett D et al Spondyloarthropathies: ankylosing spondulitis and psoriatic arthritis. Radiol Clin North Am. 2004;42:121–34
6. Quagliano PV et al Vertebral pseudoarthrosis with diffuse idiopathic skeletal hyperostosis. Skeletal Radiol. 1994;23:353–5
7. Jordana X et al The coexistence of ankylosing spondylitis and diffuse idiopathic skeletal hyperostosis-a postmortem diagnosis. Clin Rheumatol. 2009;28:353–6
8. Jevtic V et al Marginal erosive discovertebral "Romanus" lesions in ankylosing spondylitis demonstrated by contrast enhanced Gd-DTPA magnetic resonance imaging. Skeletal Radiol. 2000;29:27–33
9. Tsuchiya K et al Discovertebral lesion in ankylosing spondylitis: differential diagnosis with discitis by magnetic resonance imaging. Mod Rheumatol. 2002;12:113–7

7.3 Gout Arthritis

Gout is a clinical condition characterized by increased serum uric acid levels (hyperuricemia) with deposition of uric acid monocrystals in the synovial fluid, initiating acute inflammatory reaction that leads to arthritis. Gout is the most common cause of inflammatory arthritis in men >40 years of age.

Hyperuricemia is defined as urate levels >7 mg/dL in men and menopausal women, or urate levels >6 mg/dL in premenopausal women. Plasma urate level >7 mg/dL exceeds the saturation for urate solubility at normal body temperature and blood PH.

Not every patient with hyperuricemia develops symptoms of gout. Gout can result from impaired uric acid clearance by the kidney (primary gout), or due to increased production of uric acid for a variety of causes, increased turnover of nucleic acids, or from decreased clearance of uric acid (secondary gout). Up to 80% of cardiac transplant patients develop hyperuricemia, and 10% develop gout after a mean of 1.5 years posttransplantation.

Uric acid monocrystals are needle-shaped negatively birefringent crystals, and they are the main product of purine catabolism. They deposit within the synovium or the renal parenchyma forming chalky-white deposits that initiate painful arthritis and renal disease. High uric acid precipitation within the renal tubules can result in uric acid renal stones formation.

In gout arthritis (GA), deposition of the urate crystals (tophi) within the synovial fluid and the synovial membrane causes inflammation. With time, a soft tissue pannus forms within the joint which will start to erode the intra-articular cartilage and the subchondral bone. The monosodium urate crystals may also deposit in the tendon, ligaments, bursae, and other organs like the ear, nose, and skin.

Rarely, gout can involve the spines resulting in sclerotic bony lesions, cervical pain, or paraplegia if the spinal cord is affected.

It takes 4–6 years for gout to cause detectable radiographic signs, and the patients are usually treated before the radiological signs start to appear. Because of this, GA radiographic features are not commonly seen, although they have characteristic patterns.

Signs on Plain Radiographs and MRI

- There are typically cortical bony erosions with well-defined sclerotic margin in the absence of steoporosis (Figs. 7.3.1 and 7.3.2). Disuse osteopenia may occur in late stages of the disease.
- *Podagra* is a term used to describe gout tophi affecting the metatarsophalangeal joint of the great toe; it is seen as erosion of the first metatarsal bone often associated with para-articular soft tissue swelling (Fig. 7.3.3). Podagra shows signs of inflammation when the process of tophus formation is active (Fig. 7.3.4).
- Cartilage calcification (chondrocalcinosis) can be seen in up to 40% of patients.
- Vertebral gout may present as an osteolytic vertebral lesion with sclerotic margin.

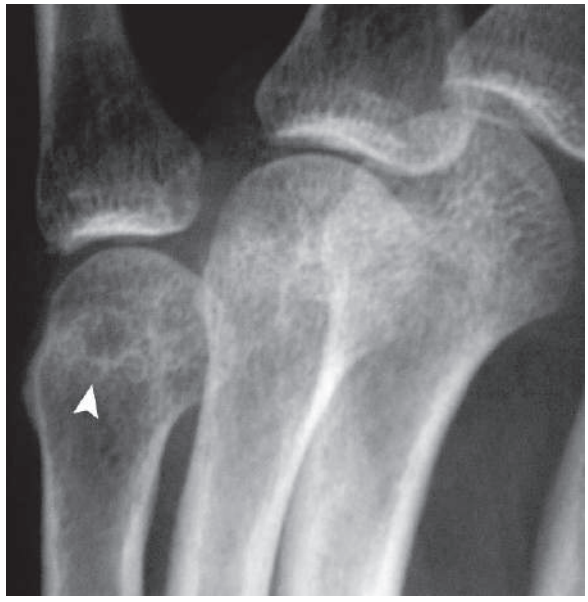

Fig. 7.3.1. Plain radiograph of the metacarpal heads shows bony erosion with sclerotic margin in the absence of osteoporosis (*arrowhead*), a typical finding of gout arthritis (GA)

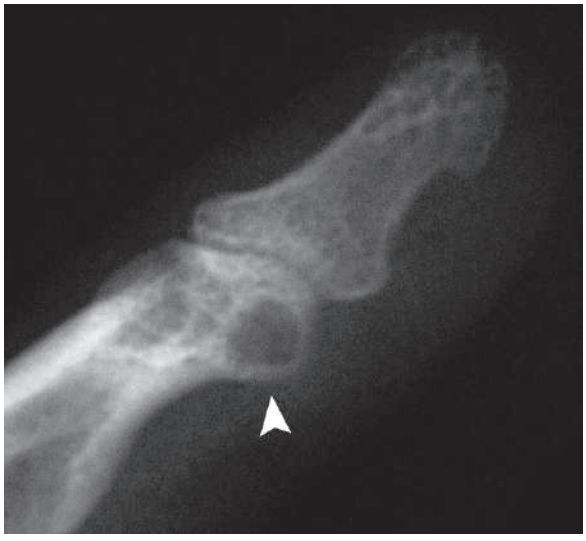

Fig. 7.3.2. Plain radiograph of a finger shows bony erosion with sclerotic rim in the middle phalanges (*arrowhead*)

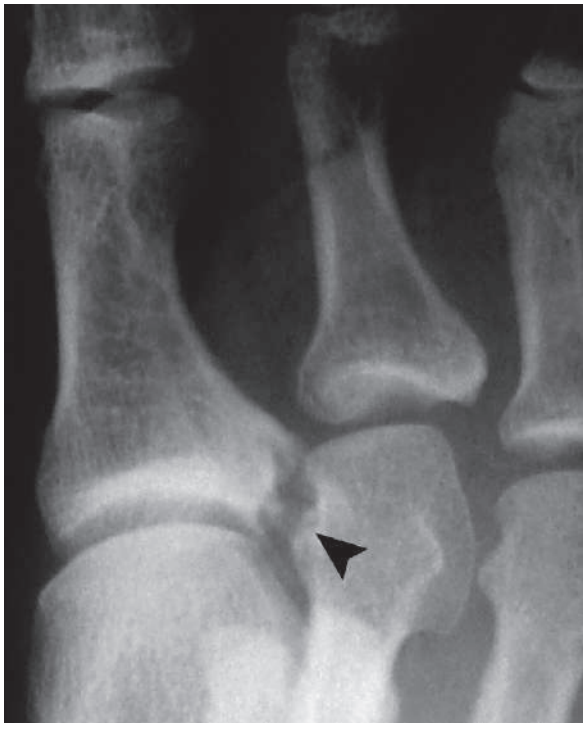

Fig. 7.3.3. Plain radiograph of the foot of a patient with chronic gout shows marginal erosion of the proximal phalanges (*arrowhead*)

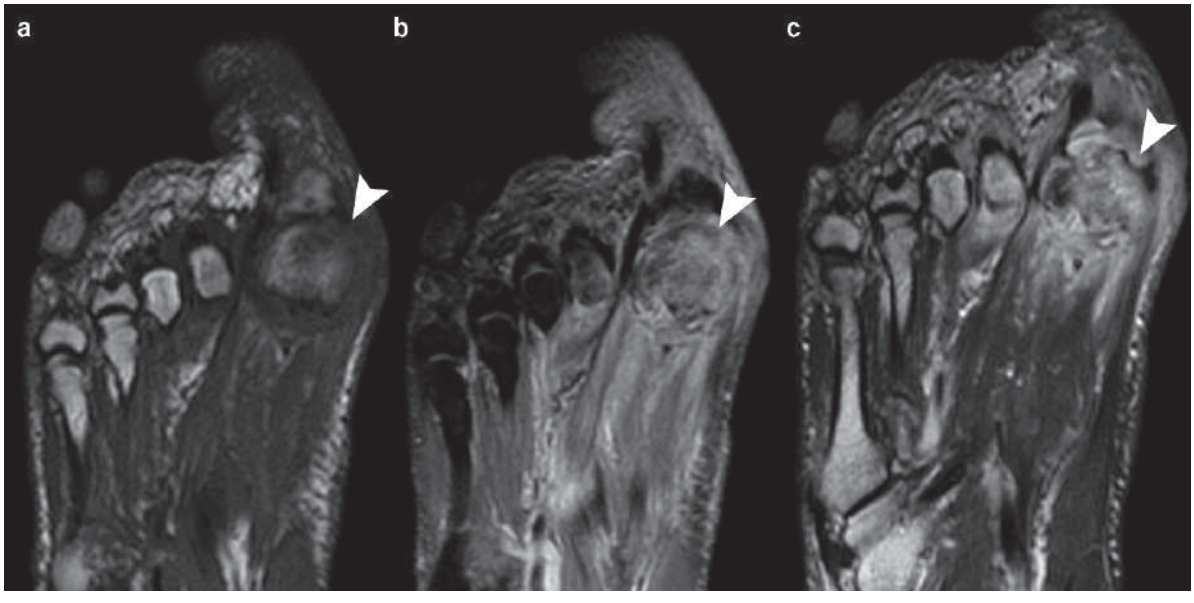

Fig. 7.3.4. Coronal T1W (**a**), STIR (**b**), and T1W postcontrast foot MRI of a patient investigated for gout with foot pain localized to the big toe show hypointense signal intensity due to edema of the first metatarsal head in (**a**), hyperintense T2 signal intensity in (**b**), and marked contrast enhancement of the first metatarsal head and the surrounding soft tissues due to active inflammatory process (*arrowhead*)

Differential Diagnoses and Related Diseases

7.3

Lesch–Nyhan syndrome (*LNS*) is an X-linked recessive metabolic disease characterized by defective purine metabolism that results in uric acid overproduction. The disease arises due to genetic absence or near absence of the enzyme hypoxanthine-guanine phosphoribosyltransferase (HGPRT). Patients with LNS present with involuntary movements in a combination of chorea and athetosis (choreoathetosis), spasticity, and psychiatric abnormalities in the form of compulsive self-mutilation. Recurrent formation of renal uric acid stones is commonly encountered in LNS due to hyperuricemia. Laboratory findings show increased levels of uric acid in the urine, cerebrospinal fluid, and serum. Plain radiographs can show GA. Renal ultrasound can be used to screen for renal stones in these patients. Brain MRI may show caudate nuclei head atrophy with widening of the anterior lateral horns of the lateral ventricles (Fig. 7.3.5). Furthermore, very prominent prepontine cisterns with mild to moderate midbrain atrophy have been reported in some patients.

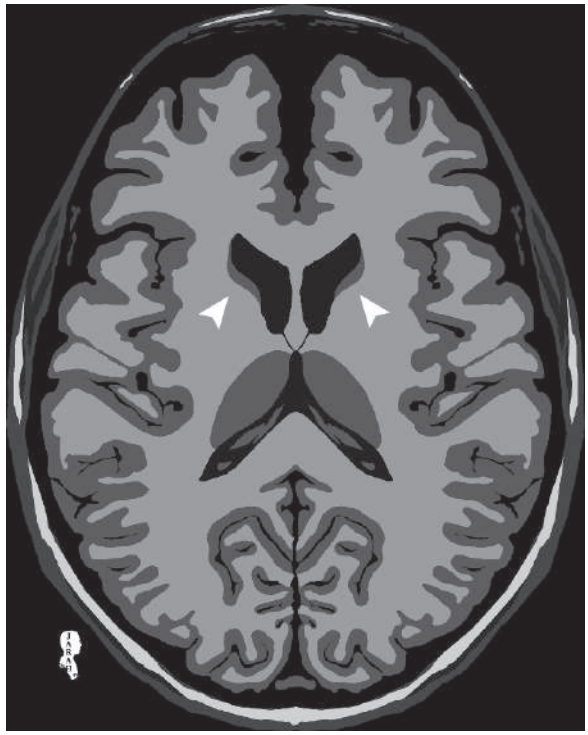

Fig. 7.3.5. Axial T1W brain MR illustration demonstrates bilateral caudate nucleus atrophy in a patient with Lesch–Nyhan syndrome (LNS)

For Further Reading

1. Monu JUV et al Gout: a clinical and radiological review. Radiol Clin North Am. 2004;42:169–84
2. Jacobson JA et al Radiographic evaluation of arthritis: inflammatory conditions. Radiology. 2008;248:378–89
3. Chang PC et al Tophaceous gout of the first costochondral junction in a heart transplant patient. Skeletal Radiol. 2006;35:684–6
4. Agarwal K et al Fine needle aspiration cytology of gouty tophi with review of the literature. J Cytol. 2007;24:142–5
5. Cabot J et al Tophaceous gout in the cervical spine. Skeletal Radiol. 2005;34:803–6
6. Jajić I et al Gout in the spine and sacro-iliac joints: radiological manifestations. Skeletal Radiol. 1982;8:209–12
7. Rosenfeld DL et al Serial renal songraphic evaluation in patient with Lesch-Nyhan syndrome. Pediatr Radiol. 1994; 24:509–12
8. Harris JC et al Craniocerebral magnetic resonance imaging measurments and findings in Lesch-Nyhan syndrome. Arch Neurol. 1998;55:547–53

7.4 CPPD and HADD

Calcium pyrophosphate dihydrate crystal deposition disease (CPPD) and hydroxyapatite crystal deposition disease (HADD) are diseases characterized by deposition of insoluble crystals within the joints and periarticular soft tissues, initiating inflammatory destructive reaction. Other clinically important calcium-containing crystals deposition diseases include tricalcium phosphate (TCP) and octacalcium phosphate (OCP) diseases.

Calcium Pyrophosphate Dihydrate Crystal Deposition Disease

CPPD, also known as *pseudo-gout* and *chondrocalcinosis*, is a disease characterized by calcium pyrophosphate crystals deposition within the *articulating cartilage*, leading to cartilage inflammation and later to joint destruction in a similar fashion to gout arthritis.

CPPD is classified based on its etiology into hereditary, idiopathic, or secondary to metabolic disorders (e.g., vitamin D intoxication). The disease is age-related, with an incidence of 5% in patients >70 years, and nearly 50% in patients >90 years. Many patients present with gout-like arthritic episodes characterized by joint synovitis, malaise, and fever that lasts from 1 day to 4 weeks. Up to 50% of patients develop progressive degeneration of multiple joints. The most frequently involved joints are the knees, wrists, metacarpophalangeal joints, and the hips.

Pyrophosphate deposition involves both hyaline cartilage and fibrocartilage joints like symphysis pubis, annulus of the spine, triangular fibrocartilagenous complex (TFCC) of the wrist, and menisci. CPPD can occur in high incidence with other diseases like gout, hyperparathyroidism and hemochromatosis.

CPPD diagnosis is established by identifying the pyrophosphate crystals within the synovial fluid after aspiration. Plasma and uric acid levels of pyrophosphate are typically not elevated (differential point from gout).

Signs on Plain Radiograph

- *Chondrocalcinosis*: cartilage calcification is the hallmark of CPPD. Chondrocalcinosis is usually observed in medial and lateral compartments of the knee, wrist TFCC, and the symphysis pubis (Fig. 7.4.1).
- *Pseudo-charcot's joint*: severe joint destruction that mimics Charcot's joint may be observed occasionally.
- Normal bone density with occasional subchondral cysts.
- *SLAC wrist deformity*: *S*capho-*L*unate *A*dvanced *C*ollapse is a pathological situation characterized by loss of the cartilage between the scaphoid bone and the radius, causing the scaphoid to indent the radius, and the capitate to collapse, thus disturbing the scapholunate joint articulation (Fig. 7.4.2).
- *Generalized chondrocalcinosis* is a pathological condition characterized by involvement of more than one group of joints with cartilage calcification (e.g., knees, wrists, plus vertebral discs).

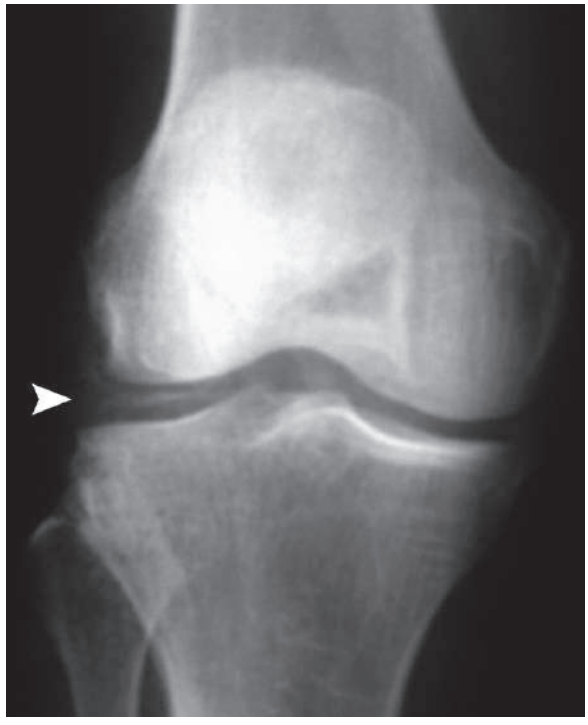

Fig. 7.4.1. Anteroposterior knee radiograph shows calcification of the lateral meniscus due to CPPD chondrocalcinosis (*arrowhead*)

7.4

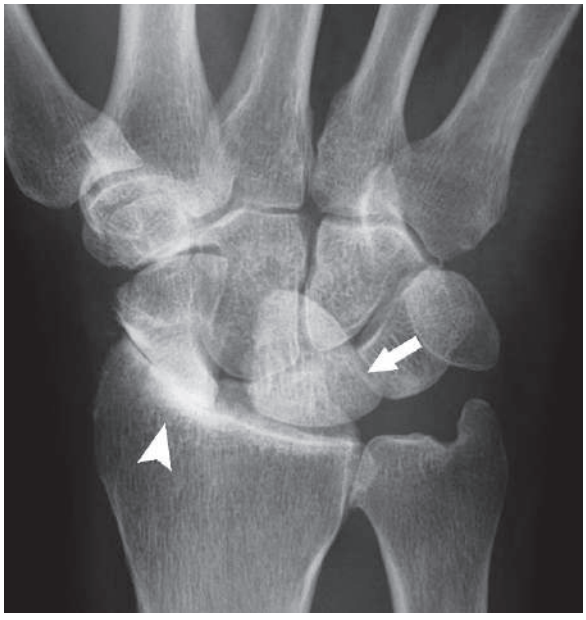

Fig. 7.4.2. Plain hand radiograph shows scaphoid indenting the distal radius with sclerosis (*arrowhead*) and collapse of the capitate from its normal position (*arrow*) (SLAC wrist deformity)

Hydroxyapatite Crystal Deposition Disease

HADD, also known as *calcific periarthritis* and *peritendinitis calcarea*, is characterized by hydroxyapatite crystal deposition in the soft tissues, especially the tendons.

The most characteristic feature of this disease is *tendon* calcification within the body, especially around the shoulder. Moreover, crystal deposition and calcification tend to occur characteristically around the joints (periarticular). HADD can be sporadic, or associated with long-term hemodialysis for renal insufficiency.

Patients with HADD can be asymptomatic, or present with recurrent attacks of arthritis in the area of crystal deposition. Shoulder pain is the commonest complaint since supraspinatus tendon calcification is common in HADD.

HADD is characterized by three pathological phases: silent, mechanical, and adhesive. The silent phase is characterized by crystal deposition that is completely within the tendon. The mechanical phase is characterized by enlargement of the deposits with starting of impingement-like symptoms (e.g., bursitis). The adhesive phase is characterized by generalized disability and limitation of motion. When the adhesive phase occurs in the shoulder, the condition is called *adhesive capsulitis* or *frozen shoulder*. Hydroxyapatite crystals are commonly deposited in damaged tissues (dystrophic calcification).

HADD calcification is often monoarticular, although it can be polyarticular. Involvement of the joints of the feet and toes are rare (<1%). There are two syndromes associated with HADD due to crystal deposition around the joints: calcific periarthritis with bone resorption (acute HADD arthritis), and rapid destructive arthritis of the shoulder (Milwaukee shoulder syndrome).

Calcific periarthritis with bone resorption is characterized by inflammation of the calcified focus with resorption of the bone beneath it. The condition mimics bone sarcoma, especially if perisotitis develops. Biopsy can be avoided if the location of the osteolytic lesion is characteristic of HADD (near a tendon insertion), and other manifestations of HADD exist in the body.

Milwaukee shoulder syndrome is a disease characterized by destructive shoulder arthropathy, blood-stained joint effusion (80%), and chronic tears of the rotator cuff tendon. Patients are typically elderly women with a mean age of 72 years. Symptoms range from none to severe shoulder pain with joint effusion. Most patients have symptoms dating from several years back. Bilateral shoulder involvement is common, and knees arthropathy is found in 50% of patients.

Differential Diagnoses and Related Diseases

Crowned dens syndrome (*CDS*) is a rare clinical condition characterized by deposition of pyrophosphate or calcium hydroxyapatite crystals around the odontoid process of the axis vertebra and its ligaments, especially ligamentum flavum. Inflammatory signs and high erythrocyte sedimentation rate (ESR) are present in up to 30% of cases.

The patients often present with acute attack of neck pain, neck rigidity, and fever, mimicking acute meningitis or spondylodiscitis. CDS affects mostly females, with up to 45% of cases found in patients above 85 years of age.

Signs on Radiographs

- Calcification of the supraspinatus and infraspinatus tendons are a very characteristic feature of HADD (Figs. 7.4.3 and 7.4.4). The calcification typically starts in the site of tendon insertion, or the critical zone. The *critical zone* is the part of the supraspinatus tendon 1 cm proximal to its insertion into the greater tubercle of the humerus.
- Areas of calcifications are noticed in the periarticular soft tissues.
- Calcification within the carpal bones, ligaments, and wrist tendons are commonly seen.
- Always suspect HADD in a calcification that is observed near a joint, at tendon insertion, near muscular attachment, or after trauma (dystrophic).
- In *Milwaukee shoulder syndrome*, there is glenohumeral joint destruction, narrowing, and sclerosis. Upward sublaxation of the humeral head can be seen indicating long-standing rotator cuff tendon disruption. Periarticular calcification is noticed in 40% of cases. Pseudo-arthrosis between the humeral head, coracoid, and acromion is common. Knees involvement is similar to that of CPPD arthropathy.
- In *crown dens syndrome*, radio-opaque calcifications with different sizes and shapes are seen around and above the superior part of the odontoid process, giving the shape of a "crown on a head" appearance. CDS can be mistaken with cervical block vertebra (Klipple-Feil anomaly type 1).

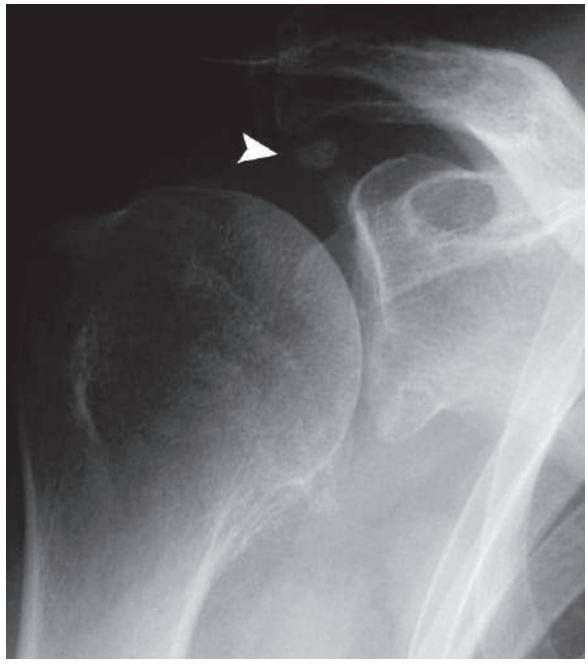

Fig. 7.4.3. Plain radiograph of the shoulder shows calcification in the area of the supraspinatus tendon due to HADD (*arrowhead*)

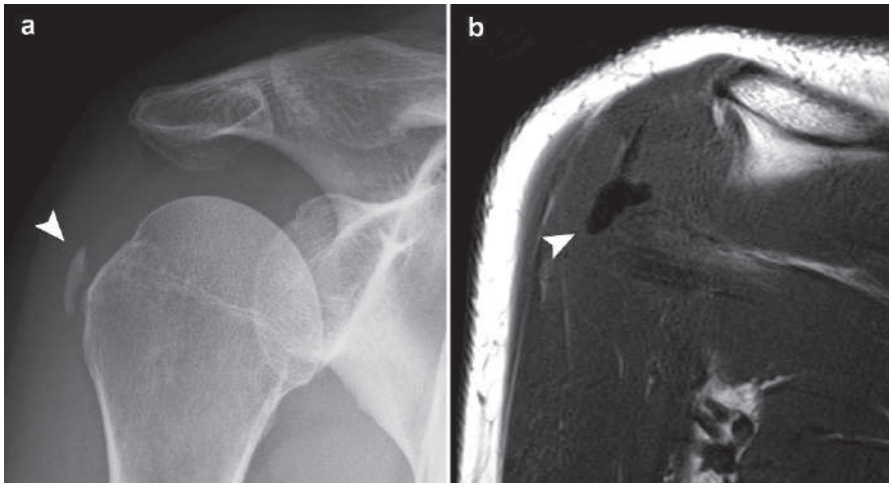

Fig. 7.4.4. Plain radiograph of the shoulder (**a**) and T1W shoulder MRI (**b**) show calcification area within the infraspinatus tendon due to HADD (*arrowheads*)

For Further Reading

1. Curtis W et al Calcium hydroxyapatite deposition disease. RadioGraphics. 1999;10:1031–48
2. Fam AG et al Hydroxyapatite pseudopodagra. A syndrome of young women. Arthritis Rheum. 1989;32:741–7
3. Vargas A et al Calcium pyrophosphate dihydrate crystal deposition disease presenting as a pseudotumor of the temporomandibular joint. Eur Radiol. 1997;7:1452–3
4. Nguyen VD. Rapid destructive arthritis of the shoulder. Skeletal Radiol. 1996;25:107–2
5. Hayashi M et al Idiopathic widespread calcium pyrophosphate dihydrate crystal deposition disease in young patient. Skeletal Radiol. 2002;31:246–50
6. Baysal T et al The crown dens syndrome: a rare form of calcium pyrophosphate dihydrate crystal deposition disease. Eur Radiol. 2000;10:1003–5
7. Steinbach LS. Calcium pyrophosphate dihydrate and calcium hydroxyapatite crystal deposition disease: imaging perspectives. Radiol Clin North Am. 2004;42:185–205
8. Talbott JH. Gout. Dis Mon. 1957;3:1–39
9. Till G et al Calcium pyrophosphate dihydrate crystal deposition disease: a report of a case. JCCA 1988;32:23–7

7.5 Osteoarthritis

Osteoarthritis (OA) is a clinical condition that arises primarily from cartilaginous defect in the joint, which leads to cartilage degeneration and bone-to-bone friction resulting in joint destruction and osteophytes formation.

The hallmarks of OA are:

- *Joint space narrowing*: due to loss of the cartilaginous surface of the joint.
- *Osteophytes formation*: osteophytes are small extra bony growths commonly seen at the margins of the affected joint. Osteophytes formation is the body's palliative attempt to increase the articular surface area. They are formed in the areas of low stress, classically at the margins of the joint, because vascularization of the subchondral bone is high.
- *Subchondral sclerosis*: new bone (callus) formation at the areas of articular cartilage loss due to bone-to-bone friction and trabecular bone micro-fractures.
- *Subchondral cysts* (*geodes*): cystic lesions formed in the subchondral bone due to trabecular bone micro-fractures with deposition of hemorrhagic, myxoid, and adipose material within these fractured trabeculae. Later, a cyst forms in these fractured trabeculae instead of bone healing.

Primary OA is a term used when OA develops with no predisposing factor (e.g., trauma), and it can be classified into three subtypes: genetically determined OA (type 1), estrogen-hormone-dependent OA (type 2), and aging-related OA (type 3). Genetically determined OA is commonly seen in middle-aged women and occurs almost exclusively in the hands. It affects the distal and proximal interphalangeal (DIP and PIP) joints, and the base of the thumb in bilateral symmetrical fashion. Primary OA must be bilaterally symmetrical to be diagnosed. Estrogen-dependent OA is seen in females after menopause, or patients with hysterectomy due to loss of the effect of estrogen on the cartilage, bone, synovium, ligaments, and muscles. It affects mostly the knees, and is seen perimenopausally or within 5 years of natural menopause or hysterectomy.

Secondary OA is the most common form, which develops after a pathological event that violates the articular cartilage integrity. Joint trauma, metabolic abnormalities (e.g., ochronosis), and bleeding into joints (hemoarthrosis) are common causes of secondary OA. The incidence of OA increases with age, but it is not a natural outcome of it (not every old person develops OA).

Erosive OA is a severe form of primary OA that presents clinically with an acute inflammatory process of swelling, erythema of the joint, and limitation in function. Erosive OA is predominantly seen in the hands of postmenopausal women, and it can be confused with rheumatoid arthritis. It has the same distribution as primary OA (bilateral and symmetrical), but is associated with severe osteoporosis and erosions in the hands (it occurs only in hands). Erosions of erosive OA affect the central portion of the articular surface, unlike rheumatoid arthritis which affects margins of the articular surface.

Rapid destructive osteoarthritis (*Postel's osteoarthritis*) is an uncommon type of hip OA where destruction of the bone and cartilage occurs within a matter of weeks to months. The cause of this disorder is unknown. Cases might be seen with disorders like ochronosis, hemochromatosis, and drug-induced arthropathy (especially indomethacin). Patients are usually women presenting with severe progressive pain classically in a single hip joint.

Signs on Plain Radiographs and MRI

- The radiological hallmarks for OA are its four main signs: narrowing of joint space, bone sclerosis, subchondral cysts, and osteophytes formation (Fig. 7.5.1)
- *Normal bone density* (no osteoporosis): this differentiates OA from rheumatoid arthritis which is characteristically associated with osteoporosis of the affected joint due to hyperemia and synovial inflammation.
- *Subchondral cysts* (*geodes*) are seen as cystic lesions located below the articular cartilage. On MRI, the cysts show fluid signal intensity on T2W images (high signal) (Fig. 7.5.2).
- *Heberden's nodes* are osteophytes that are seen at the DIP joints. They are commonly seen in primary OA, mainly in the index and the middle fingers (Fig. 7.5.3).
- *Bouchard's nodes* are osteophytes that are seen at the PIP joints (Fig. 7.5.3).
- *Gangelion cyst formation*: a gangelion cyst is a myxoid, tumor-like, cystic lesion that is surrounded by dense connective tissue and filled with gelatinous material. It is

typically located in the epiphysis of long bones. Gangelion cysts are typically round or tubular, unilocular or multilocular lesions with often sharply defined internal septa (Fig. 7.5.4). They may show rim enhancement following contrast injection. Gangelion cysts can be found juxta-articular, intra-osseus, and periosteal in location. Sometimes they are difficult to differentiate from synovial cysts based on imaging alone.

- *Gullwing sign* describes wavy contours of the base of the distal phalanx resembling the wings of a seagull due to small osteophytes formation on both sides of the articular surface.
- *Thumb-base osteoarthritis* (*rhizarthrosis*) is OA that occurs at the trapeziometacarpal joint and the trapeziometacarpal joint of the thumb. (Fig. 7.5.5)
- *Central erosions* of the interphalangeal joints (characteristic of erosive arthritis).
- *Hallux rigidus* is a term used to describe OA of the first metatarsophalangeal joint (the big toe). The appearance of accentuated transverse skin crease overlying the big toe at the DIP joint is commonly associated with hallux rigidus (Fig. 7.5.6).
- *Rapid destructive osteoarthritis*: the radiographic features may mimic osteonecrosis of the hip joint. Septic arthritis must be excluded by synovial fluid aspiration before diagnosing rapid erosive OA.
- In OA of the hip joint, superior migration of the femoral head may occur (Fig. 7.5.7).

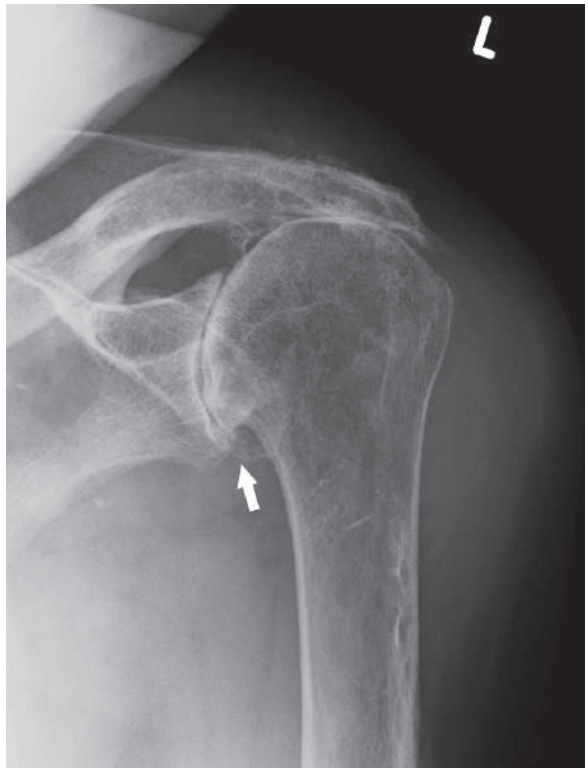

Fig. 7.5.1. Plain shoulder radiograph shows the classical signs of OA: narrowing of the joint space, sclerosis of the humeral head and the glenoid fossa, and osteophyte formation at the base of the humeral head (*arrow*)

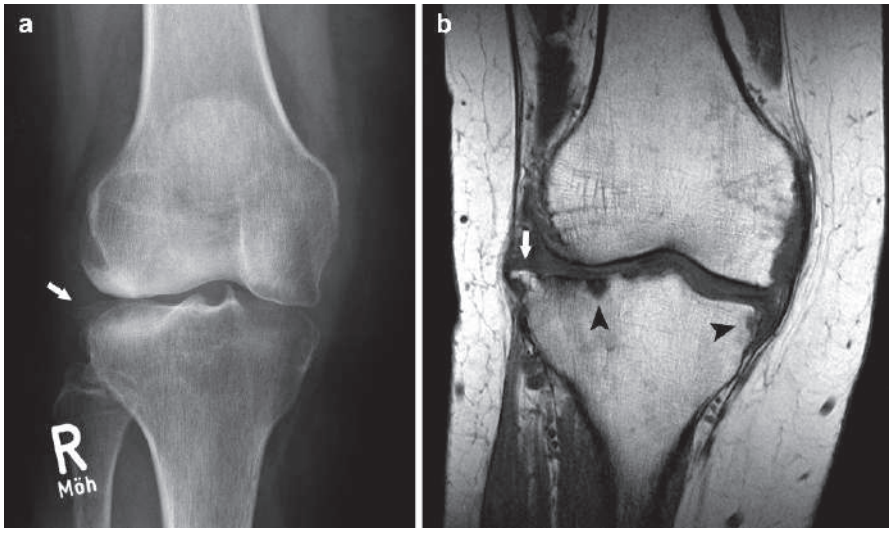

Fig. 7.5.2. Plain knee radiograph (**a**) and coronal T1W knee MRI of the same patient shows subchondral cysts (*black arrowheads*) and marginal osteophyte in the lateral tibial plateau (*white arrows*)

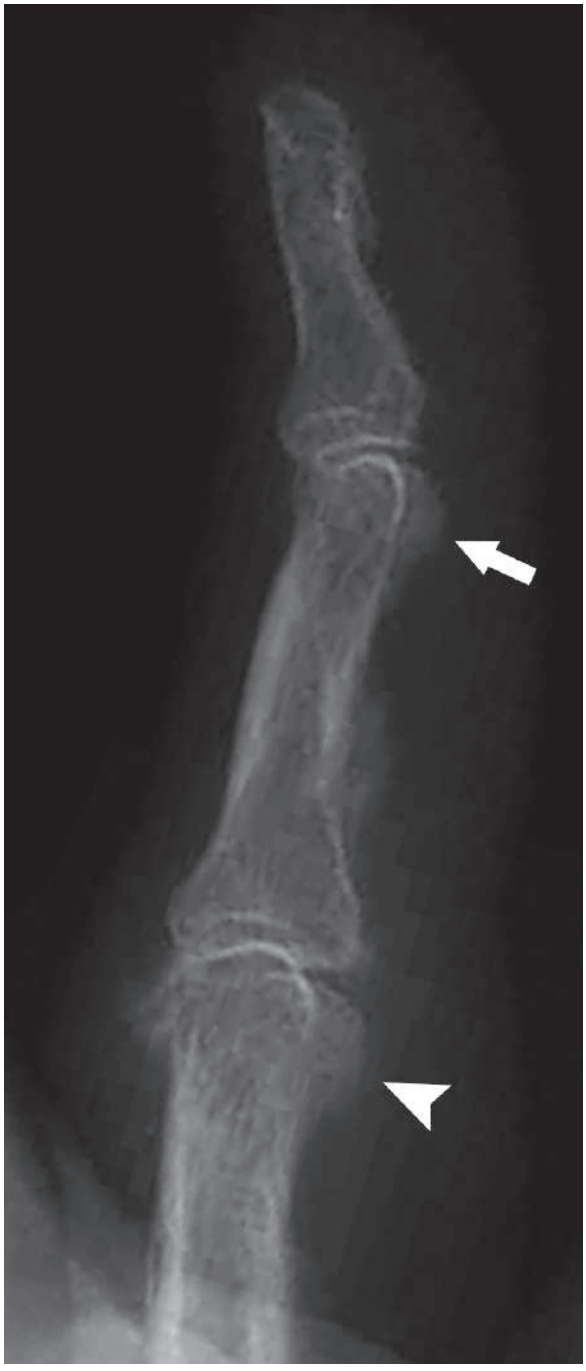

Fig. 7.5.3. Plain radiograph of the finger shows both Heberden's node (*arrow*) and Bouchard's node (*arrowhead*)

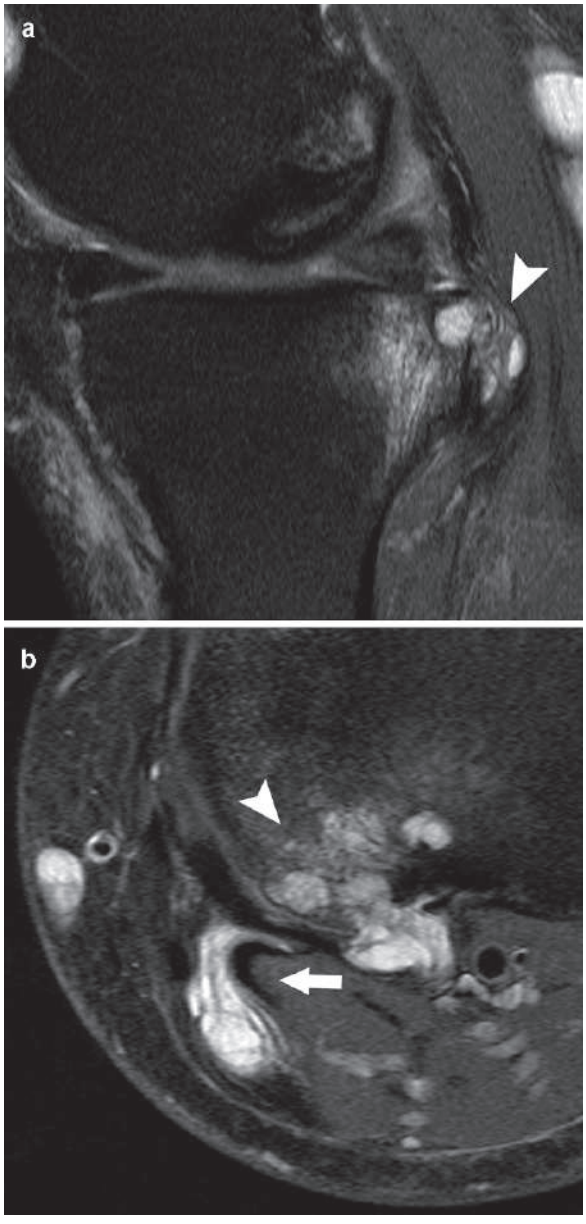

Fig. 7.5.4. Sagittal (**a**) and axial (**b**) PD knee MRI shows juxta-articular intra-osseus gangelion cysts formation in the posterior part of the tibia with bone marrow edema due to knee OA (*arrowheads*). A small Baker cyst can be seen as a secondary finding (*arrow*)

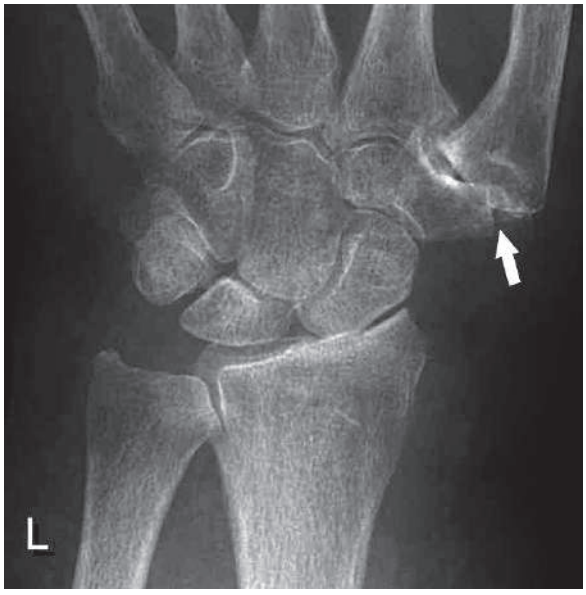

Fig. 7.5.5. Plain radiograph of the hand shows OA of the base of the thumb (*arrow*)

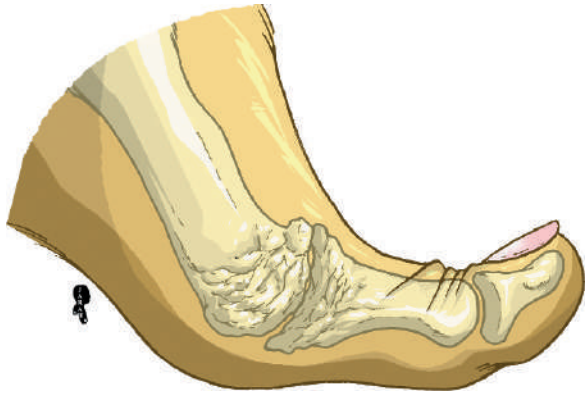

Fig. 7.5.6. An illustration demonstrates hallux rigidus with its accentuated transverse skin crease

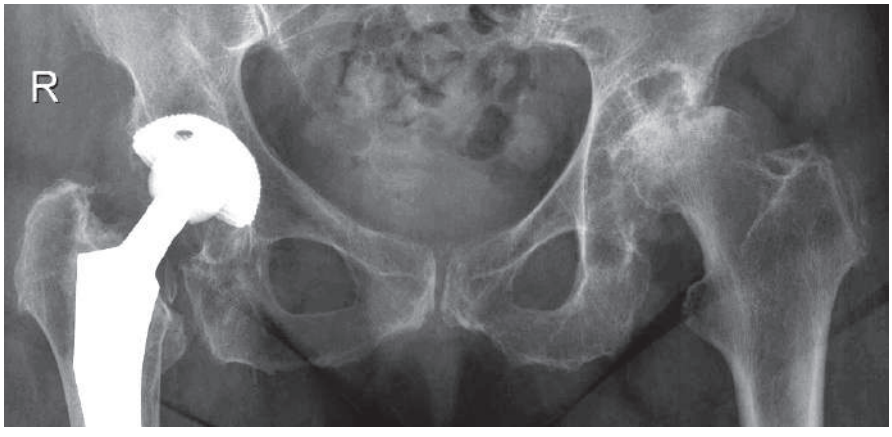

Fig. 7.5.7. Anteroposterior plain radiograph of the pelvis shows severe OA of the left hip joint with superior displacement of the femoral head. Notice the total right hip joint replacement due to previous OA of the right hip joint

For Further Reading

1. Gupta KB et al Radiographic evaluation of osteoarthritis. Radiol Clin North Am. 2004;42:11–41
2. Corrà T et al Ochronotic arthropathy: Rapid destructive hip osteoarthritis associated with metabolic disease. Clin Rheumatol. 1995;14:474–7
3. Theiler R et al Reduced vitamin A tolerance in a hyperlipidemia patient with rapid destructive and hyperostotic osteoarthritis of the hip. Clin Rheumatol. 1994;13:293–8
4. Kijowski R et al Correlation between radiographic findings of osteoarthritis and arthroscopic findings of articular cartilage degeneration within the patellofemoral joint. Skeletal Radiol. 2006;35:895–902
5. Weiss E et al Osteoarthritis revisited: A contemporary review of aetiology. Int J Osteoarchaeol. 2007;17:437–50
6. Beaman FD et al MR imaging of cysts, ganglia, and bursae about the knee. Radiol Clin North Am. 2007;45:969–82

7.6 Psoriasis and Psoriatic Arthritis

Psoriasis is an idiopathic genetic, multifactorial disease characterized by the formation of large, sharply defined, sliver-white scaly cutaneous plaques on the extensor surfaces of the knees and elbows, genitalia, scalp, and lumbosacral area. Psoarisis comes from the Greek word "spora," which means itch.

Psoriasis can present as erythematous plaques (psoriasis vulgaris), or pustules (psoriasis pustulosa). The psoriatic skin lesions are characterized by hyperproliferation of the epidermal keratinocytes, and inflammatory cell cutaneous infiltration in which neutrophils and lymphocytes predominate. The earliest psoariatic lesion is an erythematous papule surmounted by a fine scale, and is characteristically sharply demarcated from surrounding normal skin. If the scale of psoriasis is lifted, multiple, minute areas of bleeding will form (*Auspitz sign*).

Predisposing factors of psoriasis include: emotional trauma, infections (e.g., β-hemolytic streptococci), sunlight, hormonal changes (e.g., pregnancy), medications (e.g., antimalaria drugs), and cigarette smoking. Many patients experience worsening symptoms in winter. *Köbner's phenomenon* is a term used to describe the formation of psoriatic lesions in an area of previous trauma. *Inverse psoriasis* is a term used to describe a condition in which the psoriasis involves the flexor surfaces rather than the extensor surfaces.

Psoriatic arthritis (*PsA*) is an inflammatory, rheumatoid factor-negative arthritis that is associated with psoriasis. PsA is found in 5–7% of patients with psoriasis. PsA can occur in up to 40% of severe psoriasis cases. Up to 60% of PsA patients are HLA-B27 positive, and they are young adults aged 35–55 years.

Skin psoriasis precedes PsA in 70% of cases, and occurs concomitantly with PsA in 15% of cases. However, PsA may precede psoriasis skin lesions in 10–30% of cases.

PsA is characterized by bone erosions with new bone formation, which is the most distinguishing character of PsA differentiating it from other seronegative spondyloarthritis disorders. PsA is characterized by the formation of periostitis, enthesitis, and distal joint distribution in the extremities. Moreover, PsA arthritis can be symmetrical mimicking rheumatoid arthritis, asymmetrical, and affecting the axial skeleton mimicking ankylosing spondylitis. Because of these reasons, the history of psoriasis plus the absence of serological tests for rheumatoid factor are essential criteria to establish the diagnosis of PsA.

Hyperuricemia may be found in association with PsA as a result of increased purine metabolism due to high cell turnover. However, gout arthropathy is rarely developed in association with PsA.

Enthesitis is the inflammation at the site of attachment of a tendon or a ligament to the joint capsule (e.g., plantal fasciitis). The concept of an "enthesis organ" states that the enthesis together with the adjacent fibrocartilage, periosteium, synovial and bursal membrane should be viewed as a unique "organ." PsA is considered as a disease affecting the enthesis organ, unlike rheumatoid arthritis which is a disease essentially affecting the synovium. Entheses may be fibrous (located at the metaphyses or diaphyses of long bones), or fibrocartilaginous (located at the apophyses and epiphyses of long bones). Both types are found in the spine.

Sinus tarsi syndrome may occur in patients with PsA. The sinus tarsi is a bony compartment bounded by the talus, the calcaneus, the talonavicular and posterior subtalar joints, and is continuous with the tarsal canal medially. The sinus tarsi contains fat, nerve endings, vessels, and ligaments (cervival and interosseus ligaments). Sinus tarsi syndrome is a clinical condition characterized by pain and paresthesia in the lateral side of the ankle. The causes of sinus tarsi syndrome include hemorrhage or inflammation of the synovial recesses of the sinus tarsi. Other causes include ganglion cyst formation within the sinus tarsi.

Differential Diagnoses and Related Diseases

SAPHO syndrome is a disease characterized by *S*ynovitis, *A*cne, *P*ustulosis the palmar and plantar skin surface (psoriasis vulgaris), *H*yperostosis of bones (e.g., sterno-clavicular joint), and *O*stitis. SAPHO syndrome can occur with PsA in 2% of cases.

7.6

Signs on Radiographs (In General, the Radiographic Features Are Either Erosive or Proliferative Changes)

- Osteoporosis is mild or absent in spite of severe bone erosions. Erosions typically start at the margins then progress toward the center.
- Bone erosions start from the periphery of the joint and extend to the articular surface. The distal interphalangeal joints (DIPJs) of the hands and feet are commonly affected.
- The sacroiliac joint is affected in a unilateral or bilateral pattern (sacroiliitis occurs in up to 40%).
- Periosteal reaction is seen at the affected bones as fuzzy appearance, which is characteristic for the bony proliferation associated with psoriatic arthritis (Fig. 7.6.1).
- *Sausage fingers or toes*: soft tissue swelling of the affected fingers or toes due to tenosynuvitis. It is seen in 40% of psoriatic patients (Fig. 7.6.2).
- *Ivory phalanx* is a characteristic lesion of PsA that most often occurs in the distal phalanx of the great toe. It is seen as a dense appearance of the distal interphalangeal joint due to sclerosis plus periosteal and endosteal new bone formation.
- *Pencil and cup deformity*: this deformity is seen in a severe form of marginal erosion, with one end of the joint forming the cup and the other a pencil that projects into this cup. It is mostly seen in the DIP joints of the fingers. The pencil tip is represented by the distal end of the metatarsal or metacarpal bone with the cup represented by the eroded articular surface of the apposing phalanx.
- *Non-marginal bridging*: this is seen in the axial skeleton as excess bone formation that usually begins toward the vertebral bodies and curves upward. In contrast, syndesmophytes in ankylosing spondylitis begin at the corner of the vertebral body and extend vertically.

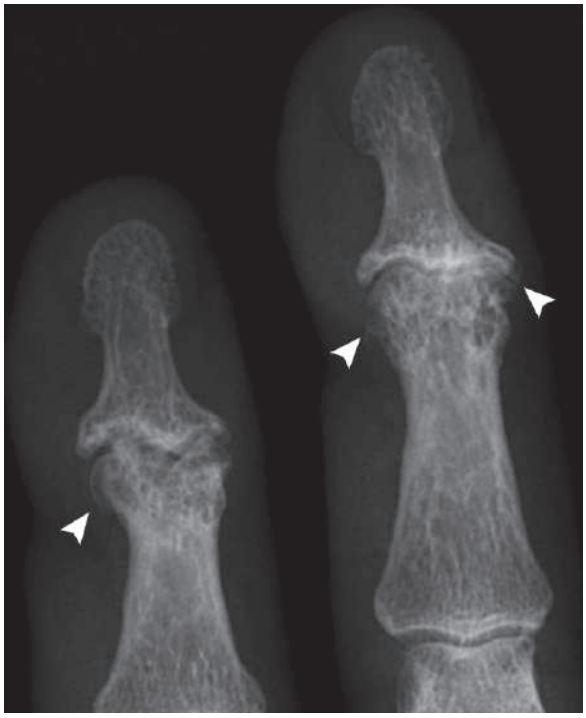

Fig. 7.6.1. Plain radiograph of the distal fingers in a patient with psoriasis shows narrowing of the DIP joints and marginal new bone formation (*arrowheads*)

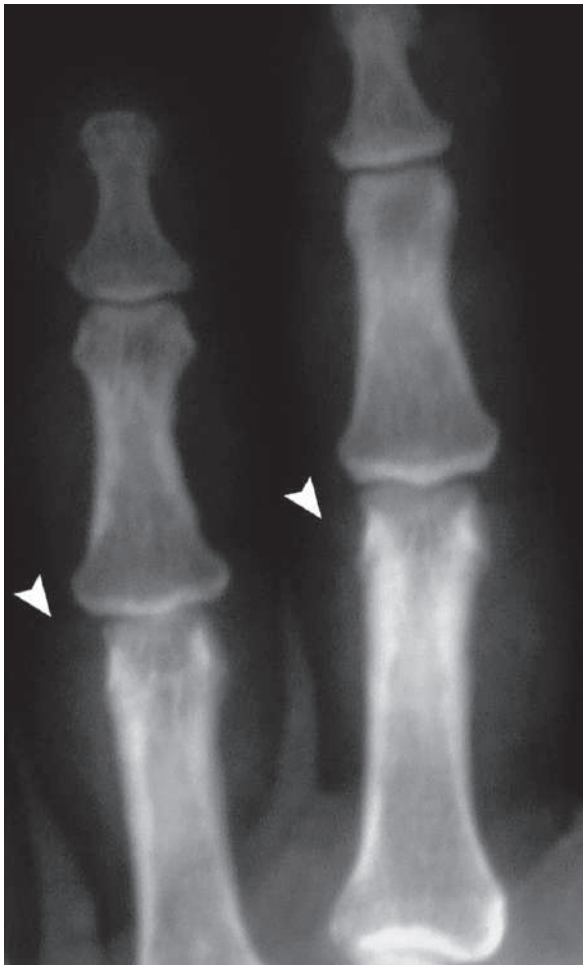

Fig. 7.6.2. Plain radiograph of the fingers in a patient with psoriasis shows soft tissue swelling (*arrowheads*) of the PIP joints (sausage fingers)

Signs on MRI

- Tenosynovitis is defined as high T2 signal intensity surrounding a low T2 intensity tendon (Fig. 7.6.3).
- In the foot, PsA can develop Achilles tendinitis, which is seen as thickened Achilles' tendon with high signal intensity within the tendon (Fig. 7.6.3).
- Plantal fasciitis is seen as a T2 high signal intensity at the site where the plantar fascia is inserted into the calcaneus (enthesitis) (Fig. 7.6.3).
- In sinus tarsi syndrome, there are low T1 and high T2 signal intensities within the sinus tarsi, with or without loss of the cervical or the interosseus ligaments (Figs. 7.6.3 and 7.6.4).

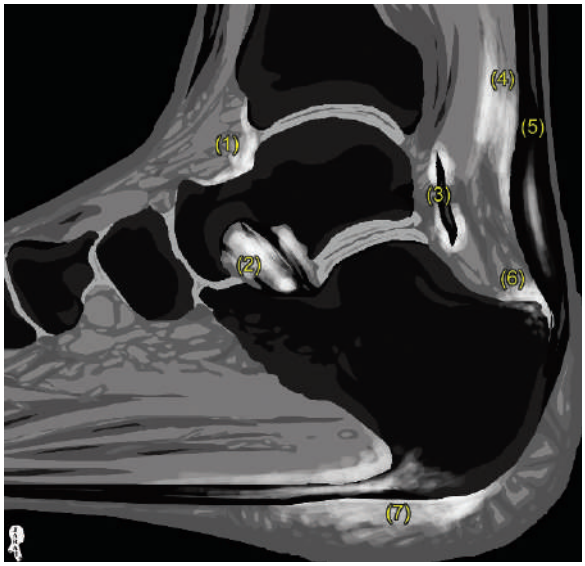

Fig. 7.6.3. Sagittal STIR ankle MR illustration demonstrates types of foot pathologies seen in psoriatic arthritis: (*1*) synovitis, (*2*) sinus tarsi syndrome, (*3*) tenosynovitis, (*4*) Achilles peritendinitis, (*5*) Achilles tendonitis, (*6*) retrocalcaneal bursitis, and (*7*) plantar fasciitis

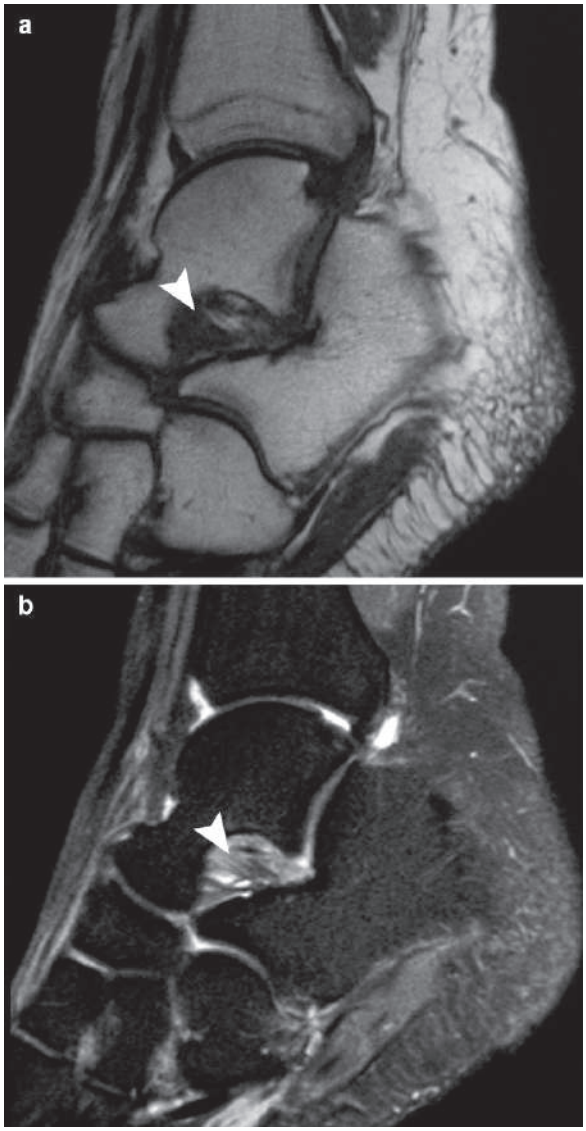

Fig. 7.6.4. Sagittal T1W (**a**) and STIR (**b**) ankle MRI of a patient with chronic sinus tarsi syndrome show mild hyperintense signal within the sinus tarsi with disruption of the interosseus ligament (*arrowhead*)

For Further Reading

1. Baden HP et al Psoriasis. Dis Mon. 1973;19:1–45
2. Prasad PVS et al A clinical study of psoriatic arthropathy. Indian J Dermatol Venerol Leprol. 2007;73:166–70
3. Jacobson JA et al Radiographic evaluation of arthritis: inflammatory conditions. Radiology. 2008;248:378–89
4. Zuhal Erdem C et al MR imaging features of foot involvement in patients with psoriasis. Eur J Radiol. 2008;67: 521–5
5. Tan AL. Imaging of seronegative spondyloarthritis. Best Pract Res Clin Rheumatol. 2008;22:1045–59
6. Leung YY et al Psoriatic arthritis as a distinct disease entity. J Postgrad Med. 2007;53:63–71
7. Zelickson BD et al Generalized pustular psoriasis in childhood. Report of thirteen cases. J Am Acad Dermatol. 1991; 24:186–94
8. Vun YY et al Generalized pustular psoriasis of pregnancy treated with narrowband UVB and topical steroids. J Am Acad Dermatol. 2006;54:S28–30
9. Bellet JS et al Intertriginous pustular psoriasis. J Am Acad Dermatol. 2009;60:679–83
10. Herbst RA et al Guttate psoriasis triggered by perianal streptococcal dermatitis in a four-year-old boy. J Am Acad Dermatol. 2000;42:885–7
11. Jiaravuthisan MM et al Psoriasis of the nail: anatomy, pathology, clinical presentation, and a review of the literature on therapy. J Am Acad Dermatol. 2007;57:1–27
12. Lee Bennett D et al Spondyloarthropathies: ankylosing spondulitis and psoriatic arthritis. Radiol Clin North Am. 2004;42:121–34
13. Benjamin M et al Magnetic resonance imaging of entheses. Part 1. Clin Radiol. 2008;63:691–703

7.7

Baastrup's Disease (Spinout Process Impingement Syndrome)

Baastrup disease (BD) is a pathological condition characterized by close approximation and contact of adjacent spinout processes, an appearance known as "kissing spines," leading to reactive bone and cartilage formation in the spinous processes causing sclerosis, enlargement, and flattening of the involved spines, with calcification of the interspinous and supraspinous ligaments (Fig. 7.7.1).

BD most commonly occurs in the lumbar spines. Cervical spines can be affected rarely. Patients typically present with back pain exacerbated on spine extension, which is relieved by flexion. The pain arises due to irritation of the periosteum or adventitial bursae between abutting spinous processes.

Signs on Plain Radiograph

There is close approximation of the spinous processes with sclerosis, osteophytes formation, and hyperlordosis (Fig. 7.7.2).

Signs on MRI

There is approximation of the spinous processes, usually in the lumbar spines. Bone marrow edema is often seen in active disease, typically located in the spinous processes.

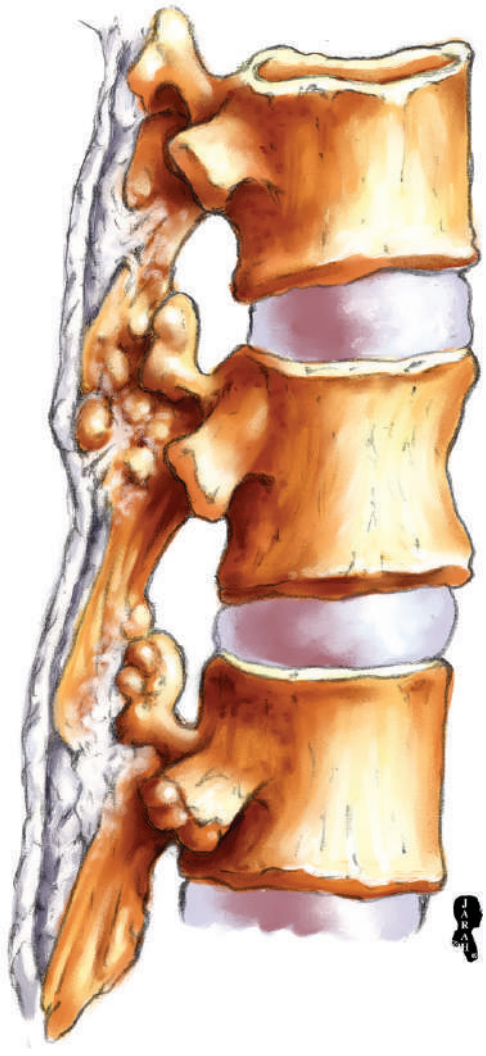

Fig. 7.7.1. An illustration of the thoracic vertebrae demonstrates the gross appearance of the kissing spines and the calcification of the interspinous and supraspinous ligaments in Baastrup's disease

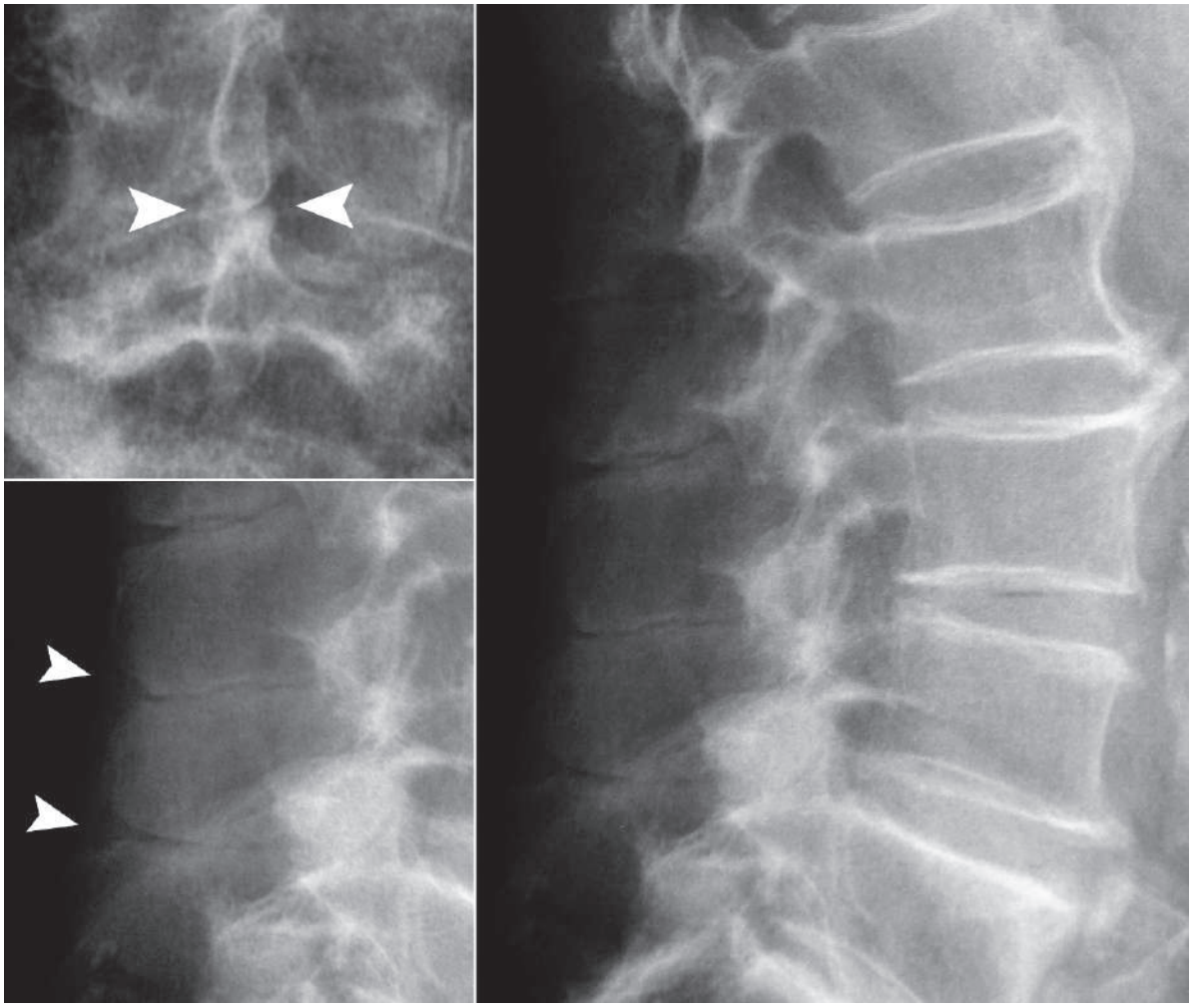

Fig. 7.7.2. Lateral and anteroposterior plain radiograph of the vertebral column in the thoracolumbar region shows flattened spinous processes of the lumbar vertebrae with sclerosis and close approximation (*arrowheads*), typical findings in Baastrup's disease of the spines

For Further Reading

1. Lin E. Baastrup's disease (kissing spine) demonstrated by FDG/PET CT. Skeletal Radiol. 2008;37:173–5
2. Pinto PS et al Spinous process fracture associated with Baastrup disease. J Clin Imaging. 2004;28:219–22
3. Hui C et al Two unusual presentations of Baastrup's disease. Clin. Radiol. 2007;62:495–7

7.8

Scheuermann's Disease (Juvenile Kyphosis Dorsalis)

Scheuermann's disease (SD) is a disease characterized by juvenile thoracic kyphosis with minimal deformity and few clinical symptoms (Fig. 7.8.1). The disease has an autosomal dominant pattern of inheritance, with an incidence of 1% of population.

The normal disc space is composed of two end plates, central nucleus pulposus, and an outer annulus fibrous tissue (annulus fibrosus) surrounding the nucleus pulposus. Due to age process or repetitive trauma, the nucleus pulposus loses its watery content and the annulus fibrosus develops cracks and fissures. When this occurs, the nucleus pulposus extrudes through the annulus fibrosus fissures. Extrusion of the nucleus pulposus into the vertebral end plates results in Schmorl node and limbus vertebra, while extrusion through the annulus fibrosus results in disc degenerative disease (disc hernia). *Schmorl node* is nucleus pulposus extrusion into the end plates and then into the vertebral body. In contrast, *limbus vertebra* is extrusion of the nucleus pulposus below the ring apophysis separating it from the body of the vertebra. SD is characterized by the presence of Schmorl node and multiple end plate irregularities due to nucleus pulposus extrusion.

Although the etiology of SD is unknown, Scheuermann proposed that the kyphosis resulted from avascular necrosis of the vertebral body's apophysis ring, but it is now generally believed to be a form of disc degeneration. *Kyphosis* is a term used to describe posterior convex curvature of the spine. Normal vertebral kyphosis is located in the cervico-lumbar areas and does not exceed 25–45°. Any kyphosis exceeding this range is considered pathologic. Kyphosis is classified into:

- *Arcuate kyphosis*: kyphosis with long arc. This type is seen in SD, osteoporosis, and ankylosing spondylitis.
- *Angular kyphosis*: kyphosis with short arc. This type is seen in vertebral pathologic or compressive fractures, and spondylities.

SD can be associated with scoliosis in 15% of cases. *Scoliosis* is defined as an abnormal lateral curvature of the vertebral column. It can be classified into:

- *Rotoscoliosis*: scoliosis with rotation of the vertebra in the axial plane (Fig. 7.8.2).
- *Kyphoscoliosis*: scoliosis plus kyphosis
- *S-shaped scoliosis*: double lateral deviation of the vertebral column (Fig. 7.8.3).
- *C-shaped scoliosis*: single lateral curve of the vertebral column.

Fig. 7.8.1. An illustration demonstrates thoracic kyphosis in a young patient with Scheuermann's disease (SD)

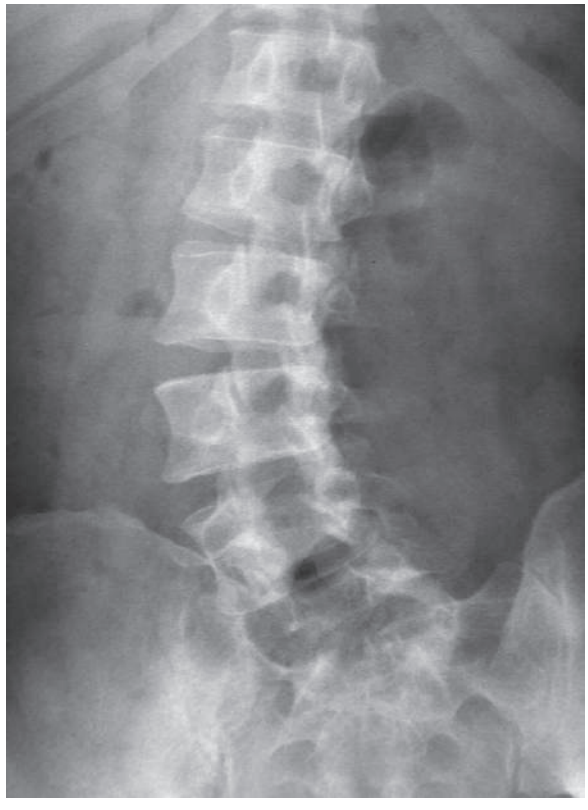

Fig. 7.8.2. A plain abdominal radiograph of a patient shows right rotoskoliosis

7.8

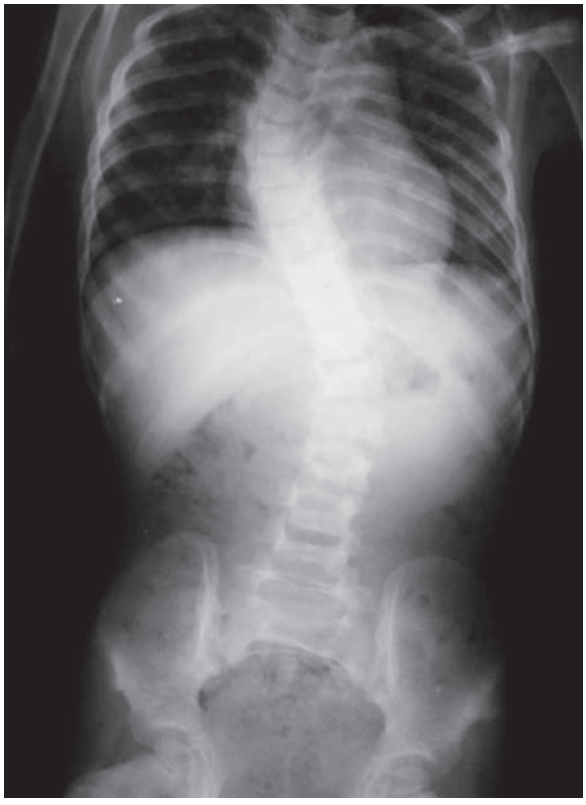

Fig. 7.8.3. A plain abdominal radiograph of a patient with Marfan's syndrome shows right S-shaped skoliosis

Neurological symptoms of SD are rare in general, and usually arise due to spinal cord compression. There are three types of neural compression reported in SD:

- Extradural spinal cyst.
- Compression of the cord at the apex of the kyphos.
- Disk hernia at the apex of the kyphos.

Criteria for Scheuermann's Disease Diagnosis

- More than 5° of wedging of at least three adjacent vertebrae at the apex of the kyphosis.
- End plate irregularities.
- A thoracic kyphosis of more than 45°.

Signs on Radiographs, CT, and MRI

- Increased thoracic kyphosis with compensatory lumbar hyperlordosis (Fig. 7.8.4).
- Wedging of at least three consecutive vertebrae (>5°) with end plate irregularities (Fig. 7.8.4).
- End plate irregularities, loss of disc space height, and Schmorl nodes. Schmorl node is defined as localized depression of the superior or inferior end plates >3 mm in diameter (Fig. 7.8.5).
- Limbus vertebra is visualized as separation of the ring apophysis from the vertebral body (Fig. 7.8.6).
- Scoliosis in 15% of cases.

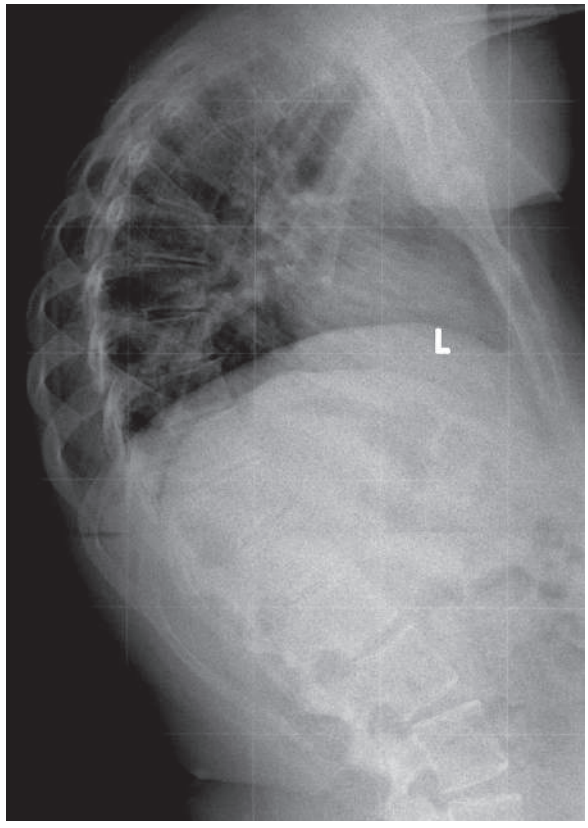

Fig. 7.8.4. Lateral plain radiograph of the thoracic spine of an 18-year-old girl with SD shows marked thoracic kyphosis with wedging of more than three adjacent vertebrae

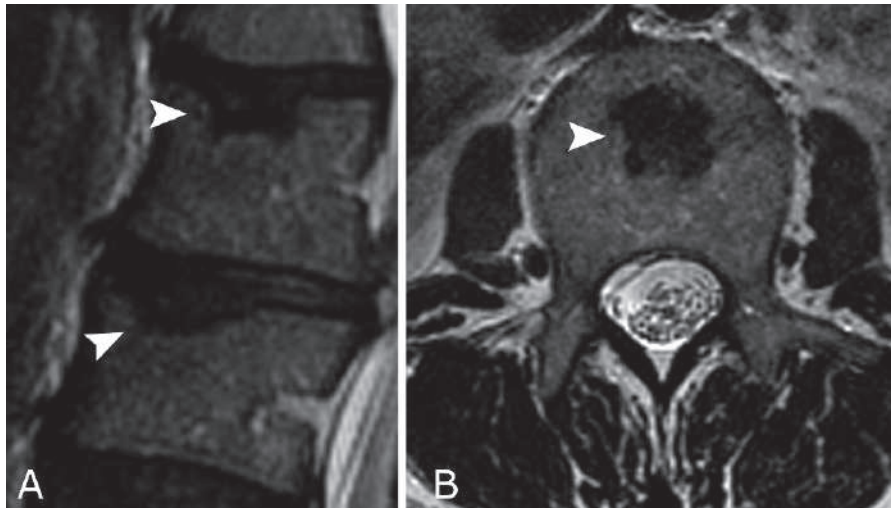

Fig. 7.8.5. Sagittal (**a**) and axial (**b**) T2W image MRI of a patient with SD shows Schmorl's node seen as localized depression of the superior end plates >3 mm in diameter due to extrusion of the nucleus pulposus into the end plates (*arrowheads*)

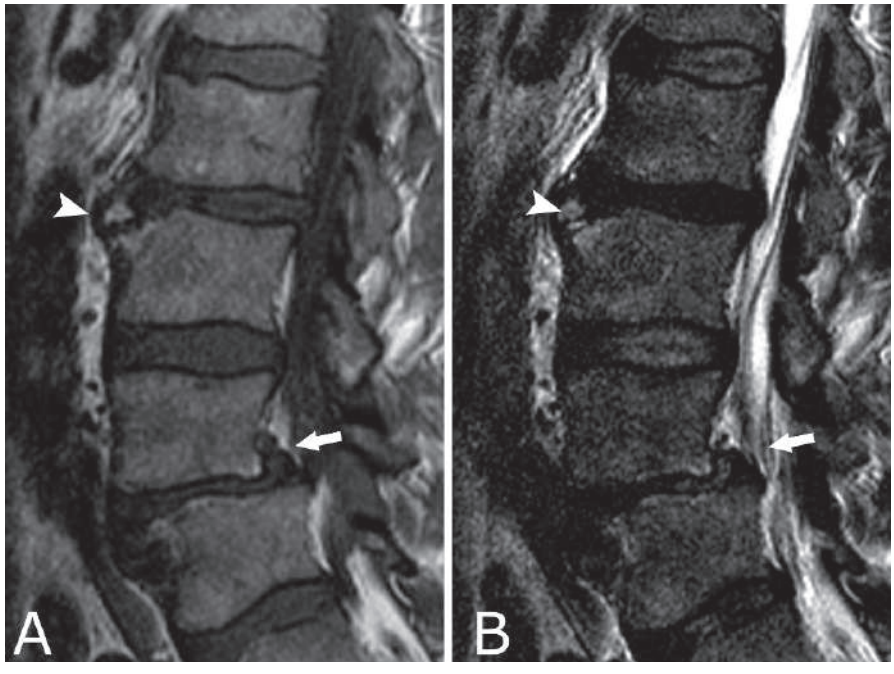

Fig. 7.8.6. Sagittal T1W (**a**) and T2W (**b**) MRI of a patient with vertebral column osteochondrosis shows L2 limbus vertebra (*arrowheads*) and L4/L5 grade 1 (<25%) spondylolisthesis (*arrows*). Notice the active bone marrow edema around the bone fragment of the anterior superior end plate of L2 in (**b**)

For Further Reading

1. Swischunk LE et al Disk degeneration in childhood: Scheuermann's disease, Schmorl's nodes, and the limbus vertebra: MRI findings in 12 patients. Pediatr Radiol. 1998;28:334–8
2. Arlet V et al Scheuermann's kyphosis: surgical management. Eur Spine J. 2005;14:817–27
3. Kapetanos GA et al Thoracic cord compression caused by disk herniation in Scheuermann's disease. A case report and review of the literature. Eur Spine J. 2006;15(suppl. 5): S553–8
4. Alexander CJ. Scheuermann's disease. Skeletal Ardiol. 1977; 1:209–21
5. Paajanen H et al Disc degeneration in Scheuermann disease. Skeletal Radiol. 1989;18:523–6

7.9

Sjögren Syndrome (Myoepithelial Sialadenitis)

Sjögren syndrome (SS) is a chronic, systemic autoimmune disease characterized by infiltration of the acinar cells of the salivary and lacrimal glands by lymphocytes, causing dry eye (*xeropthalmia*), dry mouth (*xerostomia*), and inflammation of the cornea and the conjunctiva (*keratoconjunctivitis*).

SS is classified as secondary (*Sicca syndrome*) when it is associated with other connective tissue disorders (e.g., rheumatoid arthritis), and primary when it occurs without any manifestation of other connective tissue disorders.

Criteria to Diagnose SS Include

- Symptoms and signs of ocular dryness (e.g., positive Schrimer's test).
- Symptoms and signs of mouth dryness.
- Evidence of autoimmune disease (e.g., positive rheumatoid factor).
- Exclusion of lymphoma, sarcoidosis, and acquired immunodeficiency syndrome.

SS causes salivary glands inflammation (*sialeadenitis*) that leads to parenchymal destruction and salivary gland dilatation (*sialectasia*).

Patients with SS are commonly perimenopausal women who often develop multiple systemic manifestations that include mouth dryness, which affects eating, speaking, and may lead to teeth decay; extreme fatigue occurs in 50% of patients, which is more troublesome than the exocrine symptoms; intermittent polyarthritis affecting the small joints in asymmetrical fashion; dry skin (50%), esophageal dysmotility (up to 90%), vaginal atrophy and dyspareunia, and interstitial nephritis. Patients with SS have risk for developing lymphoma, and they should be closely monitored.

Patients with SS may also develop neuropsychiatric manifestations. Brain manifestations include aseptic meningoencephalitis and multiple sclerosis-like symptoms (25% of cases). Psychiatric manifestations include Alzheimer-type dementia, poor attention and concentration, and memory deficits. Rarely, neuromyelitis optica may coexist in patients with SS. In children, although it is rare, SS is characterized by bilateral parotid enlargement. Very rarely, SS may be associated with amyloidosis.

Laboratory investigation reveals high titer of SS-A antibodies and SS-B antibodies plus rheumatoid factor in 50% of cases.

Signs on Sialography

On both conventional and MR-sialography, the affected salivary gland shows mottled appearance with cystic changes due to destruction of the gland parenchyma (sialectasia). Four stages of sialectasia are classically described:
Stage 1 (*punctuate*): multiple dots <1 mm in size (Fig. 7.9.1).
Stage 2 (*globular*): multiple dots 1–2 mm in size.
Stage 3 (*cavitary*): multiple dots >2 mm in size.
Stage 4 (*destructive*): multiple irregular and widened ducts due to gland inflammation (*sialodochitis*).

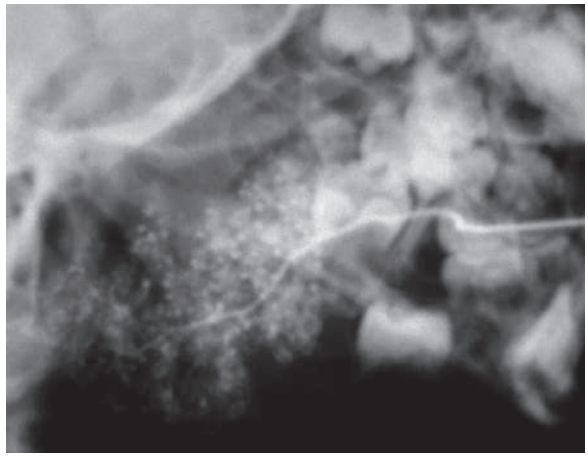

Fig. 7.9.1. Lateral conventional sialography radiograph in a patient with submandibular sialectasis grade 1-2 seen as diffuse multiple punctuated dots between 1-2 mm in diameter

Signs on CT

- In the acute phase, the affected glands are bilaterally enlarged with parenchymal nodules of variable size and formation of cysts, giving a honeycomb appearance (Fig. 7.9.2).
- The salivary glands often show signs of fibrosis and size shrinkage in advanced stages of the disease.
- The lacrimal glands might be bilaterally and symmetrically enlarged (Fig. 7.9.3).

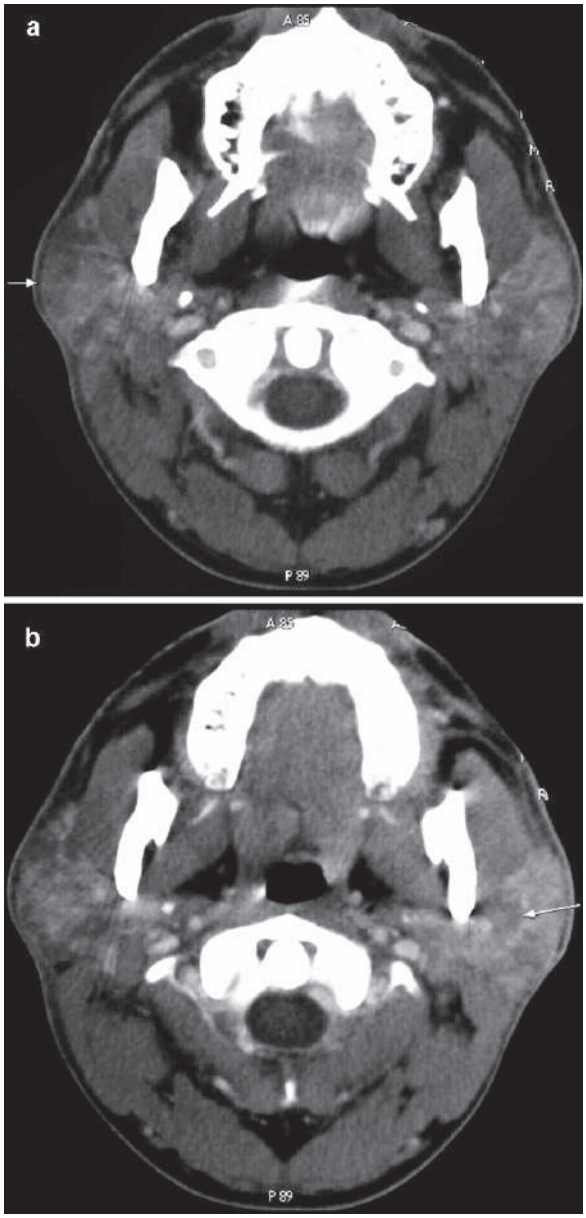

Fig. 7.9.2. Sequential postcontrast head CT images (**a**) and (**b**) of a patient with Sjögren syndrome (SS) show bilateral parotid gland bulging and enlargement (*arrows*)

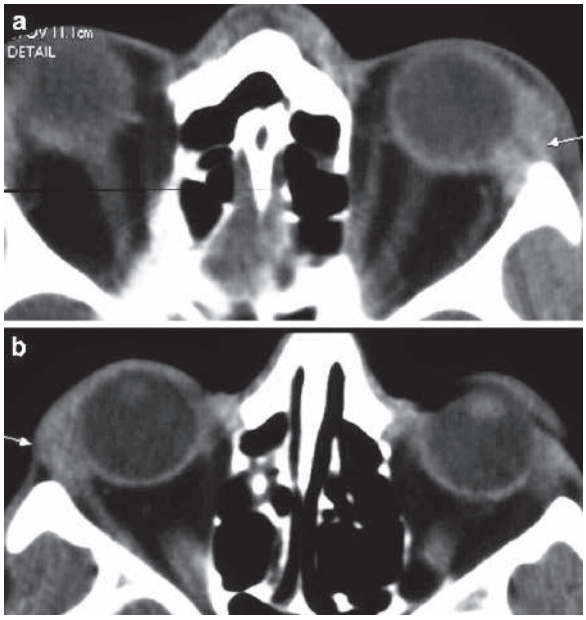

Fig. 7.9.3. Sequential nonenhanced orbital CT images of the same patient with Sjögren syndrome (SS) show bilateral lacrimal glands enlargement (*arrows*)

Signs on Brain MRI

Brain MRI shows multifocal T2 hyperintensities located in the subcortical and periventricular white matter (Fig. 7.9.4), enlargement of the sulci, and ventricular dilatation. These manifestations are often seen in 50% of patients with focal neurological deficits or psychiatric manifestations.

7.9

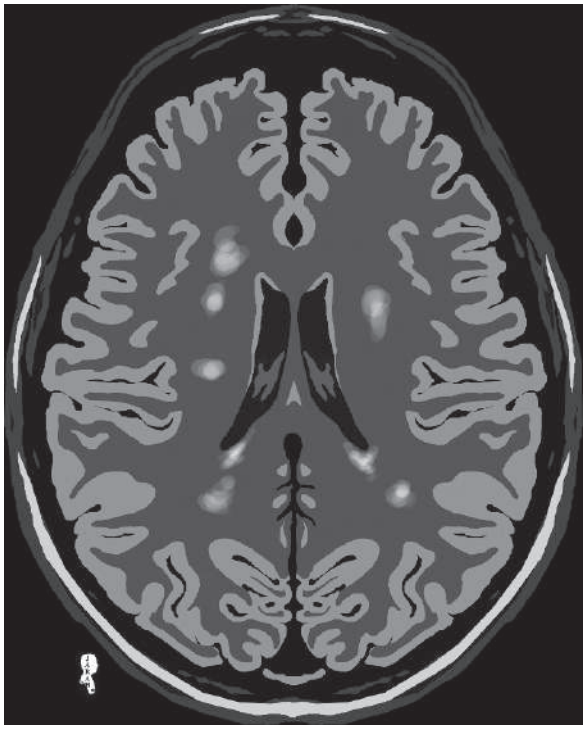

Fig. 7.9.4. Axial FLAIR brain MR illustration demonstrates patchy areas of high T2 signal intensity lesions within the white matter as presentation of neuro-Sjögren syndrome (SS)

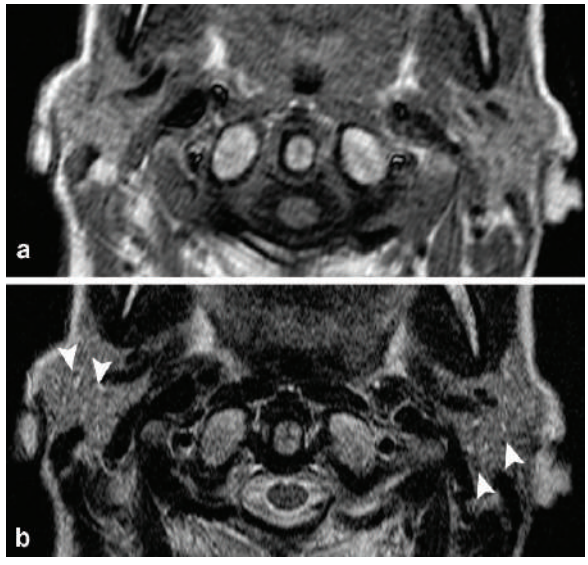

Fig. 7.9.5. Axial T1W (**a**) and T2W (**b**) images of a patient with Sjögren syndrome (SS) show bilateral moderate parotid glands enlargement with fine, small cysts formation within the gland (*arrowheads*)

Signs on Parotid MRI

- Bilateral, almost symmetrical enlargement of the parotid glands (Fig. 7.9.5).
- Low T1/high T2 multiple cysts are seen within the parotid and lack of enhancement ("salt and pepper" appearance) (Fig. 7.9.5).
- Chronic disease can lead to gland shrinkage, microcysts formation, and calcifications.

For Further Reading

1. Mataró M et al Magnetic resonance abnormalities associated with cognitive dysfunction in primary Sjögren syndrome. J Neurol. 2003;250:1070–6
2. Mizuno Y et al Recurrent parotid gland enlargement as an initial manifestation of Sjögren syndrome in children. Eur J Pediatr. 1989;148:414–16
3. Kobayashi I et al Complications of childhood Sjögren syndrome. Eur J Pediatr. 1996;155:890–4
4. Tristano AG et al A case of Sjögren's syndrome with acute transverse myelitis and polyneuropathy in a patient free of sicca symptoms. Clin Rheumatol. 2005;25:113–14
5. Adžić TN et al Multinodular pulmonary amyloidosis in primary Sjögren's syndrome. Eur J Int Med. 2008;19:e97–8
6. Ohbayashi N et al Sjögren syndrome: Comparison of assessments with MR sialography and conventional sialography. Radiology 1998;209:683–8
7. Yoon YH et al Sialectasis of Stensen's duct: an unusual case of recurrent check swelling. Eur Arch Otorhinolaryngol. doi: 10.1007/s00405–008–0702–0
8. Varghese JC et al A prospective comparative study of MR Sialography and conventional sialography of salivary duct disease. AJR 1999;173:1497–503
9. Kalk WWI et al Parotid sialography for diagnosing Sjögren syndrome. Oral Surg Oral Med Oral Pathol Oral Radiol Endod. 2002;94:131–7
10. Kassan SS et al Clinical manifestations and early diagnosis of Sjögren's syndrome. Arch Intern Med. 2004;164:1275–84
11. Madani G et al Inflammatory conditions of the salivary glands. Semin Ultrasound CT MRI. 2006;27:440–51

7.10 Behçet Disease

Behçet disease (BD) is a relatively rare rheumatological disease characterized by the triad of apthus oral ulcers, genital ulcers, and ocular inflammation (uveitis). The disease is named after its first describer, the Turkish dermatologist Hulusi Behçet, in 1937.

Clinical Criteria to Diagnose BD Require a Combination of Three or More of the Following Findings

- Recurrent aphthous stomatitis (79%). The lesions are punched out with rolled edges.
- Recurrent genital ulcers, mainly seen on the scrotum or labial majora, which heal by scar formation.
- Anterior or posterior uveitis, presenting with pain, blurry vision, and redness.
- Vasculitis of cutaneous or large vessels.
- Mono-or oligoarthritis affecting the knees in particular.
- Meningoencephalitis.
- Cutaneous hyperactivity to minor trauma.

BD lesions are characterized by chronic inflammation of the soft tissues with neutrophilic infiltration, which is characteristic of BD lesions regardless of the disease stage.

BD is a multisystemic disease with many manifestations. Documented complications of BD are those that affect the gastrointestinal tract (GI), large vessels (vasculitis and thrombophlebitis), muskuloskeletal system (myonecrosis and arthritis), renal system (proteinuria and hematuria), and the nervous system (neuro-BD).

Myonecrosis should be considered in patients with known BD presenting with acute onset of muscle pain and edema in the absence of signs and symptoms of infection. Renal BD is mainly caused by secondary amyloidosis (AA-type) and glomerulonephritis.

Neuro-BD has three patterns of presentation: the first pattern is seen as brain parenchymal lesions presenting in stroke-like lesions and brain stem syndrome; the second pattern is migraine headache (64%), papilledema, and increased intracranial hypertension; and the third pattern presents in the form of meningitis-like disease.

The esophagus is involved in 50% of patients usually in its mid-portion. Patients with esophageal involvement often present with substernal pain, dysphagia, and occasional hematemesis. Esophageal varices may develop when the superior vena cava is obstructed due to thrombophlebitis (*superior vena cava syndrome*). Thrombophlebitis may involve the hepatic veins resulting in *Budd–Chiari syndrome* (liver congestion and cirrhosis due to hepatic veins outflow obstruction).

GI manifestations of BD may mimic the manifestations of Crohn's disease (CD) radiologicaly, and even pathologically. However, involvement of the rectum and anus is rare in BD; perforation is more common in BD than CD, no cobbelstoning in BD, and the GI disease is usually milder in BD than in CD.

Diagnosis is essentially clinical, and atypical presentation can be misleading and delay the diagnosis.

Signs on Enteroclysis

Distal ileum inflammation and aphthous ulceration are seen in up to 80% of patients with GI manifestations of BD.

Pseudopolyp formation is seen in 35% of cases.

Signs on MRI

- In the muscles, myonecrosis presents with soft tissue inflammation in the form of soft tissue mass with high signal intensity on T2W images and rim contrast enhancement on postgadolinium injection images.
- In the brain, multiple, round, small (>5 mm) white matter high T2 signal intensity lesions on FLAIR and T2W images, usually in the juxtacortical region (Fig. 7.10.1). Brain stem lesions and atrophy can be seen.

7.10

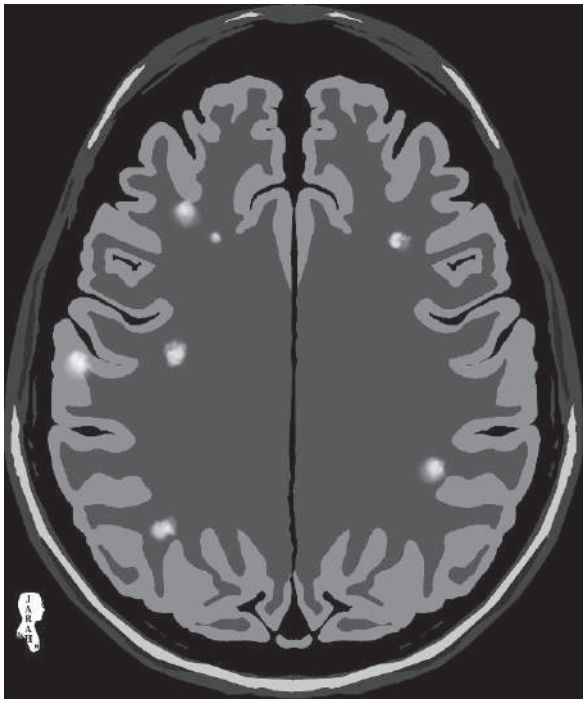

Fig. 7.10.1. Axial FLAIR brain MR illustration demonstrates the neurological findings in neuro-Behçet disease

For Further Reading

1. Stubbs AY et al Myonecrosis in Behcet's disease. Skeletal Radiol. 2008;37:357–60
2. Hwang I et al Necrotizing villitis and decidual vasculitis in placentas of mothers with Behçet disease. Human Pathol. 2009;40:135–8
3. Benjilali L et al Chylothorax and chylopericardium in a young man with Behçet disease. Joint Bone Spine 2008;75: 740–52
4. Akpolat T et al Renal Behçet's disease: an update. Semin Arthritis Rheum. 2008;38:241–8
5. Korman U et al Enteroclysis findings of intestinal Behcet disease: a comparative study with crohn disease. Abdom Imaging 2003;28:308–12
6. Oktay Kaçmaz Ret al Ocular inflammation in Behçet disease: incidence of ocular complications and loss of visual acuity. Am J Opthalmol. 2008;146:828–36
7. Ebert EC et al Gastrointestinal manifestations of Behçet's disease. Dig Dis Sci. doi: 10.1007/s10620–008–0337–4
8. Bank I et al Dural sinus thrombosis in Behçet's disease. Arthritis Rheum. 1984;27:816–8
9. La Mantia L et al Headache and inflammatory disorders of the central nervous system. Neurol Sci. 2004;25:S148–53
10. Jäger HR et al MRI in neuro-Behcet's syndrome: Comparison of conventional spin-echo and FLAIR pulse sequences. Neuroradiology 1990;41:750–8

7.11 Sharp Syndrome (Mixed Connective Tissue Disease)

Mixed connective tissue disorder (MCTD) is a rare disease characterized by a combination of clinical features similar to systemic lupus erythematosus (SLE), scleroderma, and polymyositis, and unusually high titers of antibody to RNase-sensitive ribonuclear protein complex (RNP).

MCTD patients have mixed features of rheumatological symptoms that do not match a certain rheumatological category. For example, polyarthritis, myositis, and hypergammaglobulinemia are more common in MCTD than in scleroderma. Also, polyarthritis and hypergammaglobulinemia are more frequently found in MCTD than in polymyositis. Esophageal hypermotility, pulmonary hypertension, and absence of renal disease are typical features of MCTD. Moreover, the detection of serological antibodies to RNP is very specific for MCTD, and very rarely found in other rheumatic or connective tissue disorders.

Patients with MCTD may show neurological signs like seizures, psychosis, headache, gait disturbance, and polyneuritis. Trigeminal neuralgia has been reported in patients with MCTD, and seen frequently when the patient has more symptoms toward scleroderma. In contrast, MCTD with more symptoms toward SLE shows neurological symptoms like gait ataxia, transverse myelitis, and optic neuropathy. MCTD is one of the rare causes of "treatable dementia."

MCTD should be considered in a patient when his/her symptoms and signs cannot be confined to a sole rheumatological disease.

Signs on Radiograph and CT

Chest radiograph or CT may show signs of pulmonary hypertension (e.g., prominent pulmonary trunk) (Fig. 7.11.1).

Signs on Brain MRI

- Optic or trigeminal neuritis is seen as contrast enhancement of the nerve after gadolinium injection due to the hyperemia and inflammation (the normal nerve does not enhance after contrast injection).
- Transverse myelitis shows enlargement of the cord with diffuse hyperintense signal of the spinal cord on T2W images in the affected segment (Fig. 7.11.2). The affected segment enhances in an inhomogeneous pattern after contrast administration. Cord atrophy occurs in chronic cases. On axial segments, the high signal on T2W images occurs on both sides of the cord giving a "snake-eye appearance."

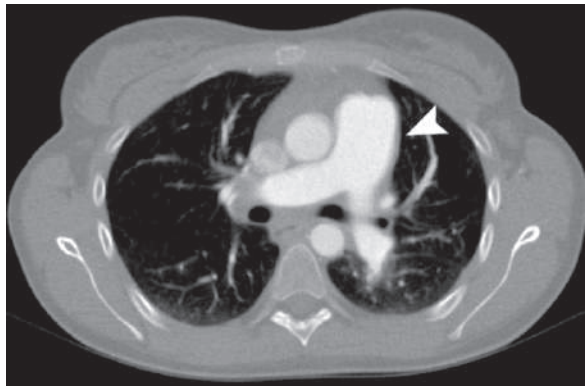

Fig. 7.11.1. Axial postcontrast CT-angiography of the pulmonary vessels in 32-year-old woman with Sharp's syndrome shows mildly dilated pulmonary trunk (28 mm) due to newly developed pulmonary hypertension (*arrowhead*)

7.11

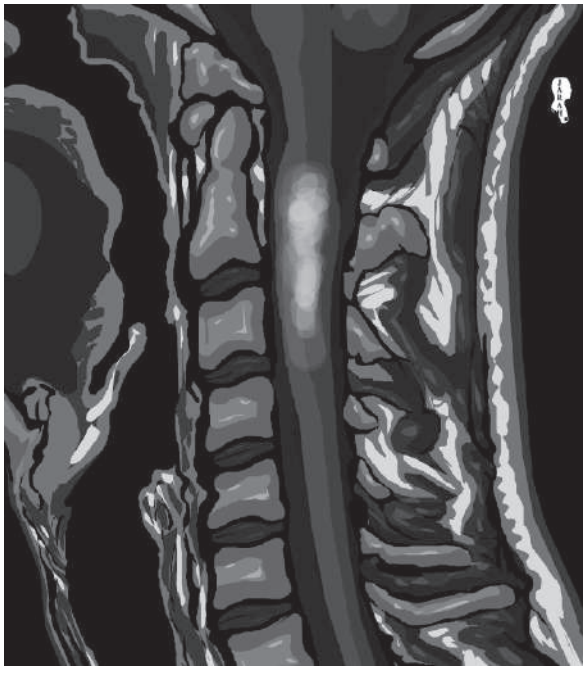

Fig. 7.11.2. Sagittal T1W postcontrast cervical spine MR-illustration demonstrates transverse myelitis as thickened spinal cord with

For Further Reading

1. Colombo A et al Mixed connective tissue disease (Sharp syndrome): Description of two cases. Ital J Neurol Sci. 1983;2:203–5
2. Matsui H et al Encephalopathy and sever neuropathy due to probable systemic vasculitis as an initial manifestation of mixed connective tissue disease. Neurol India. 2006;54: 83–5
3. Malaviya AN et al Sharp's syndrome (mixed connective tissue disease) with extensive inflammatory panniculitis complicated with pyoderma gangrenosum–a case report. J Indian Rheumatol Assoc. 2003;11:45–50

Chapter 8

Hematology

CONTENTS

J. A. Al-Tubaikh: *Internal Medicine* – An Illustrated Radiological Guide
DOI: 10.1007/978-3-642-03709-2_8, © Springer-Verlag Berlin Heidelberg 2010

8.1 Hemosiderosis and Hemochromatosis

Hemosiderosis, or iron overload, is a pathological condition characterized by deposition of excess iron within the body tissues that normally do not containing iron. Hemosiderosis is usually secondary to a primary cause such as multiple blood transfusion, chronic hemodialysis, or hemolytic anemia (e.g., thalassemia).

When iron is released into the cytoplasm, it enters a cellular compartment called "labile iron pool" (LIP). Both ferrous (Fe^{2+}) and ferric (Fe^{3+}) iron forms are poorly bound with proteins, and are highly toxic to the cells within this compartment. The unneeded iron from LIP is stored in the form of ferritin, which is organic and nontoxic. When the LIP iron content exceeds the ferritin capacity, hemosiderin is generated from ferritin denaturation. Iron in the form of hemosiderin is thought to be more toxic to the body tissues. Hemosiderin initially accumulates in the reticuloendothelial system (spleen, bone marrow, and Kupffer cells in the liver). When the reticuloendothelial system is saturated, deposition occurs in normal body tissues such as the hepatocytes, heart muscles, and the endocrine system. Chelation therapy (e.g., desferrioxamine) removes mainly the extracellular iron and only a fraction of the intracellular LIP iron.

Hemosideroses have different body manifestations according to the area of deposition:

- *Cardiac hemosiderosis*: myocardial iron deposition results in dilated cardiomyopathy that will lead to heart failure.

Signs on Chest Radiograph

The heart appears larger than normal in cases of cardiac damage and development of dilated cardiomyopathy.

Signs on MRI

MRI can detect early myocardial siderosis via obtaining T2* images, which show a dark, hypointense rim located within the myocardium in short-axis sequences, representing myocardial siderosis (Fig. 8.1.1).

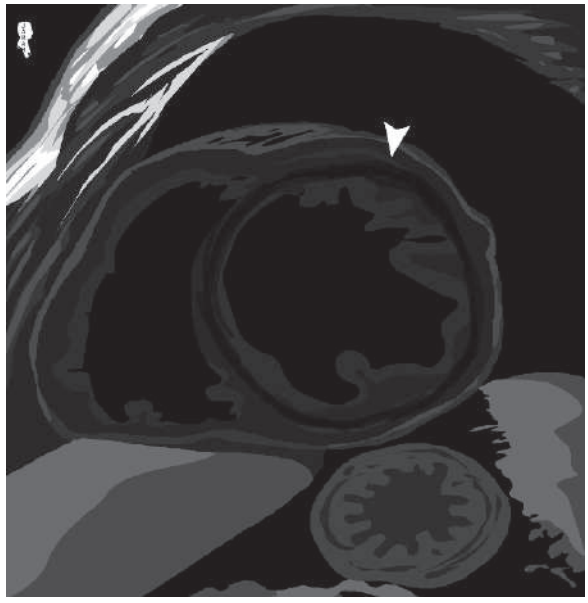

Fig. 8.1.1. Short-axis cardiac MRI illustration demonstrates a black ring within the myocardium, a sign of cardiac siderosis (*arrowhead*)

- *Hepatic hemosiderosis*: iron deposition in hepatocytes results in liver cirrhosis.

Signs on CT and MRI

- On CT, the liver appears hyperdense compared to the spleen.
- On MRI, the liver appears extremely hypointense, with an almost black signal on all pulse sequences, depending on the severity of the iron overload.
- *Anterior pituitary gland hemosiderosis*: loss of the endocrine function of the anterior pituitary results in hypogonadism and loss of libido.

Signs on MRI

The anterior pituitary shows a hypointense signal intensity area on both T1 and T2 images.

- *Pancreatic hemosiderosis*: deposition of iron in the pancreases results in impairment of both exocrine and endocrine functions. Diabetes mellitus may result due to pancreatic siderosis.

Signs on US

- The normal pancreas has almost the same echogenicity as the liver on ultrasound. In siderosis, the pancreas may appear hyperechoic compared to the liver, due to iron overload. Other causes of hyperechoic pancreas include fatty infiltration and pancreatic calcification.

Signs on MRI

Hypointense signal intensity areas are seen within the pancreas on both T1W and T2W images).

Hemochromatosis is a disease characterized by deposition of excess iron in the body as a result of genetic defect (primary hemosiderosis).

In hemochromatosis, iron deposition initially occurs in the hepatocytes and spares Kupffer cells (the reverse situation to hemosiderosis). The age of presentation is usually between 50 and 60 years of age. Menstruation blood loss in women has a protective effect against hemochromatosis due to iron loss.

Hemochromatosis is asymptomatic in early stages. As the iron deposition progresses, liver failure, skin hyperpigmentation, arthropathy (especially in the metacarpophalangeal joints), and cardiac failure may occur. Deposition of hemosiderin in the subcutaneous tissues results in increased skin tanning and darkening.

Bronze diabetes is a term used to describe maturity-onset diabetes seen in hemochromatosis. The term "bronze" is used because the diabetes is associated with skin tanning that mimics bronze coloring.

Diagnosis is confirmed by measuring serum ferritin level, transferrin saturation testing, liver biopsy, genetic testing, and MRI.

Differential Diagnoses and Related Diseases

- *Bantu siderosis* a type of hemosiderosis only found in Africa. It is associated with liver cirrhosis, diabetes, and heart disease. The disease is linked with higher rates of tuberculosis infection.
- *Juvenile hemochromatosis* is a form of hemochromatosis that present in the second decade of life. Patients often present with abdominal pain, cardiac arrhythmias, impaired glucose tolerance, and hypogonadotrophic hypogonadism.
- *Ferroportin disease* is a genetic disease characterized by mutation in the gene responsible for the production of ferroportin, a protein that exports iron from body cells. Ferroportin is expressed mainly in Kupffer cells and splenic macrophages. Patients present with isolated hyperferritinaemia and normal or slightly elevated transferrin saturation. In contrast to hemochromatosis, iron is mainly deposited within Kupffer cells.
- *Pulmonary hemosiderosis* is a rare condition that arises due to repeated episodes of bleeding within the lung alveoli. Iron overload within the lungs results in pulmonary fibrosis, anemia, and (rarely) death due to pulmonary hemorrhage. The disease has an incidence of less than 1:1,000,000 live births, and occurs usually in children <7 years old (it is extremely rare in adults). Symptoms include coughing blood (hemoptysis) and iron-deficiency anemia.
- *Superficial brain siderosis*: superficial siderosis of the brain is a condition characterized by deposition of hemosiderine within brain tissues, often secondary to subdural hemorrhage and bleeding into the brain cisterns. When siderosis affects the vestibulocochlear nerve, tinnitus may result.

Signs on MRI

- The liver appears extremely hypointense on all pulse sequences, depending on the iron overload severity.
- Muscles and kidneys may appear hyperintense, due to iron deposition.
- The spleen is characteristically spared and unaffected in hemochromatosis. In contrast, the spleen is almost always affected in hemosiderosis.
- In *superficial brain siderosis*, a characteristic band of low T1 and T2 signal intensity is seen around the brain tissue, especially the pons, due to its location within the pontine cistern (Fig. 8.1.2).

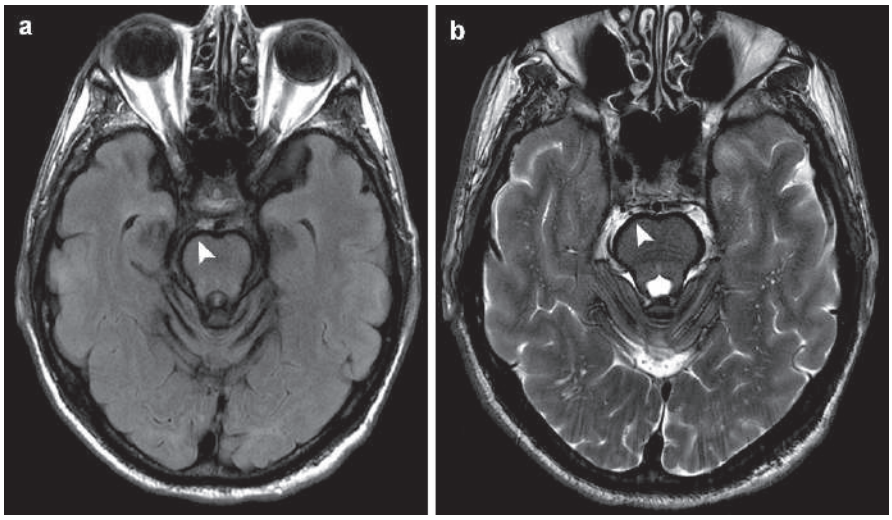

Fig. 8.1.2. Axial T1W (**a**) and T2W (**b**) brain MRI show a hypointense rim that surrounds the pons (*arrowhead*) due to superficial brain siderosis

For Further Reading

1. Rosenberg W. Haemochromatosis. Medicine. 2007;35:89–92
2. Rosenberg W et al Haemochromatosis. Medicine. 2002;30: 63–4
3. Koçak R et al The liver siderosis in beta-thalassemia intermedia and hemoglobin disease. J Islamic Acad Sci. 1993;6: 42–5
4. Flyer MA et al Transfusional hemosiderosis in sickle cell anemia: another cause of an echogenic pancreas. Pediatr Radiol. 1993;23:140–42
5. Brasch RC et al Magnetic resonance imaging of transfusional hemosiderosis complicating thalassemia major. Radiology. 1984;150:767–71
6. Chen CH et al Idiopathic pulmonary hemosidernossis: favorable response to corticosteroid. J Chin Med Assoc. 2008;71:421–24
7. Deugnier Y et al Iron and the liver: update 2008. J Hepatol. 2008;48:S113–23
8. Argyropoulou MI et al MRI evaluation of tissue iron burden in patients with β-thalassemia major. Pediatr Radiol. 2007;37:1191–200
9. Bonetti MG et al Hepatic iron overload in thalassemic patients: proposal and validation of an MRI method of assessment. Pediatr Radiol. 1996;26:650–56
10. Positano V et al Improved T2* assessment in liver iron overload by magnetic resonance imaging. Magn Reson Imaging. 2008. doi:10.1016/j.mri.2008.06.004

8.2

β-Thalassemia Major (Cooley's Anemia)

β-thalassemia major is a hereditary hemolytic anemia, characterized by deficiency in the hemoglobin beta chain synthesis. Patients with β-thalassemia major are prone to repeated attacks of intravascular hemolysis that requires repeated hospitalization and blood transfusions.

Patients with β-thalassemia major present with microcystic hypochromic anemia with signs of fatigue and cardiac tachycardia.

Repeated blood transfusion predisposes to hemosiderosis and tissue iron burden, which is the most severe complication of this disease. Hemosiderosis causes cardiomyopathy, hepatic failure, hypogonadism (pituitary siderosis), and endocrinal abnormalities. *Bronze diabetes* is a term used to describe diabetes mellitus induced in a patient with thalassemia due to pancreatic hemosiderosis. The term "bronze" refers to skin darkening and hyperpigmentation that is seen in patients with chronic thalassemia, due to deposition of hemosiderin in the subcutaneous tissues. Hypoparathyroidism is one of the most important endocrinal complications of thalassemia.

Extramedullary hematopoiesis is commonly observed in these patients due to increased body demands. Extramedullary hematopoiesis can be appreciated on plain radiographs as abnormally widened, flat bones.

Within the past few years, MRI has emerged as a powerful diagnostic tool to detect hemosiderosis through the body. Techniques for tissue iron burden quantification are well-established for the liver and the heart. Early treatment with chelating agents (e.g., Desferrioxamine) reduces the severity of the iron burden complication. MRI iron burden quantification helps in monitoring chelation therapy.

Signs on Skeletal Radiograph

- *Skull hair-on-end appearance*: increase of the trabeculae within the skull bones, due to extramedullary hematopoiesis that widens the clavarial flat bones (Fig. 8.2.1).
- Square-shaped metacarpals and thin cortex, due to bone marrow proliferation (Fig. 8.2.2).
- Dilated ribs due to extramedullary hematopoiesis (Fig. 8.2.3).
- Splaying of the femoral metaphysis (erlenmeyer flask deformity).

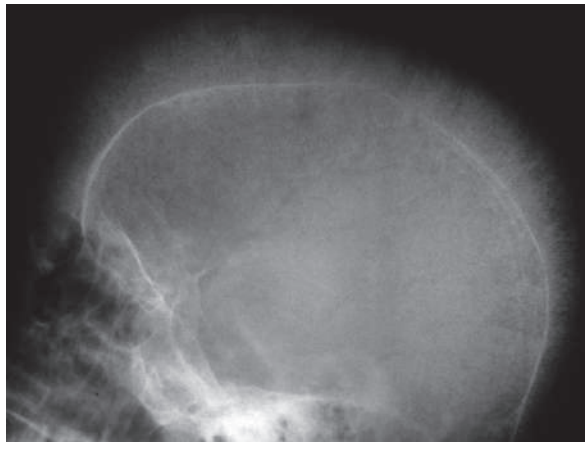

Fig. 8.2.1. A plain radiograph of the lateral skull of a patient with thalassemia shows hair-on-end-appearance

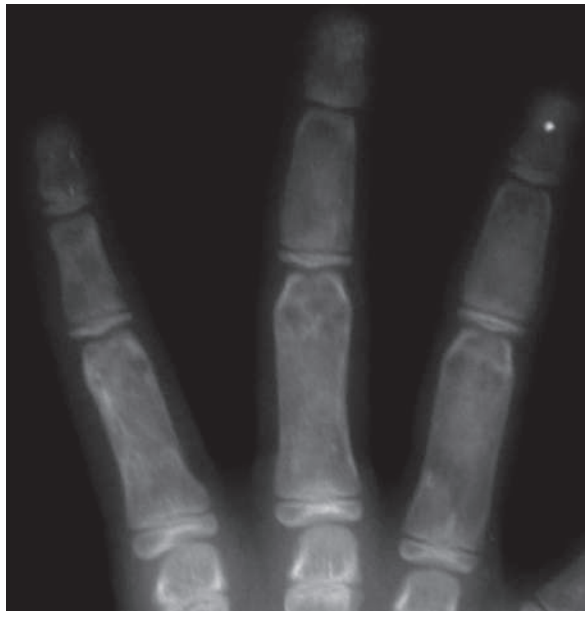

Fig. 8.2.2. A plain radiograph of the hand shows squaring and expansion of the phalanges due to extramedualllry hematopoiesis in a young patient with thalassemia

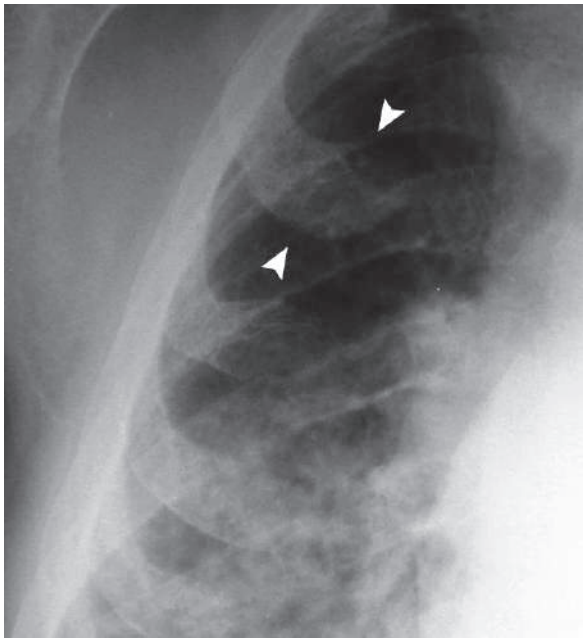

Fig. 8.2.3. AP plain radiograph shows expansion of the ribs due to extramedualllry hematopoiesis (*arrowheads*)

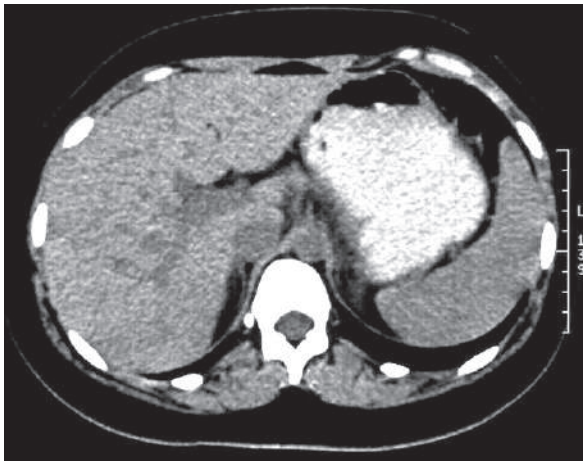

Fig. 8.2.4. Axial nonenhanced CT of the abdomen shows high-density liver

Signs on CT

- Hepatic hemosiderosis is one of the main causes of high-density liver on nonenhanced CT images (Fig. 8.2.4). The liver density will show high HU difference compared to the muscles and the spleen, with a range of 80–140 HU. Other causes of nonenhanced CT high-density liver are Wilson's disease due to copper deposition, and hepatic iodine deposition, rarely seen in amiodarone toxicity.
- Hepatosplenomegaly often occurs due to extramedullary hematopoiesis (Fig. 8.2.5).
- Thoracic paraspinal masses and enlarged lymph nodes may be seen due to extramedullary hematopoiesis (Fig. 8.2.6).
- Cerebral calcification may be seen due to hypoparathyroidism in thalassemia patients. Patients may uncommonly show bilateral symmetrical basal ganglia calcifications (Fig. 8.2.7).

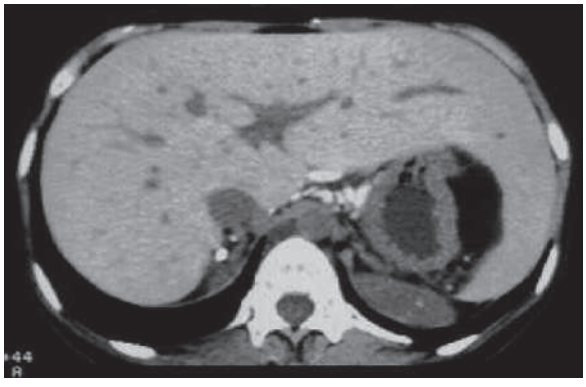

Fig. 8.2.5. Axial nonenhanced CT of the abdomen shows hepatomegaly with left liver lobe hypertrophy

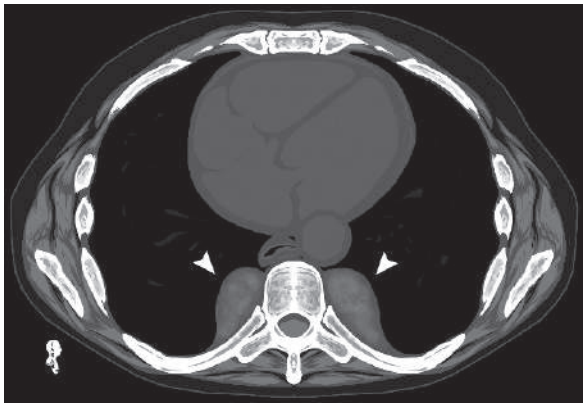

Fig. 8.2.6. Axial nonenhanced CT illustration of the thorax shows bilateral paraspinal masses due to extramedullary hematopoiesis (*arrowheads*). These masses can be easily mistaken for tumors. Other signs of extramedullary hematopoiesis support the diagnosis

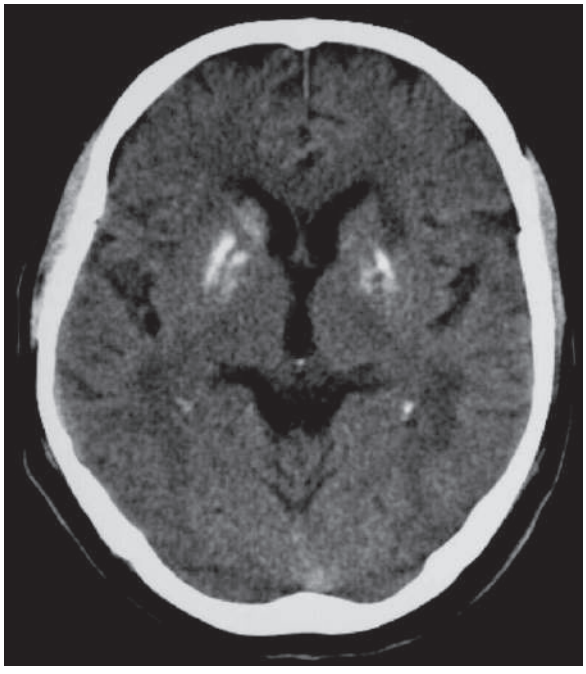

Fig. 8.2.7. Axial nonenhanced brain CT shows bilateral, almost symmetrical, basal ganglia calcifications

Signs on MRI

- Iron burden quantification is done with the use of T2* sequences (Fig. 8.2.8). The supraparamagnetic properties of the iron deposited within the tissues cause decreased signal intensity of the tissues containing iron. As a result, hepatic parenchyma, splenic parenchyma, and cardiac muscles with siderosis appear hypointense compared to normal parenchyma.
- In mild liver siderosis, the liver appears hypointense only on T2* images, compared to muscles. In moderate to severe cases, the liver appears hypointense to spleen and muscles in all sequences. The spleen shows almost the same picture as the liver, due to iron deposition. In primary hemochromatosis, only the liver shows decreased signal intensity, while the spleen is spared.
- In the heart, iron overload appears as a dark ring on T1W, T2W, and T2* images.
- In bronze diabetes, the pancreas and sometimes the adrenals show low signal intensity due to iron deposition.
- In hypogonadism and signs of pituitary failure, the anterior pituitary shows low signal intensity on T1W, T2W, and T2* images, reflecting severe iron deposition.

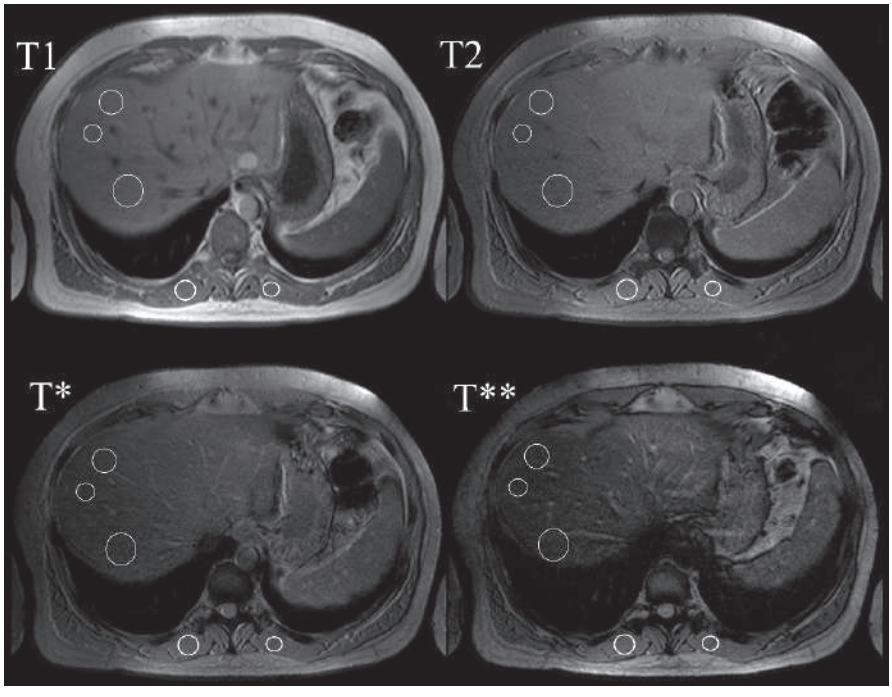

Fig. 8.2.8. Axial abdomen section in different sequences illustrates the method of liver iron burden quantification in the liver and the paraspinal muscles

For Further Reading

1. Papakonstantinou O et al MR imaging of spleen in beta-thalassemia major. Abdom Imaging. 2006. doi: 10.1007/s00261.006.9138–4
2. Lal A et al Focal splenic lesions as a cause of extramedullary hematopoiesis in a case of thalassemia. Eur J Radiol Extra. 2008;68:e125–7
3. Karimi M et al Hypoparathyroidism and intracerebral calcification in patients with beta-thalassemia major. Eur J Radiol. 2008. doi: 10.1016/j.ejrad.2008.02.003
4. Drakonaski E et al Adrenal glands in beta-thalassemia major: magnetic resonance (MR) imaging features and correlation with iron store. Eur Radiol. 2005;15:2462–68
5. Louis CK Low growth of children with β-thalassemia major. Indian J Pediatr. 2005;72:159–64
6. Mavrogeni S et al Magnetic resonance evaluation of liver and myocardium iron deposition in thalassemia intermedia and β-thalassemia major. Int J Cardiovasc Imaging 2008;24:849–54
7. Karimi M et al Prevalence of hepatosplenomegaly in beta thalassemia minor subjects in Iran. Eur J Radiol. 2007. doi: 10.1016/j.ejrad.2007.09.027
8. Argyropoulou MI et al MRI evaluation of tissue iron burden in patients with β-thalassemia major. Pediatr Radiol. 2007;37:1191–200
9. Positano V et al Improved T2* assessment in liver iron overload by magnetic resonance imaging. Magn Reson Imaging. 2008. doi:10.1016/j.mri.2008.06.004

8.3

Sickle Cell Disease

Sickle cell disease (SCD) is an autosomal recessive genetic disorder, characterized by episodic attacks of hemolytic anemia and vaso-occlusive attacks due to "sickeling" of the red blood cells (RBCs) under certain body conditions that include dehydration, metabolic acidosis, and low oxygen saturation.

SCD results from abnormal production of hemoglobin (Hb-S). Sickle cell patients are homozygous (HbSS), while heterozygous patients have "sickle cell trait". SCD can also arise when Hb-S is combined with abnormal hemoglobin (e.g., Hb-S-thalassemia). Hb-S differs from the normal Hb-A only in the substitution of valine for glutamic acid in the sixth position of the β chain.

In SCD, the normal, discoid RBCs shape is transform into a sickle-shaped, sticky mass during deoxygenation. These sickle cells can stick together, forming a hard mass that may lead to emoblization and arterial infarction in different parts of the body.

Approximately 50% of patients with SCD experience painful crises by the age of 5 years. Patients with sickle cell disease have natural protection against malaria; the reasons are unknown.

The Lungs in SCD

Patients with SCD have greater susceptibility to pneumonia (100 times more than other children), due to impaired immune status. The infective agents are commonly *Streptococcus pneumoniae, Hemophilus influenzae,* and *Salmonella*. *Acute chest syndrome* (ACS) is a term used to describe newly developed pulmonary consolidation. accompanied by fever, chest pain, dyspnea, and cough. The underlying cause is known, and presumably due to fat emboli. ACS is the second most common cause for hospital admissions in children with SCD, after painful crises. ACS is also seen in up to 10% of SCD patients after general anesthesia.

The Skeletal System in SCD

Skeletal manifestations in SCD range between vaso-occlusive crises, extramedullary hematopoiesis, osteomyelitis, and vertebral changes. Bone infarction is the most common cause of pain crises in SCD. However, silent infarctions do exist in patients with SCD. There are four zones seen in bone infarction by histology: the zone of cell death located in the center, the zone of ischemic tissue, the zone of hyperemia, and the outer zone of normal bony tissue.

Osteomyelitis means inflammation of the bone and the bone marrow. Osteomyelitis is commonly caused by *Salmonella* infection in sickle cell patients. In nonsickle cell patients, the most common cause of osteomyelitis is *Staphylococcus aureus*.

Differential Diagnoses and Related Diseases

Hand-foot syndrome is an uncommon disease seen in sickle cell patients in up to 20% of cases, characterized by bilateral inflammation and swelling of the fingers and toes (dactylitis). Patients present with fever, bilateral digital swelling in the hands and feet, leucocytosis, and pain. It can be mistaken for osteomyelitis in the initial presentation. Osteomyelitis is uncommonly known to cause bilateral infection in the hands and feet simultaneously. Also, osteomyelitis often involves the long bones, not the small bones of the hands and feet. Most patients experience this syndrome before 4 years of age, and the disease has not been reported beyond 7 years. The condition is self-limiting, with a duration that varies from a week to a month.

What is the difference between osteonecrosis, avascular necrosis, and bone infarction?

Osteonecrosis is ischemic death of the bone and bone marrow.

Avascular necrosis is osteonecrosis that occurs in the epiphyses.

Bone infarction is osteonecrosis that occurs in the metaphyses or diaphyses.

8.3

The Brain in SCD

In SCD, the brain may be damaged due to infarction from sickle cell emboli, or from vasculitis. Up to 25% of patients with SCD will have a neurological complication over their lifetime; 11% of these complications will occur by the age of 20 years. *Silent infarction* is defined as MRI manifestation of cerebral infarction in the absence of clinical symptoms, and occurs in up to 22% of patients with SCD.

The Spleen in SCD

Multiple spleen infarctions due to vaso-occlusive crises are a very common feature in SCD. With time, the spleen is replaced by fibrous tissue and by calcium and hemosiderin deposition (called *autosplenectomy*). Up to 94% of patients are asplenic by the age of 5 years.

Patients with splenectomy are susceptible to infection with *Staphylococcus pneumoniae, Salmonella,* and *Haemophilus influenzae*. Pneumococcal vaccine is often started between 2 and 5 years of age.

Sequestration syndrome is another condition that commonly occurs in SCD patients, characterized by rapid pooling of the blood within the spleen, resulting in intravascular volume depletion and dropping hematocrite levels. When the sequestration is severe, patients present with abdominal fullness, thirst, tachycardia, and tachypnea that may rapidly progresses into circulatory collapse. Up to 30% of patients experience sequestration syndrome between the ages of 6 months and 3 years.

Signs on Chest Radiograph

- Pneumonia is seen as areas of patchy lung infiltration with air bronchogram. The airspace disease may be lobar or diffuse.
- *Acute chest syndrome* is seen as single or multiple patchy areas of airspace disease, often confined to the middle and lower lobes. Up to 60% of patients with ACS show normal chest radiograph.

Signs on Skeletal Radiograph

- *Bone infarction*: seen as a radiolucent area surrounded by the sclerotic rim, typically in the epiphyses and the medullary cavity (Fig. 8.3.1). Later, sclerosis of the infarcted areas causes the appearance of dense bone within the affected bone (bone-in-bone appearance).
- *H-shaped vertebra*: there is central end plate depression, with sparing of the anterior and posterior margins due to previous infarctions of vertebral bodies. An H-shaped vertebra is a characteristic sign of SCD (Fig. 8.3.2).
- Expansion of the diploic medullary spaces of the skull due to increased hematopoietic demands (hair-on-end appearance).
- *Osteomyelitis*: the early changes seen radiographically are soft-tissue swelling or a mass, occasionally gas, periosteal reaction, and (later) cortical destruction. There are usually no signs on plain radiograph in the first 2 weeks of infection. The cortical destruction first appears as small lucent holes (permeative destruction), followed later by larger coalescent lesions (moth-eating destruction). Osteomyelitis can be difficult to differentiate from infarction.
- *Hand-foot syndrome*: the typical signs of dactylitis include soft-tissue swelling of the digits, cortical thinning, multiple intramedullary radiolucent deposits, and thick periosteal new bone formation (Fig. 8.3.3). The radiological manifestations are completely reversible after 8 months.
- Protrusio acetabuli may occur in SCD in up to 20% of cases.

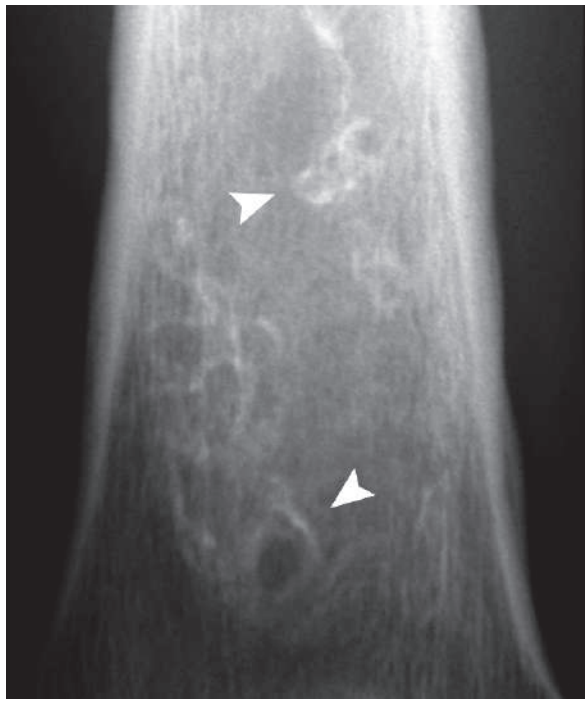

Fig. 8.3.1. Plain radiograph of the distal femur metaphysis shows radiolucent areas surrounded by sclerotic rims (*arrowheads*) due to old bone infarction in a patient with sickle cell disease (SCD)

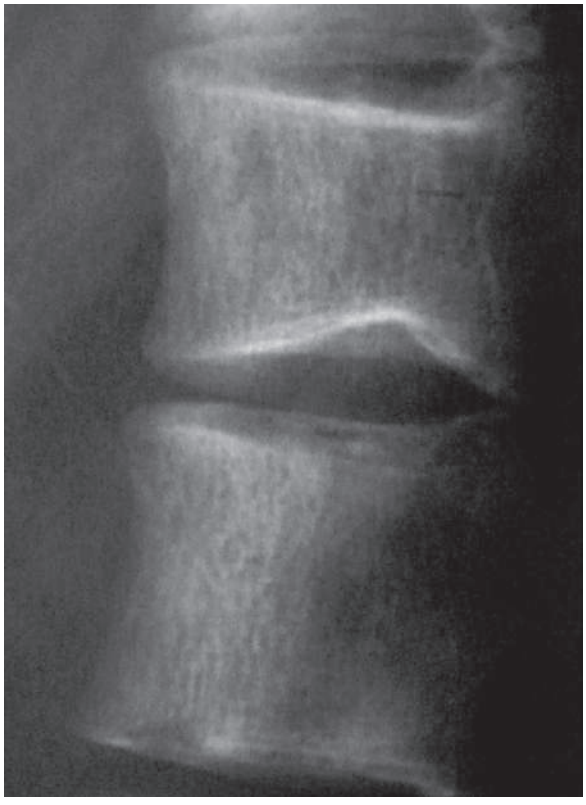

Fig. 8.3.2. Lateral vertebral plain radiograph of a patient with SCD shows H-shaped thoracic vertebra

Signs on Chest CT

Extramedullar hematopoiesis may be found as bilateral or unilateral, smooth or lobulated paraspinal masses in the lower thoracic spine, without vertebral erosions. History of hematological disease is the key diagnosis to differentiate these masses from tumors.

Signs on Abdominal CT

- *Spleen infarction* is seen on noncontrast enhanced images as a hypodense, wedge-shaped area, which typically starts from the periphery toward the center, with no contrast enhancement (Fig. 8.3.4).
- *Sequestration syndrome* is seen as splenomegaly with hypodense peripheral areas.

Signs on Skeletal MRI

- MRI is important in the early detection of bone infarction. On T2W images, there is an area surrounded by a hyperintense line and an outer hypointense line (*Double-line sign*). The

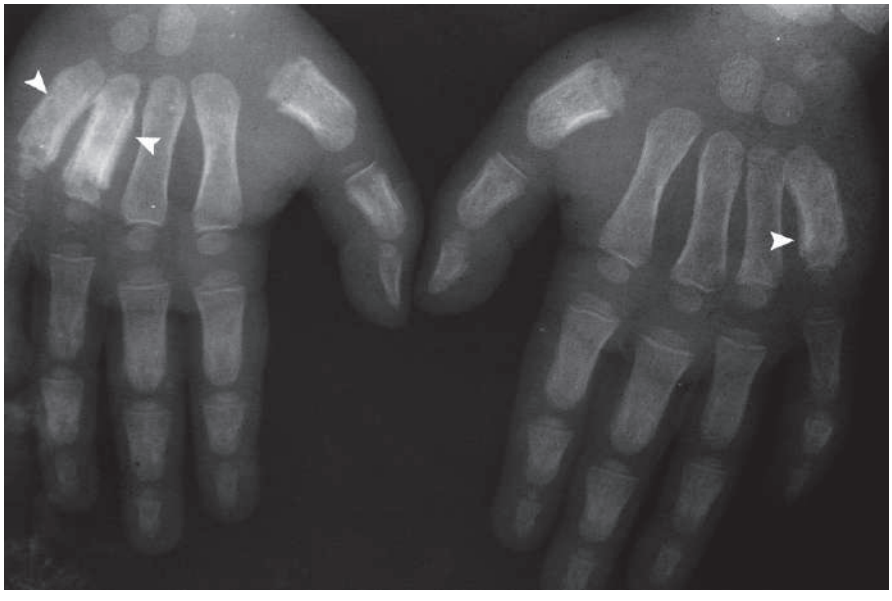

Fig. 8.3.3. Plain radiograph of both hands in a sickle-cell patient shows thick periosteal new bone formation affecting the fifth and fourth right metacarpal bones and the fifth left metacarpal bone (*arrowheads*), changes indicating hand-foot syndrome

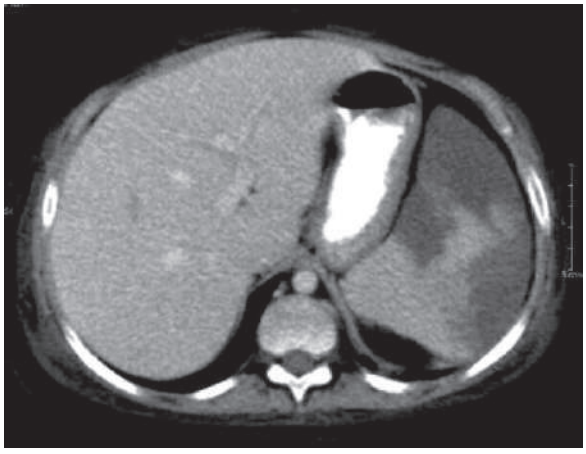

Fig. 8.3.4. Axial abdominal postcontrast CT shows multiple hypodense wedge-shaped areas within the spleen, due to multiple areas of infarction

high-intensity line represents the zone of hyperemia. Double-line sign is found in up to 80% of cases of bone infarction.

- The yellow marrow is made of 80% fat, 15% water, and 5% proteins. On MRI, it gives high signal in T1W images. In contrast, the red marrow is made of 40% fat, 40% water, and 20% proteins. This high water content gives low signal in both T1W and T2W images. Extracellular hematopoiesis, especially within the vertebrae, can be suggested by observation of the intervertebral disc signal. Normally, the vertebral bodies have higher signals than the intervertebral discs on T1W images, due to the fatty marrow. In extracellular hematopoiesis, the yellow marrow is reconverted into red marrow due to the hematpoietic demands, resulting in low signal intensity of the vertebral bodies compared to the intervertebral discs on T1W images (*high-density disc sign*). This sign is observed in any disease with bone marrow infiltration.

Signs on Brain MRI

- *Silent infarction* is detected as a high signal intensity lesion within the white matter on T2W or FLAIR images.
- *Moyamoya disease* is detected by its classical "puff of smoke" appearance on MR-angiography, and occlusion of the ipsilateral internal carotid artery.

For Further Reading

1. Lonergan GJ et al Sickle cell anemia. RadioGraphics. 2001; 21:971–94
2. Ejindu VG et al Musculoskeletal manifestations of sickle cell disease. RadioGraphics. 2007;27:1005–21
3. Schatz J et al Sickle cell disease as a neurodevelopmental disorder. Ment Retard Dev Disabil Res Rev. 2006;12:200–7
4. John N. Lukens. Sickle cell disease. Dis Mon. 1981;27:1–56
5. Babhulkar SS et al The hand-foot syndrome in sickle-cell haemoglobinopathy. J Bone Joint Surg (Br). 1995;77-B:310–2
6. Janet Watson R et al The hand-foot syndrome in sickle-cell disease in young children. Pediatrics. 1963;31;975–82
7. John N. Lukens. Sickle cell disease. Dis Mon. 1981;27:1–56

8.4

Pernicious Anemia

Pernicious anemia (PA) is a disease characterized by the development of megaloblastic anemia due to destruction of the gastric parietal cells. *Megaloblastic anemias* are a subgroup of macrocystic anemias (large volume red blood cells), which most commonly arise due to vitamin B_{12} and folate deficiencies.

Normally, the parietal cells in the gastric mucosa secret an intrinsic factor, which is important for absorption of vitamin B_{12} from the gastrointestinal tract. The fundus of the stomach contains parietal cells, the body contains the cells responsible for the secretion of pepsin and hydrochloric acid, and the antrum contains G cells. Patients with PA develop antigastric parietal cells (GPC) and anti-intrinsic factor antibodies (gastric parietal cells antibodies, or AGPA), which attack the parietal cells and cause autoimmune gastritis. Destruction of the gastric parietal cells leads to gastric mucosal atrophy, and compromises the production of the intrinsic factor. Moreover, the atrophic gastritis also compromises the gastric acid pump, leading to deficiency in the secretion of gastric acids (hypo- or achlorhydria). Loss off vitamin B_{12} causes defective synthesis of the bone marrow cellular activities, leading to the development of megaloblastic erythropoiesis and macrocytic anemia.

Chronic gastritis induces enterochormaffin-like cell hyperplasia, which may result in the development of gastric carcinoid tumors. Compared to the general population, gastric adenocarcinoma is 3–5 times more frequent among patients with PA. The activity of natural killer cells, which participate in immunosurveillance against tumor dissemination, is believed to be compromised in patients with PA.

Atrophic gastritis is divided into two types. Atrophic gastritis type (a) is characterized by mucosal atrophy affecting the fundus and the body of the stomach, with antral sparing. In contrast, atrophic gastritis type (b) is characterized by antral mucosal atrophy, with limited involvement of the fundus and body.

AGPAs are found in 20% of patients with diabetes mellitus type 1 (DMT1). Researchers suggest that patients with DMT1 should be regularly screened for atrophic gastritis. PA is rare found in the general population, with an incidence of 0.1–2% of the population. On the other hand, patients with DMT1 have a threefold increased incidence of PA, with a prevalence of 2.5–4%.

Diagnosis is confirmed by detecting AGPA levels in the serum by the Schilling test.

Signs on Barium Meal

- In a normal double-contrast barium meal examination, the stomach mucosal folds (rugae) are observed arranged in an irregular fashion through the fundus, body, and antrum (Fig. 8.4.1). At the lesser curvature near the pylorus, the mucosal folds become longitudinal and are known as magenustrass. *Area gastrica* is an area of nodular mucosal elevation located near the antrum (Fig. 8.4.2).
- In PA, there is tubular-shaped fundus <8 cm in diameter absent or reduced amount of the normal gastric rugae in the fundus of the body (bald fundus), and small or absent area gastrica (Fig. 8.4.3).

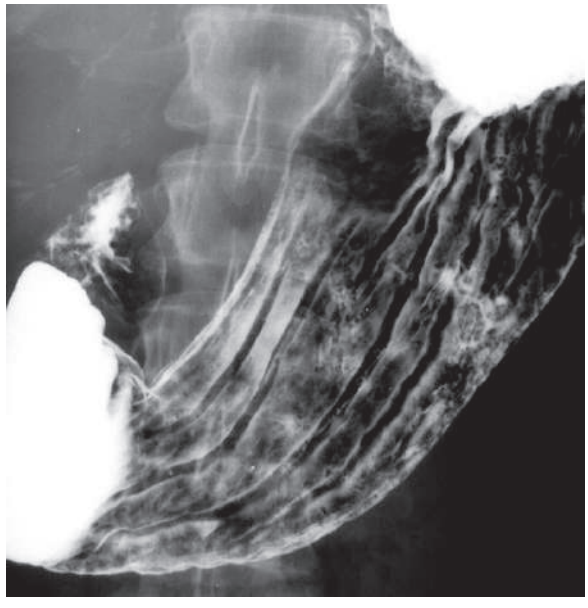

Fig. 8.4.1 Double-contrast barium meal shows the normal configuration of the stomach with the mucosal folds (rugae) nicely demonstrated

8.4

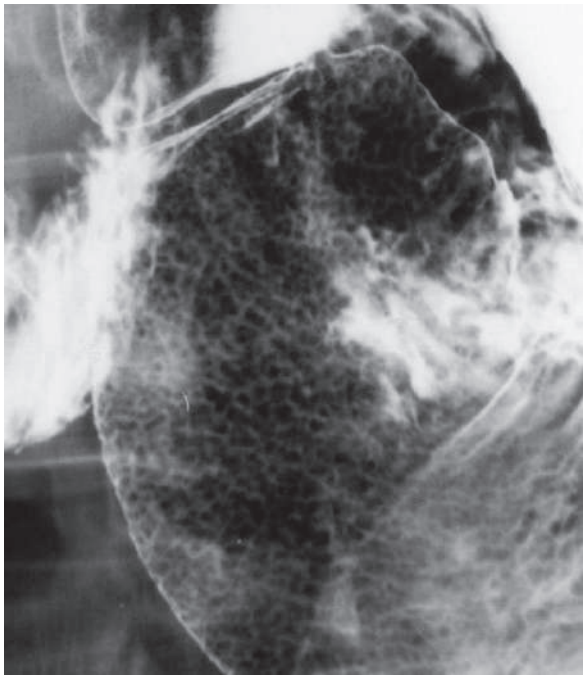

Fig. 8.4.2 Double-contrast barium meal shows area gastrica, seen as an area with nodular mucosal pattern

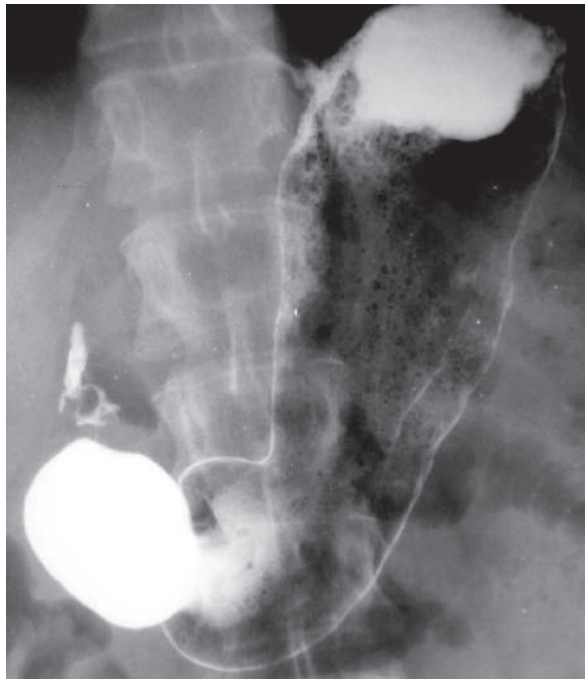

Fig. 8.4.3 Double-contrast barium meal of a patient with pernicious anemia demonstrates severe atrophic gastritis with loss of the normal mucosal folds. Compare this image with Fig. 8.4.1

For Further Reading

1. Levine MS et al Atrophic gastritic in pernicious anemia: diagnosis by double-contrast radiography. Gastrointest Radiol. 1989;14:215–19
2. Varis K et al An Appraisal of tests for severe atrophic gastritis in relatives of patients with pernicious anemia. Dig Dis Sci. 1979;24:187–91
3. Wickramasinghe SN. Diagnosis of megaloblastic anemias. Blood Rev. 2006;20:299–318
4. Vargas JA et al Natural killer cell activity in patients with pernicious anemia. Dig Dis Sci. 1995;40:1538–41
5. Tzellos TG et al Pernicious anemia in a patient with type 1 diabetes mellitus and alopecia areata universalis. J Diabet Complicat. doi:10.1016/j.jdiacomp.2008.o5.003

8.5 Hemophilia

Hemophilia is a rare, chronic X-linked genetic disease, characterized by the body's inability to form clotting factors necessary for the blood clotting cascade to occur, resulting in a tendency toward spontaneous bleeding or bleeding after minor body trauma.

The word "*hemo"* means bleeding, and the word "*philia*" means tendency toward something. Patients with hemophilia have a tendency for slow bleeding, at a constant rate and without clotting, into muscles, joint spaces, and body cavities.

Blood clotting is a complicated process that involves three primary steps. The first step involves immediate constriction of the blood vessels in the area of injury. The second step involves the formation of a platelet plug that stops the bleeding. The third step involves the activation of 12 clotting factors (identified by Roman numerals) that transform the platelet plug into a more stable clot by transforming it into fibrin. The activation of clotting factors is referred to as the "clotting cascade," because each factor stimulates the next factor in the series, until the formation of the fibrin. Deficiency of one factor will stop the cascade, and a stable clot will not form.

There are three types of hemophilia

- *Hemophilia A* results from deficiency of clotting factor VIII, and it is the most common form of hemophilia (80%). The incidence is 1:10,000 people.
- *Hemophilia B* (*Christmas disease*) results from deficiency of clotting factor IX, and constitutes up to 23% of hemophilia cases. The disease was named after a young boy, Stephen Christmas, who was the first patient identified with this disease. The incidence is 1:40,000 people.
- *Hemophilia C* results from deficiency of clotting factor XI. It is a much rarer form, and constitutes less than 2% of all cases of hemophilia.

Patients with hemophilia are prone to slow, steady, and continuous bleeding after minor trauma. Bleeding can also occur spontaneously without trauma. The most important complications include bleeding into joints (*hemoarthrosis*), internal bleeding, intracranial bleeding, and susceptibility from hematological infections due to recurrent blood transfusions.

Bleeding into the joints can occur in any joint, but it commonly affects the knees and the elbows. "*Target joint*" is a term used in hemophiliacs to indicate a joint with more frequent bleeding than other joints, commonly the knee. The joint synovium is rich in blood vessels, causing it to bleed easily. Multiple bleeding within the joint causes synovium hypertrophy, which later causes articular joint destruction and osteoarthritis. Patients with joint bleeding experience severe pain, due to swelling of the affected joint with stretching of the intra-articular structures by the entrapped blood. Recurrent joint bleeding can stimulate the growth plate, resulting in bony hypertrophy.

Bleeding into the muscles (e.g., the psoas muscle), if not controlled, may lead to muscular swelling, nerve damage, and development of compartment syndrome. *Hemophilic pseudotumor* is a rare complication of hemophilia, occurring in 1–2% of hemophiliacs. It results from a chronic, encapsulated, slow-growing intramuscular hematoma that displaces the surrounding tissues. Limb enlargement, bone resorption, muscle and skin necrosis all can be seen in severe cases.

Internal bleeding can be seen as skin bruising, nose bleeding, or blood in the urine (hematuria). Moderate hemophiliacs may bleed 5–6 times per year. Severe hemophiliacs may have 2–3 bleeding episodes per month.

Intracranial bleeding may occur within the brain parenchyma or within the subarachnoid space. Altered consciousness, headache, nausea, and vomiting in a patient with hemophilia after a minor head injury should be considered intracranial bleeding, and investigated with a head CT without delay.

Myositis ossificans (*MO*), also known as "Sterner's tumor", is a rare, non-neoplastic condition characterized by formation of bone within muscles. The disease may be hereditary (fibrodysplasia ossificans progressiva, Munchmeyer disease), nontraumatic (e.g., in hemophilia), or traumatic, which is the most common form (e.g., after muscle trauma). The previous classification is applied to intramuscular MO; however, MO can arise against a bone (parosteal MO) or evolve as periostitis (periosteoma).

In the early stages of MO, there are richly vascularized fibroblastic cells proliferations with prominent mitotic activity that mimic malignancy (early pseudosarcomatous phase). As the cells mature, the lesion typically shows three distinct zones. The first zone is composed of rapidly proliferating fibroblasts with areas of hemorrhage and necrosis; the intermediate layer is

8.5

composed of osteoblasts with osteoid matrix with islands of enchondral ossification; the third outer zone is composed of mature bone, separated from the surrounded tissue by myxoid-fibrous tissue. The peripheral zone usually calcifies at 6–8 weeks after lesion initiation, and complete lesion ossification can be seen 5—6 months from the onset of symptoms. Up to 30% of lesions regress and resolve spontaneously with maturation.

Patients with MO typically present with painful swelling, commonly in the lower limbs (60–75% of cases). Patients, especially children, may not recall the incidence of trauma. Diagnostic imaging approach for a patient with painful swelling, with suspicion of MO, should start with conventional radiography, US, CT, and later MRI, as the MRI appearance of MO is generally nonspecific unless the lesion starts to mature. History of trauma is important to suspect MO; however, the absence of history of trauma does not exclude it.

Differential Diagnoses and Related Diseases

Von Willbrand's disease is a bleeding disorder that mimics hemophilia, and results from deficiency of von Willbrand factor.

Signs on Radiographs

- Enlargement of the epiphysis (100%), joint swelling with soft-tissue swelling (81%), and osteoporosis (95) are commonly found in hemophilic arthropathy. Reduction of the joint space and signs of osteoarthritis are also commonly found (Fig. 8.5.1).
- *Genu recurvatum* is a disabling deformity condition, characterized by hyperextension of the knee to >5°. This deformity may occur in patients with hemophilia after recurrent knee hemoarthrosis.
- Hemophilic pseudotumor is seen as an expanding limb with soft-tissue mass and lytic destruction of the bone within the mass. Bones that are often affected by pseudotumors are the femur, tibia, pelvis, and bones of the hands.
- MO is detected classically as bone within areas of soft tissue. The calcification is typically peripheral with a radiolucent center depending on the level of maturation. This pattern of ossification is important to differentiate MO from osteosarcoma, which typically shows a dense center and sun-ray peripheral edges. The ossification may appear as nonspecific flocculent areas of soft-tissue calcification called "dotted veil pattern", or may characteristically follow the course of muscle fibers (Fig. 8.5.2).

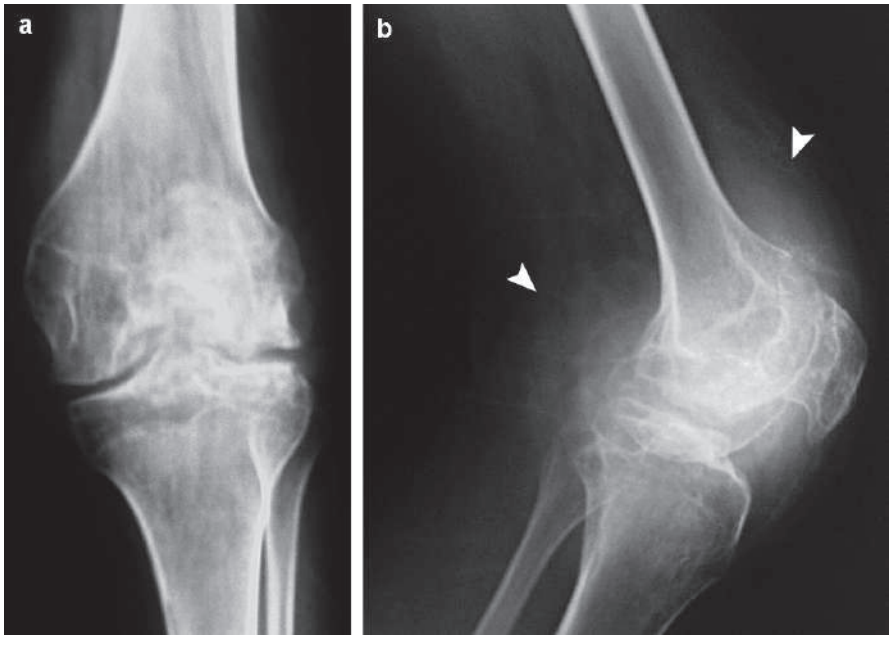

Fig. 8.5.1 Anteroposterior (**a**) and lateral (**b**) plain knee radiographs in a patient with hemophilic arthropathy. Notice the knee with obvious osteoarthritis, sclerosis, and joint effusion (*arrowheads*)

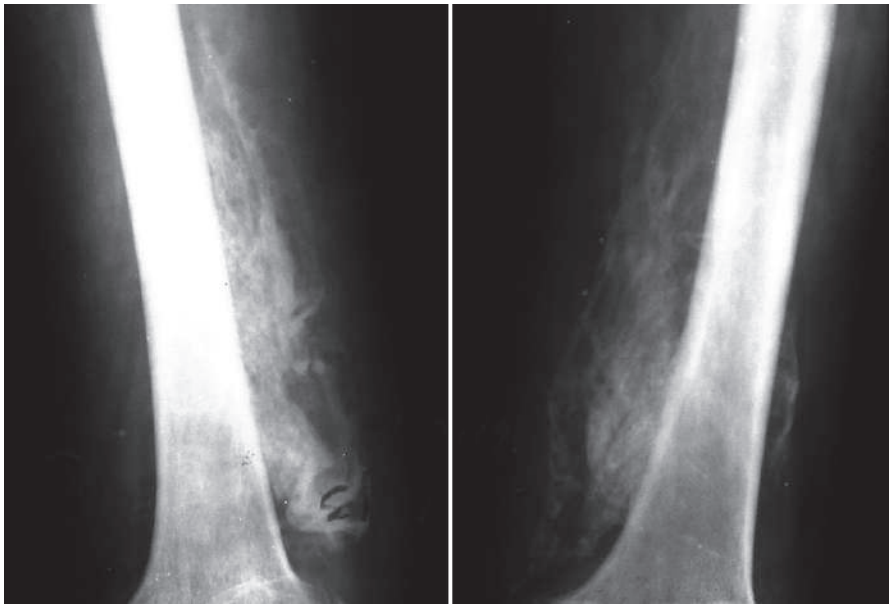

Fig. 8.5.2 Anteroposterior bilateral radiograph of the legs and distal femur shows bilateral calcification that involved the vastus medialis and the rectus femoris muscles in a patient with myositis ossificans. Notice how the calcification follows the muscle fibers

Signs on US

In the early stage of myositis ossificans, the mass is detected as a hypoechoic mass with an outer hypoechoic zone enclosing a broader hyperechoic zone, which again encloses a central hypoechoic zone. After maturation, the outer layer becomes hyperechoic due to ossification.

Signs on MRI

- In general, the MRI findings of MO are nonspecific; however, a peripheral rim with low T1 and T2 signal intensities surrounding a heterogeneous intramuscular mass can be a clue for MO. The dark rim represents the calcified peripheral zone. It should be remembered that, at the initial stage, MO resembles musculoskeletal sarcomas, even when a biopsy is done.
- After contrast injection, MO shows peripheral rim enhancement in the early stages, which can lead to mistaking it for an abscess or a necrotic tumor.

For Further Reading

1. Gupta AD et al Genu recurvatum in hemophilia: a case report. Arch Phys Med Rehabil. 2007;88:791–3
2. Nguyen DD et al Evaluation and management of hereditary hemophilia in the emergency department. J Emerg Nurs. doi: 10.1016/j.jen.2008.09.009
3. Stafford JM et al Hemophilic pseudotumor: radiologic-pathologic correlation. RadioGraphics. 2003; 23:852–56
4. Christopher S. Kovacs. Hemophilia, low bone mass, and osteopenia/osteoporosis. Transfus Apher Sci. 2008;38:33–40
5. Bae DK et al Total knee arthroplasty in hemophilic arthropathy of the knee. J Arthroplasty. doi:10.1016/j.arth.2005.01.008
6. Dauty M. Iliopsoas hematoma in patients with hemophilia: a single-center study. Joint Bone Spine. 2007;74:179–83
7. Malhotra R et al Elbow arthropathy in hemophilia. Arch Orthop Trauma Surg. 2001;121:152–57
8. Yoon KH et al Arthroscopic synovectomy in haemophilic arthropathy of the knee. Int Orthop (SICOT). 2005;29:296–300
9. Llauger J et al Nonseptic monoartheritis: imaging features with clinical and histopathologic correlation. RadioGraphics. 2000;20:S263–78
10. Gindele A et al Myositis ossificans traumatica in young children: Report of three cases and review of the literature. Peditar Radiol. 2000;30:451–59
11. Hatano H et al MR imaging findings of an unusual case of myositis ossificans presenting as progressive mass with features of fluid-fluid level. J Orthop Sci. 2004;9:399–403

8.6 Lymphomas

Lymphoma is a disease characterized by malignant transformation of lymphoid cells or other cells native to lymphoid tissues.

Lymphoma can be nodal (affecting lymph nodes) or extranodal (arising from lymphoid tissues within the organs). If left untreated, many lymphomas turn into leukemias. Not every lymphoma transforms into leukemia, but all lymphocytic leukemias are originally lymphomas. Lymphomas are divided into Hodgkin's and non-Hodgkin's diseases.

Hodgkin's lymphoma (HL), also known as *Hodgkin's disease,* constitutes <1% of all cancers worldwide, and is a lymphoma with features of systemic inflammatory disease (33% of cases). HL is characterized by fever, pruritus, fatigue, and loss of weight. It predominantly affects young men, except in its nodular sclerosis subtype, which predominantly affects young women. HL has a bimodal incidence curve, with the first incident occurring in young adulthood, and the second at >50 years of age. HL is diagnosed pathologically based on identification of *Reed-Steinburg cells*, which are multinucleated giant cells with eosinophilic inclusions-like nucleoli. History of previous infection with infectious mononucleosis increases the risk of developing HL by up to three times the normal incidence rate.

Non-Hodgkin's lymphoma (*NHL*) is a diverse group of diseases with almost 40 distinct entities. NHL is divided into two main groups according to the cell of origin: either B-cell neoplasms (precursor B-cell) or T-cell neoplasm (precursor T-cell). Each type is made up of well-differentiated cells (low-grade lymphomas), or undifferentiated cells (high-grade lymphomas). In general, NHL has a worse prognosis than does HL. *Composite lymphoma* is a term used to describe simultaneous occurrence of two histologically different types of lymphomas situated in one location.

T-cell lymphomas are often related to previous viral infection with human T-cell leukemia virus-1 (HTLV-1) and Epstein–Barr virus (EBV). EBV can also be responsible for the development of B-cell lymphomas (e.g., Burkitt's lymphoma). T-cell lymphomas constitute 10–15% of NHL, and they are commonly present with extranodal manifestations. Lymphomas and tuberculosis are generally more common in immunocompromised people than immunocompetent people.

Extranodal marginal zone B-cell lymphoma of MALT type (MALToma) is a form of lymphoma that develops in areas of chronic inflammation or autoimmune diseases. MALT stands for "mucosa-associated lymphoid tissue." This type of NHL is often seen in malignant transformation of chronic or autoimmune diseases like Hashimoto's thyroiditis, Sjögren's syndrome, and chronic gastritis caused by *Helicobacter pylori* infection.

NHL can be further divided into two groups based on growth rate: indolent lymphomas and aggressive lymphomas. Indolent lymphomas are slow-growing and have fewer symptoms (e.g., MALT lymphoma), whereas aggressive lymphomas are rapidly growing with multiple symptoms (e.g., Mantel cell lymphoma).

Gastric lymphoma develops from the neoplastic MALT transformation as a result of long-standing *Helicobacter pylori* gastritis. Intestinal lymphoma develops from Peyer's patches neoplasia. Most cases are seen in the ileum (62.7%), followed by the jejunum (22%). Low-grade NHL often presents as polyposis. Salivary gland lymphoma is seen in chronic cases of *sialadenitis* (obstruction of the salivary gland outflow with superimposed infection). Orbital lymphoma can arise due to chronic lachrymal gland inflammation, as in cases of Sjögren's syndrome (primary), or secondary to dissemination. Urinary bladder lymphoma is either primary MALT type, or secondary to dissemination. Testes lymphomas are commonly due to disseminated acute lymphoblastic leukemia/lymphoma (ALL). Hepatic lymphoma is commonly secondary to primary lymphoma elsewhere, and is associated with poor prognosis. Primary bone lymphomas are seen in < 5% of all bone tumors, and commonly seen in male patients above 45 years of age.

Testicular NHL accounts for up to 7% of all testicular neoplasms and 25–50% of testicular neoplasms in patients >50 years of age. The testes are affected in <1% of patients with lymphoma, and it is usually bilateral when it occurs (40% of cases). The testes may be the only site involved in NHL in 10% of cases.

Childhood lymphoma is a lymphoma that occurs in a patient <15 years old. In children <15 years old, NHL is more common than HL, while in adults >15 years, HL is more common than NHL. Most childhood lymphomas present with gastrointestinal manifestations. Up to 70% of childhood Burkitt's lymphoma cases present with an abdominal mass. Intussusception in

childhood Burkitt's lymphoma is not uncommon. According to some investigators, childhood lymphoma staging is less important than in adults, because the disease is considered to be disseminated even if the radiological findings suggest localized disease.

Cotswold Staging of Lymphoma

Stage I: involvement of a single lymph node region or lymphoid structure (e.g., spleen) or involvement of a single extralymphatic site.
Stage II: involvement of two or more lymph node regions on the same site of the diaphragm.
Stage III: involvement of lymph node regions on both sites of the diaphragm.
Stage IV: distant metastases with disseminated involvement of one or more extranodal structures.

Criteria for Therapy Response Assessment

Complete remission: no signs or symptoms of disease.
Partial remission: at least 50% decrease in tumor size.
Stable disease: neither partial remission nor progressive disease.

Progressive/relapse disease: at least 50% increase in disease or new lesions.
Cutaneous T-cell lymphoma (*CTCL*) is a group of disorders characterized by proliferation of homing T-cell in the skin. Almost all CTCLs have the potential to transform into high-grade T-cell lymphomas. CTCL are divided into mycosis fungoides (MF) CTCL (50%) and non-MF CTCL.
Mycosis fungoides (*MF*) is a rare form of NHL, characterized by skin patches composed of dermal T-cells infiltrations. The name comes from the first description of this disease, which shows mushroom-like tumors developed on the skin of a patient with advanced disease. There are three common clinical presentations of MF. The first presentation is a skin plaque with hypopigmented and hyperpigmented areas. The second presentation is dermatosis that mimics psoriasis, lichen planus, vitiligo, or atopic dermatitis. The third presentations include pruritus or lichenification. *Lichen planus* is an inflammatory disease characterized by reddish-purple skin lesions that can be very itchy. The name *lichen planus* comes from the word "lichen," which refers to the plant which grows on rocks or trees, and "planus" means flat.

Diagnosis of MF requires >5 cm skin lesions that show arcuate polymorphic hyperpigmented and hypopigmented areas, with the classical distribution that involves the hip, buttocks, and the inguinal area (bathing suit distribution). The breasts, face, palms, and soles maybe affected atypically. Biopsy classically shows Pautrier microabscesses, and epidermal lymphocytes larger than dermal lymphocytes.

Differential Diagnoses and Related Diseases

- *Sézary syndrome* is a rare variant of MF, characterized by a triad of erythroderma, lymphadenopathy, and neoplastic atypical lymphocytes with cerebriform nuclei (Sézary cells) in the peripheral circulation and in the skin infiltrates. *Erythroderma* is defined as diffuse reddish infiltration of the skin that lacks the sharp demarcation from the normal skin as seen in patch or plaque type MF. When erythroderma involves the skin on the face, it can produce markedly exaggerated facial lines producing the finding of "leonine facies," or the face of a lion. Rarely, Sézary syndrome can present with white, vitiligo-like skin lesions, a leukemic variant of MF referred to as "*leukoderma.*"
- *Pseudolymphoma* (*Anticonvulsant hypersensitivity syndrome*) is a rare drug-induced reaction characterized by an infectious mononucleosis-like reaction that is characterized by fever, rash, lymphadenopathy, hepatitis, and nephritis. Phenytoin is the most common drug to cause this reaction, which is typically seen 3–4 weeks after initiation of therapy. Laboratory investigations often show leucocytosis, eosinophilia, lymphocytosis, positive rheumatoid factor, and anti dsDNA antibodies. Dermal biopsy of the skin eruptions often shows lymphocytic infiltration of the dermis. Rarely, biopsy shows changes that are indistinguishable from MF.
- *Tolosa–Hunt syndrome* is a disease characterized by painful ophthalmoplegia caused by a nonspecific, granulomatous inflammatory condition within the cavernous sinus or the superior orbital fissure. This opthalmoplegia is attributed to the involvement of the cranial nerves by the inflammatory process. The cavernous sinus contains the cranial nerves (3rd, 4th,

6th, and the maxillary and ophthalmic divisions of the 5th cranial nerve). Many diseases can infiltrate the cavernous sinus producing opthalmoplegia; therefore, Tolosa-Hunt syndrome is a diagnosis of exclusion when all other possible pathologies are excluded. Pathologies that can infiltrate the cavernous sinus and cause Tolosa-Hunt syndrome-like symptoms include chondrosarcoma of the bone, lymphoma, metastasis, cavernous sinus thrombosis, and infectious diseases such as aspergillosis.

Signs on Plain Radiographs

- Bilateral symmetrical hilar lymphadenopathy is a common feature of lymphoma (Fig. 8.6.1).
- Pleural thickening with malignant effusion can be seen. Malignant effusion is usually massive, and caused by lymphatic or venous obstruction.
- Linear interstitial lung pattern is noticed more in HL than in NHL patients, due to lymphangitis carcinomatosis.
- Bone lymphomas are classically seen as metaphyseal osteolytic lesions with a permeative appearance and layered (onion skin) perisotitis.
- Complete sclerosis of the vertebral body (ivory vertebra) can be seen in cases of vertebral body infiltration by lymphoma (Fig. 8.6.2).

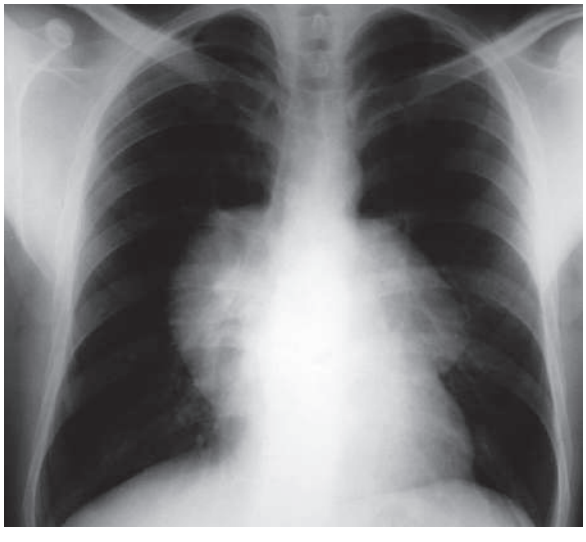

Fig. 8.6.1. Posteroanterior plain chest radiograph of a patient with NHL shows bilateral enlarged, potato-like hilar lymphadenopathy

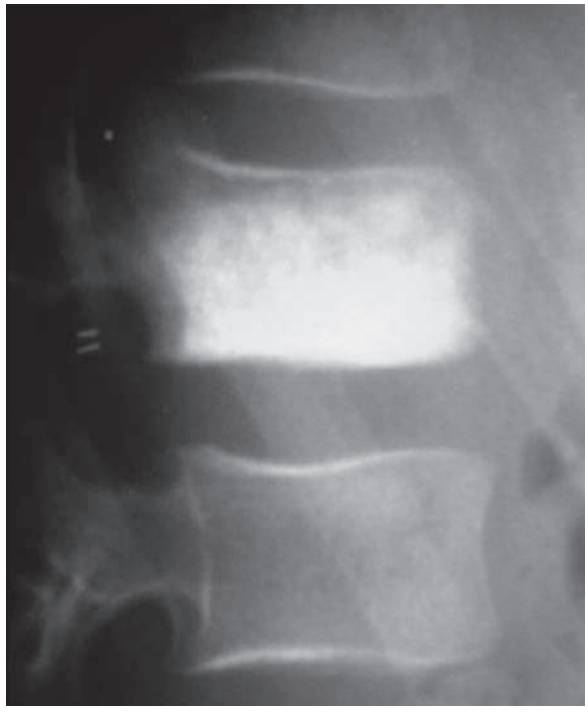

Fig. 8.6.2. Lateral plain thoracic vertebral radiograph shows complete sclerosis of a single vertebra (ivory vertebra). The differential diagnosis of ivory vertebra includes lymphoma infiltrating the vertebral body, Paget's disease, and metastases infiltrating the vertebral body

Signs on US

- Lymphoma of the spleen appears as splenomegaly or multiple focal splenic parenchymal lesions. US is more sensitive than CT in detecting splenic lesions in lymphoma. The majority of the lymphoma's foci are hypoechoic compared to the normal splenic tissue. Only 6% of lymphomas show hyperechoic lesions.
- Intestinal lymphoma (e.g., Burkitt's lymphoma) is visualized as thickened, ring-like bowel loops with a "doughnut sign" on axial sections. A layered, thickened wall is often demonstrated, with the outer hypoechoic layer corresponding to the bowel wall layers, and an inner hyperechoic layer due to intraluminal air or mucus.
- Testicular lymphoma is detected as hypoechoic, focal, or diffusely enlarged testes with a preserved oval shape. Intratesticular hemorrhage, necrosis, and calcification are rare. Extension to the epididymis and the spermatic cord is common (60% of cases). The same sonographic picture can be seen in infiltrative hematologic neoplasms such as leukemia and (rarely) plasmacytoma.

Signs on CT

- More than 80% of patients with HL present with cervical and hilar lymphadenopathy. Involvement of the Waldeyer's ring is common (50% of cases). The Waldeyer's ring is an anatomical ring of lymphoid composed of the pharyngeal tonsils, palatine tonsils, lingual tonsils, and tubal tonsils (Fig. 8.6.3). It is located at the back of the oral cavity and the pharynx. A lymphoma is considered extranodal when its main bulk of disease is located at an extranodal site.
- Splenomegaly (30% in HL and 70% in NHL). Focal splenic lesions <1 cm are common in HL, whereas large focal splenic lesions are more commonly seen in NHL. The lesions are isodense to the normal splenic tissue density on noncontrast-enhanced CT. After contrast injection, the lesions appear hypodense compared to the normal contrast-enhanced splenic tissues. Infarction of the spleen is a rare complication of lymphoma, and can typically be seen as a hypodense, peripheral, wedge-shaped area with no contrast enhancement. Lymphoma infiltrates the splenic white pulp follicles (malpighian corpuscles).
- *Orbital lymphoma*: a lymphoma usually present as a well-defined, soft-tissue mass within the orbit that may involve the lachrymal glands, the retrobulbar fat, or the muscles. Moreover, the soft-tissue mass has a tendency to coat the globe. The mass enhances homogenously after contrast injection. Orbital muscles will be diffusely enlarged with their tendons when infiltrated (lymphoma commonly involves the superior rectus muscle).
- In the *kidneys*, lymphomas can present as solitary or multiple hypodense solid masses (60%) with homogenous contrast enhancement. In 20% of cases, lymphoma can present with diffuse renal infiltration that causes nephromegaly without renal distortion. Retroperitoneal lymphadenopathy is commonly found, and it is a useful clue to lymphoma (Fig. 8.6.4). After contrast administration, lymphoma enhances homogenously, but always lower than the normal renal parenchyma (Fig. 8.6.5).
- In the *central nervous system*, lymphomas can present as solitary or multiple supretentorial lesions with hyperdense attenuation on noncontrast-enhanced CT. This native CT hyperdensity is attributed to the highly packed malignant cells within the lesion. After contrast injection, lymphomas show homogenous contrast enhancement (Fig. 8.6.6). Lymphoma does not show calcification unless treated, and it can cross from one hemisphere to the other via the corpus callosum in a butterfly pattern resembling gliobastoma multiforms. Moreover, CNS lymphoma shows minimal brain edema and no mass effect over the adjacent structures. In immunocompromised patients, lymphoma grows fast, and can have central necrosis with ring enhancement mimicking a brain abscess.

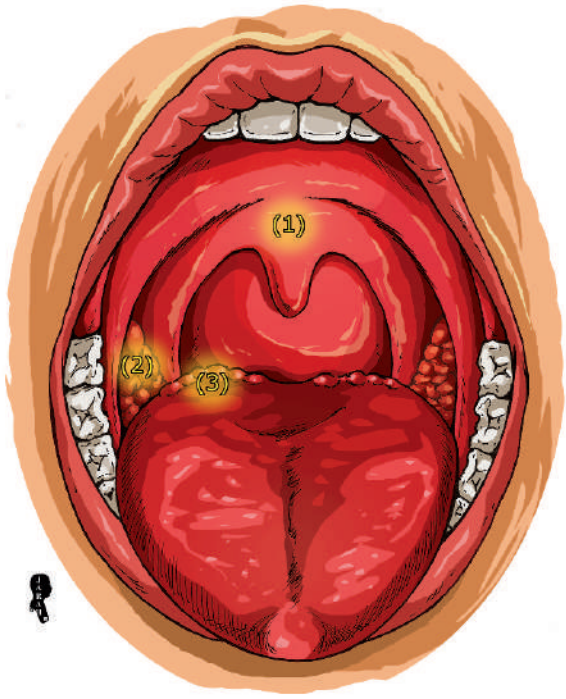

Fig. 8.6.3. An illustration of the mouth cavity demonstrates the region of the lymphatic components of Waldeyer's ring: (*1*) pharyngeal tonsils (behind the soft palate), (*2*) palatine tonsils, and (*3*) lingual tonsils

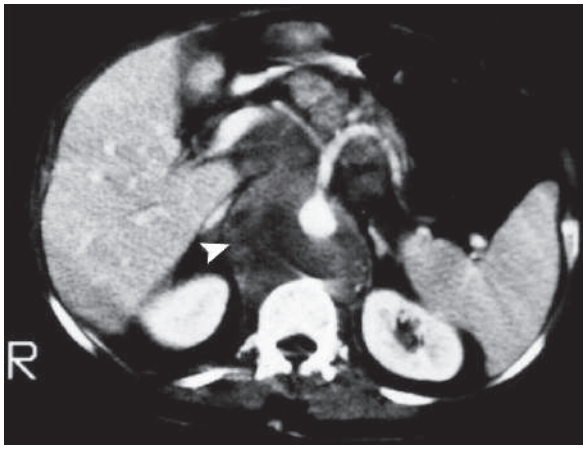

Fig. 8.6.4. Axial postcontrast CT of a patient with retroperitoneal lymphoma shows a homogenous hypodense mass surrounding the aorta (*arrowhead*)

8.6

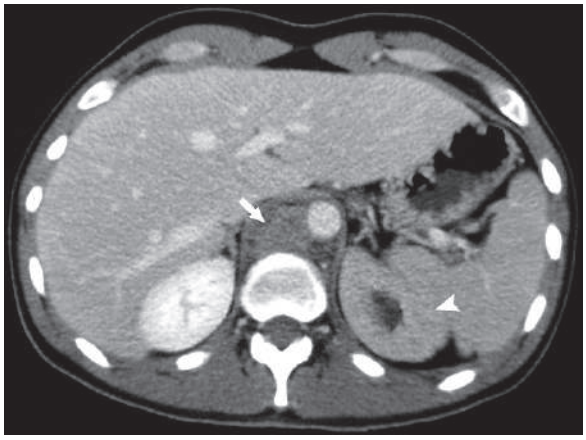

Fig. 8.6.5. Axial postcontrast CT of a patient with left renal lymphoma shows renal contrast enhancement (*arrowhead*) that is less than the normal right kidney enhancement due to diffuse parenchymal infiltration of the left kidney by lymphoma. Notice the enlarged retroperitoneal paraaortic lymph nodes, which are a good clue for lymphoma (*arrow*)

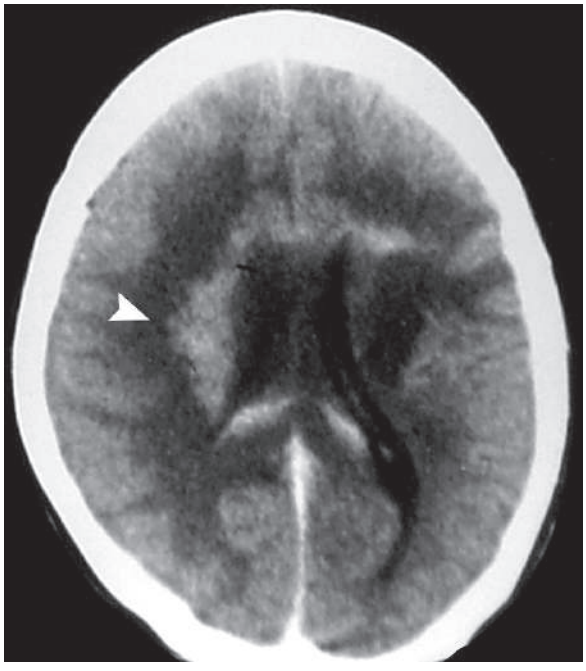

Fig. 8.6.6. Axial postcontrast brain CT of a patient with CNS lymphoma shows right-sided homogenously-enhanced subependymal mass (*arrowhead*)

- *Omental or peritoneal lymphoma* usually presents with diffusely thickened peritoneum and thickened omentum with contrast enhancement (omental cake sign). This presentation can be seen in abdominal manifestations of tuberculosis, especially in immunocompromised patients. The presence of abdominal septations near the thickened peritoneum favors tuberculosis over lymphoma (Fig. 8.6.7).
- *Faceless kidney* is uncommon feature of lymphoma where the renal parenchyma is diffusely infiltrated by lymphoma while lacking its typical familiar features of the central renal sinus structures (Fig. 8.6.8).

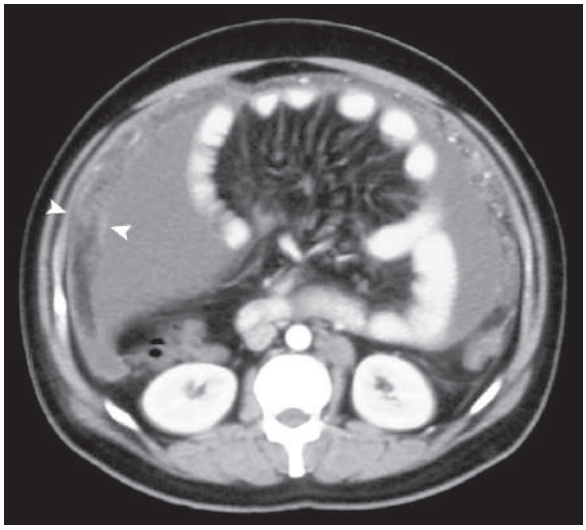

Fig. 8.6.7. Axial postcontrast abdominal CT of a patient with TB peritonitis shows thickened peritoneum and enhanced omentum (*arrowheads*) representing the "omental cake sign," with massive abdominal ascites. The same radiological picture can be caused by lymphoma

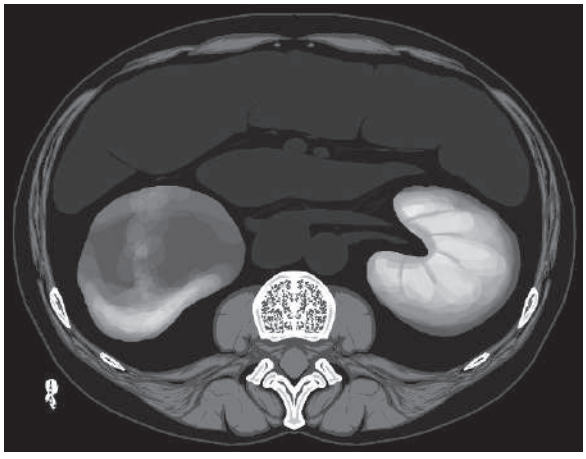

Fig. 8.6.8. Axial postcontrast abdominal CT illustration demonstrates right faceless kidney

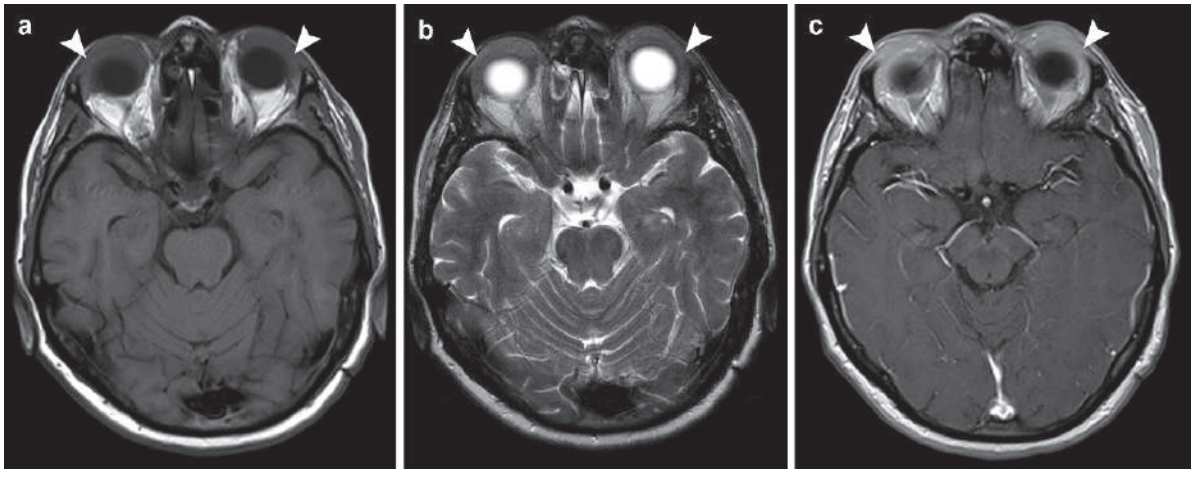

Fig. 8.6.9. Axial T1W (**a**), T2W (**b**), and T1W postcontrast MRI of a patient with orbital lymphoma shows bilateral hypointense T1, relatively hypointense T2 lesions with homogenous contrast enhancement on post-contrast image in (**c**) (*arrowheads*). Notice how the lymphoma tends to coat the globe

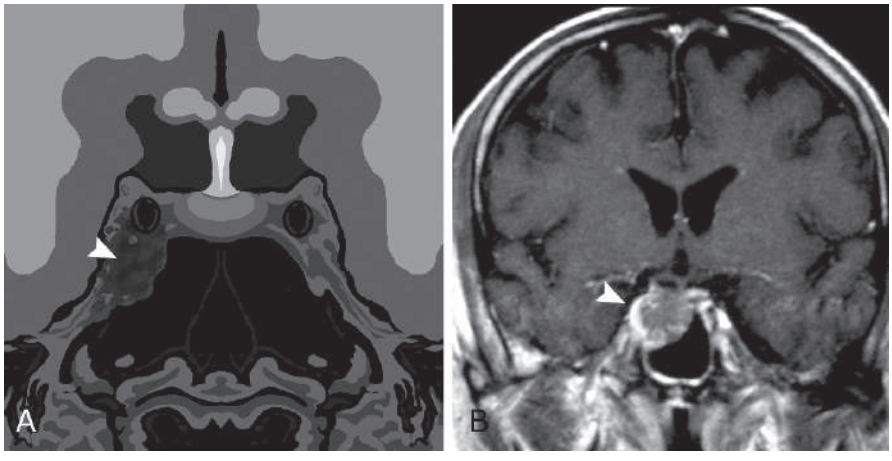

Fig. 8.6.10. Coronal native T1W magnified MR illustration of the cavernous sinus (**a**) and T1W postcontrast sellar mass on MRI show Tolosa-Hunt syndrome. In (**a**), the right cavernous sinus is infiltrated by an inflammatory mass, which often affects the cranial nerves resulting in opthalmoplegia. In (**b**), brain lymphoma infiltrating the right cavernous sinus resulting in a Tolosa-Hunt syndrome such as opthalmoplegia (*arrowheads*)

Signs on MRI

- Brain lymphoma often shows hypointense T1 signal intensity and slightly hypointense signal intensity on T2W images. This again is attributed to the highly packed cells within the tumor.
- Orbital lymphoma shows low T1 signal intensity, relatively hypointense on T2W images, with moderate contrast enhancement (Fig. 8.6.9).
- The classical *Tolosa-Hunt syndrome* shows a nonspecific mass lesion within the cavernous sinus that enhances mildly after contrast enhancement (Fig. 8.6.10). The lesion shrinks in size after therapy is initiated.

For Further Reading

1. Rademaker J. Hodgkin's and non-Hodgkin's lymphomas. Radiol Clin North Am. 2007;45:69–83
2. Jacobs P. Hodgkin's disease and the malignant lymphomas. Dis Mon. 1993;39:217–97
3. Chua SC et al Imaging features of primary extranodal lymphomas. Clin Radiol. 2009. doi:10.1016/j.crad.2008.11.001
4. Bhatia K et al Lymphoma of the spleen. Semin Ultrasound CT MRI. 2007;28:12–20
5. Weissman DE et al A case of large cell CNS lymphoma associated with a systemic small cell lymphocytic lymphoma. J Neuro-Oncol. 1990;9:171–75
6. Karaosmanoglu D et al CT findings of lymphoma with peritoneal, omental and mesenteric involvement: peritoneal lymphomatosis. Eur J Radiol. 2008. doi:10.1016/j.ejrad.2008.04.012

7. Mengiardi B et al Primary lymphoma of bone: MRI and CT characteristics during and after successful treatment. AJR Am J Roentgenol. 2005;184:185–92
8. Hinds GA et al Cutanous T-cell lymphoma in skin of color. J Am Acad Dermatol. 2009;60:359–75
9. Panda S. Mycosis fungoides: current trends in diagnosis and management. Indian J Dermatol. 2007;52:5–20
10. Nathan DL et al Carbamazepine-induced pseudolymphoma with CD-30 positive cells. J Am Acad Dermatol. 1998;38:806–9
11. Turner RB et al Anticonvulsant hypersensitivity syndrome associated with bellamine S, a therapy for menopausal symptoms. J Am Acad Dermatol. 2004;50: S86–9
12. Naik KS et al Staging lymphoma with CT: comparison of contiguous and alternate 10 mm slice techniques. Clin Radiol. 1998; 53:523–27
13. Dyer RB et al Classic signs in uroradiology. RadioGraphics. 2004;24:S247–80

8.7 Leukemia

The bone marrow manufactures the white blood cells (myeloid tissues) and the lymphocytes (lymphoid tissues), but the majority of bone marrow is myeloid tissue. Leukemia is a term used to describe a group of malignancies of either lymphoid or myeloid origin, which are characterized by malignant transformation of the leukocyte-forming tissue. The bone marrow is diffusely infiltrated with the leukemic cells that often inhibit the normal hematopoietic cell proliferation and development. Leukemias represent 30% of malignancies diagnosed in children <15 years and 25% in young adults <20 years.

If the leukemia is myeloid in origin, it will involve the myeloid tissue mainly (e.g., bone marrow), whereas if leukemia started in the lymphoid tissue, it will involve both the lymph nodes and the bone marrow lymphoid tissue. Lymphadenopathy in leukemia is seen when the leukemia is lymphocytic in origin, or the leukemic patient develops lymphoma.

Leukemia is described as "acute" when the malignant cells are immature blasts with a rapid cell proliferation rate. In contrast, leukemia is described as "chronic" when the malignant cells are more mature than those of acute leukemias. Chronic leukemias have a less devastating clinical course than do acute leukemias, but they are less responsive to treatment in comparison with acute leukemias.

Acute Lymphoblastic Leukemia

Acute lymphoblastic leukemia (ALL) is characterized by proliferation and predominance of lymphoblasts in the blood circulation and in the bone marrow. ALL is the most common type of leukemia (80%), and it has a sharp peak incidence among children 2–3 years old, which decreases by the age of 8–10 years.

Patients with leukemia classically present with fatigue, pallor, anemia, sneezing blood (epistaxis), and bruising easily (ecchymosis). Lymphadenopathy is seen in 50% of patients, and bone pain is a common complaint due to bone marrow stretching and expansion by the infiltrating leukemic cells. Cough and respiratory symptoms that mimic pneumonia may be seen in cases of mediastinal infiltration. Uncommonly, ALL can present as an isolated testicular mass.

Laboratory investigation shows anemia, thrombocytopenia, and pancytopenia. Diagnosis is essentially established by bone marrow biopsy. The presence of more than 25% blasts in the bone marrow is diagnostic of acute leukemia. Cerebrospinal fluid analysis by lumbar puncture is often included in the diagnostic workup to exclude central nervous system (CNS) infiltration. In boys with ALL, testicular ultrasound should be performed to exclude testicular enlargement.

Aleukemic leukemia is a term used to describe leukemia where the malignant blasts are not found in the peripheral blood.

Acute Myeloblastic Leukemia

Acute myeloblastic leukemia (AML) is characterized by predominance of myeloblasts and promyelocytes in the blood circulation and in the bone marrow. AML has a high incidence rate within the first 2 years of life, thereafter decreasing in incidence with a nadir at 9 years of age, and then a slow increase in incidence again during adulthood. AML is often seen in adults.

Patients present with classical symptoms as ALL. *Congenital AML* is leukemia that present in the first few years of life, often with skin infiltration (*leukemia cutis*). There is a high incidence of AML in children with Down's syndrome. AML is characterized by extramedullary manifestation called choloroma. *Choloroma (granulocytic sarcoma)* is a solid soft-tissue mass of leukemic cells that occurs anywhere in the body, and it represents extramedullary myeloblastic leukemia. The name is derived from the Greek word *chloros* meaning green, due to the green hue that these tumors demonstrate on gross specimens. The green color is due to the increase levels of the enzyme myeloperoxidase in the tumor cells.

Choloromas are rare, occuring in 2.5% of AML cases, and mostly in children <15 years of age (60%). A choloroma can be the primary presentation of AML, and the classic leukemia develops later (up to 2 years). Most cases of choloromas are seen in the head and neck region. However, any part of the body can be affected. Diagnosis of choloroma is essentially

established by biopsy. Recurrence rate after excision is up to 23%.

Hyperleukocytosis syndrome is an uncommon condition that is seen in AML and (rarely) ALL due to increased white blood cell count (>100,000/μL), which will lead to sludging of the leukemic blasts in tissue microvasculature. Patients present with neurologic or pulmonary manifestations due to blockage of the microcirculation by the leukemic cells.

Tumor lysis syndrome is another clinical condition commonly seen in patients with AML due to rapid tumor cell death and release of the intracellular contents into the circulation. Patients present with hyperkalemia, hyperuricemia, and secondary uric acid nephropathy and acute renal failure.

Differential Diagnoses and Related Diseases

- Shwachman-Diamond syndrome (SDS) is an autosomal recessive disorder of infancy, characterized by exocrine pancreas insufficiency, metaphyseal dysostosis (50%), and bone marrow dysfunction. The bone marrow dysfunction results in neutropenia (the most constant feature) and occasionally in pancytopenia (10–25%). Most infant deaths in the first year of life are due to recurrent bacterial infections. There is increased risk of leukemic transformation in these patients. SDS is the second most common cause of exocrine pancreatic insufficiency in children, after cystic fibrosis.
- Bloom syndrome: is a rare autosomal recessive disease characterized by a triad of lupus-like erythematous telangectasias of the face, stunted growth with dwarfism, and sun-sensitivity. Other manifestations include characteristic facies, immunodeficiency, azoospermia and infertility in men and subfertility in women, and well-circumscribed dermal hypo- and hyperpigmentation. The major complications in Bloom syndrome include development of different kinds of cancers, late-onset diabetes mellitus, and chronic lung disease. The most common cancers that arise in patient with Bloom syndrome are leukemia, lymphoma, and Wilms tumor.

8.7 Chronic Lymphocytic Leukemia

Chronic lymphocytic leukemia (CLL) is characterized by proliferation of lymphoid cells, almost always B cells.

CLL primary affects adults between 65 and 70 years of age. Up to 50% of patients are asymptomatic at presentation, and the disease is incidentally discovered following a routine blood investigation. Symptomatic presentations include autoimmune hemolytic anemia, lymphadenopathy, and hepatosplenomegaly. Diagnosis is essentially established by bone marrow biopsy and immunophenotyping.

Differential Diagnoses and Related Diseases

Richter's syndrome is a type of lymphoma that occurs in a patient with CLL who develops large-cell lymphoma (leukemia transforms into lymphoma). It is seen in 5–10% of CLL cases, and the survival rate is very short (2–8 months).

Chronic Myelogenous Leukemia

Chronic myelogenous leukemia (CML) is characterized by leukemia that arises from chromosomal translocation between chromosome 9 and 22 (Philadelphia chromosome), generating an aberrant tyorsin kinase. The aberrant tyorsin kinase fuels proliferation of a malignant clone of myeloid cells.

Up to 50% of CML cases are diagnosed incidentally. Patients are between 40 and 60 years of age, and present with malaise, weight loss, and splenomegaly. Laboratory investigations show neutrophil leucocytosis with basophilia and occasional eosinophilia. Diagnosis is essentially established by bone marrow biopsy and immunophenotyping.

In CML, the peripheral blood shows marked leucocytosis. Differential diagnosis of such leucocytosis includes a reactive, non-neoplastic peripheral blood leukocytosis due to an infection (e.g., infectious mononucleosis). This infectious, reactive, non-neoplastic leucocytosis is sometimes referred to as "*leukemoid reaction*."

In all types of leukemia, chemotherapy and immunosuppressive medications are used for therapy. Brain toxicity from cytotoxic agents such as methotrexate is a common complication of the medication, because methotrexate is capable of crossing the blood–brain barrier. In patients treated for leukemia, methotrexate can induce diffuse white matter lesions with demyelination and necrosis (leukoencephalopathy). *Disseminated*

necrotizing leukoencephalopathy is a fatal complication of methotrexate, characterized by multifocal areas of white matter necrosis. An insult to the tissue microvasculature and oligodendrocytes are the most likely mechanisms of injury to explain this condition. Hyperviscosity from the cytotoxic medications can lead to dural sinus thrombosis.

Signs on Plain Radiographs

- Leukemic infiltration of the bone often presents with osteopenia and linear bands of osteoporosis, observed mainly in the metaphyses of long bones (leukemic lines). However, leukemic lines can be seen normally in neonates.
- Choloroma of the bones is seen as pure lytic lesions affecting the sacrum, cranium, sternum, ribs, and spine. The lesions are typically located in the subperiosteal areas, and progress internally.

Signs on CT

- Choloroma is commonly found in the head and neck region as a sold mass with density similar to the skeletal muscle, and the mass shows homogenous contrast enhancement. Regional lymphadenopathy is commonly found (Fig. 8.7.1). If the bone is affected, lytic rather than sclerotic lesions are demonstrated.
- CNS choloroma is seen as an intermediate to hyperdense lesion (60–80 HU), with typically homogenous enhancement after contrast injection (nonspecific pattern). Mild to moderate hypervascularity can be seen on CT angiography.
- Small parenchymal brain calcifications can be seen after episodes of intracranial radiation therapy.

Signs on MRI

- Diffuse vertebral bone marrow leukemic infiltration results in low signal intensity of the vertebral bodies in relation to the intervertebral discs (*bright disc sign*) (Fig. 8.7.2). Hematopoietically active marrow is referred to as "red marrow." Red marrow is composed of water (40%), fat (40%), and proteins (20%). In contrast, hematopoietically inactive marrow is referred to as "yellow marrow." Yellow marrow is composed of fat (80%), water, (15%), and proteins (5%). The normal yellow marrow is hyperintense on T1W images. Normal red marrow is generally hypointense on MRI compared to yellow marrow, but its signal is generally greater than that of muscle. It is perhaps difficult to distinguish red marrow from infiltrative marrow processes. Infiltrative bone marrow pathology is any pathology that replaces the normal bone marrow contents. This pathological process can be diffuse or focal; neoplastic disease (e.g., leukaemia) represents the most common etiology for vertebral bone marrow infiltration.
- *CNS choloroma* shows low T1 and high T2 signal intensities with marked homogenous enhancement after contrast injection (Fig. 8.7.3).
- *Methotrexate leukoencephalopathy* is seen as areas of high signal intensities with no contrast enhancement after contrast injection (Fig. 8.7.4).
- In *disseminated necrotizing leukoencephalopathy*, there are multiple areas of high T2 signal intensities with small irregular low T2 signal foci due to coagulative necrosis. The small low T2 signal foci show enhancement after contrast injection.
- *Superior sagittal sinus thrombosis* is seen as a triangular filling defect on sagittal images (*empty delta sign*). Sinus thrombosis can also be seen on T2W images as a hyperintense vessel (Fig. 8.7.5). The vessel loses its signal void signal and appears clearly due to the thrombosed intravascular blood. The thrombus can show contrast enhancement if it is old and organized.

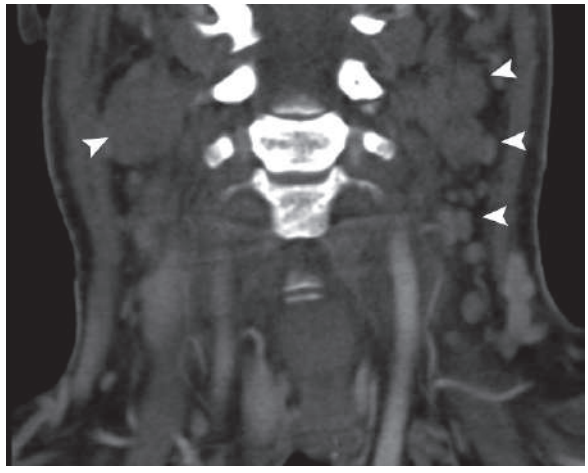

Fig. 8.7.1. Coronal postcontrast neck CT of a patient with neck choloroma shows bilateral lymphadenopathy (*arrowheads*)

8.7

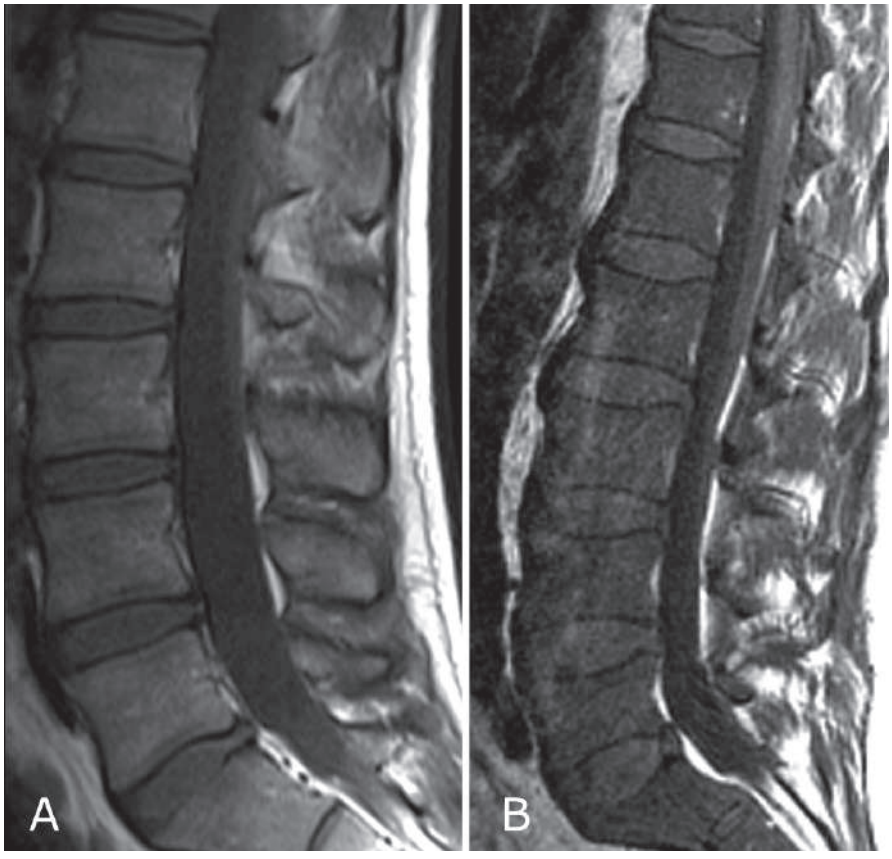

Fig. 8.7.2. Sagittal T1W thoracolumbar MRI in a normal patient (**a**) and a patient with leukemia, with diffuse vertebral bone marrow infiltration, shows the classic bright disc sign in (**b**). Notice how the vertebral body shows higher signal intensity than the intervertebral disc in (**a**) due to the presence of yellow marrow. In (**b**), the vertebral body shows lower signal intensity than the intervertebral disc, which is described as the bright disc sign

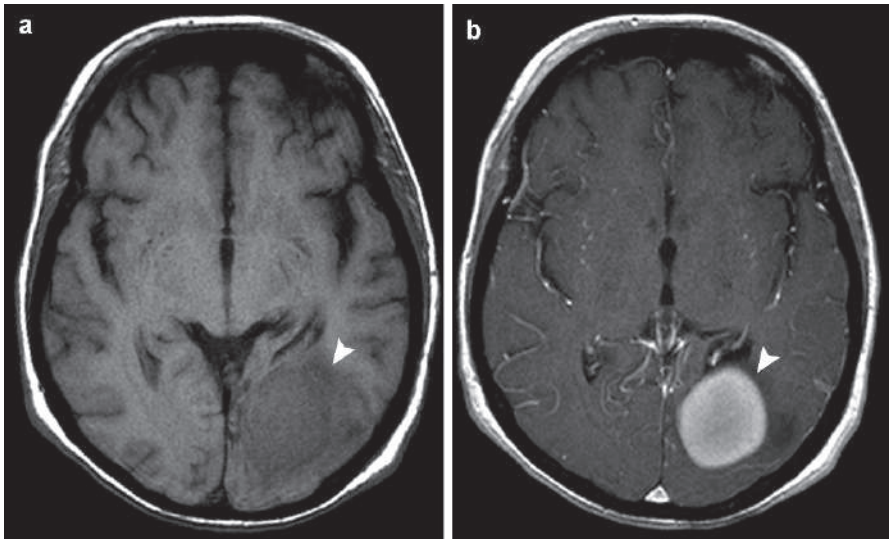

Fig. 8.7.3. Axial native T1W (**a**) and T1W postcontrast (**b**) brain MRI of a patient with biopsy-proved choloroma shows a large occipital mass with a relatively hypointense signal on the left of the T1W image, with homogenous marked enhancement (*arrowheads*)

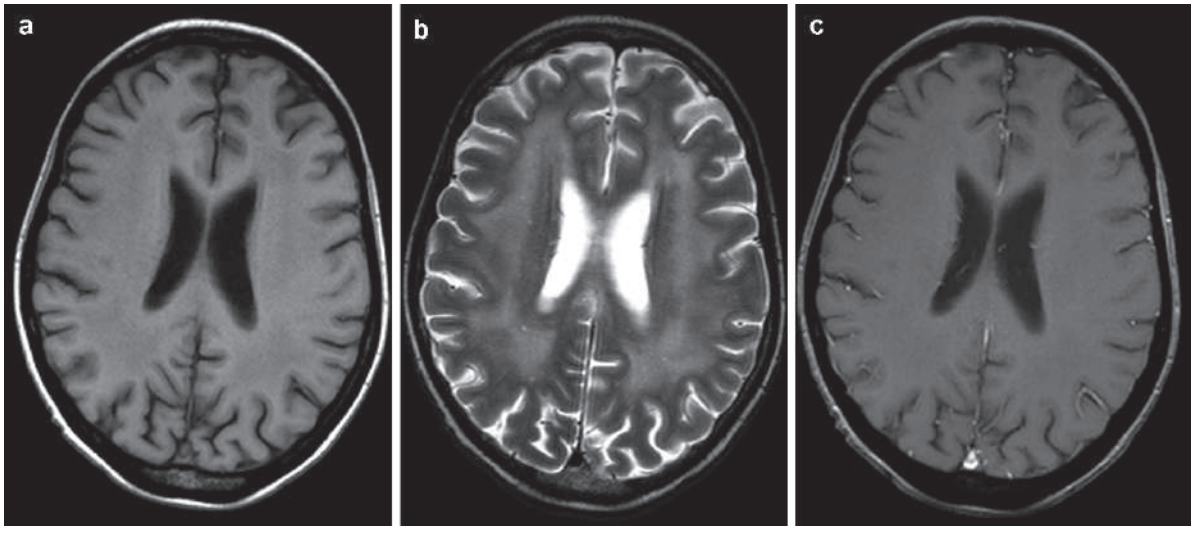

Fig. 8.7.4. Axial T1W (**a**), T2W (**b**), and T1W postcontrast brain MRI of a patient with ALL treated with methotrexate show diffuse leukoencephalopathy of the centrum semi-ovale bilaterally (**b**), with no contrast enhancement in (**c**)

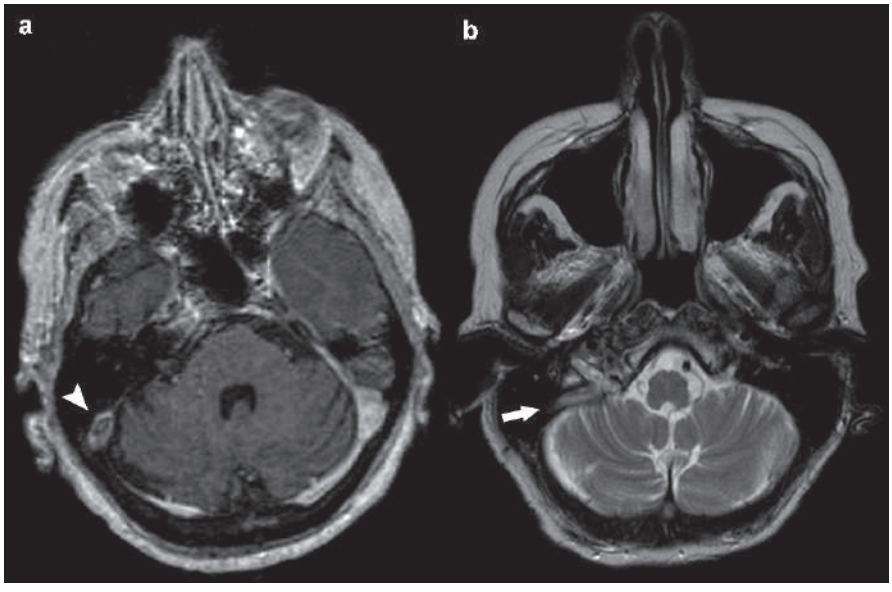

Fig. 8.7.5. Axial T1W postcontrast (**a**) and T2W (**b**) brain MRI of a patient with ALL treated with chemotherapy, who developed right transverse sinus thrombosis, show filling defect in (**a**) (*arrowhead*), and hyperintense vessel in (**b**) due to the intravascular thrombus (*arrow*)

For Further Reading

1. Jacobs P. Myelodysplasia and leukemias. Dis Mon. 1997;43:505
2. O'Brien MM et al Acute leukemia in children. Dis Mon. 2008;54:202–25
3. Kolitz JE. Acute leukemia in adults. Dis Mon. 2008;54:226–41
4. Enright H et al Chronic leukemias. Dis Mon. 2008;54:242–55
5. Lee YH et al Granulocytic sarcoma (choloroma) presenting as a lateral neck mass: initial manifestation of leukemia: a case report. Eur Arch Otorhinolaryngol. 2006;263:16–18
6. O'Brien J et al An unusual cause of persistent headache: chloroma (2008:2b). Eur Radiol. 2008;18:1071–72
7. Hermann G et al Skeletal manifestations of granulocytic sarcoma (chloroma). Skeletal Radiol. 1991;20:509–12

8. Frohna BJ et al Granulocytic sarcoma (chloroma) causing spinal cord compression. Neuroradiology. 1993;35: 509–11
9. Pande AR et al Disseminated necrotizing leukoencephalopathy following chemoradiation therapy for acute lymphoblastic leukemia. Radiat Med. 2006;24:515–19
10. Laningham FH et al Childhood central nervous system leukemia: historical perspectives, current therapy, and acute neurological sequelae. Neuroradiology. 2007;49:873–88
11. Faber J et al Schwachman-Diamond syndrome: early bone marrow transplantation in a high risk patient and new clues to pathogenesis. Eur J Pediatr. 1999;158:995–1000
12. Alkubaidan FO et al Granulocytic sarcoma (chloroma) of the shoulder in Schwachman-Diamond syndrome. Eur J Radiol Extra. 2007;64:107–10
13. Carroll KW et al Useful internal standards for distinguishing infiltrative marrow pathology from hematopoietic marrow at MRI. 1997;7:394–8
14. Jain D et al Bloom syndrome in sibs: first report of hepatocellular carcinoma and Wilms tumor with documented anaplasia and nephrogenic rests. Pediatr Dev Pathol. 2001;4:585–89
15. Cretzula JC et al Bloom's syndrome. J Am Acad Dermatol. 1987;17:479–88

8.8 Multiple Myeloma (Khaler's Disease)

Multiple myeloma (MM) is a malignant disease characterized by neoplastic proliferation of plasma cell precursors in the bone marrow. The disease can arise diffusely or focally in any region in the body. The focal form of multiple myeloma is called "*plasmacytoma.*" MM is a disease of older age groups, and typically found in patients between 40 and 70 years of age.

The cardinal features of MM are osteolytic lesions found on plain X-rays, anemia, proteinuria, and bone pain. Other features include weight loss, anorexia, hepato-splenomegaly (25%), high serum alkaline phosphatase level, and high erythrocyte sedimentation rate (ESR). Peripheral blood smears shows characteristic stacking of the red blood cells (Rouleau formation).

Anorexia in MM has been attributed to the toxic effects from breakdown products, and pain is often intense, requiring narcotics. Pain in MM can arise due to different mechanisms such as bone pain due to expansion of the bone marrow by the myelomatous tissue, root pain caused by compression or direct invasion of the nerve roots, periarticular pain mimicking arthritis, and pathologic bone fractures. Back pain commonly arises due to vertebral pathologic fractures and collapse. Back pain in MM is made worse by turning or twisting, and is aggravated by coughing or sneezing.

In MM, signs of amyloidosis may be seen in the form of macroglossia, skin papules, and alopecia. Raynaud's phenomenon, cold urticaria, and necrosis of the skin may be seen due to cyroglobulinemia. *Cryoglobulinemia* is a condition characterized by the presence of large amounts of proteins that become insoluble at reduced temperature (e.g., 4 °C). Increased plasma osmolarity due to the high plasma cell content in the blood may cause impairment of cerebral circulation due to increased plasma viscosity, a rare condition known as "*coma paraprotienemicum.*"

One of the most dramatic complications of MM is the sudden compression of the spinal cord by collapsed vertebra, or plasmacytoma. Vertebral plasmacytoma arises from the bone marrow, and tunnels through the cortex until it spreads outside the vertebra as a soft-tissue mass arising from the vertebral body.

Renal disease in multiple myeloma often arises due to amyloidosis, causing proteinuria in 60–90% of cases, and uremia in terminal stages, which is known as "*myeloma kidney.*" Renal failure in MM patients commonly arises due to infections, calculi, or nephrocalcinosis, rather than the classic myeloma kidney. In myeloma kidney, there is deposition of an abnormal globulin of small molecular weight as droplets in the cytoplasm of renal tubular epithelium. Later, fibrosis and degeneration of the renal tubules occur, resulting in replacement of the nephron by fibrous tissue. Identifying *Bence-Jones protein* in the urine is diagnostic of MM. Signs of uremia in MM are similar to those of uremia due to other causes, except that hypertension is rarely present. Intravenous urography should not be used in patients with MM to assess the renal function, as it can result in renal failure and death in some MM patients.

Rarely, multiple myeloma of the mandible may present with paresthesia of the chin and the lower lip due to infiltration of the mental nerve, a branch of the third division of trigeminal nerve, when the mandible is affected by multiple myeloma. The condition is known as "*numb chin syndrome*," and it is seen in malignancy that involves the mandible (e.g., leukemia).

POEMS syndrome, also known as *Crow-Fukase syndrome*, is a rare plasma cell disease with multisystemic involvement characterized by *p*olyneuropathy, *o*rganomegaly, *e*ndocrinopathy, *m*onoclonal gammopathy, and *s*kin changes. Patients with POEMS syndrome initially present with typical symptoms of connective tissue disorder, such as scleroderma-like skin thickening. Other manifestations include hepatosplenomegaly, Castleman's disease lymphadenopathy, hypothyroidism, hypogonadism, peripheral sensorymotor polyneuropathy, hypertrichosis, hyperpigmentation, scleroderma, and osteosclerotic plasmacytoma. POEMS syndrome has been linked to infection with human herpes-virus type 8.

How can you differentiate between POEMS syndrome from multiple myeloma with different body manifestations?

- The osteolytic lesions of plasmacytoma and MM are "purely" lytic, with punched-out appearance on skeletal radiographs. In contrast, POEMS syndrome lesions are seen as well-defined fluffy sclerotic lesions, or osteolytic lesions with sclerotic margins.

8.8

- Bone pain attributed to osteolytic lesions is common in MM, whereas bone pain is unlikely to occur due to bony lesions in POEMS syndrome.
- Patients with MM are typically elderly, >60 years of age, while patients with POEMS syndrome are usually younger.
- The monoclonal band in MM shows predominance of a kappa light chain, while in POEMS syndrome it is a lambda light chain.
- The presence of Bence-Jones protein in the serum and/or urine of classic MM patients is absent in POEMS syndrome.
- Bone scintigraphy is typically negative in MM, while it is positive in POEMS syndrome.

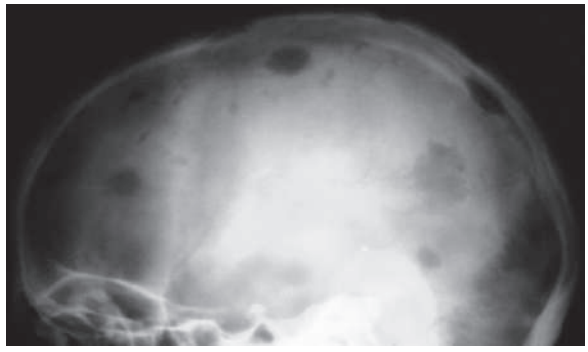

Fig. 8.8.1 Lateral plain skull radiograph of a patient with multiple myeloma shows multiple, osteolytic, sharply-defined lesions affecting the clavarium

Signs on Plain Radiographs

- The classical appearance of MM is that of punched-out, sharply-circumscribed, small osteolytic bone lesion that can be solitary or multiple. The osteolytic lesions are often found in the skull (Fig. 8.8.1), vertebrae, ribs, pelvis, and long bones. Without the clinical picture, relying on radiographs alone to diagnose MM is not always possible, as multiple osteolytic bony lesions can be also seen in metastatic cancer and other tumors.
- Diffuse osteoporosis is commonly encountered in MM.
- Pathologic fractures may be seen, especially in the vertebrae.
- Acute myeloma presents as multiple lytic lesions (Fig. 8.8.2), while chronic myeloma can presents as a dense and thick bone, mimicking Paget's disease.
- Although multiple osteolytic lesions are found in myeloma, bone scan is typically negative in MM.
- POEMS syndrome lesions are seen as well-defined fluffy sclerotic lesions, or osteolytic lesions with sclerotic margins.
- Severe complication of diffuse infiltration of the vertebral body include vertebral collapse due to pathological fracture. Severe collapse of the vertebral body (vertebra plana) can be seen (Fig. 8.8.3).

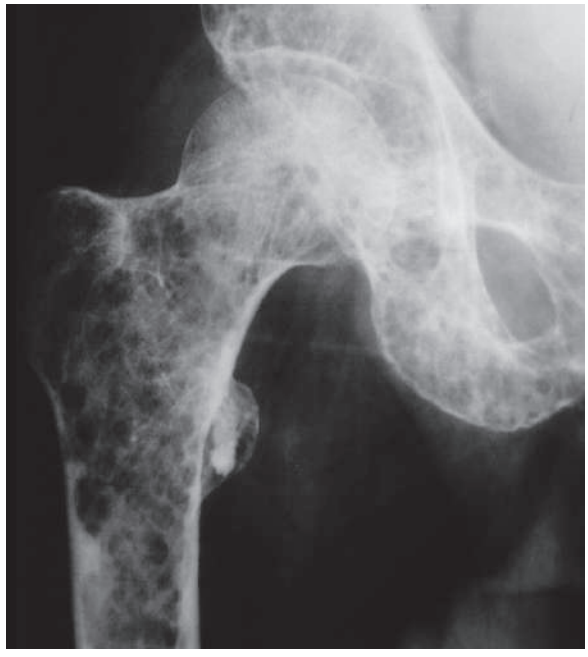

Fig. 8.8.2 Anteroposterior plain radiograph of the right hip joint shows diffuse small osteolytic lesions affecting the femur and the pelvis in a patient with acute multiple myeloma

Signs on CT

- In *numb chin syndrome*, there is an expansile bony lytic lesion that destroys the mandibular ramus and infiltrates the masticator space (Fig. 8.8.4).
- *Vertebral plasmacytoma* is seen as an osteolytic lesion with soft-tissue mass that grows externally into the adjacent surrounding tissues (Fig. 8.8.5).

Signs on MRI

- The MR appearance of lesions of MM, often in the vertebral column, is staged into four main types: normal, focal, variegated, and diffuse. The normal pattern shows no signs marrow infiltration of vertebral bodies, which is a very good sign for prognosis. The focal pattern shows localized areas of low T1 and high T2 signal intensities within the vertebral bodies.

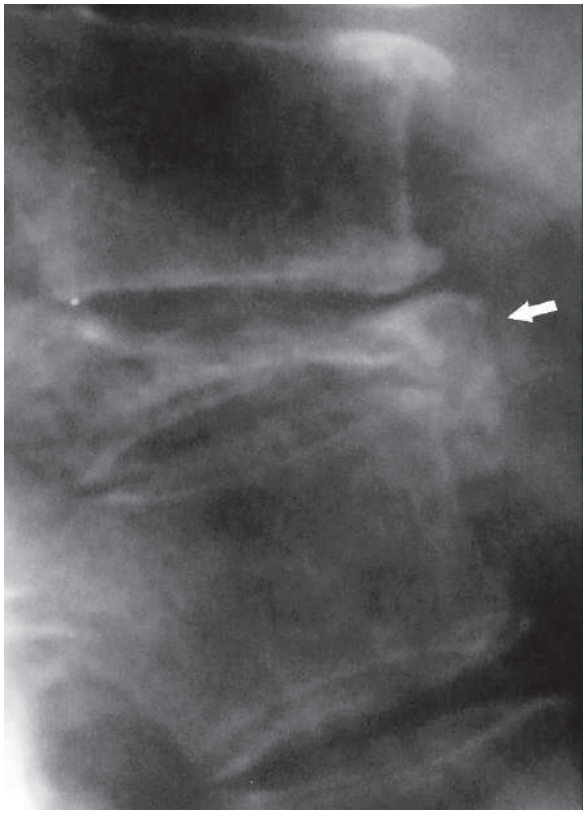

Fig. 8.8.3 Lateral plain thoracic vertebral radiograph of a patient with multiple myeloma shows vertebra plana (*arrow*)

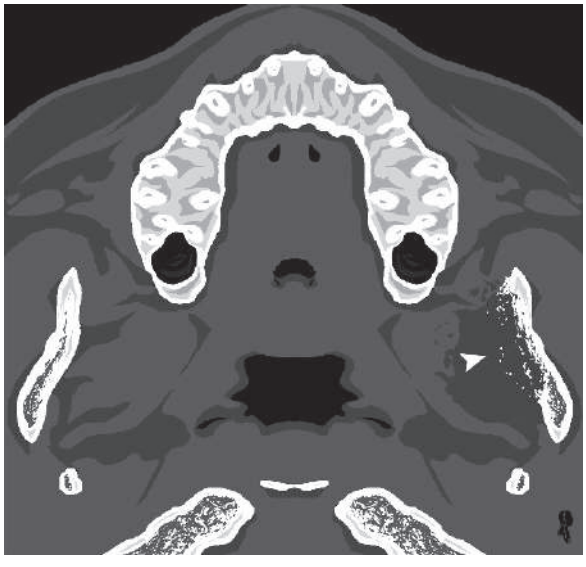

Fig. 8.8.4 Axial upper jaw dental CT illustration of a patient with numb chin syndrome due to multiple myeloma shows soft tissue mass destroying and violating the right mandibular ramus integrity (*arrowhead*)

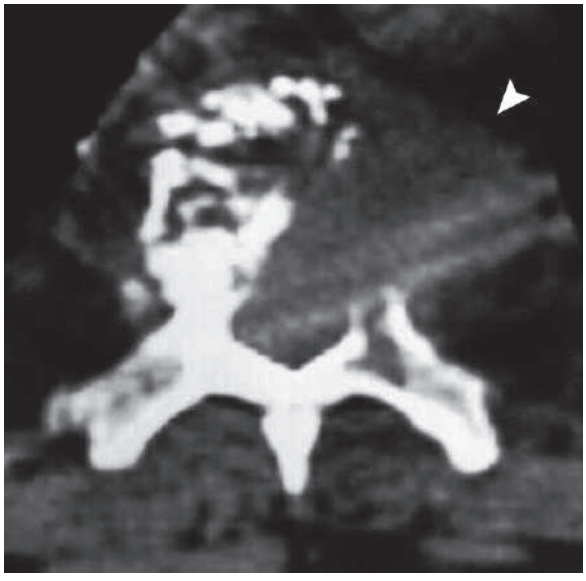

Fig. 8.8.5 Axial thoracic vertebral CT of a patient with plasmacytoma shows osteolytic soft-tissue mass with external and intraspinal canal extensions (*arrowhead*)

- The presence of multiple scattered small foci results in a variegated appearance (Fig. 8.8.6). The diffuse infiltration of the vertebral bodies results in reducing the total signal intensity of the vertebral column compared to the vertebral discs on T1W images (*positive disc sign*). In the normal vertebral MRI scan, the vertebral bodies have higher signal intensity than the vertebral discs on T1W images, due to the fatty bone marrow. The positive disc sign is commonly also found in patients with leukemia, when leukemic cells diffusely infiltrate the vertebral column.
- Infiltration of the meninges may be seen as nodular or thickened meninges with contrast enhancement (*Meningiosis carcinomatosis*).
- The degree of vertebral body bone marrow infiltration can be assessed by measuring the enhancement difference. On T1W images, this is done by applying a region of interest to the vertebral body and measuring the signal intensity (e.g., 240) is measured, and then copying the circle on the same section that was measured and applying it to the T1W postcontrast images to get the signal intensity of the vertebral body postcontrast (e.g., 320). Signal intensity (SI) difference is calculated by the following formula: (SI after contrast – SI before contrast/SI before contrast) × 100. Normal SI signal difference should be <18%. An SI difference of >24% reflects low-grade infiltration, while an SI difference of >49% reflects high-grade infiltration (Fig. 8.8.7).

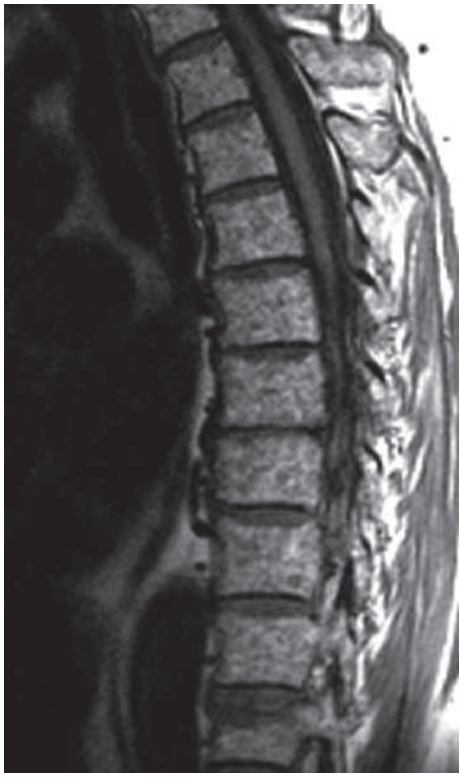

Fig. 8.8.6 Sagittal T1W thoracic vertebral MRI shows the variegated appearance of multiple myeloma bone marrow infiltration

For Further Reading

1. Jacobs P. Myeloma. Dis Mon. 1990;36:323–71
2. Magnusson S et al Multiple myeloma. Dis Mon. 1960;6:1–32
3. Leonard RCF et al Multiple myeloma: radiology or bone scanning? Clin Radiol. 1981;32:291–95
4. Winterbottom AP et al Imaging patients with myeloma. Clin Radiol. 2009;64:1–11
5. Libshitz HI et al Multiple myeloma: appearance at MR imaging. Radiology 1992;182:833–37
6. Lecouvet FE et al Stage III multiple myeloma: clinical and prognostic value of spinal bone marrow MR imaging. Radiology. 1998;209:653–60
7. Angtuaco EJC et al Multiple myeloma: clinical review and diagnostic imaging. Radiology. 2004;231:11–23
8. Hess T et al Atypical manifestations of multiple myeloma: radiological appearances. Eur J Radiol. 2006;58:280–85
9. Patriarca F et al Meningeal and cerebral involvement in multiple myeloma patients. Ann Hematol. 2001;80:758–62
10. Attwell A et al Multiple myeloma involving the porta hepatic and peritoneum causing biliary obstruction and malignant ascites. Dig Dis Sci. 2005;50:1068–71
11. Eidner T et al Clinical manifestations of POEMS syndrome with features of connective tissue disorders. Clin Rheumatol. 2001;20:70–2
12. Chong ST et al POEMS syndrome: radiographic appearance with MRI correlation. Skeletal Radiol. 2006;35:690–95
13. Narváez JA et al POEMS syndrome: unusual radiographic, scintigraphic and CT features. Eur Radiol. 1988;8:134–36
14. Sugawara Y et al Paresthesia of the lower lip as a first manifestation of multiple myeloma – a case report. Oral Radiol. 2003;19:158–66
15. Bauer A et al Neovascularization of bone marrow in patients with multiple myeloma. A correlation study of magnetic resonance imaging and histopathologic findings. Cancer 2004;101:2599–604

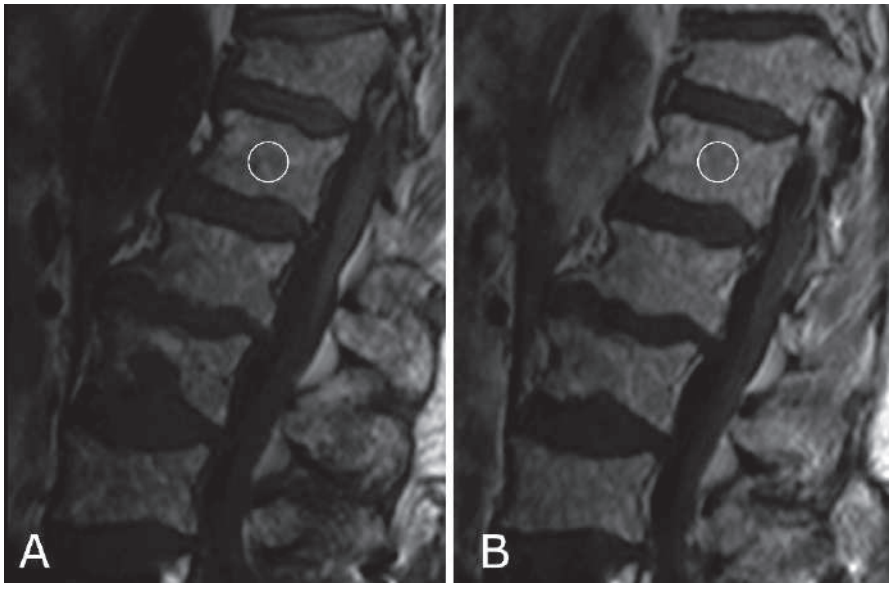

Fig. 8.8.7 Sagittal T1W (**a**) and T1W postcontrast (**b**) of a patient with multiple myeloma shows two circles that measure the signal intensity in the region of interest. By applying the formula, the signal intensity difference was 26%, reflecting low-grade diffuse vertebral bone marrow infiltration

8.9 Amyloidosis

Amyloidosis is a systemic disease characterized by amyloid protein depositions in the extracellular matrix components such as blood vessel walls, the epithelial basement membrane, and the connective tissue matrix.

Amyloid is a term used to describe any protein with a "beta-pleated sheet" configuration. Amyloid proteins stain brown with iodine stain, from which the name was derived (amyloid means "starch-like"). Characteristically, amyloid proteins stain dark red with Congo red stain. When viewed under polarized light, amyloid stained with Congo red stain displays an apple-green birefringence. Any fibrillar protein with a "beta-pleated sheet" configuration will stain as amyloid.

Amyloid protein deposition in the extracellular matrix causes thickening and narrowing of the small vessel walls, destruction of the epithelial basement membrane, and mass effect over the cells causing cellular ischemia and destruction over time. Any tissue can be affected by amyloid deposition. Amylodosis can be systemic, affecting all body tissues, or localized to a certain organ.

Classification of Amyloidosis (Clinical-Based Classification)

Systemic amyloidosis is a type of amyloidosis characterized by widespread body tissue disease and amyloid presence in the blood. The systemic form is divided into four major types:

- *B-cell dyscrasia* (*primary amyloidosis*): this form arises due to defect in the B-cell function. The B-cells produces amyloid precursor protein into the blood called "light-chain myloid," and referred to as amyloid (AL). The monocytes engulf these AL amyloid precursors and then re-secrete them in the blood in the form of the classic amyloid proteins. This type of amyloidosis is typically seen in patients with multiple myeloma and plasmacytoma (B-cell malignancies).
- *Reactive systemic amyloidosis* (*secondary amyloidosis*): this form arises due to abnormal chemical signaling that evokes the liver to manufacture amyloid precursors and secretes them into the blood. The abnormal signaling can be initiated by different diseases. The liver forms "amyloid associated protein," which is referred to as amyloid (AA). Like amyloid AL, monocytes play a major role in transforming amyloid AA precursor into complete amyloid protein form. This type of amyloidosis can be seen associated with diseases like ulcerative colitis, Crohn's disease, systemic vasculitis, tuberculosis, Hodgkin's disease, and rheumatoid arthritis.
- *Dialysis-associated amyloidosis*: this is a special form of systemic amyloidosis that occurs in patients on hemodialysis (up to 70% of cases). It is believed that this form arises due to aggregation of β_2-microglobulins within the filtration machine, which will form amyloid protein, and then these amyloid proteins re-enter the body via the machine when the clear blood returns to the body. This type of amyloid has an affinity to precipitate in the joints, ligaments, tendons, and synovial membranes.
- *Hereditary familial amyloidosis*: this form is rare, and it is seen in families and rare syndromes. An example of hereditary amyloidosis is *Muckle-Wells syndrome*, which is a rare autosomal dominant disease characterized by chronic recurrent urticaria, often combined with fever, chills, rigors, arthralgia, progressive sensorineural hearing loss, and AA-type amyloidosis in 30% of cases. Another example of hereditary amyloidosis is familial Mediterranean fever. *Familial Mediterranean fever* (*Familial paroxysmal polyserositis*) is a genetic disease with autosomal recessive mode of inheritance, characterized by episodes of fever, abdominal pain, arthritis, and amyloidosis. The disease is common among Iraqi Jews, Armenians, Turks, and Middle Eastern Arabs. Patients experience multiple attacks of fever that last 12–72 h and resolve spontaneously. Recurrent attacks of abdominal pain that mimics acute abdomen are common, with constipation and diarrhea. The abdominal attack typically improves spontaneously in 24–72 h. Arthritis, including large-joint mono- and polyarthritis, is a common feature. Sero-negative HLA-B27 sacroiliitis and ankylosing spondylitis are reported among patients with familial Mediterranean fever.

Localized amyloidosis: this type of amyloidosis is characterized by deposition in a specific tissue (e.g., renal parenchyma). In this type, the amyloid proteins

8.9

are manufactured in the affected tissue. Examples of localized amyloidosis include:

- *Amyloidoma*: this is a rare form of deposition of amyloid in a certain tissue, forming a solid mass in the absence of B-cell disease (dyscrasia) or elevation of serum proteins. Amyloidoma can occur in any body tissue, and cannot be differentiated from other tumors except by biopsy.
- *Hormonal amyloidosis*: an example of this type is seen in endocrine cancerous cells that secrete amyloid proteins rather than normal hormones (e.g., thyroid medullary carcinoma).
- *Senile amyloidosis*: deposition of amyloid proteins due to the aging process in the choroids plexus, brain, and heart.

Up to 30% of patients with B-cell dyscrasia progress to multiple myeloma, while multiple myeloma is associated with systemic amyloidosis in 15% of cases. The median survival rate in patients with AL-type amyloidosis is 1.5 years, whereas the median survival rate in patients with AA-type amyloidosis is 4.5 years.

Although the features of amyloidosis are not specific, radiologists need to be familiar with the disease manifestations in different body organs, especially in secondary amyloidosis. Secondary amyloidosis can be suspected in patients with systemic diseases that present with body manifestations that cannot be explained by the original disease symptoms.

Renal amyloidosis can be divided into early and late stages. In the early stage, the kidney is normal in size and shape, after which it starts to progressively increase in size, due to the amyloid deposition. The enlarged amyloid kidney is firm in consistency, and has a waxy appearance on postmortem gross examination. In later stages, chronic parenchymal ischemia occurs due to amyloid deposition within the renal vessels, which causes irreversible cell damage and fibrosis. The end result of renal amyloidosis is renal failure. Patients with kidney amyloidosis commonly present with *nephrotic syndrome*, a syndrome characterized by generalized edema, hyperlipidemia, hematuria, and gross protienuria (>3 g/L). Bladder amyloidosis is often seen as a solitary mass (amyloidoma), which presents clinically with hematuria.

Hepatic amyloidosis can occur, but usually does not progress into liver failure. Normally, the liver parenchymal reservation is 85% of its mass, and the renal parenchymal reservation is 75% of the kidneys' mass. Due to these facts, most patients with systemic amyloidosis rarely develop hepatic failure, because they may die from renal failure before developing complete hepatic failure. However, hepatic dysfunction is observed, but hepatic failure is rare. The amyloid proteins are deposited in the arterioles, the extracellular compartments, and the hepatic sinusoids (space of Diss) until they fill the sinusoids and exert back pressure on the hepatocytes, causing pressure atrophy.

Splenic amyloidosis is detected clinically in the form of splenomegaly. The spleen is made of white pulp (15%) and red pulp (85%). Amyloidosis of the spleen may affect the white pulp or the red pulp. When amyloidosis affects the white pulp, it results in a moderately enlarged spleen, with a patchy, waxy appearance in postmortem gross examination (sago spleen). When it affects the red pulp, it causes diffuse enlargement, with diffuse waxy appearance in postmortem gross examination (diffuse amyloid spleen).

Cardiac amyloidosis is generally a rare condition. It can arise due to senility or due to chronic systemic disease. Amyloidosis of the heart can affect the atria more than the ventricles, for unknown reasons, and it may causes restrictive cardiomyopathy. Cardiac amyloidosis is usually caused by AL-type amyloidosis, and rarely by AA-type amyloidosis.

Endocrine amyloidosis may occur, and is classically seen in the form of endocrine insufficiency of the pituitary gland (hypopituitarism) or adrenal gland insufficiency (Addison's disease).

Gastrointestinal tract amyloidosis is detected as a disease of hollow organs. The colon is the most frequently affected organ. In the intestine, amyloid accumulates within the arterioles of the intestinal villi, resulting in malabsorption and diarrhea (due to failure of the villi to function), and mucosal ulceration and bleeding (due to villi ischemia and necrosis). Esophageal and gastric involvement results in dysmotility, wall thickening, and gastroesophageal reflux disease.

Pulmonary amyloidosis is a relatively rare condition, with patients often presenting with recurrent pneumonias, which characteristically occur in the same distribution that correspond to previous antibiotic treatment, but recurs at a later time. Features of pulmonary amyloidosis include diffuse interstitial nodular pattern, tracheal and bronchial wall thickening, and (rarely) a solitary mass (amyloidoma).

Central nervous system amyloidosis is often present in the form of cerebral amyloid angiopathy (CAA)

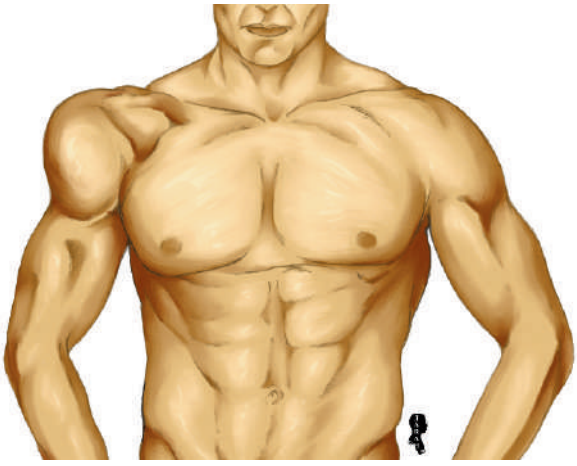

Fig. 8.9.1 An illustration demonstrates the shoulder pad sign (right shoulder)

with spontaneous nontraumatic intracranial bleeding, or (rarely) as leptomeningeal thickening.

Musculoskeletal amyloidosis generally causes muscular hypertrophy, weakness, and chronic pain. Muscular amyloidosis preferentially involves the shoulder girdle. Deposition of amyloids within the periarticular tissues of the shoulder girdle resulting in shoulder enlargement is called the "shoulder pad sign" (Fig. 8.9.1).

Amyloidosis in the head and neck region usually manifests as vocal cord thickening causing hoarseness of the voice, tongue intrinsic muscles deposition causing macroglossia, supra- and subglottic larynx, and periorbital deposition causing bleeding and ecchymoses (the raccoon sign). Amyloidosis of the paranasal sinuses can be seen as a sinusoidal mass with "fluffy-bone appearance" of the adjacent bone.

Signs on Plain Radiographs

- Pulmonary amyloidosis can be seen as a diffuse interstitial nodular patter or (rarely) as a single solitary mass (amyloidoma) (Fig. 8.9.2).
- When an amyloidoma involves a bone, it is usually visualized as an osteolytic mass lesion.
- Dialysis-related amyloid arthropathy is detected as periarticular bony cysts or erosions.

Signs on US

- Amyloidosis is one of the rare cases of enlarged kidneys with high echogenicity.
- Hepatic amyloidosis may appear as multiple foci of increased liver parenchymal echogenicity.

Signs on CT and MRI

- The affected kidney is normal or larger than normal in early stages of amyloidosis. In later stages, renal fibrosis shrinkage with parenchymal calcification is often seen.
- Hepatic amyloidosis can be seen on nonenhanced CT as a diffusely-enlarged liver with hypoattenuation. Other radiological signs are nonspecific.

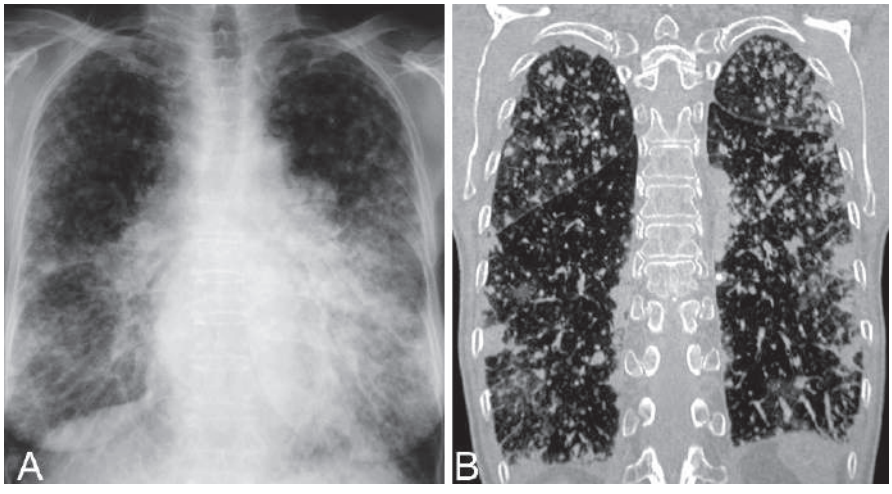

Fig. 8.9.2 Posteroanterior plain radiograph (**a**) and coronal HRCT (**b**) of a patient with multiple myeloma who developed pulmonary amyloidosis shows diffuse bilateral nodular interstitial pattern lung disease

8.9

- Splenic manifestations of amyloidosis include splenomegaly, calcification, and lack of enhancement after contrast injection. The lack of contrast enhancement is thought to be due to vascular amyloid angiopathy and diffuse parenchymal infiltration by amyloid proteins.
- Small and large bowel involvement results in diffuse or nodular wall thickening.
- Cardiac amyloidosis can show many nonspecific findings, such as biventricular hypertrophy that mimics hypertrophic cardiomyopathy (Fig. 8.9.3), thickening of the papillary muscles and the valvular leaflets, and pleural or pericardial effusion. Biatrial enlargement and enhancement is a characteristic sign, but unfortunately not always seen. On MRI, a relatively characteristic pattern of myocardial amyloidosis seen on postgadolinium injection consists of strong subendocardial and subepicardial late enhancement (zebra enhancement pattern) (Fig. 8.9.4).
- Pulmonary amyloidosis on HRCT may resemble the features of bronchiolitis obliterans, diffuse interstitial nodular pattern (nodules <15 mm in diameter) may cause a "budding tree" appearance, or may (rarely) present as a solitary solid mass with calcification (amyloidoma) (Fig. 8.9.2). Tracheal and bronchial wall thickening are other characteristic signs of amyloidosis of the bronchial tree.
- Paransal sinuses amyloidoma is seen as a mass with "fluffy-bone appearance" of the adjacent bone. However, a biopsy is required to confirm diagnosis.
- On MRI, synovial thickening that resembles pigmented villonodular synovitis can be seen, which characteristically lacks the chronic hemorrhage and hemosiderin T1 and T2 hypointense signal intensities.

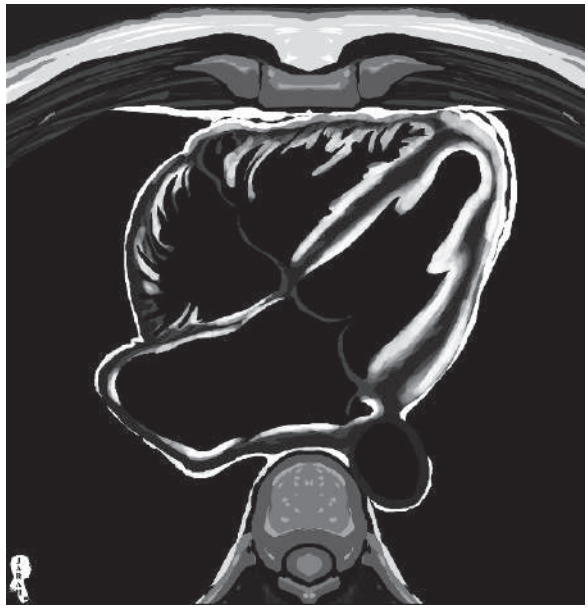

Fig. 8.9.4 Axial, four-chambers postcontrast cardiac MR illustration of a patient with cardiac amyloidosis shows subendocardial and subepicardial enhancement that is described as a zebra enhancement pattern

- Amyloid proteins on MRI typically show low T1 and T2 signal intensities and contrast enhancement. Therefore, signs of high signal intensity on T2W images in amyloidosis are usually due to the inflammatory reaction evoked by the amyloidosis, not by the amyloid proteins themselves.

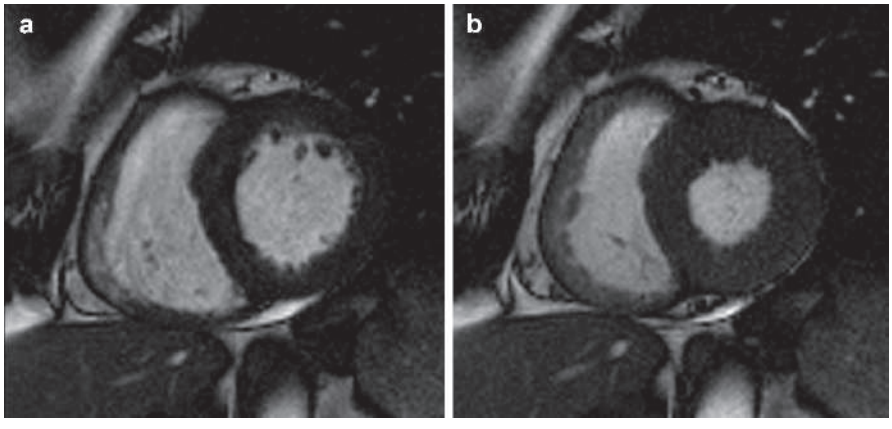

Fig. 8.9.3 Short-axis white blood pool cardiac MRI in diastolic (**a**) and systolic (**b**) phases show hypertrophy of the right and left ventricles in a patient with systemic amyloidosis

- Cerebral amyloidosis may present on noncontrast-enhanced CT as intracranial hemorrhage due to CAA or (rarely) diffuse lepromeningeal thickening and enhancement.
- Amyloidoma in any body region is usually seen as a solid tissue mass that may cause bone osteolysis and contains calcification. However, this appearance is nonspecific, and biopsy is crucial to establish the diagnosis.
- Dialysis-related amyloid arthropathy is detected on CT as bony erosions and as formation of bony cysts. On MRI, the amyloid changes are detected as thickening and irregularity of the supraspinatus tendon, thickening of the iliofemoral portion of the hip joint capsule, and fluid collection within the bursae of the joints. Soft-tissue amyloid deposition can be seen in the spine, carpal tunnel, and knee synovium as typical low signal intensity on both T1W and T2W images.

For Further Reading

1. Georgiades CS et al Amyloidosis: review and CT manifestations. RadioGraphics. 2004;24:405–26
2. Guerreiro de Moura CG et al "Shoulder pad" sign. N Engl J Med. 2004;351:25:e23
3. Geluwe FV et al Amyloidosis of the heart and respiratory system. Eur Radiol. 2006;16:2358–65
4. Urban BA et al CT evaluation of amyloidosis: spectrum of diseases. RadioGraphics. 1993;13:1295–308
5. Singh SK et al Localized primary amyloidosis of the prostate, bladder, ureters. Int Urol Nephrol. 2005;37:495–97
6. Sueyoshi E et al Cardiac amyloidosis: typical imaging findings and diffuse myocardial damage demonstrated by delayed contrast-enhanced MRI. Cardiovasc Intervent Radiol. 2006;29:710–12
7. Motosugi U et al Localized nasopharyngeal amyloidosis with remarkable early enhancement on dynamic contrast-enhanced MR imaging. Eur Radiol. 2007;17:852–53
8. Chin SC et al Amyloidosis concurrently involving the sinosoidal cavities of the larynx. AJNR Am J Neuroradiol. 2004; 25:636–38
9. Gilad R et al Severe diffuse systemic amyloidosis with involvement of the pharynx, larynx, and trachea: CT and MR findings. AJNR Am J Neuroradiol. 2007;28:1557–58
10. Urban PP et al Leptomeningeal familial amyloidosis: a rare differential diagnosis of leptomeningeal enhancement in MRI. J Neurol. 2006;253:1238–40
11. Metzler JP et al MRI evaluation of amyloid myopathy. Skeletal Radiol. 1992;21:463–65
12. Matsumoto K et al Primary solitary amyloidosis of the lung: findings on CT and MRI. Eur Radiol. 1997;7:586–88
13. Rafal RB et al MRI of primary amyloidosis. Gastrointest Radiol. 1990;15:199–201
14. Arslan A et al Laryngeal amyloidosis with laryngocele: MRI and CT. Neuroradiology 1998;40:401–3
15. Escobedo EM et al Magnetic resonance imaging of dialysis-related amyloidosis of the shoulder and hip. Skeletal Radiol. 1996;25:41–8
16. Touart DM et al Cutanous deposition diseases. Part I. J Am Acad Dermatol. 1998;39:149–71
17. Fujita Y et al Nail dystrophy and blisters as sole manifestations in myeloma-associated amyloidosis. J Am Acad Dermatol. 2006;54:712–4
18. Hidalgo E et al Amyloidoma of the skull: plain radiographs, VT and MRI. Neuroradiology. 1996;38:44–6
19. El-Darouti MA et al Muckle-Wells syndrome: report of six cases with hyperpigmented sclerodermoid skin lesions. Int J Dermatol. 2006;45:239–44
20. Asaumi J et al CT and MR imaging of localized amyloidosis. Eur J Radiol. 2001;39:83–7
21. Fonnesu C et al Familial Mediterranean fever: a review for clinical management. Joint Bone Spine. 2008. doi:10.1016/j.jbspin.2008.08.004
22. Keles¸ I et al Familial Mediterranean fever and ankylosing spondylitis in a patient with juvenile idiopathic arthritis: a case report and review of the literature. Rheumatol Int. 2006;26:846–51

8.10

Evans' Syndrome

Evans' syndrome (ES) is a disease characterized by simultaneous development of autoimmune thrombocytopenia (AITP) and autoimmune hemolytic anemia (AIHA).

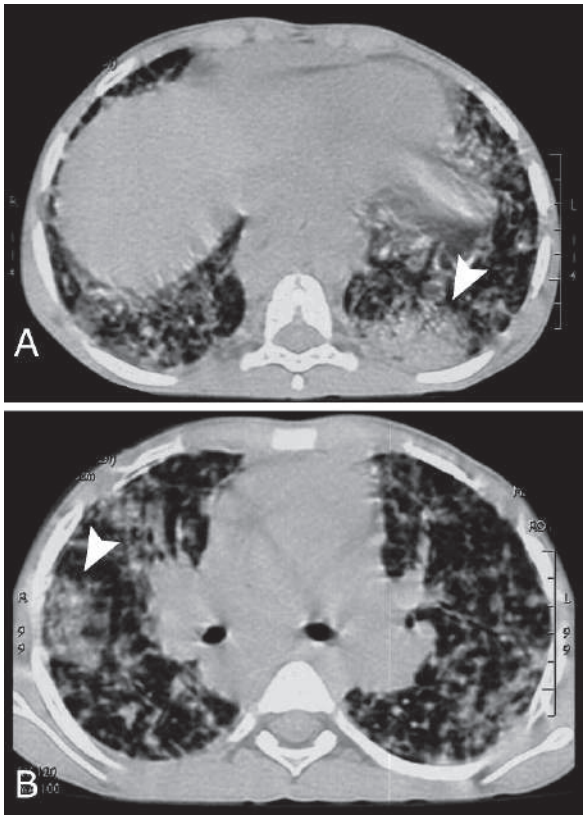

Fig. 8.10.1 Axial lung window HRCT of the lungs show bilateral patchy lung consolidation with a mass of consolidation located at the subpleural, peripheral, posterior lung lobe (*arrowhead in* **a**) and the right subpleural area in the right middle lobe (*arrowhead in* **b**) due to cryptogenic organizing pneumonia

Patients with ES develop autoantibodies against erythrocytes, platelets, and neutrophils. ES often presents with a wide variety of clinical manifestations that include lymphoid tissue hyperplasia, interstitial nephritis, eczema, and insulin-dependent diabetes mellitus. AITP and AIHA can be also the first signs of systemic lupus erythematosis.

Uncommonly, ES patients may present with progressive dyspnea due to the formation of cryptogenic organizing pneumonia. Neurological symptoms due to sagittal vein thrombosis may occur.

Investigations show low platelet count, low hemoglobin, neutropenia, and positive Coombs test. Radiology investigations are requested mainly to detect complications of the disease (Fig. 8.10.1)

For Further Reading

1. Savasan S et al The spectrum of Evans' syndrome. Arch Dis Child. 1997;77:245–4
2. Garcia-Muñoz R et al Splenic marginal zone lymphoma with Evans' syndrome, autoimmunity, and peripheral gamma/delta T cells. Ann Hematol. doi: 10.1007/s00277–008–0555-z
3. Tsang KWT et al *Rhodococcus equi* lung abscess complicating Evans' syndrome treated with corticosteroid. Respiration. 1998;65:327–30
4. Miyamae T et al An infant with γ-globulin-induced hypersensitivity syndrome who developed Evans' syndrome after a second γ-globulin treatment. Mod Rheumatol. 2004;14:314–19
5. Shiozawa Z et al Superior sagittal sinus thrombosis associated with Evans' syndrome of haemolytic anaemia. J Neurol. 1985;232:280–82
6. Ucci G et al A case of Evans' syndrome in a patient with ulcerative colitis. Dig Liver Dis. 2003;35:439–41
7. Máiz L et al Bronchiolitis obliterance organizing pneumonia associated with Evans syndrome. Respiration. 2001;68:631–34

8.11 Other Lymphatic Disorders

This topic discusses some of the uncommon lymphatic disorders occasionally encountered in radiology, and that can be mistaken initially for lymphoma or inflammatory conditions causing lymphadenopathy.

Castleman's Disease (Angiofollicular Lymph Node Hyperplasia)

Castleman's disease (CD) is a rare benign process of unknown cause, characterized by lymph nodes hyperplasia.

CD is liable to be misdiagnosed as other hypervascular tumors by radiology and pathology examinations. Lymph node hyperplasia may occur anywhere along the lymphatic chain within the body; however, it is commonly described in the mediastinum, abdomen, and pelvis.

The main pathology in CD concerns lymph nodes hyperplasia and the related small blood vessels. The lymph nodes are enlarged with high blood vessel proliferation and hypervascularity. CD is divided into two types: localized type and diffuse type.

The localized type is characterized by proliferation of the lymph nodes in a certain region within the body. Differential diagnoses of the localized type include tuberculosis lymphadenitis (ruled out by TB serology) and pheochromocytoma due to its hypervascularity (rules out by biochemistry investigations). CD diagnosis should be considered in differential diagnosis of hypervascular tumor in the retroperitonium.

The diffuse type is characterized by lymph node proliferation through the body. The main differential diagnosis is lymphoma. Lymph node biopsy is the gold standard method to diagnose CD.

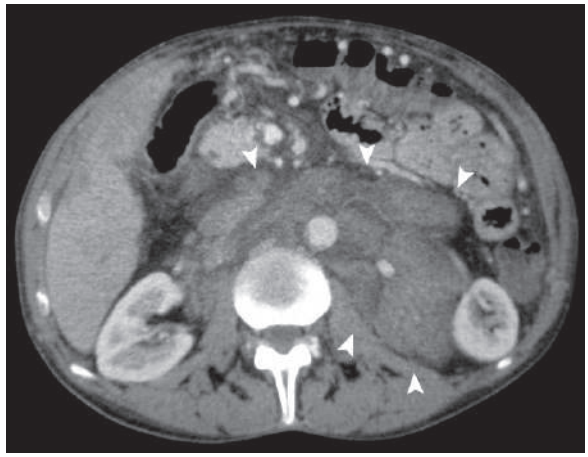

Fig. 8.11.1 Axial abdominal portal phase, contrast-enhanced CT shows diffuse lymphadenopathy in the retroperitonium around the aorta and the inferior vena cava (*arrowheads*) in a patient with Castleman's disease

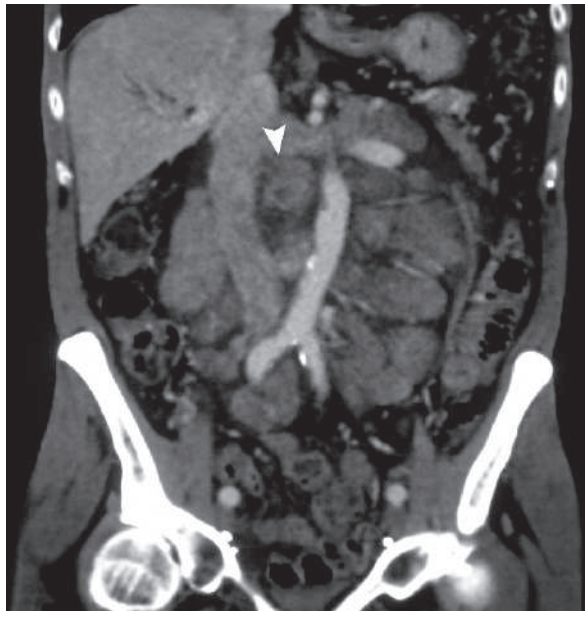

Fig. 8.11.2 Coronal abdominal portal phase, contrast-enhanced CT of the same patient shows the enlarged lymph nodes separating the inferior vena cava from the aorta (*arrowhead*)

Signs on CT

- There are enlarged lymph nodes located within the mediastinum or the retroperitonium (Figs. 8.11.1 and 8.11.2)
- The lymph nodes in CD are characterized by homogenous high-contrast enhancement in the early phase of dynamic enhancement that can exceed the enhancement of pheochromocytoma due to the hypervascularity of the lymph nodes. The high enhancement persists in the delayed phases.

8.11

- Typically, there is absence of necrosis or cystic changes within the enlarged lymph nodes, due to the abundant vascular supply. However, cystic changes may be found in 22% of cases, especially when the lymph node is > 5 cm in diameter.
- Punctuate or coarse calcification may be seen in 30% of cases (lymphomas do not calcify unless treated).
- A thin rim-like enhancement sign may be noticed in the arterial phase, with several enhancing feeding vessels that surround the nodes.
- To differentiate CD from *pheochromocytoma* in the retroperitonium, MRI should be done. Pheochromocytoma show higher signal intensity on T2W images compared to CD. Contrast-enhanced images may be similar due to the high vascular blood supply of the lymph nodes in CD.
- CD shows higher contrast enhancement than any other retroperitoneal sarcoma.

Kikuchi–Fujimoto Disease (Histocytic Necrotizing Lymphadenitis)

Kikuchi–Fujimoto disease (KFD) is a rare, self-limiting condition, characterized by the development of fever, weight loss, malaise, and lymphadenitis (commonly cervical).

KFD is often mistaken for tuberculous lymphadenitis, lymphoma, systemic lupus lymphadenitis, and infectious lymphadenitis. The misdiagnosis rate is up to 40% of cases.

The disease is self-limiting and benign, with a course lasting 6–8 weeks. The recurrence rate is 3% of cases. Laboratory findings are not specific, and usually show high C-reactive protein and erythrocyte sedimentation rate, mild lymphocytosis, leucopenia, and atypical lymphocytes. Definite diagnosis is done by fine-needle lymph node biopsy.

The disease is of unknown origin, affects mainly females (mean age of 30 years), and may be associated with Epstein-Barr virus activation and systemic lupus erythematosus.

Signs on CT

Neck and mediastinal CT often show lymphadenopathy similar to the picture seen in lymphoma and tuberculous adenitis. History, laboratory investigations, and the biopsy report are the main elements for establishing the diagnosis.

Kimura's Disease

Kimura's disease (KD) is a chronic inflammatory disease characterized by tumor-like soft tissue swelling and lymphoid tissue hyperplasia (Fig. 8.11.3).

KD is characterized histopathologically by lymphoid hyperplasia with soft-tissue infiltration by eosinophils, which is a constant finding in this disease. The cause of this disease is unknown, but it is thought to be caused by chronic allergic reaction due to the eosinophilia and high serum immunoglobulin E in patients with KD.

KD has predominance in young males, and is usually seen in Asian populations, especially in Japan and China (80%). Patients often present with asymptomatic, unilateral soft-tissue swelling involving lymph nodes or salivary glands (e.g., the parotid glands). Regional lymphadenopathy is found in 66% of cases. The head and neck region is affected in 70% of cases. Atopic disorders can be seen in patients with KD. Rare manifestations include masses formation in the external auditory meatus, tongue, orbits, epiglottis, larynx, groin (15%), and extremities (12%). Nephrotic syndrome is found in 12% of cases.

Definite diagnosis requires mass biopsy with laboratory evidence of eosinophilia that is not related to parasitic infection.

Fig. 8.11.3 An illustration demonstrating left parotid enlargement in a patient with Kimura disease

Signs on CT

- When the salivary glands are affected, an irregularly shaped subcutaneous mass with heterogeneous contrast enhancement is commonly found. The adjacent bone is often not disturbed.
- Enlargement of the lachrymal gland in a unilateral or bilateral fashion, mimicking Sjögren's syndrome, may be seen.
- Abdominal lymphadenopathy may be enlarged, mimicking lymphoma or localized CD.

Signs on MRI

MR features are nonspecific, and diagnosis is essentially by laboratory investigation and biopsy. MR examination helps to exclude other differential diagnoses.

For Further Reading

1. Zhou LP et al Imaging findings in Castleman disease of the abdomen and pelvis. Abdom Imaging. 2008;33:482–88
2. Irsutti M et al Castleman disease: CT and MR imaging features of a retroperitoneal location in association with paraneoplastic pemphigus. Eur. Radiol. 1999;9:1219–21
3. Zheng X et al Localized Castleman disease in retroperitonium: newly discovered features by multi-detector helical CT. Abdom Imaging. 2008;33:489–92
4. Chidambara Murthy S et al Kikuchi's disease associated with systemic lupus erythematosus. Indian J Dermatol Venereol Leprol. 2005;71:338–41
5. Kaicker S et al PET-CT scan in patient with Kikuchi disease. Pediatr Radiol. 2008;38:596–97
6. Chen HC et al Systemic lupus erythematosus with simultaneous onset of Kikuchi-Fujimoto's disease complicated with antiphospholipid antibody syndrome: a case report and review of the literature. Rheumatol Int. 2005;25:303–6
7. Hrycek A et al Kikuchi-Fujimoto disease: a case report. Rheumatol Int. 2005;26:179–81
8. Hiwatashi A et al Kimura's disease with bilateral auricular masses. Am J Neuroradiol. 1999;20:1976–8
9. Ching ASC et al Extranodal manifestations of Kimura's disease: ultrasound features. Eur Radiol. 2002;12:600–4
10. Ortak T et al Kimura disease: a brief clinical report. Eur J Plast Surg. 2008;31:253–57
11. Kodama T et al Kimura's disease of the lacrimal gland. Acta Opthalmol Scand. 1998;76:374–77
12. Liu PI et al Kimura's disease in upper arm: a case report and imaging findings. Chin J Radiol. 2007;32:153–6
13. Jeong YY et al Imaging of Kimura's disease involving teh abdomen. AJR Am J Roentgenol. 2006;187:W131–2

Chapter 9

Dermatology

CONTENTS

J. A. Al-Tubaikh: *Internal Medicine* – An Illustrated Radiological Guide
DOI: 10.1007/978-3-642-03709-2_9, © Springer-Verlag Berlin Heidelberg 2010

9.1 Scleroderma (Systemic Sclerosis)

Scleroderma is a systemic disease characterized by progressive fibrosis of the skin and multiple organs. The term "scleroderma" means literally "hard skin"

In scleroderma, the dermis is infiltrated by T-lymphocytes, causing abnormal fibroblasts activation, which leads to increased production of extracellular collagen type-I. This increase in collagen causes skin thickening and tightening, which is the main manifestation of this disease.

Scleroderma is divided into two major forms: diffuse and focal. In the generalized form, diffuse skin disease with organ involvement is typically seen. In the focal form, there is limited cutaneous involvement of the skin. Linear scleroderma and morphea are examples of focal scleroderma.

Females are affected by scleroderma seven times as often as males. Patients present classically with flexural contracture of the terminal phalanges (claw-hand like appearance), loss of the skin folds around the mouth (mask-like appearance), atrophied nasal alae (mouse facies), reduced opening of the mouth with jaw fixation, pathological changes of minor salivary glands mimicking Sjögren's syndrome, and uncommonly trigeminal neuralgia (4%). Laboratory investigations show positive antinuclear antibodies (70–90%), rheumatoid factor (25%), and hyperglobulinemia.

CREST syndrome is a variant of diffuse scleroderma characterized by *C*alcinosis cutis, *R*aynaud's phenomenon, *E*sophageal dysmotility with dysphagia, *S*clerodactyly, and *Telangiectasia*. *Calcinosis cutis* is deposition of calcium in the skin producing hard cutaneous nodules. *Raynaud's phenomenon* is a series of finger discoloration after exposure to either temperature alternation or emotional disturbance. First, fingers become pale (white) due to small vessels vasoconstriction, then turn blue as the vessels dilate to keep blood flow, and finally turn red as blood flow returns (Fig. 9.1.1). *Sclerodactyly* means skin thickening of the fingers and toes that produces claw-hand deformity. *Telangiectasia* is dilatation of the small vessels over the skin and the mucus membranes ranging between 0.51 mm in diameter. They are commonly seen over the face and the neck as small red marks on the skin.

Morphea is a superficial localized form of scleroderma characterized by a plaque of thickened skin, often with an active, violaceous border with a yellow to white center. It is commonly seen in children, with an incidence of 1 per 100,000 individuals. *Generalized morphea* is a term used to describe morphea lesions covering >30% of the body surface. *Pansclerotic disabling morphea (Deep morphea)* is a term used to describe morphea that extends deep into the soft tissues with fixation to the underlying structures.

Nodular (keloid) scleroderma is a rare form of cutaneous scleroderma that can occur in association with diffuse scleroderma or morphea. It is seen as keloidal hyperpigmented papules that develop early in the course of the disease. An inflammatory infiltrate is present during the period of active fibrosis.

Linear scleroderma, also known as *(en coup de sabre)*, is a localized form of scleroderma seen as a linear, ivory-colored, deforming depression on the scalp and the forehead mimicking a blow of a sword, which is described as "coup de sabre" (Fig. 9.1.2). The lesion usually results in furrowing of the forehead causing significant facial asymmetry and cosmetic deformity. Linear scleroderma lesions can be seen following "*Blaschko's lines*" (Fig. 9.1.3). These lines determine

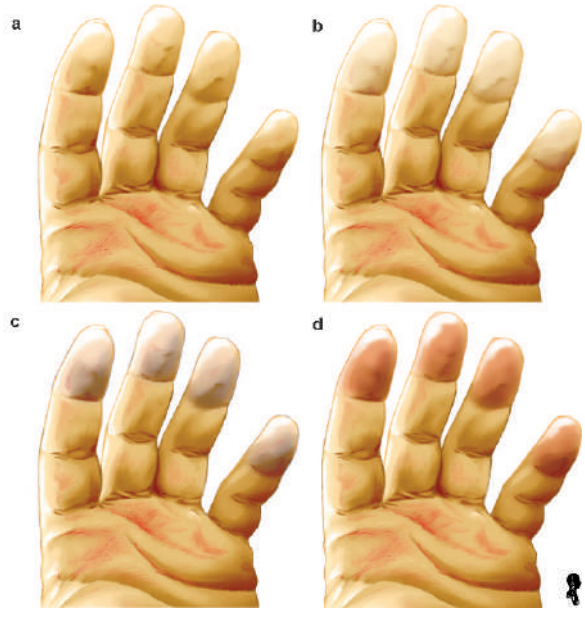

Fig. 9.1.1 An illustration demonstrates the finger discoloration stages of Raynaud's phenomenon: (**a**) normal fingers, (**b**) pale fingers, (**c**) bluish discoloration due to ischemia, and (**d**) reddish discoloration due to postischemic hyperemia

Fig. 9.1.2. An illustration demonstrates linear scleroderma affecting the left forehead

Fig. 9.1.3. An illustration demonstrates Blaschko lines over the right forehead. The same lines can be found on the left side

the distribution of many congenital and acquired skin diseases (e.g., epidermal nevi). Many authors believe that these lines represent the pattern of embryonic migration of skin cells.

Linear scleroderma is usually seen in children and in the young population, and it can affect the limbs, especially the lower limbs, resulting in unilateral, atrophic limb. Linear scleroderma is usually confused with *Parry-Romberg syndrome* when it extensively affects half of the face. Brain involvement in linear scleroderma usually presents in the form of epilepsy, with or without brain abnormalities.

Differential Diagnoses and Related Diseases

- *Hypothenar hammer syndrome:* hypothenar hammer syndrome (HHS) is a rare condition characterized by episodic digital ischemia as a result of occlusion of the distal ulnar artery at the level of the hamate bone, typically due to repetitive blunt trauma to the ulnar artery at the hypothenar eminence. The ulnar injury usually results from thrombosis or aneurysms from the repetitive trauma. The distal ulnar artery is most vulnerable to trauma at the level of the hook of the hamate, which works as an anvil against the dital ulnar artery as the patient uses his/her hypothenar eminence of the hand. The disease usually occurs in males who engage in activities that expose the hypothenar eminence to repetitive hand injuries. Workers using vibrating hand tools are commonly affected. Sportsmen who use their hands extensively in sports activities such as baseball, handball, karate, and weightlifting or dumbbell training are also affected. Patients usually present with palm pain, paraesthesia, and numbness with cold fingers and pallor, usually affecting the dominant hand. HHS can be mistaken for Raynaud's disease. Raynaud's disease is defined as episodic ischemia of the fingers and toes, clinically presenting as pallor (arterial vasospasm), cyanosis (deoxygenated static venous blood), and rubor (reactive hyperemia).
- *Eosinophilic fasciitis* (*Shulman's syndrome*) is a rare condition with scleroderma-like illness characterized clinically by inflammatory swelling and induration of the arms and legs. Patients with eosinophilic fascitis are usually females presenting with painful thickening and induration of the skin and subcutaneous tissues of the affected limb. The disease may affect the upper limbs, trunk, and lower limbs but spares the face. Raynaud's phenomenon is usually not present, and organs are not affected. The skin is typically thickened with orange-peel appearance. Bilateral symmetrical muscle weakness and stiffness of the joint may occur. Pathologically, there is inflammation and infiltration of the superficial muscle fasciae by lymphocytes, plasma cells, and occasionally eosinophils. Laboratory findings show high ESR, blood eosinophilia (characteristic), and hyperglobulinemia. Diagnosis is usually based on MRI and laboratory findings; however, definite diagnosis requires full-thickness skin-to-muscle biopsy.

How can you differentiate between hypothenar hammer syndrome and Raynaud's disease?

- HHS has a male predominance, while Raynaud's disease has a female predominance.
- HHS is an occupational disease, while Raynaud's disease is a primary disease or secondary to systemic disease.
- HHS has an asymmetric distribution (affects one hand), while Raynaud's disease is typically symmetrical, affecting the hands or toes.

9.1

Signs on Radiographs

- Resorption of the terminal phalanges (acro-osteolysis) of the hands and the distal portion of the radius and ulna are the most common radiological features of scleroderma (80%).
- Mandibular resorption resembling "Gorham syndrome osteolysis" may be seen.
- Soft-tissue calcinosis may be seen, especially in the digits (Figs. 9.1.4 and 9.1.5).
- Widening of the periodontal space on dental radiographs may be seen.
- Pulmonary fibrosis can be seen in advanced chronic stages of scleroderma.

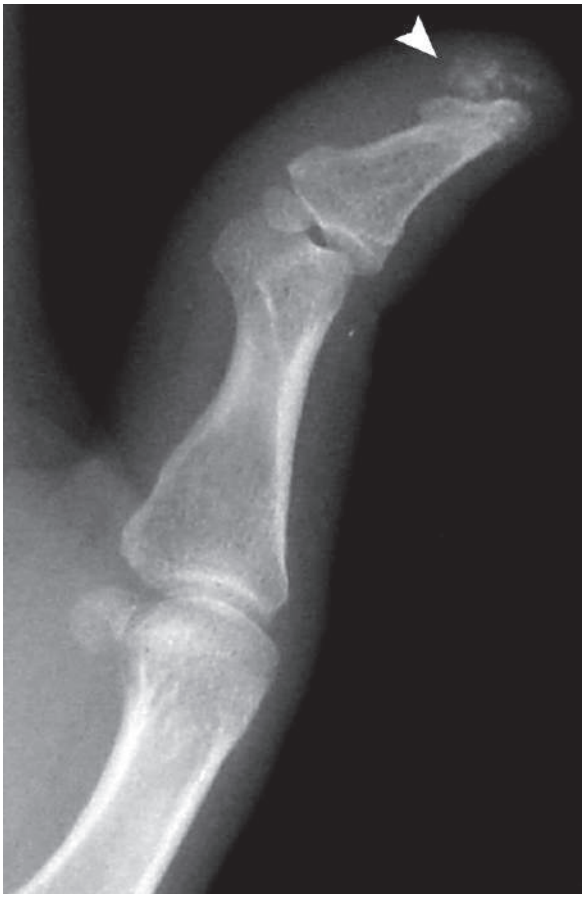

Fig. 9.1.4. Plain thumb radiograph of a patient with scleroderma shows fingertip calcinosis (*arrowhead*)

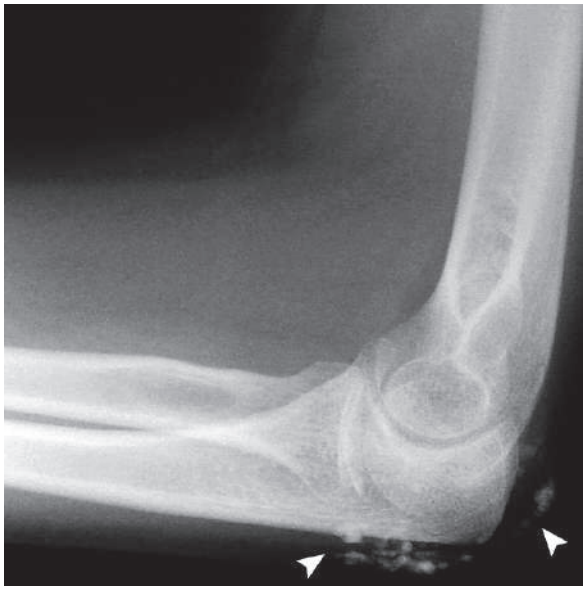

Fig. 9.1.5. Lateral plain elbow radiograph of a patient with scleroderma shows calcinosis around the elbow joint (*arrowheads*)

Signs on Barium Swallow

The esophagus in CREST syndrome shows weak peristalsis with no stripping waves (Fig. 9.1.6). The esophagus may show fine, wavy horizontal lines due to muscular contraction of the esophagus wall (*Feline esophagus*).

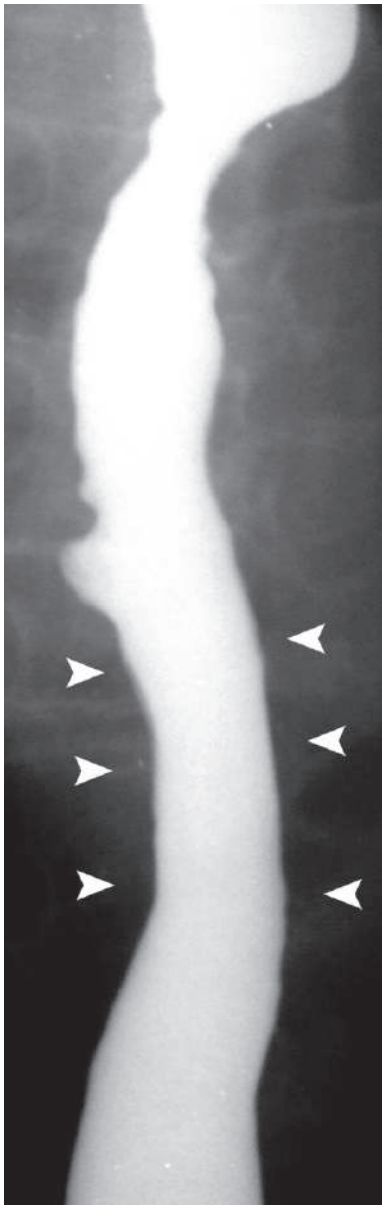

Fig. 9.1.6. Anteroposterior barium swallow radiograph of the esophagus in a patient with scleroderma shows poor esophageal motility (*arrowheads*)

Signs on MRI

- In *linear scleroderma*, there are intracranial parenchymal calcifications affecting mainly the thalami, and the basal ganglia ipsilateral to the skin lesion may be seen. Progressive multiple brain aneurysms can be seen in linear scleroderma.
- In *hypothenar hammer syndrome*, the axial wrist images will show hyperintense mass usually seen on T1W images located around the ulnar artery at the level of the hook of the hamate, representing hematoma or thrombus (Fig. 9.1.7).
- In *deep morphea*, there is T2 hyperintensity signal observed over the skin and subcutaneous tissue that may involve the muscles and the bone beneath. The bone shows bone marrow edema signal without bone erosions. Contrast enhancement of the affected tissues reflects ongoing inflammatory reaction. Enhancement around the tendons may be observed due to inflammation of the synovial sheath (synovitis).
- In *eosinophilic fasciitis*, there is increased thickening and T2 signal intensity of the superficial muscle fasciae with marked contrast enhancement after contrast injection (Fig. 9.1.8). Characteristically, there is little or no signal change within muscles and the pathological changes are confined only to the superficial muscle fasciae, and to a lesser degree to the deep muscle fasciae.

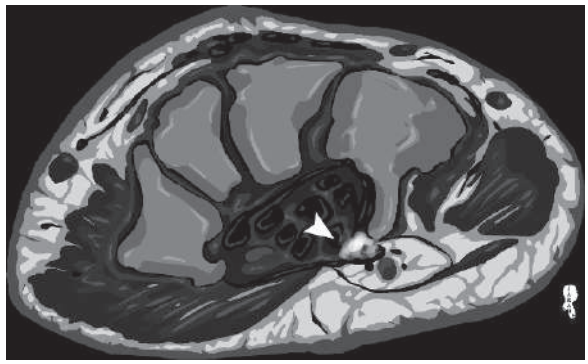

Fig. 9.1.7. Axial T2W wrist MR illustrations show high signal intensity at the tip of the hook of hamate within the Gyon's canal representing hematoma of the ulnar artery (*arrowhead*)

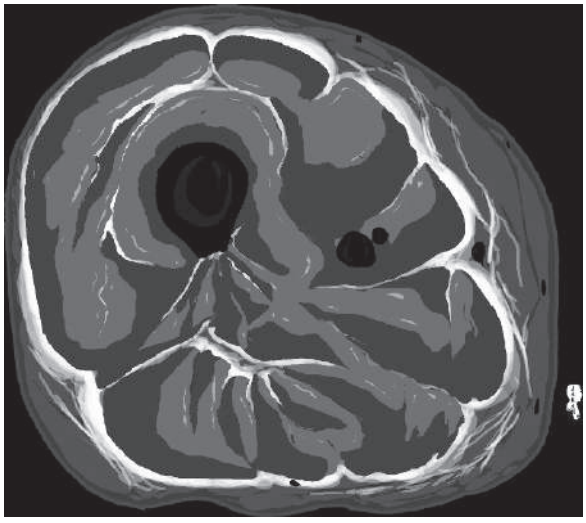

Fig. 9.1.8. Axial T1W postcontrast, fat-sat, thigh MR illustration demonstrates the typical findings in eosinophilic fasciitis. Notice the marked thickening and enhancement of the superficial and deep fascial planes with no signal intensity or contrast enhancement of the muscles of the subcutaneous tissues

For Further Reading

1. Ahathya RS et al Systemic sclerosis. Indian J Dent Res 2007; 18:27–30
2. Jacobson et al Superficial morphea. J Am Acad Dermatol 2003;49:323–5
3. Christen-Zaech et al Pedatric morphea (localized scleroderma): review of 136 patients. J Am Acad Dermatol 2008; 59:385–96
4. JM et al Nodular scleroderma. J Am Acad Dermatol 1995; 32:343–5
5. WD et al Nodular (keloidal) scleroderma. J Am Acad Dermatol 11:111–114
6. Soma et al Frontoparietal scleroderma (en coup de saber) following Blaschko's lines. J Am Acad Dermatol 1998;38: 366–8
7. Grosso et al Linear scleroderma associated with progressive brain atrophy. Brain Dev 200357–61
8. Robitschek et al Treatment of linear scleroderma "en coup de saber" with AlloDerm tissue matrix. Otolaryngol Head Neck Surg 2008138540–1
9. Bologina et al Lines of Blaschko. J Am Acad Dermatol 1994; 31:157–90
10. Genchellac et al Hypothenar hammer syndrome: gray-scale and color Doppler sonographic appearance. J lin ltrasound 2008; 362. doi 10.1002/jcu
11. Mueller et al Hypothenar hammer syndrome in sports. Knee Surg Sports Traumatol Arthroscopy 19964:167–70
12. Kreitner et al Hypothenar hammer syndrome caused by recreational sports activities and muscle anomaly in the wrist. Cardiovasc Intervent Radiol 199619:356–9
13. Abudakka et al Hypothenar hammer syndrome: rare or underdiagnosed? Eur J Vasc Endovasc Surg 32257–60
14. Horger et al MRI findings in deep and generalized morphea (localized scleroderma). AJR 2008;190:32–9
15. Baumann et al MRI for diagnosis and monitoring of patients with eosinophilic fasciitis. AJR 2005;184:169–74

9.2

Lipoid Proteinosis (Urbach-Weithe Disease)

Lipoid proteinosis (LP) is a rare, autosomal recessive disease characterized by infiltration of the skin, oral cavity, larynx, vocal cords, and internal organs by a hyaline material composed of carbohydrates, proteins, and lipids.

LP is caused by defective basement membrane collagen metabolism. The patient commonly presents with hoarseness of voice since infancy due to deposition of the hyaline material within the vocal cords. Beaded, whitish papules along the margins of the eyelids (*Blepharosis moniliformis*) are classical features of this disease (Fig. 9.2.1). Pock-like scars over the face and the body, waxy papules, less mobile tongue, and thickened oral mucosa with yellowish tinges are other common findings. Deposition of the hyaline material in the scalp can lead to patchy loss of hair (*alopecia areata*).

Hyaline deposition can be found in some cases in the trachea, stomach, esophagus, testes, pancreas, and vagina.

Diabetes mellitus, epilepsy, and calcified cerebral vessels can be seen associated with LP occasionally. Diagnosis can be confirmed by pathological skin biopsy. The hyaline material shows positive periodic-acid-Schiff (PAS) stain result. Differential diagnoses of LP in adults include amyloidosis, lipoidoses, and myxoedema.

Signs on Chest Radiographs

In severe cases, LP can present as a bilateral alveolar lung disease that mimics lung edema. This pattern is seen due to deposition of the hyaline material within the alveoli.

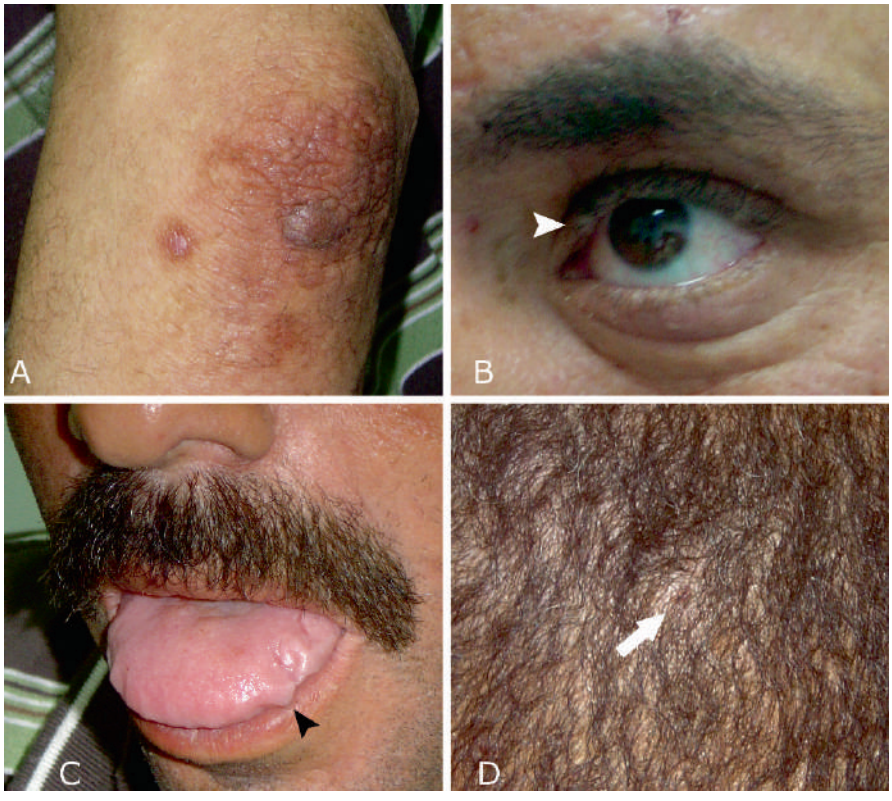

Fig. 9.2.1. Multiple images from a 28-year-old patient with lipoid proteinosis show the dermatological features of this disease. In (**a**), there are multiple psoriatic-like lesions over the elbow. In (**b**), a whitish papule (blepharosis moniliformis) along the margin of the upper eyelid can be seen (*white arrowhead*). In (**c**), the tongue is thickened and shows multiple nodules (*black arrowhead*). In (**d**), there is a focal area with reduced hair on the scalp (*arrow*). The patient has a history of hoarseness of voice since the age of 3 years

9.2

Signs on CT

- Thickening and infiltration of the vocal cords by a hypodense hyaline material can be observed (Figs. 9.2.2 and 9.2.3).
- Calcification within the cerebral hemispheres can be seen when calcified vessels are present.

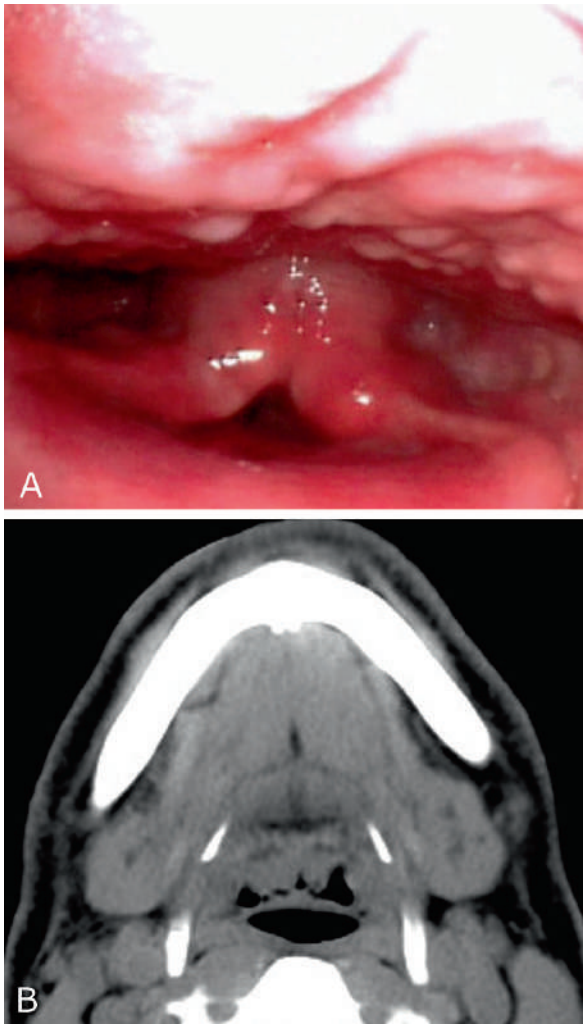

Fig. 9.2.2. Bronchoscopic image (**a**) correlated with axial CT image (**b**) of the hypopharynx shows multiple submucosal nodules. After biopsy these lesions, the results stated that these nodules are composed of hyaline lipoid material deposited within the submucosa. The nodules in (**b**) are almost completely replacing the valleculae (*arrowheads*)

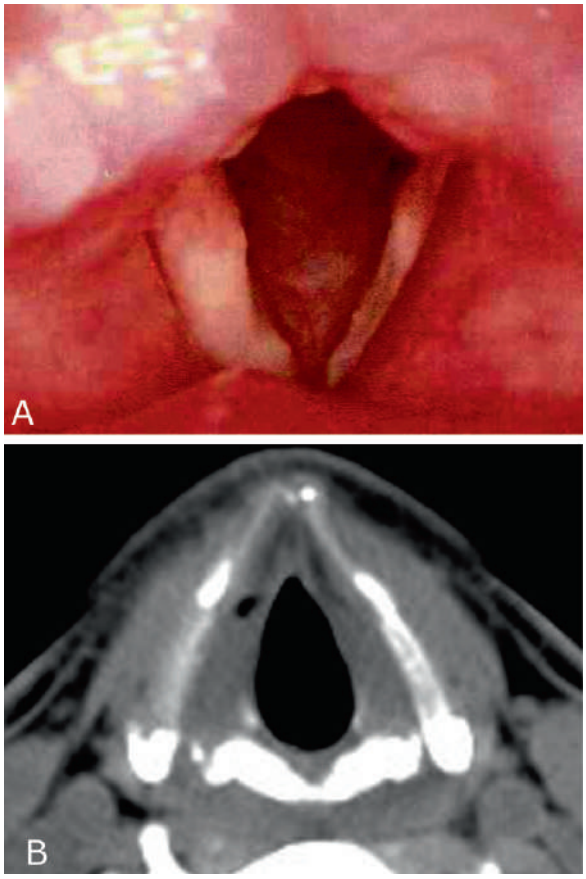

Fig. 9.2.3. Bronchoscopic image (**a**) correlated with axial CT image (**b**) of the vocal cords of the same patient shows thickening of both vocal cords, with the right one markedly thickened compared to the left one in (**a**). In (**b**), the CT image shows hypodense areas found in the anterior aspect of both vocal cords bilaterally involving the anterior commissure (*arrowheads*), with subtle left vocal cord thickening anteriorly

For Further Reading

1. Mukhija P et al Lipoid proteinosis. Ind J Dermatol. 2006; 51(1):51–2
2. Sen S et al Lipoid proteinosis. Ind J Dermatol. 2006; 51(1):49–50
3. Behera SK et al Lipoid proteinosis in two siblings. Ind J Dermatol. 2006;51(1):47–8
4. Simpson HE. Oral manifestations in lipoid proteinosis. Oral Surg. 1972;33(4):528–31
5. Savage MM et al Lipoid proteinosis of the larynx: a cause of voice change in the infant and young child. Int J Pediatr Otorhinolaryngol. 1988;15:33–8
6. Orton CI et al Lipoid proteinosis - The oro-facial manifestations. Br J Oral Surg. 1975;12:289–91
7. Mirancea N et al Vascular anomalies in lipoid proteinosis (hyalinosis cutis et mucosae): Basement membrane components and ultrastructure. J Dermatol Sci 2006;42:231–9

9.3 Dermatomyositis

Dermatomyositis (DM) is an inflammatory connective-tissue disorder characterized by inflammation of the muscles and skin. DM is closely related to another inflammatory muscle disease called "polymyositis" (PM).

DM is diagnosed by specific criteria that include:

- *Proximal symmetrical muscle weakness:* the typical clinical presentation is bilateral symmetrical muscle weakness of the limb-girdle muscles, often affecting the shoulders and anterior neck flexors. Progressive weakness is experienced over weeks to months. Patients often first note an inability to groom their hair or to rise from a sitting position. Proximal dysphagia may be seen if the cricopharyngeus muscle and muscles of the pharynx are involved. Respiratory muscles of the chest wall can be affected.
- *Muscle biopsy:* muscle biopsy classically shows muscle necrosis and inflammatory changes; however, muscle biopsy can be normal in 10–15% of cases.
- *Elevated muscle enzymes:* elevated muscle enzymes like creatine kinase (CK), serum transaminases, and lactic dehydrogenase (LDH) is a common finding in DM and PM. CK is a normal serum enzyme with three isoenzymes: CK-MM (found in skeletal muscles), CK-MB (found in cardiac muscles), and CK-BB (found in neural tissue). In PM and DM, CK-MM and CK-BB are often elevated. However, up to 40% of DM cases have normal CK levels. CK is not so specific to muscular diseases, as it can be elevated in metabolic and neurological diseases as well.
- *Specific dermatological lesions:* two cutaneous lesions are very specific for DM, among other dermatological nonspecific manifestations. The first lesion is *Gottron's sign* (80% of cases), which is characterized by erythematous papules and plaques that are found over bony prominences, particularly the metacarpal-phalangeal and proximal and distal interphalangeal joints (Fig. 9.3.1). They can also be found over the elbows and knees. The second lesion is *heliotrope rash* (60% of cases), which is composed of violaceous to erythematous hue rash with or without edema located in the periorbital region (Fig. 9.3.2).

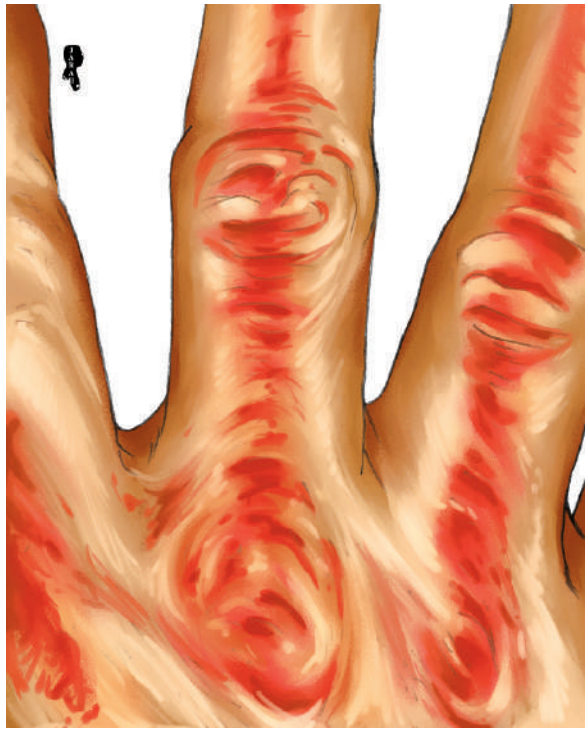

Fig. 9.3.1. An illustration demonstrates Gottron's signs

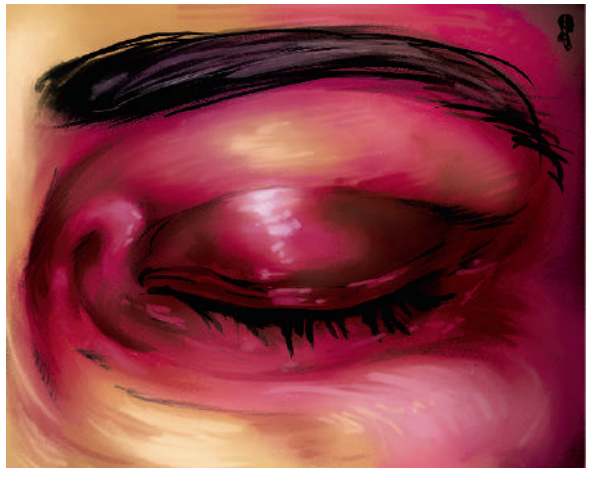

Fig. 9.3.2. An illustration demonstrates heliotrope rash

Photosensitivity occurs in 75% of patients with DM. Some patients with DM may develop poikiloderma of Civatte with Gottron's papules. *Poikiloderma of Civatte* is defined as a skin area with extra-pigmentation demonstrating a variety of shades and associated with widened capillaries (telangiectasia).

- *Exclusion of other disorders causing a myopathy:* like endocrinopathies, neurological diseases, and muscular dystrophies.

9.3

DM can be precipitated by viral infections (e.g., retrovirus), or parasitic infections (e.g., toxoplasmosis). DM can also be associated with autoimmune disorders (e.g., scleroderma) and tumors. Arthlargia, Raynaud's phenomenon, and polyarthritis are seen with DM overlapped with autoimmune diseases. Cardiac symptoms are uncommonly seen in DM. When the heart is affected, atrioventricular (AV) conduction disturbance, arrhythmias, and mitral valve prolapse are commonly seen.

DM can be classified into four groups:
Group 1: pure PM.
Group 2: PM with cutaneous lesions (DM).
Group 3: DM with autoimmune disease.
Group 4: DM with malignant neoplasm.

DM has a juvenile form that affects young adults <12 years old. It is often associated with high serum levels of Coxsackie-virus B antibody titers. Patients show same signs and clinical manifestations as the adult form. Esophageal dysmotility occurs in 50% of cases.

Signs on Radiographs

- DM patients show soft tissue calcifications in up to 40% chronic cases. The calcifications can be superficial or deep, and often located mainly within the girdle muscle areas. The calcifications are described as linear, reticular, or calcareal (Fig. 9.3.3).
- Pulmonary fibrosis is seen in advanced stages of the disease.

Signs on MRI

- In the early stages of PM, there is tissue edema and high signal intensity of the muscles on T2W images.
- In chronic cases, the muscles are replaced by fat. There is high T1 signal intensity within the muscles due to fat replacement of the muscular tissue, with reduced muscle size due to chronic muscle wasting and inflammation.

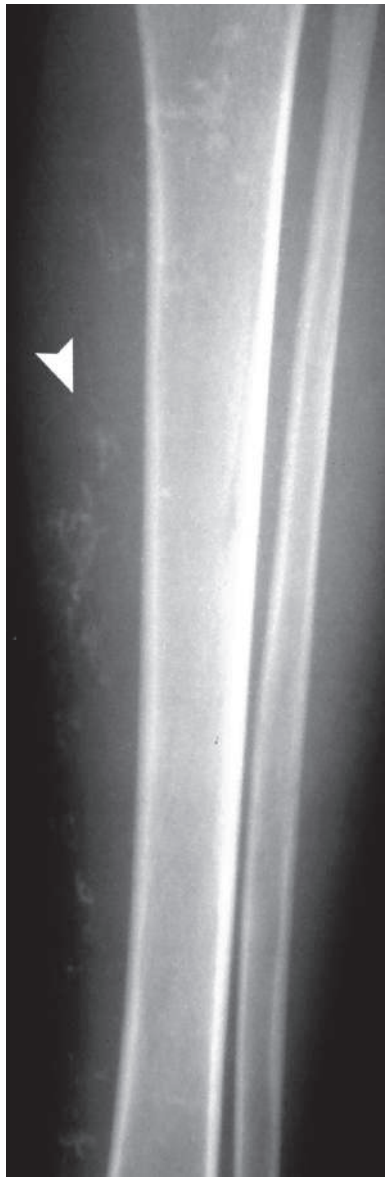

Fig. 9.3.3. Anteroposterior plain radiograph of the left leg shows multiple fine soft tissue calcifications in a patient with dermatomyositis (*arrowhead*)

What is the difference between calcification and ossification?

- *Calcification* is the presence of an area of calcium deposition within soft tissue that does not form a trabecular or cortical structure (no real bone formation within the soft tissue, only small area of calcium deposition).
- *Ossification* is the presence of an area of calcium deposition within the soft tissue that forms a trabecular or cortical structure (a real bone formation within the soft tissue).

What are the types of calcifications and ossifications?

- Calcification can be divided into *metastatic calcification* (calcium and phosphate metabolism disturbance that leads to ectopic calcification in normal tissues), *dystrophic calcification* (deposition of calcium in damaged tissues while the serum calcium level is normal), and *calcinosis* (deposition of calcium in soft tissue in the presence of normal calcium level). Dystrophic calcification is seen usually in posttrauma or after neoplastic therapy. Calcinosis is typically seen in rheumatic diseases and DM.
- Ossification is typically seen in cases like posttraumatic ligamentous ossification (e.g., *Pellegrini-Stedia disease*), neurogenic heterotopic ossification (soft tissue ossification after long period of denervation), *myositis Ossificans traumatica* (*Sterner's tumor*), and *fibrodysplasia ossificans progressiva* (*Munchmeyer disease*). Pellegrini-Stedia disease is characterized by ossification of the medial collateral ligament of the knee, commonly after trauma. Myositis ossificans is a rare condition characterized by progressive skeletal muscles ossification, usually after a major trauma. Fibrous dysplasia ossificans is a rare disease characterized by disabling ossification of muscles, tendons, ligaments, and fascial planes (the normal soft tissues are transforming into bones).

For Further Reading

1. Marfatia YS et al Dermatomyositis in a human immunodeficiency virus infected person. Indian J Dermatol Venerol Leprol. 2008;74:241–43
2. Agarwal V et al Calcinosis in juvenile dermatomyositis. Radiology. 2007;242:307–11
3. Lee LA et al Lipodystrophy and metabolic abnormalities in a case of adult dermatomyositis. J Am Acad Dermatol. 2007;57:S85–7
4. Magill HL et al Duodenal perforation in childhood dermatomyositis. Pediatr Radiol. 1984;14:28–30
5. Stiglbauer R et al Polymyositis: MRI-appearance at 1.5 T and correlation to clinical findings. Clin Radiol. 1993;48:244–48

9.4

Ochronosis (Alkaptonuria)

Ochronosis, also known as alkaptonuria, is a very rare autosomal recessive metabolic disease characterized by accumulation of homogentisic acid (HGA) in body tissues due to an inherited deficiency of the enzyme HGA oxidase. HGA is a main product of the amino acids tyrosine and phenylalanine. Acquired form of ochronosis can be seen after exposure to some chemicals like hydroquinone.

Ochronosis has an incidence of 1:1,000,000 in the general population. The urine of patients with ochronosis turns dark when it is exposed to air or alkaline environment because of HGA polymerization after its exposure to oxygen. The name "alkaptonuria" comes from Arabic and Greek words referring to the relationship between oxygen and urine kept standing.

Although HGA deposition may occur in any body tissue, the disease severity is mainly related to the musculoskeletal system. HGA accumulates particularly in the tendon ligament tissues and cartilage-rich joints. The tissues acquire black color grossly due to the HGA pigment.

Patients typically present in the third decade of life complaining of back pain and stiffness. Skin and soft tissue lesions are seen in the fourth and fifth decades. HGA acts as a chemical irritant that leads to joint degeneration and inflammation. Patients develop osteoarthritis arthropathy in almost all large joints, but the main severity is classically observed in the vertebral column. The typical feature of this disease in the vertebral column involves intervertebral disc calcification.

Bluish-brownish discoloration of the skin is seen due to deposition of HGA in the subcutaneous tissues, and it is a pathognomonic finding of this disease. The skin pigment is observed in cartilage-rich tissue as the ear (70%) and nose (Fig. 9.4.1). The bluish pigment can also be seen in the cornea and the sclera (Fig. 9.4.1). It may also be excreted in the sweat, causing changes of color in clothing.

Rarely, cardiac involvement of ochronosis may be seen in advanced stages. Mitral and aortic valve stenoses are the main pathologic complications seen. Renal function can deteriorate when the pigment accumulates in the prostate. Prostatic calcification causes obstructive renal uropathy and hydronephrosis.

Signs on Radiographs

- Typically, the intervertebral discs are calcified in ochronosis, with severe intervertebral disc narrowing (Fig. 9.4.2). The disease affects the lumbar region first, and then progresses to the thoracic and the cervical vertebrae.
- Osteoarthritic changes of the large joints with sclerosis and osteophytes formation.
- Progressive formation of marginal intervertebral bridges and obliteration of disc spaces resulting in "pseudo-block vertebrae."

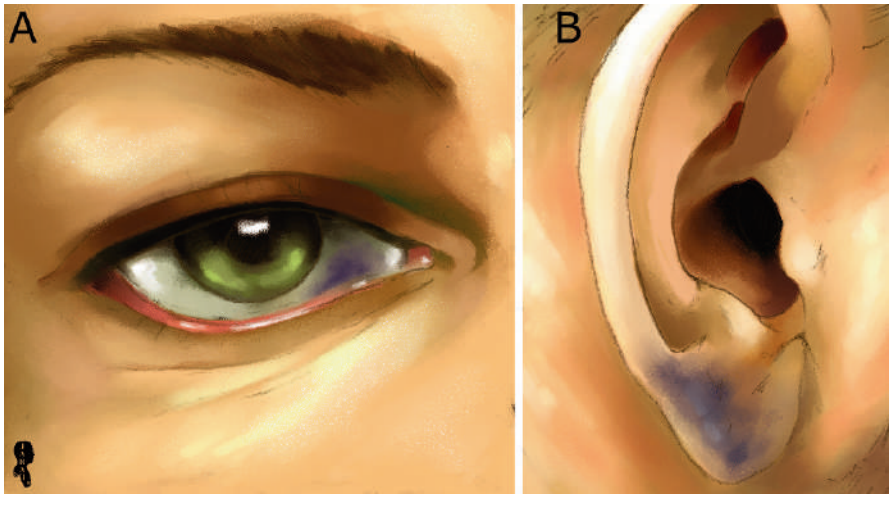

Fig. 9.4.1. Two illustrations show bluish discoloration of the sclera (**a**) and the earlobe (**b**) in a patient with ochronosis

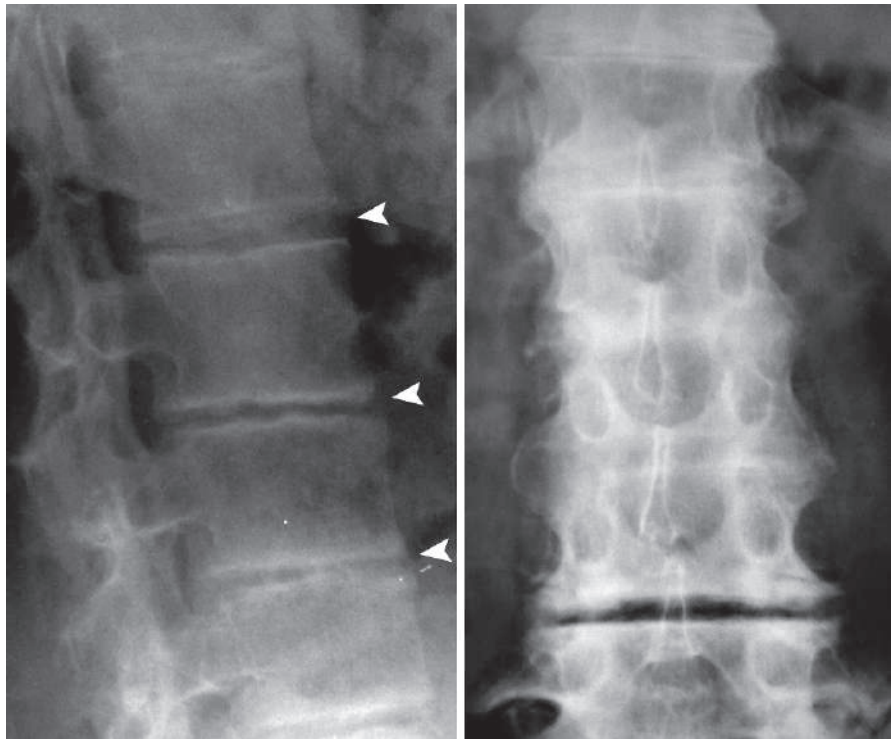

Fig. 9.4.2. Anteroposterior and lateral plain radiograph of the lower thoracic vertebrae in a patient with ochronosis shows severe intervertebral disc space narrowing (*arrowheads*)

The main differential diagnosis of ochronotic changes of the vertebral column is ankylosing spondylitis. How can you differentiate between the two diseases?

- Ankylosing spondylitis affects the sacroiliac joint in a bilateral symmetrical fashion, while sacroiliac joint affection is not necessarily observed in ochronosis.
- Ankylosing spondylitis shows syndosmophytes, bamboo spine appearance on radiographs, and positive HLA-B 27. All the past features are not part of ochronosis.
- Bluish skin pigmentation and calcification of the intervertebral discs are not features of ankylosing spondylitis.

For Further Reading

1. Çapkin E et al Ochronosis in differential diagnosis of patients with chronic back ache: a review of the literature. Rheumatol Int. 2007;28:61–4
2. Demir S. Alkaptonuric ochronosis: a case with multiple joint replacement arthropathies. Clin Rheumatol. 2003;22: 437–39
3. Lagier R et al Hip arthropathy in ochronosis: anatomical and radiological study. Skeletal Radiol. 1980;5:91–8
4. Güar D et al Ochronosis and lumbar disc. Acta Neurochir (Wien). 2006;148:891–94
5. Şahin G et al A case of ochronosis: upper extremity involvement. Rheumatol Int. 2001;21:78–80
6. Bal S et al Ochronosis with cardiovascular involvement: a case report. Rheumatol Int. 2008;28:479–82

Chapter 10

Diabetology

CONTENTS

J. A. Al-Tubaikh: *Internal Medicine* – An Illustrated Radiological Guide
DOI: 10.1007/978-3-642-03709-2_10, © Springer-Verlag Berlin Heidelberg 2010

10.1 Diabetic Hand and Diabetic Foot

Diabetes mellitus (DM) is a chronic metabolic disease that arises due to insulin deficiency (type 1 DM), or insulin receptor insensitivity (type 2 DM). Type 2 DM is more common than type 1.

Diabetic complications arise due to cellular ischemia, angiopathy, peripheral neuropathy, osteopathy, infections, skin changes, and atherosclerosis. The hands and feet are uncommonly affected in diabetes, but when they are affected, it may be severe enough to cost the patient loss of a limb.

Radiology offers great tools for early detection of diabetic complications by ultrasound and MRI. For diabetic foot screening, a Doppler scan is performed to detect arterial flow anomalies. If the Doppler scan shows abnormalities in the vessels, MRI can be done to detect hidden signs of diabetic foot complications. Adults with long-term DM should be annually examined for lower limb vascular abnormalities.

Diabetic Angiopathy

Diabetic angiopathy is divided into two types: microangiopathy and macroangiopathy. Microangiopathy arises due to chronic hyperglycemia that impairs the walls of the microvessels, causing leakage of exudates and blood. Later, these exudates may lead to obstruction of the microvessels causing ischemia. This type is typically seen in diabetic retinopathy and diabetic nephropathy. Macroangiopathy, on the other hand, damages the arterial vessels due to atherosclerosis affecting the coronary, cerebral, and lower limb vessels. Arteriosclerosis occurs 10 years earlier in diabetics than in normal people.

Chronic limb ischemia and compromised vascular supply can lead to tissue necrosis and dry gangrene. This is often complicated by bacterial infection that may cause wet gangrene; this scenario is often seen in the feet. Amputation is the tragic end of severe limb osteomyelitis, extensive lower limb calcifications, and uncontrolled diabetes that suppresses the immune system. Within 2 years of amputation of one leg, the other leg has a 50% chance of complications that might lead to a 50% chance of contralateral amputation.

Gangrene can be divided into dry, wet, and infected. *Dry gangrene* arises due to an occluded artery with a patent vein; with tissue liquefaction occurs at a very slow rate. It is seen in senile gangrene (due to atherosclerosis and vascular stasis) and Buerger's disease (thromboangiitis Obliterance). Senile gangrene is seen in 50% of elderly patients wearing tight shoes, and commonly affects the big toe. *Wet gangrene* arises due to an occluded artery and vein, with rapid tissue liquefaction and sever toxemia. This type is classically seen in DM, crush injuries (accidents), and bedsores. *Infected gangrene* arises due to bacterial infection, and is typically seen in lung abscess, necrotizing fasciitis, synergistic gangrene, and gas gangrene (due to muscular lesion with anerobic fermentation of the tissues with *Clostridia defficile*).

As previously mentioned, patients with gangrene are treated by amputation of the gangrenous part of the lower extremity, which can be above or below the knee, depending on the extension of the compromised vascular supply. The amputee may develop stump pain after surgery, which can be attributed to stump infection, inflammation, impaired vasculature, or development of neuromas. A *neuroma* is a focal, nodular, noncapsulated soft-tissue mass that forms at the distal segment of peripheral nerves after surgery or traumatic avulsion injury. Schwann cells regenerate the peripheral nervous system axons and myelin sheath after trauma. In an amputated limb, regeneration of the nerve axon is unstoppable, because there is no distal end pathway for the regenerated nerve axon to fuse with, resulting in aggregation of the Schwann cells at the stump end, forming a mass of nerve tissue. Postamputation neuromas are usually multiple, and may appear 1 month after amputation. Patients typically present with stump pain, usually in the absence of inflammation or stump infection.

Signs on Radiographs

Calcification of pedal vessels occurs in 24% of diabetic patients, and it is seen radiologically as classic "tramline "or "pipestem "calcification (Fig. 10.1.1).

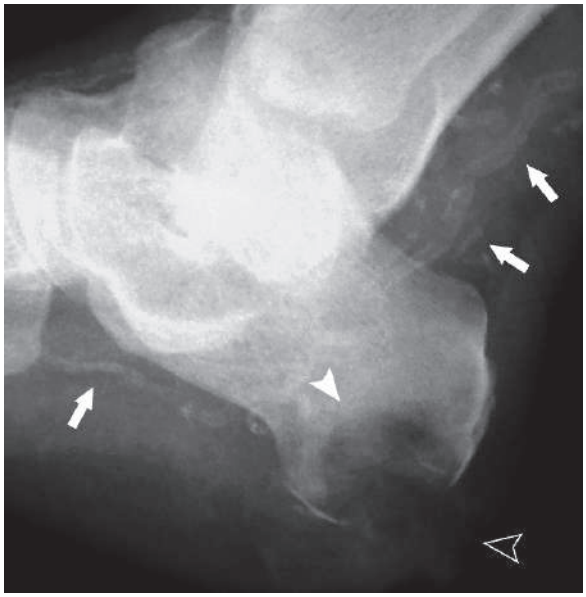

Fig. 10.1.1. A lateral plain radiograph of a patient with severe diabetic foot shows calcaneal ulcer (*hollow arrowhead*), osteomyelitis causing bone resorption and necrosis (*solid arrowhead*), and calcified arteries due to macroangiopathy (*arrows*)

Signs on MRI

Postamputation neuromas are detected as ovoid, bulbous, or rounded soft-tissue mass expansions at the end of a proximally transected nerve (e.g., peroneal nerve in above-knee amputation) that classically measure 1–2 cm in diameter. The mass shows low T1 and moderately high T2 signal intensity, with a characteristic dark rim seen on both T1W and T2W images due to focal fibrous tissue condensation around the neuroma.

Diabetic Peripheral Neuropathy, Osteopathy, and Infections

Diabetic peripheral neuropathy often affects both hands and feet in a bilateral symmetrical fashion (*glove and stocking phenomenon*). Loss of the deep knee tendon reflex is the earliest sign of diabetic neuropathy, even before any sensory or motor disturbances manifest. Diabetic neuropathy is attributed to metabolic abnormalities affecting Schwann cells, the myelin-forming cells of the peripheral nervous system.

In the neuropathic diabetic foot, sympathetic denervation is the main pathological injury. Somatic and autonomic denervation causes numbness and loss of heat and pain sensation, along with reduction in the sensation of touch and vibration. Sympathetic denervation causes arteriovenous shunts within hands and feet, causing abnormal increase in the venous flow within the limbs. Moreover, the intracutaneous pressure causes the development of calcification within the medial layer of the arterial vascular wall (*Monckeberg's sclerosis*).

There are two types of neuroarthropathies in DM: atrophic and hypertrophic (*Charcot's joint*). Atrophic neuroarthropathy is characterized by osteoporosis, bone resorption, and dislocation. In contrast, Charcot's joint is characterized by the 5Ds: *d*istention, *d*islocation, *d*isorganization, *d*ebris, and increased bone *d*ensity. In the absence of diabetes, atrophic neuroarthropathy is commonly caused by syrinx in the cervical spine, while Charcot's joint is commonly caused by neurosyphilis of the posterior columns of the spinal cord (*tabes dorsalis*). A syrinx is also the commonest cause of Charcot's joint of the shoulder.

Diabetic peripheral neuropathy affects 10–15% of patients, and it can be diffuse or focal. The diffuse form presents in the form of bilateral, symmetrical denervation and sensory deficits of the hands and feet (glove and stocking phenomenon). In contrast, the focal form presents in the form of "mononeuritis," commonly affecting the cranial nerves CN III, CN IV, CN VI, and CN VII. Involvement of both sympathetic and sensory fibers leads to mechanical overuse, loss of the protective joint pain, proprioceptive sensation, and active hyperemia due to loss of vasoconstrictive neural impulses, which all result in atrophic neuroarthropathy. In contrast, sensory fiber denervation in the absence of sympathetic fiber involvement results in the development of Charcot's joint. The atrophic joint tends to involve the forefoot, while Charcot's joint tends to affect the mid- or hindfoot.

Diabetic lumbosacral radiculoplexus neuropathy (DLRPN), also known as *Burns-Garland syndrome*, is an uncommon condition, characterized by asymmetric lower extremity pain, weakness, and muscle atrophy commonly affecting the thigh muscles. The mechanism of injury is thought to be a result of microvasculitis and resultant ischemic injury to the sacral plexus and/or peripheral nerves. Patients with DLRPN are commonly between 46 and 71 years of age, often presenting with acute or subacute onset of severe asymmetric lower limb pain and paresthesia involving the

10.1

anterolateral thigh region. The pain is described as aching and burning, and tends to be worse at night or in contact with cloths or bed sheets (contact allodynia). DLRPN pain is usually followed by limb weakness, evolving over weeks or months, and commonly affects the quadriceps and iliopsoas muscles. Wasting of the quadriceps muscle plus absence or reduction in the knee jerk reflex are classic features. DLRPN is commonly preceded by unintentional weight loss. Laboratory findings in DLRPN include high erythrocytes sedimentation rate, occasional positive rheumatoid factor (RF) and antinuclear antibody (ANA), and elevated cerebrospinal fluid protein content.

Osteomyelitis occurs in up to 90% of cases in the diabetic foot, due to neurotropic pedal ulcers. Diabetic ulcers tend to occur at the sites of pressure over bony or joint protuberance (e.g., metatarsal heads or the calcaneus).

The diabetic foot can be rarely associated with tarsal tunnel syndrome. *Tarsal tunnel syndrome* is a condition characterized by entrapment of the posterior tibial nerve as it passes beneath the flexor retinaculum. The condition is analogous to carpal tunnel syndrome in the wrists. Patients often present with a burning sensation and paresthesia in the toes, sole of the foot, or medial heel, aggrevated by weight bearing.

Uncommonly, Freiberg's disease may arise in patients with diabetic foot. *Freiberg's disease* is a disease characterized by infarction of the metatarsal heads. The disease typically develops 3–4 times more frequently in women than men, during late childhood or adolescence. Patients present clinically in the acute phase with local foot pain with tenderness, confined to the area of the metatarsal heads. In the chronic phase, which is characterized by osteonecrosis and repair, patients are typically asymptomatic.

Signs on Plain Radiographs

- Charcot's joint is destruction of the affected with sclerosis (increased bone density), osteophytes (debris), dislocation, and destruction (Fig. 10.1.2).
- Calcified vessels may be seen as radio-opaque tubular structures.
- An atropic joint often shows osteoporosis with resorption of the metatarsal distal ends resulting in "pencil and cup" or "sucked candy stick" deformities, similar to those seen in leprosy.
- Osteomyelitis is seen as cortical bone destruction with a moth-eaten appearance of the affected bone (Figs. 10.1.1 and 10.1.3).
- *Lisfranc's fracture* is a clinical condition where the entire forefoot is displaced laterally. Lisfranc's fracture is diagnosed radiographically when the second metatarsal bone is displaced laterally >2 mm from its articulation with the intermediate cuneiform bone (Fig. 10.1.4).
- Charcot's joint of the hip can results in osteolysis of the acetabulum with loss of its boarders (*wandering acetabulum*), and hypertrophic sclerosis of the femoral head resulting in a "drumstick" appearance.
- The talo-navicular joint is a preferred site for Charcot's joint in the hindfoot.
- *Freiberg's infarction* is detected as subtle flattening and sclerosis of the metatarsal head, with widening of the metatarsophalangeal joint (Fig. 10.1.5). The widening of the metatarsophalangeal joint is attributed to the subchondral trabeculation, with collapse of the articular surface (subchondral fractures). The most common metatarsal head involved is the second metatarsal head (sometimes referred to as *second ray syndrome*).

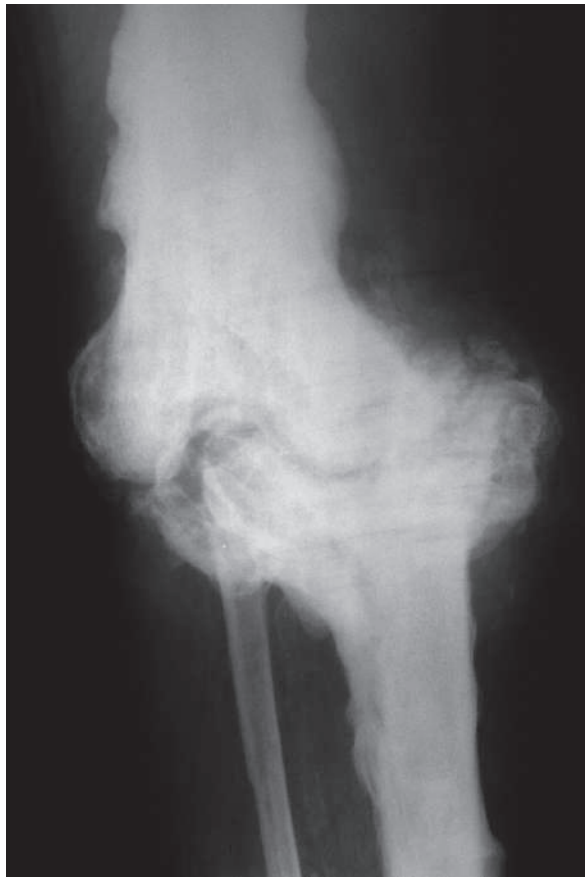

Fig. 10.1.2. Anteroposterior plain knee radiograph of a patient with sever Charcot's knee joint demonstrates disorganization, debris, and increased bone density

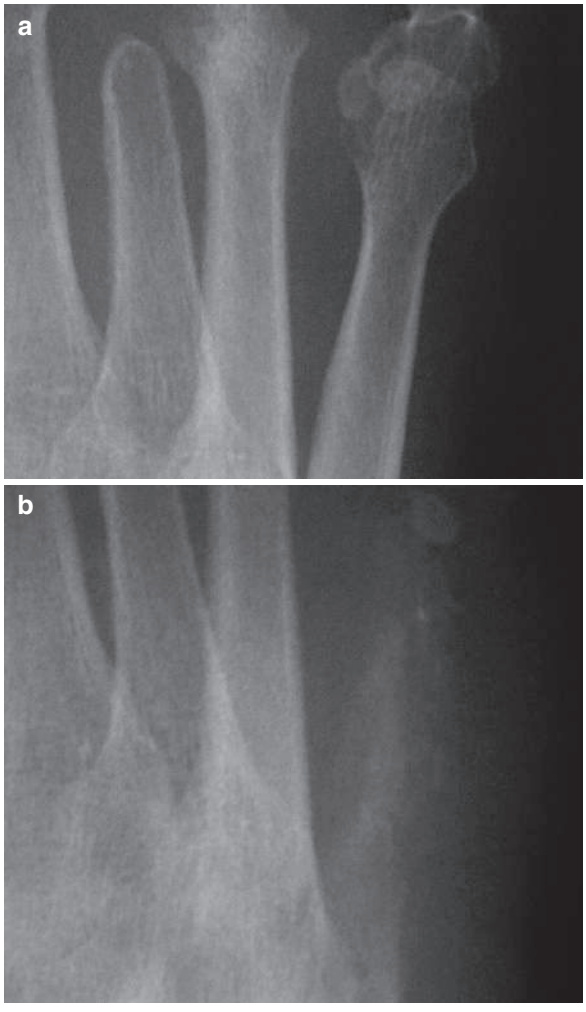

Fig. 10.1.3. Plain foot radiographs of a patient with diabetic foot show acute osteomyelitis. In (**a**), the patient was investigated for a pain in the fifth toe, which shows mild osteoporosis compared to the rest of the metatarsals (note the third toe amputation). After 3 months, the patient showed moth-eaten osteomyelitis bone destruction of the fifth metatarsal bone, with complete cortical destruction

Signs on MRI

- In DLRPN, the scan show enhancement of the lumbosacral nerve roots and plexus after contrast injection.
- In *Freiberg's infarction*, the metatarsal head shows low T1 signal intensity, high T2 signal intensity, with contrast enhancement (Fig. 10.1.5).

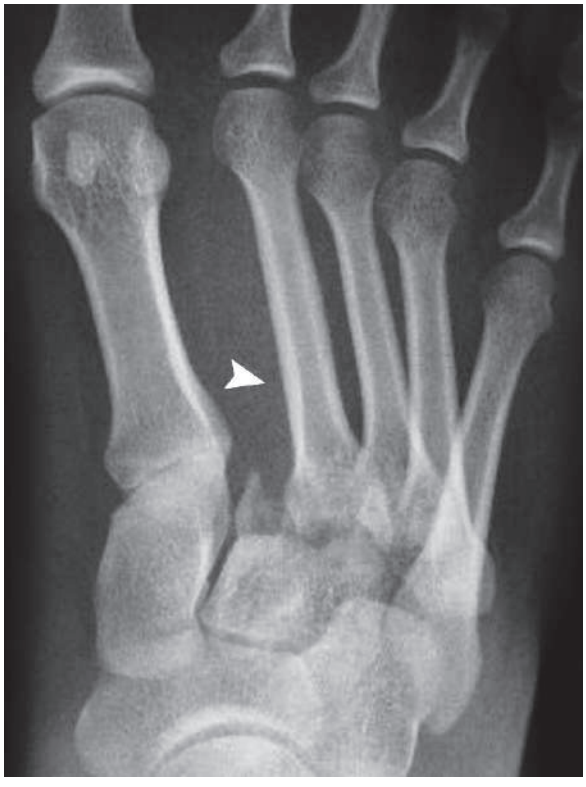

Fig. 10.1.4. Plain radiograph of the forefoot show Lisfranc's fracture, with lateral displacement of the metatarsals (*arrowhead*)

Diabetic Myonecrosis

Diabetic myonecrosis is a rare complication of diabetes, characterized by muscle infarction. Most patient affected with diabetic myonecrosis are patients with type 1 DM (74%), type 2 DM (26%), or patients with prolonged poorly controlled diabetes. Diabetic myonecrosis occurs in association with diabetic retinopathy (60%), nephropathy (80%), or neuropathy (64%). It almost always occurs in the lower extremities, and often affects the quadriceps muscles.

Patients with diabetic myonecrosis commonly present with a painful limb, swelling, and resting pain that is aggravated by walking. If one limb is affected by diabetic myonecrosis, the contralateral limb may be involved up to 2 years after the initial manifestation.

The main differential diagnosis of diabetic myonecrosis includes deep venous thrombosis (DVT) and pyomyositis.

10.1

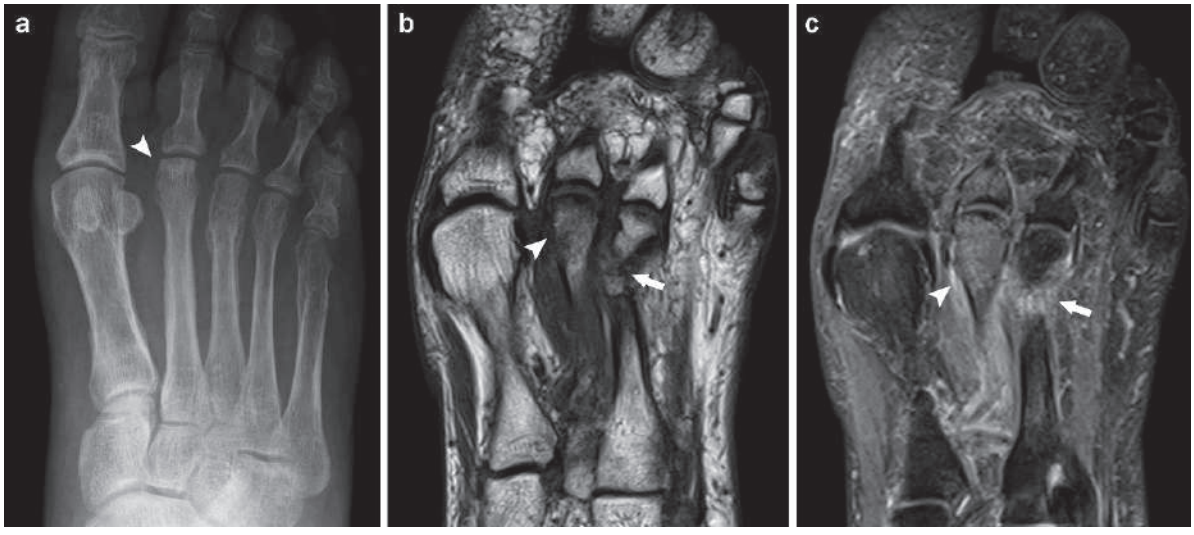

Fig. 10.1.5. Plain foot radiograph (**a**), T1W (**b**), and Sagittal short tau inversion recovery (STIR) (c) foot MRI of a patient show the signs of Freiberg's infarction. In (**a**), there is mild flattening and sclerosis of the second metatarsal head (*arrowhead*). Later, the patient underwent a foot MRI that confirmed bone infarction of the second metatarsal head seen as low T1 signal intensity in (**b**) and high signal intensity in (**c**). The MRI shows also fracture of the third metatarsal neck (*arrows*), which was not well appreciated in the plain radiograph (**a**)

DVT can be ruled out by Doppler sonography. Pyomyositis is a severe muscle infection with formation of an intramuscular abscess. In 90% of cases, it is caused by *Staphylococcus*. In contrast, diabetic myonecrosis does not show positive culture of *Staphylococcus*, because it is mostly caused by ischemia and infarction rather than infection.

Signs on MRI

The affected muscle shows extensive edema and swelling, with high signal intensity on T2W images involving the muscle and the subcutaneous tissues.

Diabetic Skin Changes and Infections

Diabetic hand lesions are not as common as diabetic foot lesions, perhaps due to the stress load on the feet compared to the hands. The main lesions of the hands in diabetes are related to dermatological diseases rather than neuro- osteopathic diseases such as those of the feet.

Diabetic dermopathy is characterized by the formation of multiple skin thickening on the back of the fingers (finger pebbles), scleroderma-like skin and stiff joints of the fingers and dorsum of the hand, and brown atrophic macules over the shin. *Acanthosis nigricans* is hyperpigmentation and velvety brown thickening of the major skin flexures, which is often seen with type 2 DM and obese patients.

Diabetic hand syndrome refers to a condition of neuropathy denervation of the hand. It is characterized by intrinsic wasting of the hand muscles, atrophy of the palmar tissues, with flexion contractures of the fingers that may mimic Dupuytren's contracture. Patients with diabetic hand syndrome often complain of *carpal tunnel syndrome*, with paresthesia in the palmar distribution of the median nerve (the first three fingers), and positive *Tinel's sign* (pain and paresthesia initiated in the palmar sensory distribution of the median nerve by tapping over the palmar aspect of the wrist). Moreover, sever neuropathic denervation may lead to (Sudeck's atrophy) *(shoulder-hand disease)*. Sudek's atrophy is a disease characterized by osteoporosis and swelling in one limb, especially the ankles, wrists, and elbows, after a minor trauma. It results from abnormal sympathetic innervations and secondary vascular changes after minor trauma, and typically affects the distal part of a limb below the trauma.

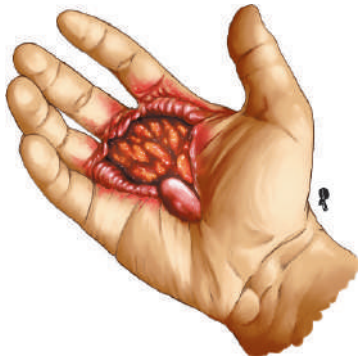

Fig. 10.1.6. An illustration demonstrates severe synergistic gangrene of tropical diabetic hand syndrome

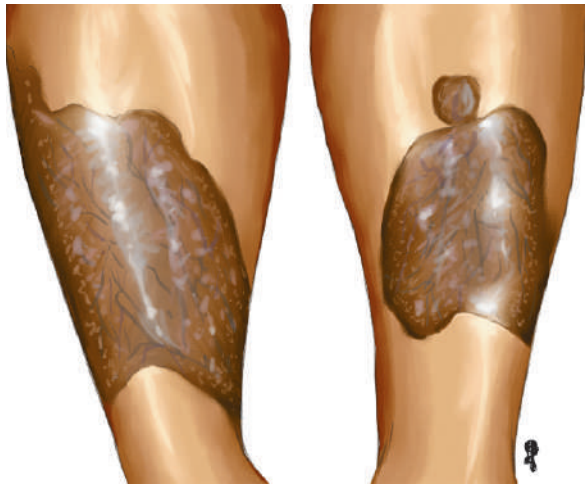

Fig. 10.1.7. An illustration demonstrates necrobiosis lipoidica diabeticorum lesions on both shins

Tropical diabetic hand syndrome, a terminology used to describe a specific infection of the hands in diabetics, usually occurs in tropical areas, and is characterized by progressive synergistic gangrene (*Meleney's gangrene*) of the hand following minor trauma. The cause of this syndrome is a progressively severe form of cellulitis caused by multibacterial infection, usually after a history of minor trauma or a scratch (Fig. 10.1.6).

Necrobiosis lipoidica diabeticorum (NLD) is a rare, degenerative, granulomatous skin disease that often affects the lower extremities in diabetic patients (0.3% of diabetics). Lesions are red papules or oval plaques that grow peripherally and become atrophic and yellowish at the center, with elevated and erythematous edges (Fig. 10.1.7). With time, these lesions become more brownish-yellow, telangiectatic, and porcelain-like. In most cases they are bilateral. Ulceration, the most common complication of NLD (35%), usually arises after a minor trauma. Lesions in NLD are granulomatous, mainly affecting the subcutaneous tissues and the dermis, and the epidermis is often normal or atrophic. NLD is classically found in young Caucasian diabetic patients, with female predominance (80%); however, it may occur also with sarcoidosis, rheumatoid arthritis, and inflammatory bowel disease.

When normal skin is stroked with a dull object, it rises and swells to assume the shape of the stroke, due edema and local erythema. In rare situations, exaggeration of this response may be seen in diabetic patients, a condition known as *dermatographism (mechanical urticaria)*. Skin stroke erythema in normal skin develops and subsides in less than 5–10 min, whereas in dermatographism, it can last up to 30 min.

Fournier's gangrene, also known as necrotizing fasciitis of the scrotum, is a medical emergency that is characterized by rapidly progressing gangrene of the penis and scrotum, usually in diabetic males aged 50–70 years. Fournier's gangrene is commonly seen after perineal trauma, urinary tract infection, or urological surgical procedures. Fournier's gangrene is initiated by perianal, perirectal, and ischiorectal abscesses, fissures, or urinary extravasation. Systemic findings include leucocytosis, fever, hypoglycemia, tachycardia, and dehydration.

The skin of the back of the neck is surrounded by tough deep fascia that attaches to the epidermis layer by fibrous bands, creating separated compartments. In diabetics, subcutaneous infection on the back of the neck is localized by these fibrous bands laterally and inferiorly, forcing the abscess to spread to the surface via a sinus. Multiple intercommunicating abscesses that open into the surface via multiple sinuses in diabetic patient is a special type of abscess called "*carbuncle*."

Signs on Plain Radiographs

Changes in the hand due to Sudeck's atrophy are typically seen as severe osteoporosis, which occurs at the ends of all the phalanges, and up to 70% of metatarsal heads (Fig. 10.1.8). Pseudoperiostitis may be seen as striation of the cortices due to new bone formation. Severe sublaxation of the phalangeal joints may occur later in the course of the disease.

10.1

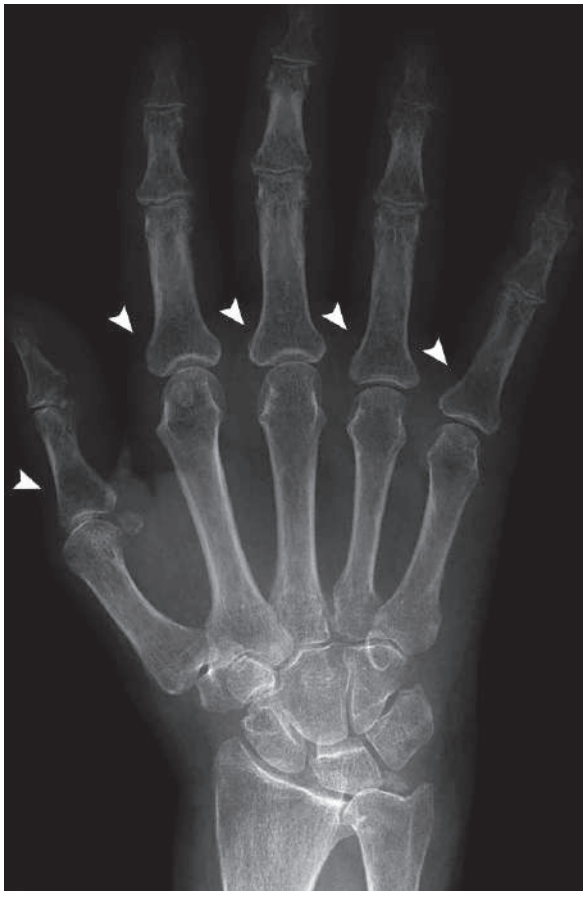

Fig. 10.1.8. Plain hand radiograph of a patient with Sudeck's atrophy shows marked osteoporosis of the hand that is localized to the phalanges and the metatarsal heads (*arrowheads*)

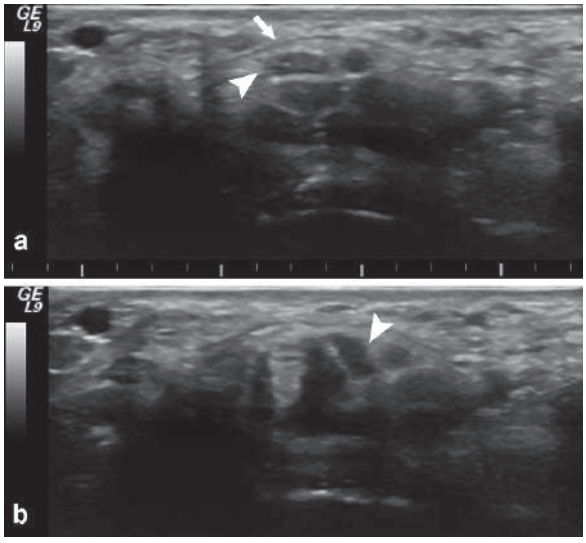

Fig. 10.1.9. Median nerve ultrasound in a healthy volunteer shows the normal median nerve (*arrowhead*) seen below the flexor retinaculum (*arrow*) as a hypoechoic structure in (**a**) and (**b**). The median nerve transverse diameter was 4 mm. In the flexion pinch maneuver, the patient is asked to flex his wrist, forcefully oppose the thumb to the index finger, hold the position for 3–5 s, and then release. In this maneuver, the median nerve moves in a sagittal motion deep into the carpal tunnel (*arrowhead* in **b**), and then returns to its normal position. Failure of the nerve to return to its normal position or to move deep into the carpal tunnel with this maneuver is a sign of entrapment

Signs on US

- Carpal tunnel syndrome can be diagnosed with wrist ultrasound by identifying the nerve below the flexor retinaculum. Diagnosis of nerve entrapment is achieved when the nerve transverse diameter exceeds 10 mm due to edema, or when the nerve fails to return to its normal position when performing the flexion pinch maneuver (Fig. 10.1.9).
- Fournier's gangrene is characterized by thickening of the scrotal skin, with gas formation within the subcutaneous skin, seen as hyperechoic foci surrounded by dirty shadowing.

Signs on CT

Fournier's gangrene is seen as thickened scrotal and/or penile skin with hypodense soft-tissue fluid collection surrounded by rim-contrast enhancement (abscess). Air within the mass and the subcutaneous tissues is a typical sign of necrotizing faciitis (Fig. 10.1.10).

Signs on MRI

In patients with carpal tunnel syndrome, there is a typical flattening of the median nerve, with high signal intensity in T2W images with contrast-enhancement, due to inflammation.

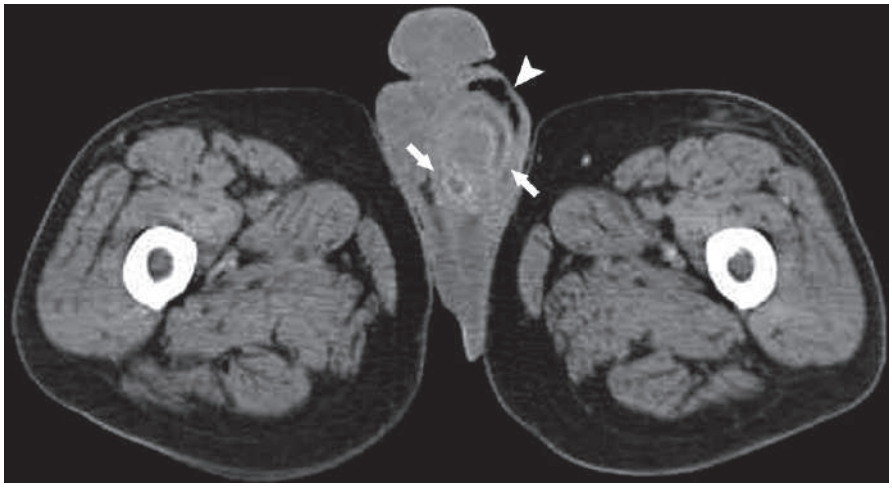

Fig. 10.1.10. Axial postcontrast CT of the scrotum and the upper thighs shows scrotal abscess with areas of ring contrast enhancement (*arrows*) and gas formation (*arrowhead*); a radiological stigma of Fournier's gangrene

The Role of Doppler Sonography in DM

Doppler sonography is used to detect stenosis within the arterial system of the lower extremities. Arteriosclerosis is the most common cause of arterial stenosis with the formation of atheromas and calcium plaques within the arterial walls. Analysis of the Doppler wave spectrum is essential to detect the hemodynamic abnormalities of circulation in the lower limbs. Different spectral waves are observed, according to the degree of stenosis.

Signs of Peripheral Vascular Disease on Doppler Scan *(Can Be Detected Even Before the Appearance of Clinical Symptoms)*

- Medial arterial wall calcification with acoustic shadowing "*string of beads sign*" (Fig. 10.1.11).
- Increased diastolic flow with reduced resistance index (RI) in the spectral flow analysis (Fig. 10.1.12). The increase in diastolic flow is due to arteriovenous shunting.
- Spectral flow abnormalities.

Spectral Flow Abnormalities on Doppler Scan of the Lower Limbs

- The normal arterial spectrum is triphasic, with peak systolic velocity (PSV) <120 cm/s.

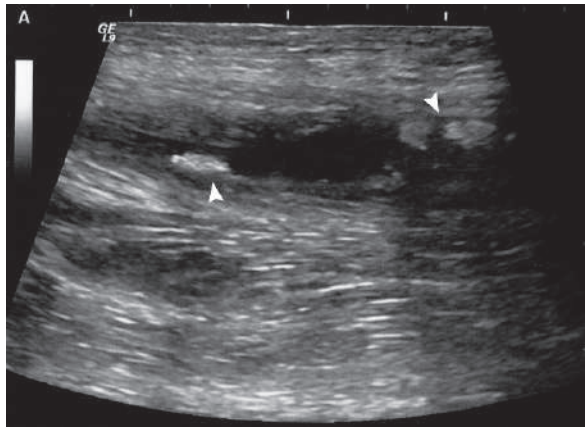

Fig. 10.1.11. Sagittal ultrasound image of the superficial femoral artery in a diabetic shows multiple dense calcifications of the arterial wall (*arrowheads*)

- 0–50% stenosis: shows triphasic or biphasic arterial spectrum (due to loss of the reversal flow pattern), with PSV <180 cm/s.
- 50–75% stenosis: shows biphasic or monophasic arterial spectrum, with PSV >180 cm/s (Fig. 10.1.13).
- 75–99% stenosis (high grade): shows biphasic or monophasic arterial spectrum, with PSV >250 cm/s.
- As the stenosis becomes generalized and affects a long segment of the artery, the flow spectrum becomes biphasic or monophasic, the acceleration upstroke is reduced, and the systolic peak becomes rounded (Fig. 10.1.14).

10.1

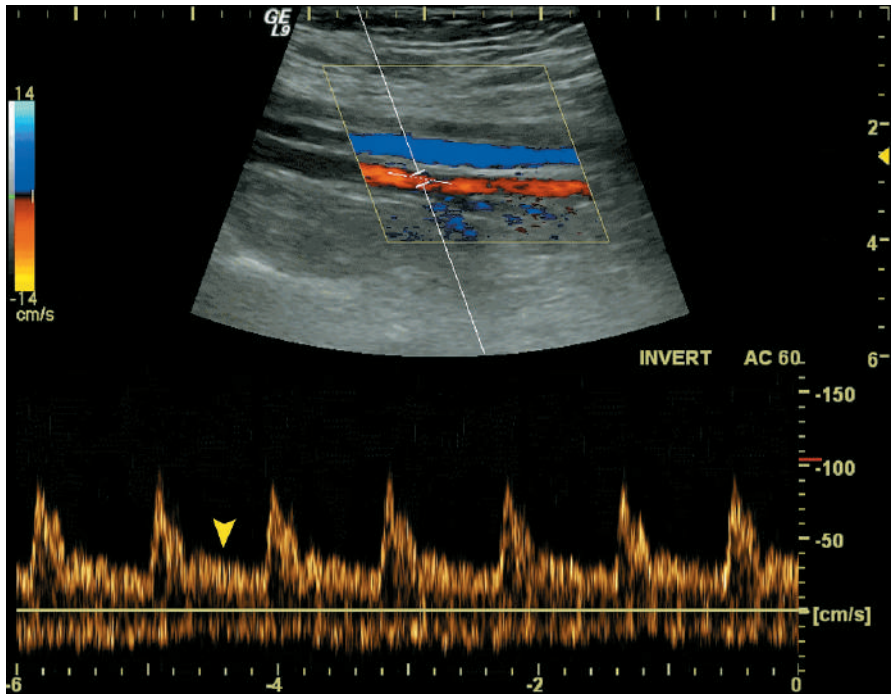

Fig. 10.1.12. Sagittal ultrasound image of the superficial femoral artery in a patient with peripheral vascular disease due to diabetes mellitus (DM) shows monophasic arterial spectral wave with increased diastolic flow (*arrowhead*)

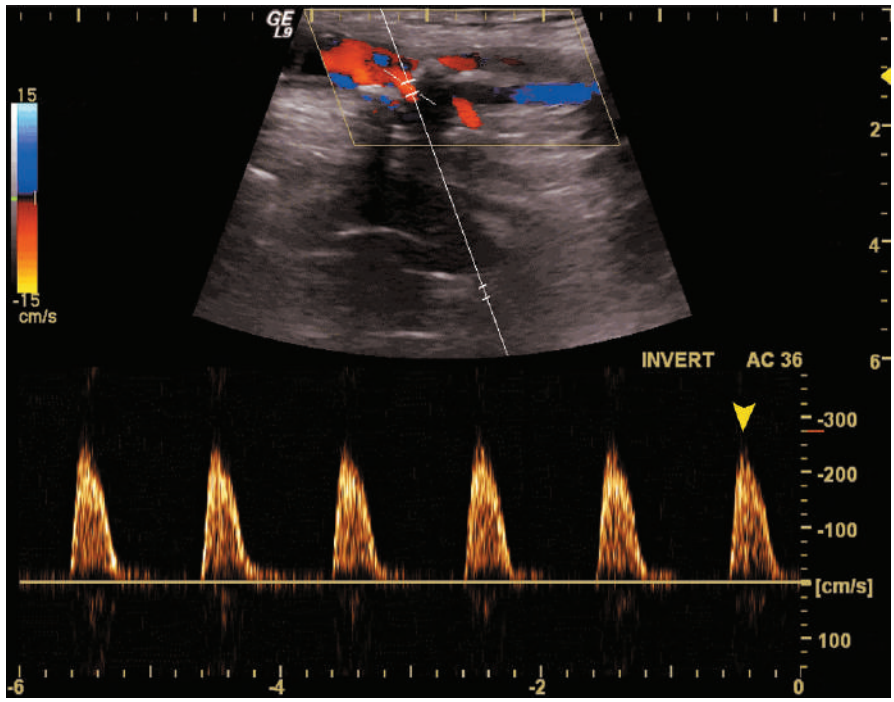

Fig. 10.1.13. Sagittal ultrasound image of the superficial femoral artery in a patient with peripheral vascular disease due to DM shows monophasic arterial spectral wave with PSV >250 cm/s (*arrowhead*), representing >75–99% arterial stenosis

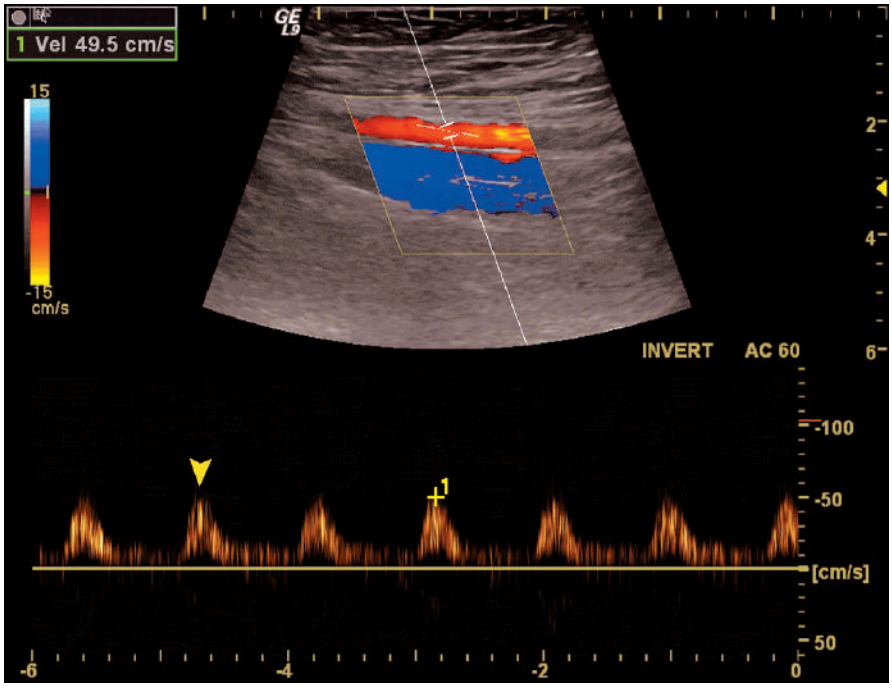

Fig. 10.1.14. Sagittal ultrasound image of the superficial femoral artery in a patient with peripheral vascular disease due to DM shows monophasic arterial spectral wave with PSV <50 cm/s (*arrowhead*). As mentioned earlier, the normal peripheral arterial spectral wave for the superfical femoral artery is triphasic, with PSV <120 cm/s

Signs of Diabetic Nephropathy on Doppler Scan

- Increased renal length and parenchymal thickness due to glomerular hyperfiltration. The normal kidney size is 10–12 cm in the longitudinal diameter and 4–6 cm in the transverse diameter; the normal renal parenchymal thickness is 1.6 cm.)
- RI of arcuate arteries is >0.7.
- In advanced renal disease, there is increased echogenicity of the renal cortex, with reduction of its thickness.

The Role of MRI in DM

MRI is a powerful tool to detect early bone changes that may not be seen on plain radiographs or evoke complaints unless they are severe and destructive. Contrast-enhanced studies should be done to detect signs of soft tissue inflammation, abscess formation, sinus tract detection, and devitalization.

Signs of Diabetic Foot on MRI

- A *callus* is detected on MRI as a soft-tissue area of low T1 signal intensity with intense contrast enhancement after contrast injection. It is typically found at the first and fifth metatarsal heads, the malleoli, and the calcaneus (Fig. 10.1.15).
- *Devitalization* is an area of soft tissue that is devoid of vascular supply (tissue infarction). It is detected on MRI as a soft tissue area with low T1 and low T2 signal intensities, which shows no contrast enhancement after contrast injection (like any other tissue infarction in the body). It is important to inform the surgeon about devitalization areas for tissue debridement planning.
- An *ulcer* is detected as an area of skin and soft tissue defect, with low signal intensity on T1W images, and intense enhancement after contrast administration.
- *Cellulitis* is an area of soft tissue inflammation, and is detected on MRI as an ill-defined area of soft tissue with low T1 and high T2 signal intensities, with ill-defined enhancement after contrast administration (Fig. 10.1.16).

10.1

- An *abscess* is a localized area of pus collection, and typically detected as acystic area of low T1 and high T2 signal intensities, with ring enhancement after contrast administration (Fig. 10.1.17).
- *Reactive bone marrow* is detected as a normal (isointense) signal intensity of the bone marrow on T1W images, with high signal intensity on T2W images (Fig. 10.1.18).
- *Osteomyelitis* is inflammation of the bone and the bone marrow. It is detected on MR as areas of cortical bone defect characterized by the following characteristics: diffuse bone marrow edema, may show sequestrum, shows no bone deformities (unless complicated by neuropathic joint), usually underlying an ulcer (e.g., metatarsal heads), may show sinus formation into the skin surface, and the soft tissue around it is usually inflamed and shows marked contrast enhancement. (Fig. 10.1.19). Signs of periostitis may be found, which is seen as linear contrast enhancement surrounding the outer cortical margin. An intraosseous abscess may occur in subacute osteomyelitis (*Brodie's abscess*), which is characterized by the "*penumbra sign*." The penumbra sign is detected on MRI as a discrete zone of peripheral T2 hyperintensity signal surrounding a high T2 signal intensity intraosseous abscess (Fig. 10.1.19). Osteomyelitis is classically located in a single focus. However, multiple lesions may be seen in 20% of cases.
- *Septic arthritis* is inflammation of a joint due to infection. It is detected on MRI as high T2 signal intensity within a joint and its surrounded soft tissue, with signs of joint effusion and cartilage destruction. There is intense enhancement of the joint and its surrounding soft tissue after contrast administration (Fig. 10.1.20).
- A *foreign body* is detected on MRI as an object of low T2 signal intensity, surrounded by a high intensity signal in the soft tissues on T2W images (due to edema around the foreign body). (Fig. 10.1.21)
- *Neuroarthropathic joint (Charcot's joint)* has the same presentation and signal intensities as osteomyelitis, with destruction of the subchondral cortices. Neuropathic joint is characterized by: midfoot predominance, subchondral cyst formation, normal surrounding tissue with intact overlying skin, juxta-articular edema, signs of joint disorganization and deformity (5Ds), and no signs of fluid collection or abscess (Fig. 10.1.22). Osteomyelitis, in contrast to neuropathic joint, predominates in pressure areas such as the metatarsal heads in the forefoot and the calcaneus in the hindfoot. The only common location for osteomylitis in the midfoot is in the cuboid bone, which occurs in severe midfoot neuropathic joint. However, bone biopsy remains the definite diagnostic method to differentiate osteomyelitis from neuropathic joints in diabetics.
- *Tenosynovitis*: is detected as normal tendon size, surrounded by high T2 fluid-signal intensity on T2W images.
- *Calcaneal insufficiency avulsion fracture*: is an extra-articular fracture affecting the posterior third of the calcaneus (Fig. 10.1.23). It is seen almost exclusively in diabetics.
- Sinus tract is detected as a hypodense line extending from an area of bone destruction to the adjacent soft tissues (Fig. 10.1.19). It is best detected on postcontrast fast-suppressed T1W images.

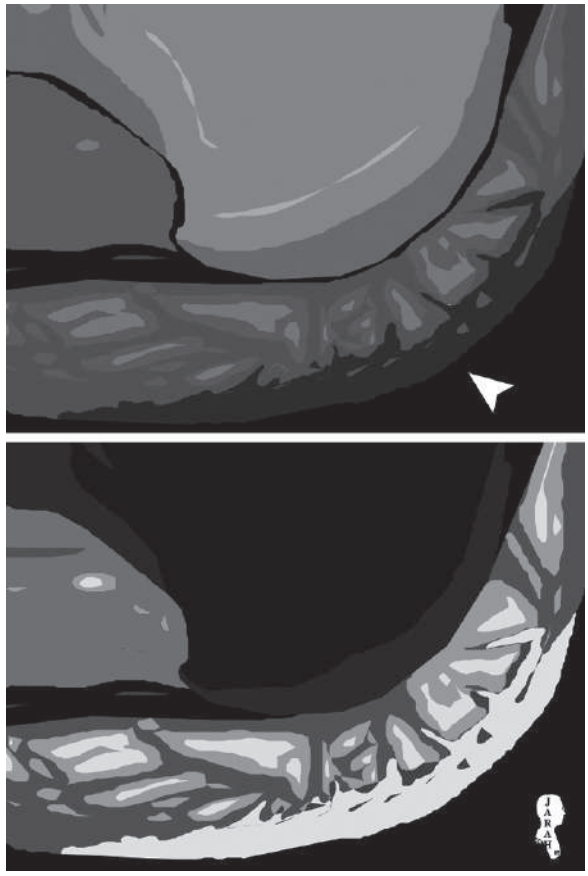

Fig. 10.1.15. Sagittal T1W (**a**) and STIR (**b**) ankle MR illustrations demonstrate callus seen as an area of soft tissue with low T1 signal intensity in (**a**) and with high T2 signal intensity in (**b**) (*arrowheads*)

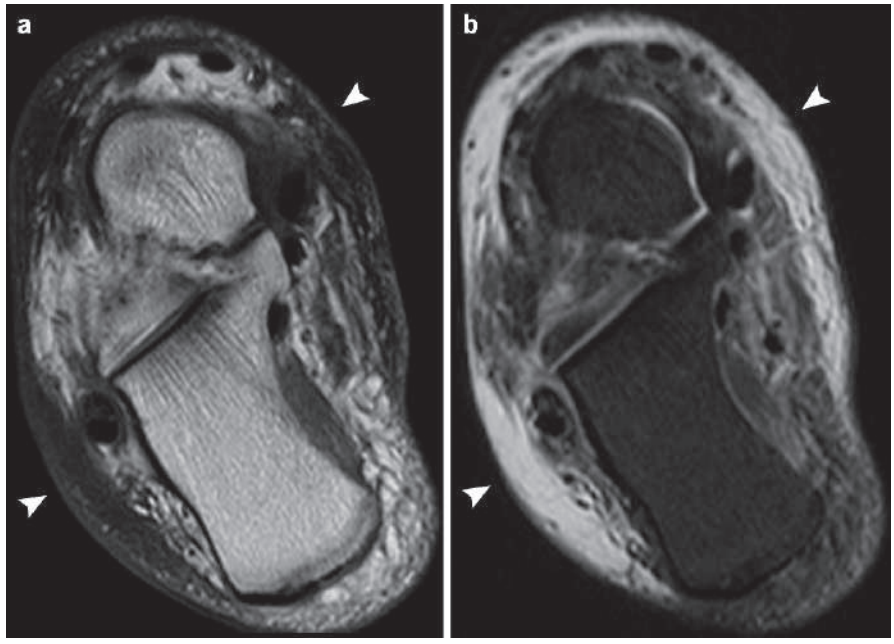

Fig. 10.1.16. Sagittal T1W (**a**) and STIR (**b**) ankle MRI show areas of low T1 and high T2 signal intensity lesions confined to the skin and the subcutaneous tissue, without signs of bone marrow edema or joint effusion (*arrowheads*), representing cellulites

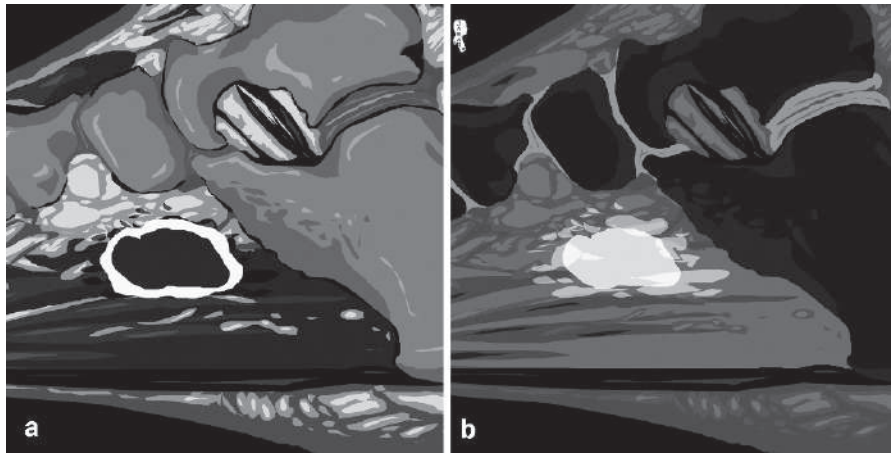

Fig. 10.1.17. Sagittal T1W postcontrast (**a**) and STIR (**b**) ankle MR illustrations demonstrate abscess formation, seen as a cystic area surrounded by rim contrast enhancement in (**a**), and seen as an area of cystic fluid collection in (**b**)

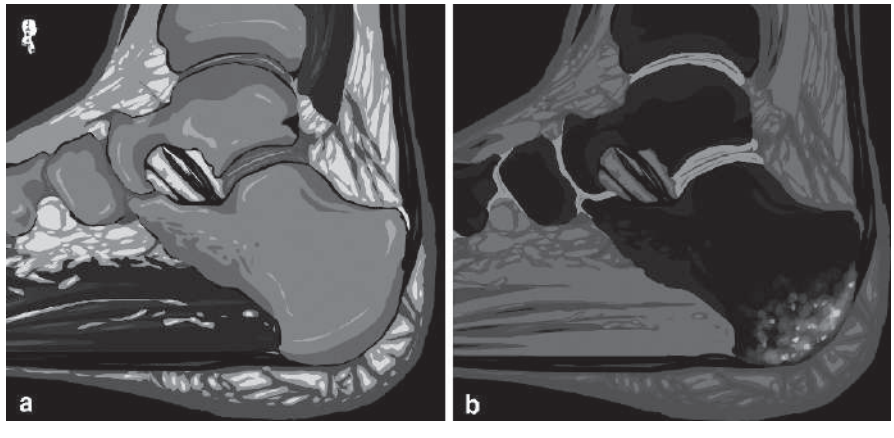

Fig. 10.1.18. Sagittal T1W (**a**) and STIR (**b**) ankle MR illustrations demonstrate reactive bone edema affecting the posterior third of the calcaneus

10.1

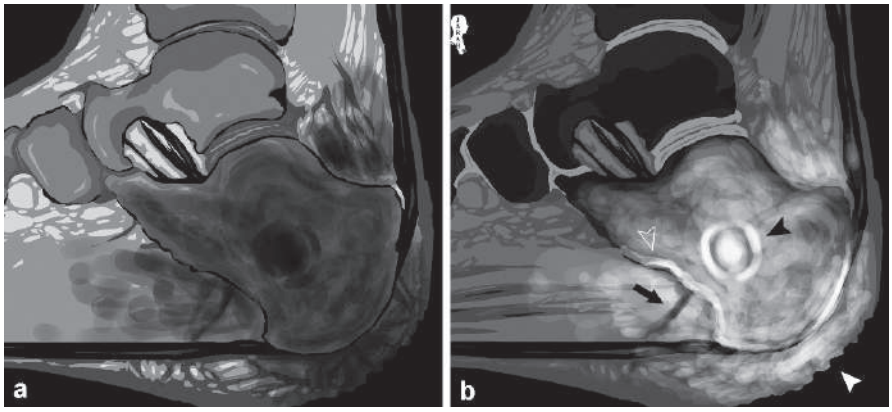

Fig. 10.1.19. Sagittal T1W postcontrast (**a**) and STIR (**b**) ankle MR illustrations show signs of osteomyelitis. Notice the calcaneal ulcer with edema (*white arrowhead*), the penumbra sign (*black arrowhead*), sinus tract from the osteomyelitis spreading infection to the nearby soft tissues (*arrow*), and signs of periostitis seen as linear high signal intensities located around the cortex of the calcaneus (*hollow arrowhead*)

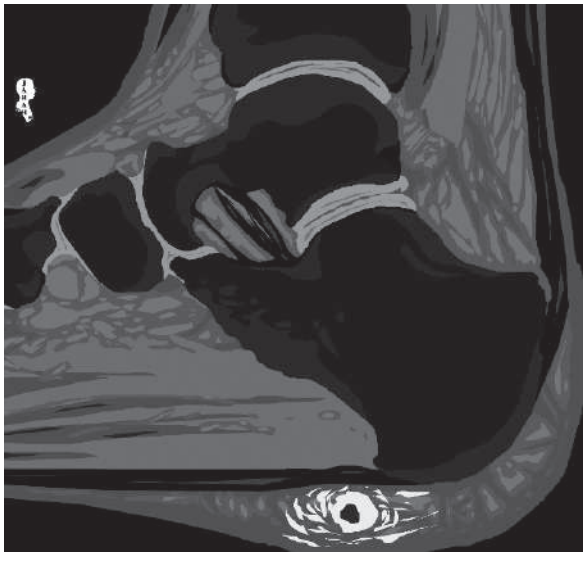

Fig. 10.1.21. Sagittal STIR ankle MR illustration demonstrates a foreign body surrounded by tissue edema located within the infracalcaneal soft tissue region

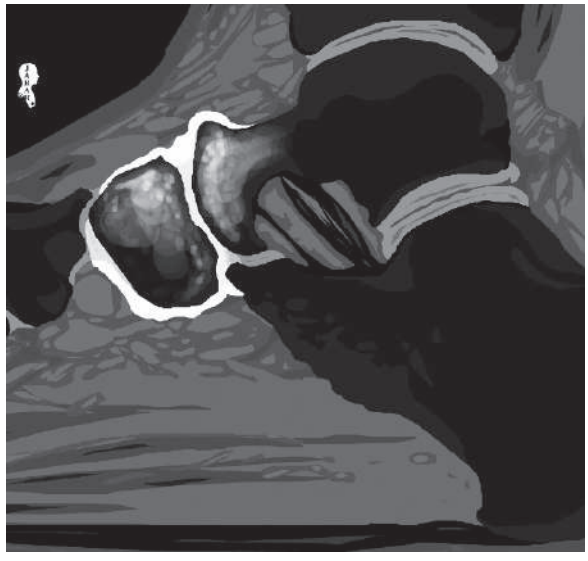

Fig. 10.1.20. Sagittal STIR ankle MRillustration demonstrates talo-navicular joint septic arthritis, seen as bone marrow edema affecting the articular bones with joint effusion

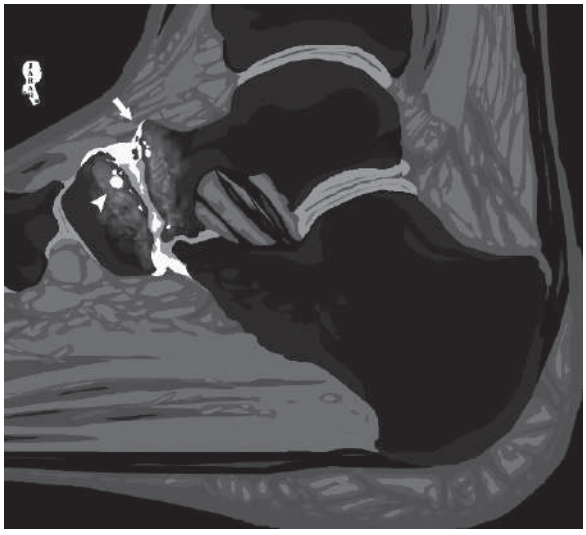

Fig. 10.1.22. Sagittal STIR ankle MR illustration demonstrates talo-navicular Charcot's joint. Notice the midfoot location, the joint deformity (*arrow*), the subchondral cysts (*arrowhead*), and the mild joint effusion due to reactive inflammation

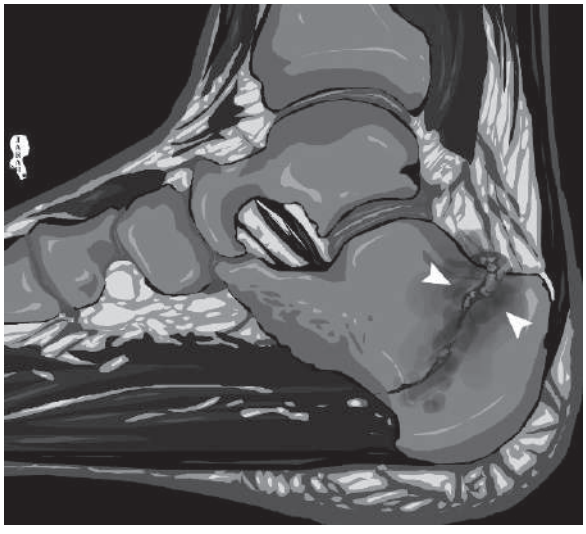

Fig. 10.1.23. Sagittal T1W ankle MR illustration demonstrates avulsion fracture of the posterior third of the calcaneus (*arrowheads*)

Differential Diagnoses and Related Diseases

Congenital insensitivity to pain (CIPA): CIPA, also referred to as *hereditary sensory and autonomic neuropathy type IV*, is a rare disorder characterized by the inability to perceive pain stimuli due to peripheral autonomic nervous system demyelination and reduced fiber caliber. CIPA patients respond to normal pain stimuli, but not to painful stimuli. Early symptoms include decreased sweating (anhydrosis), which causes episodes with extreme hyperpyrexia, multiple healed tongue bites since infancy, and multiple missing teeth due to auto-extraction (50% of cases). Characteristically, CIPA patients present with multiple bony features at varying stages of the healing process. Interestingly, patients with CIPA develop aseptic necrosis and osteochondritis in the juxta-articular regions of the weight-bearing long bones (hip, knees, and ankles). Joint radiographs of CIPA patients show changes similar to those of chronic Charcot's joint and osteomyelitis.

For Further Reading

1. Chatha DS et al MR imaging of the diabetic foot: diagnostic challenges. Radiol Clin N Am. 2005;43:747–59
2. Puttemans T et al Diabetes: the use of color Doppler sonography for the assessment of vascular complications. Eur J Ultrasound. 1998;7:15–22
3. Beltran J et al The diabetic foot: magnetic resonance imaging evaluation. Skeletal Radiol. 1990;19:37–41
4. Gefen A et al Integration of plantar soft tissue stiffness measurements in routine MRI of the diabetic foot. Clin Biomech. 2001;16:921–25
5. Marcus CD et al MR imaging of osteomyelitis and neuropathic osteoarthropathy in the feet of diabetics. RadioGraphics. 1996;16:1337–48
6. Biswal N et al Congenital indifference to pain. Indian J Pediatr. 1988;65:755–69
7. Abdel-Hafez HZ et al Congenital insensitivity to pain with anhidrosis (CIPA). Egyptian Dermatol Online J. 2007; 3(1):5
8. Purewal TS. Charcot's diabetic neuroarthropathy: pathogenesis, diagnosis and management. Pract Diab Int. 1996; 13(3):88–91
9. Chuter V et al Limited joint mobility and plantar fascia function in Charcot's neuroarthropathy. Diabet Med. (2001);18, 558–61
10. Tiwari S et al Tropical diabetic hand syndrome. Int J Diab Dev Ctries. 2008;28(4):130–31
11. Jung Y et al Diabetic hand syndrome. Metabolism. 1971; 20 (11), 1008–1015
12. Peyri J et al Necrobiosis Lipoidica. Semin Cutan Med Surg. 26:87–89
13. McGuinness M et al Necrobiosis Lipoidica diabeticorum. Foot. 1997;7:47–51
14. Nguyen K et al Necrobiosis Lipoidica diabeticorum treated with chloroquine. J Am Acad Dermatol. 2002;46:S34–6
15. Naderi ASA et al Diabetic muscle necrosis. J Diabet Complications. 2008;22:150–52
16. Glauser SR et al Diabetic muscle infarction: a rare complication of advanced diabetes mellitus. Emerg Radiol 2008;15: 61–65

17. Gold RH et al Imaging the diabetic foot. Skeletal Radiol. 1995;24:563–71
18. Beltran J et al The diabetic foot: magnetic resonance imaging evaluation. Skeletal Radiol. 1990;19:37–41
19. Reinhardt K. The radiological residua of healed diabetic arthropathies. Skeletal Radiol. 1981;7:167–72
20. Chantelau E et al "Silent" bone stress injuries in the feet of diabetic patients with polyneuropathy: a report on 12 cases. Arch Orthop Trauma Surg. 2007;127:171–77
21. Erickson SJ et al MR imaging of the tarsal tunnel syndrome and related spaces: normal and abnormal findings with anatomic correlation. AJR. 155:323–28
22. Bhute D et al Dermatographism. Ind J Dermatol Venerol Leprol. 2008;74:177–79
23. Piedra T et al Fournier's gangrene: a radiologic emergency. Abdom Imaging. 2006;31:500–502
24. Bhanushali MJ et al Diabetic and non-diabetic lumbosacral radiculoplexus neuropathy. Neurology India. 2008;56(4): 420–25
25. Nguyen VD et al Freiberg's disease in diabetes mellitus. Skeletal Radiol. 1991;20:425–28
26. Tan PL et al MRI of the diabetic foot: differentiation of infection from neuropathic change. Br J Radiol. 2007;80: 939–48
27. Singson RD et al Postamputation neuromas and other symptomatic stump abnormalities: detection with CT. Radiology. 1987;162:743–45
28. Singson RD et al Postamputation neuromas. Skeletal Radiol. 1990;19:259–62

10.1

10.2 Diabetic Brain and Nervous System

In advanced stages, diabetes mellitus (DM) can affect the brain, due to microangiopathy and prolonged exposure to hypoglycemia. Over the past decade, many researches have evaluated the anatomical and functional status of the brain in diabetics compared to the normal population. This topic presents the most common, well-documented brain changes in diabetics, as reported in the medical and radiological literature.

DM type 1 can be associated (rarely) with chorea-ballismus episodes due to nonketotic hyperglycemia (NKH). The cause of these chorea-ballismus episodes is unknown, but it is believed that they are vascular in origin.

Chorea is defined as involuntary, continuous, random, fast, jerking, dance-like movements in the distal parts of the limbs. *Ballismus* shows a picture similar to chorea, but the movements are more irregular, of large amplitude, and violent, affecting the proximal portion of limbs.

Nonketotic hyperglycemia (NKH) is a severe form of hyperglycemia with hyperosmolarity and intracellular dehydration, with little or no ketoacidosis. It is typically observed in diabetic patients >50 years of age. NKH is characterized by partial insulin deficiency with enough insulin to inhibit ketoacidosis, but not enough to transport glucose into the cells. Hyperglycemia causes an osmotic diuresis, with progressive dehydration, resulting in NKH. Up to 40% of patients with NKH develop seizures beside the chorea-ballismus episodes.

The incidence of stroke is six times higher in patients with DM than in nondiabetics. This high stroke risk can be explained by the high incidence of atherosclerosis of the internal carotid artery in diabetics.

Many researchers reported high cerebral brain atrophy among long-term diabetics. Patients with DM type 2 were found to have an increased risk of Alzheimer's disease (AD) and vascular dementia. AD in diabetics is believed to be due to the increase in advanced glycation end products, which increase aggregation of proteins involved in AD development. Furthermore, dysfunction of insulin signaling in the brain has been implicated in the pathogenesis of AD. Subcortical arteriosclerosis encephalopathy can develop in diabetics due to brain vessel atherosclerosis.

Cranial nerve involvement in DM is a rare complication. A single cranial nerve (*diabetic mononeuritis*) or multiple cranial nerves (*mononeuritis multiplex*) can be involved. DM classically affects the cranial nerves CN III, CN IV, CN VI, and CN VII. Cranial nerve involvement in diabetes is thought to be a result of microvasculitis and resultant ischemic injury to the nerves.

Patients with *diabetic ketoacidosis (DKA)* can develop subclinical cerebral edema for unknown reasons. The brain edema can start before or after treatment initiation. Patients with DM type 1 are most commonly affected, and it occurs in > 1% of cases. Typically, patients present with severe headaches that can progress (rarely) into brain herniation. Other manifestations of symptomatic brain edema due to DKA include a drop in heart rate, altered mental status that ranges from dizziness to coma, and increased blood pressure.

Signs on CT and MRI

- Stroke is seen as a hypodense area on CT or a hyperintense area on T2W MR images. Focal neurological deficits and the clinical picture suggest the diagnosis.
- In *NKH-ballismus episode*, CT scan of the basal ganglia (caudate and putamen) are hyperdense compared to the rest of the brain parenchyma (Fig. 10.2.1). Normal basal ganglia attenuation is between 33 and 36 HU. In diabetic chorea, the basal ganglia show attenuation between 40 and 51 HU. This finding is believed to be caused by multiple petechial hemorrhages within the basal ganglia. On MRI, the basal ganglia show hyperintense signal intensity on both T1W and T2W images (Fig. 10.2.1). This sign is not specific, and can be observed in cases of hepatic encephalopathy, carbon monoxide toxicity, Wilson disease, and neurofibromatosis.
- Generalized brain atrophy is seen in diabetics with signs of dementia. The hippocampus and the amygdale volume are reduced in diabetics who develop signs of dementia.
- Signs of subcortical arteriosclerosis encephalopathy may be seen when the clinical status of the patient suggests dementia.
- *Diabetic mononeuritis* is detected as enhancement of the affected cranial nerve after contrast injection ipsilateral to the site of cranial nerve clinical deficits. Multiple cranial nerve enhancements are seen in mononeuritis multiplex.
- *Diabetic ketoacidosis* brain edema often shows signs of loss of gray-white matter differentiation, effacement of the sulci, and decrease in ventricular size

10.2

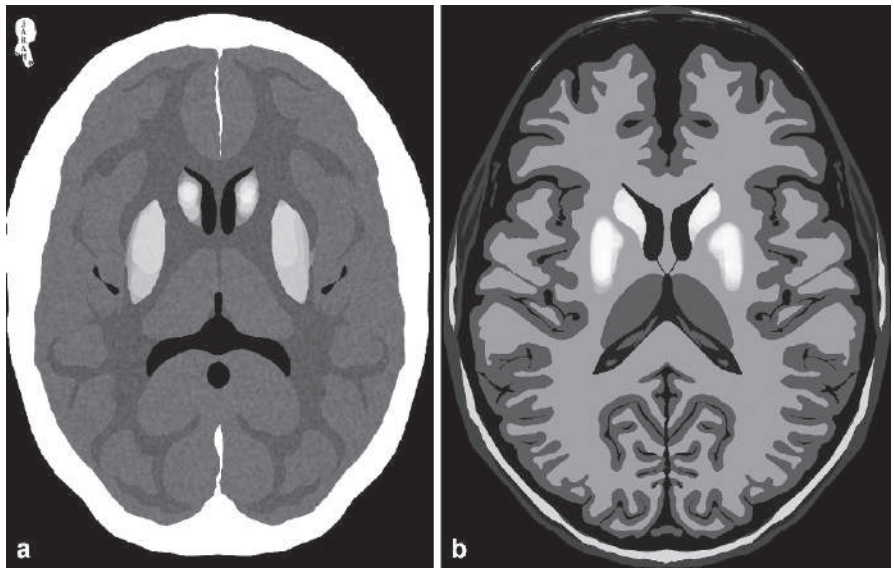

Fig. 10.2.1. Axial nonenhanced brain CT (**a**) and MR (**b**) illustrations demonstrate high density basal ganglia (**a**) and high intensity signal of the basal ganglia (**b**), which is a sign detected in patients with ballismus episodes and in patients with nonketotic hyperglycemia

For Further Reading

1. Araki Y et al MRI of the brain in diabetes mellitus. Neuroradiology. 1994;36:101–3
2. Lai PH et al Chorea-ballismus with nonketotic hyperglycemia in primary diabetes mellitus. AJNR Am J Neuroradiol. 1996;17:1057–64
3. Lavin PJM. Hyperglycemic hemianopia: a reversible complication of non-ketotic hyperglycemia. Neurology. 2005;65: 616–19
4. den Heijer T et al Type 2 diabetes and atrophy of medial temporal lobe structures on brain MRI. Diabetologia. 2003; 46:1604–10
5. Harten BV et al Brain imaging in patients with diabetes. A systematic review. Diabetes Care. 2006;29(11):2539–46
6. Brands AMA et al Cognitive functioning and brain MRI in patients with type 1 and type 2 diabetes mellitus: a comparative study. Dement Geriatr Cogn Disord. 2007;23: 343–50
7. Kelkar P et al Mononeuritic multiplex in diabetes mellitus: evidence for underlying immune pathogenesis. J Neurol Neurosurg Psychiatry. 2003;74;803–6
8. Witzke KA et al Diabetic neuropathy in older adults. Rev Endocr Metab Disord. 2005;6:117–27
9. Pacheco E et al Pathophysiology and computed tomography findings in a case of diabetic ketoacidosis. Int Pediatr. 1999;14(2):118–20

10.3 Diabetic Syndromes

Diabetic syndromes are a group of diseases characterized by the development of diabetes mellitus (DM) in childhood. Most of these diseases are originally syndromes, with DM constituting a major manifestation of these syndromes. This topic describes the most common pediatric syndromes associated with DM.

Alström Syndrome

Alström syndrome (AS) is a very rare genetic disease, characterized by infantile dilated cardiomyopathy, diabetes mellitus, pigmentary retinal dystrophy causing blindness, sensorineural hearing loss, and obesity.

The disease has an autosomal recessive mode of inheritance, and it is linked to mutation in the short arm of chromosome 2. Dilated cardiomyopathy is the earliest manifestation of this syndrome, and classically starts in the third to fourth week of life. Blindness and sensorineural hearing loss in an obese child should trigger the suspicion of AS.

Diagnostic and key features of AS include:

Ophthalmoloic Clinical Findings

- Atypical pigmentary retinopathy without classical bone specules is a constant finding (*diagnostic criterion*).
- Nystagmus usually appears during the first 1–2 years of life.
- Visual deterioration occurs during the first decade of life.
- Loss of the papillary reactions appear during the second decade of life.

Auditory Clinical Findings

Progressive, bilateral sensorineural hearing loss is found within the first decade of life (*diagnostic criterion*).

Metabolic and General Clinical Findings

- Obesity with hypertriglyceridemia from birth (*diagnostic criterion*).
- Hyperinsulinemia and noninsulin dependent DM (*diagnostic criterion*).
- Hepatic failure and hypogonadism are found occasionally.

Renal Clinical Findings

Renal deterioration is a constant finding, and it is age-related, often starting within the second decade of life.

Dermatological Clinical Findings

Areas of hyperpigmentation and papillary hypertrophy on the neck and flexor creases (acanthosis nigricans) may be found occasionally.

Signs on Chest Radiographs

Increased cardiaothoracic ratio and signs of dilated cardiomyopathy can be seen in advanced stages.

Signs on US and CT

Multiple hyperechoic or hypodense liver lesions may be found with heterogeneous contrast enhancement. The lesions are usually due to hepatocellular adenoma with pericellular fibrosis.

10.3 Bardet-Biedl Syndrome

Bardet-Biedl syndrome (BBS) is a rare, genetically heterogeneous disease, characterized by noninsulin dependent DM in adulthood, ocular abnormalities, mental retardation, obesity, polydactyly, and renal dysfunction.

BBS has an autosomal recessive mode of inheritance, with prevalence of 1 in 125,000 live births. Key features of BBS include pigmentary (rod-cone) retinal dystrophy in the second decade of life (95% of cases), truncal obesity with normal appetite (85% of cases), genital hypoplasia (74% of cases), mental retardation (70% of cases), postaxial polydactyly (80% of cases), and renal anomalies. Chronic end-stage renal failure is a constant feature (100% of cases). Renal anomalies are the main cause of mortality in BBS patients.

Signs on IVU

- Bilateral small kidney size.
- Multiple calyceal clubbing and blunting, with medullary cysts in the absence of reflux on voiding cystourethrogram.
- Persistent fetal lobulation.

Signs on US

- Loss of differentiation between the medulla and the cortex.
- Hyperechogenic parenchyma with multiple cysts.
- Moderately dilated renal pelvis.

Signs on Plain Radiographs

Postaxial polydactyly and cutaneous syndactyly are classically found.

The main differential diagnosis of BBS is AS. How can you differentiate between the two conditions?

- Dilated cardiomyopathy is a feature of AS, not a feature of BBS.
- Mental retardation is a feature of BBS, not a feature of AS.
- Bilateral sensorineural hearing loss is found in AS, but not in BBS.

Leprechaunism (Donohue Syndrome)

Leprechaunism (Donohue syndrome) is a very rare genetic metabolic disease, characterized by insulin-resistant DM with fasting hypoglycemia due to severe insulin receptor mutation. Infants with leprechaunism exhibit severe DM at birth, postnatal growth retardation, atrophy of the subcutaneous fat, characteristic facial features, and acanthosis nigricans.

Leprechaunism is a fatal disease, and most afflicted infants die before the age of 1 year. The disease has an incidence of 1: 4 million live births. The term "leprechaunism" is derived from"leprechaun", a green, man-like creature with magical powers, according to Irish folklore. The infant's features are acclaimed to be similar to the features of this mythical creature.

The key features of leprechaunism include hirsutism, severe failure to thrive (that might lead to death in the early months of life), growth retardation and failure to thrive, and areas of hyperpigmentation and papillary hypertrophy on the neck and flexor creases (acanthosis nigricans). Notice that all these features are seen in an infant. Laboratory investigations typically show hyperinsulinemia, hyperandrogenism, and elevated cord human chorionic gonadotropin (hCG).

Prader-Willi Syndrome

Prader-Willi syndrome (PWS) is an autosomal dominant, multisystemic disease, characterized by multiple features that are almost all related to hypothalamic dysfunction. PWS has a prevalence rate of 1 in 15,000 live births.

PWS is characterized by hyperphagia and obesity, starting in the teens. Obesity is the major cause of morbidity and mortality in PWS. DM (19%), hypertension, obstructive sleep apnea, lower limb edema and varicosity, all can be explained by the morbid obesity caused by this disease.

Key features of PWS include almond-shaped palpebral fissures, dolichocephalic (wide) skull, micropenis, hypoplastic scrotum and hypogonadism, and history of fetal hypotonia and poor sucking. Body habitus features include sloping shoulders, genu valgum, and heavy mid-section. Patients with PWS have high serum levels of "gherlin," a peptide released from the stomach that can stimulate food intake.

Signs on Plain Radiographs

Lateral skull radiograph shows small sella turcica with prominent posterior clinoid process.

Wolcott-Rallison Syndrome

Wolcott-Rallison syndrome (WRS) is a rare disease characterized by neonatal permanent DM, with multiple epiphyseal dysplasia causing short stature (dwarfism).

WRS has an autosomal recessive mode of inheritance, and the affected child has tendency to long bone fractures. WRS patients have a waddling gait, lordotic posture, with genu valgum.

Other abnormalities of WRS include hypoplastic pancreas, blue sclera, brown mottling of the teeth, mental retardation, seizures, and renal, hepatic and cardiac abnormalities. Mild chronic neutropenia is reported in many cases, but without immune deficiency.

Multiple epiphyseal dysplasia (Fairbank disease) is a genetic disease with autosomal dominant mode of inheritance, characterized by abnormalities in maturing epiphyses, resulting in dwarfism and stubby digits. The disorder is almost always bilateral. The disease is divided into a severe form (Fairback subtype), and a milder form. Patients usually present with severe flexion contractures, juvenile osteoarthritis, limb deformities, and limping during early childhood, with a duckling gait.

Signs on Radiograph

- Multiple epiphyseal dysplasia is characterized by bilateral hypoplastic epiphyses with irregular contour in the Fairbank form. Flattening of the epiphyses may be seen in the mild form (Figs. 10.3.1 and 10.3.2). The most common joints affected are the hips (100%), knees, and ankles. There is no epiphyseal sclerosis. Hands and wrists are involved in the severe form. The fingers and toes are short and thick. Hypoplastic tarsal and carpal bones may be seen. Persistent calcified cartilage within the bone may be found.
- Osteoporosis.

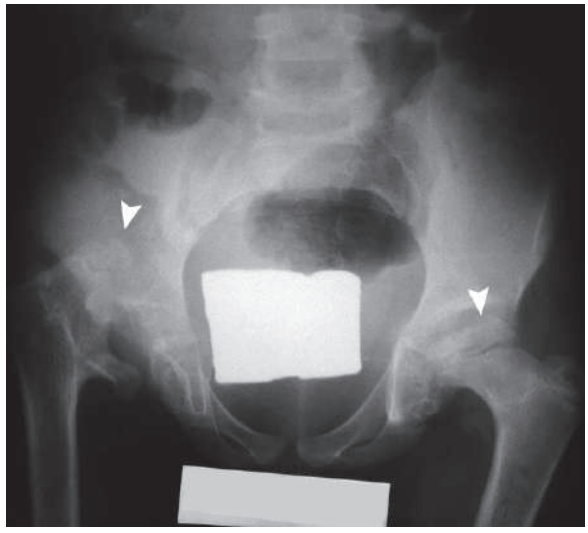

Fig. 10.3.1. Anteroposterior plain hip radiograph of a child with multiple epiphyseal dysplasia shows bilateral femoral epiphyses fragmentation and flattening (*arrowheads*), with right hip dislocation

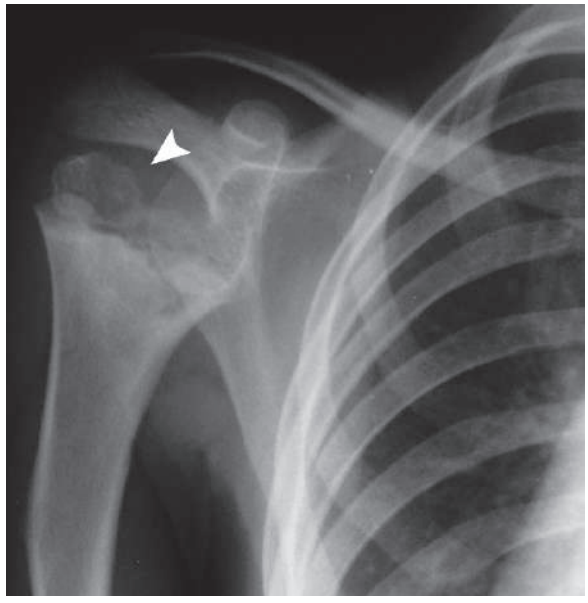

Fig. 10.3.2. Plain right shoulder radiograph of the same patient shows severe humeral epiphysis hypoplasia and dysplasia (*arrowhead*)

Wolfram Syndrome (DIDMOAD)

10.3

Wolfram syndrome (WS) is a rare disease characterized by *d*iabetes *i*nsipidus, *d*iabetes *m*ellitus, *o*ptic *a*trophy, and sensorineural *d*eafness, making the acronym DIDMOAD.

WS has an autosomal recessive mode of inheritance, and it is caused by mutation in chromosome 4. Incidence of WS is estimated to be 1 in 100,000 live births.

Diagnostic and key features of DIDMOAD include:

Ophthalmoloic Clinical Findings

Bilateral progressive optic atrophy (98% of cases) (*diagnostic criterion*).

Auditory Clinical Findings

Bilateral sensorineural hearing loss is found in up to 12% of cases (*diagnostic criterion*).

Metabolic and General Clinical Findings

- Diabetes insipidus (35% of cases) (*diagnostic criterion*).
- DM (99% of cases) (*diagnostic criterion*).
- Hypogonadism (occasionally).

Renal Clinical Findings

- Dilatation of the urinary tract with unknown cause (*diagnostic criterion*).
- Testicular atrophy (occasionally).

Neurological Clinical Findings

- Ataxia due to cerebellar atrophy.
- Short-term memory loss and dementia.
- The mean age at death is 30 years, most commonly due to brain stem atrophy and central respiratory failure.

Signs on Brain MRI

- Generalized brain atrophy, especially in the cerebellum, medulla, and pons.
- Loss of the posterior pituitary signal.
- Atrophy of the optic nerves, tracts, and radiations.
- Patchy areas of white matter demyelination may be seen occasionally.

Rabson-Mendenhall Syndrome

Rabson-Mendenhall syndrome (RMS) is a rare genetic disease with various somatic abnormalities, characterized by noninsulin dependent DM due to severe insulin resistance, caused by insulin receptors mutation. The disease has an autosomal recessive mode of inheritance.

Diagnostic and key features of RMS include:

Metabolic and General Clinical Findings

- Noninsulin dependent DM, postpardinal hypoglycemia, and hyperinsulinemia (*diagnostic criterion*).
- Dysmorphic facial features, with large ears (*diagnostic criterion*).
- Generalized hypertrichosis, with coarse head hair.
- Genital (phallic) enlargement (*diagnostic criterion*).
- Premature dentition.

Renal Clinical Findings

- Bilateral renal enlargement with medullary sponge kidney may be found. *Medullary sponge kidney* is a congenital disease characterized by dilatation of the collecting tubules in one or more renal papillae, affecting one or both kidneys. There is a high incidence of renal calculi formation in medullary sponge kidney, with hypercalciuria found in up to 50% of patients. Gross hematuria can be found in 10–20% of patients.
- Nephrocalcinosis.

Dermatological Clinical Findings

Typically, there are areas of hyperpigmentation and papillary hypertrophy on the neck and flexor creases (acanthosis nigricans).

Signs on IVU

Sponge kidney is diagnosed by the presence of typical cystic collection of contrast material in the collecting ducts in a form of "bouquet of flowers or paintbrush appearance" (Fig. 10.3.3).

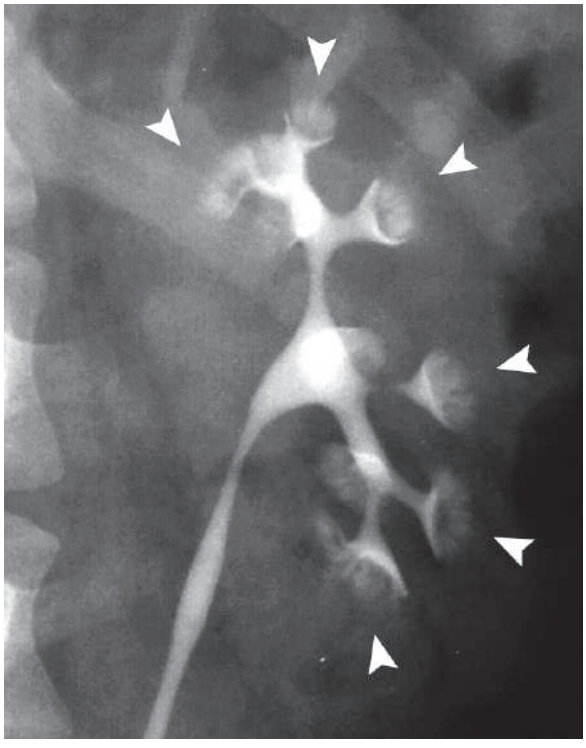

Fig. 10.3.3. Intravenous urography radiograph of a patient with sponge kidney shows the classical collecting duct paintbrush appearance (*arrowheads*)

For Further Reading

1. Makaryus AN et al A rare case of Alström syndrome presenting with rapidly progressing severe dilated cardiomyopathy diagnosed by echocardiography. J Am Soc Echocardiogr. 2003;16:194–96
2. Barrett TG. Mitochondrial diabetes, DIDMOAD and other inherited diabetes syndromes. Best Prac Res Clin Endocrinol Metab. 2001;15(3):325–43
3. Benso C et al Three new cases of Alström syndrome. Graefe's Ach Clin Exp Opthalmol. 2002;240:622–27
4. Morgan J et al US, CT, and MRI imaging of hepatic masses in Alström syndrome: a case report. Clin Imaging. 2008; 32:393–95
5. Tobin JL et al Bardet-Biedl syndrome: beyond the cilum. Pediatr Radiol. 2007;22:926–36
6. Dippell J et al Early sonographic aspects of kidney morphology in Bardet-Biedl syndrome. Pediatr Nephrol. 1998;12: 559–63
7. Fralick RA et al Early diagnosis of Bardet-Biedl syndrome. Pediatr Nephrol. 1990;4:264–65
8. Urben SL et al Otolaryngologic features of Laurence-Moon-Bardet-Biedl syndrome. Otolaryngol Head Neck Surg. 1999; 120:571–74
9. Donohue WL et al Leprechaunism. A Euphuism for a rare familial disorder. J Pediatr. 1954;45(5):505–18
10. Summitt RL et al Leprechaunism (Donohue's syndrome): a case report. J Pediatr. 1969;74(4):601–10
11. Papavramidis ST et al Prader-Willi syndrome-associated obesity treated by biliopancreatic diversion with duodenal switch. Case report and literature review. J Pediatr Surg. 2006;41:1153–58
12. Miller J et al Neurocognitive findings in Prader-Willi syndrome and early-onset morbid obesity. J Pediatr. 2006; 149:192–98
13. Cohen MM Jr. Syndromology: an updated conceptual overview. V. Aspects of aneuploidy. Int J Oral Maxillofac Surg. 1998;18:333–38
14. Stöß H et al Wolcott-Rallison syndrome: diabetes mellitus and spondyloepiphyseal dysplasia. Eur J Pediatr. 1982;138: 120–29
15. Barrett TG. Mitochondrial diabetes, DIDMOAD and other inherited diabetes syndromes. Best Pract Res Clin Endocrinol Metab. 2001;15(3):325–43
16. Bin-Abbas B et al Wolcott-Rallison syndrome: clinical, radiological, and histological findings in a Saudi child. Ann Saudi Med. 2001;21(1–2):73–4
17. Genis D et al Wolfram syndrome: a neuropathological study. Acta Neuropathol. 1997;93:426–29
18. Shannon P et al Evidence of widespread axonal pathology in Wolfram syndrome. Acta Neuropathol. 1999;98:304–8
19. Tekgül S et al Urological manifestations of the observation in 14 patients. J Urol. 1999;161:616–17
20. Verri A et al A case of Wolfram syndrome: neurological features. Ital J Neurol Sci. 1982;4: 351–53
21. Galluzzi P et al MRI of Wolfram syndrome (DIDMOAD). Neuroradiology. 1999;41:729–31
22. Harris AM et al Rabson-Mendenhall syndrome: medullary sponge kidney, a new component. Pediatr Nephrol. 2007;22: 2141–44
23. Gupta S et al Medullary sponge kidney. Ind J Pediatr. 2002; 69(12):1091–92
24. Parveen BA et al Rabson-Mendenhall syndrome. Int J Dermatol. 2008;47:839–41
25. Hatori M et al Multiple epiphyseal dysplasia – report of two families. Arch Orthop Trauma Surg. 2000;120:372–75
26. Sebik A et al The orthopaedic aspects of multiple epiphyseal dysplasia. Int Orthopaed (SICOT). 1998;22:417–21
27. Rubin EL et al Cystic disease of the renal pyramids ('sponge kidney'). J Fac Radiol. 1959;10(3):134–37

10.4 Diabetes Insipidus

Diabetes insipidus (DI) is a disease characterized by increased frequency of urination (polyuria), with increased fluid intake (polydypsia) secondary to inappropriate secretion of the antidiuretic hormone (ADH) vasopressin from the posterior pituitary gland.

ADH is secreted by the supraoptic and paraventricular hypothalamic nuclei, and stored in the terminals within the posterior pituitary. *Neurohypophysis* is a term used to describe the posterior pituitary, the infundibular stalk, and the supraoptic and paraventricular hypothalamic nuclei. ADH regulates fluid and electrolytes balance within the body by promoting water reabsorption in the distal tubules in the kidneys.

According to its origin, DI is classified into three types:

- *Neurogenic DI:* can be idiopathic (50%), genetic (5%), secondary to tumor (e.g., craniopharyngioma), or secondary to inflammatory reactions (e.g., Langerhans cell histocytosis).
- *Nephrogenic DI:* can be due to primary renal disease, or secondary to chronic renal failure or hypercalcemia.
- *Dipsogenic DI:* arises due to compulsive polydipsia, or due to hypothalamic disorders affecting the thirst center.

DI has a prevalence of 1:25,000 of the population. Patients typically present with polyuria and polydipsia. The polyuria is not reduced by cessation of fluid intake. Signs of dehydration, such as dry skin, hypotension, and tachycardia, are often found. Serum electrolyte investigations show high plasma osmolarity, hypernatremia, hypokalamia, hyperglycemia, and hypercalcemia.

The most common hypothalamic tumors associated with DI are metastases, geminoma, and craniopharyngioma. *Craniopharyngioma* is a benign, slow-growing tumor that arises from the remnant of *Rathke's pouch* (craniopharyngeal duct). It can occur in children between 6–15 years of age, and adults between 50 and 60 years of age. Up to 50% of suprasellar lesions in children are craniopharyngiomas. Patients usually present with visual disturbance (bitemporal quadrianopia), headache, and hypothalamic dysfunction.

As previously mentioned, the neurohypophysis is composed of the posterior pituitary lobe, the infundibular stalk, and the median eminence of the hypothalamus. The normal posterior pituitary shows high signal intensity on native T1W images (Fig. 10.4.1). It is thought that this bright spot is due to the macrogranules composed of the ADH neurophysin complex. *Ectopic posterior pituitary* is a condition where the posterior pituitary bright signal spot on MR imaging is not located in the posterior pituitary lobe, but is typically seen in the median hypothalamic eminence.

The anterior pituitary gland (*adenohypophysis*) normally shows the same signal characteristic as the rest of the brain on T1W images. However, the adenohypophysis can show a bright signal on native T1W images during the first 2 years of life, due to secretory activity, or in preterm babies during the first 2 months of life. The bright signal of the adenohypophysis is best demonstrated with the magnetization transfer MR sequence.

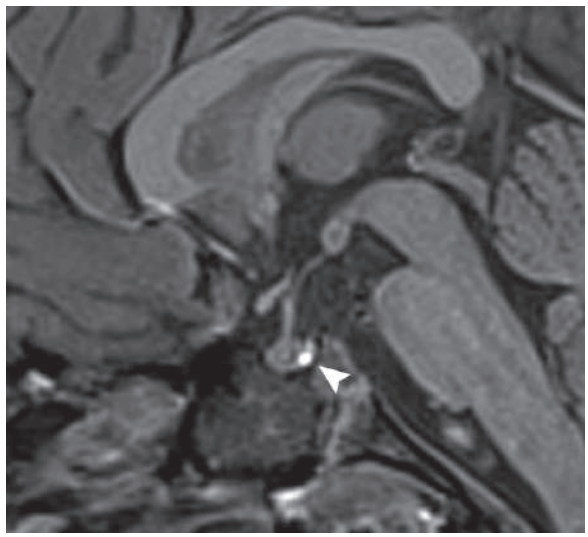

Fig. 10.4.1. Sagittal nonenhanced T1W MRI of the sella shows the physiological bright signal of the posterior hypophysis (*arrowhead*)

Signs on Brain MRI (Done in Patients with Suspected Neurogenic DI)

- *Genetic cause*: there is loss of the typical posterior pituitary hyperintensity signal on T1W contrast-enhanced images (Fig. 10.4.2). However, the neurohypophysis bright spot can be absent in 10–20% of normal individuals.
- *Craniopharyngioma*: on CT, the main bulk of the lesion is located in the suprasellar region, and has cystic (90%) and solid components with rim-like or nodular calcifications in up to 80% of cases (Fig. 10.4.3). The solid component enhances after contrast administration. On MRI, the lesion has high T1 signal and high/low T2 signal according to the fat and thick protinaceous (motor oil) consistency within the lesion. The solid component enhances after contrast administration.
- *Langerhans cell histiocytosis*: there is typical enlargement of the central part of the infundibulum (>2.5 mm) when Langerhans cell histiocytosis is the main cause of DI (Fig. 10.4.4).
- Bilateral, symmetrical brain calcifications within the basal ganglia and the subcortical area has been reported as unusual manifestations of DI. These findings are best evaluated on CT.
- *Ectopic posterior pituitary* is seen as a bright spot, typically located in the hypothalamic eminence (Fig. 10.4.5).

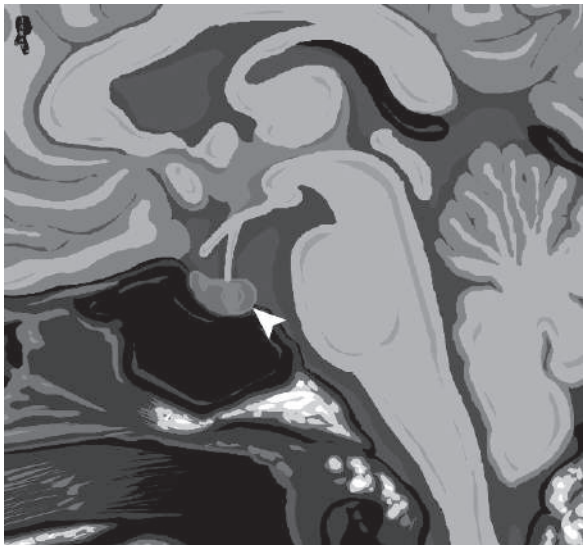

Fig. 10.4.2. Sagittal nonenhanced T1W MR illustration of the sella shows loss of the physiological posterior pituitary bright spot, which is a characteristic finding in idiopathic or genetic diabetes insipidus

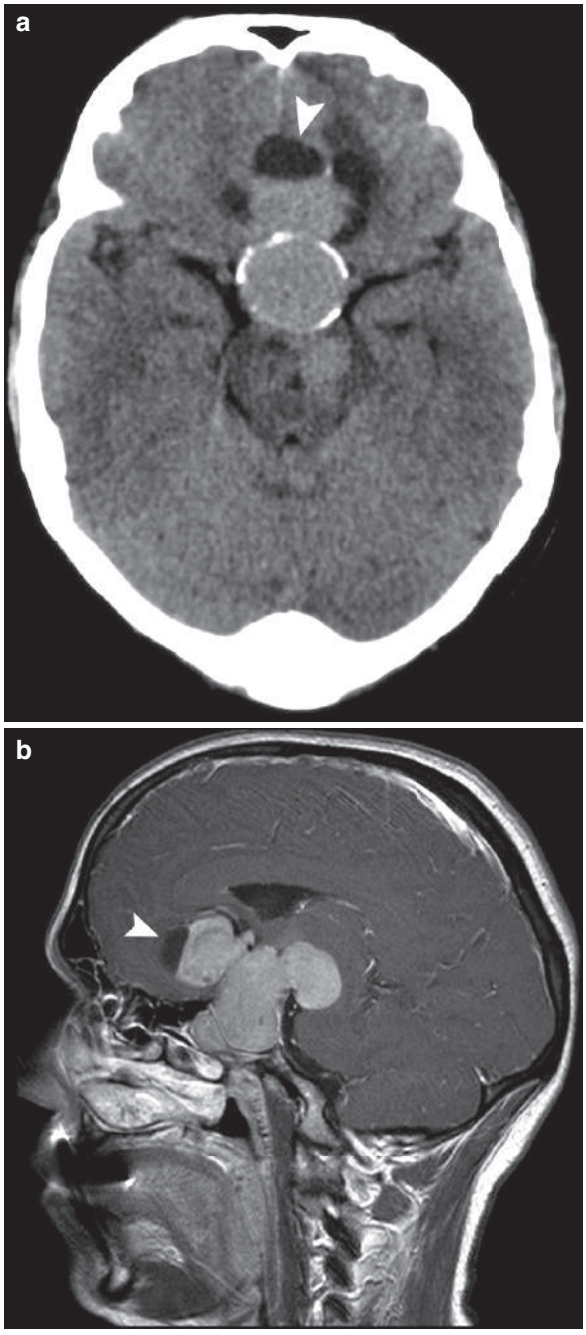

Fig. 10.4.3. Axial nonenhanced brain CT (**a**) and sagittal contrast-enhanced T1W MRI of the sella show craniopharyngioma in a 40-year-old patient. In (**b**), the main bulk of the lesion is located in the suprasellar area, with infiltration of the sella turcica and the sphenoid sinus. The lesion is mostly solid, with anterior cystic component located in the inferior frontal region (*arrowhead*). In (**a**), a calcified rim that surrounds the lesion is nicely illustrated

10.4

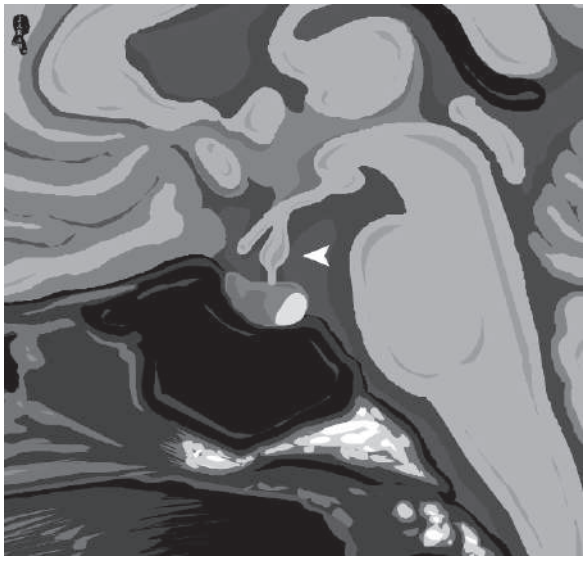

Fig. 10.4.4. Sagittal nonenhanced T1W MR illustration of the sella shows thickened infundibulum due to Langerhans cell histiocytosis (*arrowhead*)

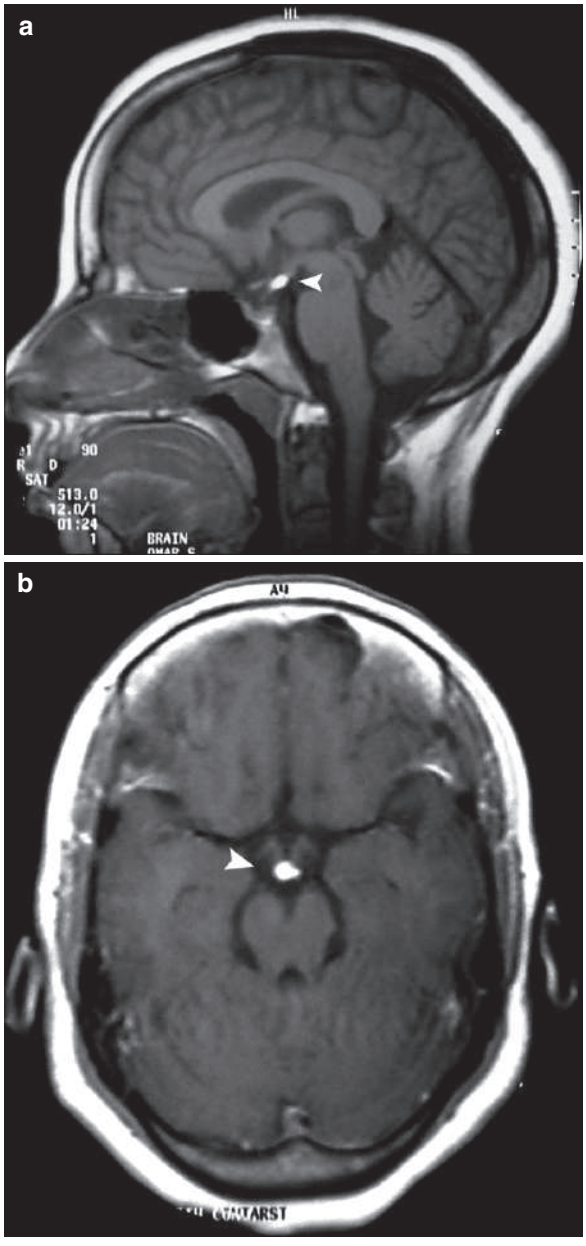

Fig. 10.4.5. Sagittal (**a**) and axial (**b**) T1W MRI shows an ectopic high signal intensity spot located at the proximal part of the infundibulum (ectopic posterior pituitary)

For Further Reading

1. Al-Kandari SR et al Intracranial calcification in central diabetes insipidus. Pediatr Radiol. 2008;38:101–3
2. Maghnie M et al Central diabetes insipidus in children and young adults. N Eng J Med. 2000;343:998–1007
3. Hadjizacharia P et al Acute diabetes insipidus in severe head injury: a prospective study. J Am Coll Surg. 2008;207: 477–84
4. Jane JA Jr. et al Neurogenic diabetes insipidus. Pituitary. 2006;9:327–29
5. Kassebaum N et al Diabetes insipidus associated with propofol anesthesia. J Clin Anesth. 2008;20:466–68
6. Mavrakis AN et al Diabetes insipidus with deficient thirst: report of a patient and review of the literature. Am J Kidney Dis. 2008;51(5):851–59
7. Schmitt S et al Pituitary stalk thickening with diabetes insipidus preceding typical manifestations of Langerhans cell histiocytosis in children. Eur J Pediatr. 1993;152: 399–401
8. Mitchell LA et al Ectopic posterior pituitary lobe and periventricular heterotopia: cerebral malformation with the same underlying mechanism. AJNR Am J Neuroradiol. 2002;23:1475–81
9. Saeki N et al MRI of ectopic posterior pituitary bright spot with large adenomas : appearances and relationship to transient postoperative diabetes insipidus. Neuroradiology. 2003;45:713–16
10. Maria IA. MRI of the hypothalamic-pituitary axis in children. Pediatr Radiol. 2005;35:1045–55

10.5 Obesity, Gastric Banding, and Liposuction

Obesity is a disease characterized by an increase in the size and number of fat cells. Fat cell size differs from region to region within the body, and the number of fat cells may increase 3–5-fold during adolescence. Overweight is defined as a body weight of 101–120% of the ideal, while obesity is defined as fat accumulation >120% of the ideal.

Obesity is defined by the world health organization (WHO) as the ratio of body mass to body height (kg/m^2), the so-called "*body mass index*" (BMI). A BMI of 25–30 kg/m^2 is considered "overweight", >30 kg/m^2 is defined as "obesity", and >40 kg/m^2 is defined as "morbid obesity". BMI is used as a marker for estimating the risks for diseases such as diabetes mellitus and cardiovascular diseases. Women usually have gynecoid fat distribution around the hips, while men have android fat distribution where adiposity is predominantly central.

Patients with obesity suffer from many systemic diseases such as diabetes mellitus and insulin insensitivity, cardiovascular diseases, obstructive sleep apnea, osteoarthritis, venous stasis and varicosities, and gout.

There are different causes of obesity. Apart from a sedentary lifestyle and high-carbohydrate food intake, hormonal, syndromic/pathologic, and drug-induced lipomatosis are other common causes of obesity. Each cause induces obesity by a different mechanism.

Hormonal Obesity

- *Hypothalamic obesity*: obesity that arises after paraventricular ventromedial hypothalamic injury, causing hyperphagia due to loss of the serum leptin level sensitization.
- *Cushing's syndrome*: obesity is a cardinal sign of Cushing syndrome. Patients classically present with truncal (android) obesity.
- *Hypothyroidism*: obesity in hypothyroidism is mainly due to a slow metabolic rate. The weight gain is often modest, without marked obesity.
- *Polyscystic ovary disease*: up to 50% of patients with polycystic ovary disease are overweight with insulin resistance.
- *Growth hormone deficiency*: growth hormone deficiency causes a reduction in lean body mass and an increase in fat body mass.

Syndromic/Pathologic Obesity

- Lipoma is defined as the localized, encapsulated accumulation of fat. It can be single or multiple, and can be seen in any part of the body (Fig. 10.5.1). Multiple lipomas can be seen in Maffuci's syndrome and neurofibromatosis type 1 (*von Ricklinghausen disease*).
- *Lipomatosis* is a condition characterized by proliferation of nonencapsulated fat cells (Fig. 10.5.2).
- *Liposarcoma* is a rare malignant tumor characterized by neoplastic proliferation of fat cells (Fig. 10.5.3).
- *Lipodystrophy* is a condition characterized by loss of body fat in one or more areas. It can be genetic or acquired (e.g., HIV drug-induced lipodystrophy).
- *Binge-eating disorder* is a psychiatric disorder, characterized by uncontrolled episodes of eating, usually in the evening.
- *Night-eating syndrome* is a psychiatric disorder, characterized by consumption of at least 25% of daily energy between the evening meal and the next morning. Patients often awake at night to eat, three or more times per week.

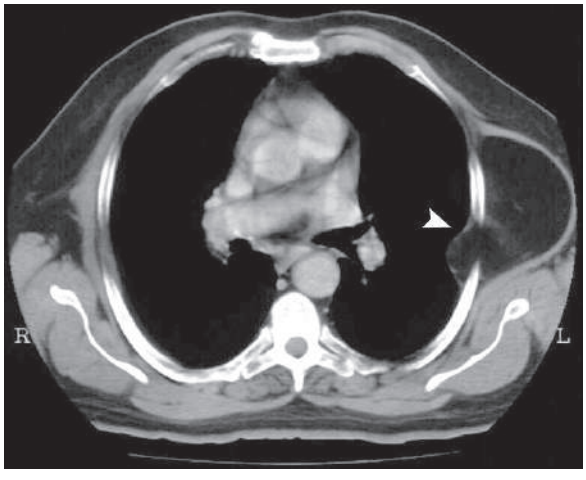

Fig. 10.5.1. Axial nonenhanced chest CT shows left chest wall lipoma, seen as a typically well-circumscribed mass with fat-attenuation (*arrowhead*)

10.5

- *Dercum's disease (Lipomatosis dolorosa)* is a rare disease, characterized by painful subcutaneous fatty tissue with inflammatory characteristics. Patients are typically young obese women 25–40 years of age, presenting with vague pain that can be focal or generalized. Many patients live with this disease while being unaware of it, either because the disease sometimes shows mild symptoms or because patients receive a wrong diagnosis.

Lipomatosis dolorosa can be mistaken for fibromyalgia rheumatica. Unlike fibromyalgia rheumatica, the pain in lipomatosis dolorosa increases with body weight gain. The pain often has insidious onset, and progresses with time. The pain in lipomatosis dolorosa is chronic (>3 months duration), aching, stabbing, or burning, and usually symmetrical (Fig. 10.5.4). However, localized pain maybe seen in the upper limbs or around the knee. The face and hands are typically not involved.

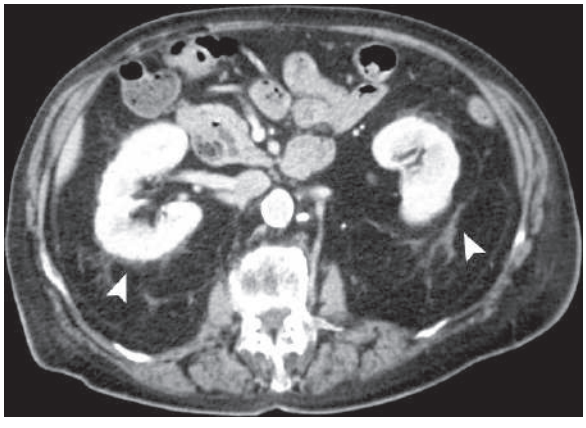

Fig. 10.5.2. Axial abdominal postcontrast CT shows retroperitoneal lipomatosis, with increased fat content of the retroperitonium pushing the kidneys anteriorly in a bilateral fashion (*arrowheads*)

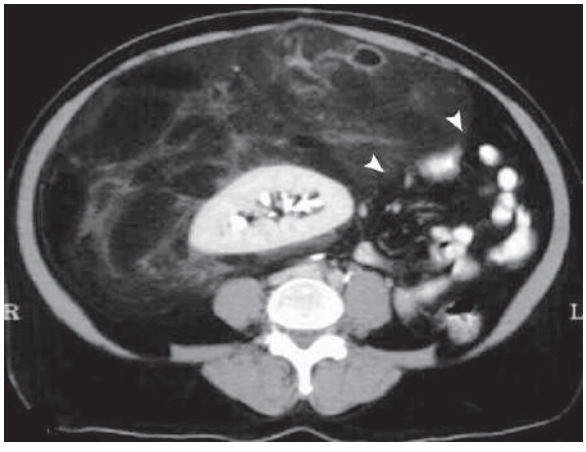

Fig. 10.5.3. Axial abdominal postcontrast CT shows severe abdominal fatty proliferation that pushes the left kidney and the intestines to the left abdominal cavity region (*arrowhead*) due to proliferating retroperitoneal liposarcoma

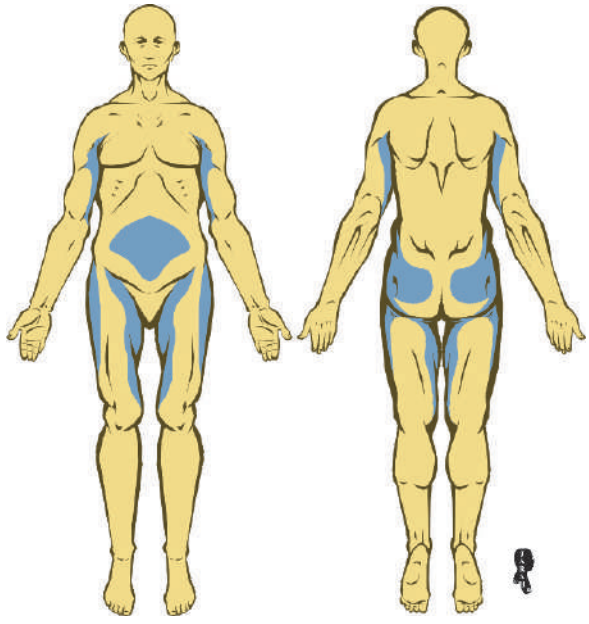

Fig. 10.5.4. An illustration demonstrates the typical pain distribution in dercum dolorosa

The pain characteristically arises from the subcutaneous fat. The pain may worsen on any light touch or pressure (allodynia), wearing tight clothes, or taking a shower. Also, the pain is temperature- and humidity-dependent, and usually reduces when the weather is hot and dry. Hot baths may reduce the pain, but only temporarily. The pain is thought to be caused by fat masses pressing upon the nerve root endings, or by releasing cytokines that induce pain (e.g., tumor necrosis factor-α).

Three types of lipomatosis dolorosa are described: *Type 1 (juxta-articular)*, with painful subcutaneous folds around the knees or the hips; *Type 2 (diffuse)*, which affects the whole body symmetrically; and. *Type 3 (nodular)*, characterized by intense pain around lipomas.

- *Weber-Christian disease (WCS)* is a disease characterized by painful subcutaneous nodules found mainly on the trunk and the extremities, with constitutional symptoms like fever, fatigue, polymyalgia, and arthralgia. The subcutaneous nodules are composed of lobular panniculitis (subcutaneous tissue inflammation). When the panniculitis is systemic, WCS can be fatal in up to 10% of patients. Patients commonly show elevated erythrocyte sedimentation rate and C-reactive protein levels.

- *Madelung's disease (Benign symmetric lipomatosis/ Launois-Bensaude syndrome)* is a rare condition, characterized by massive symmetric deposits of non-encapsulated adipose tissue in the head, the neck, and the upper trunk.

Madelung's disease (MD) is typically seen in middle-aged males of Mediterranean origin with a history of excessive alcohol consumption (90% of cases). Patients with MD typically consume more than 80 g of alcohol per day for more than 10 years. MD is considered a "sight diagnosis" because of the typical patterns of fat distribution in the head and neck region. Lipomatosis is typically seen accumulating in both parotid regions (hamster cheeks appearance), cervical region (horse collar appearance), and the posterior neck region (buffalo hump appearance) (Fig. 10.5.5). The disease is divided into two types: *type 1 MD* is characterized by symmetric body lipomatosis that gives the patient a "pseudo-athletic" appearance (Fig. 10.5.5). *Type 2 MD* is characterized by diffuse lipomatosis that gives the patient a generalized obese appearance.

Sensory, motor, or autonomic polyneuropathy is seen in up to 85% of patients with MD. Rarely, the tongue or the mediastinum is involved in lipomatosis, resulting in dysphagia and dyspnea.

- *Metabolic syndrome (Syndrome X)* is defined by the WHO as the presence of impaired glucose regulation or diabetes, with two of the following risk factors: hypertension, dyslipidemia, central obesity, and microalbuminuria. There is a strong association between the development of metabolic syndrome and increase in visceral adipose tissue (VAT).
- *Fröhlich syndrome* is a rare hypothalamic disorder, characterized by obesity, stunned growth, and genital hypoplasia.
- *Obesity-hypoventilation (Pickwickian) syndrome*) is a disease characterized by the triad of morbid obesity, hypoventilation, and irresistible hypersomnolence (drowsiness). Hypoventilation in Pickwickian syndrome is defined clinically by an arterial blood gas as a $PaCO_2 > 45$ and/or a $PO_2 < 55$ in the presence of morbid obesity. This hypoventilation is attributed to obstructive sleep apnea in these patients, and by the ventilation/perfusion mismatch that results from the irregular shallow breathing with or without compression by a thick chest wall.

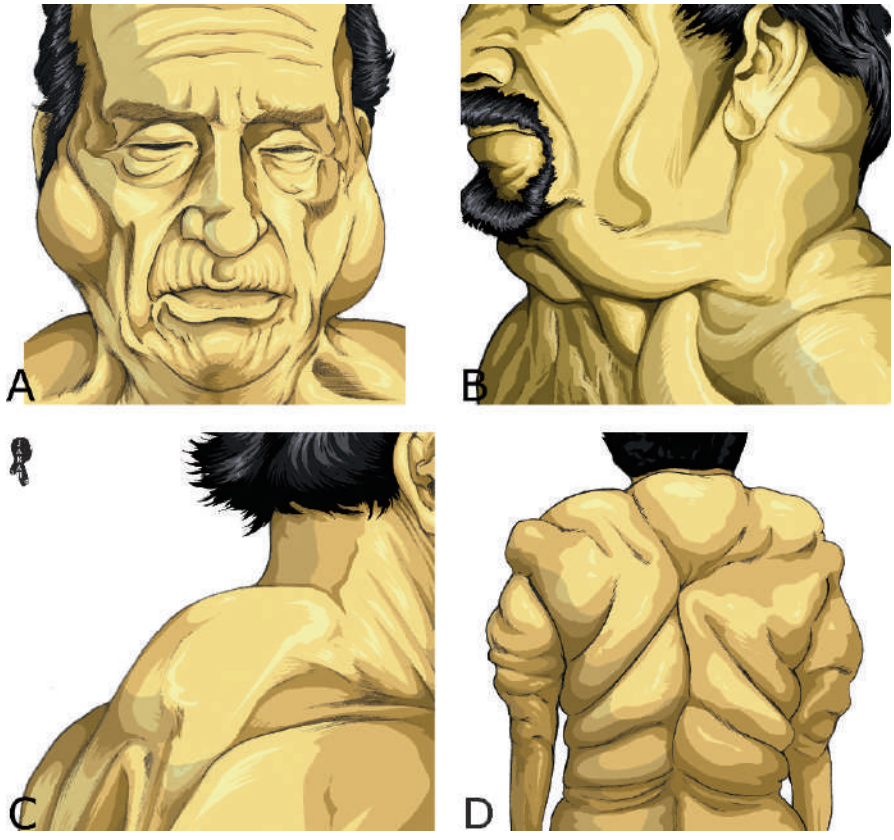

Fig. 10.5.5. An illustration demonstrates the typical clinical signs of Madelung's disease: (**a**) hamster cheeks appearance, (**b**) horse collar appearance, (**c**) buffalo hump appearance, and (**d**) pseudo-athletic appearance

Drug-Induced Obesity

10.5

- *Glucocorticoids use*: glucocorticoids cause fat accumulation in the body in a similar fashion to people with Cushing's syndrome. Glucocorticoid obesity is seen in patients with chronic prednisolon intake >10 mg/day or its equivalent.
- *Cessation of smoking*: Patients who quit smoking can gain up to 4–5 kg on average, and it is partly mediated by nicotine withdrawal.

Evaluation of Fat within the Body

There are several techniques used to estimate body fat. Anthropometry is a technique used to estimate BMI by measuring waist circumference and skinfold thickness. BMI is a good indicator of obesity, but it provides indirect measurement of body fat, and is unable to differentiate lean body mass from body fat. The inability of BMI to discriminate lean body mass from fat body mass leads to defining lean, muscular individuals as obese.

The metabolism of adipocytes varies with fat sites. Fat deposits in the abdomen and flank are more metabolically active than fat deposits in the buttocks or thighs. Upper-body obesity is more associated with hypertension, glucose intolerance, and serum cholesterol levels than is lower-body obesity. Recent research emphasizes the high risks of cardiovascular diseases and metabolic abnormalities associated with increased intra-abdominal VAT. VAT is defined as the fatty tissue that accumulates beneath the abdominal muscle wall and surrounding the abdominal viscera. VAT mass is pathologically more important than subcutaneous fat thickness over the trunk. Also, visceral fat is a major determinant of whole body insulin resistance.

Adipose tissue is a specialized loose connective tissue that is laden with adipocytes. It works as a source of energy, thermal insulation (e.g., brown fat), and as a mechanical cushion in mammals. A 70-kg man normally has 15 kg of adipose tissue, representing 21% of body mass. In contrast, fat is a term used to describe the chemical lipid component in the form of triglycerides. It can be found within adipocytes, or in pathological conditions like fatty liver. Modern methods use ultrasound, CT, and MRI as useful and accurate tools for VAT quantification.

Quantitative Assessment of Visceral Fat by US

Ultrasound can be used as a fast and easy method to quantify visceral and subcutaneous fat. Although it is not as standard as CT quantification, it is reported by many investigators to be an accurate method to quantify the abdominal wall fat thickness and preperitoneal fat thickness.

Quantitative Assessment of Visceral Fat by CT and MRI

An axial body section is taken at the level of the navel or (L4/L5), and assessment is done via a computer software program to calculate the percentage of visceral fat distribution (Figs. 10.5.6 and 10.5.7). Excess visceral fat typically separates the intra-abdominal structures. The drawbacks of the CT method are the use of radiation and the limited gantry diameter to patients less than 70 cm wide (the standard CT gantry diameter). MRI, on the other hand, is radiation-free, but more expensive in its use as a regular monitoring method. The MRI method uses the same procedures as the CT method of quantification.

Gastric Banding

Gastric banding is a widely performed surgical procedure as a surgical therapy for morbid obesity. The procedure consists of placing a silicon band around the upper part of the stomach to create a small gastric pouch that works as a stomach (neostomach). The pouch is connected to the rest of the stomach via a narrow stoma. The silicon band contains an adjustable inner balloon that can be inflated with air or fluid up to 5 cm^3, and it is connected to a reservoir that is typically sutures to the anterior rectus sheath. The stoma width normally should be within 3–4 mm.

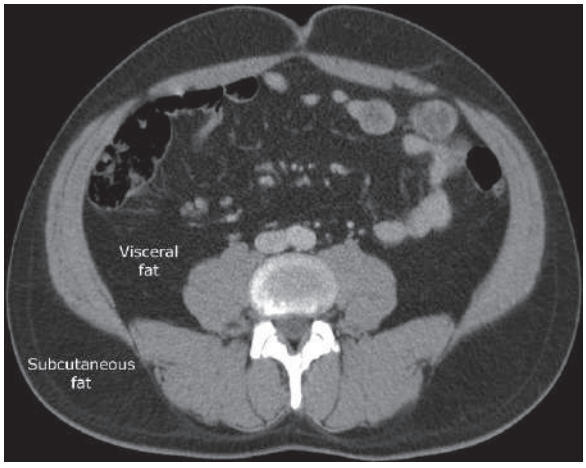

Fig. 10.5.6. An axial CT section obtained at the level of L4/L5 vertebra

The gastric banding procedure controls obesity by restricting food administration to the stomach into a small gastric pouch and narrow stoma, which creates early satiety when the pouch is full. Although gastric banding is a relatively safe procedure, several complications may arise later in up to 35% of cases. Additional surgery may be required in up to 11% of cases.

Early complications of gastric banding include esophageal perforation (0.5% of cases), dysphagia (14% of cases), gastroesophageal reflux disease, and early slippage of the band (1% of cases). Late complications include eccentric pouch dilatation (25%), slippage of the band (24%), intra-gastric band migration, and gastric necrosis (<0.3%). Patients with diabetes show early gastric dilatation due to diabetic gastroparesis.

Fluoroscopic barium meal examination is performed to detect abnormalities and complications of gastric banding. Initially, a scout supine abdominal image is taken to identify the place of the band and the reservoir. Water-soluble contrast media is initially administered in the early stages to confirm the absence of leakage. The normal images should reveal a small upper gastric pouch, a narrow stoma extending through the gastric band, and opacification of the rest of the stomach (Fig. 10.5.8). CT can be performed after the fluoroscopic examination to detect other abnormalities.

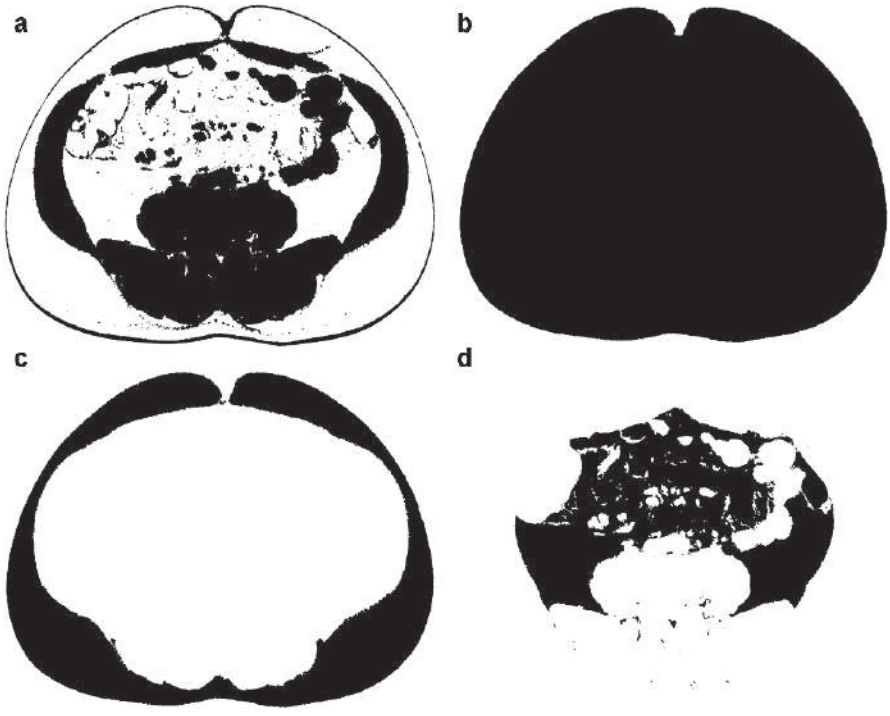

Fig. 10.5.7. Computer-generated histogram segmentation of the same CT section as (Fig. 10.5.6) done by using image analysis software (Image J). The image in (**a**) reflects fat density (represented in *white*) and the other nonfatty tissues are removed (represented in *black*). Image (**b**) represents total body volume, image (**c**) represents subcutaneous tissue volume (in back after inversion of the original *white color*), and image (**d**) represents VAT volume (in *black*). The volume of VAT or subcutaneous tissue in this image is gained in cm^2. The volume must be multiplied by the slice thickness of the original image to get the fat volume in cm^3

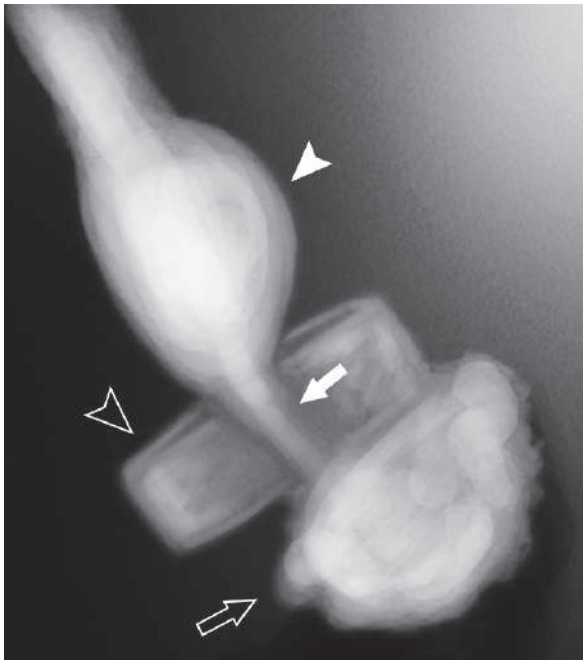

Fig. 10.5.8. Barium meal illustration shows the normal radiographic findings in gastric banding: the gastric pouch (*solid arrowhead*), the stoma (*solid arrow*), the gastric band (*hollow arrowhead*), and the gastric fundus (*hollow arrow*)

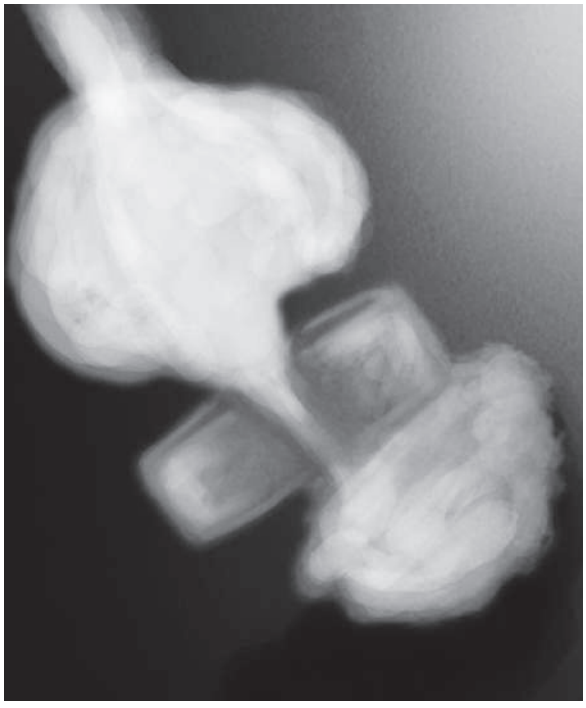

Fig. 10.5.9. Barium meal illustration shows eccentric pouch dilatation

Signs on Barium Meal

- Eccentric pouch dilatation is seen as an abnormally dilated gastric pouch. It is usually seen in patients with dietary noncompliance (Fig. 10.5.9). The gastric pouch is dilated due to chronic overfilling. The stoma is usually in its normal position.
- Pouch dilatation may also occur due to narrow stoma (Fig. 10.5.10). The scan shows pouch dilatation, with narrow stoma (2–3 mm). Patients with this kind of obstruction often present with esophageal dysmotility, vomiting, and pseudoachalasia.
- Band slippage is seen as stomach herniation above the band, resulting in pouch dilatation (Fig. 10.5.11). Patients may be asymptomatic (20%), or may present with epigastric pain, vomiting, and progressive gastroesophageal reflux disease. If not corrected, band slippage can lead to gastric volvulus and gastric necrosis.
- Intragastric migration of the band is a serious complication, in which the band gradually erodes into the gastric wall until it perforates the stomach. It is a rare complication, seen in 0.2–2% of cases. Patients present with nonspecific gastric pain, gastrointestinal bleeding, and perotinitis when perforation occurs. The herniated band edge is seen as a barium filling defect within the stomach on barium examination (pathognomonic).

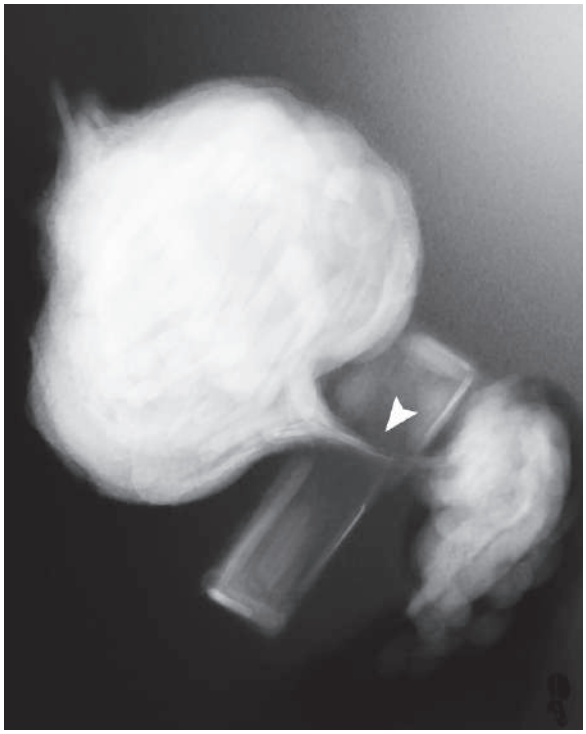

Fig. 10.5.10. Barium meal illustration shows pouch dilatation due to narrow stoma (*arrowhead*)

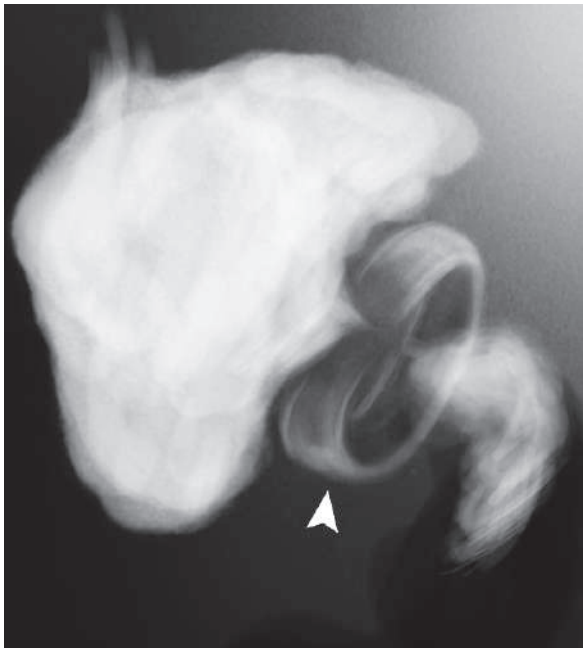

Fig. 10.5.11. Barium meal illustration shows band slippage into the dilated gastric pouch (*arrowhead*)

Liposuction

Liposuction is a procedure that allows surgical removal of excess adipose fat in healthy individuals. It is a very common and popular aesthetic surgical procedure that is performed in many countries around the world.

The main complications in fat removal procedures lies in the degree of hemostasis achieved after detachment of the subcutaneous fat layer from the skin in the area of desired fat removal. Poor hemostasis results in the formation of hematoma, seroma, infection, necrosis, and even shock and death, which was commonly seen in the old fat removal techniques that used cutting instruments. In modern liposuction techniques, the detachment of subcutaneous fat is accomplished by injecting fluid under the skin in the desired region through a blunt-edged cannula (hydrodissection). The cannula is used to create multiple tunnels within the subcutaneous fat, inject the dissecting fluid, and then pulled (rather than cut) from the neighboring structures. The liquefied dissected fat is then sucked into a container via the same cannula that injects the dissecting fluid. Classically, the amount of injected fluid equals the amount of fat to be removed (Illouz technique). The dissecting fluid is composed of isotonic saline, hyaluronidase, and perhaps lidocain, epinephrine, and sodium bicarbonate.

Liposuction is a relatively safe procedure, with overall complications occurring in approximately 5–10% of patients. Most of these complications include the formation of hematoma, seroma, edema, and skin pigmentation problems. Removal of more 3,000 mL of fat may carry the risk of severe systemic complications that require resuscitation and blood transfusion. The amount of fat removed should not exceed 6–8% of the patient's body weight and 30% of patient's body surface area. Also, blood loss should not exceed 1–1.5 units.

Causes of severe complications and death in liposuction include the development of crush syndrome and fat embolism syndrome (FES). *Crush syndrome* is a pathological condition characterized by severe shock and hypotension, anuria, coma, and death. Classically, the disease is caused by muscle disintegration that releases myoglobin into the circulation, which has toxic effect over the renal glomerule. During liposuction, the numerous tunnels created through the fat create a mechanism of subcutaneous injury similar to crush syndrome. Also, uncontrolled cannula movements may cause muscle injury, creating crisscrossed tunnels that may produce large cavities. These large cavities result in third space fluid loss, which produces severe symptoms. *FES* is a pathological situation characterized by the development of metastatic fat emboli in multiple body organs, resulting in a triad of pulmonary insufficiency, cerebral involvement, and petechial rashes. FES can result due to fat droplets leaking into the systemic circulation via ruptured veins at the site of cannula tunneling (mechanical theory), or due to the liberation of free fatty acids such as "chylomicrons" from the detached adipocytes. These free fatty acids are toxic to the pneumocytes and the capillary epithelium, producing chemical pneumonitis. FES typically manifests within 24–72 h after trauma or liposuction procedure. Neurological manifestations due to fat emboli to the brain include seizures, altered level of consciousness, focal neurological deficits, and even coma. Patients develop petechial skin rash on the head and neck region and on the upper body, which is believed to be the only pathognomonic feature (seen in 50% of cases). Laboratory findings show decreased hematocrit level, increased serum lipase level, hypoxemia,

and hypokalemia. These findings are observed during the first 24–72 h. Fluminant FES is a term reserved for severe manifestations of cardio-pulmonary obstruction by fat produced by a sudden intravascular liberation of a large amount of fat. Severe heart failure, shock and even death occur within the first 1–12 h of injury.

10.5

Signs on Radiographs

Pulmonary edema may be seen on chest radiograph if a large amount of fluid is injected subcutaneously or intravenously, or if the patient develops ARDS due to multiple pulmonary fat emboli. When pulmonary manifestations develop, the radiological signs may remain for up to 3 weeks.

Signs on US

Seromas are detected as localized fluid (anechoic) collections below the skin, whereas hematoma is seen as hypoechoic to hyperechoic masses, depending on the age of the hematoma.

Signs on MRI

When FES affects the brain, it usually results in multiple diffuse foci of hyperintensity located in the white matter of the subcortical, periventricular, and centrum semiovale regions. Characteristic multiple hyperintense foci lesions in the centrum semiovale may be seen in DWI, resulting in a "starfield pattern" (Fig. 10.5.12).

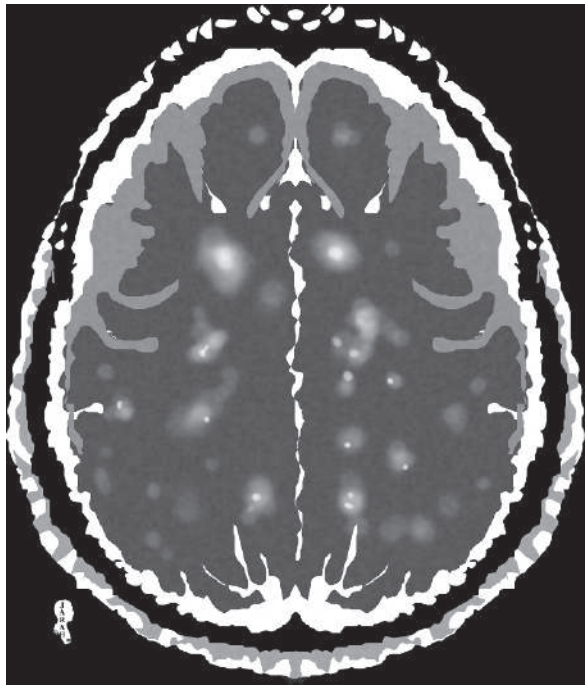

Fig. 10.5.12. Axial brain DW-illustration of a patient with fat embolism syndrome shows the starfield pattern

For Further Reading

1. Bray GA. Obesity. Dis. Mon. 1979;26(1):1–85
2. Buckley O et al European obesity and radiology department. What can we do to help? Eur Radiol (2009);19: 298–309
3. Koda M et al Sonographic subcutaneous and visceral fat indices represent in the distribution of body fat volume. Abdom Imaging. 2007;32:387–92
4. Valchos IS et al Sonographic assessment of regional adiposity. AJR Am J Roentgenol. 2007;189:1545–53
5. Bulum T et al Madelung's disease: case report and review of the literature. Diabetologia Croatica. 2007;36-2, 25–30

6. Lange U et al Dercum's disease (lipomatosis dolorosa): successful therapy with pregabalin and manual lymphatic drainage and a current overview. Rheumatol Int. 2008;29:17–22
7. Yoshida T et al Weber-Christian disease presenting with ocular manifestations. Clin Rheumatol. 2003;22:339–42
8. Nakai M et al Weber-Christian disease presenting with retroperitoneal panniculitis. Eur J Radiol Extra. 2006;60: 89–92
9. Raguse JD et al Benign symmetric lipomatosis (Madelung's disease) complicated by involvement of the facial nerve. Eur J Plast Surg. 2004;27:306–308
10. Verna G et al Launois-Bensaude syndrome: an unusual localization of obesity disease. Obes Surg. 2008;18:1313–17
11. Adami GF et al Metabolic syndrome in severely obese patients. Obes Surg. 2001;11:543–45
12. Shen W et al Adipose tissue quantification by imaging methods: a proposed classification. Obes Res. 2003;11(1): 5–16
13. Carucci LR et al Adjustable laparoscopic gastric banding for morbid obesity: imaging assessment and complications. Radiol Clin N Am. 2007;45:261–74
14. Landen S et al Complications of gastric banding presenting to the ED. Am J Emerg Med. 2005;23:368–70
15. Wiesner W et al Adjustable laparoscopic gastric banding in patients with morbid obesity: radiographic management, results, and post-operative complications. Radiology. 2000; 216:389–94
16. Trekner SW et al Imaging of morbid obesity procedures and their complications. Abdom Imaging. 2008. doi: 10.1007/s00261–008–9389–3
17. Pomerri F et al Radiological assessment of complications after laparoscopic suprabursal adjustable gastric banding for morbid obesity. Obes Surg (2009);19: 146–152
18. Illouz YG. Complications of liposuction. Clin Plast Surg. 2006;33:129–63
19. Wang HD et al Fat embolism syndromes following liposuction. Aesth Plast Surg. 2008;32:731–36
20. Chen JJS et al MR imaging of the brain in fat embolism syndrome. Emerg Radiol. 2008;15:187–92
21. Reddix RN Jr. et al Crush syndrome presenting three days after injury. Injury Extra. 2004;35:73–75

10.6

Lipoatrophic–Lipodystrophic Syndromes

Lipoatrophy syndromes are a wide group of disorders, characterized by diffuse or focal paucity of fatty tissue within the body.

Loss of fat is known as "*lipoatrophy*," whereas abnormal fat distribution is known as "*lipodystrophy*." When diabetes mellitus occurs with lipoatrophy, it is called "*lipoatrophic diabetes*."

Patients with lipoatrophy syndromes are clinically characterized by focal or diffuse loss of fatty tissue, diabetes mellitus, acanthosis nigricans, hyperandrogenism and amenorrhea in females, cardiomyopathy and muscular hypertrophy, increased appetite and high basal metabolic rate, and nonalcoholic liver steatosis or cirrhosis.

Focal lipoatrophy refers to a condition where the loss of fat involves a single region in the body. An example of focal lipoatrophy is loss of fat in the gluteal area, usually following intramuscular injection (Fig. 10.6.1).

Laboratory investigations in lipoatrophy syndromes typically show hyperinsulinemia, hyperglycemia, hypertriglyceridemia, abnormal cholesterol profile, elevated free fatty acids, and low leptin and other adipocytes hormones.

In general, radiological features show normal bone mineral density on DEXA scan and hepatic steatosis on ultrasound. However, the conventional radiographic and MRI features depend on the syndrome. Different lipoatrophy syndromes and their characteristic radiological features are discussed below.

Congenital Generalized Lipodystrophy (Seip-Berardinelli Syndrome)

Seip-Berardinelli syndrome (SBS) is a disease characterized by generalized absence of fat within the first year of life (primarily affects neonates).

As neonates grow up, they develop diabetes mellitus type 2 before the teenage years. Acanthosis nigricans, hypertriglyceridemia, and frequent bouts of pancreatitis are other common features.

The syndrome has an autosomal recessive mode of inheritance; with females showing more severe lipid profile abnormalities than males. Features of gigantism are often found in patients with SBS.

Talon cusp has been reported in cases with SBS. *Talon cusp*, also known as "eagle cusp," is an extra cusp of an anterior tooth. In the premolar teeth, an extra tooth-cusp is referred to as "*dens envaginatus*." When dens envaginatus occurs in an anterior tooth such as an incisor or a canine, it is referred to as a talon cusp (Fig. 10.6.2).

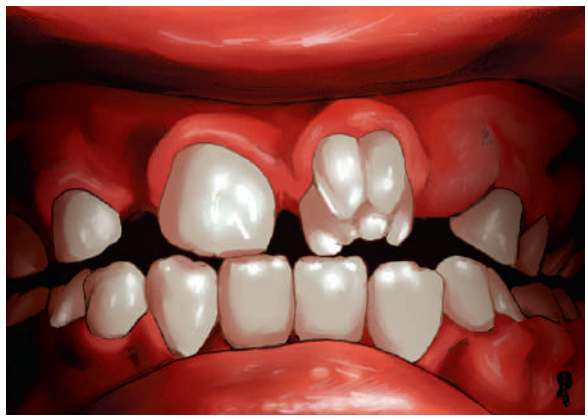

Fig. 10.6.2. An illustration demonstrates talon cusp

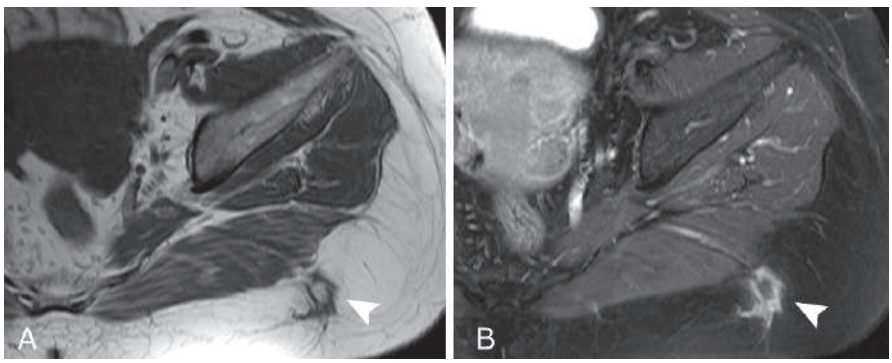

Fig. 10.6.1. Axial T1W (**a**) and T1W postcontrast fat-saturation (**b**) images show focal fatty necrosis with enhancement due to previous intramuscular injection (*arrowhead*)

Signs on Plain Radiographs

- Skeletal radiographs usually show advanced bone age plus loss of subcutaneous fat.
- Craniosynostosis may be seen in some patients (e.g., dolichocephaly).

Signs on CT and MRI

- Transverse sections of the torso at the level of the fifth lumbar vertebra often show markedly deficient subcutaneous fat and loss of the visceral fat.
- Liver cirrhosis or steatosis is a common feature of SBS.

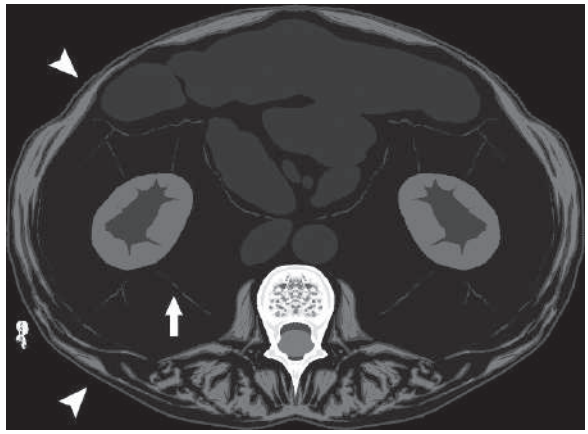

Fig. 10.6.3. Axial abdominal CT illustration demonstrates profound proliferation of the visceral fat in the retroperitonium (*arrow*), with almost complete absence of subcutaneous fatty tissue (*arrowheads*), which is a typical finding in a patient with familial partial lipoatrophy

Familial Partial Lipodystrophy (Dunnigan-Kobberling Syndrome)

Dunnigan-Kobberling syndrome (DKS) is a rare autosomal dominant disease, characterized by normal fat distribution at birth, with progressive loss of subcutaneous fat, mainly that located in the extremities and the trunk, as the patient reaches puberty. The loss of subcutaneous fat from the extremities and the trunk is associated with increased fat deposition in the face and the neck as puberty is complete.

Like SBS, DKS shows a more severe course in females than in males. Diabetes and dyslipidemia are seen in much earlier ages in females compared to males. Polycystic ovary disease is often seen in females with DKS.

The presentation of DKS may be clinically mistaken for Cushing's syndrome. The absence of fat and the well-reserved muscles in the extremities enable establishing the correct diagnosis.

Signs on CT and MRI

- The patient's body shows loss of the subcutaneous fat in the extremities and increased subcutaneous fat in the head and neck region.
- Transverse sections of the torso at the level of the fifth lumbar vertebra often show markedly reduced subcutaneous fat and increased visceral fat (Fig. 10.6.3).

Mandibuloacral Dysplasia

Mandibuloacral dysplasia (MAD) is a very rare, multisystemic, autosomal recessive disease, characterized by mandibular and clavicular hypoplasia (Fig. 10.6.4), joint contractures, acro-osteolysis, joint and skin problems, and lipodystrophy.

Patients with MAD present with loss of the subcutaneous fat of the extremities with increased visceral fat deposition.

Fig. 10.6.4. An illustration demonstrates the clinical findings in a patient with mandibuloacral dysplasia. Notice the hypoplastic mandible (micrognathia)

10.6

Signs on Plain Radiographs

- Hypoplastic clavicle and mandible (micrognathia).
- Loss of the terminal phalangeal tufts (acro-osteolysis).
- Widened skull sutures.

Acquired Generalized Lipoatrophy (Lawrence-Seip Syndrome)

Lawrence-Seip syndrome (LSS) is an acquired generalized lipodystrophy disorder. Its clinical features are similar to SBS (congenital form), but it often arises after a triggering event (e.g., infection). The key diagnosis between the two conditions is the age of presentation. SBS typically starts in neonates, while LSS starts in much older patients after a triggering event.

Fat loss in LSS is usually severe, and may lead to a dramatic change in the physical appearance. Patients often develop diabetes mellitus within 4 years from the time they starting losing fat. The fat loss is profound, and it may affect the retro-orbital fat, hands, feet, the genital area, and the bone marrow. Nephrotic syndrome is often seen in patients with LSS.

Signs on Plain Radiographs

Skeletal radiographs usually show advanced bone age plus loss of subcutaneous fat.

Signs on CT and MRI

Almost the same radiological features as SBS.

Acquired Partial Lipoatrophy (Barraquer-Simon Syndrome)

Barraquer-Simon syndrome (BSS) is a disease with a wide-range of variations, with a few shared features. Patients with BSS are typically women in their second or third decade of life, who also have autoimmune disorder (e.g., scleroderma), presenting with partial loss of fat.

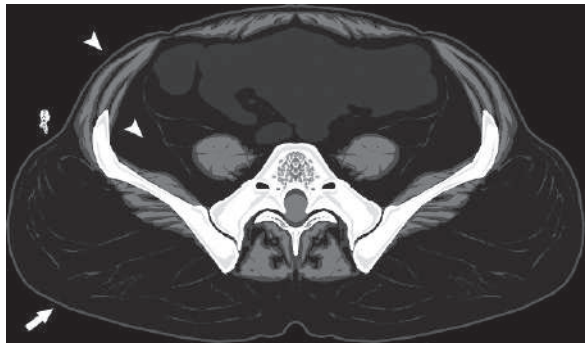

Fig. 10.6.5. Axial abdominal CT illustration demonstrates profound proliferation of the subcutaneous fat in the buttocks (*arrow*) compared to the visceral fat and the anterior abdominal wall subcutaneous fat (*arrowheads*), which is a characteristic finding in acquired partial lipoatrophy

The loss of fat in BSS typically starts from the face and descends downward until the gluteal line, with increased fat deposition in the lower extremities. Not all patients with BSS develop diabetes mellitus and dyslipidemia (only 50%).

Signs on CT and MRI

A body section of the upper abdomen shows marked reduced subcutaneous fat compared to the lower pelvis and the lower extremities (Fig. 10.6.5).

Parry-Romberg Syndrome (Progressive Facial Hemiatrophy)

Parry-Romberg syndrome (PRS) is a sporadic disease of unknown origin, characterized by slow, progressive atrophy of the face with all its components, involving the skin, subcutaneous tissues, muscles, cartilage, and bones (Fig. 10.6.6). Some authors consider PRS a focal form of lipoatrophy affecting the face, while other authors consider it a form of phakomatosis.

PRS starts at a young age, and slowly progresses as the patient gets older. Patients commonly present with epilepsy and brain abnormalities ipsilateral to the facial atrophy. Bilateral facial atrophy is seen in 5–10% of cases, and atrophy of the ipsilateral eye or enopthalmus is seen in 10–35% of cases.

Fig. 10.6.6. An illustration demonstrates the facial features in Parry-Romberg syndrome (PRS). Notice the hypoplasia of the right side of the face with mouth deviation, reduced mandible size, and eye size compared to the normal, unaffected left side of the face

Histological examinations of the facial specimens of the disease reveal proliferative interstitial neurovasculitis. PRS may be mistaken for an extensive form of linear scleroderma.

Signs on MRI

The MRI in PRS usually shows cerebral hemiatrophy, cortical calcifications, focal areas of white matter abnormalities, and meningeal enhancement, all ipsilateral to the atrophic side of the face.

For Further Reading

1. Oral EA. Lipoatrophic diabetes and other related syndromes. Rev Endocr Metab Disord. 2003;4:61–77
2. Premkumar A et al Lipoatrophic-lipodystrophic syndromes: the spectrum of findings on MR imaging. AJR Am J Roentgenol. 2002;178:311–18
3. Garg A et al Lipodystrophies: rare disorders causing metabolic syndrome. Endocrinol Clin N Am. 2004;33:305–31
4. Owen KR et al Mesangiocapillary glomerulonephritis type 2 associated with familial partial dystrophy (Dunnigan-Kobberling syndrome). Nephron Clin Pract. 2004;96:c35–8
5. Spranger S et al Barraquer-Simon syndrome (with sensorineural deafness): a contribution to the differential diagnosis of lipodystrophy syndromes. Am J Med Genet. 1997;71:397–400
6. Janaki VR et al Lawrence-Seip syndrome. Br J Dermatol. 1980;103:693
7. Lt Col Prasad AN. Berardinelli Seip syndrome. MJAFI. 2006;62:83–4
8. Sheh JJ et al Mandibuloacral dysplasia caused by homozygosity for the R527H mutation in lamin A/C. J Med Genet. 2003;40;854–57
9. Babu P et al Berardinelli Seip syndrome in a 6-year-old boy. Indian J Dermatol Venerol Leprol. 2008;74:644–46
10. Kobashi Y et al Berardinelli Seip lipodystrophy. Skeletal Radiol. 2007;36:999–1003
11. Solanski M et al Talon cusps, macrodontia and aberrant tooth morphology in Berardinelli Seip syndrome. Oral Surg Oral Med Oral Pathol Oral Radiol Endod. 2008; 105:e41–7
12. Goldberg-Stern H et al Parry-Romberg syndrome: follow-up imaging during suppressive therapy. Neuroradiology. 1997;39:873–76
13. Mako SB et al Parry-Romberg syndrome: intracranial MRI appearances. J Cranio-Maxillofacial Surg. 2003;31:321–24
14. Mazzeo N et al Progressive hemifacial atrophy (Parry-Romberg syndrome), case report. Oral Surg Oral Med Oral Pathol Oral Radiol Endod. 1995;79:30–5
15. Novelli G et al Mandibuloacral dysplasia is caused by a mutation in *LMNA*-enconding lamin A/C. Am J Hum Genet. 2002;71:426–31

Chapter 11

Infectious Diseases and Tropical Medicine

CONTENTS

J. A. Al-Tubaikh: *Internal Medicine* – An Illustrated Radiological Guide
DOI: 10.1007/978-3-642-03709-2_11, © Springer-Verlag Berlin Heidelberg 2010

11.1 Fever

Fever is a condition characterized by elevation of body temperature above the normal daily variation, along with an increase at the hypothalamic thermal set point. A substance that induces fever is called a pyrogen.

Some infections produce exogenous toxins that induce the synthesis of endogenous pyrogenic cytokines such as interleukin-1, interleukin-6, and tumor necrosis factor. These endogenous pyrogens induce the synthesis of prostaglandin E_2 (PGE_2), which elevates the hypothalamic core temperature set point. When the hypothalamic set point is raised, vasoconstriction occurs, decreasing heat loss from the skin.

Fever can be caused by infections (e.g., abscess and septicemia), neoplasms (e.g., lymphoma), inflammatory diseases (e.g., collagen vascular disease), and other causes (e.g., Kawasaki syndrome).

Pyrexia of unknown origin (*PUO*) is defined as an illness of more than 3 weeks' duration, fever >38.3°C on three occasions, and necessary initial investigations that fail to reveal the cause of the fever. The necessary initial investigations include detailed history and physical examination, complete blood count, antinuclear antibodies, rheumatic factor, urinalysis, three blood cultures, urine culture, chest radiograph, abdominal sonography, and tuberculin skin test. In 25–35% of PUO patients, a diagnosis cannot be made.

Central fever is a term used to describe fever that arises after intracerebral hemorrhage, in the absence of infection, inflammation, or a tumor explaining the fever. This fever has been attributed to cytokine-related elevation of the hypothalamic set point.

Signs on CT and MRI

In patients with suspected central fever, the examination classically shows bleeding into the thalamus and the hypothalamus (Fig. 11.1.1).

What is the difference between fever and hyperthermia?

- Hyperthermia is a condition characterized by uncontrolled increase in body temperature that exceeds the body's ability to lose heat, in conjunction with a normal hypothalamic thermal set point.
- Hyperthermia does not involve pyrogens, and does not respond to antipyretics.

For Further Reading

1. Chantal PBR et al Fever. Medicine. 2009;37(1):28–34
2. Chantal PBR et al Pyrexia of unknown origin. Medicine. 2005;33(3):33–6
3. Rudd P. Pyrexia of unknown origin (PUO). Curr Paediatr. 1996;6:105–7
4. Deogaonkar A et al Fever is associated with third ventricle shift after intracerebral hemorrhage: pathophysiological implications. Neurol India. 2005;53(2):202–7

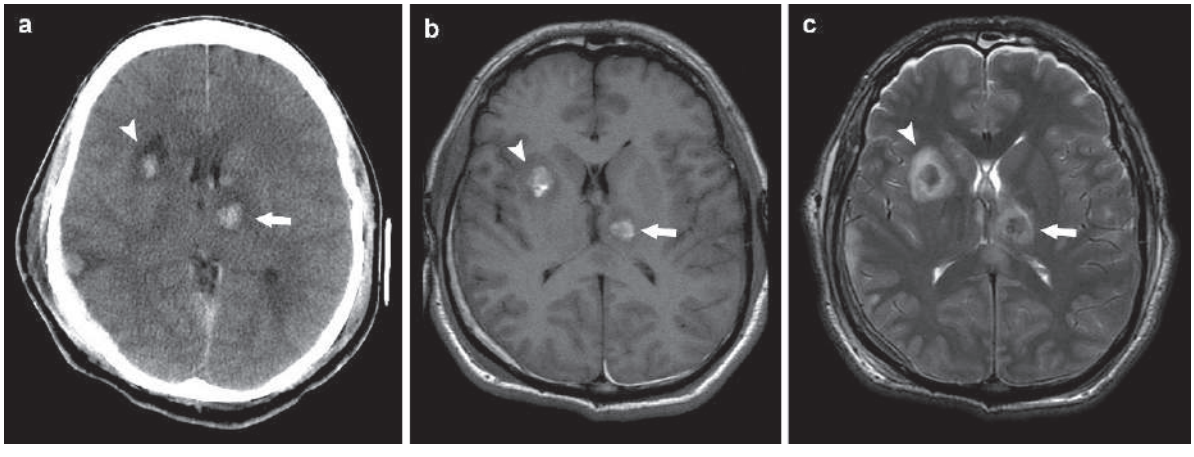

Fig. 11.1.1. Axial CT (**a**), MR-T1W (**b**), and MR-T2W (**c**) images of a 26-year-old patient with intracranial bleeding after a car accident show multiple foci of intracranial bleeding. The patient developed high-grade fever, with no signs of infection detected in the serum or the cerebrospinal fluid. The scans showed focal intracranial hemorrhage involving the right lentiform nucleus (*arrowhead*) and the left thalamus (*arrow*). The patient was finally diagnosed as having central fever and was managed accordingly

11.2 Giardiasis

Giardiasis is an infectious disease inducing fatty diarrhea caused by the intestinal protozoa *Giardia lamblia*. Protozoa are single-celled living organisms with two cell layers: an outer layer (ectoplasm) and an inner layer (endoplasm). In cases of environmental changes, the protozoa secrete a protective coat and shrink into a round, armored, infectious form called a "cyst." When humans ingest the cyst, it transforms again into the motile form and is called "trophozoite."

Giardiasis outbreak often occurs after sewage contamination of drinking water, or after drinking from clear mountain streams contaminated with *G. lamblia*. After ingestion of the cysts, the parasites transform into trophozoites in the duodenum and jejunum, and adhere to the intestinal wall. The parasites coat the duodenal and jejunal walls and interfere with fat absorption from the gut, resulting in fatty diarrhea. The parasites do not invade the intestinal wall, only coat it. The ileum is rarely affected by giardiasis.

Most patients with giardiasis are asymptomatic. Children and patients with low immunity may show mild abdominal discomfort, along with fatty diarrhea resembling celiac sprue or celiac disease diarrhea. Rarely, *G. lamblia* may invade the gallbladder, causing cholecystitis and jaundice. A concomitant infection with *Entamoeba histolytica* may be overlooked in cases of infection by a large number of *G. lamblia*.

There is an increased incidence of giardiasis in patients with hypogammaglobulinemia. Intestinal lymphoid hyperplasia (*Peyer's patches hyperplasia*) may be found in cases of giardiasis infecting a patient with hypogammaglobulinemia. Diagnosis of giardiasis is confirmed by identifying the cysts in the stool.

Differential Diagnoses and Related Diseases

Gay bowel syndrome: there is an increased incidence of giardiasis in male homosexuals with diarrhea.

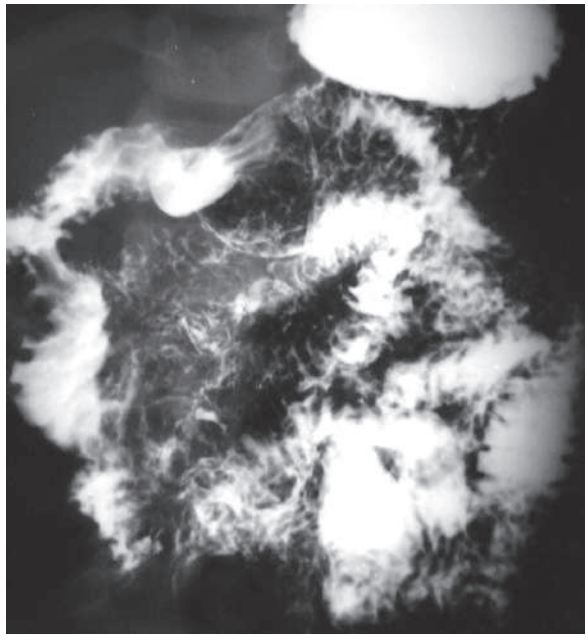

Fig. 11.2.1. Barium enteroclysis examination in a patient with giardiasis shows some irregularity and mucosal thickening of the second part of the duodenum. The proximal jejunum loops show edema, irritability, and poor filling, with thickening and separation of mucosal folds

Active male homosexuals may show cysts in the stool in up to 20% of cases.

Signs on Barium enteroclysis

As giardiasis mainly affects the duodenum and jejunum, bowel fold thickening, edema, and barium filling defects are usually seen in the duodenum and jejunum. Occasional barium segmentation or fragmentation may be seen (Fig. 11.2.1).

For Further Reading

1. Maurice MR. Radiological diagnosis of giardiasis. Semin Roentgenol. 1997;32(4):291–300
2. Heymans HSA et al Giardiasis in childhood: an unnecessarily expensive diagnosis. Eur J Pediatr. 1987;146:401–3
3. David BH et al An update review on *Cryptosporidium* and *Giardia*. Gastroenterol Clin N Am. 2006;35:291–314

11.3 Amebiasis

Amebiasis is a parasitic infectious disease caused by the protozoan *Entamoeba histolytica*. It is the second most common cause of deaths from parasitic diseases after malaria.

Amebiasis is endemic in Mexico, India, Central and South America, and East and South Africa. There is a high incidence of amebiasis among homosexual patients.

The infectious form of the parasite is the "mature cyst," which is resistant to the gastric and gastrointestinal (GI) secretions. The mature cyst can survive harsh environmental conditions, and is resistant to the conventional chlorine used to purify drinking water.

Amebiasis is initiated by ingestion of the mature cyst from infected water or food. The disease is often asymptomatic; however, multiple manifestations may be seen throughout the body, including bloody diarrhea in a small percentage of patients. Diagnosis is confirmed by identification of the amebic trophozoites in the stool or by serological identification of ameba-specific antibodies, usually 7 days after the initial symptoms of amebiasis.

Intestinal Amebiasis

Amebic invasion of the GI tract can results in different manifestations, each with its own radiological imaging features:

- *Ulcerative amebic rectocolitis (ambulatory dysentery)*: in 10% of children, the trophozoites invade and penetrate the intestinal mucosa, resulting in intestinal erosions and bleeding. This is usually manifested as 4–6 episodes of bloody diarrhea per day without systemic manifestations or fever. Complications of ambulatory dysentery include anemia due to bloody diarrhea, intussception, and/or rectal prolapse due to high-speed peristalsis.
- *Ameboma*: a granulomatous colonic lesion of ameba, with necrosis, edema, and inflammation, resembling a pseudotumor superimposed by secondary infection. It arises from the cecum or the ascending colon wall, measuring 5–30 cm. Ameboma is often solitary, but can be multiple. Patients complain of bloody diarrhea, abdominal pain, and a colonic mass.
- *Amebic appendicitis*: cannot be differentiated from classic appendicitis, unless the patient's history of bloody diarrhea is known.
- *Fulminant colitis with toxic megacolon*: a rapidly progressing disease with up to 20 episodes of bloody diarrhea within 24 h. Patients present with abdominal pain, anorexia, fever, rapid pulse, hypovolemia, and intense, constant tenesmus. There is a high mortality rate, especially when massive thrombosis of the colonic wall venules and intestinal ischemia develop.
- *Chronic amebic colitis*: this term is used to describe patients with chronic, nonspecific abdominal pain with occasional *E. histolytica* evidence in the stool.

Signs on Plain Abdominal Radiograph

Abdominal radiograph may show a dilated colon with loss of the haustrations (0.5% of cases) (Fig. 11.3.1).

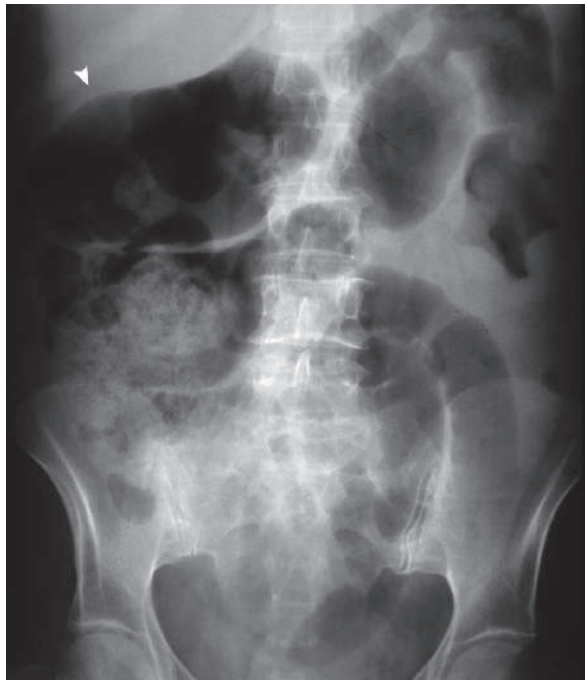

Fig. 11.3.1. A plain abdominal radiograph of a patient with chronic amebic dysentery shows toxic colonic dilatation of the ascending and the transverse colon (*arrowhead*)

Signs on Barium Enema

- *Ulcers*: seen as fine granular appearance of the mucosa with margin speculations. Deep ulcers penetrate the mucosa and result in "collar-button" ulcers.
- *Thumbprinting*: a term used to describe the shape of barium distribution inside the intestinal or colonic lumen due to edema. The barium will show filling defects at the mucosal edges as if a person's thumb has erased the barium from the edges (Fig. 11.3.2).
- *Conical cecum*: a term used to describe a rigid, ulcerated, and conical-shaped cecum. Conical cecum is often seen in intestinal tuberculosis, Crohn's disease, and amebiasis, because the cecum is affected in 90% of cases (Fig. 11.3.3).
- *Ameboma*: seen as barium filling defect that resembles a carcinoma.

Signs on CT

Colitis is seen as marked irregular thickening of the colonic wall, with enhancement after contrast administration.

Fig. 11.3.2. Intestinal barium CGI shows thumbprinting appearance (*arrowheads*)

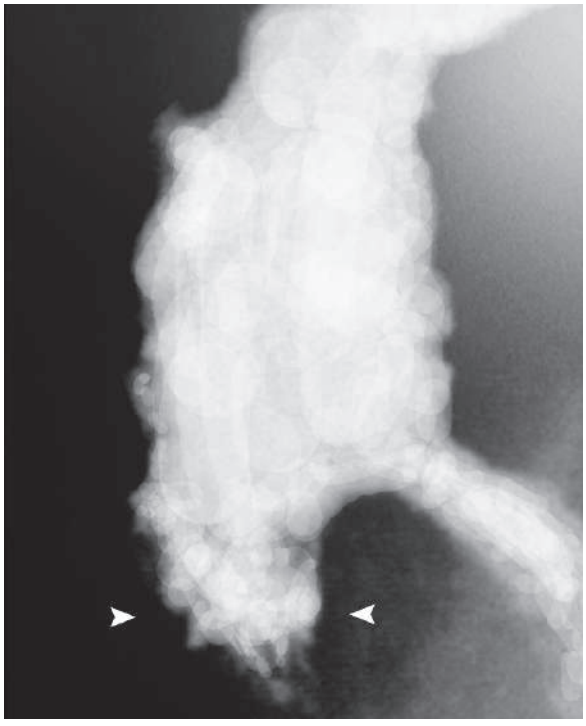

Fig. 11.3.3. Intestinal barium CGI shows the classical appearance of conical cecum (*arrowheads*)

Hepatic Amebiasis

Occasionally, the amebic trophozoites can reach the liver via the portal system and form an abscess (30% of cases). GI invasion is often seen in children, with a mortality rate of 1%, while the formation of liver abscess is often seen in adults, with a mortality rate of 0.2–2%.

Hepatic abscess may not be preceded by a history of diarrhea (59% of cases). Patients often present with sudden onset of right hypochondriac pain radiating to the shoulder or the subscapular area. There is associated fever, anorexia, vomiting, and the pain is exacerbated by deep inspiration or sitting in the right lateral decubitus position. The abscess is often seen in the right lobe of the liver. Differentiation between amebic and pyogenic hepatic abscess is important for proper patient management.

Signs on Plain Chest Radiograph

Hepatic abscess may often reveal itself in the form of a raised right hemidiaphragm (Fig. 11.3.4).

11.3

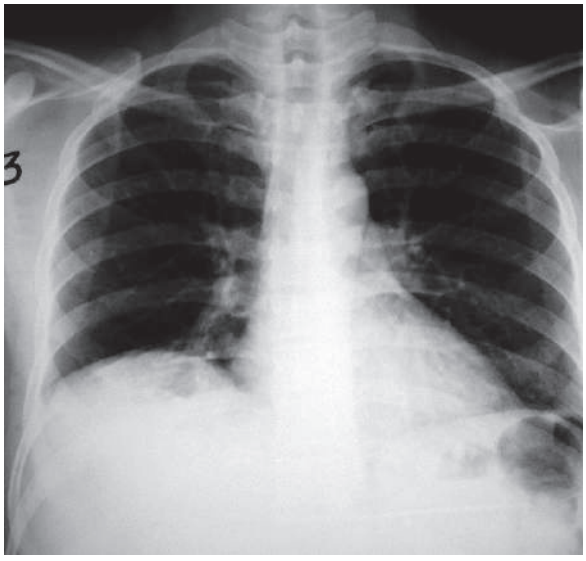

Fig. 11.3.4. A plain chest radiograph shows a raised right diaphragm due to hepatic abscess

Signs on US

Abscesses are seen as masses of heterogeneous echogenicity, with irregular wall and poor peripheral definition. Internal fluid-fluid level might be seen.

Signs on CT

Hepatic abscesses can be either *pyogenic* (bacterial) or *amebic* (parasitic) in origin. It is often difficult to differentiate between amebic and pyogenic liver abscesses based on CT appearance alone, but some radiological clues may be of use:

- *Pyogenic abscess* can present without any signs of infection, shows uniform ring enhancement after contrast injection, air fluid level may be seen inside the abscess, and it shows microabscesses (satellite lesions), which are occasionally seen as hypodense lesions >2 cm around the main abscess. A pyogenic abscess classically reveals yellowish fluid after aspiration.
- *Amoebic abscess* characteristically shows a halo of hypodensity surrounding the enhanced ring of the abscess, due to peripheral edema (Fig. 11.3.5). After aspiration, an amebic abscess classically reveals brown fluid (*anchovy sauce*

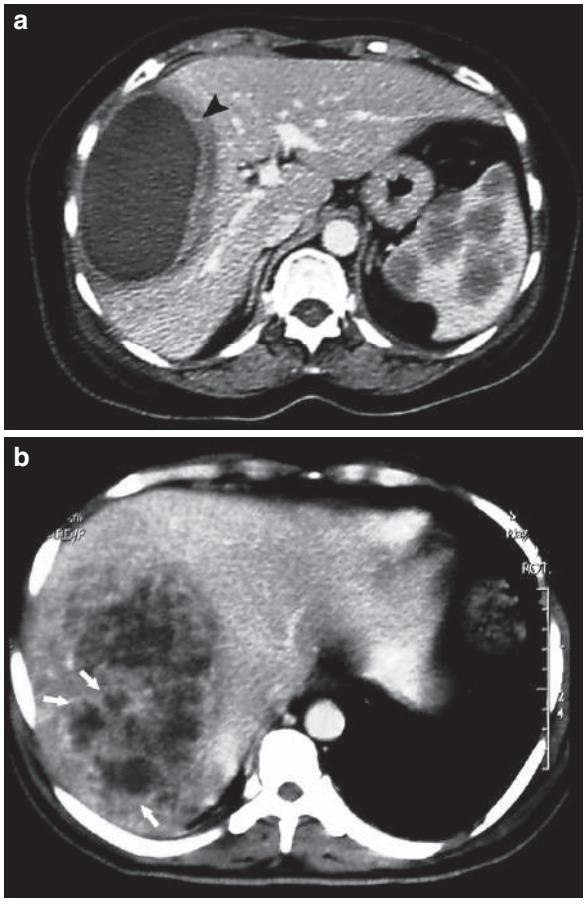

Fig. 11.3.5. Axial hepatic postcontrast-enhanced CT images in two different patients with hepatic abscesses. In one patient (**a**), an amebic liver abscess is illustrated with its characteristic halo (*arrowhead*). Notice the multiple splenic microabscesses. In the other patient (**b**), a pyogenic liver abscess is demonstrated for comparison. Notice the lack of the surrounding halo, with the presence of multiple small satellite lesions (*arrows*)

appearance), although it may be a pyogenic abscess mixed with hemorrhage from the needle. An acute amoebic abscess can transform into a chronic abscess, which is characterized by fibrosis and hard mass formation that can be mistaken for hepatocellular carcinoma.

Differential Diagnoses and Related Diseases

Meleney's synergistic gangrene is a rare complication of progressive postoperative gangrene, which arises after empyema or intra-peritoneal abscess drainage. This complication can arise due to *Staphylococcus*

aureus infection or cutaneous amebiasis. Patients often present 10–14 days post empyema or intraperitoneal abscess drainage, with truncal ulcer and severe pain. Pathologically, the ulcer is sharply demarcated, with three zones of colors: an outer bright red zone, an inner raised purple zone, and a central zone of red granulation tissue obscured by yellowish exudates.

Thoracic Amebiasis

Amebiasis from liver abscess may extend to the right lower lung lobes via invading the diaphragm. This rare complication is often seen in adults. Thoracic amebiasis is almost always secondary to amebic hepatic abscess. Empyema, pericarditis and medistinitis may occur due to amebic extension into the thoracic structures.

Signs on Plain Chest Radiograph

Chest radiograph often shows a raised right hemidiaphragm along with right basal pleural effusion, pneumonic patch, or atelectasis.

Brain Amebiasis

Brain amebiasis is a rare complication seen in 1% of patients with amebic dysentery. The parasites often reach the brain via the hematogenous route. Patients often present with convulsions, hemiplegia, meningitis, or cranial nerve lesions.

Signs on Brain CT

Amebic abscess is seen as a nonspecific parenchymal hypodense area with peripheral, uniform ring enhancement.

For Further Reading

1. Kimura K et al Amebiasis: modern diagnostic imaging with pathological and clinical correlation. Semin Roentgenol. 1997;32(4):250–75
2. Yin LS et al Left lobe amoebic liver abscess mimicking a perforated gastric tumor. Eur J Radiol Extra. 2008;66:e25–7
3. Davson J et al Diagnosis of Meleney's synergistic gangrene. Br J Surg. 1988;75:267–71
4. Cade D et al Amoebic perforation of the intestine in children. Br J Surg. 1974;61:159–61
5. Avron B et al Biochemistry of *Entamoeba*: a review. Cell Biochem Funct. 1988;6:71–86

11.4 Leprosy (Hansen Disease)

Leprosy is a chronic, granulomatous, infectious disease that mainly affects the skin and the peripheral nerves, and is caused by acid- and alcohol-fast bacilli *Mycobacterium leprae* (*M. leprae*).

Leprosy is divided into different clinical subtypes based on the capacity of the patient's immune system to resist the disease:

- *Indeterminate leprosy*: the initial form that either resolves spontaneously or progresses into the other forms according to the degree of cell-mediated immunity.
- *Tuberculoid leprosy* (*TL*): a form of leprosy that results from strong cell-mediated immune response to the disease. This type is characterized by the formation of multiple skin and nerve granulomas (tubercles), often restricted to a few locations. The granulomatous reaction in TL mimics tuberculosis, but is non-caseating.
- *Borderline leprosy*: this form represents an intermediate state between the tubeculoid and the lepromatous forms of leprosy.
- *Lepromatous leprosy* (*LL*): this form results from low immunity of the infected host, resulting in widespread, extensive disease damage. The granulomatous reaction in LL is characterized by the formation of "lepromas," which are granuloma formations mediated by macrophages engulfing live bacteria (lepra cells).

The clinical features of leprosy are determined by the host response to *M. leprae*. Skin, nerves, eyes, mucosa, and bone may all be affected by leprosy. Laboratory results often show high erythrocyte sedimentation rate, and increased finding of rheumatoid factor in LL (rheumatoid factor is positive in 58% of cases).

Diagnosis of leprosy is established via clinical examination, and identification of the acid- and alcohol-fast bacilli on skin or buccal mucosa smears stained by the Ziehl–Neelsen technique. Clinical diagnostic features of leprosy include skin lesions with definite sensory loss and thickened peripheral nerves.

Skin Involvement

In TL, the early skin manifestation is hypopigmented macules or plaques. A macule is a localized area with textural or color change of the skin, while a plaque is a palpable, plateau-like elevation of skin >2 cm in size. TL is characterized by few skin lesions, which are often dry, scaly, and hairless.

In LL, widespread symmetrically distributed macules are often seen as early skin changes. The macules are poorly defined and show erythema (redness due to vascular dilatation). If the macules are untreated, dermal infiltration occurs, which causes skin thickening. When skin thickness occurs in the face, it is called *leonine facies* (Fig. 11.4.1). The eyebrows and the eyelashes may be lost (*madarosis*). *Leprous alopecia* is characterized by scalp hair loss with preservation of the hair over the course of scalp arteries. Dystrophic nail changes, with development of peripheral edema of the legs and ankles, often occur. *Souza Campos nodule* is a rare form of TL seen in endemic areas of Brazil, where leprosy infection may infect patients during a kiss, and the highly resistant child develops a nodule at the site of the inoculation. *Lucio phenomenon* is a very rare reactional state of LL characterized by painful irregular skin patches that become purpuric and form bullae that break down, leaving widespread areas of ulceration. Healing is with scar formation. Lucio phenomenon arises due to cutaneous vasculitis.

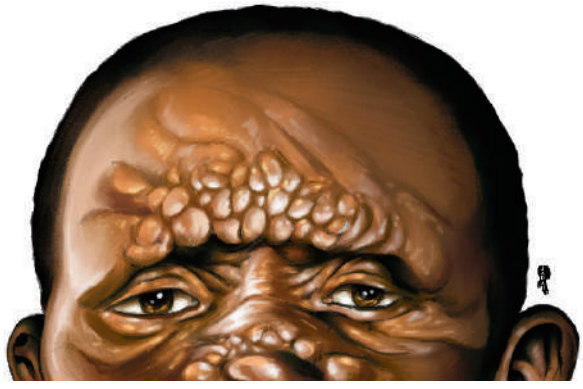

Fig. 11.4.1. Forehead skin thickening and plaques (leonine facies) with loss of the eyebrows (madarosis)

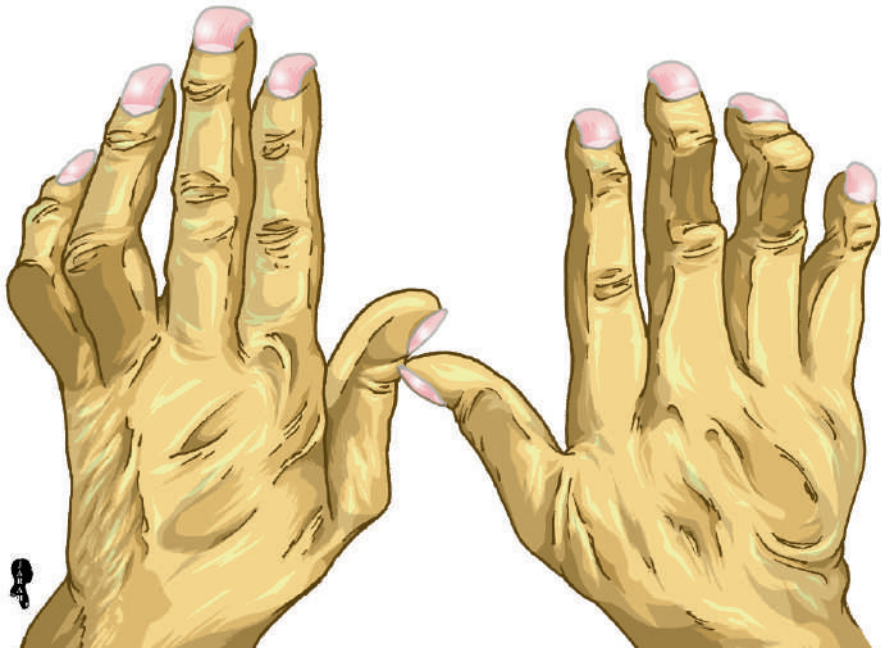

Fig. 11.4.2. Bilateral claw-hand deformities of leprosy

Nerve Involvement

Nerve involvement in leprosy affects sensory, motor, and autonomic peripheral nerves. The posterior tibial nerve is mostly affected, resulting in anesthesia of the soles and feet. Involvement of the peripheral autonomic fibers results in loss of skin sweating, with glove-and-stocking hypohidrosis, a situation similar to the changes seen in diabetic peripheral neuropathy. Loss of peripheral joint sensation causes repetitive trauma and osteomyelitis, later resulting in the development of Charcot's joint. Motor denervation of the hand causes progressive hand contracture deformity, known as "claw hand" (Fig. 11.4.2).

Eye Involvement

Blindness may occur in up to 5.3% of patients with leprosy, due to an inability to close the eyes normally (*Lagophthalmos*), corneal ulceration, secondary cataract, and chronic iridocyclitis.

Mucosal Involvement

Both the nasal and the oral mucosa may be affected by LL. Nasal mucosa involvement results in sneezing blood (epistaxis) due to ulceration, and nasal stuffiness due to formation of polyps.

The oral mucosa is affected in TL and LL patients, who are often neglected and who receive delayed treatment. Oral mucosal lesions in LL include yellowish-white plaques, nodular infiltration of the tonsils, deep ulceration of the soft palate, and elongation of the uvula (Fig. 11.4.3).

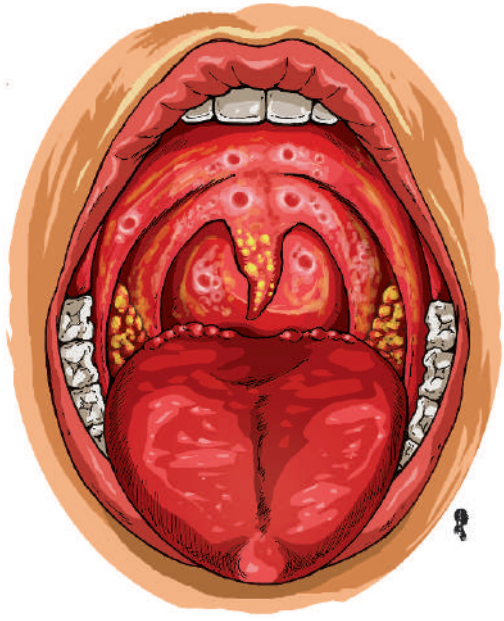

Fig. 11.4.3. Oral mucosal involvement in leprosy. There is deep ulceration of the soft palate, tonsillar abscess formation, and elongation of the uvula

11.4

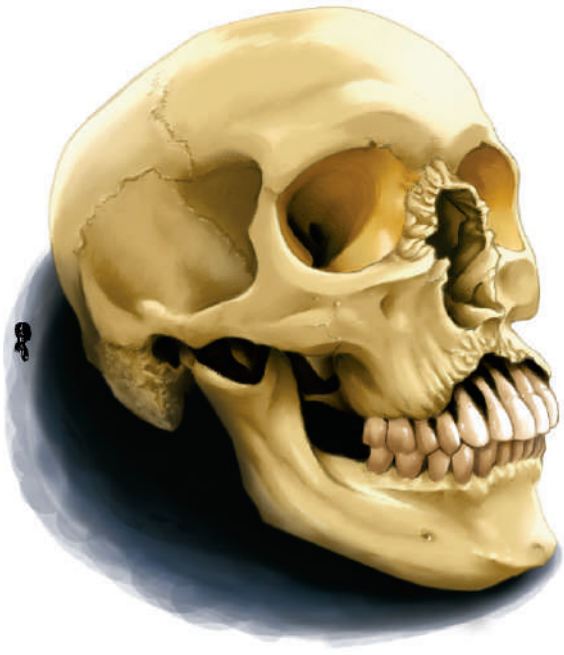

Fig. 11.4.4. Bony changes of facies leprosa. Notice the destruction of the nasal spine and the recession of the alveolar processes of the maxillae

Bone Involvement

Bone involvement in leprosy may be seen due to reactional state arthritis (explained later), development of Charcot's joint due to peripheral neuropathy, osteomyelitis, or due to destruction of facial bones by leprosy. In osteomyelitis, the bacteria directly invade the articular bone and its bone marrow, causing infection and destruction of the joint. Up to 80% of bone changes in leprosy are seen in the hands and feet.

Facies leprosa describes a triad of facial skull lesions that has been used by paleopathologists as a reliable marker for leprosy in ancient skeletal remains. The triad includes atrophy of the anterior nasal spine, atrophy and recession of the alveolar processes of the maxillae, and endonasal inflammatory changes (Fig. 11.4.4).

Post-Therapy Leprosy

When therapy is started to eliminate *M. leprae*, a cell-mediated autoimmunity may result which starts to fight both the bacteria and the normal cells, known as *reactional states*. Reactional states may also occur spontaneously, without treatment. The eyes, skin, nerves, and ears become swollen and painful. Reactional states are mainly divided into two types:

- *Type 1 (reversal) reaction*: this type of reaction is seen in patients with BL (30% of cases) and is characterized by skin and nerve inflammation, edema, and ulceration.
- *Type 2 reaction* (*erythema nodosum leprosum*): this type of reaction is seen mainly in LL (20%) and TL (10%). Symmetrical joint arthritis that involves small or large joints is a characteristic feature of patients with erythema nodosum leprosum (ENL). The arthritis can be monoarticular, oligoarticular, or polyarticular. The arthritis can be infective or sterile (reactive) arthritis. Reactive arthritis in leprosy has almost the typical clinical presentation as rheumatoid arthritis. In general, the severity of the arthritis parallels the severity of the ENL.

Signs on Radiographs

- In joint osteomyelitis, there is destruction of the juxta-articular bone, with joint collapse (Fig.11.4.6).
- Diffuse osteoporosis.

- Joint destruction due to neuropathic arthropathy (Charcot's joint) (Fig. 11.4.5).
- The phalanges often show thinning of the bone with reduction in thickness, a finding that is usually called "sucked lollipop appearance" (Fig. 11.4.6).
- *Osteitis leprosum* are localized cortical bone erosions of the phalanges and metacarpals.
- Acroosteolysis (bone resorption) of the terminal phalangeal tufts (Fig. 11.4.6).
- Contracture of the hands, with soft-tissue swelling (claw-hand deformity).

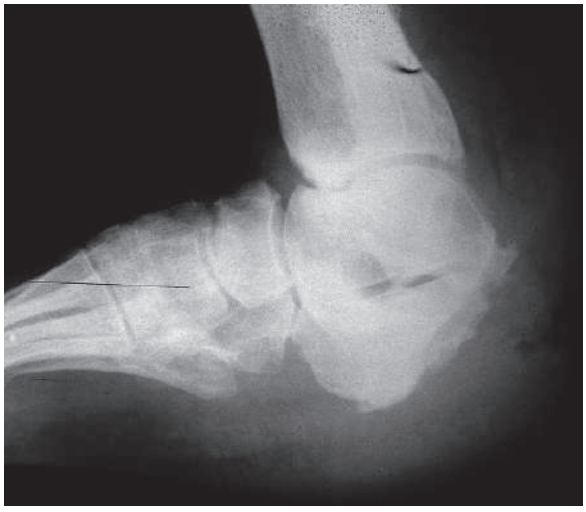

Fig. 11.4.5. A lateral ankle radiograph of a patient with leprosy shows severe calcaneus destruction

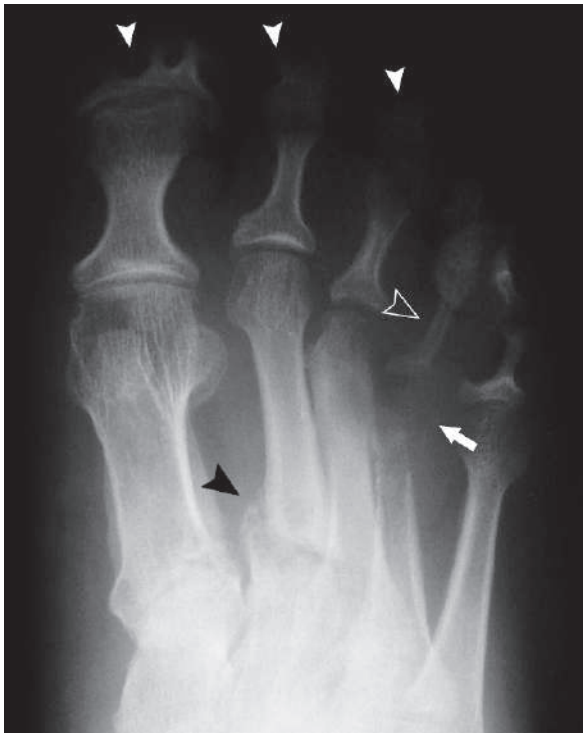

Fig. 11.4.6. An anteroposterior radiograph of the forefoot of the other foot of the same patient shows acroosteolysis of the distal phalanges (*white arrowheads*), fracture of the second metatarsal diaphysis (*black arrowhead*), sucked lollipop appearance of the fourth phalange (*open arrowhead*), and cortical destruction of the fourth metatarsal head due to osteomyelitis (*arrow*)

For Further Reading

1. Walker SL et al Leprosy. Clin Dermatol. 2007;25:165–72
2. Gibson T. Bacterial infections: the arthritis of leprosy. Baillière's Clin Rheumatol. 1995;9(1):179–91
3. Rostom S et al Neurogenic osteoarthropathy in leprosy. Clin Rheumatol. 2007;26:2153–5
4. Paira SO et al The rheumatic manifestations of leprosy. Clin Rheumatol. 1991;10(3):274–6
5. de Abreu MAMM et al The oral mucosa in paucibacillary leprosy: a clinical and histopathological study. Oral Surg Oral Med Oral Pathol Oral Radiol Endod. 2007;103:e48–52
6. David MS et al Oropharyngeal leprosy in art, history, and medicine. Oral Surg Oral Med Oral Pathol Oral Radiol Endod. 1999;87:463–70
7. Boddingius J. Ultrastructural and histopathological studies on the blood-nerve barrier and perineural barrier in leprosy neuropathy. Acta Neuropathol. 1984;64:282–96
8. Lupi O et al Tropical dermatology: bacterial tropical diseases. J Am Acad Dermatol. 2006;54:559–78

11.5 Toxoplasmosis

Toxoplasmosis is an opportunistic, protozoan infection of humans by *Toxoplasma gondii*. The name of the parasite is derived from the Greek word "toxon" meaning bow (the shape of the parasite) and "gondi," which is a local name for a desert rodent in North America that hosts this parasite.

The life cycle of *T. gondii* occurs commonly between cats and mice. The cat (definite host) harbors the parasite in its intestinal mucosa, where sexual reproduction occurs to produce the oocysts. The oocysts are passed through the cat feces into the soil. The oocysts mature into the infective form within the soil, depending on the temperature and other conditions. In the mouse, the sporozoites invade the intestinal mucosa and are distributed via the blood and lymphatics through the body. The cycle is completed when the cat ingests a mouse infected with the parasite.

Humans get *T. gondii* incidentally, as intermediate hosts, by ingestion of the oocyst in uncooked meat (pork mutton), or food contaminated with household cat feces. The transplacental route of infection from mother to fetus is also a common method of toxoplasmosis infection. Ingestion of uncooked meat is an important route of transmission worldwide. Cooking meats at high temperatures (>66°C) or freezing the meat for one day is sufficient to kill the parasite. Fast food that is improperly grilled or barbecued may still be infective, as the parasite is not killed.

Pregnant women should avoid cats, as *t*oxoplasmosis infection is one of the known infections that can pass through the placenta from the mother to her fetus, along with other infections, such as rubella, cytomegalovirus, and herpes simplex virus (collectively called the TORCH complex). Infection of the mother before pregnancy rarely results in the birth of a congenitally infected child. Half the women who are infected with *T. gondii* during pregnancy do not transmit the parasite to their fetus. Fetal infection commonly occurs in the third trimester. The effect on the fetus is more significant when transmission occurs in the first trimester. Diagnosis is confirmed by serological detection of *T. gondii* antibodies in the amniotic fluid.

Multiple manifestations are noticed in patients infected with toxoplasmosis, depending on host immunity. In immunocompetent patients, fever, hepatosplenomegaly, enlarged lymph nodes, and headache may be seen. In contrast, immunocompromised patients show more extensive clinical symptoms that include lymphadenitis, fever, myocarditis, rash, meningitis, pneumonia, and encephalitis (50% of cases). Moreover, fundoscopic examination of the retina often reveals yellowish, cotton-like patches within the globe.

In immunocompromised patients, toxoplasmosis can cause rheumatic diseases such as acute myositis that resembles polymyositis or dermatomyositis due to direct infection of the muscles, or due to autoimmune reaction affecting the muscles. Other rheumatic manifestations include fever and rheumatic-like arthritis of the small joints, with fever that resembles adult-Still's disease, and development of vasculitis and (rarely) Raynaud's phenomenon.

Signs on US

In immunocompromised patients with toxoplasmosis, hepatosplenomegaly with retroperitoneal lymphadenopathy may be detected by ultrasound.

Signs on Brain CT

- Toxoplasmosis commonly involves the basal ganglia, but other regions may be involved.
- In *congenital toxoplasmosis*, brain CT characteristically shows hydrocephalus, parenchymal atrophy, and multiple scattered parenchymal calcifications often found around the lateral ventricles and the basal ganglia (Fig. 11.5.1). Hydrocephalus almost always arises due to aqueductal stenosis.
- Retinal calcifications may rarely be seen on CT in congenital toxoplasmosis due to retinochoroiditis (pathognomonic sign of ocular toxoplasmosis) (Fig. 11.5.2).
- In immunocompromised patients, solitary or multiple hypodense lesions surrounded by vasogenic edema, with ring contrast enhancement are often detected (Fig. 11.5.3). Localization of the lesions in the basal ganglia is characteristic.

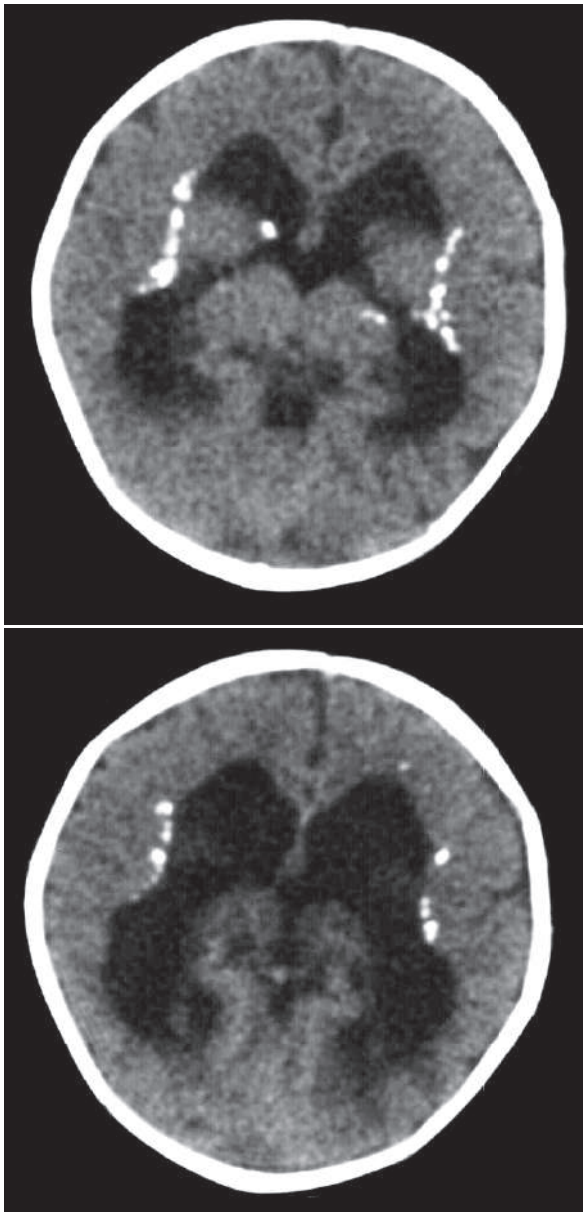

Fig. 11.5.1. Axial nonenhanced sequential CT images of a child born with congenital toxoplasmosis show brain parenchymal atrophy, moderate ventricular system dilatation (hydrocephalus), and characteristic calcification along the ventricular edges

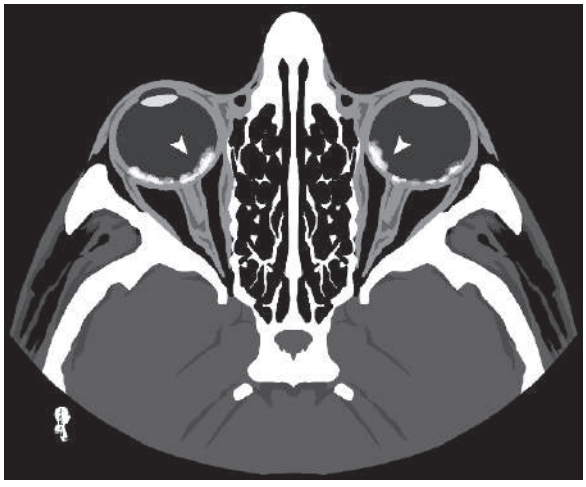

Fig. 11.5.2. Axial orbital CT illustration shows bilateral retinal calcification as a rare manifestation of toxoplasmosis (*arrowheads*)

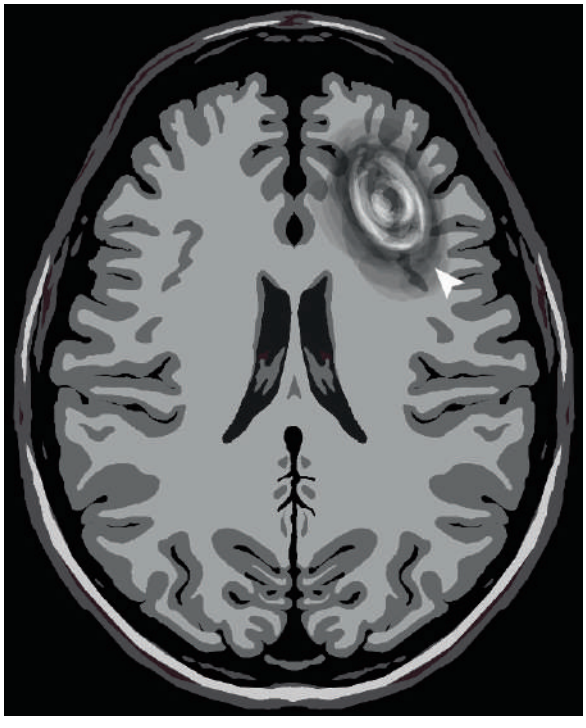

Fig. 11.5.3. Axial T1W postcontrast MRI shows toxoplasmosis lesion seen in an immunocompromised patient as a rounded lesion with vasogenic edema and ring enhancement (*arrowhead*)

11.5

- *Assymetric target sign* is a very characteristic sign of toxoplasmosis. There is an enhancing ring abscess that contains a similarly enhancing, eccentrically located nodule (Fig. 11.5.4). It is found in 30% of cases.
- A ring-like calcification may be seen in unenhanced images of treated toxoplasmosis lesions.
- Toxoplasmosis is often difficult to differentiate from lymphoma. The subcortical location of toxoplasmosis compared with the subependymal location of lymphoma, and the involvement of the corpus callosum in lymphoma that is not often seen in toxoplasmosis are helpful differentiating clues. Also, lymphoma is usually hyperdense on nonenhanced CT images, while toxoplasmosis becomes hyperdense on nonenhanced images only when the lesion is hemorrhagic or calcified.

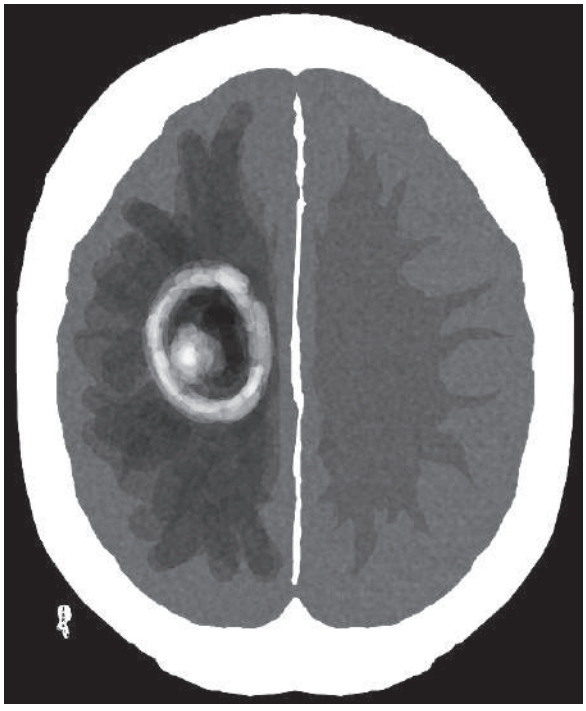

Fig. 11.5.4. Axial postcontrast brain CT illustration demonstrates toxoplasmosis asymmetric target sign in the right centrum semiovale surrounded by vasogenic edema

For Further Reading

1. Diebler C et al Congenital toxoplasmosis. Clinical and neuroradiological evaluation of the cerebral lesions. Neuroradiology. 1985;27:125–30
2. Dunn IJ et al Toxoplasmosis. Semin Roentgenol. 1998;33(1): 81–5
3. Palm C, et al Diagnosis of cerebral toxoplasmosis by detection of *Toxoplasma gondii* tachyzoites in cerebrospinal fluid. J Neurol. 2008;255:939–41
4. Yanagisawa S et al Ocular toxoplasmosis in Brazilians living in Japan. Ann Opthalmol. 2002;34(1):54–7
5. Surendrababu NRS et al Globe calcification in congenital toxoplasmosis. Indian J Pediatr. 2006;73(6):527–8
6. Navia BA et al Cerebral toxoplasmosis complicating the acquired immune deficiency syndrome: clinical and neuropathological findings in 27 patients. Ann Neurol. 1986;19: 224–38
7. Mombró M et al Congenital toxoplasmosis: assessment of risk to newborns in confirmed and uncertain maternal infection. Eur J Pediatr. 2003;162:703–6
8. Alappat JP et al A case of cerebral toxoplasmosis. Neurology India. 2000;48:185–6
9. Singh S. Mother-to-child transmission and diagnosis of *Toxoplasma gondii* infection during pregnancy. Indian J Microbiol. 2003;21(2):69–76
10. Peng SL. Rheumatic manifestations of parasitic diseases. Semin Arthritis Rheum. 2002;31:228–47

11.6

Brucellosis (Malta Fever)

Brucellosis, also known as "Malta fever," is a zoonotic disease caused by intracellular, gram-negative coccobacilli bacterium. Zoonosis is a term used to describe infections that are transmitted to humans from infected animals. The disease is named after the discoverer of the bacterium "David Bruce" in 1887. The name "Malta fever" is derived from the geographic endemic region where the fever is originally described.

Brucellosis is almost always transmitted to humans from infected animals. Different species of the bacteria are identified, and four species are responsible for most human infections: *Brucella melitensis* (found in sheep and goats), *Brucella abortus* (found in cattle), *Brucella suis* (found in swine), and *Brucella canis* (found in dogs). *B. melitensis* is the most common species infecting humans. The organism name is derived from *Melita* (honey), the Roman name for the Island of Malta.

Humans develop brucellosis after ingesting raw infected milk or dairy products such as cheese, yogurt or ice cream prepared from unpasteurized milk. Camel milk is an important source of brucellosis infection in the Middle East and Mongolia.

For *B. melitensis*, a small infective dose of ten organisms is sufficient to initiate the disease. The incubation period is between 1 week and 10 months.

Brucellosis can infect any organ, and may present with a variety of symptoms, depending on the infected organ. Patients typically present with a fever that can be acute (<2 months), subacute (2–12 months), or chronic (>1 year). The fever is typically normal during the early part of the day and rises during the night. Brucellosis is one of the common causes of pyrexia of unknown origin.

Other symptoms include influenza-like illness, sweating, malaise, myalgia, headaches, weight loss, lymphadenopathy, hepatosplenomegaly, and joint pain (arthralgia). Joint and back pain may be the first manifestations of brucellosis, and is seen in up to 40% of cases. Back pain arises either due to sacroiliitis or spondylitis. Peripheral arthritis is a common complaint, and usually affects the knees, hips, and ankles.

Unilateral epididymoorchitis is the most frequent complication affecting the genitourinary system.

The liver is commonly affected in brucellosis, and laboratory investigations often show liver enzyme abnormalities.

In 5–7% of patients, the central nervous system is affected in the form of transient ischemic attacks, meningitis, encephalitis, and demyelinating diseases. Cranial nerves may be affected in neurobrucellosis, especially the optic, abducens, facial, and the cochlear branch of the vestibulocochlear nerve in the form of neuritis. Headache due to intracranial hypertension is a common symptom in neurobrucellosis. Diagnosis can be confirmed by identifying *Brucella* antibodies in the cerebrospinal fluid (CSF) or the serum. The organism is rarely isolated from the CSF.

The spine is commonly infected by brucellosis via hematogenous spread though the lumbar venous plexus. The lumbosacral region is the most frequently affected (60%), followed by the thoracic region. Spondylodiscitis and vertebral osteomyelitis are common findings. Back pain and large joints arthralgia are described in up to 15% of cases of chronic spinal brucellosis.

The skin is involved in 1–12% of patients, mostly females, in the form of vasculitis or erythema nodosum. Up to 2% of brucellosis deaths are attributed to *Brucella* endocarditis.

Brucellosis diagnosis is confirmed by demonstrating *Brucella*-specific antigens in the serum, blood culture (definite diagnosis), or by polymerase chain reaction performed on any clinical specimen.

Signs on Plain Radiographs

- Spondylitis often begins in the superior vertebral end plates. The organisms are located in the anterior part of the end plate, initiating epiphysitis. Erosion and destruction of the anterior-superior part of the end plates with new bone formation is a characteristic sign of vertebral brucellosis (*Pons' sign*) (Fig. 11.6.1).
- The healing process is marked by dense sclerosis, with the formation of anterior-superior end plate "parrot-peak" osteophytes.

11.6

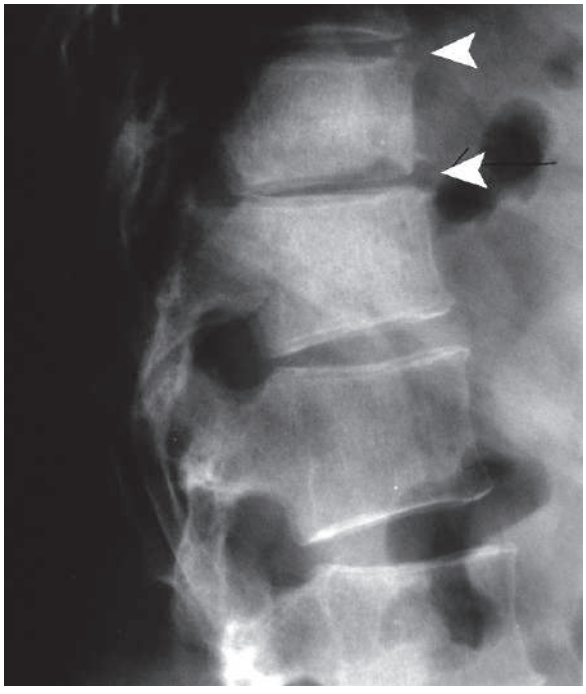

Fig. 11.6.1. Lateral plain radiograph of the lower thoracic vertebrae in a patient with brucellosis shows spondylitis affecting the anterior-superior and the anterior-inferior vertebral end plates (*arrowheads*)

Signs on US

- Brucellosis epididymoorchitis is seen as a focal, hypoechoic mass near the testes, with marginal flow signal on color flow Doppler sonography, reflecting hyperemia. The normal epididymus does not show high flow signal on color flow Doppler sonography.
- Hydrocele and scrotal skin thickening may be found.
- The resistance index may be reduced due to hyperemia, with low-resistance arterial flow pattern seen on pulsed Doppler sonography.

Signs on MRI

- Signs of encephalitis or meningitis may be seen.
- Enhancement of the cranial nerves is detected when neuritis is suspected clinically.

The main problem in diagnosing brucellosis of the spine is to differentiate it from tuberculosis (TB) of the spine. How can you differentiate between the two conditions?

- Brucellosis commonly affects the lumbosacral vertebrae, while TB commonly affects the thoracic vertebrae.
- The vertebral height is preserved in brucellosis, while it is severely damaged in TB.
- The posterior elements and the epidural sac are usually spared in brucellosis, while they are affected in TB.

For Further Reading

1. Mantur BG et al Review of clinical and laboratory features of human brucellosis. Indian J Med Microbiol. 2007;25(3):188–202
2. Metin A et al Cutaneous findings encountered in brucellosis and review of the literature. Int J Dermatol. 2001;40:434–8
3. Glasgow MMS. Brucellosis of the spine. Br J Surg. 1976;63: 283–8
4. Mays SA. Lysis at the anterior vertebral body margin: evidence for brucellar spondylitis? Int J Osteoarchaeol. 2007;17:107–18
5. Koc Z et al Gonadal brucellosis abscess: imaging and clinical findings in 3 cases and review of the literature. J Clin Ultrasound. 2007;35:395–400
6. Bayram MM et al Scrotal gray-scale and color Doppler sonographic findings in genitourinary brucellosis. J Clin Ultrasound. 1997;25:443–7
7. Estevão [AU1]MHL et al Neurobrucellosis in children. Eur J Pediatr. 1995;154:120–2
8. Bilen S et al Four different clinical manifestations of neurobrucellosis. Eur J Intern Med. 2008;19:e75–7
9. Jochem T et al Neurobrucellosis with thalamic infarction: a case report. Neurol Sci. 2008;29:481–3
10. Guney F et al First case report of neurobrucellosis associated with hydrocephalus. Clin Neurol Neurosurg. 2008;110:739–42
11. Tali ET et al MRI of brucella polyneuritis in a child. Neuroradiology. 1996;38:S190–2

11.7 Neurocysticercosis

Cysticercosis is a parasitic disease caused by human infection with *Taenia solium*, the pork tapeworm.

The definitive host of *T. solium* is the pig. The larvae are ingested by humans in improperly prepared, infected pork meat. After ingestion, the larvae attach themselves to the intestinal mucosa and develop into adult tapeworms in 5–12 weeks. The tapeworm eggs contain active embryos (oncospheres), which are excreted in the stool. Pigs ingest the infected stool and the oncospheres are liberated into pigs' gastrointestinal tract, enter the mesenteric circulation, and develop into larvae in various tissues, completing the life cycle. Cysticercosis is endemic in parts of Asia, Thailand, India, Europe, and Latin America.

Cysticerci are found in various human tissues, but they have affinity for the central nervous system (neurocysticercosis). The clinical findings in neurocysticercosis are often nonspecific, and diagnosis is confirmed only by imaging and laboratory cerebrospinal fluid (CSF) studies. Patients commonly present with headaches, seizures (70%), and neurological deficits. Arachnoiditis, infarction, and obstruction of the ventricular system by intraventricular lesions or reactive ependymitis may occur.

Neurocysticercosis can be found within the brain parenchyma, within the arachnoid space, the intraventricular space, and (very rarely) within the spinal cord (<1% of cases).

Cisternal or subarachnoid cysticercosis is caused by two types of larval worms: *Cysticercus cellulosae* and *Cysticercus racemosus*. They are usually found in the basal cisterns, sylvian fissures, or ventricles.

Signs on Plain Radiographs

When the larval cysts are killed by the inflammatory reaction within muscles and subcutaneous tissues, calcification of the dead cysts is seen as ovoid flecks of calcification resembling grains of rice (rice grain calcification). These calcifications are characteristic of cysticercosis, and usually parallel the long axis of the muscle.

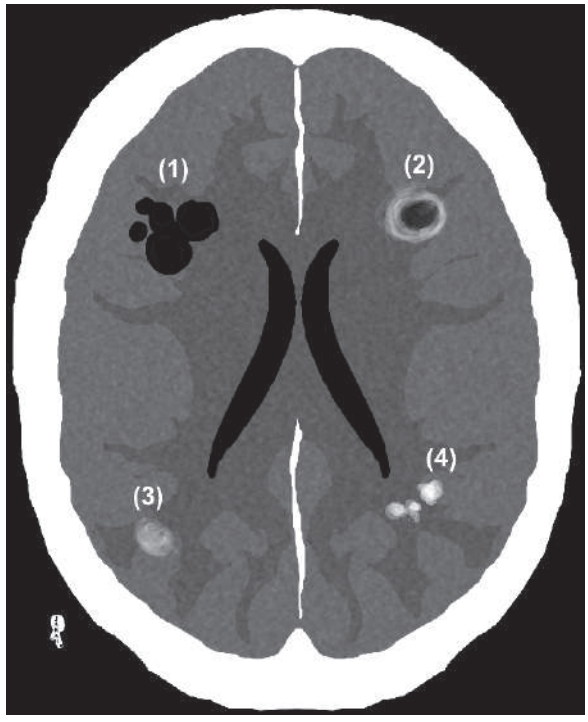

Fig. 11.7.1. Axial brain CT illustration shows the four stages of neurocysticercosis: (1) vesicular stage, (2) colloidal stage, (3) granular stage, and (4) calcified stage

The CT and MRI findings in neurocysticercosis mainly depend on the stage of the disease; four stages are recognized:

- *Stage 1 (vesicular stage)*: in this stage (Fig. 11.7.1), the cysticerci are viable, with immune tolerance. There is a cystic lesion in the brain with little or no sign of acute inflammation, because the cyst is able to escape the host's immune system surveillance. The cyst shows no contrast enhancement. A small eccentric nodule may be found within the cyst, which represents the parasite's head or scolex (Fig. 11.7.2). This is referred to as *hole-with-dot sign*, and it is almost a pathognomonic sign of neurocysticercosis. Single or multiple cysts may be found anywhere within the brain. Patients are often asymptomatic in this stage.
- *Stage 2 (colloidal stage)*: this stage develops after years, when the larvae start to die. The immune system starts an inflammatory response, and the fluid within the cyst becomes opaque. The cyst wall is thickened and shows contrast enhancement

11.7

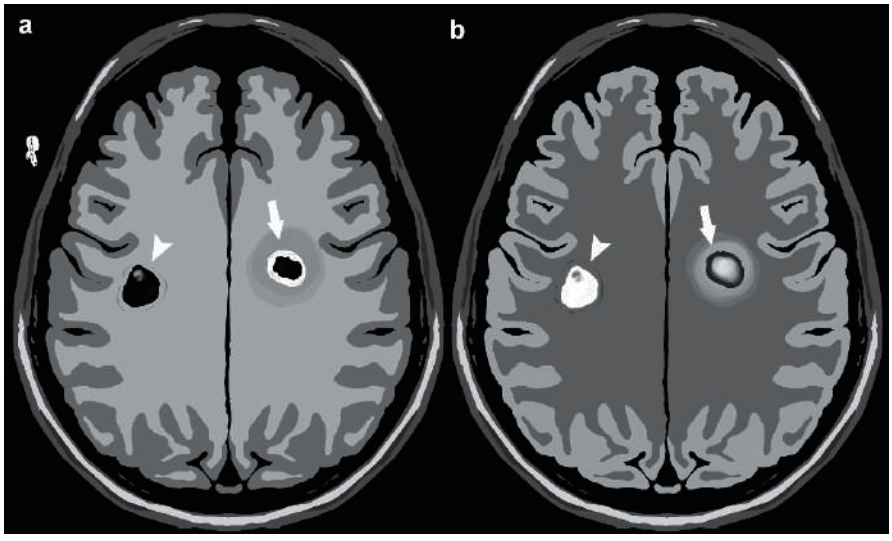

Fig. 11.7.2. Axial T1W postcontrast (**a**) and T2W (**b**) brain MR illustrations show different neurocysticercosis stages. In (**a**) and (**b**), the right cyst represents the vesicular stage, with eccentric scolex (*arrowheads*). The left cyst represents the colloidal stage, with rim contrast enhancement and edema around the cyst (*arrows*)

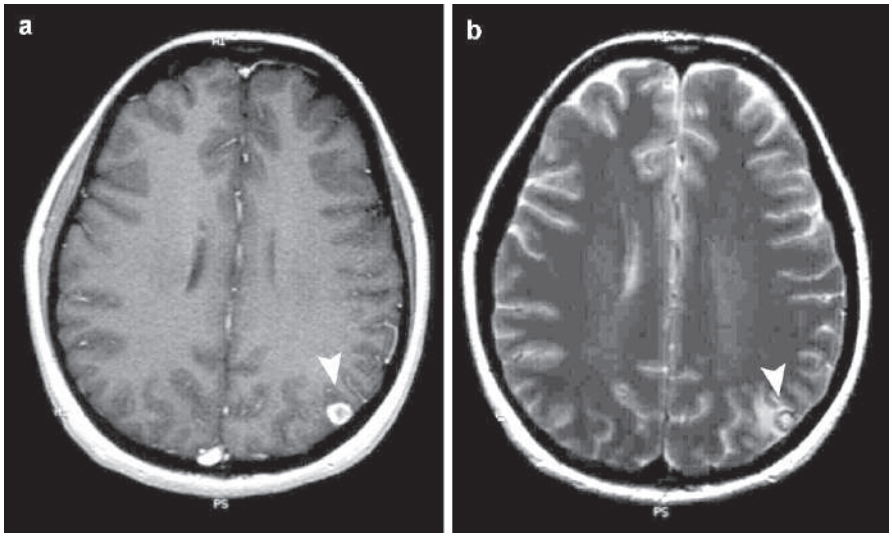

Fig. 11.7.3. Axial T1W postcontrast (**a**) and T2W (**b**) brain MR images of colloidal stage neurocysticercosis (*arrowheads*)

(Figs. 11.7.2 and 11.7.3). Edema around the lesions is demonstrated on T2W and FLAIR images.

- *Stage 3 (granular stage)*: in this stage, the colloid cyst is transformed into a nodular granuloma (Fig. 11.7.1). The lesion is nodular, with low T1/T2 signal intensities, surrounded by perifocal edema.
- *Stage 4 (calcified stage)*: in this stage, deposition of calcium occurs within the granuloma, and the lesion is calcified (Fig. 11.7.1). This stage is best demonstrated by CT.
- *Miliary neurocysticercosis*: this uncommon form of neurocysticercosis is characterized by small (3–5 mm), bilateral symmetrical nodular cystic parenchymal lesions with marked edema (Fig. 11.7.4). This form is often seen in children and young adults.
- *Racemose neurocysticercosis* is found in the subarachnoid space or the basal cisterns, with a similar signal and density to the CSF on MRI or CT, respectively. Racemose neurocysticercosis may manifest as a large lobulated (resembling bunch of grapes) cyst compressing the adjacent structures. It also frequently infiltrates the basal meninges, causing extensive meningitis and fibrosis. The cyst typically shows no scolex or contrast enhancement. The combination of a large lobulated cyst with no mural nodule inside it and enhanced basal meninges strongly suggests

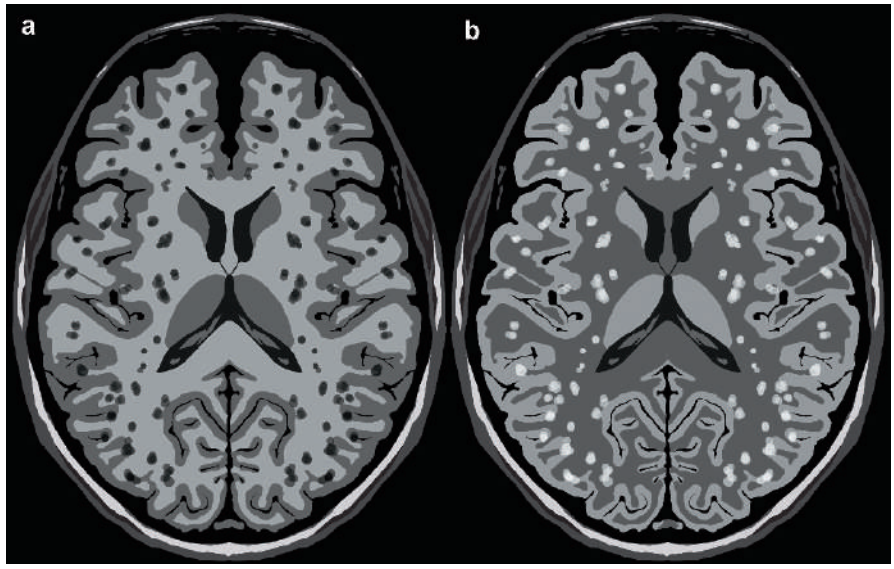

Fig . 11.7.4. (Axial T1W (**a**) and T2W (**b**) MR-illustrations show the radiological appearance of miliary neurocysticercosis)

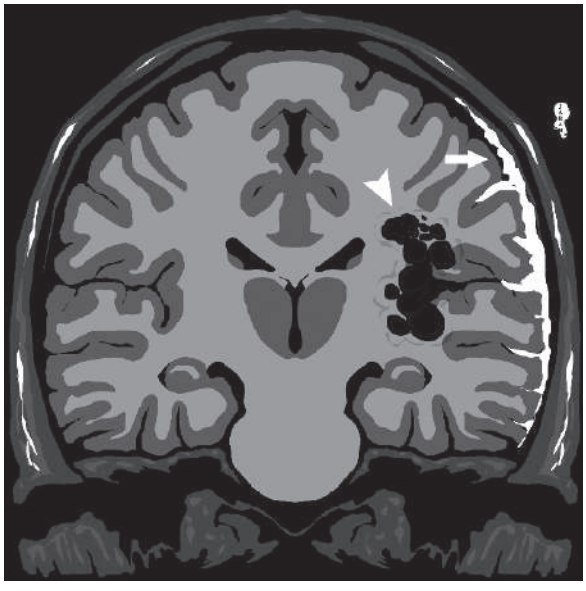

Fig. 11.7.5. Coronal postcontrast T1W brain MR illustration demonstrates left lobulated cystic lesions within the sylvian fissure (*arrowhead*), representing racemose neurocysticercosis with leptomeningitis ipsilaterally (*arrow*)

racemose neurocysticercosis, especially in endemic areas (Fig. 11.7.5).

- *Intraventricular neurocysticercosis* is seen as intraventricular round lesions with signs of hydrocephalus due to ventricular obstruction.
- *Intraspinal neurocysticercosis* is seen on MRI as an intramedullary cystic mass with fluid signal with wall enhancement according to the stage. Serological testing of the CSF is helpful to establish the diagnosis.

For Further Reading

1. Palacios E et al Computed tomography and magnetic resonance imaging of neurocysticercosis. Semin Roentgenol. 1997;32(4):325–34
2. Dumas JL et al Parenchymal neurocysticercosis: follow-up and staging by MRI. Neuroradiology. 1997;39:12–8
3. Yeh SJ et al Neurocysticercosis presenting with epilepsia partialis continua: a clinicopathologic report and literature review. J Formos Med Assoc. 2008;107(7):576–81
4. Ruiz-García M et al Neurocysticercosis in children. Clinical experience in 122 patients. Child's Nerv Syst. 1997;13:608–12
5. Chang KH et al MRI of CNS parasitic diseases. JMRI. 1998; 8:297–307
6. Roche CJ et al Selections from the buffet of food signs in radiology. RadioGraphics. 2002;22:1369–84

11.8 Ascariasis

Worms, also known as "helminthes," are parasitic infections. Diagnosis is usually made by identifying the worm eggs in the stool.

Ascariasis is a parasitic disease that arises due to ingestion of food contaminated by the eggs of the roundworm (nematodes) *Ascaris lumbricoides*. Most patients are children between 1–15 years of age. Consuming uncooked vegetables and drinking polluted water from wells are important sources of ascariasis infection.

After ingestion of the eggs, the larvae hatch from the eggs before they reach the intestine, due to stimulation by gastric juices. The larvae penetrate the intestinal wall, enter the bloodstream, and travel via the portal venous or the lymphatic systems to the liver and then to the thoracic cavity. When they reach the lungs, the larvae grow and mature within the lung alveoli. When the worms are mature enough, they migrate from the lungs into the bronchi and from the trachea to the epiglottis, from where they are swallowed into the intestine for the second time. The matured larvae grow into adult worms in the intestine, especially the jejunum, and produce eggs that pass out in the feces. Up to 99% of ascarids are found in the jejunum and ileum.

Most patients are asymptomatic, although severe ascariasis infection can cause abdominal cramps and malnutrition. The worms may also invade the gallbladder, appendix, liver, or bile duct. Ileocecal intestinal obstruction, ascending cholangitis, cholecystitis, appendicitis, and liver abscess are documented complications of ascariasis.

Respiratory symptoms in the form of fever, hemoptysis, cough and pneumonia (*ascariasis pneumonia*) occur 5–26 days postinfection. The alveoli are filled with eosinophils and white blood cells attacking the larvae. Ascariasis is one of the most common causes of *Loffler's syndrome* (fever, systemic eosinophilia, asthma, cough with sputum, and signs of alveolar infiltration on chest radiograph). The adult worm can produce a neurotoxin that can result in neurological manifestations (*ascariasis encephalopathy*).

Diagnosis is made by identifying the ascaris eggs in the feces, and pronounced eosinophilia on complete blood count.

Differential Diagnoses and Related Diseases

Visceral larva migrans (*VLM*) is a disease characterized by the invasion and residence of animal parasites in human tissues for a long time. The disease is often seen in children, and often caused by *Toxocara canis* (from dogs) *and Toxocara cati* (from cats). Rarely, VLM can be caused by pig's roundworm, *Ascaris suum*, which is closely related to human roundworm, *Ascaris lumbricoides*.

Signs on Chest Radiograph

- Signs of patchy alveolar infiltration.
- A pulmonary nodule can occur if the larvae form a granulomatous lesion when they die.

Signs on Ultrasound

- In the gallbladder, the ascaris worm is identified as a tubular structure with nondirectional movement causing a zig-zag sign. The tubular structure has 3–4 parallel echogenic lines in longitudinal axis and a target sign in transverse axis.
- When the gallbladder is full of worms, echogenic, intraluminal, and spaghetti-like structures are seen.

Signs on Barium enteroclysis

- The ascarides are seen as long, tubular filling defects within the intestinal lumen in the jejunum or the ileum (Fig. 11.8.1).
- The worm may ingest the barium, which will cause its gastrointestinal opacification, resulting in *double contrast* worm appearance around the barium (Fig. 11.8.1).

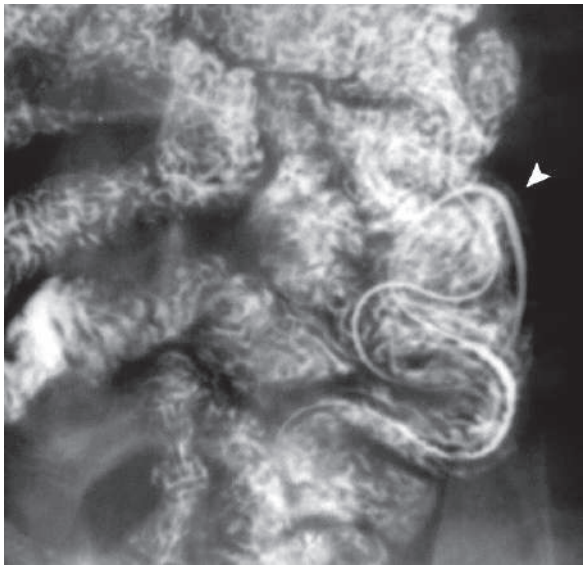

Fig. 11.8.1. Barium enteroclysis radiograph of a patient with ascariasis shows a long, tubular filling defect in the jejunum, with a double contrast sign representing ascaris worm with barium ingestion (*arrowhead*)

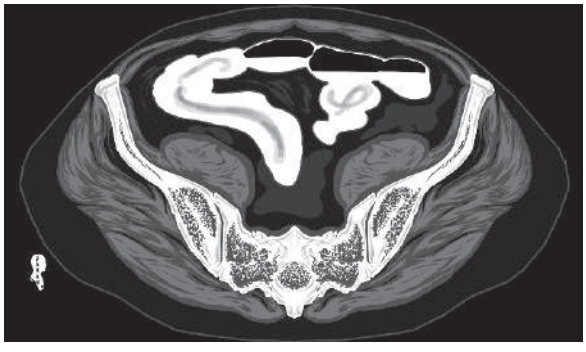

Fig. 11.8.2. Axial CT illustration demonstrates ascaris worms within the intestinal bowel loops

Signs on CT

- On bowel oral contrast-enhanced CT, the worm is seen as a tubular filling defect within the bowel loops (Fig. 11.8.2). A thin enhanced line within the tubular defect can be seen representing contrast within the gastrointestinal tract of the worm due to contrast ingestion.
- In the gallbladder, the worms are seen as tubular, coiled soft-tissue structures within the gallbladder with no contrast enhancement. Speckles of curvilinear calcifications may be seen.

For Further Reading

1. Kakihara D et al Liver lesions of visceral larva migrans due to *Ascaris suum* infection: CT findings. Abdom Imaging. 2004;29:598–602
2. Robbani I et al Worms in liver abscess: extensive hepatobiliary ascariasis. Dig Liver Dis. 2008;40(12):962. doi: 10.1016/j.dld.2008.03.008
3. Ochoa B. Surgical complications of ascariasis. World J Surg. 1991;15:222–7
4. Maheshwari PR. Gall bladder ascariasis. Clin Radiol Extra. 2004;59:8–10
5. Sherman SC et al The CT diagnosis of ascariasis. J Emerg Med. 2005;28(4):471–2
6. Slesak G et al Obstructive biliary ascariasis with cholangitis and hepatic abscess in Laos: a case report with gall bladder ultrasound video. J Infect. 2007;54:e233–5
7. Reeder MM. The radiological and ultrasound evaluation of ascariasis of the gastrointestinal, biliary, and respiratory tracts. Semin Roentgenol. 1998;33(1):57–78
8. Hayashi K et al Hepatic imaging studies on patients with visceral larva migrans due to probable *Ascaris suum* infections. Abdom Imaging. 1999;24:465–9

11.9 Guinea Worm Disease (Dracunculiasis)

Dracunculiasis is an infection of the body by *Dracunculus medinensis*, a tissue-invasive round worm (nematode).

The name "Medinensis" is derived from the frequency of human guinea worm infestation near Medina, a city in Saudi Arabia. It is a disease that is seen in the Middle East, Asia, and Africa.

The parasite enters the body through drinking water infected with the larvae, which penetrate the intestine and enter the blood stream to lie deep within the subcutaneous tissues. The worm can grow under the skin up to 100 cm, and usually exposes its uterus out of the host body through the skin to release its larvae into the water.

Patients infected with *D. medinensis* often present with allergic symptoms, nausea, and vomiting. Patients also present with skin blisters, sterile abscess, and (uncommonly) septic arthritis. The worm can be sensed under the skin within the abscess.

D. medinensis tends to migrate into the lower extremities, breast, and scrotum. Other sites in the body might be affected as well. It rarely affects the viscera.

The adult worm can directly invade any joint, resulting in monoarthritis. The knee is the most common joint involved, resulting in an intense destructive arthropathy (*Ibadan knee*). Other manifestations include sterile monoarthritis due to immune complexes, also commonly affecting the knee.

The worm is often removed from the skin by driving a small stick under the part of the worm that is looped out of the skin, and the worm is slowly twisted to pull it out of the subcutaneous tissues (Fig. 11.9.1).

Fig. 11.9.1. An illustration demonstrates the classical method of extracting the guinea worm from the body. The worm is wrapped around a stick and slowly pulled out. The worm can be very long, and the process of pulling the worm out may take days

Signs on Radiograph

When the female worm dies, it will calcify, giving an intact, long, curvilinear, and beaded radio-opaque shadow in the radiograph, and this is diagnostic. No other parasite condition simulates this long, beaded full worm calcification within the muscles or the soft tissues in the body (Figs. 11.9.2 and 11.9.3).

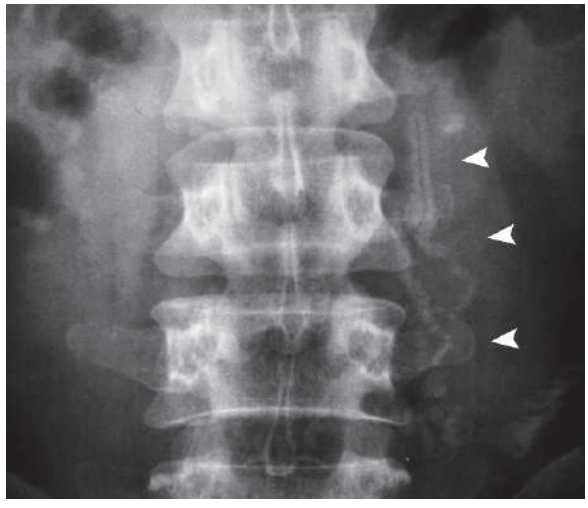

Fig. 11.9.2. Anteroposterior plain radiograph of the thoracic spine shows linear, beaded, radio-opaque shadow in the left paraspinal region in a patient with dracunculiasis, representing a dead worm (*arrowheads*)

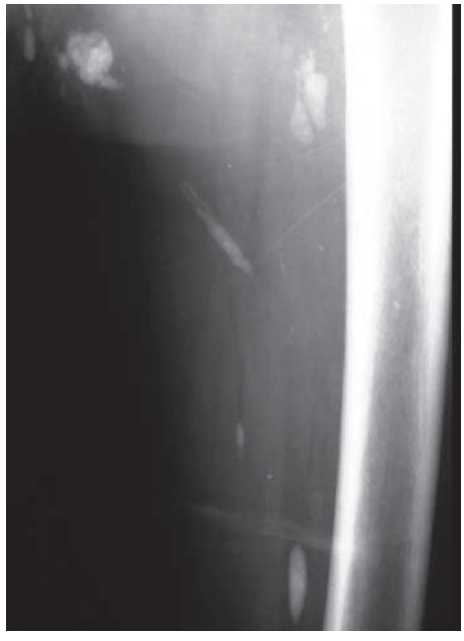

Fig. 11.9.3. Plain radiograph of the soft tissue of the posterior thigh in the same patient shows multiple linear and rounded calcified lesions, representing dead intramuscular worms

For Further Reading

1. Iriemenam NC et al Dracunculiasis – the saddle is virtually ended. Parasitol Res. 2008;102:343–7
2. Legmann P et al Epidural dracunculiasis. A rare cause of spinal cord compression. Neuroradiology. 1980;20:43–5
3. Watts S. An ancient scourge: the end of dracunculiasis in Egypt. Soc Sci Med. 1998;46(7):811–9
4. Muller R. Dracunculiasis medinensis: diagnosis by indirect fluorescent antibody technique. Exp Parasitol. 1970;27: 357–61
5. Peng SL. Rheumatic manifestations of parasitic diseases. Semin Arthritis Rheum. 2002;31:228–47

11.10 Hydatid Cyst (Echinococcosis)

Echinococcosis is a disease caused through infection from the human tapeworms *Echinococcus granulosus* and *Echinococcus multilocularis*. Each infection behaves in a different manner within the human body. *Echinococcus granulosus* produces cystic lesions within the body, while *Echinococcus multilocularis* produces tumor-like lesions.

Fig. 11.10.1. An illustration shows the gross pathological appearance of hydatid cysts

Echinococcus granulosus Disease

Infection with *E. granulosus* is found in the Middle East, Africa, Mediterranean countries, and Eastern Europe. The definitive hosts for the parasite are dogs and sheep. Humans are intermediate hosts who are infected with the parasite by ingesting food contaminated by the definitive hosts' feces or by direct contact with the definitive hosts.

After the parasite is ingested, the eggs hatch, and the embryos penetrate the intestinal mucosa, enter the portal circulation, and are carried to various organs. Any organ can be infected by *E. granulosus*, but the liver (75%) and lungs are considered the most common areas for hydatid cyst disease. The original cyst grows 2–3 cm per year; as the cyst enlarges, it starts to form internal daughter cysts (Fig. 11.10.1).

Patients with *E. granulosus* infection are often asymptomatic, unless a cyst is ruptured. A ruptured cyst usually results in fever, pruritus, eosinophilia, and fatal anaphylactic shock.

Grading of the Liver Lesions by E. granulosus

On the different radiological imaging modalities, different shapes of the hydatid cyst may be encountered. This is due to the fact that the cysts undergo different stages of life and death during the course of the disease (Fig. 11.10.2).

The hydatid cyst walls are composed of three layers. The first layer (pericyst) is made up of compressed host tissue and inflammatory cells. The second and the third walls are the true cyst walls. The second wall is an outer acellular layer (ectocyst), and the third is an inner cellular wall (endocyst). The daughter cysts arise from the endocyst wall.

- *Grade 1 lesion* (purely cystic lesions): This grade is seen on ultrasound, CT, or MRI as a pure cyst without internal inhomogeneities. This grade is explained by intact endocysts, and patients with grade 1 lesions benefit from percutaneous aspiration and scolecidal injection therapy.

Signs on Chest Radiograph

Hydatid cyst lesions are seen as a well-circumscribed, round mass, with no internal texture (Figs. 11.10.2 and 11.10.3). It mimics a solid pulmonary mass, and may lead to a false diagnosis of pulmonary tumor. Absence of symptoms and presence of other cystic lesions within the liver are important clues.

Signs on US

On ultrasound, the hydatid cyst shows a double wall (*double-line sign*). This is an important sign that differentiates a grade 1 hydatid cyst from a simple hepatic cyst, which shows a thin single wall.

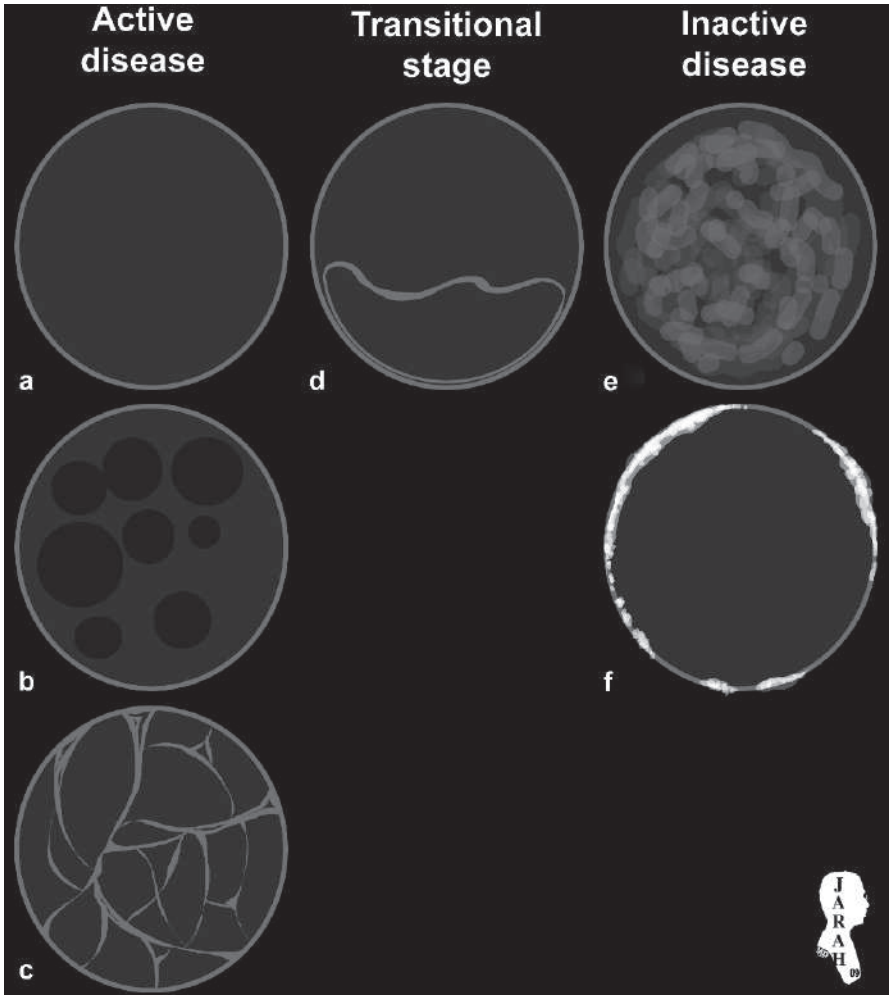

Fig. 11.10.2. An illustration shows the different stages of hydatid cysts that may be encountered during CT examination: (**a**) pure cystic form, (**b**) a cyst with multiple hypodense lesions within it, (**c**) a cyst with internal septations, (**d**) floating water lily sign, (**e**) ball of wool sign, and (**f**) calcified cystic wall

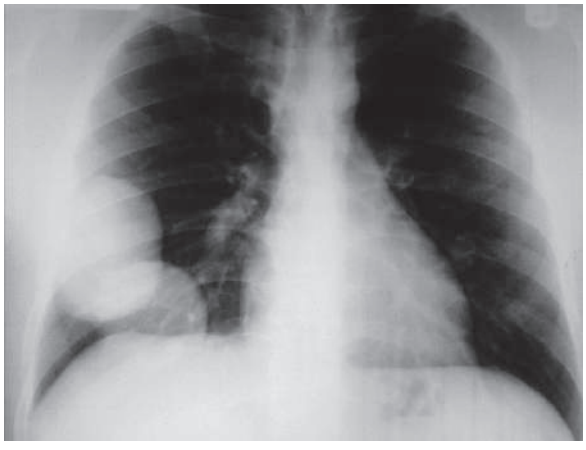

Fig. 11.10.3. Posteroanterior plain chest radiograph shows two large masses located at the right middle and lower lung fields in a patient with hydatid liver disease. The masses represent intact hydatid cysts within the lung

Signs on CT

The cyst appears as a simple cyst with no internal septations, densities, or contrast enhancement (Fig. 11.10.4).

- *Grade 2 lesions* (lesions with complex morphology with or without biliary dilatation around the lesion): This grade is characterized by the appearance of different intracystic textures. These textures arise due to previous rupture of an endocyst, with hydatid fluid leakage into the potential space between the endocysts and the pericyst. Later, this fluid causes different intracystic textures seen on ultrasound, CT, or MRI.

11.10

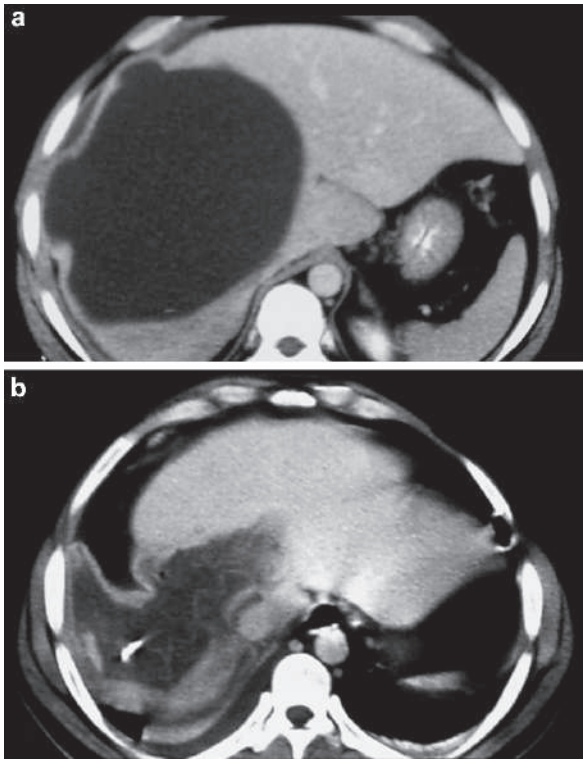

Fig. 11.10.4. Axial abdominal CT images show a very large hydatid cyst that occupies almost the entire right lobe of the liver (**a**), and the cyst appearance after aspiration of the cyst contents (**b**)

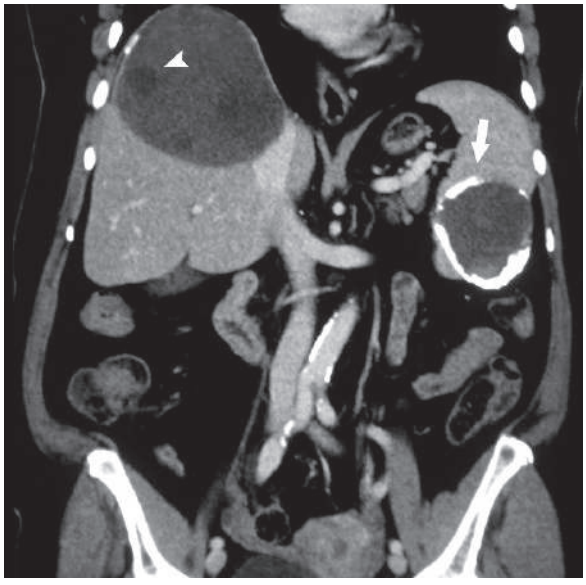

Fig. 11.10.5. Coronal abdominal CT image in a patient with hepatic and splenic hydatid cyst shows hepatic hydatid cyst with internal hypodense lesions (*arrowheads*) and splenic hydatid cyst with calcified wall (*arrow*)

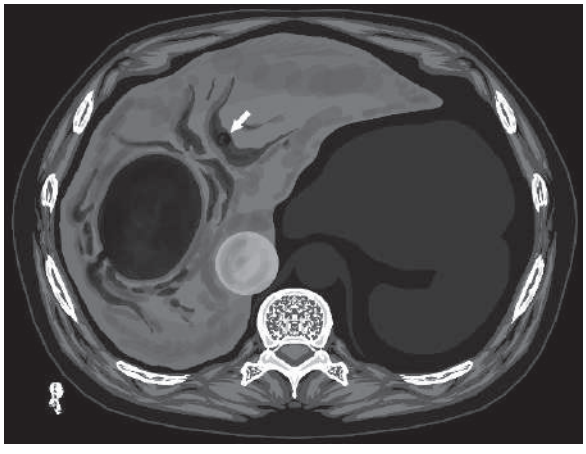

Fig. 11.10.6. Axial CT illustration demonstrates grade 3 hydatid cyst disease. Notice the right lobe cyst with dilated biliary radicals around it, with an intrabiliary daughter cyst (*arrow*)

Signs on US, CT, and MRI

- Internal septations with honeycomb-like appearance can be seen on ultrasound, CT, and MRI. (Fig. 11.10.2)
- Small internal echoes may be seen on ultrasound, reflecting floating protoscoleces (*snow flakes sign*).
- The daughter cysts may be seen as multiple hypodense lesions, compared to the density of the original cyst on CT (Figs. 11.10.5 and 11.10.2).

- *Grade 3 lesions* (lesions with intrabiliary rupture): Because the cyst is originally formed within the liver tissue, which in turn contains biliary canaliculi, cysto-biliary communication may occur as an uncommon complication. This grade is characterized by intrahepatic biliary dilatation with hydatid vesicle escape from the mother cyst into the biliary radicals, causing regional biliary obstruction (Fig. 11.10.6).

- *Grade 4 lesions*: This grade is characterized by rupture of the pericyst and the endocysts, with spillage of the cyst content into the neighboring organs or spaces. Leakages of the hydatid fluid into the peritoneum causes severe irritation and-peritonitis. Later, peritoneal calcification arises (Fig. 11.10.7).

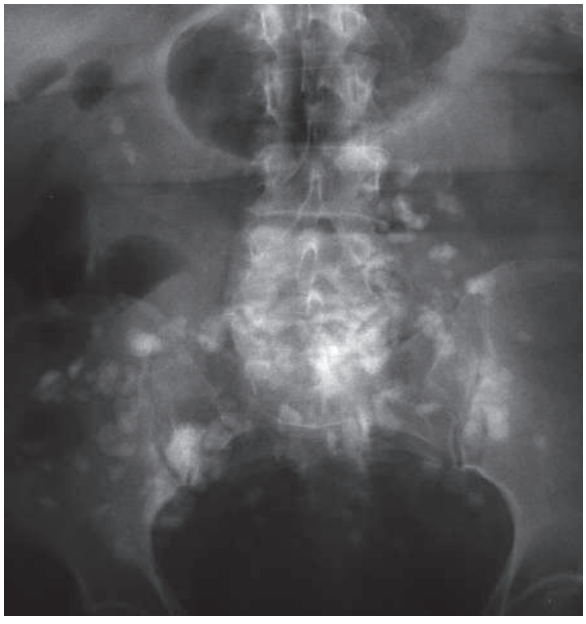

Fig. 11.10.7. Plain abdominal radiograph in a patient with previous intraperitoneal ruptured hydatid cyst shows multiple calcifications involving the mesentery and the intraperitoneal structures

- *Grade 5 lesions*: This grade is characterized by death of the cyst (inactive disease). It is seen as collapse of the hydatid membrane (pericyst) over the residual endocysts. This is seen on plain radiographs, CT, and MRI as a thick wall plus an irregular, wavy, water-fluid level floating on top of the residual hydatid fluid.

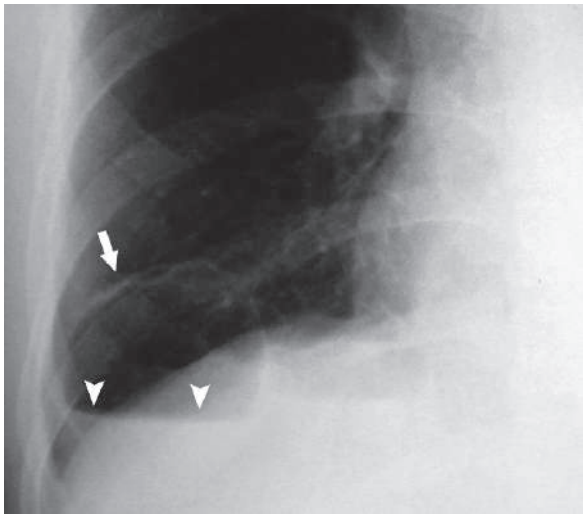

Fig. 11.10.8. Posteroanterior plain chest radiograph shows ruptured hydatid cyst with floating water lily sign (*arrowheads*). Notice the cystic wall mimicking a cavity (*arrow*)

This sign is known as the "*floating water lily sign*" (Figs. 11.10.8 and 11.10.2). Degeneration of cysts is seen as multiple, solid-like lesions within the mother cyst, resulting in a pseudotumor appearance on ultrasound or CT, known as the "*ball of wool sign*" (Figs. 11.10.9 and 11.10.2). Finally, circular or curvilinear calcification of the hydatid cyst wall is a sign of inactive disease (Figs. 11.10.10 and 11.10.2).

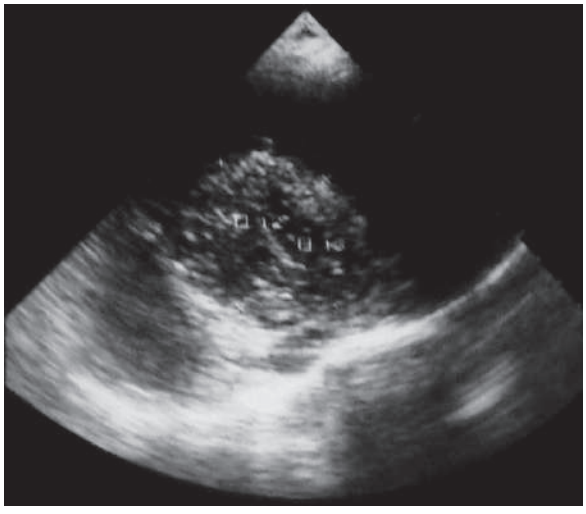

Fig. 11.10.9. Ultrasound image of a liver hydatid cyst shows internal, multiple, solid-like lesions within the cyst (ball of wool sign)

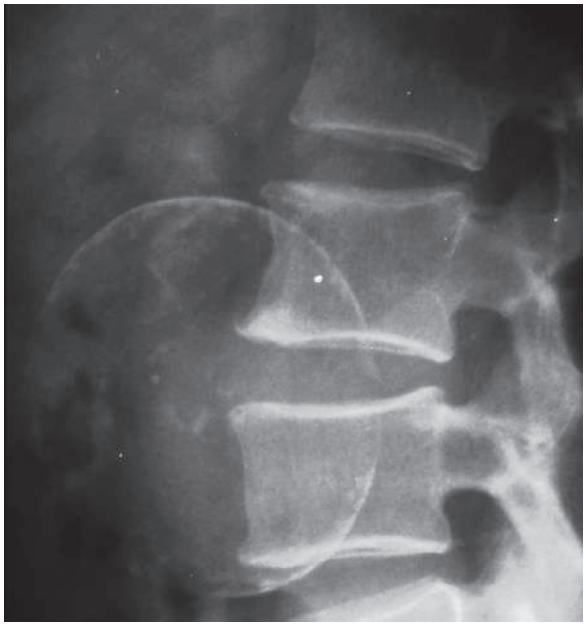

Fig. 11.10.10. Lateral plain radiograph of the thoracic spine shows a calcified hydatid cyst in the paraspinal region

11.10

Differential Diagnoses and Related Diseases

Hepatic atrophy–hypertrophy complex (HAHC): obstruction of a major hepatic or portal vein or biliary tree branch results in atrophy of the hepatic segment supplied by this vein or biliary branch. As the liver has the ability to regenerate, compensatory hypertrophy of the liver is usually seen when a large segment of the liver parenchyma is atrophied. This phenomenon is known as the HAHC. HAHC may occur uncommonly as a complication of hydatid cyst disease, especially when the cyst occupies a large area within the right lobe of the liver. It is important for HAHC to be documented by the radiologist, because it informs the surgeon that the cyst is tightly involved with one or more of the portal triad structures or a major hepatic vein (Fig. 11.10.11).

How does one differentiate between ruptured hydatid cyst and acute abscess?

- The wall of the abscess is enhanced after contrast injection on CT, while the hydatid cyst wall will not enhance.
- The air-fluid level surface is straight in the abscess, while in the hydatid cyst it has a wavy water surface due to the collapsed pericyst (floating water lily sign).

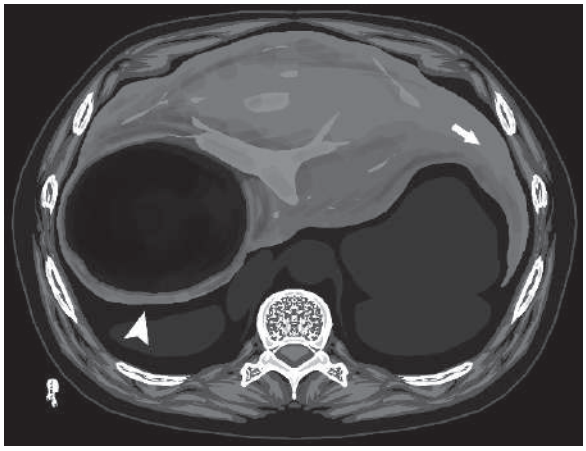

Fig. 11.10.11. Axial CT illustration shows the hepatic atrophy–hypertrophy complex. Notice the large hydatid cyst occupying a large portion of the right lobe of the liver (*arrowhead*), with compensatory hypertrophy of the left liver lobe (*arrow*)

Echinococcus alveolaris Disease

Infection with *E. multilocularis* is found in the United States, Canada, Japan, and Central and Northern Eurasia. The definitive hosts for *E. multilocularis* are foxes and rodents. Like *E. granulosus*, humans are intermediate hosts who are infected via ingesting food or water contaminated with the eggs or by direct contact with the definitive hosts.

In contrast to *E. granulosus*, *E. multilocularis* cysts are not confined within a pericyst layer, and grow by external vesiculation. The cyst is small (1–10 mm in diameter), and forms multilocular alveolar cysts that resemble lung alveoli, hence the name *alveolaris*. The external parasitic proliferation initiates a fibroinflammatory response of the host within the affected organ, commonly the liver. This will later result in a fibrous, tumor-like lesion composed of *E. multilocularis* embedded in a keloid scar and necrotic liver tissue. Stenosis of the porta hepatic with the hepatic veins within the lesion is commonly found. When the lesion heals, multiple, punctuate calcifications arise within the lesion, which makes the lesion increasingly resemble a malignant hepatocellular carcinoma (HCC) or metastasis of the liver.

Signs on US

In the liver, there are multiple echogenic nodules embedded within irregular and indistinct margins from the normal hepatic parenchyma (*hailstorm sign*).

Signs on CT

- The liver often shows a hypodense mass with a "geographic map" appearance and inhomogeneous internal texture (Fig. 11.10.12).
- Areas of punctuate calcifications within the lesions are very common in healed lesions (90% of cases). (Fig. 11.10.12)
- Unlike HCC, the lesion shows no enhancement or mild enhancement in the portal venous phase because of the fibrous stroma within the mass (characteristic and diagnostic).

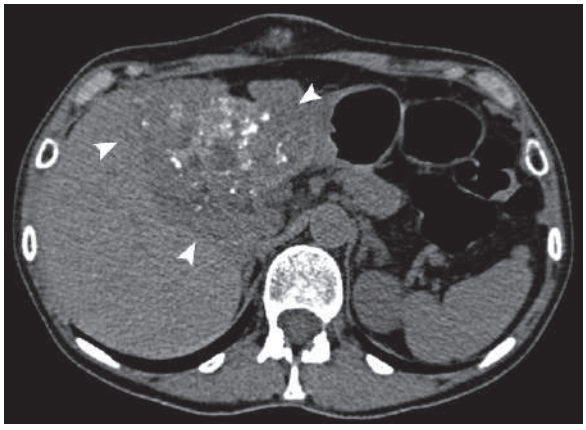

Fig. 11.10.12. Axial nonenhanced abdominal CT in a patient with *Echinococcus alveolaris* disease affecting the left lobe of the liver shows liver mass with geographic edges (*arrowheads*) and internal punctuated calcifications

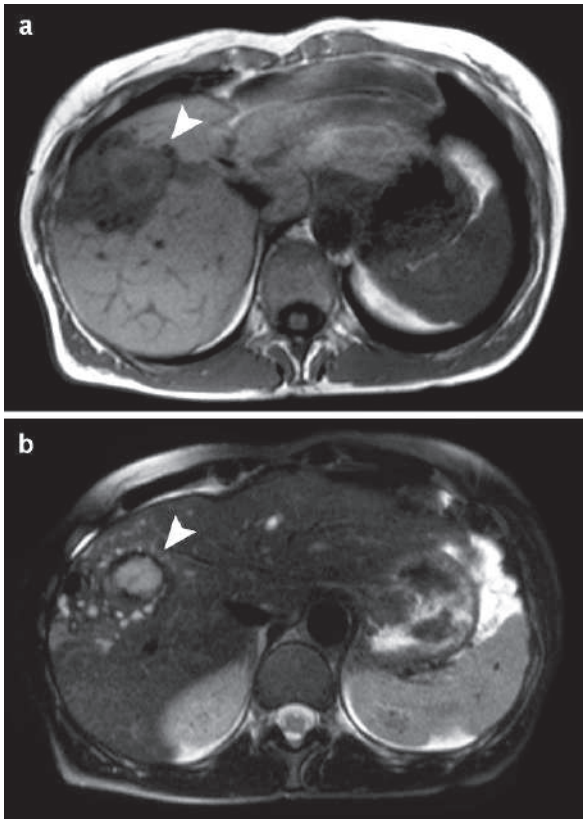

Fig. 11.10.13. Axial T1W (**a**) and T2W (**b**) nonenhanced MR images in a patient with *Echinococcus alveolaris* disease show a mass that resembles HCC (*arrowheads*), with multiple cystic lesions within the mass. Notice that the mass bulk is hypointense on T2W image (**b**) due to the fibrous (keloid) nature of the lesion

- Areas of central liquefaction may be seen.
- There are no signs of retroperitoneal lymphadenopathy (another differentiating point from HCC).

Signs on MRI

The scan shows an inhomogeneous mass with geographic margins and characteristically low T1 and low T2 signal intensities, with no enhancement or mild enhancement after contrast enhancement in the portal venous phase (Fig. 11.10.13).

For Further Reading

1. Czermak BV et al Echinococcosis of the liver. Abdom Imaging. 2008;33:133–4
2. Etlik Ö et al Contrast-enhanced CT and MRI findings of atypical hepatic *Echinococcus alveolaris* infestation. Pediatr Radiol. 2005;35:546–9
3. Rozanes I et al Grading of liver lesions caused by *Echinococcus granulosus*. Eur Radiol. 1993;3:429–33
4. Karabulut K et al Hepatic atrophy-hypertrophy complex due to *Echinococcus granulosus*. J Gastrointest Surg. 2006;10:407–12
5. Katranci N et al Correlation CT, MRI and histological findings of hepatic *Echinococcus alveolaris*: a case report. Comput Med Imaging Graph. 1999;23:155–9
6. Sasaki F et al Alveolar echinococcosis of the liver in children. Pediatr Surg Int. 1994;9:32–4

11.11 Chagas' Disease (American Trypanosoma)

Chagas' disease (CD) is an infectious, multi-systemic disease caused by *Trypanosoma cruzi* (*T. cruzi*), a blood-borne flagellate. *T. cruzi* was first described in Brazil by Carlos Chagas, in 1909. The disease is one of the most common public health problems in South America from Texas to Argentina.

CD often affects children and young adults living in rural areas and mud huts. *T. cruzi* is transmitted to humans by the defecation of a vector bug known as the "kissing bug" (reduviid bug). The bite occurs around the face, often at night, and the parasite is found in the bug's feces. The bite can be painless or painful depending on the toxins found in the bug's saliva.

At the bite site, *T. cruzi* penetrates the skin and travels via the blood to the body organs. The parasite invades and enters the host cells, particularly the muscles, the glia, and the reticuloendothelial system. Multiplication occurs by binary fission until the cells rupture, and the parasite enters the blood or invades more tissues. At the site of multiplication, severe inflammatory reaction occurs with local lymphangitis, which is known as "*chagoma*." Soon after that, lymphatic spread to regional lymph nodes occurs, which is usually seen in the first 2 weeks post-infection.

Although the parasite can be found in any body tissue, *T. cruzi* often has a distinct predilection for striated and cardiac muscles, glial, and nerve cells.

There are four distinct phases of CD, each with its own pathological and radiological features.

Acute Chagas's Disease

The main pathological process during this stage is chagoma affecting the heart and the central nervous system (CNS). The acute stage is frequently seen in neonates, although it may occur at any age.

After an incubation period of 2 weeks, patients often present with fever that can persist for months, malaise, loss of appetite (anorexia), vomiting, diarrhea, and muscle pain.

In the heart, there is severe lymphocytic myocarditis with focal areas of endocardium and epicardium inflammation, which leads to dilated cardiomyopathy and pericardial effusion. Hyaline necrosis of isolated myocardial fibers (*Magarinos-Torres' lesion*) is a characteristic feature of Chagas' myocarditis.

In the CNS, encephalitis or meningoencephalitis is often seen, and may be the primary manifestation of CD. The trypanosomes may enter the conjuctiva in up to 50% of patients, causing upper or lower eyelid edema, conjuctiva chemosis, and preauricular lymph nodes enlargement (*Romana's sign*).

Hepatosplenomegaly, and pneumonia when the trypanosoma affect the lungs, may be seen.

ECG Abnormalities

The most common changes in electrocardiogram (ECG) are prolonged P-R interval, low voltage in an ECG rhythm showing electrical activity in the ventricles (QRS complex), and prolonged Q-T interval.

Signs on Ultrasound

- Hepatosplenomegaly that may persist for up to 5 months from the onset of the disease.
- Liver fatty infiltration.
- Regional lymph node enlargement.

Signs on Cardiac MRI

- Chagas' myocarditis is seen as focal, segmental high T2 signal intensity areas, with contrast enhancement localized in the mid-wall or the outer wall of the ventricle below the pericardium (Fig. 11.11.1).
- There are areas of wall motion abnormalities, along with areas of aneurismal wall dilatation. Apical aneurysm with thrombus formation is a common finding.

Subacute Chagas' Disease

This stage is often seen in young adults, and the patient presents without any fever, with severe heart failure that does not respond to therapy.

Fig. 11.11.1. Sagittal short-axis, T1W postcontrast cardiac MR illustration demonstrates the type of myocarditis enhancement seen in Chagas' disease (mid- to outer-wall enhancement) (*arrowhead*)

Latent Chagas' Disease

After the acute stage subsides, many patients completely recover, while others may pass into a latent or chronic stage. In this stage, 2–5% of patients become symptomatic annually.

The number of ganglion cells in the Auerbach plexi in the gastrointestinal (GI) tract starts to diminish in this stage. All patients who recovered from the acute CD stage, or live in endemic areas, have a positive complement fixation test (*Machado-Guerreiro reaction*).

Chronic Chagas' Disease

This stage develops after many years, and is characterized by dilated cardiomyopathy, with esophageal and colonic dilatation. The main pathology is attributed to reduction in the motor ganglia of the GI tract, resulting in loss of motor function (aperistalsis), which results in dilatation and flaccidity of the affected organs.

In the esophagus, early stages are characterized by hypercontractility and hypertrophy of the circular smooth muscles. Later, denervation of the esophageal muscles results in marked esophageal dilatation. Food may become lodged in the esophagus. Carcinoma and esophageal abscess may develop in 7% of patients with chronic CD.

In the colon, massive dilatation and chronic constipation is often seen. Sigmoid volvulus may occur in 10% of patients.

Signs on Plain Chest Radiograph

- The dilated esophagus is seen as a medistinal mass along the entire right side of the mediastinum with air or air–fluid level.
- The heart is often dilated due to dilated cardiomyopathy of chronic CD.
- Raised left hemidiaphragm due to splenic flexture dilatation may be found.

Signs on Barium Swallow and CT

- The esophagus is massively dilated (>7 cm), with bizarre, dysrhythmic contractions that mimic achalasia (Fig. 11.11.2). Food may be found lodged within the esophagus.
- On CT, megacolon with massive rectosigmoid dilatation is usually found.

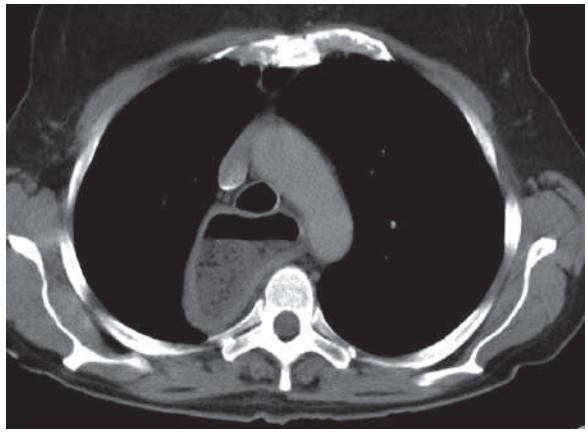

Fig. 11.11.2. Axial thoracic CT in a patient with chronic Chagas' disease shows massive dilatation of the esophagus, with food lodged inside the esophagus, mimicking achalasia

For Further Reading

1. Felippe L et al Radiological diagnosis of Chagas' disease (American trypanosomiasis). Semin Roentgenol. 1998;33(1): 26–46
2. Rochitte CE et al Myocardial delayed enhancement by magnetic resonance imaging in patients with Chagas' disease: a marker of disease severity. J Am Coll Cardiol. 2005;46:1553–58. Originally published online 22 Sep 2005. doi: 10:1016/j.jacc.2005.06.067
3. Barros MVL et al Doppler tissue imaging to access systolic function in Chagas' disease. Arq Bras Cardiol. 2003;80(1): 36–40
4. de Souza AP et al Magnetic resonance imaging in experimental Chagas disease: a brief review of the utility of the method for monitoring right ventricular chamber dilatation. Parasitol Res. 2005;97:87–90
5. Ferreira-Santos R. Aperistalsis of the esophagus and colon (megaesophagus and megacolon) etiologically related to Chagas' disease. Am J Digest Dis New Ser. 1961;6(8), 700–726

11.12 Schistosomiasis (Bilharziasis)

Schistosomiasis is an infectious disease caused by freshwater schistosoma. Schistosoma are flatworms that do not have a digestive tract, and are commonly known as trematodes or blood-flukes. Schistosomiasis is commonly known as "Bilharziasis," after Bilharz, the discoverer of the parasite in 1815.

Schistosoma Life Cycle

Schistosoma release their eggs in freshwater. Later, the eggs are hatched into larvae, which maturate in freshwater snails. After maturation, the mature larvae (cercariae) leave the snails and enter into humans by penetrating the exposed human skin in the freshwater. After skin penetration, the parasites travel within the lymphatic system through the thoracic duct to enter the circulation. The parasites lie in the lymphatic system for almost 21 days before they enter the hepatic portion of the portal venous system into the liver, where they further mature and mate. Depending on the type of the schistosoma, the parasites migrate into the intestinal or the bladder venous system to lay their eggs. The adult worms are strictly intravenous and do not evoke the immune system, while both the cercariae and the eggs stimulate the immune system, resulting in the formation of granulomas around the eggs and the systemic cercariae, which will cause tissue fibrosis and calcification of the affected organ in advanced stages of the disease. Dead worms can be embolized almost anywhere within the body.

There are four types of Schistosoma worldwide:

- *Schistosoma japonicum* is found within eastern Asia, is located within the intestinal tract veins, and releases its eggs in the feces.
- *Schistosoma mansoni* is found within South America and Africa, is located within the intestinal tract veins, and releases its eggs in the feces.
- *Schistosoma haematobium* is found within Africa and the Middle East, is located within the bladder and ureters venules, and releases its eggs in the urine.
- *Schistosoma intercalatum* is found only in equatorial Africa, and mainly affects the intestinal tract and the portal system.

The first symptom of the disease starts when patients develop itchy skin after larvae penetration, due to hypersensitivity reaction type 1 and type 4 (cercarial dermatitis or swimmer's urticaria). Weeks later, systemic manifestations like hematuria, fever, weight loss, diarrhea and abdominal pain arise.

The living worm lives between 4 and 30 years. The living worm engulfs the red blood cells (RBCs) and excretes them as hemozoin, which is engulfed later by the macrophages. The other action by the living worm is laying eggs (ova). As the ova penetrate the wall of the intestine or the urinary bladder, they may cause chronic bleeding (resulting in anemia), be trapped in the wall of the organ, or enter the blood and circulate as emboli. The dead worms initiate a severe inflammatory reaction within the veins, causing thrombophlebitis, which can block the affected vein.

Diagnosis of schistosomiasis is confirmed by identifying the schistosoma eggs in urine or feces, and eosinophilia in the complete blood count (CBC).

The clinical and radiological manifestations of schistosomiasis can be classified according to the parasite type.

Schistosomiasis by *S. japonicum*

S. japonicum lives in the mesenteric veins, and mainly affects the liver, small bowel, and lungs. In the small bowel, the duodenum and the jejunum are mainly affected.

In the liver, the parasite eggs are deposited in the portal venules along the liver periphery. When the eggs die, fibrosis within the venules results in a polygonal network of periportal fibrosis that makes the liver look like a "turtle back" on gross appearance (Fig. 11.12.1). The eggs are also deposited within the liver capsule, resulting in capsule thickening and fibrosis. There is a high incidence of liver carcinoma with *S. japonicum* infection.

11.12

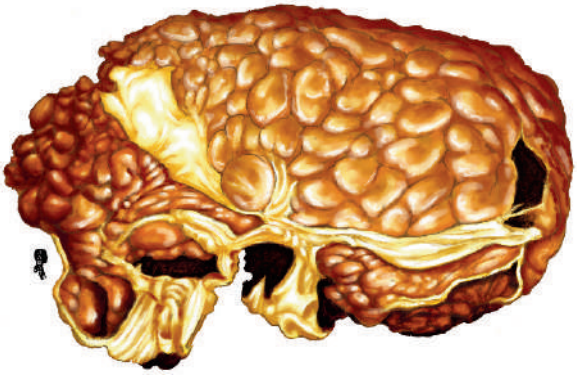

Fig. 11.12.1. An illustration demonstrates the gross turtle-back appearance of *S. japonicum* liver schistosomiasis

Signs on Ultrasound

The liver shows an internal echogenic polygonal network due to periportal fibrosis and calcification, which causes a "fish-scale" appearance (30% of cases).

Signs on Abdominal CT

There is internal periportal fibrosis (low-density bands) or calcification (high-density bands) within the liver parenchyma, along with liver contour irregularities (turtle-back appearance) (Fig. 11.12.2).

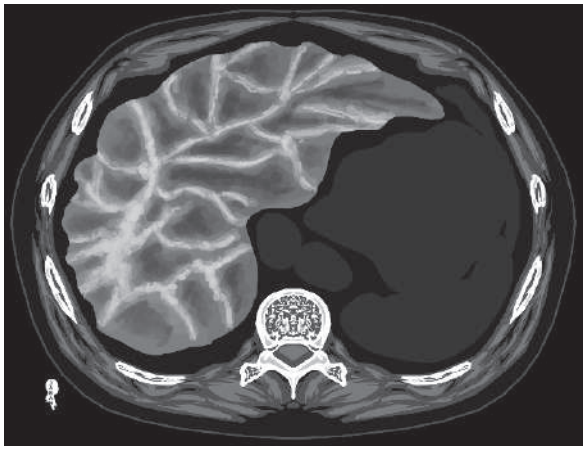

Fig. 11.12.2. Axial CT illustration of the liver in *S. japonicum* schistosomiasis demonstrates the internal periportal calcification and fibrosis causing the turtle-back appearance

Schistosomiasis by *S. mansoni*

S. mansoni mainly affects the liver, bowel, central nervous system, and lungs. In the bowel, the parasite causes granulomatous colitis, which causes loss of haustration and strictures later on, mimicking Crohn's disease. If the small intestine is affected, regional ileitis and protein-losing enteropathy may develop. In uncommon cases, when the calcification is so severe as to include all the layers of the colon wall, the ova start to accumulate freely within the peritoneal cavity outside the wall. This causes inflammation and fibrosis within the peritoneal cavity and the pericolic region, resulting in a pericolic mass that cannot be differentiated from carcinoma on imaging.

In the liver, the parasite deposits its eggs around the main portal vein at the liver hilum, later resulting in Symmer's pipestem fibrosis. *Symmer's pipestem fibrosis* is a condition that arises when egg granulomas aggregate around the portal vein, resulting in vascular fibrosis that causes obstruction of the small veins and presinusoidal cirrhosis. Portal hypertension (HTN), esophageal varices, and splenomegaly are common complications of this type of fibrosis.

In uncommon cases, *angiomatoid lesions* can develop within the liver. These angiomatoid lesions emerge as a secondary action taken by the body against severe fibrosis of the hepatic veins and portal HTN. The emergence of such lesions can be explained by the fact that in severe portal HTN, the blood within the veins cannot flow normally, which results in opening of sideway channels and collaterals to decrease liver congestion. This can result in angiomatoid formation of lesions (e.g., hemangiomas). These lesions seen in the liver represent a severe stage of portal HTN.

Splenomegaly in bilharziasis occurs at an early stage due to antigen stimulation, causing splenic parenchymal hyperplasia, and later in the course of the disease due to portal hypertension.

If eggs are embolized into the pulmonary vessels via the venous system, they damage the vascular wall by initiating an inflammatory reaction. The inflammatory reaction results in a characteristic "dumbbell" granuloma blocking the vessel, or forms a pseudoaneurysm. Pulmonary hypertension may develop in advanced stages (20% of cases). All schistosoma species can affect the lungs.

Rheumatic manifestations are uncommonly seen with bilharziasis, resembling reactive arthritis or seronegative

spondyloarthropathies and sacroiliitis. Rheumatoid-like disease affecting the metacarpophalangeal (MCP) and proximal interphalangeal (PIP) joints, wrists, ankles, and knees have been reported. Some of these manifestations are due to immune complexes or direct infection by the parasite.

In the central nervous system, *S. mansoni* produces conus medullaris thickening and arachnoiditis (*bilharzioma*).

Signs on Plain Chest Radiograph

- Signs of pulmonary hypertension and enlarged pulmonary trunk in advanced stages.
- Localized bilharzias granulomas within the lung may be mistaken for a neoplastic nodule or mass.
- Calcification of the bowel walls may be seen (rarely) on plain radiographs (Fig. 11.12.3).

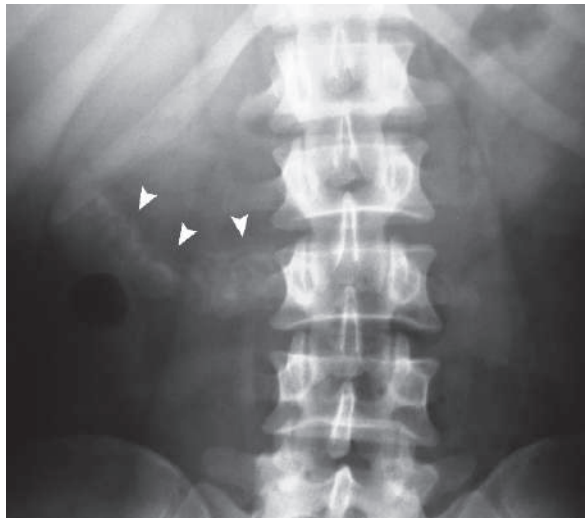

Fig. 11.12.3. Plain abdominal radiograph shows calcification of the transverse colon walls in a patient with schistosomiasis (*arrowheads*)

Signs on Ultrasound

- Hyperechoic lesions are noticed around the portal vein due to Symmer's pipestem fibrosis.
- Thrombosis of the portal vein may be seen as loss of Doppler signal flow within the portal main stem.
- Signs of liver cirrhosis and portal hypertension (e.g., splenomegaly).
- Gallbladder wall thickening is found in 80% of cases.

Signs on Abdominal CT

- The portal venous tracts are replaced by fibrous tissue, seen as low-attenuation bands or rings, with peripheral fibrosis radiating from the center of the liver around the main portal vein branches. Marked enhancement is noticed on postcontrast images.
- Shrunken liver, portal venous thrombosis, splenomegaly, and esophageal varices are commonly noticed (Fig. 11.12.4).
- Splenic siderotic nodules (*Gamna-Gandy bodies*) are commonly seen within the enlarged spleen.

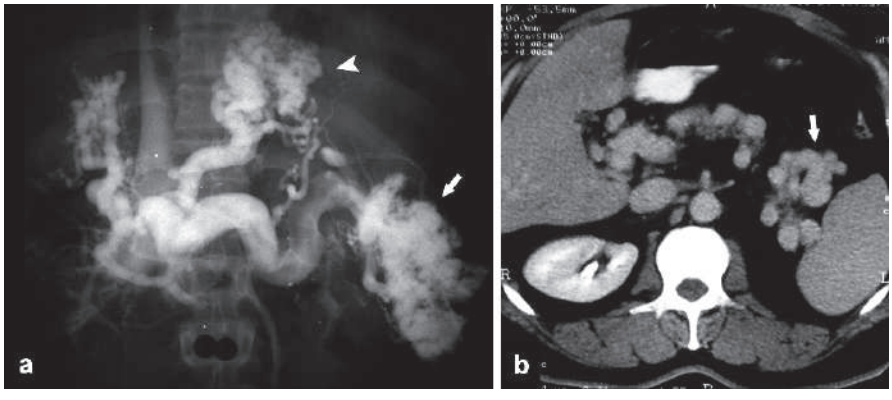

Fig. 11.12.4. Portal cavography (**a**) and axial CT-urography (**b**) in a patient with schistosomiasis and portal vein thrombosis shows a severely dilated portal vein, with development of esophageal varices (*arrowhead*) and splenic varices (*arrows*)

11.12

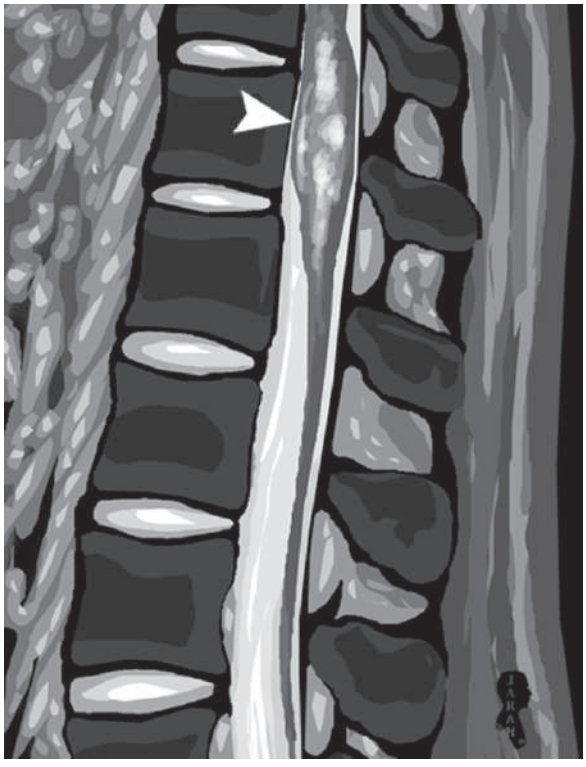

Fig. 11.12.5. Sagittal T2W lumbar MR illustration demonstrates enlarged conus medullaris with multiple high signal intensities representing bilharzioma (*arrowhead*)

Signs on Spinal Cord MRI

Bilharzioma is seen as localized conus medullaris thickening, with high signal intensity on T2W images and heterogeneous contrast enhancement postgadolinium injection (Fig. 11.12.5).

Schistosomiasis by *S. haematobium*

S. haematobium mainly affects the bladder and the ureters. The posterior part of the bladder is the most vascular area of the bladder, and it is the area where most ova within the vesical veins are seen. *S. haematobium* lays more ova than *S. mansoni*. The eggs are trapped within the ureter and the bladder mucosa as they are carried by the urine to be excreted. The immune system surrounds the eggs, and starts an aggressive granulomatous reaction that causes death and calcification of the eggs. As the disease advances, calcification can occur within the ureters, bladder, and seminal vesicles. When the ureters are calcified, obstructive uropathy and renal hydronephrosis may occur.

Complications of the ova within the bladder and intestinal walls:

- *Sandy patch* occurs when a huge number of ova die and calcify, causing the overlying mucosa to degenerate and atrophy.
- *Bilharzial polyp* occurs due to localized deposition of a huge number of ova, with hyperplasia of the wall. This is mainly seen in the intestine (*S. mansoni*).
- *Bilharzial ulcers* can arise due to penetration of huge numbers of ova, falling of the atrophic mucosa over a sandy patch lesion, or due to detachment of a bilharzial polyp.
- *Fibrosis* can arise as a consequence of chronic inflammation of the organ wall.
- *Urothilial changes* (only seen in the bladder) comprise a chronic reactive inflammatory disorder characterized by transitional epithelial hyperplasia in the form of nests called von Brunn's nests, due to an irritant (e.g., schistosomal ova). These nests may undergo central cystic degeneration, forming a condition called "cystitis cystica." The cystitis cystica transitional epithelium may undergo metaplasia into columnar mucin-secreting epithelium, causing another condition called "cystitis glandularis." The ova may cause squamous metaplasia of the transitional cell nest, causing leukoplakia, which may transform into dysplasia and carcinoma in situ. *Leukoplakia* is a thick, white patch of skin, commonly seen on the tongue, vulva, or the bladder. It is composed of thick layers of stratified epithelium with keratin, with chronic inflammation of the submucosa. Pathologically, it is explained by squamous metaplasia followed by cellular hyperplasia.

Signs on Plain Abdominal Radiographs

- There is striking calcification of the ureters or the bladder (Fig. 11.12.6). The uniform and linear calcification of the schistosomiasis bladder is pathognomonic. In contrast, bladder calcification due to tuberculosis or radiation is often patchy and focal.

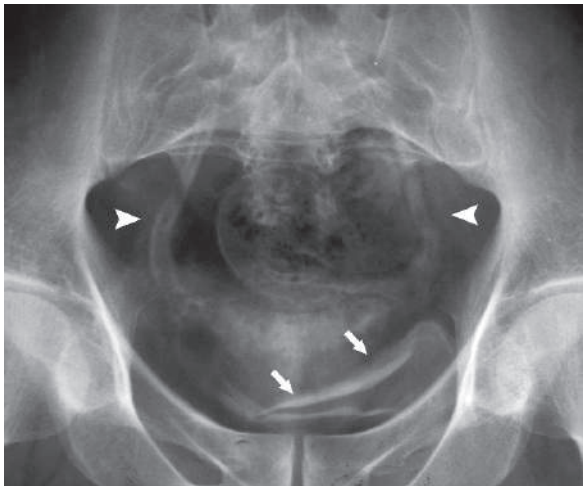

Fig. 11.12.6. Plain radiograph of the pelvis shows complete bilateral calcification of the ureters (*arrowheads*) and the bladder (*arrows*) in a patient with bilharziasis

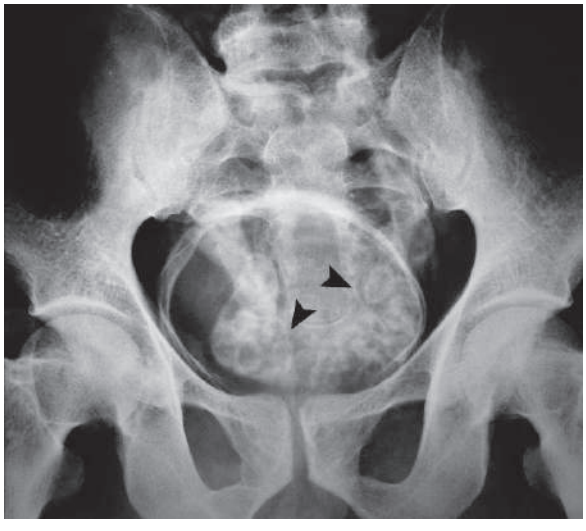

Fig. 11.12.7. Plain radiograph of the pelvis shows complete calcification of the bladder with the seminal vesicles (*arrowheads*) in a patient with bilharziasis

- Bilateral ureters calcification (Fig. 11.12.6) with hydronephrosis is a common finding.
- Calcification of the seminal vesicles, testes, and spermatic cords may be seen (Fig. 11.12.7).
- Fallopian tubes or cervical calcifications may occur in women.

Signs on Ultrasound

- Hyperechoic bladder wall, due to calcification.
- Bilateral, nonsymmetrical, hyperechoic dilated ureters are often seen.

Signs on Intravenous Urography

- Bilateral ureteric dilatation with hydronephrosis is often seen.
- Marked bladder dilatation may be seen due to bladder neck stenosis and hypertrophy of the trigon. This finding is only reported in Egypt.

Signs on CT and MRI

Cystitis cystica and cystitis glandularis are seen on MRI as hypervascular polypoid tissue with low T1 and T2 signal intensity, with central hyperintensity forming a branching pattern. The branching central areas show contrast enhancement. The muscular layer of the bladder should be intact and not disturbed or infiltrated, a characteristic feature that distinguishes cystitis cystica and cystitis glandularis from a real bladder tumor. On CT, the scan shows irregular bladder wall thickening and multiple polypoid masses arising, often from both the lateral walls of the bladder and the base of the trigone (Fig. 11.12.8).

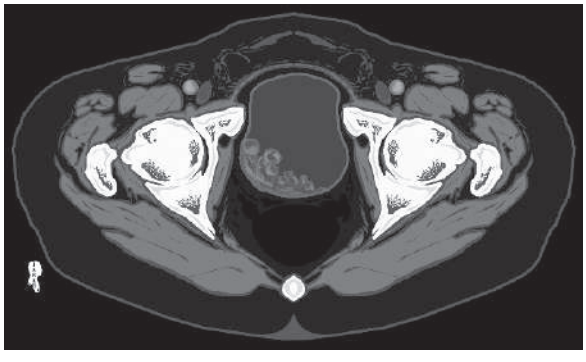

Fig. 11.12.8. Axial postcontrast CT illustration of the pelvis shows multiple polypoid masses arising from the right lateral posterior wall of the bladder with contrast enhancement representing the radiological findings in cystitis cystica and cystitis glandularis

Differential Diagnoses and Related Diseases

11.12

Katayama syndrome is a disease characterized by acute systemic immune reaction similar to the one seen in schistosmiasis patients but is not caused by mature worms or eggs. The patient typically has no immunity, presenting with skin redness and irritation or urticaria (swimmer's urticaria) after 1–2 days of swimming or washing in infected water. Weeks later, the affected patient often presents with fever, headaches, chills, lack of appetite (anorexia), and abdominal pain. Neck stiffness and coma may occur. CBC shows esinophilia in almost 90% of cases. Imaging investigations are often nonspecific. The disease is believed to be caused by esinophil-mediated toxicity leading to vasculitis and small vessel thrombosis.

For Further Reading

1. Palmer PES. Schistosomiasis. Semin Roentgenol. 1998;33(1): 6–25
2. Manzella A et al Schistosomiasis of the liver. Abdom Imaging. 2008;33:144–50
3. Maia ACM Jr et al Spinal cord compression secondary to epidural bilharzioma: case report. J Neuroimaging. 2007;17:367–70
4. Jauréguiberry S et al Neurological involvement during Katayama syndrome. Lancet Infect Dis. 2008;8(1):9–10
5. Wong-You-Cheong JJ et al Inflammatory and nonneoplastic bladder masses: radiologic-pathologic correlation. RadioGraphics. 2006;26:1847–68
6. Singh I et al Cystitis cystica glandularis masquerading as a bladder tumor. Int Urol Nephrol. 2001;33:635–6
7. Lee G et al Case report: cystitis glandularis mimics bladder tumor: a case report and diagnostic characteristics. Int Urol Nephrol. 2005;37:713–5
8. Peng SL. Rheumatic manifestations of parasitic diseases. Semin Arthritis Rheum. 2002;31:228–47

11.13 Tuberculosis

Tuberculosis (TB) is a multi-systemic, granulomatous disease caused by the bacilli *Mycobacterium tuberculosis*. There are two main groups of gram-negative bacilli that infect humans: *Mycobacterium tuberculosis* and *Mycobacterium bovine*. *M. tuberculosis* is an infection from human to human. Humans are infected by inhalation (pulmonary TB), by ingesting infected food or drinks (tonsillar and intestinal TB), or by wound contamination (rare). *M. bovine*, on the other hand, infects humans who come into contact with an infected mastitis cow.

TB bacteria have a body composed of protein with an attached polysaccharide, and a capsule composed of lipids. TB bacteria do not produce endotoxins and are noninvasive. When neutrophils engulf the TB bacilli, they do not digest the bacilli because neutrophils lack the enzyme lipase, which is necessary to dissolve the bacterial capsule. The bacteria remain alive within the neutrophils until the neutrophils die, when the bacteria are again released into the blood stream. The pathogenesis of TB is due to the antibody reaction evoked by the protein nature of the bacteria. The body produces antibodies against the bacteria antigen, resulting in a hypersensitivity reaction causing granulomas (tubercles).

Tubercle (*proliferative tissue reaction*) is the unit reaction of TB. It is grossly composed of a grayish nodule 1–2 mm in size. Microscopically, it is composed of caseating necrosis of epithelioid cells. The epithelioid cells can join together to form large cells with horseshoe-shaped peripheral nuclei, called Langerhan's giant cells. A tubercle is a granuloma with a caseating center. An infected person becomes tuberculin-test positive usually 1–2 months after initial exposure. The caseous lesion has three prognoses: it may heal, it may enlarge and spread to the lymphatic or the blood stream, or it may form a cavity.

Necrotic TB lesions are the result of hypersensitive immune reactions to the bacteria in different body systems (hypersensitivity necrosis), and ischemia, because granuloma do not form angiogenesis, and the vessels within the area of the granuloma develop endarteritis obliterans due to the chronic inflammatory reaction (ischemic necrosis). *Exodative tissue reaction* is of a special type and is seen in TB when the inflammatory reaction affects serosal tissue. This reaction is characterized by serous fluid formation and a few epitheloid cells and macrophages.

As TB is a multi-systemic disease, manifestations of TB are different from organ to organ, with many manifestations having characteristic radiological features that are best addressed separately.

Pulmonary TB

Patients with pulmonary TB classically present with fever, weight loss, chills, night sweats, cough, and hemoptysis. Diagnosis is established by staining *M. Tuberculosis* with acid-fast bacilli stain. Laboratory investigations often show an elevated erythrocyte sedimentation rate (ESR), anemia, mild hyponatremia (43%), moderate leucocytosis, and hypercalcemia (27%).

In the lungs, there are four outcomes of TB infection:

- *TB clearance*: the disease is cleared from the body with dormant residuals, as long as the immune system is functioning properly.
- *Primary (acute) TB*: this type is usually seen in children with widespread disease and less tissue destruction. The rate of primary TB is 90%, and depends on the body's innate immunity and hypersensitivity. The infection in primary TB is called "*primary complex*," composed of tuberculous focus, regional lymphangitis, and lymphadenitis. It can occur in the lung (by inhalation), the tonsils, or the intestine (by ingestion), or (rarely) in the spleen (by wound infection via hematogenous spread). Primary pulmonary TB is classically located in the apical segment of the lower lobes or middle lobes. When the lesion is healed, it results in a focal calcified lesion known as *Ghon focus*. Ghon focus is composed of multiple aggregated tubercles, with TB lymphangitis due to the spread of the bacteria in the nearby lymphatic vessels. The disease can spread from one region of the lung to another via the bronchi (bronchogenic spread). It generally heals without sequelae, with few cases of generalized spread.
- *Latent (chronic) infection*: a condition characterized by *M. tuberculosis* infection without any clinical signs of active disease. The patient is at risk of reactivation.

11.13

- *TB reactivation*: a situation where an old latent TB infection gets reactivated into an acute disease, and mostly occurs in patients with low immunity, such as HIV patients, diabetics or children. TB reactivation occurs in the lung apices; it is thought that this location is preferred by the bacilli due to the high oxygen tension or the low lymph flow at the lung apices. Cavity formation in the lung apices is seen in up to 40% of reactivation TB patients.

Signs on Chest Radiographs

- Primary TB presents with a pneumonic patch in the middle or lower lobes, with ipsilateral hilar lymphadenopathy (Fig. 11.13.1). When the TB pneumonic patch regresses and calcifies, it results in Ghon Lesion.
- *Ranke's complex*: Ghon lesion with ipsilateral calcified hilar lymphadenopathy.
- *Tuberculoma*: a round, smoothly circumscribed pulmonary nodule (<3 cm) that usually contains central calcification. It is seen at the common areas of TB infection (upper lobes and apical segment of lower lobes). The main differential diagnosis of tuberculoma is "pulmonary hamartoma," which has the same tuberculoma features, central popcorn calcifications, and occurs anywhere within the lungs. Tuberculoma is diagnosed by its features and locations.
- *Apical fibrosis (Simon's focus)*: old TB in the lung apices may results in chronic granulomatous reaction that causes lung fibrosis (Fig. 11.13.2). The term "old TB" should be used with caution, as the TB may be chronic but still active. "Stable TB disease" requires 6 months of unchanged radiological features to be acclaimed.
- TB reactivation is classically seen as lung apices cavitary lesions (40%) or noncavitary lung infiltration (4–9%). A TB cavity tends to have thick irregular walls (Fig. 11.13.3), and air–fluid level may be seen (9–21%). Superimposed infection of the cavity with fungi can result in fungal ball (mycetoma/aspergilloma) within the cavity (halo sign).
- *Cicatrization atelectasis*: atelectasis of the upper lobes due to previous fibrosis from TB infection, with retraction of the hilum upward.
- *Bronchiectasis* may occur in up to 87% of patients due to bronchial wall and parenchymal destruction. Bronchiectasis is seen as focally dilated bronchi with honeycomb, cystic interstitial pattern.
- *Broncholithiasis* is an uncommon complication of TB characterized by the presence of calcified materials within the bronchial tree.
- Pleural calcification is often seen unilaterally, especially with previous empyema.

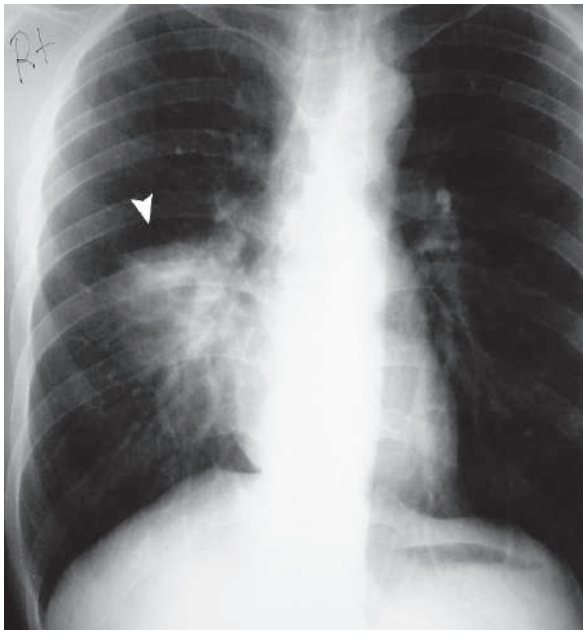

Fig. 11.13.1. Posteroanterior plain chest radiograph in a patient with primary TB shows a pneumonic patch in the right middle lung zone (*arrowhead*) with ipsilateral lymphadenopathy

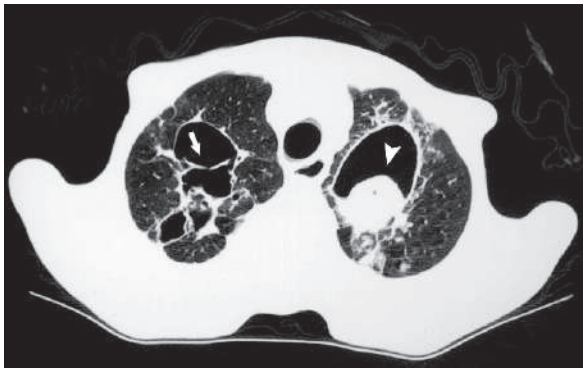

Fig. 11.13.4. Axial lung window HRCT in a patient with TB shows apical left mycetoma with a halo sign (*arrowhead*) and marked bronchiectasis in the right lung (*arrow*)

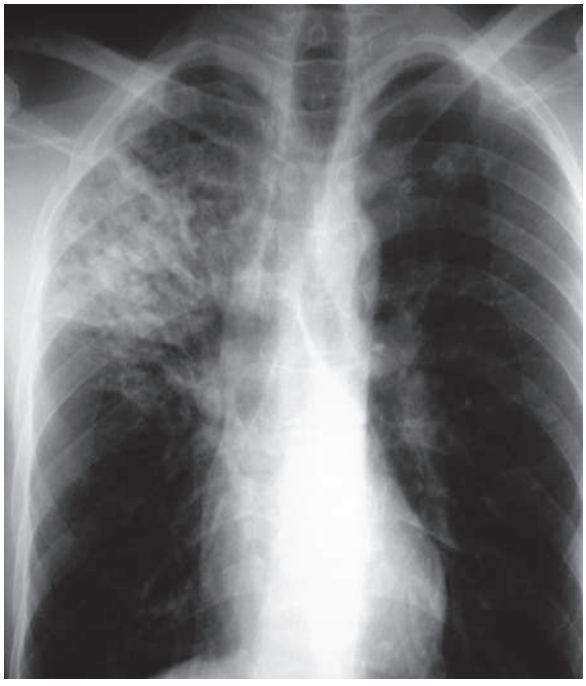

Fig. 11.13.2. Posteroanterior plain chest radiograph in a TB patient shows right apical fibrosis (Simon's focus)

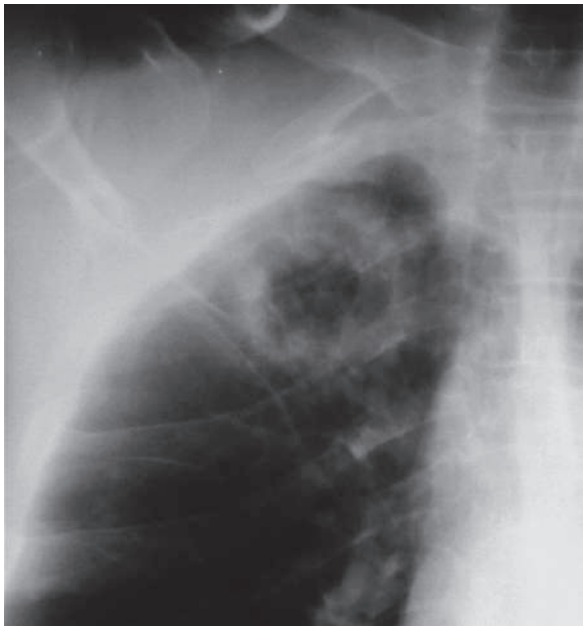

Fig. 11.13.3. Posteroanterior plain chest radiograph shows right apical TB cavity

Signs on HRCT

- *Mycetoma* is seen as a fungal ball within a TB cavity at the lung apices in up to 55% of patients (*halo sign*) (Fig. 11.13.4).
- *Tree-in-bud appearance* represents terminal bronchiole impaction with mucus, pus, or fluid, resulting in enhanced appearance of the normal branching bronchial tree that is normally invisible (Fig. 11.13.5). It is seen in diseases that affect the peripheral airways and cause material plugs deposition within them, such as TB, cystic fibrosis, and panbronchiolitis.

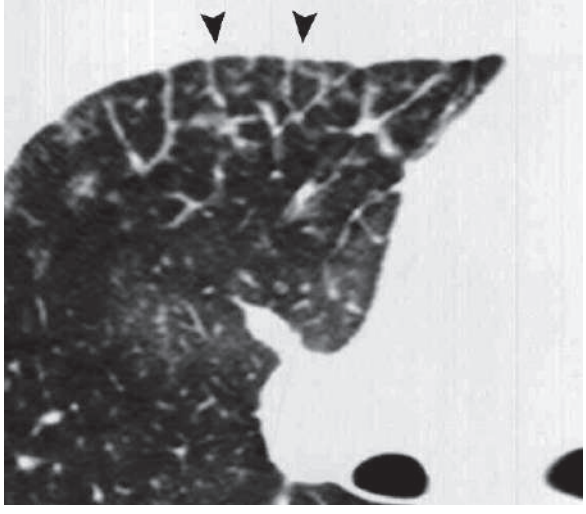

Fig. 11.13.5. Axial lung window HRCT in a patient with TB shows peripheral tree-in-bud appearance (*arrowheads*)

11.13

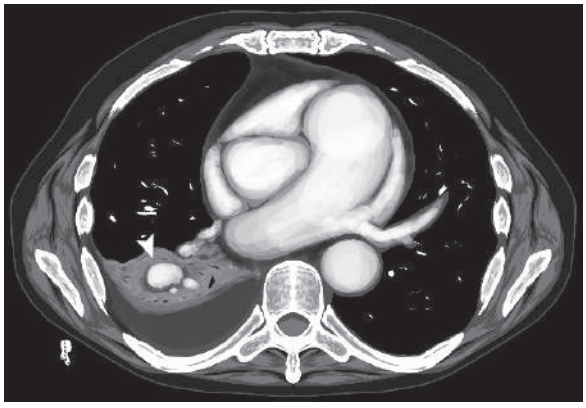

Fig. 11.13.6. Axial postcontrast chest CT illustration demonstrates a mass of TB associated with dilated pulmonary vessels representing Rasmussen pulmonary aneurysm (*arrowhead*)

Signs on CT

Rasmussen pulmonary aneurysm is a rare phenomenon characterized by dilatation and weakening of the peripheral pulmonary artery wall from an adjacent TB cavity (Fig. 11.13.6). It is seen in up to 5% of patients, and it may cause life-threatening hemoptysis. It is detected as TB inflammatory reaction or cavitary mass, with dilatation of the peripheral pulmonary artery adjacent to it.

Pleural TB

Pleural TB is the most common extra-pulmonary manifestation of primary or reactivation TB, and it can alone be the only manifestation of primary TB.

The pleural fluid often contains granulomata and a few organisms. When the fluid contains pus, high protein content (>3 g/dL), and a large number of organisms, it is called "*empyema*." Tuberculous empyema can be rarely caused by spinal TB draining into the pleural space via a sinus.

Patients with pleural TB present with pain during deep inspiration (pleuritic pain), fever, weight loss, and anorexia.

Chyliform (lymphatic) pleural effusion may occur in TB, with deposition of cholesterol within the pleural space. Fat-fluid or fat calcium level with calcified pleural margins may be seen on CT.

Empyema necessitates is a rare situation that arises when the empyema spontaneously discharge through the parietal pleura into the chest wall, forming a subcutaneous abscess.

Signs on Chest Radiograph and HRCT

- On plain radiograph, pleural effusion is seen as loss of the posterior and lateral costo-phrenic angles along with meniscus sign.
- Pleura thickening on CT is confirmed when the pleura is >2 mm in width.
- When the empyema calcifies, the CT scan shows empyema with calcified edges, a clinical condition called "*fibrothorax*" (Fig. 11.13.7).
- Empyema necessitates is detected as thickened pleural effusion with abscess formation that opens into the chest wall (Fig. 11.13.8).

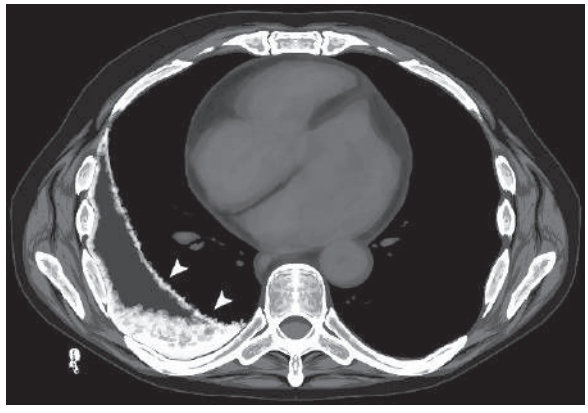

Fig. 11.13.7. Axial chest CT illustration demonstrates fibrothorax (*arrowheads*)

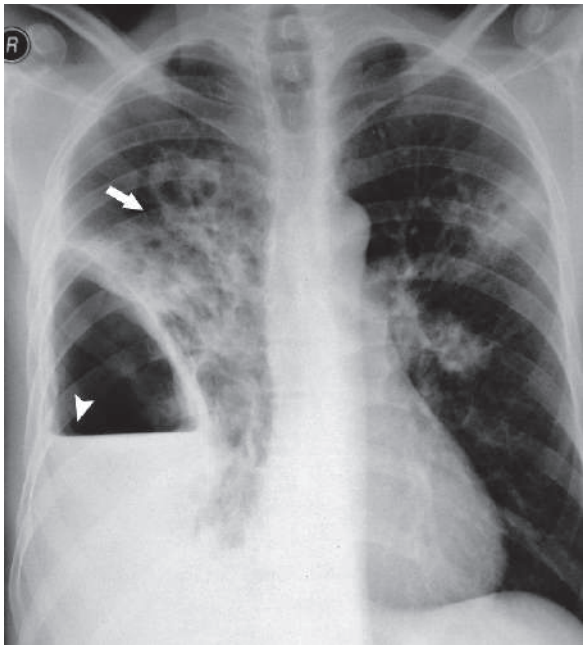

Fig. 11.13.8. Posteroanterior plain chest radiograph in a patient with old TB and chronic empyema that transformed into a lung abscess shows a huge right lung abscess (*arrowhead*) and bronchiectasis (*arrow*). The patient needed several pleural taps, and the abscess was beginning to open into the right lateral chest wall

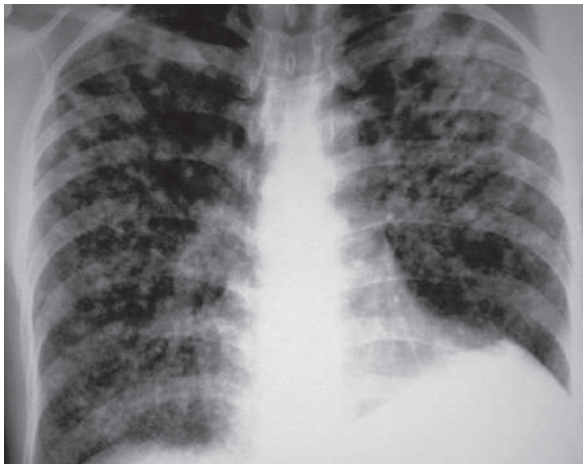

Fig. 11.13.9. Posteroanterior plain chest radiograph in a patient with miliary TB shows bilateral diffuse nodules in the lung fields representing miliary TB

Signs on Chest Radiograph

- Miliary TB is seen as bilateral symmetrical interstitial nodular pattern (Fig. 11.13.9). Absence of miliary pattern on chest radiograph does not rule out miliary TB.
- Bilateral pleural effusion may occur.

Miliary TB

Hematogenous spread of TB can be in small numbers causing no harm, moderate amount affecting one or two organs (isolated-organ TB), or in a diffuse large amount (miliary TB). In 5% of primary TB patients, the infection is not contained within an organ, and is disseminated into the blood stream and the lymphatic system, resulting in miliary TB. The term "miliary" is given because the disseminated lesions (granulomas) are round and small, mimicking numerous millet seeds. Miliary TB in HIV patients arises when the CD4 count is <300/mL.

Miliary TB is divided into acute miliary TB or cryptic miliary TB. Acute miliary TB may be associated with hyponatremia, inappropriate secretion of antidiuretic hormone, or adrenal insufficiency. Cryptic miliary TB is characterized by silent TB foci that seed bacilli into the blood stream from time to time; TB foci may be located within the lungs, kidneys, or lymph nodes.

Signs on HRCT

Miliary TB shows multiple, bilateral small nodules (<3 cm in size) randomly distributed through the lungs (Fig. 11.13.10).

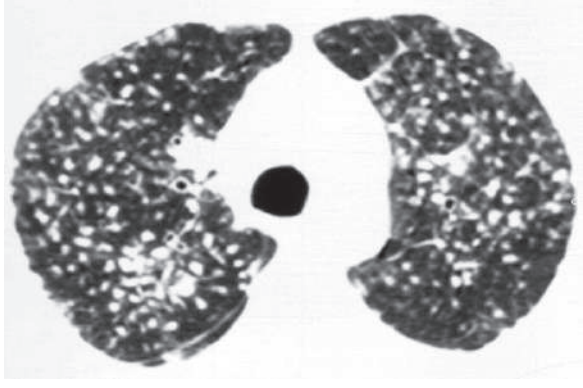

Fig. 11.13.10. Axial lung-window HRCT in the same patient of figure 11.13.19 shows the multiple nodular interstitial pattern of miliary TB

Abdominal TB

11.13

Abdominal TB invades the abdomen, peritoneum, and pancreato-biliary system via hematogenous spread from a primary lung or reactivation TB, or from swallowing infected milk. Although any structure can be involved, the ileocecal valve is the most frequently affected by granulomas, fibrosis and later scarring.

Patients may present with fever, weight loss, diarrhea, and abdominal pain and distension. Duodenal TB may results in dyspepsia, while rectal TB may results in constipation (30%) and passing fresh blood (hematochezia). Fistula-in-ano may arise due to anal TB. The chest radiograph may be normal in patients with abdominal TB in up to 60% of cases.

TB peritonitis may develop causing ascites, and omental and peritoneal thickening. TB peritonitis is divided into three forms: wet, fibrotic, and dry. Wet peritonitis is characterized by a large amount of viscous ascetic fluid (90% of cases). Fibrotic peritonitis is characterized by large omental masses and intestinal adhesions, causing the omentum to form a hard mass on palpation. Dry or plastic peritonitis is characterized by fibrous peritoneal reaction, dens adhesions, and caseous nodules.

Differential Diagnoses and Related Diseases

- *Bauhin's ileocecal valve syndrome* is a rare sporadic disease characterized by hypertrophic ileocecal valve in the absence of intestinal pathology. Patients classically present with vague abdominal pain, nausea, vomiting, diarrhea or constipation, and even active bleeding or melena. Differential diagnoses include TB, lymphoma, adenocarcinoma, and inflammatory bowel diseases.
- *Nonreactive TB* is a rare form of TB characterized by the formation large abscesses with large quantities of bacilli without granulomata. The abscesses may develop in the liver, lungs, or kidneys. Patients often present with fever, sepsis syndrome, and splenomegaly. This form of TB has been associated with AIDS, lymphoma, chronic steroid users, diabetics, and patients with hematological disorders.

Signs on Barium enteroclysis and Enema

- Ileocecal valve deformity, ulceration, and fibrosis. Wide gaping between the valve and the narrowed terminal ileum is called "*Fleischner sign*."
- *Coned cecum* is a deformity of the cecum into a cone-shaped structure due to prolonged infection and inflammation. Conical cecum with a widely open ileocecal valve and fixed terminal ileum is called "*Stierlin's sign*."

Signs on CT

- Thickened peritoneum may be seen as a tiny nodules or a thick nodular line surrounding the viscera beneath the abdominal walls, with marked enhancement after contrast injection.
- Irregular or focal omental thickening (*omental cake sign*).
- TB ascetic fluid with septations is seen in 30–100% of cases. The fluid typically has attenuation between 25 and 45 HU, which may reflect its exodative nature.
- Retroperitoneal (e.g., parao-aortic) nodes enlargement.
- Intestinal adhesions are identified on CT as intestinal loops sticking to the abdominal wall.
- In *Bauhin's ileocecal valve syndrome*, the CT show hypertrophic ileocecal valve with dilated small bowel loops proximally. The absence of abnormal contrast enhancement, pathologic intestinal manifestations, and iliocecal mass are supportive signs that assist in establishing the diagnosis. Definite diagnosis requires colonic biopsy that typically shows hypertrophic muscularis layer with absence of inflammatory or malignant changes.

Hepatic TB

Hepatic TB is seen as a part of miliary TB, and is characterized by hepatomegaly and liver failure. The bacilli reach the liver via hematogenous spread through the hepatic artery. TB can be one of the causes of hepatic peliosis.

Hepatic peliosis is a pathological condition characterized by segmentally or focally dilated liver sinusoids,

with or without macroscopically visible blood-filled cysts formation, with no preferential location in the liver. The blood-filled cysts can be lined by hepatocytes (parenchymal type) or lined by endothelium, and are based on aneurysmal dilatation of the central vein (phlebectatic type). Hepatic peliosis is caused by chronic wasting diseases like TB and malignancies, and it is also reported in long-term abuse of anabolic steroids or prolonged oral contraceptive use. Hepatic peliosis can be asymptomatic or causes liver failure, portal hypertension, or fatal intra-abdominal bleeding. Peliosis may also occur in the spleen, bone marrow, and lymph nodes.

Signs on CT

- Liver tuberculomas are abscesses that are seen on CT as multiple, scattered, hypodense lesions through the liver, 1–3 cm in size (Fig. 11.13.11).
- Large abscesses show ring enhancement after contrast injection.
- Hepatic peliosis has nonspecific features, and most reported features are variable. Histopathology is the definite diagnosing method. The most constant reported features are hypodense liver lesions that do not show mass effect over the adjacent vessels. The masses show a variable degree of enhancement, depending on the connection with the normal liver sinosoids. These masses represent areas of hepatic necrosis with internal hemorrhagic cysts formation.

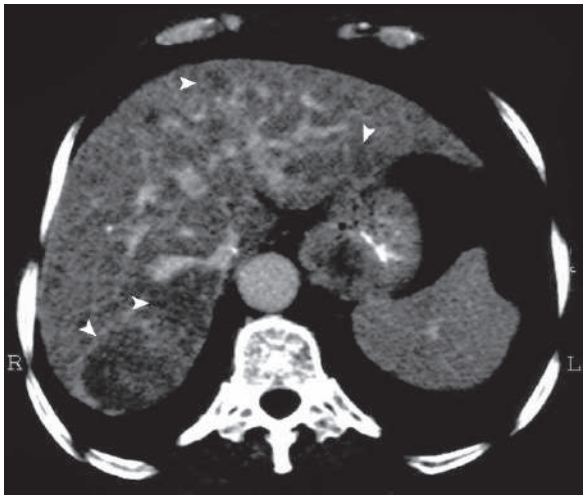

Fig. 11.13.11. Axial abdominal-enhanced CT shows multiple hypodense lesions in a patient with liver TB representing tuberculomas (*arrowheads*)

Central Nervous System TB

Intracranial TB can occur without evidence of pulmonary TB. It occurs in 10% of AIDS patients. Up to 60% of patients with intracranial TB are younger than 20 years.

TB of the central nervous system may occur in the form of meningitis (often in children), abscess, tuberculomas, or spinal cord disease. Patients may present with seizures, cognitive changes, or neurological deficits.

Signs on CT and MRI

- *Tuberculous meningitis*: there is thickening and enhancement of the meninges after contrast injection, along with signs of hydrocephalus due to basal meninges obstruction. Tuberculous meningitis usually occurs due to rupture of parenchymal granuloma into the subarachnoid space. Meningeal enhancement may persist for years after successful TB therapy.
- *Tuberculomas*: seen as multiple nodular, ring enhancing lesions (<1 cm). Only active tuberculomas enhance with contrast, while nonactive tuberculomas will not enhance. Tuberculoma may show mass effect over the adjacent brain parenchyma.
- *Tuberculous Abscess*: seen as a hypodense area surrounded by edema and uniform ring enhancement postcontrast injection (Fig. 11.13.12).

11.13

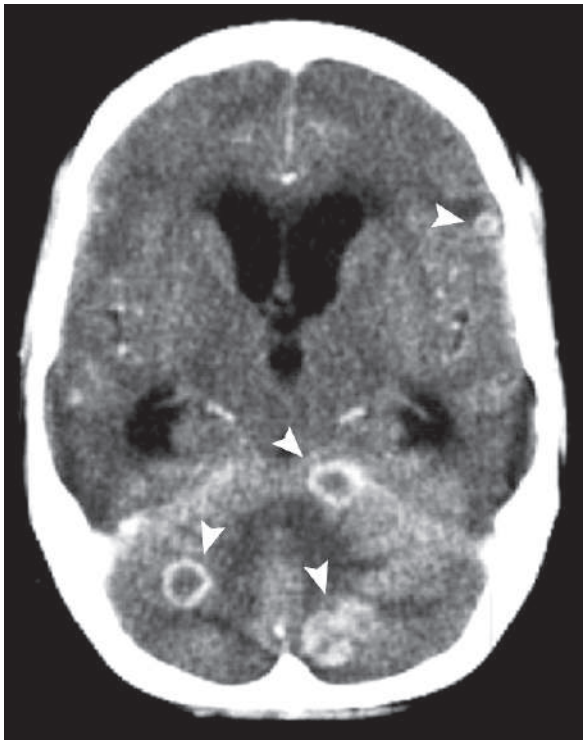

Fig. 11.13.12. Axial postcontrast CT image show multiple tuberculous abscesses in a patient with disseminated TB (*arrowheads*)

Genitourinary TB

Renal TB commonly occurs due to hematogenous spread of *M. tuberculosis* from adjacent primary focus, usually from the lungs. The urinary tract is infected in 15% of patients.

In the kidneys, there are papillary lesions forming multiple granulomas, and irregular renal cavities that may communicate with the calyces.

Patients classically present with burning micturation, frequent urination due to contracted bladder (29%), renal colic (13%), and (uncommonly) hematospermia. Patients with TB urinary symptoms do not respond to the usual antibiotics.

Epididymitis in males and tubo-ovarian abscess and infertility in females may be seen when the genital organs are infected with TB.

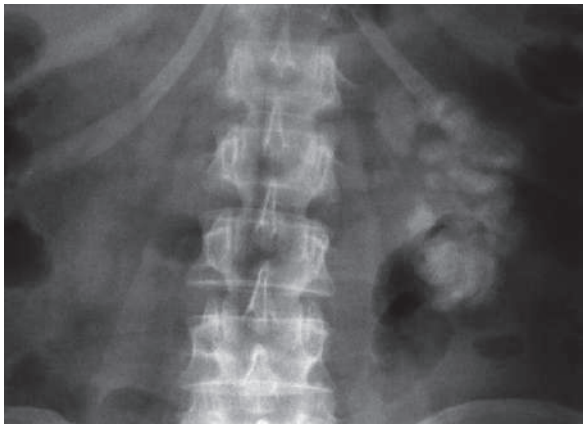

Fig. 11.13.13. Plain abdominal radiograph shows unilateral left renal parenchymal calcification in a patient with TB

Signs on IVU

- There are strictures of the calyces and calcifications within the renal parenchyma (Classic) (Fig. 11.13.13).
- The presence of psoas abscess supports the diagnosis of renal TB.
- Ureteral strictures may present at the infundibulum, the ureteropelvic junction, or the distal ureters (saw tooth appearance). The ureter may become a straight rigid tube, known as "*pipestem ureter*."
- End-stage renal TB results in a small, shrunk, and fibrotic kidney with poor function and parenchymal calcifications (putty kidney).

Signs on CT

- Calcifications within the renal parenchyma are seen in up to 50% of cases.
- Fibrotic strictures of the infundibulum, renal pelvis, and ureters (diagnostic).
- *Putty kidney* is a term used to describe end-stage TB kidney, characterized by a shrunken kidney with extensive calcification that is associated with autonephrectomy (Fig. 11.13.14).
- *Phantom calyx* is a kidney in which no collecting system element can be identified.
- *Thimble bladder* is a very small bladder with reduced capacity due to thick extensive calcification of the bladder wall.

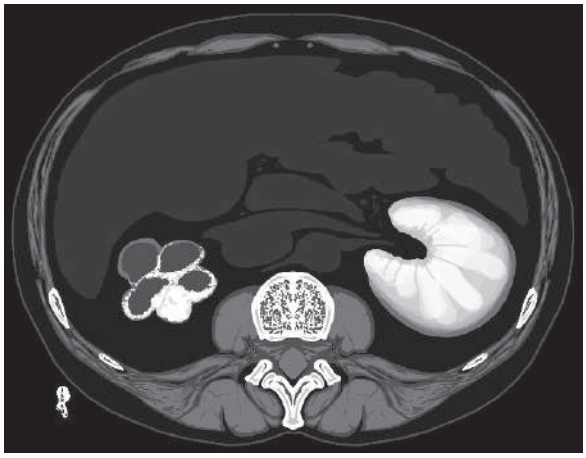

Fig. 11.13.14. Axial postcontrast abdominal CT illustration demonstrates right putty kidney

Musculoskeletal TB

Musculoskeletal TB is an uncommon condition that occurs in 1–3% of patients. *M. tuberculosis* often infects the musculoskeletal system via hematogenous spread.

Any bone can be affected, but the spine, hip, and knee are commonly affected, usually in young patients. Spinal TB is called "*Pott's disease*," and it often affects the thoracic spine (50% of cases). Pott's disease is characterized by kyphosis, cold abscess, and paraplegia. *Cold abscess* is a localized caseous collection that can be seen in the lymph nodes, TB of joints, and in Pott's disease. In Pott's disease, it occurs due to collapsed TB-infected vertebra with pus released into the adjacent paraspinal compartments. It can be seen as a retropharyngeal abscess (cervical Pott's disease), retrocardial abscess (thoracic Pott's disease), and psoas abscess (lumbar Pott's disease).

Patients often present with progressive focal back pain and muscle spasm. Neurological deficits, cauda equine compression syndrome, and paraplegia due to cord compression are uncommon neurological complications of Pott's disease. Paraplegia occurs in Pott's disease (10% of cases) due to cord compression from a collapsed vertebra or due to spinal cord infarction from closed vessels due to endarteritis obliterans.

Tuberculous arthritis commonly affects one joint (monoarthritis). The hip or the knee joint is frequently affected. Patients present with progressive pain, swelling of the affected joint with loss of function due to septic arthritis, and synovial pannus formation.

Spina ventosa is a term used to describe a form of TB osteomyelitis where there is underlying bone destruction, overlying periosteal thickening, and fusiform expansion of the bone. Very rarely, TB osteomyelitis can result after vaccination with Bacille-Calmette-Guérin (BCG) vaccine (*BCG osteomyelitis*). BCG vaccine is used for preventing TB in many areas of the world, and it is composed of a live attenuated strain of *Mycobacterium bovis*. BCG osteomyelitis usually arises in infants and children with low immunity, with a very low incidence (1 or 2 per several million vaccine recipients). Symptoms arise during a period ranging from a few months to 5 years postvaccination. The lesions occur in the epiphysis and metaphysis, and may cross the growth plate. BCG osteomyelitis is radiographically identical to TB osteomyelitis. Diagnosis requires culture of the BCG strain for conformation.

Differential Diagnoses and Related Diseases

Mycobacterium marinum flexor tenosynovitis: *M. marinum* is an atypical mycobacterial infection that inhabits saltwater fish and swimming pools. Patients are often infected with *M. marinum* after abrasions or puncture to the hand while working with aquariums. Lesions start to appear 2–4 weeks after inoculation in the form of focal tenosynovitis of the hand, usually with lymphadenopathy in the ipsilateral arm. Diagnosis is often delayed for months due to lack of clinical suspicion, and is often mistaken for rheumatoid arthritis or gout arthropathy. Diagnosis is usually difficult and requires open surgical biopsy of the synovium with histological examination. Ziehl-Nielson stain is often negative, and diagnosis is established by modified AFB (Fite) stain, which will stain the *M. marinum*. On MRI, there is flexor tenosynovitis with hypertrophied synovium und contrast enhancement similar to the image seen in chronic granulomatous diseases. Unlike acute purulent tenosynovitis, the bone and the underlying muscles are rarely affected (characteristic finding). Tenosynovitis with normal muscle and bone marrow signal on postcontrast MRI in a fisherman or a patient dealing with aquariums should bring *M. marinum* tenosynovitis to mind.

11.13

Signs on Radiograph

- Vertebral end plate irregularities with decreased high of the disk intervertebral space (Fig. 11.13.15). In contrast to Pott's disease, metastases destroy the vertebral bodies and spare the disc spaces, while in Pott's diseases both vertebral body destruction and intervertebral disc space reduction are found.
- *Step-off kyphosis*: there is loss of the anterior vertebral endplates with herniation of the intervertebral disk into the vertebral bodies, causing kyphosis.
- *Gibbus deformity* is referred to as destruction of multiple thoracic vertebrae, causing angular kyphosis.
- Paraspinal (cold abscess) and psoas abscesses may develop due to extension of the infection to the nearby structures.
- The affected joint in tuberculous arthritis shows soft-tissue mass swelling with loss of the joint surface definition (Fig. 11.13.16). Articular cartilage destruction and erosion are commonly seen.
- *Phemister's triad*: juxta-articular osteoporosis, gradual joint-space narrowing, and peripheral osseous erosions. It suggests TB arthritis, but is not specific.
- *Spina ventosa* is typically seen in the short bones of the hands and feet as cyst-like cavities with expansion of the diaphyses and soft-tissue swelling (*TB dactylitis*).

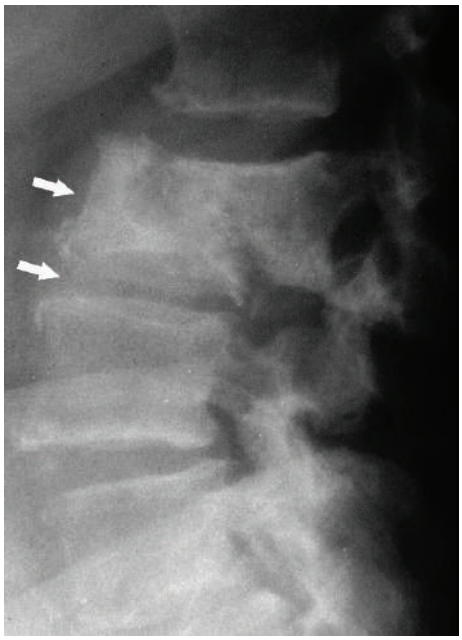

Fig. 11.13.15. Lateral plain radiograph of the thoracic spine in a patient with thoracic Pott's disease shows destruction of the vertebral body and narrowing of the intervertebral disc space (*arrows*)

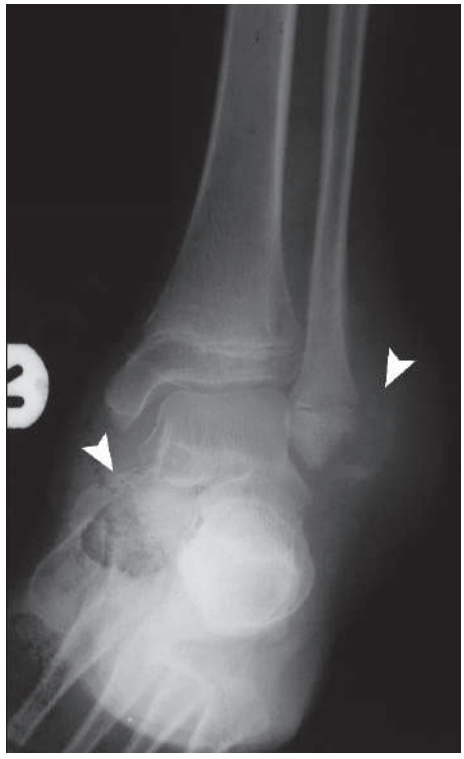

Fig. 11.13.16. Plain radiograph of the ankle in a young patient with tuberculous arthritis shows lateral ankle soft-tissue swelling with bone destruction of the distal fibular epiphysis and the metatarsal bones, suggesting osteomyelitis (*arrowheads*)

Signs on CT

- Psoas abscess is seen as an enlarged psoas muscle with a hypodense center due to abscess formation (Fig. 11.13.17). Rim enhancement after contrast injection is typically seen.
- Paraspinal cold abscess is detected as abnormal fluid collection adjacent to vertebral destruction (Fig. 11.13.18).
- *Borrowing abscess* is a pathological situation characterized by tracts (sinuses) linking the infected vertebra with the peritoneal cavity. There may also be sinuses linking the infected vertebra with the muscles or the skin.
- Formation of an epidural abscess is the most feared complication of Pott's disease, and it develops in 10–47% of patients.

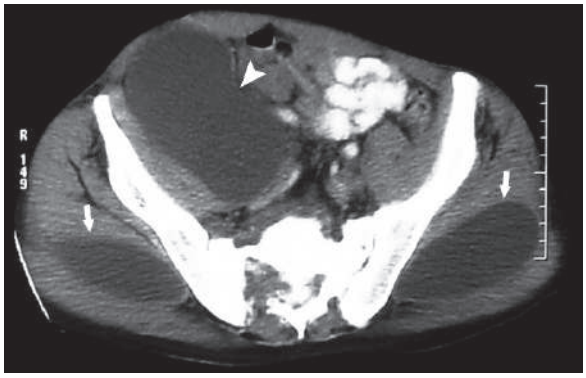

Fig. 11.13.17. Axial pelvic CT in a patient with Pott's disease shows a large right psoas abscess (*arrowhead*), which drains into both gluteal muscles (*arrows*)

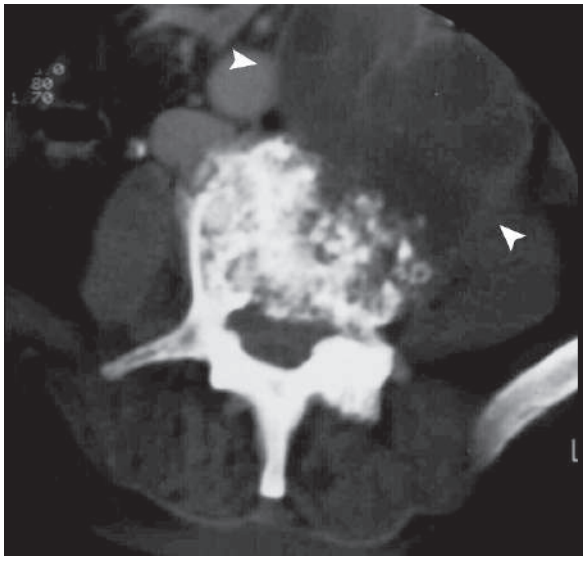

Fig. 11.13.18. Axial nonenhanced vertebral CT shows vertebral destruction in a patient with Pott's disease, with left paraspinal cold abscess formation (*arrowheads*)

Tuberculous Lymphadenitis

Tuberculous lymphadenitis is a common cause of lymphadenopathy in primary TB patients. It may occur in the pulmonary hilar nodes, cervical lymph nodes (called *scrofula*), the mesenteric nodes, the para-aortic nodes, the axillary and the inguinal nodes. *Tabes mesenterica* is a term used to describe primary TB lymphadenopathy of the mesentery.

Nodal infection arises from hematogenous or lymphatic TB dissemination. Clinical presentation depends on the lymph nodes affected. The affected nodes may erode into the adjacent organs, resulting in draining sinuses.

Tuberculous pericarditis that may lead to constrictive pericarditis may occur due to invasion of the pericardium from the adjacent tuberculous hilar lympha denitis. It is a rare complication that may occur in 1% of cases. Also, direct bacilli invasion of the mediastinum from the adjacent hilar tuberculous lymphadenopathy may result in inflammation of the mediastinal structures (mediastinitis).

Signs on Sonography and PD

- TB cervical lymphadenopathy shows different flow pattern signals on power Doppler sonography. The most frequent pattern is *hilar* flow, in which the flow signal branches from the hilus radially. The second pattern is *peripheral*, where the signal is spotted flowing along the periphery of the enlarged node. A mixed pattern between the hilar and the peripheral can be seen.
- Avascular nodes with no flow signal on PD may be seen, and attributed to caseous necrosis within the nodes.

Signs on CT

- Enlarged, circular nodes with a mean size of 20 mm. Calcification may be seen.
- Center caseation of the nodes is seen as low-attenuated center of the enlarged nodes (Fig. 11.13.19).
- After contrast administration, enhancement can be peripheral (characteristic of TB lymphadenopathy), homogeneous, or homogeneous mixed with peripheral enhancement.

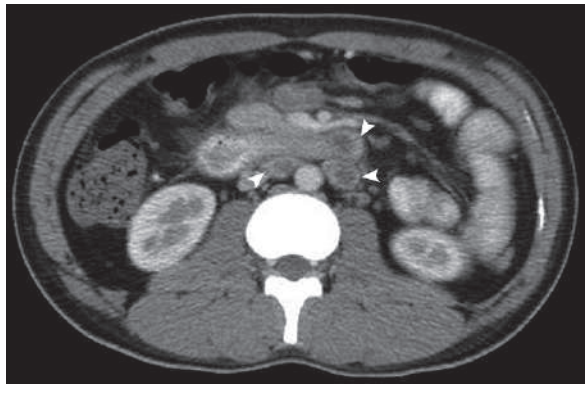

Fig. 11.13.19. Axial abdominal postcontrast CT in a patient with TB shows enlarged para-aortic lymph nodes with a hypodense center (*arrowheads*)

Dermatological TB

11.13

Cutaneous TB is generally classified into true cutaneous TB or tuberculid TB. In true cutaneous TB, also known as *tuberculous gumma*, multiple, painless cold abscesses form on the skin due to secondary metastasis of the bacteria from a primary focus via hematological routes. In contrast, tuberculid is a skin reaction to tuberculous lesions in other organs.

Tuberculous gumma is a very rare lesion, and it has been reported to occur in patients with no primary TB infection after trauma or venous blood test with a sterile needle, a phenomenon known as "*Pseudo-Köbner's phenomenon*." The lesion arises at the site of the trauma or the needle injection.

Scrofuloderma is an atypical dermatological manifestation of TB in tropical countries. Scrofula is a Latin word meaning "weal resistance to disease." Scrofuloderma arises due to infection of the skin with TB overlying another TB process, usually tuberculous lymphadenitis. It is commonly seen in the pediatric age group, and typically located in the parotid, submandibular, supraclavicular, and lateral aspect of the neck regions (Fig. 11.13.20).

Fig. 11.13.20. An illustration demonstrates scrofula at the lateral side of the neck

Lupus vulgaris is TB of the skin characterized by reddish-brown plaques located on the skin of the face and the neck. The term "lupus vulgaris" was given to the lesion because the skin looks as if the patient were attacked by a wolf (Fig. 11.13.21). The condition may transform into squamous cell carcinoma.

Erythema induratum (Bazin's disease) is a rare form of nodular vasculitis and lobular panniculitis (Fig. 11.13.22). The dermal lesions are typically seen in the legs. The lesions are caused by hypersensitivity reaction to the tubercle bacillus antigen. Patients with erythema induratum have a positive tuberculin skin test.

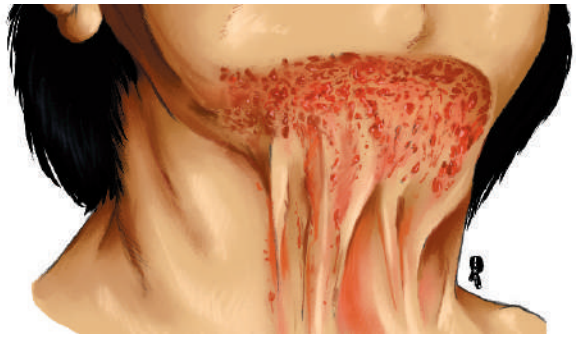

Fig. 11.13.21. An illustration demonstrates lupus vulgaris

Fig. 11.13.22. An illustration demonstrates erythema induratum of Bazin

For Further Reading

1. Quast TM et al Pathogenesis and clinical manifestations of pulmonary tuberculosis. Dis Mon. 2006;52:413–9
2. Yun JS et al Latent tuberculosis infection. Dis Mon. 2006; 52:441–5
3. Johnson MD et al Tuberculosis and HIV infection. Dis Mon. 2006;52:420–7
4. Lazarus AA et al Pleural tuberculosis. Dis Mon. 2007;53: 16–21
5. Lazarus AA et al Tuberculous lymphadenitis. Dis Mon. 2007;53:10–15
6. Lazarus AA et al Abdominal tuberculosis. Dis Mon. 2007; 53:32–8
7. Ludwig B et al Musculoskeletal tuberculosis. Dis Mon. 2007; 53:39–45
8. Myers JN et al Miliary, central nervous system, and genitourinary tuberculosis. Dis Mon. 2007;53:22–31
9. Picard C et al Massive hemoptysis due to Rasmussen aneurysm: detection with helicoidal CT angiography and successful steel coil embolization. Intensive Care Med. 2003;29: 1837–9
10. Pereira JM et al Abdominal tuberculosis: imaging feature. Eur J Radiol. 2005;55:173–80
11. Lee JJ et al High resolution chest CT in patients with pulmonary tuberculosis: characteristic findings before and after antituberculous therapy. Eur J Radiol. 2008;67:100–4
12. Kim HY et al Thoracic sequelae and complications of tuberculosis. RadioGraphics. 2001;21:839–60
13. Miller WT et al Tuberculosis in the normal host: radiological findings. Semin Roentgenol. 1993;28(2):109–18
14. Castaner E et al Congenital and acquired pulmonary artery anomalies in the adult: radiologic overview. RadioGraphics. 2006;26:349–71
15. Kanabar P. Tuberculosis of the lumbar spine. Indian J Orthop. 2005;39(2):18–89
16. Ahuja A et al Power Doppler sonography of cervical lymphadenopathy. Clin Radiol. 2001;56:965–9
17. Dyer RB et al Classic signs in uroradiology. RadioGraphics. 2004;24:S247–80
18. Vidal D et al Tuberculous gumma following venepuncture. Br J Dermatol. 2001;144:601–3
19. Aslam N et al Pseudo-Koebner phenomenon: unusual manifestation of tuberculosis after venepuncture. Injury Extra. 2005;36:479–82
20. Lupi O et al Tropical dermatology: bacterial tropical diseases. J Am Acad Dermatol. 2006;54:559–78
21. Nesher E et al Bauhin's ileocecal valve syndrome – a rare cause for small-bowel obstruction: report of a case. Dis Colon Rectum. 2006;49:527–9
22. Rademarker M et al Erythema induratum (Bazin's disease). J Am Acad Dermatol. 1989;21:750–5
23. Steinke K et al Unusual cross-sectional imaging findings in hepatic peliosis. Eur Radiol. 2003;13:1916–9
24. Funato M et al Refractory osteomyelitis caused by bacilli Calmette-Guérin vaccination: a case report. Diagn Microbiol Infect Dis. 2007;59:89–91
25. Wongworawat MD et al A prolonged case of Mycobacterium marinum flexor tenosynovitis: radiographic and histological correlation, and review of the literature. Skeletal Radiol. 2003;32:542–5

11.14

Typhoid Fever (Salmonellosis)

Typhoid fever (TF) is a disease caused by systemic infection with the bacterium *Salmonella typhi*. The occurrence of TF is high in developing countries due to poor sanitation.

Between 1900 and 1907, TF was notoriously linked to the name of an Irish cook in New York City named "Mary Mallon." Mallon, notoriously known as "typhoid Mary," was the first person defined as a "healthy carrier" of TF in the United States. Patients who are silent carriers of *S. typhi* can transmit the disease to other persons via feco-oral transmission. The carrier can transmit the bacteria by touching food or water with a dirty hand.

Typical manifestations of salmonellosis include fever, constipation during the first week of fever, diarrhea during the second week of fever, splenomegaly, rose spots, encephalopathy (*typhoid state*), leucopenia, and abdominal distension that may be complicated by intestinal perforation in the third week of fever (commonly in the terminal ileum). Typhoid encephalopathy typically occurs in the third week of fever.

Atypical manifestations of TF include psoas pyomyositis, splenic abscess, and (later) rupture, hepatic abscess, cerebellar ataxia, pneumonia, and vertebral osteomyelitis. These atypical manifestations are attributed to the bacteremia encountered during the first week of fever.

Typhoid osteomyelitis is a very rare complication of TF, with widespread bacteremia. It may develop years after the initial infection with a widespread disease. Usually, the patient does not show any spinal or skeletal involvement during the active intestinal disease. Patients with typhoid osteomyelitis often present with nonspecific lower back pain, without fever. A previous history of TF may be the only clue to the diagnosis of typhoid osteomyelitis. Raised erythrocyte sedimentation rate and positive blood cultures are found in 50–70% of cases.

The liver manifestations of TF fall into three categories: asymptomatic patient, hepatomegaly with abnormal liver functions, and hepatic disease as the main manifestation of TF (*typhoid hepatitis*). On histopathology, the bacteria are found within the reticuloendothelial system, causing hyperplasia of the Kupffer cells (*typhoid nodules*).

Clinicopathologically, TF is diagnosed by a positive *Widal test*; however, a negative test result does not rule it out. The Widal test is only positive in the second week. Bacterial culture or isolation of the bacteria from the urine or the stools confirms the diagnosis of TF. Ultrasound is helpful in diagnosing TF within the first week, especially with high suspicion.

Signs on US

- Hepatosplenomegaly may be present, especially during the second week.
- Uncommonly, splenic or hepatic abscesses may be found as multiple hypoechoic lesions.
- Increased bowel wall thickness is a common finding due to diarrhea and intestinal infection (commonly at the terminal ileum).
- Enlarged mesenteric lymph nodes with a diameter ranging from 8 to 34 mm.
- The gall bladder wall may be distended and thickened (>4 mm). Positive sonographic Murphy's sign plus increased vascular Doppler signal of the gallbladder wall indicate acute acalculus cholecystitis. In sonographic Murphy's sign, the probe has to be kept steady in the subcostal region in the right upper quadrant and the patient must be asked to take a deep breath. If the patient stops breathing while the probe is still, then the sign is positive (exactly like the manual surgical Murphy's sign examination).

Signs on CT

- Hepatic and splenic abscesses may be encountered on contrast-enhanced liver CT as multiple hypodense lesions, with characteristic rim enhancement within enlarged liver and spleen (Fig. 11.14.1).
- Rarely, splenic infarction may be seen in cases of severe bacteremia as a hypodense area, commonly located at the periphery, with no contrast enhancement after contrast injection.

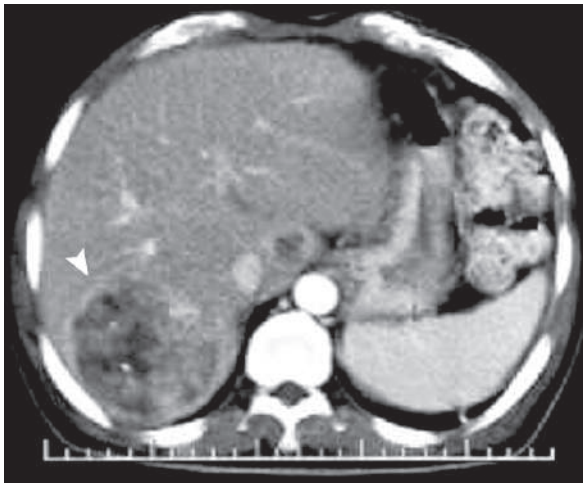

Fig. 11.14.1. Axial postcontrast abdominal CT shows liver abscess developed in a patient after typhoid septicemia (*arrowhead*)

Signs on Vertebral Plain Radiograph and MRI

- On plain radiographs, erosion of the vertebral end plates may be seen without evidence of diffuse vertebral destruction, according to the stage and severity of the osteomyelitis (Fig. 11.14.2).
- On MRI, irregular end plates, erosions, vertebral disc infiltration, with high signal intensity on T2W images representing edema may be seen.

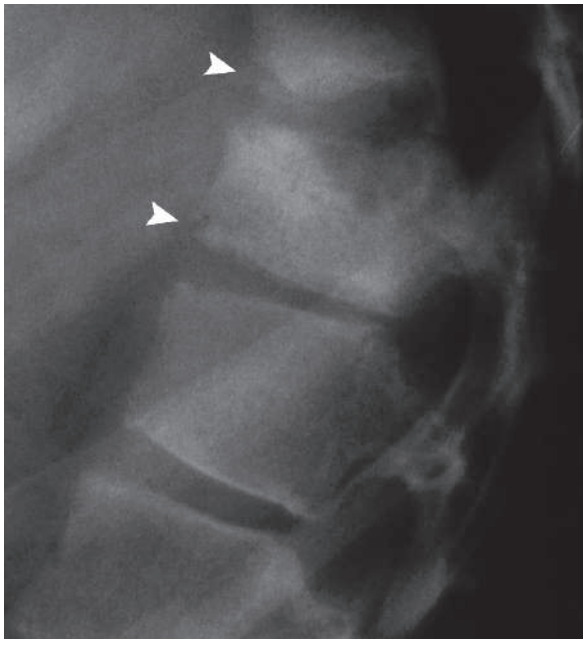

Fig. 11.14.2. Lateral plain radiograph of the thoracic vertebrae in a patient with a history of previous typhoid fever infection who presented with erosions of the inferior end plates due to typhoid osteomyelitis (*arrowheads*)

For Further Reading

1. Khan FY et al Typhoid osteomyelitis of the lumbar spine. Hong Kong Med J. 2006;12:391–3
2. Crichton EP et al Typhoid osteomyelitis of spine treated with chloramphenicol. Can Med Assoc J. 1953;69:529–30
3. Mateen MA et al Ultrasound in the diagnosis of typhoid fever. Indian J Pediatr. 2006;73(8):681–5
4. Mehta LK et al Infarction of spleen in typhoid fever. Saudi Med J. 2007;28(2):271–2
5. Mirsadraee M et al Typhoid myelopathy or typhoid hepatitis: a matter of debate. Indian J Med Microbiol. 2007;25(4):351–3
6. George P et al A sinister presentation of typhoid fever. Indian J Nephrol. 2007;17(4):176–7
7. Pandey A et al Typhoid sigmoid colon perforation in an 18-month-old boy. World J Pediatr. 2008;4(4):305–7
8. Hart JL et al Life-threatening colonic haemorrhage in typhoid fever: Successful angiographic localization and platinum microcoil embolization of several resources. Clin Radiol. 2008;63:727–30
9. Yüksel M et al Multiple splenic abscesses in a child as a complication of typhoid fever. Firat Tip Dergisi. 2005;10(2):80–2
10. Dutta TK et al Atypical manifestations of typhoid fever. J Postgrad Med. 2001;47:248–51
11. Karande SC et al Typhoid fever in a 7 month old infant. J Postgrad Med. 1995;41(4):108–9

11.15 Malaria

Malaria is a mosquito-borne disease, caused by the protozoan parasite *Plasmodium*. There are four main varieties of the genus *Plasmodium*: *P. falciparum*, *P. vivax*, *P. malariae*, and *P. ovale*.

Transmission of malaria is by the anopheline mosquito, or occasionally by blood transfusion. The majority of the endemic areas are located within sub-Saharan Africa and Southeast Asia.

The clinical presentation of malaria is variable, ranging from a simple, mild flu-like illness to the full-blown disease of encephalopathy and intermittent fever. It must be on the list of differential diagnosis in any patient with unexplained symptoms returning from areas where malaria is endemic. Some patients possess immunity against malaria, especially people in endemic areas who have repeated infections, or patients with hemoglobinopathies such as sickle cell disease and β-thalassemia.

Most mortality cases of malaria are related to the *P. falciparum* variant. The classical presentation is a febrile illness with cyclical fever, rigors, and chills; however, the disease is rarely present with its classical description. Additional symptoms include abdominal pain, vomiting, and mild diarrhea. The nonsevere malaria illness may be indistinguishable from any febrile illness caused by any infection. The severe form often presents with anemia, hypoglycemia, acidosis, and multi-systemic manifestations.

The most common neurological symptom of *P. falciparum* encephalopathy is deep coma, which is defined as the inability to localize a painful stimulus in a patient with *P. falciparum* in whom other causes of encephalopathy have been excluded. Patients with *P. falciparum* coma typically have their eyes open, and seizures develop in approximately 70% of cases. Sequelae of *P. falciparum* encephalopathy include hemiplegia (42%), behavioral disorder (24%), epilepsy (24%), and blindness (8%).

Respiratory abnormalities due to malaria have one or more of four abnormalities: deep, gasp-like breathing due to metabolic acidosis (*Kussmaul's breathing*), hyperventilation without acidosis, hypoventilation with nystagmus and excessive salivation due to status epilepticus, and periodic respiration associated with abnormalities in the papillary reflexes.

Anemia in malaria arises due to the parasitic infection of the red blood cells during the asexual life cycle, bone marrow suppression by the disease, or from iron deficiency due to poor intake. Hepatic disease with elevated liver enzymes is common due to the parasite cycle.

Rarely, malaria can cause rheumatic-like arthritis or polymyositis-like syndrome. The role of radiology in malaria is to monitor disease progression and therapy response, or to detect complications. Diagnosis is essentially made by identifying the parasite by thick and thin blood films under microscopy.

Differential Diagnoses and Related Diseases

Hyperactive malarious splenomegaly (HMS) (tropical splenomegaly syndrome) is a pathological condition characterized by splenomegaly due to disturbance in the T-lymphocyte control of the humoral response to recurrent malaria. HMS is recognized as a distinct entity from the splenic enlargement directly resulting from malarial parasitemia. Patients are typically young adults from a malarious area, presenting with persistent moderate to marked splenomegaly, which may be progressive or fluctuating in degree but does not spontaneously regress, and which may at times give rise to severe pain. Laboratory investigations in HMS show pancytopenia with very high serum IgM levels and malaria antibody titers, and an absence of malaria pigment in circulating erythrocytes, circulating monocytes, or tissue macrophages.

Signs on Radiographs

Chest radiographs may show signs of bronchoalveolar edema or patchy pneumonic infiltrations.

Signs on US

- Nonspecific splenomegaly is often found, while hepatomegaly is classically absent. However, absence of splenomegaly does not rule out malaria.
- Splenic infarction may be seen as a hypoechoic peripheral wedge-shaped area.
- Signs of portal hypertension may be seen in advanced liver disease.

Signs on CT

- In the acute stage of the coma, profound brain edema with compressed ventricles is often found due to intraparenchymal inflammation.
- In the chronic stage, ventricular dilatation and brain parenchymal atrophy are commonly found.
- Severe brain edema may cause life-threatening brain herniation.

Signs on MRI

MRI of reported cases of cerebral malaria show that cytotoxic edema often involves the centrum semiovale in a bilateral fashion, and show cortical and subcortical ischemic lesions, central pontine myelinolysis, and myelinolysis of the upper medulla. *Central pontine myelinolysis*, or osmotic myelinolysis, is a disease characterized by focal demyelination in the middle of the pons, often seen as a consequence of excessively rapid correction of chronic hyponatremia. It is classically seen on MRI as a central area of high T2 signal intensity within the pons, sparing the periphery and the descending corticospinal tracts, with no enhancement or mass effect (Fig. 11.15.1).

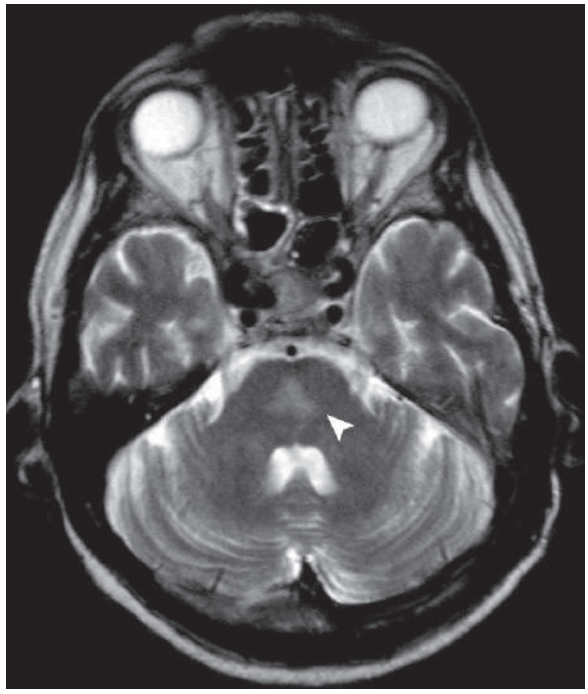

Fig. 11.15.1. Axial T2W brain MRI shows central pontine high intensity signal in a patient with central pontine myelinolysis (*arrowhead*)

For Further Reading

1. Medana IM. Human cerebral malaria and the blood brain barrier. Int J Parasitol. 2006;36:555–68
2. Dunn IJ et al Malaria. Semin Roentgenol. 1998;33(1):79–80
3. Richter J et al Is ultrasound a useful adjunct for assessing malaria patients? Parasitol Res. 2004;94:349–53
4. Idro R et al Pathogenesis, clinical features, and neurological outcomes of cerebral malaria. Lancet Neurol. 2005;4: 827–40
5. Gamanagatti S et al MR imaging of cerebral malaria in a child. Eur J Radiol. 2006;60:46–7
6. Agrawal A et al Symmetric peripheral gangrene with mixed malaria. Indian J Pediatr. 2007;74:587–8
7. Peng SL. Rheumatic manifestations of parasitic diseases. Semin Arthritis Rheum. 2002;31:228–47
8. Crane GG. Hyperactive malarious splenomegaly (tropical splenomegaly syndrome). Parasitol Today. 1986;2(1):4–9

11.16 Animal Bites and Stings

Animal bites and stings are uncommon medical conditions encountered in emergency rooms, but when encountered, they can present a life-threatening situation. In this topic, some of the most common animal bites are discussed, with radiological features that were occasionally reported in the radiological literature.

Rabies

Rabies is a zoonotic disease arising due to human infection with the rabies virus, which is a single-stranded RNA virus that belongs to the genus *Lyssavirus* of the family *Rhabdoviridae*. The term rabies is derived from an old Indian root word *rabh*, meaning to make violent.

The rabies virus infects humans after a bite from an animal host, because the virus is abundant in high concentrations in the animal host's saliva. Almost any animal is capable of contracting rabies. The main hosts are foxes in Europe, raccoons in the United States, dogs in Asia, jackals in Africa, and vampire bats in Latin America.

The incubation period is typically 2–8 weeks, but it can be as long as 1 year (7% of cases). There is no laboratory test to determine whether a person is infected with the rabies virus during the incubation period. Other modes of transmission are through inhalation, and contact of infected saliva with an open wound or mucous membrane.

After the animal bite, the virus is introduced deep into the human soft tissues via the animal's saliva. The virus replicates in muscles, then starts its journey toward the central nervous system (CNS) through retrograde axoplasmic flow of approximately 12–24 mm per day. The virus enters the CNS via the dorsal spinal root ganglia, and then propagates in a retrograde flow to the brain. The clinical manifestations start when the virus reaches the CNS.

In the CNS, rabies may present in one of two forms: encephalitic (furious) and paralytic (dumb). The encephalitic form is the classical form, which is characterized by fever, malaise, anorexia, hydrophobia (fear of water), aerophagia (swallowing too much air), hyperirritability, hyperactivity, seizures, and mood swings. In contrast, paralytic rabies has a clinical presentation that resembles Guillain-Barré syndrome with flaccidity and lack of hydrophobia and aerophagia. Both forms of the disease are fatal, and death is 100% within 10 days of the onset of neurologic symptoms.

The rabies virus has an affinity to the gray matter. On histological examination of rabies specimens, neuronal *Negri bodies* are classically found. Negri bodies are eosinophilic cytoplasmic inclusions that contain the rabies virus in the neurons. They are commonly seen in the pyramidal cells of the hippocampus, cerebral cortex, and Purkinje cells.

Signs on CT

A CT scan shows focal or diffuse hypodense areas involving the basal ganglia, periventricular white matter, brain stem, and hippocampus.

Signs on MRI

- Bilateral high T1 and T2 signal intensities are seen in the basal ganglia, thalami, periventricular white matter, and the cervical spinal cord. The high T1 signal intensities are attributed to area of hemorrhage (Fig. 11.16.1a).
- The spinal cord may show signs of transverse myelitis or dorsal root ganglionitis (enhanced dorsal root after contrast injection).
- Moderate brachial plexus contrast enhancement ipsilateral to the site of the bite may be seen. This finding is due to neuronal inflammation in response to the presence of the rabies virus during its retrograde axoplasmic flow (Fig. 11.16.1b).
- MRI of the brain in a patient with the paralytic form may mimic the MRI of postvaccinial acute disseminated encephalomyelitis (ADEM). Rabies affects the gray matter, while ADEM predominantly affects the white matter.

Viper Bite

Viperidae are a family of venomous snakes possessing long fangs that permit deep-tissue penetration and venom injection.

After a snake bite, vesicular and hemorrhagic reaction starts to develop from 8 to 24 h. Local manifestations include swelling, pain, and perhaps tissue necrosis.

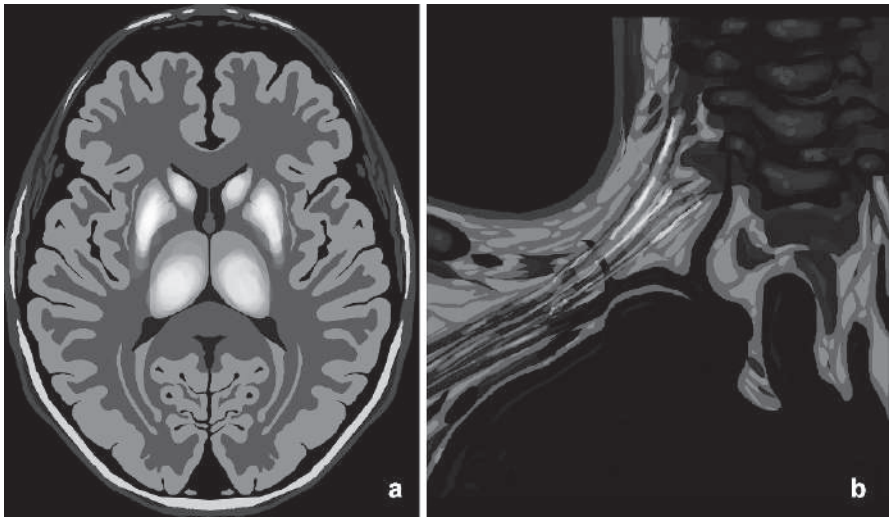

Fig. 11.16.1. Axial FLAIR (**a**) and coronal T1W postcontrast brachial plexus MR illustrations show signs of rabies. In (**a**), the axial brain shows hyperintensity signal involving the basal ganglia and the thalami bilaterally in a symmetrical fashion. In (**b**), the brachial plexus illustration shows brachial plexus cords and roots enhancements

Systemic manifestations include faintness, weakness, hypotension, abnormal bleeding and clotting, hematuria, and renal failure. Most of the systemic manifestations of a viper bite are related to abnormal coagulopathy.

Snake venom enhances bleeding tendency due to blood depletion of fibrinogen and clotting factors V, VII, II, and XIII. Diffuse intravascular consumptive coagulopathy (DIC) with thrombosis of small and large vessels may occur. Uncommonly, a stroke may arise a after snake bite, which may be hemorrhagic in nature due to bleeding tendency, or ischemic in nature due to thrombosis of the middle cerebral artery. Suspicion of stroke may be raised in a patient with drowsiness and altered consciousness after a snake bite.

Signs on CT

Cerebral infarction may be seen as a hypodense ischemic lesion or a hemorrhagic area within the cerebral parenchyma.

Differential Diagnoses and Related Diseases

Kounis syndrome is a disease characterized by development of angina pectoris after an allergic reaction (allergic angina pectoris). Kounis syndrome may develop in patients with snake bites due to immunological reaction and body hypersensitivity toward the snake venom.

Hymenoptera Stings

Hymenoptera is a large group of membranous wing insects. There are three large families of stinging hymenoptera: *Vespidae* (wasps, yellow jackets, hornets), *Apidae* (honeybees and bumblebees), and *Formicidae* (stinging ants).

Insect stings cause localized or generalized reaction due to their venom. Localized reaction includes swelling, urticaria, and blister formation. Generalized reaction includes anaphylactic shock, which typically develops within 10 min, or is delayed for up to 5 h after the insect bite. Rare complications include rhabdomyolysis that induces renal failure, multi-system failure, nephrotic syndrome, and coagulopathy.

Necrotizing fasciitis (*flesh-eating disease*) is a rare complication of insect bites. It is a severe form of deep layer inflammation involving the skin and the subcutaneous tissues, commonly caused by group A *streptococcus* bacteria. Patients present with limb erythema, edema, crepitus, and pain out of proportion to the physical findings. Development of necrotizing fasciitis after an insect bite is attributed to superimposed infection of the bite site.

Signs on CT

Necrotizing fasciitis presents as hypodense muscles and subcutaneous tissues, with gas formation in the subcutaneous tissues (Fig. 11.16.2). Areas of ring contrast enhancement may be seen due to abscess formation.

11.16

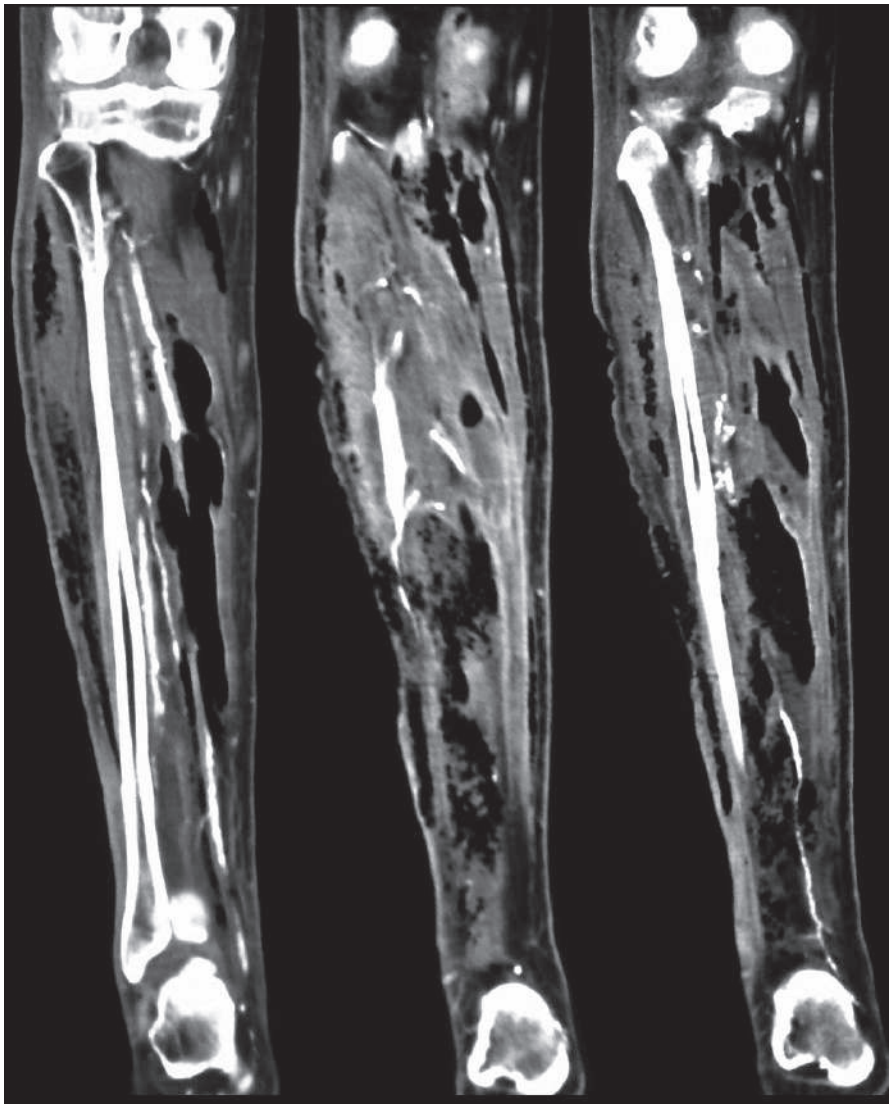

Fig. 11.16.2. Coronal sequential leg CT images of a patient with necrotizing fasciitis. Notice the severe muscle necrosis and deep tissue gas formation involving the soleus and the gastrocnemius muscles

For Further Reading

1. Awasthi M et al Imaging findings in Rabies encephalitis. Am J Neuroradiol. 2001;22:677–80
2. Takayama N. Rabies: a preventable but incurable disease. J Infect Chemother. 2008;14:8–14
3. Loathamatas J et al MR imaging in human rabies. Am J Neuroradiol. 2003;24:1102–9
4. Mani J et al Magnetic resonance imaging in rabies. Postgrad Med J. 2003;79:352–4
5. Dubinsky I. Rattlesnake bite in a patient with horse allergy and von Willebrand's disease: case report. Can Fam Physician. 1996;42:2207–11
6. Bashir R et al Cerebral infarction in a young female following snake bite. Stroke. 1985;16;328–30
7. Polo JM et al Aphasia in a farmer following viper bite. Lancet. 2002;359:2164
8. Hanchanale VS et al A costly sting! preputial gangrene following a wasp sting. Indian J Urol. 2006;22:370–1
9. George P et al Wasp sting: an unusual fatal outcome. Saudi J Kidney Dis Transplant. 2008;19(6):969–72
10. Ryssel H et al Necrotizing fasciitis after a honey bee sting. Eur J Plast Surg. 2007;30:11–14
11. Tasic V. Nephrotic syndrome in a child after a bee sting. Pediatr Nephrol. 2000;15:245–7
12. Soufras GD et al Penicillin allergy in cancer patients manifesting as Kounis syndrome. Heart Vessels. 2005;20:159–63

Index

R